EPRI | ELECTRIC POWER RESEARCH INSTITUTE

# Fire Modeling Enhancements for Fire Probabilistic Risk Assessment

## Fire Location Factor, Transient Fires, and Liquid Spill Heat Release Rate

2015 TECHNICAL REPORT

# Fire Modeling Enhancements for Fire Probabilistic Risk Assessment

## Fire Location Factor, Transient Fires, and Liquid Spill Heat Release Rate

**3002005303**

Final Report, November 2015

EPRI Project Manager
A. Lindeman



ELECTRIC POWER RESEARCH INSTITUTE
3420 Hillview Avenue, Palo Alto, California 94304-1338 ▪ PO Box 10412, Palo Alto, California 94303-0813 ▪ USA
800.313.3774 ▪ 650.855.2121 ▪ askepri@epri.com ▪ www.epri.com

## DISCLAIMER OF WARRANTIES AND LIMITATION OF LIABILITIES



THE FOLLOWING ORGANIZATION, UNDER CONTRACT TO EPRI, PREPARED THIS REPORT:

**Jensen Hughes, Inc.**



## NOTE

For further information about EPRI, call the EPRI Customer Assistance Center at 800.313.3774 or e-mail askepri@epri.com.

# ACKNOWLEDGMENTS

The following organization, under contract to the Electric Power Research Institute (EPRI), prepared this report:

Jensen Hughes, Inc.
3610 Commerce Drive, Suite 817
Baltimore, MD 21227

Principal Investigators
S. Hunt
F. Joglar
S. LeStrange
V. Ontiveros
G. Ragan
J. Williamson

This report describes research sponsored by EPRI.

This publication is a corporate document that should be cited in the literature in the following manner:

*Fire Modeling Method Enhancements for Fire Probabilistic Risk Assessment: Fire Location Factor, Transient Fires, and Liquid Spill Heat Release Rate.* EPRI, Palo Alto, CA: 2015. 3002005303.

# PRODUCT DESCRIPTION

In 2005, *EPRI/NRC-RES Fire PRA Methodology for Nuclear Power Facilities* (published jointly as Electric Power Research Institute [EPRI] 1011989 and NUREG/CR-6850) described a set of methods and data for performing a modern fire probabilistic risk assessment (PRA). Since the publication of that report, research has been underway continuously to improve the methods and to assemble and analyze additional data to better characterize nuclear power plant (NPP) risk due to fire. This report addresses three areas in which technical refinements of existing guidance or new methods have been developed:

- The development of guidance for accounting for the impacts of fires that originate near walls or in corners of rooms. In such cases, the characteristics of the fires (that is, the manner in which they grow and the heat transfer to targets in the room) are different from those for fires that originate in the middle of a room. These impacts are reflected by applying a fire location factor for the ignition source.
- The characterization of transient fire ignition frequency to account for the probability of a transient ignition source that could be located near a secondary transient combustible material.
- The characterization of heat release rate (HRR) profiles and durations for liquid spills.

The guidance included in this report is intended to promote consistency in the manner in which these conditions are treated and to increase the degree of realism associated with characterizing the fire risk for the resulting fire scenarios.

## Background

Internal fires may threaten the safe shutdown of a NPP, especially as the initial fire progresses and involves secondary combustibles such as electrical cables. EPRI 1011989 (NUREG/CR-6850) provides a framework and data for the calculation of fire frequency and size; however, some of these elements may lead to over-estimating the aggregate fire risk. Since the publication of EPRI 1011989 in 2005, additional research in many areas has led to an increased understanding of the risk contributors from fire. This report provides the results of some of that research; additional research relating to the frequency and size of fires is ongoing.

## Objectives

The objective of this report is to provide the ability to address specific elements of the fire modeling process in a more realistic manner in order to better understand the contributions to plant fire risk.

## Approach

Three specific areas for refinement are identified in this technical report. The approach for each method is described individually in more detail below.

*Fire Location Factor*. Currently, literature and experimental data are associated with the fire location factor phenomenon in fire protection engineering. However, no guidance is available for the treatment of an ignition source located near wall or corner surfaces. Such configurations are found commonly in NPPs; therefore, more explicit guidance for addressing fire scenarios associated with these locations is needed for NPP fire PRAs. In order to explore the impacts for such fires, the Fire Dynamics Simulator (FDS) software tool was used to simulate fire conditions in the open, near walls, and in corner configurations. FDS served as a tool for understanding how parameters such as HRR and distance to wall or corner influence the fire behavior and for developing the guidance for modeling such fires.

*Transient Fires*. A review of the EPRI Updated Fire Events Database (1025284) was performed to develop insights from transient fire events occurring either at power or during low-power or shutdown operating modes. The review revealed that many of the ignition sources associated with actual fires did not have the potential to develop into larger fires due to lack of nearby combustibles or minimal combustible material within the ignition source itself. Based on these insights, a factor, Wp, has been developed based on the event data to represent the likelihood of having a transient ignition source integral or near to a secondary combustible.

*Liquid Spill Heat Release Rate and Duration.* Recent experimental data for a large number of liquid fuel fire tests conducted for the U.S. National Institute of Justice were used to improve an empirical model to more realistically characterize the HRR and duration of liquid spill fires.

## Results

The results of the research documented in this report include:

1. New guidance defining the treatment of fire scenarios postulated near wall and corner surfaces. Specific conditions are described for applying the wall and corner location factor in fire plume temperature calculations.
2. A new quantification factor has been defined for characterizing the probability of transient fire scenarios. This factor improves the realism of the risk equation by incorporating the probability of transient ignition sources within or near transient combustible packages.
3. A set of equations used for characterizing the HRR profile and duration for liquid spill fires.

This research is documented such that it facilitates its implementation in fire PRAs developed over the past 10 years, using the framework described in EPRI 1011989/NUREG/CR-6850.

## Applications, Value, and Use

The results of this report can be incorporated into fire PRAs. It is expected that these methods will provide a more realistic characterization of the fire hazards for selected ignition sources or scenarios that is commensurate with operating experience. Improving the realism of these fire PRAs will allow more meaningful identification of risk contributors and more effective evaluation of potential plant improvements to reduce fire risk further.


## Keywords

| | | |
|---|---|---|
| Fire probabilistic risk assessment (FPRA) | Fire hazard | Fire location factor |
| Oil fires | Transient fires | |

# LIST OF ACRONYMS AND ABBREVIATIONS

| | |
|---|---|
| AFFF | aqueous film-forming foam |
| ASTM | American Society for Testing and Materials |
| CFD | computational fluid dynamics |
| CFAST | Consolidated Fire and Smoke Transport |
| FM/SNL | Factory Mutual/Sandia National Laboratories |
| FDS | Fire Dynamics Simulator |
| FDTs | Fire Dynamics Tools |
| $k_F$ | fire location factor |
| FPA | fire propagation apparatus |
| FIVE | fire-induced vulnerability evaluation |
| FLASH-CAT | flame spread over horizontal cable trays |
| FP | fluoroprotein |
| FAQ | frequently asked questions |
| HRR | heat release rate |
| HRRPUA | heat release rate per unit area |
| HGL | hot gas layer |
| kW | kilowatts |
| LPSD | low power-shutdown |
| MW | megawatt |
| NFPA | National Fire Protection Association |
| NIJ | National Institute of Justice |
| NIST | National Institute of Standards and Technology |
| NPP | nuclear power plant |
| NRC | Nuclear Regulatory Commission |
| OMA | operator manual action |

| | |
|---|---|
| PRA | probabilistic risk assessment |
| SDP | significance determination process |
| SFPE | Society of Fire Protection Engineers |
| THIEF | thermally induced electrical failure |
| TP | thermoplastic |
| TS | thermoset |
| TIS | transient ignition source |
| Wp | transient propagation factor |
| U.S. | United States |
| V&V | verification and validation |
| ZOI | zone of influence |

# NOMENCLATURE

## Nomenclature for Sections 5 and 6

### *Roman*

| | |
|---|---|
| A | Area (m²) |
| C | Empirical coefficient (–) |
| D | Diameter (m) |
| H | Energy (kJ) |
| k | Empirical constant for pool fire burning rate model (m-1) |
| m | Mass (kg) |
| M | Mass (kg) |
| P | Power law constant |
| q | Heat (kW) |
| Q | Heat (kW) |
| r | Radial coordinate (m) |
| R | Radius (m) |
| t | Time (s) |
| T | Temperature (°C) |
| v | Velocity (m/s) |
| V | Volume (m³) |

### *Subscript*

| | |
|---|---|
| ∞ | Limiting or maximum value; ambient value |
| δ | Relating to the fuel depth |
| act | Actual value |
| b | Relating to the burning duration at a fixed point in a liquid pool |
| c | Relating to combustion |
| cr | Critical value |

| | |
|---|---|
| d | Duration |
| e | Equivalent |
| lag | Relating to the lag or heat release rate development time |
| o | Outer |
| p | Peak value |
| pred | Predicted value |
| v | Relating to the velocity spread time |

### *Superscript*

| | |
|---|---|
| . | Per unit time (1/s) |
| “ | Per unit area (1/m²) |

### *Greek*

| | |
|---|---|
| β | Empirical constant for pool fire burning rate model (–) |
| δ | Fuel depth (m) |
| Δ | Change operator |
| θ | Angular coordinate (radians) |
| ρ | Density (kg/m³) |
| σ | Surface tension (mN/m) |

# CONTENTS

# LIST OF FIGURES

# LIST OF TABLES

# 1
# INTRODUCTION

In 2005, the Electric Power Research Institute (EPRI) and the U.S. Nuclear Regulatory Commission (NRC) jointly published a framework and methodology to support the development of modern fire probabilistic risk assessment (PRA) known as EPRI 1011989/NUREG/CR-6850 (referred to here as NUREG/CR-6850). Since publication, this methodology has been widely implemented in support of risk-informed applications such as National Fire Protection Association (NFPA) 805. Since that time, technical areas have been identified where the current methods, assumptions, and data may produce conservative results. This has resulted in the need to further examine these areas and understand how prior simplifications, assumptions, or conservatisms could affect insights and decision making.

This report examines a more detailed treatment of three technical areas: fire location factor (Sections 2 and 3), transient fire frequency (Section 4), and liquid spill fire heat release rate (HRR) treatment (Sections 5 and 6). For each method, the scope, technical basis, and revised treatment are discussed.

## 1.1 Fire Location Factor

The fire location factor is a parameter used to modify the plume equation for fires that are located near a wall or corner to reflect the effects of air entrainment in the plume temperature. This modifier produces higher plume temperatures above the ignition source and, consequently, a larger vertical zone of influence when compared to fires postulated in the open (that is, away from wall or corner surfaces).

Section 2 of the report is structured to provide the background, literature review, and scoping of Fire Dynamics Simulator (FDS) software simulations that were used to investigate the assignment of fire location factors. A literature review of existing studies, including a comparison of FDS results to earlier experimental data, was performed. Influencing parameters, such as HRR, fire diameter and distance from the wall, are discussed, and a simulation matrix details the FDS simulations performed in support of this effort.

Section 3 of this report presents the results of the FDS simulations. Over 50 simulations were performed to explore the behavior of fire near walls and corners. Sensitivities to wall parameters and a treatment of uncertainty are provided. Also, fire PRA implementation guidance and examples are discussed.

## 1.2 Transient Fire Frequency

Transient fire propagation is the next method addressed in this report. Available fire event data from the U.S. commercial nuclear industry capture general transient ignition events. A review of the data suggests that many of the ignition sources do not contain sufficient combustibles to grow into larger fires and thus may need to be within close proximity to secondary combustibles to become challenging fires. Therefore, the current transient fire frequency may be overestimated.

Section 4 of this report presents the concept of the propagation factor, Wp, that accounts for the likelihood of having a transient ignition source integral or nearby to secondary combustibles. The parameter, Wp, has been developed to modify the ignition frequency of transient fires during all modes, at-power, and low-power shutdown (LPSD) operating modes.

## 1.3 Liquid Spill Fire Heat Release Rate Treatment

The characterization of the HRR profile and duration associated with liquid spill fires is the final method explored in this report. This research is based on fire tests conducted for the U.S. National Institute of Justice, which provided a wealth of data to enhance existing methods for characterizing liquid spill fires.

Section 5 of this report discusses the current methods available for determining the fire hazard and duration for liquid spill fires. Additionally, a discussion of the assumptions and limitations of the methods are discussed. Finally, experimental results for confined and unconfined liquid spills are presented.

Section 6 of the report reviews the experimental data. The data have been classified to provide a more realistic method to characterize the HRR profiles. Updated implementation guidance is provided in Section 6.2 along with common pre-solved HRR profiles and durations in Appendix C.

# 2
# GUIDANCE ON THE IMPLEMENTATION OF FIRE LOCATION FACTORS NEAR WALLS AND IN CORNERS FOR THERMAL PLUMES

## 2.1 Introduction

Fire plume temperatures are routinely calculated in fire modeling and fire PRAs in the commercial nuclear power industry. This is because numerous fire scenario configurations consist of risk-contributing equipment above potential fire sources. The latest guidance available for determining fire plume temperatures includes the use of fire location factors when the fire is postulated near corners or along walls to account for the increased thermal exposure in those configurations [1]. This report provides detailed guidance on the appropriate use and selection of fire location factors suitable for fire plume temperature predictions in fire PRA. The guidance provided in this report is intended for field application, and the results are ultimately presented in a simplified manner for ease of use.

Fires that are located near a wall or a corner may experience reduced air entrainment and a force imbalance on the plume that tends to push the flames against the boundary [2]. The offset distance between a fire and a wall or a corner boundary at which the boundary influences the entrainment likely varies with the fire size and other parameters. In practice, distances from walls and corners used in fire modeling analyses range from as little as a few inches to several feet as documented in the *Technical Basis for Fire Protection Significance Determination Process* [5].

When a fire is considered to be influenced by a wall or a corner boundary, the "image" method is used to quantify the effect on the entrainment. The image method treats a fire adjacent to a wall as one-half of a virtual fire with a symmetry plane coincident with the wall boundary. This is accomplished by application of fire location factors when the fire is postulated in corners or along walls to account for the potentially increased thermal plume temperatures in those configurations [4, 5]. The term *fire location factor* refers to a variable, which is typically expressed in equations by the symbol $k_F$, used in calculating fire plume temperatures in wall and corner configurations. The location factor can be equated to the number of reflections of the analyzed configuration required to equate it with an open fire plume configuration. The location factor has the effect of increasing the resulting plume temperature to account for two conditions that may be related to each other:

- Less entrainment of fresh air into the fire plume is due to the wall surfaces surrounding the fire. That is, fire away from wall surfaces is able to entrain ambient air into the fire plume around its entire circumference. The concept of *air entrainment* refers to the fire-induced movement of fresh air into the fire plume due to density differences in the ambient air and

the warmer fire plume gases. In contrast, a fire in a corner or along a wall would be able to entrain air only along the portions of its circumference that are not blocked by the wall surfaces. Less entrainment of fresh air into the fire plume produces higher plume temperatures.

- Fires in contact with wall and corner surfaces tend to produce longer flames, which in turn may produce higher plume temperatures. The longer flames are due to flames being forced toward the wall surfaces by the momentum of the air entrainment on the open side, effectively "pushing" the flames against surfaces and potentially stretching the reaction zone over a greater height. The longer flames can also be due to the reduced rate of entrainment relative to the open burning configuration, and the fuel requires more entrainment height in order to draw in sufficient oxygen to complete the combustion reaction.

The location factor application does not currently account for the potential that the wall surfaces may reduce the thermal plume temperatures by convective heat transfer losses. Limited guidance is currently available in the method for how to apply the fire location factor in commercial nuclear power plant (NPP) applications. Two specific clarifications are necessary for plume temperature exposure analysis: 1) when to use the fire location factor, and 2) what value of the location factor to use.

The first clarification refers to how far the fire needs to be from the wall surfaces for the location factor to be applicable. There is no clear guidance on what the distance should be. Current guidance in the fire protection engineering literature recommends values ranging from "zero" distance (that is, the fire should be flush with the wall surfaces [3], to conservative applications for fires 0.6 m from the surfaces [5].

The second clarification refers to the numerical value assigned to the fire location factor. Current guidance suggests a value of 4 for fires in a corner and a value of 2 for fires along a single wall surface [4, 5, 7].

In commercial NPP applications, the concept of fire location factors is most relevant for calculating the zone of influence (ZOI). A ZOI is the region surrounding a fire where a cable or component can be damaged by fire-generated conditions [4]. For the same HRR, the ZOI will be different for fires in corners or along walls if the fire location factor is applied. Since the fire plume temperature is expected to increase for fires near walls or corners, the corresponding ZOI associated with these fires is expected to be larger.

Given the relative importance of fire location factors in the analysis of NPP fire scenarios, and the need to maintain the fire modeling calculations that are part of fire protection programs, the clarifications described above are necessary. This report documents research developed with the objective of understanding fire plume temperatures near wall surfaces (that is, corners and walls) so that specific guidance can be provided on applying fire location factors to plume temperature calculations. The research and guidance described in this report is intended to clarify the question of when to apply location factors and what value to use when analyzing commercial NPP fire scenarios. It is anticipated that this guidance can also be applied to other types of analyses such as hot gas layer types of exposures.

## 2.2 Purpose and Scope

### 2.2.1 Purpose

Consistent with the two main clarifications listed earlier, the purpose of this study is twofold:

1. Describe the research, providing the technical basis for the application of fire location factors in plume temperature exposure calculations.
2. Describe the recommended methodology for applying fire location factors in typical commercial NPP fire scenarios. Specifically, this report provides guidance on when to apply the fire location factor and which values to use.

### 2.2.2 Scope

The scope of the research includes the investigation of fire plume temperatures near wall surfaces using the National Institute of Standards and Technology (NIST) Fire Dynamics Simulator (FDS), Version 6.01. In addition, existing experimental data available in fire protection engineering literature have been considered. It should be noted that the guidance described in this report is limited to thermal plume ZOI applications without hot gas layer conditions. That is, the analysis does not cover room heat-up effects associated with a ceiling obstruction on the plume temperature. As such, it is intended to be used in plume temperature calculations supporting the characterization of the ZOI in the early stages of the fire (that is, before significant room temperature increases). Additionally, the presence of an obstruction, such as a fire located in a cabinet, forced ventilation, and changes in fire source elevation are not explored in this investigation.

Understanding the thermal plume behavior in the presence of wall surfaces is a necessary first step to understanding the effects on hot gas layer types of exposures. It is anticipated that the plume temperature guidance can also be applied to other types of analyses such as hot gas layer types of exposures; however, this effort does not attempt to encompass such effects. This study will establish the framework for analyzing fire modeling data that will allow future studies to build upon the knowledge of fire behavior related to NPP fire scenarios.

## 2.3 Assumptions and Limitations

The assumptions and limitations that follow are applicable to this research.

### 2.3.1 Heskestad's Fire Plume Correlation

A mathematical model for characterizing fire plume flows based on the conservation of mass, energy, and momentum has not been developed in this research to address restricted flows by walls and corners. Instead, the Heskestad fire plume correlation is used as a surrogate for characterizing axi-symetric fire plumes. The following considerations influenced this decision:

- The Heskestad correlation is a widely used model for calculating fire plume temperatures as identified in fire PRA methodology [4] and validation of fire models for NPP applications [1, 12].
- The Heskestad correlation has been verified and validated for commercial nuclear applications [1, 12].

- As an algebraic mathematical model, the Heskestad correlation can be easily evaluated and applied for the purposes of this research and for fire PRA applications.
- A review of a multitude of thermal plume correlations [21] concluded that several reported correlations use a nearly identical approach to that used by Heskestad.

Note that the Heskestad correlation assumes axi-symetric plumes with the source of energy concentrated at a point in space near the base of the fire (that is, the virtual source, see Heskestad [13]). Consequently, the research documented in this report includes fires modeled as axi-symetric plumes, and the results are compared with FDS simulations with similar fire sources.

The application of the guidance documented in this report to other plume configurations such as "line fires" has not been investigated. The existing guidance has allowed the application of location factors to other types of analyses. These applications are typically justified by the fire modeler for the specific configuration being explored. This document does not seek to limit those applications, but rather to begin the process of improving the guidance for future applications.

### 2.3.2 Fire Dynamics Simulator

The Fire Dynamics Simulator (FDS), Version 6.0.1 [8], was used to develop simulations of wall and corner effects. FDS is a computational fluid dynamics (CFD) model of fire-driven fluid flow. FDS solves numerically a form of the Navier-Stokes equations appropriate for low-speed, thermally driven flow with an emphasis on smoke and heat transport from fires. The formulation of the equations and the numerical algorithm are contained in the *FDS Technical Reference Guide* [9]. Verification and validation (V&V) of the FDS are discussed in the FDS V&V guides [10, 11].

Although FDS is routinely used for solving practical fire problems in fire protection engineering, including fire reconstruction investigations, sprinkler design, smoke management, and so on, it is also useful as a tool to study fundamental fire dynamics and combustion [9], including low-speed transport of heat and combustion products from fire. This latter purpose serves as motivation for using FDS 6.0.1 as the source of the "virtual fire experiments" developed in this research.

The following reasons justify the use of FDS 6.0.1:

- FDS provides the flexibility to model the scenarios with the selected influencing factors required for supporting the study of fire location factors.
- FDS has been verified and validated for commercial nuclear applications in Verification and Validation of Selected Fire Models for Nuclear Power Plant Applications [12]. Additionally, NIST updates the FDS V&V study with each new release.
- There is precedent in the commercial nuclear industry in using FDS for fire PRA applications. For example:
- An FDS simulation provides the technical basis in the approach described in Fire PRA FAQ 13-0004 dealing with "sensitive electronics" inside electrical cabinets.
- A number of fire PRAs have used FDS in support of the fire modeling calculations for estimating time to control room abandonment due to fire generated conditions.

- In comparison to an experimental program, FDS models can be revised and reproduced at very little cost or time delay.
- FDS base case simulations for fire plumes (that is, plume applications away from wall surfaces) have been compared with fire plume temperature correlations as a benchmark.

### 2.3.3 Zone of Influence Applications

The information developed here applies to determining the fire plume component (that is, the vertical ZOI distance of the plume) generated in the initial stages of the fire.

The guidance provided in this report does not consider room heat-up effects (that is, development of a hot gas layer). The practical implication of this limitation is that the guidance is focused on the "early stages" of a fire where substantial smoke accumulation and room heat-up has not occurred. This limitation also prevents any direct evaluation of the potential effects of a wall surface on the smoke visibility reduction in a compartment. Existing guidance on smoke visibility reduction is still applicable and should be used without modification.

This analysis also does not provide any justification for altering the treatment of the thermal radiation horizontal ZOI. Thermal radiation effects are often used to determine the horizontal ZOI. The existing guidance should be used to determine the thermal radiation horizontal ZOI.

### 2.3.4 Flame Height

The guidance provided in this report covers only the non-combusting region of the fire plume (that is, the smoke rising above the fire source). The combusting region of the fire plume (that is, the flames) is not addressed. Specifically, the effects that proximity to a wall or corners may have on flame heights have not been investigated. The maximum extent of the ZOI described in this report is not directly affected by the flame interaction with the boundary as this has been implicitly captured in the results of the FDS simulations. The outcome of this study will have no impact on the damage predictions for targets exposed to direct flame impingement.

### 2.3.5 Ceiling Jet

As stated previously, the guidance provided in this report is limited to the "early stages" of a fire where substantial smoke accumulation and the development of a hot gas layer has not occurred. Consequently, the guidance provided does not consider the development of a ceiling jet. The authors have no evidence to support applying the results of this investigation to ceiling jets and are reluctant to speculate.

### 2.3.6 Other Limits of Applicability

The research and guidance documented in this report are based on typical commercial NPP fire scenarios, such as the following:

- The simulations that were developed in FDS consist of wall boundaries with concrete thermo-physical properties. Concrete walls are common in NPP scenarios for which this guidance is provided. Additional simulations are performed to show in Section 3.1.4 that the results presented in this analysis are no different for gypsum and steel wall surfaces.

- Temperature measurements above the fire are made up to 6 m above the fire source, which is the typical elevation of room heights in NPPs.
- Evaluated HRRs were up to 1 MW, which is approximately equal to the 98$^{th}$ percentile HRR value recommended for ignition sources in Appendix G of NUREG/CR-6850. The current investigation does not consider the effects of secondary combustibles, such as cable trays ignited above the initiating fire source.
- The current analysis applies to relevant temperature exposures for thermoplastic and thermoset cable targets. Lower temperatures are not considered to be relevant to risk, and the existing guidance for exposure to flame temperatures is appropriate.
- The current investigation does not consider the effect of forced or augmented ventilation.
- The effect of obstructions, such as cabinet walls and ceiling around a fire source, on fire plume flows is not considered in this investigation. This topic is being studied independently of the wall and corner effects on thermal plumes in NUREG-2178/EPRI 3002005578 [28].
- FDS simulations performed in this investigation do not vary the elevation of the fire (vent) above the floor. Variation in the fire source elevation is not considered to be a substantial factor without the presence of a ceiling to allow the accumulation of heat.
- The current investigation applies to defining the thermal plume exposure and extent of the ZOI, assuming relevant temperature exposures for thermoplastic (TP) and thermoset (TS) cable targets. The range of relevant temperatures includes 130°C to 800°C as defined in Section 2.4.6.4.
- Since FDS has the inherent capability to predict plume temperatures under the influence of wall surfaces, FDS results should never be adjusted in post-processing calculations to account for the presence of a wall surface. The bias correction developed in this analysis does not apply to results obtained directly from FDS and is intended for use with the Heskestad fire plume temperature correlation only. A qualified user of FDS should develop an appropriate set of inputs to address the effects of wall surfaces directly and not by adjusting the output data with a bias correction.

## 2.4 Technical Approach (Methodology)

The fire location factor, $k_F$, is a variable that has the effect of increasing the resulting plume temperature used in calculating fire plume temperatures when fires are located in corners or along walls.

To improve upon the limited guidance provided in how to apply the fire location factor and to address the previously identified specific clarifications necessary for plume temperature exposure analysis, the Heskestad plume correlation is modified to include a fire location factor. This factor is estimated through a comparison of the correlation results to those of a fire model simulation.

In the following information, the historical development of the fire location factor, the modification of the Heskestad fire plume correlation, and the simulations used in this investigation are reviewed.

### 2.4.1 Background

A number of studies have explored the effects of wall and corner effects on fire plumes. Works by Zukoski [15]; Hasemi and Tokunaga [16, 17]; Alpert and Ward [7]; Takahashi et al. [18]; and Poreh and Garrad [19] note that corner and wall configurations restrict entrainment of air into the fire plume. The phenomenon of air entrainment refers to the fire-induced movement of fresh air into the fire plume due to density differences in the ambient air and the warmer fire plume gases. Fires away from wall surfaces are able to entrain air into the fire plume around its entire circumference. In contrast, a fire in a corner or along a wall would be able to entrain air only along the portions of its circumference that are not blocked by the wall surfaces. Less entrainment of fresh air into the fire plume produces higher plume temperatures.

The effect of this, often referred to as the *image* or *mirror method*, can be treated as shown in Figures 2-1 and 2-2. For a corner geometry, a pseudo HRR of four times the actual HRR is used to represent the effect of the corner on the entrainment. Following this representation, the actual entrainment is only one-quarter of the perimeter of the pseudo fire.

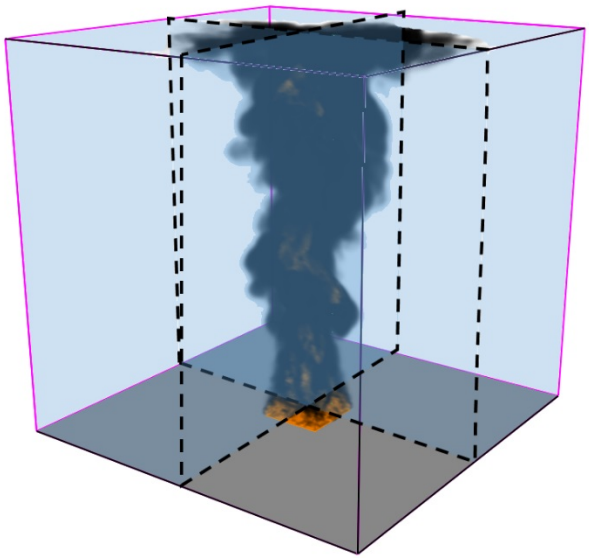

**Figure 2-1**
**Corner pseudo-fire representation**

A similar representation of a fire located next to a wall can be made, with a pseudo fire two times as large as the actual fire.

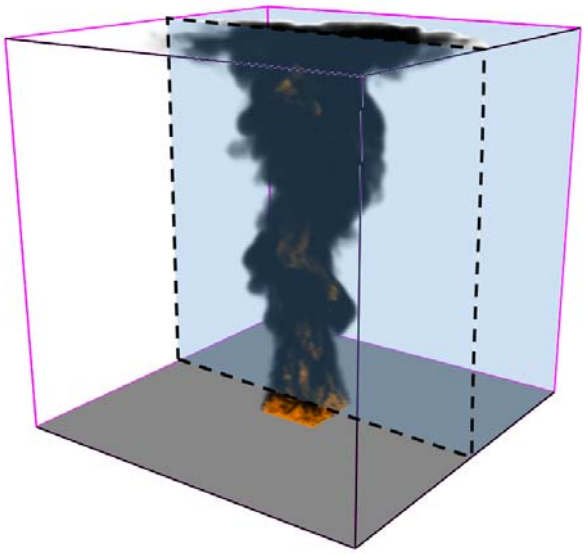

**Figure 2-2**
**Wall pseudo fire representation**

A considerable amount of the research performed on the effects of walls and corners on fire plumes focused on the mass flux and flame height. However, observations on the plume temperatures are available. Results from Hasemi and Tokunaga [17] showed that doubling the HRR as outlined in the image method resulted in an overestimation of the flame height on the order of 30%. Similar differences are expected for applying a factor of four with fires located in corners as the mirror method does not consider wall drag and suppression of large-scale flame structures by the wall surface [21].

The same results from Hasemi and Tokunaga showed that the excess plume temperatures are inversely proportional to the entrainment of fresh air and that the measured plume temperature increase is greater than what would be predicted using the image method described in the journal article, “Some experimental aspects of turbulent diffusion flames and buoyant plumes from fire sources against a wall and in a corner of walls” [17].

This investigation will consider the conclusions presented by Hasemi and Tokunaga, using the recommended corner treatment. Plume temperature measurements subject to wall and corner effects for a single HRR are presented; however, this evidence is not sufficient to develop detailed recommendations on the application of fire location factors and is, at best, a single point of comparison. Other studies provide normalized data that are not easily tailored for comparison with the results of this investigation. These results will be reviewed and compared with results from this investigation.

Experiments performed by Takahashi et al. [18] showed an excess temperature increase, when compared to the model presented by McCaffrey [22], as the fire source moved closer to a corner or wall surface. Additionally, a decrease in the plume mass flux was observed when compared to the correlation provided by Zukoski et al. [15]. Following observations that air entrainment mass flux is almost constant along upward velocity for a fire located along walls and near corners, results from Takahashi et al. [18] showed that mixing of air is restricted and laminarization of the plume flow occurs along vertical walls. These results suggest a dependence on turbulence for plume flows. It should be noted that the HRRs used in this study were below values of 25 kW.

Experiments performed by Poreh and Garrad [19] follow earlier observations that adjacent walls decrease mass flux and increase flame height. These results also showed that the dimensionless span of the flame height fluctuations in confined fires is larger than that of free fires, so that the increase of the peak values due to walls is larger than the increase on their mean values [19].

Experiments performed by Mowrer and Williamson [20] explored the effects of walls and corners on hot gas layer (HGL) temperatures. This investigation does not consider room heat-up effects, such as the development of an HGL. However, some of the observations made by Mowrer and Williamson are comparable to this investigation. One experimental observation made was that moving the fire source only 0.05 m away from a wall surface decreased the HGL temperatures measured when compared with a fire located directly adjacent to a wall surface [20]. A similar decrease in plume temperatures was observed as the fire source moves away from wall and corner surfaces from the FDS simulations. Additionally, Mowrer and Williamson [20] concluded that a fire located in a corner was equivalent to having a fire approximately twice as large located in the open. The factor increase was around 1.5 for a fire located along a single wall surface. These factors are lower than the values of 4 and 2 postulated by the mirror method to modify an HRR for a fire located near wall and corner surfaces.

Alpert and Ward [7] developed relations to estimate the increase in plume temperature at heights above a fuel source. Within these equations, to account for the decreased entrainment and its effect on the plume temperature, a fire location factor, $k_F$, was proposed. The relation proposed by Alpert and Ward [7] is:

$$\Delta T = \frac{0.22(k_F \dot{Q})^{2/3}}{z^{5/3}} \qquad \textbf{Eq. 2-1}$$

Where:

$\Delta T$ is the temperature increase above ambient in degrees centigrade.

$k_F$ is the fire location factor, 2 for near walls and 4 for corners.

$\dot{Q}$ is the HRR in watts.

$z$ is the height above the fuel source in meters.

However, values of $k_F$ greater than 1 have been applied in fire scenarios where the postulated fire is flush against the wall to distances of 0.6–0.9 m [5], independent of the fuel source width or diameter.

While providing considerable insight into the effects of walls and corners on fire plume temperatures, the Alpert and Ward research does not provide sufficient evidence to develop detailed guidance on the application of fire location factors.

### 2.4.2 Plume Theory

The point source solution of turbulent plume flow has shown a remarkable ability to correlate velocities, temperatures, and mass flow rates above the flame tip [21, 26]. This solution assumes the fire to be a single point source of heat. The details of the point source become less observable as the distance from the point increases until only the total output becomes relevant. This investigation will focus on the near field plume behavior, where the temperatures of interest are comparable to the damage thresholds of cables used in NPPs.

#### 2.4.2.1 Plume Scaling

As identified in the references presented above, significant effort has been undertaken in the study of plume theory. Relations developed by Zukoski et al. [15] are capable of estimating plume temperatures and velocities for fires uninfluenced by wall surfaces. Using these relationships, the following simplified proportionality allows for an estimation of the plume centerline temperatures at different elevations above a fire source [21]:

$$\Delta T_m \sim \dot{Q}^{2/3} z^{-5/3} \quad \textbf{Eq. 2-2}$$

Where:

$\Delta T_m$ is the rise in plume temperature above ambient in kelvin.

$\dot{Q}$ is the HRR in kW.

$z$ is the height above the fire source in meters.

Constants of proportionality have been determined by a number of investigators. The constant of proportionality, $A$, modified to include the virtual origin, $z_0$, can be estimated as:

$$A \approx \frac{\Delta T_m}{\dot{Q}^{2/3}(z-z_0)^{-5/3}} \quad \textbf{Eq. 2-3}$$

When comparing these constants of proportionality determined by various investigators, a value of 26 is suggested for use when the convective HRR is known [21]. This value is consistently reported among the several studies reviewed by Beyler [21]. One of the relations that follows the above proportionality is the Heskestad fire plume correlation.

#### 2.4.2.2 Heskestad Plume Temperature

The objective of this study is to develop a modification to the Heskestad fire plume correlation using the results from fire model simulations and provide guidance for the use of the fire location given these results.

In this investigation, the correlation used to predict the changing fire plume temperature was developed by Heskestad [13, 26]:

$$\Delta T = 9.1 \left[\frac{T_0}{(g c_p^2 \rho_0^2)}\right]^{1/3} \dot{Q}_c^{2/3} (z - z_0)^{-5/3} \quad \textbf{Eq. 2-4}$$

Where:

$\Delta T$ is the change in temperature above ambient (K).

$g$ is the acceleration due to gravity (m/s$^2$).

$c_p$ is the specific heat of air (kJ/kg·K).

$\rho$ is the density of air (kg/m$^3$).

$\dot{Q}_c$ is the convective HRR (kW).

$z$ is the height above the top of the combustible (m).

$z_0$ is the height of the virtual source (m) calculated as:

$$z_0 = -1.02D + 0.083\dot{Q}^{2/5} \quad \textbf{Eq. 2-5}$$

Where:

$D$ is the diameter of the fire source (m).

$\dot{Q}$ is the HRR (kW).

This correlation is valid only above the mean flame height $F_h$. The mean flame height can be calculated as:

$$F_h = -1.02D + 0.230\dot{Q}^{2/5} \quad \textbf{Eq. 2-6}$$

The Heskestad fire plume correlation was chosen for this study because it is identified as the correlation for use in calculating the damage temperature in vertical plume ZOI applications. However, unlike the correlation developed by Alpert and Ward, this correlation does not include a location factor to account for the fire source being located in a corner or near a wall.

In this investigation the Heskestad correlation is modified to account for the effects of a fire located in a corner or near a wall. The purpose of this modification is to expand the Heskestad fire plume correlation so that it better captures the effects of more complicated geometries such as when located near wall or corner surfaces.

#### 2.4.2.3 Modified Heskestad Plume Equation

Following the approach used by Alpert and Ward [7], the modified Heskestad equation becomes:

$$T_{pl} = T_0 + 9.1\left[\frac{T_0}{(gc_p^2\rho_0^2)}\right]^{1/3}\left(k_F\dot{Q}_c\right)^{2/3}(z - z_0)^{-5/3} \quad \textbf{Eq. 2-7}$$

Where:

$T_{pl}$ is the plume temperature (K).

$T_0$ is the ambient temperature (K).

$g$ is the acceleration due to gravity (m/s$^2$).

$c_p$ is the specific heat of air (kJ/kg·K).

$\rho$ is the density of air (kg/m$^3$).

$k_F$ is the fire location factor identified in Table 3-3.

$\dot{Q}_c$ is the convective HRR (kW).

$z$ is the distance above the fuel source (m).

$z_0$ is the virtual origin (m).

Since the virtual origin, $z_0$, makes use of the HRR as well, it too must be modified:

$$z_0 = -1.02D_F + 0.083\left(k_F\dot{Q}\right)^{2/5} \quad \textbf{Eq. 2-8}$$

The effective diameter used in Equation 2-8 also includes the fire location factor and is determined as:

$$D_F = D\sqrt{k_F} = \sqrt{\frac{k_F\dot{Q}}{\dot{q}''}\cdot\frac{4}{\pi}} \quad \textbf{Eq. 2-9}$$

where $\dot{q}''$ is the HRRPUA (kW/m$^2$), for the fuel source.

In this study, $k_F$ was estimated by comparing the temperatures predicted by the Heskestad fire plume correlation to those predicted by FDS. The fire location factor was determined such that the modified Heskestad fire plume correlation estimations matched the temperature measurements from the FDS simulations. To achieve this, $T_{pl}$ used in the modified Heskestad fire plume correlation is taken from the FDS simulations, and the value of $k_F$ is estimated such that the correlation prediction matches the FDS simulation result. The values of $k_F$ estimated in this approach not only captured the effect of walls and corners located near fires, but also the differences between the FDS simulations and the Heskestad fire plume correlation.

The inclusion of $k_F$ in the virtual origin means that a numerical solution must be used to determine $k_F$. This was accomplished using the Newton-Raphson method of approximation. For more on the Newton-Raphson method, see Ypma [24].

### *2.4.3 Configuration Definitions*

No clear description of what constitutes a wall or corner configuration is presented in the literature. As discussed above, a primary reason that fires located next to wall surfaces produce higher fire plume temperatures results from a reduced entrainment of fresh air. Therefore, for a fire to be subject to the guidance outlined in this report, the following definitions are provided:

A *wall configuration* consists of a single wall surface at least 1 m (3.2 ft.) in length that extends past the fire source in both directions parallel to the closest edge of the fire source (as shown in Figure 2-3).

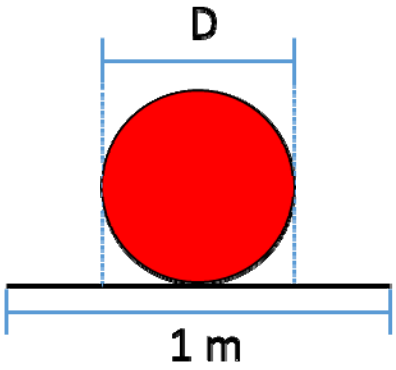


**Figure 2-3**
**Wall configuration geometry**

A *corner configuration* consists of two adjoining wall surfaces at least 1 m (3.2 ft.) in length with an angle between 45° and 135° and that extends past the fire source in both directions (as shown in Figure 2-4).

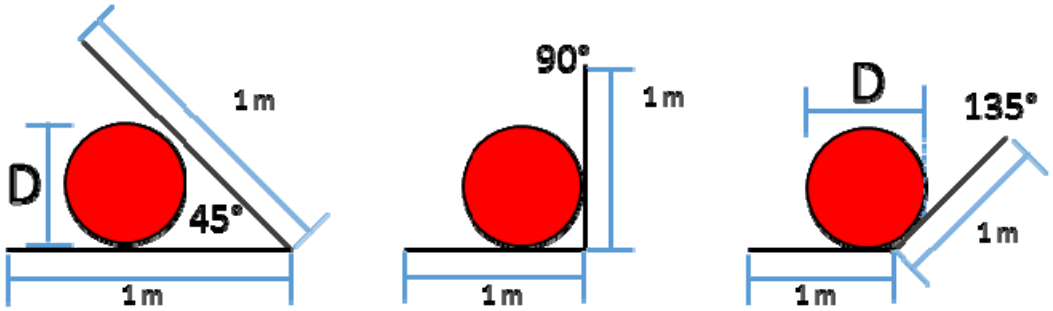


**Figure 2-4**
**Corner configuration geometry**

For both wall and corner configurations, the wall surface(s) must extend to the full height from the source to the target.

Configurations not meeting the wall or corner definitions in Figures 2-3 and 2-4 should be treated as an open configuration. These definitions are based on observations of plume behavior made with this investigation.

### *2.4.4 FDS 6.0.1 Validation*

FDS 6.0.1 has undergone a significant V&V exercise [11]. In this section, FDS simulations will be compared with experimental evidence to develop confidence that the simulations used in this analysis are capable of representing actual experimental evidence.

#### 2.4.4.1 Factory Mutual/Sandia National Laboratories Data

Of particular interest to this investigation are the validation exercises conducted in which plume temperatures for fires located in corners and near walls were studied. The series of experiments conducted by Factory Mutual under the direction of Sandia National Laboratories (FM/SNL) were done in a manner to simulate typical power plant conditions [23]. Of these experiments, seven were conducted with a fuel source located adjacent to a wall, and two were conducted with the fuel source located in a corner. The general layout of the test series is shown in Figure 2-5.

Results from this test series were used to determine the capability at which FDS 6.0.1 could accurately simulate fire plume temperatures. FDS 6.0.1 does a reasonable job estimating the plume temperature with little bias (1.18) and uncertainty (0.20) [11]. In Figure 2-5, the locations of both the fire source and the temperature measurements (taken at stations and expanded stations) were identified for the experiments, and FDS simulations were taken at 5 and 10 second intervals, respectively.

As noted with the assumptions outlined in Section 2.3, this investigation does not consider substantial smoke accumulation and room heat-up effects that are present in the FM/SNL experimental measurements and FDS simulated results through the development of an HGL. Since the values for $k_F$ estimated for the FDS results are consistently larger than the experimental

results, the potential effects of the model bias and the smoke accumulation need to be considered in the design and evaluation of the FDS simulations. The FM/SNL test series was designed to simulate typical NPP conditions. The test series provides results for fires located near wall surfaces and within corners and is included in the FDS V&V for fire plume temperature rise. This test series provides the best available experimental data for comparison with this investigation. However, the results are not directly applicable to the goal of this investigation due to the smoke and heat accumulation effects; the results are used more as proof of concept to show that FDS is capable of predicting fire plume temperature rise and is appropriate for this investigation.

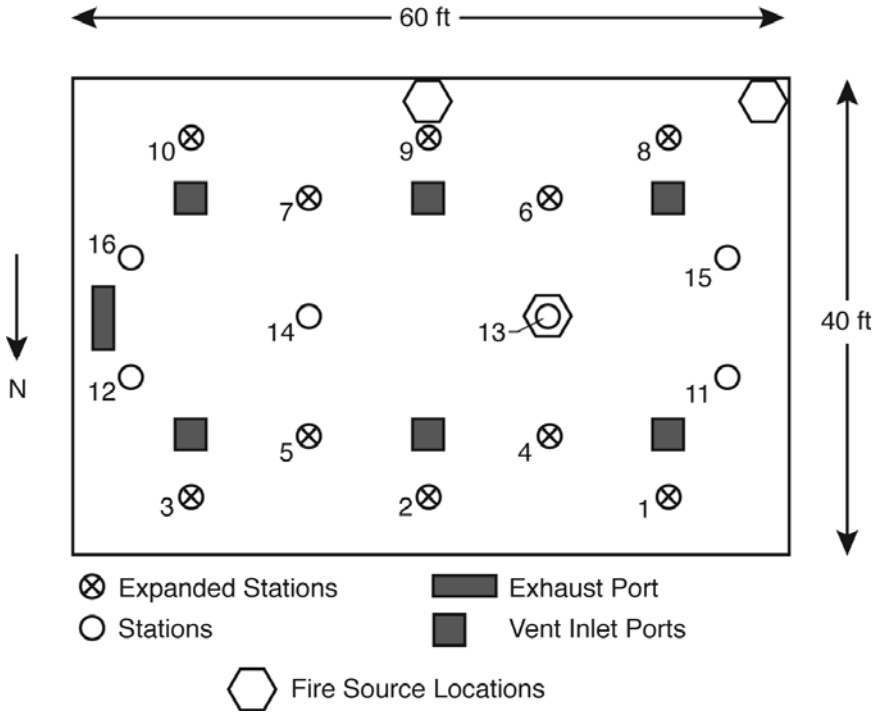


**Figure 2-5**
**FM/SNL compartment layout (modified from Reference 23)**

Data from these validation exercises have been reviewed to compare the fire location factors estimated using the FM/SNL experimental data to those estimated using the FDS simulation data. As shown in Figure 2-5, for the fire sources located near a single wall surface and within a corner, the temperature measurements are not taken directly over the fire source (temperatures are taken at expanded stations 8 and 9). Therefore, the temperature data used in this analysis are more representative of the ceiling jet next to the plume, not within the plume.

In Figure 2-6, the estimated values of $k_F$ as a function of time for two experiments with fire sources located near a single wall surface are presented. These values of $k_F$ were determined using the experimentally measured temperatures and the temperatures simulated by FDS. The values of $k_F$ estimated using the FDS simulations are presented as solid lines. The estimated values of $k_F$ using the experimentally measured data are presented as dashed lines. In each case, it appears that the values of $k_F$ estimated using the temperatures from the FDS simulations are greater than those using the experimentally measured temperatures. The estimated values for $k_F$

from FM/SNL Experiment 14, determined using the FDS simulated temperatures as well as the experimentally measured temperatures are similar and greater than the historical value of 2. The values for $k_F$ using data from FM/SNL Experiment 15 show less agreement with the FDS temperature, determined values of $k_F$ are greater.

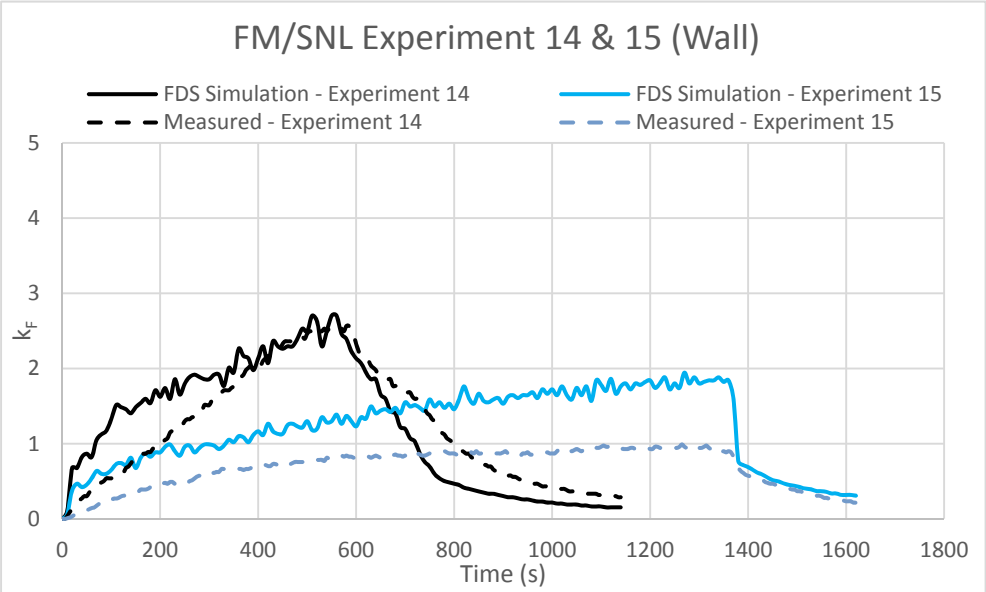


**Figure 2-6**
**$k_F$ vs. time – FM/SNL wall configuration experiments**

A similar comparison for the experiments using fires located in the corner are presented in Figure 2-7. For the fires located in the corners, once again the estimated values for $k_F$ are greater for the FDS simulations than for those values estimated using the experimentally measured temperatures. For both experiments, the estimated values of $k_F$ do not reach the historical value of 4. The results presented for $k_F$ in Figures 2-6 and 2-7 are shown as a function of time over the course of different experiments from the FM/SNL test series. These results show that while FDS on average over-predicts temperatures by about 18% [11], the impact of this variation on $k_F$ is considerably larger and can be up to a factor of two in this case. However, the location factor in this case is also being affected by the accumulation of heat within the room, so it is difficult to isolate all of the potential effects.

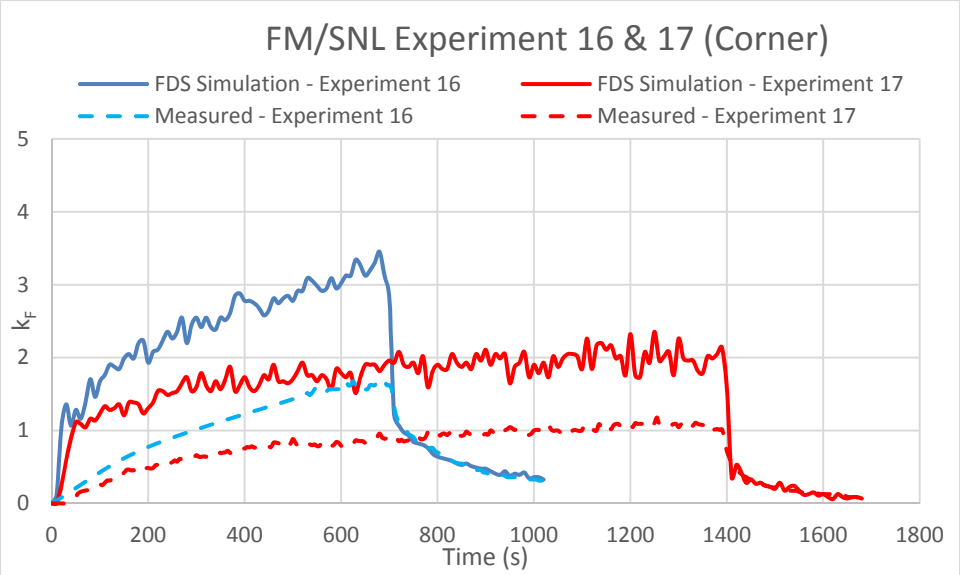


**Figure 2-7**
**$k_F$ vs. time – FM/SNL corner configuration experiments**

In Table 2-1, a comparison between the maximum values of $k_F$ estimated using the temperature data reported during different FM/SNL experiments are compared to those estimated using plume temperatures from FDS simulations of the FM/SNL test series [23] for fires located in corners and near walls. This is achieved by taking the largest temperature data from the experiment or FDS, regardless of time, and mathematically determining the appropriate value of $k_F$ required to match the data to the modified Heskestad correlation.

**Table 2-1**
**Fire location factors FM/SNL test series**

| Experiment | Geometry | kF: Exp* | kF: FDS | HRR (kW) |
|---|---|---|---|---|
| 6 | Wall | 1.40 | 2.56 | 500 |
| 10 | Wall | 2.06 | 2.34 | 1000 |
| 11 | Wall | 1.49 | 1.47 | 500 |
| 12 | Wall | 1.72 | 2.50 | 2000 |
| 13 | Wall | 1.52 | 2.31 | 2000 |
| 14 | Wall | 2.56 | 2.70 | 500 |
| 15 | Wall | 0.94 | 1.94 | 1000 |
| 16 | Corner | 1.74 | 3.64 | 500 |
| 17 | Corner | 1.22 | 2.46 | 500 |

*As presented in Figure 2-5, measurements were not taken directly in the plume. For a discussion, see Section 2.4.4.1.

The results in Table 2-1 show that the FDS simulations result in slightly larger estimations of $k_F$ than those estimated using the experimental data. The values for $k_F$ estimated by FDS range from 1–3 for wall geometries and are larger, ranging from 2–4, for corner geometries. These values are close to those expected from the literature; however, the values for $k_F$ estimated using the experimental data are, in most cases, slightly lower. This is consistent with the observed bias reported for FDS for predicting plume gas temperatures such that FDS has a tendency to predict higher temperatures relative to the reported experimental validation data [11].

This may also be a result of the difference in how the temperatures are measured between the experiment and FDS. The temperatures are measured in the FM/SNL experiments using aspirated and bare-bead thermocouples. In the FDS simulations, temperatures were measured using device parameters that report the gas temperature directly and do not account for the thermal mass and other physical characteristics associated with thermocouples.

While potential differences between the experimental results and FDS simulations used in this analysis may affect the observed results, the differences are not significant enough to invalidate the outlined approach. These differences are observed and discussed in order to carefully consider their impact on the conclusions generated in this work. While this experimental study and model comparison adds value to this work, it offers no conclusive answer to the application of location factors.

#### 2.4.4.2 Hasemi and Tokunaga Data

Experimentally measured plume temperatures for a fire with a 60 kW HRR located within a corner and along a single wall surface are provided by Hasemi and Tokunaga [17]. These results are comparable to the lower HRRs used in this investigation and are reviewed below.

In Figure 2-8, plume temperatures at different elevations from Hasemi and Tokunaga [17] for a 60 kW fire are compared with plume temperatures predicted by FDS for fires with two of the closest HRRs used in this investigation, 40 kW and 78 kW for a corner configuration. For consistency, the data selected from the Hasemi and Tokunaga report are the highest measurements at any given height. The results show that the plume temperatures measured by Hasemi and Tokunaga are almost completely bounded by the temperatures predicted by FDS. The temperatures measured by Hasemi and Tokunaga in the 60 kW experiment are closer to those predicted by FDS for the 40 kW HRR. The flame height, estimated using Equation 2-6, for the 60 kW fire used by Hasemi and Tokunaga is estimated to be 0.86 m. Therefore, the Figure 2-8, may be within the flame.

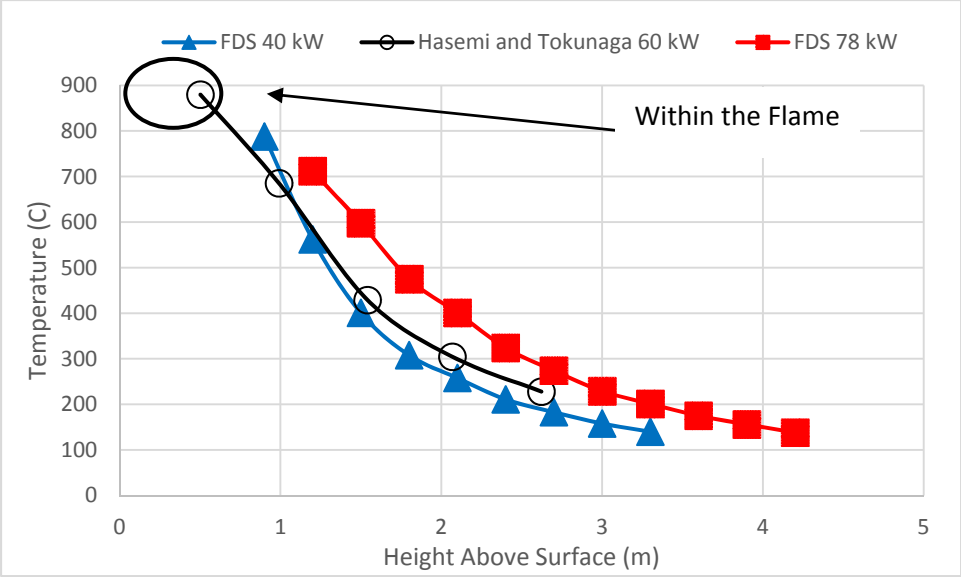


**Figure 2-8**
**Plume temperatures at different elevations, corner configuration – Hasemi and Tokunaga and FDS simulations**

A similar comparison can be made with the results presented for a fire located near a single wall surface. These results are presented in Figure 2-9. For the wall configuration results, the plume temperatures measured by Hasemi and Tokunaga for a 60 kW fire are very close to the temperatures estimated by FDS for a fire with an HRR of 78 kW. For consistency, the data selected from Hasemi and Tokunaga report are the highest measurements at any given elevation. Once again, with an estimated flame height of 0.86 m, the highest temperature plotted in Figure 2-9 using the Hasemi and Tokunaga [17] results may be within the flame.

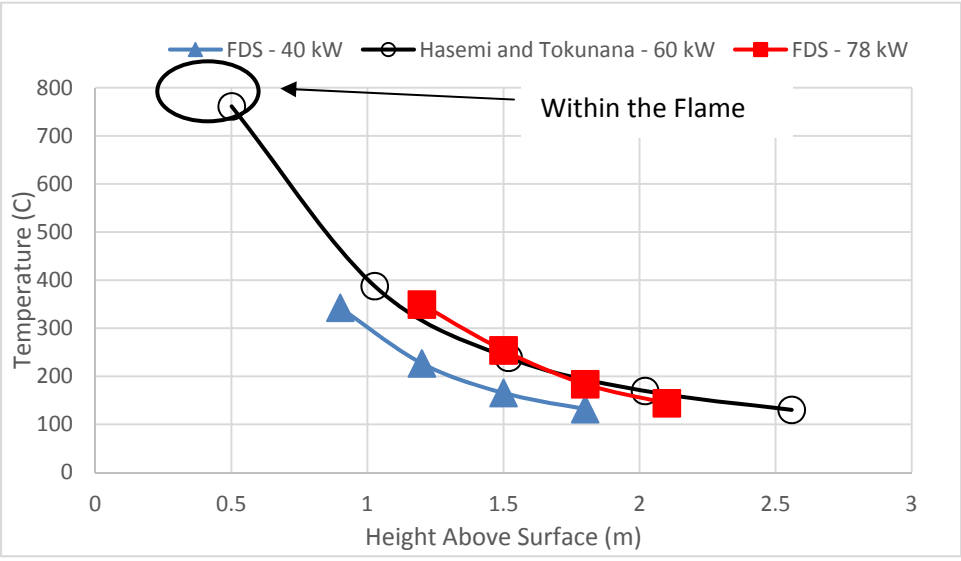


**Figure 2-9**
**Plume temperatures at different elevations: wall configuration – Hasemi and Tokunaga and FDS simulations**

Estimated values of $k_F$ at different elevations using the plume temperatures measured by Hasemi and Tokunaga are compared with estimated values of $k_F$ from the 40 kW and 78 kW FDS simulations in Figure 2-10. The results in Figure 2-10 show that the estimated values for $k_F$ are comparable between the measured and simulated results.

In Figures 2-10 and 2-11, the low values of $k_F$ estimated are likely within the flame region. It was observed that near the flame, the estimated values of $k_F$ are lower than those estimated at higher elevations where plume temperatures decrease. The larger estimated values of $k_F$ plotted in Figure 2-11 correspond to temperatures lower than cable damage thresholds and are not considered to be significant to this application.

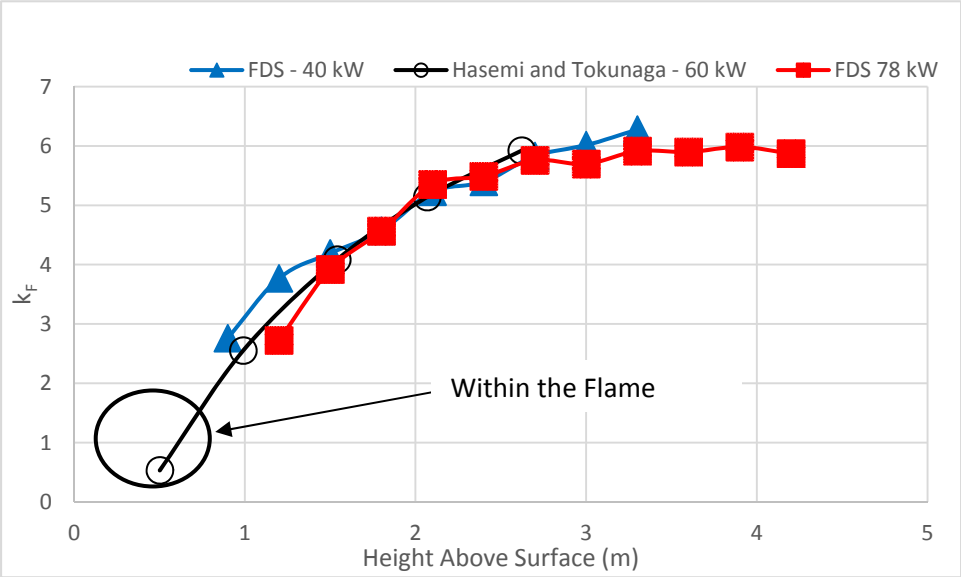


**Figure 2-10**
**Estimated values of $k_F$ at different elevations: corner configuration – Hasemi and Tokunaga and FDS simulations**

The estimated values of $k_F$ for a wall configuration are presented in Figure 2-11. For the wall configuration, the estimated values of $k_F$ for the experimental data presented by Hasemi and Tokunaga are larger than those estimated using the FDS simulations. This differs from the results seen for the fires located within corners, which were in agreement with the current results. Differences in experimental conditions and assumptions made for modeling purposes between the experiments performed by Hasemi and Tokunaga when compared with the FDS simulations used in this investigation may provide a possible explanation:

- The walls used by Hasemi and Tokunaga were constructed of calcium silicate, which is more insulating than the concrete boundaries used with the FDS simulations performed as part of this investigation.
- Fire location factors for the experimental measurements were calculated using a radiative fraction of 0.27 [27] to account for the use of propane [17]. The FDS simulations use fuel properties for the polyethylene-jacketed electrical cables, which have a notably higher soot yield and an assumed radiative fraction of 0.3.

- The HRR per unit area (HRRPUA) for the burner used in the experiments performed by Hasemi and Tokunaga is lower than the HRRPUA used in the corresponding FDS simulations (see Section 2.4.5.2). Results of this investigation show that lower HRRPUAs are often associated with higher estimates of $k_F$. This is thought to be tied to differences in turbulence and will be discussed later in this report.

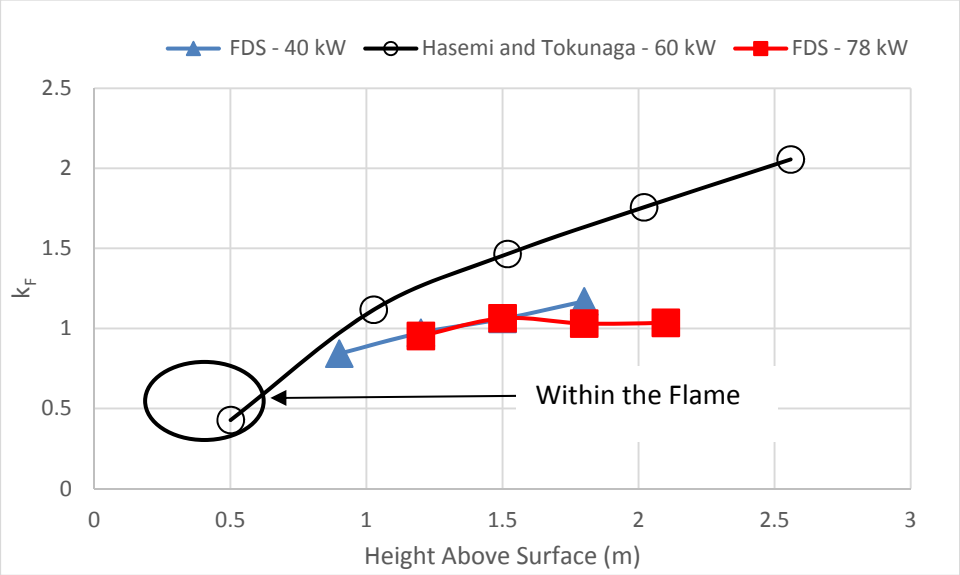


**Figure 2-11**
**Estimated values of $k_F$ at different elevations: wall configuration – Hasemi and Tokunaga and FDS simulations**

### *2.4.5 The FDS Simulations*

Fifty-one simulations using the Fire Dynamic Simulator (FDS) software were used to develop the simulation data for this study. Four influencing factors were identified in order to define a "test matrix":

- HRR
- Fire diameter
- Elevation above the fire where the plume temperature is measured
- Distance of the fuel package from wall surfaces

These factors are based on the study of fire plume flows currently available in the fire protection engineering literature and the specific needs of this research. The influencing factors are described in the information that follows.

#### 2.4.5.1 Heat Release Rate

The HRR is perhaps the most important influencing factor in all fire modeling applications. In the specific case of axi-symetric fire plumes, it represents the energy released at a point in space near the base of a fire, generating the upward movement of flows. HRR values selected for this study range from approximately 40 kW–1000 kW. This range is based on the range of 98$^{th}$

percentile HRR recommendations for ignition sources in commercial NPP applications in Appendix G of NUREG/CR-6850 [4]. This range of HRRs covers the most applicable variations for which the thermal plume exposure is used for detailed fire modeling in support of fire PRA development.

#### 2.4.5.2 Fire Diameter

The fire diameter characterizes the size of the fire base. It has been identified as an important parameter governing fire plume temperatures, velocities, and flame heights. Consequently, it is included as an influencing factor to evaluate its impact on fire plume temperatures near wall surfaces. Fire diameters are varied based on the interactions between the HRR and the HHRPUA. The width of the fuel source used in the simulations is determined by taking the square root of the HRR divided by the HRRPUA. HRRPUAs used in this investigation were 500 kW/m$^2$, 1000 kW/m$^2$ and 2000 kW/m$^2$. The majority of cases were evaluated at 1000 kW/m$^2$ and a few cases at lower and higher values to approximate the sensitivity to this parameter. The resulting range of fire diameters selected for this study was 0.23 m (0.75 ft.) to 1.13 m (3.7 ft.). These values were also appropriate for the validation range of the Fire Froude Number (Q*) as reported in EPRI 1011999 and NUREG-1824 [12].

#### 2.4.5.3 Elevation Above the Fire

The elevation above the fire refers to distance from the base of the fire where the plume temperature is measured. Typical fire plume flow behavior in terms of velocity and temperature is characterized by decreasing magnitudes as the elevation increases. The elevation ranges from 0 m (0 ft.), representing measurements at the base of the fire, to approximately 6 m (20 ft.) above the fire. The upper limit of 6 m was selected because that is the maximum height of many rooms in commercial NPPs. This is a relatively large distance at which the fires usually modeled would not generate damaging temperatures. Fire plume temperatures were measured in the FDS simulations at 0.3 m (1 ft.) intervals. At each elevation, three temperature measurements were recorded at different locations within the fire plume in order to capture the plume centerline temperature while accounting for plume shifting to the corners and walls.

#### 2.4.5.4 Distance from Wall Surfaces

The distance from wall surfaces refers to how far the fire source is from a wall or a corner. This was a necessary factor for the specific application addressed in this report. As the distance from the wall surfaces to the fire source was varied in the different FDS simulations, the temperature in the plume was measured for evaluating the impact of boundary effects on the fire plume temperature. The range of variation for this factor is from 0 m, representing fires flush with the wall surfaces, to 1.5 m, representing fires in the open (that is away from walls or corners). Distances used in this investigation were 0 m, 0.24 m, 0.48 m, 0.76 m, 1.0 m, and 1.48 m, commensurate with the numerical grid resolution.

Test matrices of simulations performed in this investigation are presented in Tables 2-2 and 2-3.

**Table 2-2**
**FDS corner configuration simulation test matrix**

| Heat Release Rate (kW) | Fire Source Separation Distance from Corner, L (m) | | | | | |
|---|---|---|---|---|---|---|
| | **0** | **0.24** | **0.48** | **0.76** | **1** | **1.48** |
| 40 | X | x | x | x | x | x |
| 78 | X | x | x | x | x | x |
| 250* | X | x | x | x | x | x |
| 500 | X | x | x | x | x | x |
| 1000* | X | x | x | x | x | x |

x – FDS simulation was performed.
* – Additional simulations were performed to vary the fire source diameter.

**Table 2-3**
**FDS wall configuration simulation test matrix**

| Heat Release Rate (kW) | Fire Source Separation Distance from Wall, L (m) | | | | | |
|---|---|---|---|---|---|---|
| | **0** | **0.24** | **0.48** | **0.76** | **1** | **1.48** |
| 40 | X | x | x | x | x | x |
| 78 | X | x | x | x | x | x |
| 250* | X | x | x | x | x | x |
| 500 | X | x | x | x | x | x |
| 1000 | X | x | x | x | x | x |

x – FDS simulation was performed.
* – Additional simulations were performed to vary the fire source diameter.

### 2.4.5.5 Simulation Compartment

The compartment used in this investigation measures 6 m x 6 m x 6 m. The compartment is bounded on two sides by concrete walls and includes a concrete floor. In this investigation room, heat-up effects are not included. Therefore, the other three surfaces, including the ceiling, are modeled as open (see Figure 2-12). A mesh of 150 x 150 x 150 was used for each simulation resulting in a grid resolution of 4 cm. The values of $D^*/\delta x$ ranged from 6.6 to 24.0, which falls within or exceeds the values of $D^*/\delta x$ used in the validation study of FDS sponsored by the U.S. NRC and EPRI [12].

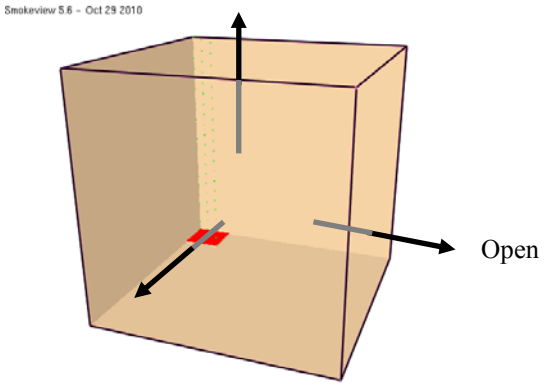


**Figure 2-12**
**Simulation compartment**

In Figure 2-13, the different configurations used in the investigation are presented. The different configurations include a base configuration of a fire located sufficiently away from wall surfaces. The other configurations presented are of fires located near a single wall surface and fires located in corners. The configurations presented in Figure 2-13 for fires located near a wall surface and in a corner are of those with a distance away from the surface equal to zero. In Figure 2-14, the change in distance as the fuel source moves away from the wall surfaces in a corner configuration is presented. In Figure 2-14, a fire with an HRR of 40 kW is shown located flush against the wall at a distance of 0 m and at two additional distances, 0.76 m and 1.48 m, from the corner.

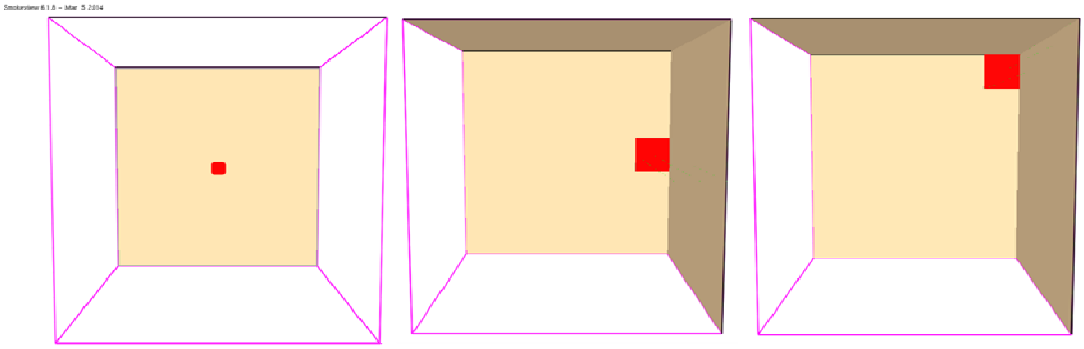

**Figure 2-13**
**Simulation compartment configurations (open, wall, corner)**

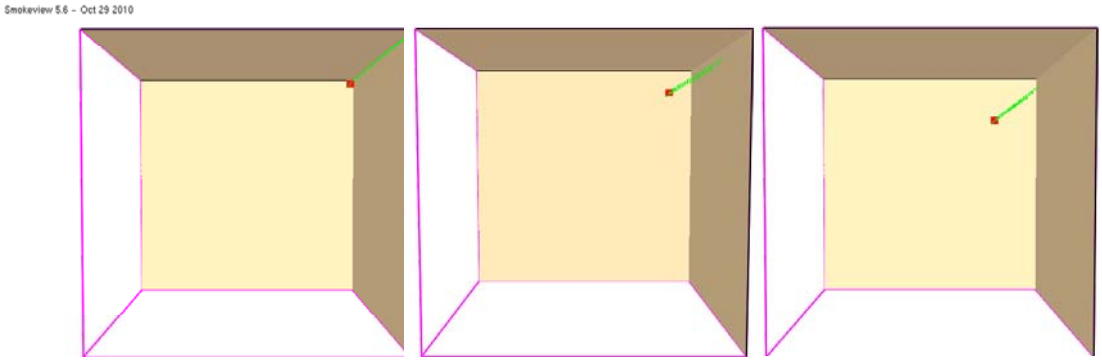


**Figure 2-14**
**Fuel source locations – distance from corner, 0 m, 0.76 m, 1.48 m**

Data gathered from these simulations are used to estimate the value for $k_F$ from fires at different locations, of various HRRs, and with different fuel source diameters.

#### 2.4.5.6 Temperature Measurement Plane

Above the fuel source, temperature predictions are obtained using slice files in FDS every 0.03 seconds. Slice files save horizontal planar slices of data at user-specified locations (see Figure 2-15). This is the equivalent of experimentally placing thermocouple devices at 4 cm (1.6 in) spacing in the horizontal plane at each elevation. Temperatures used in this investigation were averaged over a period of 10 seconds in order to determine averaged plume centerline data in a manner similar to that used to develop plume correlations by Heskestad. Each simulation predicts a total time of 30 seconds which, as discussed in Section 2.4.6.1, is longer than necessary to achieve steady-state plume conditions. The slice files are included at elevations spaced every 0.3 m (1 ft.) from the floor to the top of the 6 m tall compartment. Using the slice file to record temperature measurements ensures that the maximum plume temperature can be recorded for analysis, regardless of the location, within the compartment. The maximum plume temperature at elevations above the fire source is used to determine the effect of wall surfaces on plume temperatures and develop information for any resulting change in the ZOI.

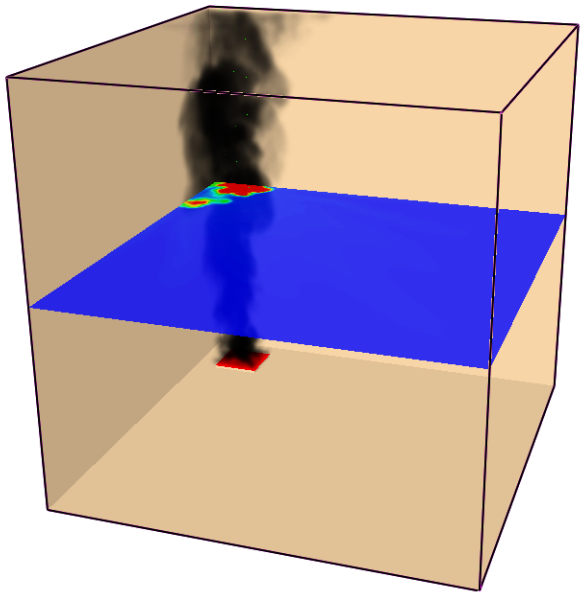

**Figure 2-15**
**Slice file simulation temperature measurements**

As outlined above, data gathered from these simulations were used to estimate the value for $k_F$ from fires at different locations, of various HRRs, and with different fuel source diameters for fires located near walls or corners.

### *2.4.6 Preliminary FDS Simulations*

In the following sections, the results for simulations with fuel sources located in corners and near walls are reviewed and analyzed to ensure proper implementation of the model and to confirm that the results provided appropriate data. First, results for open configurations, fires unaffected by corners and walls, will be reviewed. Second, four example simulations used in this investigation are reviewed. The simulations reviewed are for 40 kW and 1000 kW fires in corner and wall configurations.

#### 2.4.6.1 Open Configuration – Control

Simulations with the fire source subject to no wall or corner effects for each of five HRRs used in this investigation were performed. In Figure 2-16, fires with HRRs for 40 kW and 1000 kW located in the open are shown. The 40 kW and 1000 kW fire represent the smallest and largest HRRs simulated in this investigation.

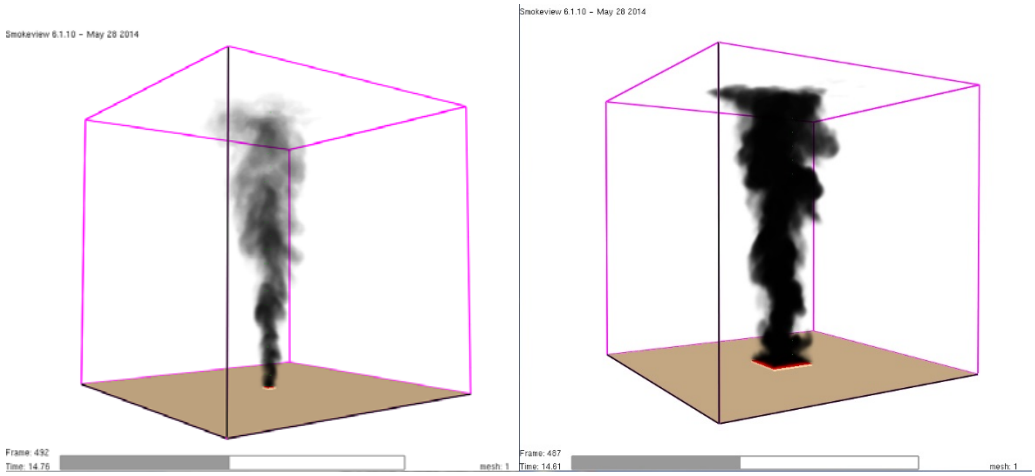

**Figure 2-16**
**40 kW and 1000 kW – open configuration**

Figures 2-17 and 2-18 show the HRR vs. time for the two open configuration simulations presented in Figure 2-16. The HRRs shown are the FDS default described by:

$$\dot{Q}(t) = \dot{Q}_0 \cdot tanh\left(\frac{t}{\tau}\right) \qquad \textbf{Eq. 2-10}$$

Where:

$\dot{Q}_0$ is the user-specified HRR in kW.

$t$ is time in seconds.

$\tau$ is the time for the HRR to ramp up to its prescribed value in seconds.

The default value (1) for $\tau$ in FDS was not modified in this investigation. This fire growth rate was considerably faster than that recommended by NUREG/CR-6850 [4], and was applied here to achieve a fast steady-state performance and limit simulation time. The HRR for the two simulations quickly reached the user-specified values of 40 kW and 1000 kW and varied throughout the remainder of the simulation due to turbulent fluctuations simulated by FDS. In Figures 2-17 and 2-18, the 1 second time-averaged HRR is presented along with the resulting HRR described by Equation 2-10 directly to verify that the HRR has been implemented correctly.

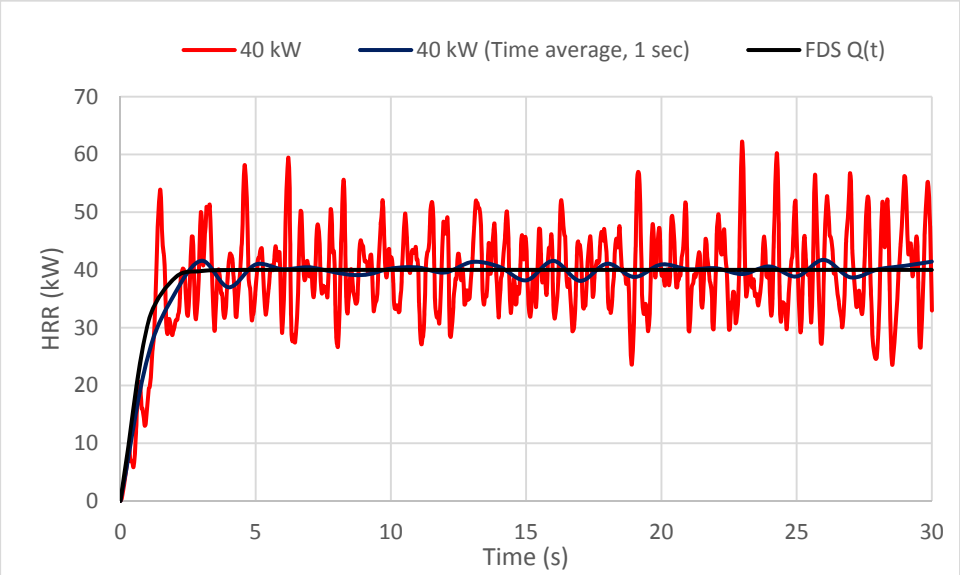


**Figure 2-17**
**HRR vs. time, open configuration – 40 kW**

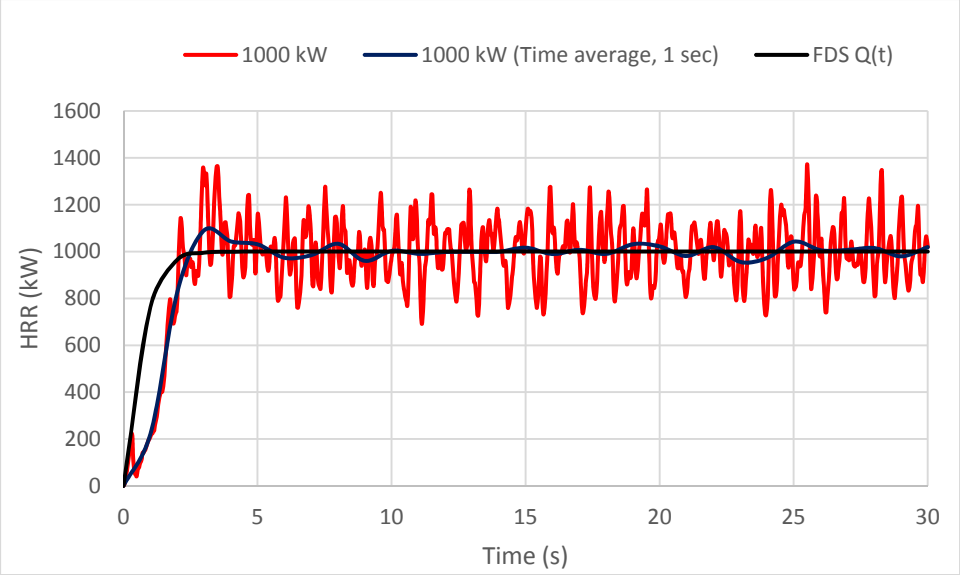


**Figure 2-18**
**HRR vs. time, open configuration – 1000 kW**

In Figure 2-19, the temperature at different elevations (Ht.) in meters vs. time for the 1000 kW fire is presented. These results show that the temperature became sufficiently steady after 15 seconds and within the 30 second duration of the simulations used in this investigation. Additional simulations using 40 kW, 250 kW, and 1000 kW HRRs showed no significant increase or decrease in plume temperatures over a period of 180 seconds. The up and down variations in the data were associated with the 5 second data interval and will be addressed by averaging over a 10 second interval (with slice data) that improves the statistics.

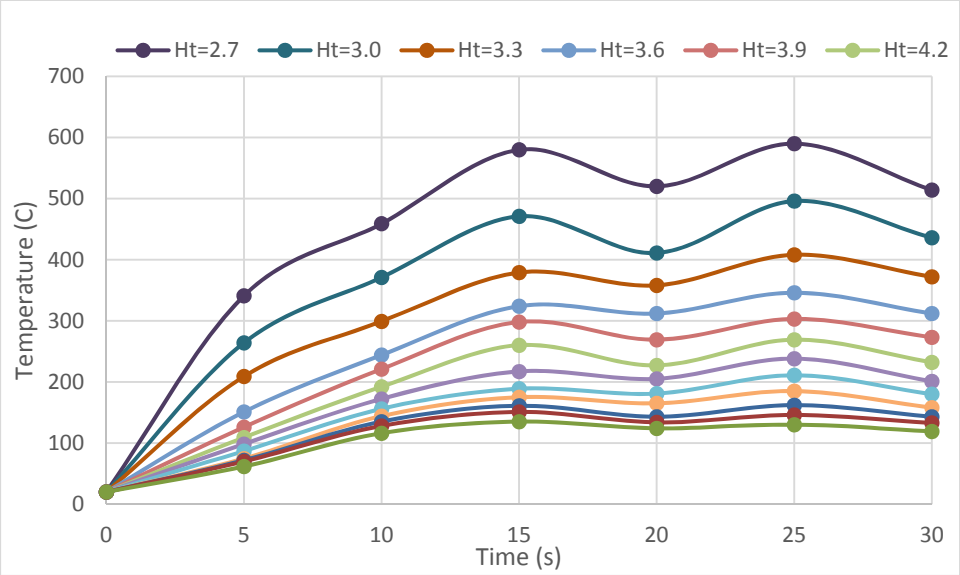


**Figure 2-19**
**Temperature vs. time, open configuration – 1000 kW, different elevations above the fuel source**

In Figure 2-20, the fire plume temperatures predicted by FDS and the Heskestad fire plume correlation are presented. For the 40 kW fire, the Heskestad fire plume correlation appears to be slightly conservative with respect to the FDS simulated plume temperatures. For the 1000 kW fire, the FDS simulated plume temperatures are greater than the temperatures predicted by the Heskestad fire plume correlation.

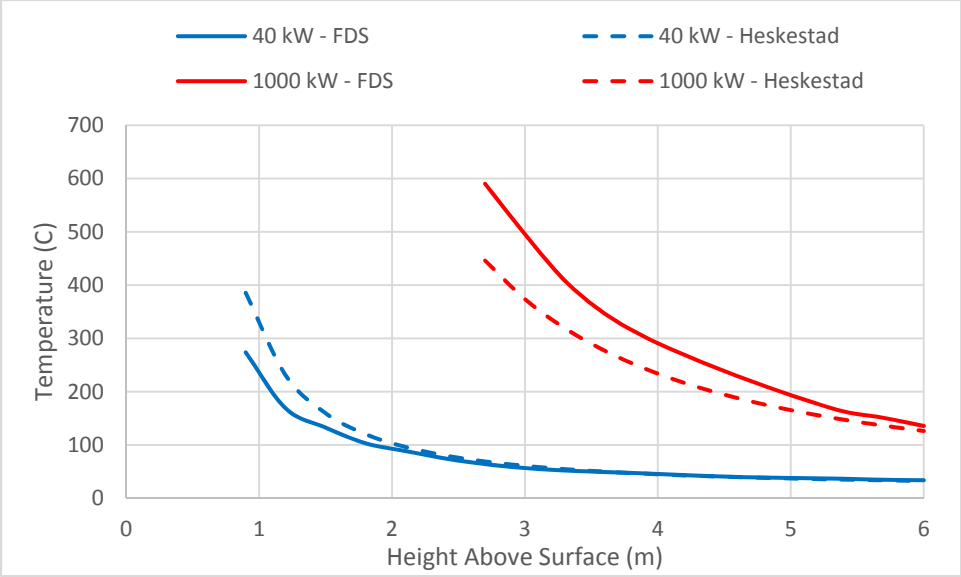


**Figure 2-20**
**Temperature vs. elevation above floor, open configuration – 40 kW and 1000 kW**

Also shown in Figure 2-20 is the different elevations at which data are taken for the two HRRs. The Heskestad fire plume correlation is applied only above the mean flame height as described by Equation 2-6. Temperatures within the flame region of the fire have been reported to produce consistent temperatures that are not likely to be affected in a meaningful way by the wall or corner. A typical NPP fire PRA application would treat all targets within the flame height of the source fire to fail very quickly, and additional specificity for the temperature in this region is unnecessary. For this investigation, the flame height was predicted by the Heskestad flame height equation. Any simulation data from elevations below the predicted flame height were excluded from this investigation. For the 40 kW HRR simulation, a height of 0.9 m above the floor was predicted. That height increases to 2.7 m for the 1000 kW size fire as a result of the higher predicted flame height.

The following sections will compare outputs between Heskestad and FDS for fires located in corners and adjacent to walls.

### 2.4.6.2 Corner Configuration

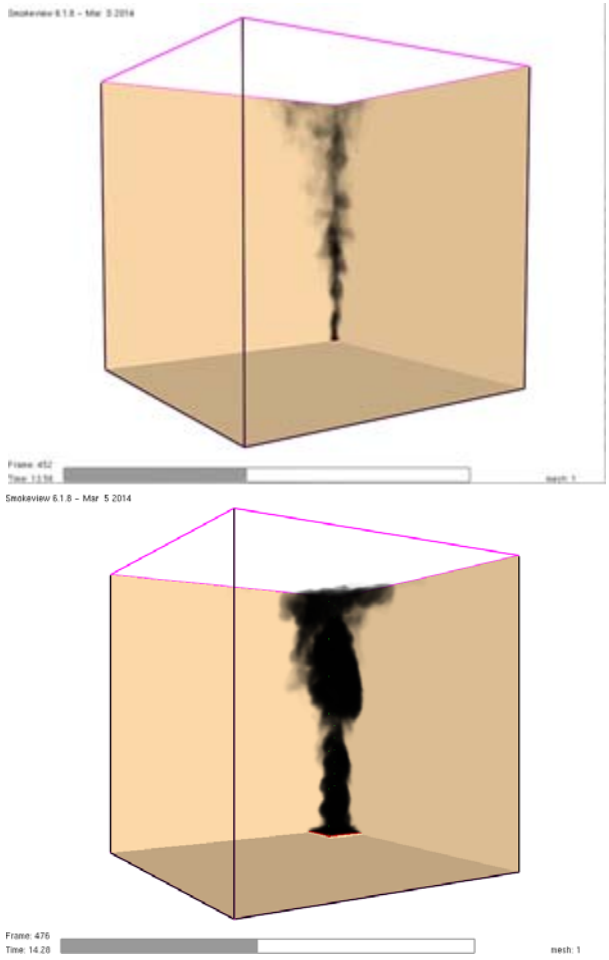


**Figure 2-21**
**40 kW and 1000 kW – corner configuration**

In Figure 2-21, fires with HRRs of 40 kW and 1000 kW located in corners are shown.

The HRRs for the simulations are similar to those presented in Figures 2-17 and 2-18.

In Figure 2-22, the temperature profiles for the 40 kW and 1000 kW HRRs in corners are presented. Also included are the unmodified Heskestad (Equation 2-4) fire plume correlation temperatures. A comparison between the results suggests that a modification to the Heskestad plume temperature equation is required when the fire source is located in a corner. The simulations for fires in corners show a clear underestimation of the plume temperature predicted by the unmodified Heskestad fire plume correlation when compared to the plume temperatures simulated by FDS.

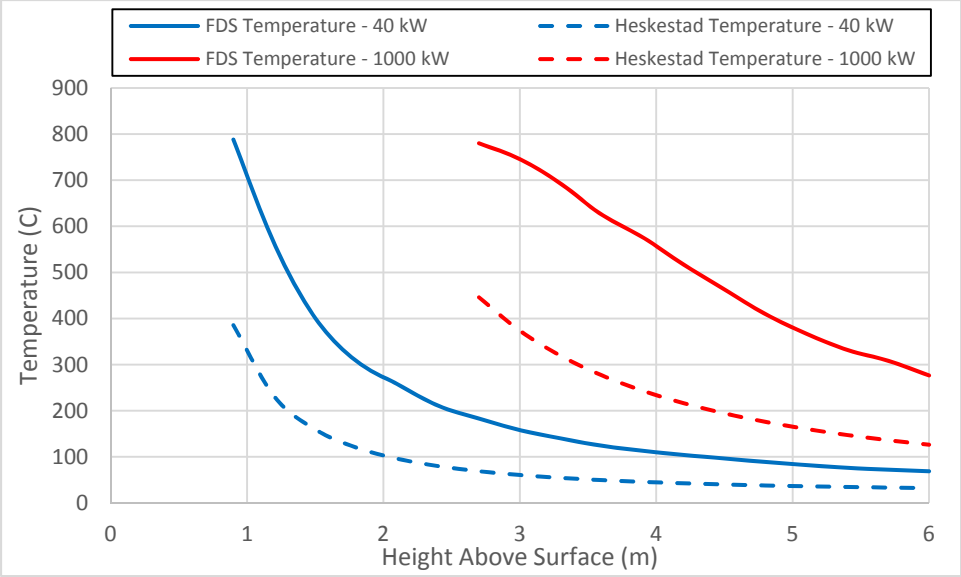


**Figure 2-22**
**Temperature vs. elevation above floor, corner configuration – 40 kW and 1000 kW**

### 2.4.6.3 Wall Configuration

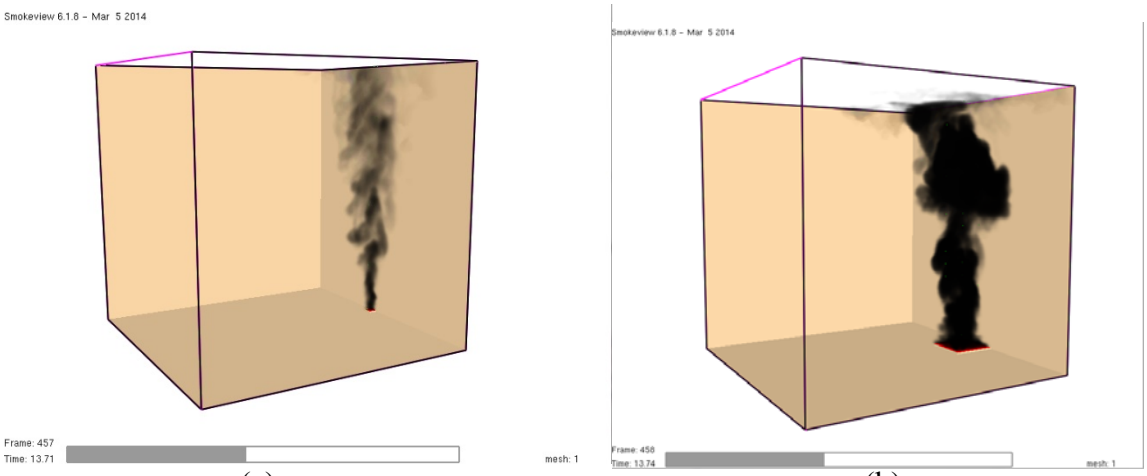


**Figure 2-23**
**40 kW and 1000 kW – wall configuration**

Figure 2-23 shows simulations of a 40 kW and 1000 kW fire against a wall surface. The HRR trends observed are similar to those seen in Figures 2-17 and 2-18 for open configuration simulations.

Temperature profiles for the two simulations are presented in Figure 2-24.

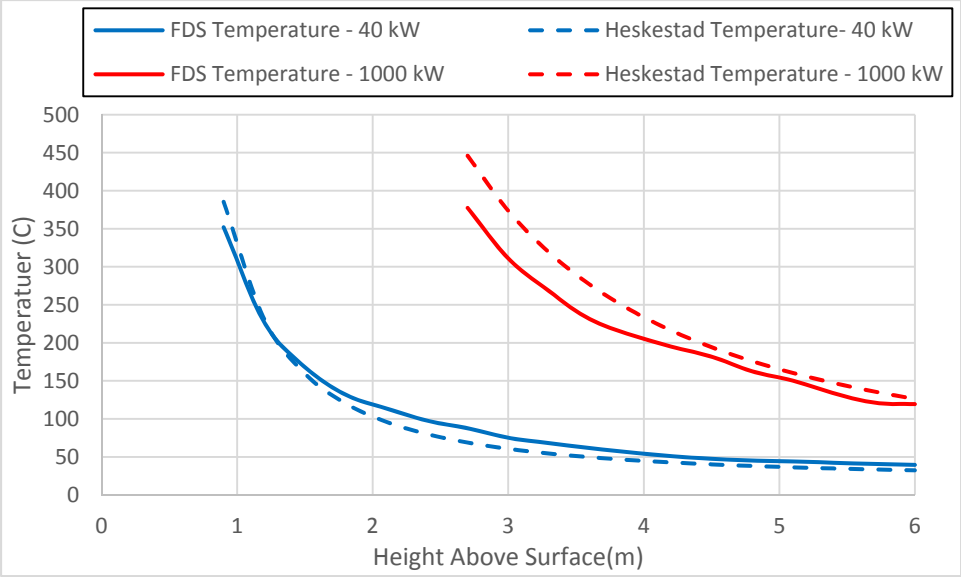


**Figure 2-24**
**Temperature vs. elevation above floor – wall configuration, 40 kW and 1000 kW**

Figure 2-24 presents the unmodified Heskestad equation for plume temperatures. For the 40 kW fire size, it appears that only a small modification, if any, to the Heskestad fire plume correlation is needed. However, the difference between the simulation results and Heskestad fire plume correlation are a little more significant for the 1000 kW fire. Here, the Heskestad fire plume correlation is over-estimating relative to the simulated FDS temperatures, suggesting that, in this example, the Heskestad fire plume correlation is conservative.

From these plots, we can begin to determine what parameters may be influential in the estimation of the fire location factor $k_F$.

### 2.4.6.4 Data Selection

Review of the preliminary simulations reported above indicated the necessity to define valid limits on the selection of temperature data for this analysis. As discussed above, temperatures within the flame region were filtered out of the analysis. Temperatures within the flame height are typically not applied in NPP fire PRA in favor of more conservative treatments of damage. This effectively limits the data used in this analysis to temperatures less than approximately 800°C.

Additionally, temperatures below 130°C are lower than temperatures that are used for target damage in NPP applications (that is, 205°C and 330°C for TP and TS cables, respectively [4]). The temperature of 130°C was chosen because it results in a negligible probability of causing damage for the 205°C limit using the bias (1.18) and normalized standard deviation (0.20) calculated for FDS 6.0.1 [11]. A simple means of assessing the probability that a given prediction will exceed a threshold value due to model uncertainty is provided in *Nuclear Power Plant Fire Modeling Analysis Guidelines* [1]. This probability may be determined from the following equation:

$$P(x > x_c) = \frac{1}{2}\text{erfc}\left(\frac{x_c - \mu}{\sigma\sqrt{2}}\right) \qquad \textbf{Eq. 2-11}$$

Where:

$P$ is the probability.

$x$ is a parameter value.

$x_c$ is a threshold parameter value.

$\mu$ is mean "true" predicted mean value of the parameter.

$\sigma$ is the standard deviation of the model prediction for the parameter of interest.

The mean value is determined from the model bias [1] as follows:

$$\mu = M/\delta \quad \textbf{Eq. 2-12}$$

Where:

$M$ is the model prediction.

$\delta$ is the model bias.

The standard deviation is computed from the normalized standard deviation as follows:

$$\sigma = \tilde{\sigma}_M(M/\delta) \quad \textbf{Eq. 2-13}$$

Where $\tilde{\sigma}_M$ is the normalized standard deviation.

The model bias and normalized standard deviation for the FDS Version 6.0.1 model are as follows [11]:

- Plume temperature (model bias): 1.18
- Plume temperature (normalized standard deviation): 0.20

Following the procedures above, temperatures of 130°C would result in a 0.00006% chance of causing damage to a target with a 205°C critical temperature.

Simulations similar to those reviewed above were used to estimate the value of $k_F$ for different configurations. In this investigation, no values for temperatures lower than 130°C were used to estimate $k_F$, based on the low probability that damage might occur at this temperature. It was observed that as the elevation above the fuel source increased and the plume temperatures decreased, the values for $k_F$ also increased. Examples of this trend are shown in Figure 2-25.

Values approaching 8 were estimated for $k_F$ using the 40 kW fire, but these values were predicted for very low plume temperatures that are typically below the damage thresholds considered in targets of interest for NPP applications. As the estimation of $k_F$ includes not only the effects of fires located in corners and near walls, but also the difference between the Heskestad fire plume correlation and the FDS simulated temperatures, it was believed that these larger values of $k_F$ were not appropriately capturing the effect of the wall or corner on the plume temperature. This indicated that the difference between the fire plume correlation and the CFD simulation may be caused by application of the plume correlation beyond the appropriate limits of its applicability.

Lower temperature predictions were thought to be associated with reduced levels of turbulence caused by the viscous influence of the wall surfaces and the reduced entrainment. Since turbulence strongly influences entrainment, and it is inherently built into the plume correlations, these elevated location factors were likely caused by the suppression of turbulence by the corner or wall. These lower temperatures were also statistically irrelevant to NPP damage analysis; therefore, they were filtered out of the calculations.

It was also observed during this investigation that simulations with lower HRRs and larger fuel source diameters often resulted in unexpectedly large estimated values of $k_F$ when the fire was located in the corner. A functional relationship between the observed values of $k_F$ and changes in the HRR and the fuel source diameter has not been determined. It is suspected that this relationship may also be related to different regimes of turbulence in the plume, and, in this case, the reduced turbulence is defined by the buoyancy of the source fire and the presence of the corner.

Turbulence is very important for entrainment (one of the primary drivers of plume temperature), and a plume with less turbulence will remain hotter than one that is fully turbulent. It is important to note that the Heskestad plume correlation was developed to match the observed behavior of turbulent fire plumes. Any effects that noticeably reduce the level of turbulence below that which was originally assumed in the Heskestad correlation will result in higher temperatures.

In this case, the absolute difference in temperature is relatively small, but the overall impact on the fire location factor is noticeable. It is unclear if this effect should be filtered out of the analysis; therefore, no data limits were defined to filter out the effects of reduced turbulence. Further research into this matter may indicate if a valid limit can be applied, although no specific recommendation has been defined here.

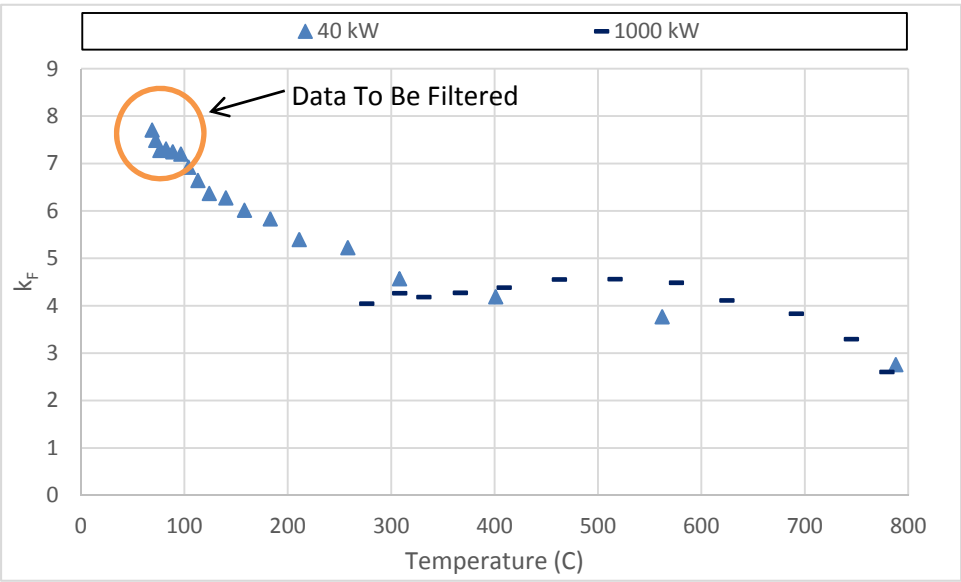


**Figure 2-25**
**$k_F$ vs. temperature**

### 2.4.7 Important Parameters – Corner Configurations

A number of different parameters have been identified as important to the modeling of the fire location factor, $k_F$:

- HRR, $\dot{Q}$
- Distance from the corner/wall surface, *L*
- Fuel source diameter, *D*
- Height above the fuel source, *H*

In the following sections, changes made in these different parameters are explored for their effect on the value of $k_F$. Following a discussion of the experimentally observed important parameters, a more detailed analysis will be provided for the determination of wall surface effects.

In Figure 2-28, the largest estimated values of $k_F$ for each simulation are presented. This artificially distorts the results as only the highest estimated values of $k_F$ are presented. As discussed in Section 2.4.6.4, it was observed that as the elevation above the fuel source increased and the plume temperatures decreased, the values for $k_F$ also increased. The temperatures associated with the higher values of $k_F$ are typically much less than the damage criteria for electrical cables and therefore are not directly applicable to damage estimates. Ultimately, the entirety of valid data as established in Section 2.4.6.4 is used to develop recommendations for the use of the fire location factor in Section 3.

#### 2.4.7.1 Distance from Surfaces, *L*

Current guidance for NPP applications is that $k_F$ should be applied from distances of flush against wall surfaces up to 0.6–0.9 m from the wall or corner [5]. A major part of this investigation is to determine at what distances from a corner the fire location factor should be applied. In Figure 2-26, the largest estimations of $k_F$ for all the different HRRs used in this investigation are shown at different distances from the corner normalized by D*, which is a characteristic fire diameter or length scale. The parameter D* is used to incorporate the HRR into the length scaling presented. The equation for D* is:

$$D^* = \left(\frac{\dot{Q}}{\rho c_p T_0 \sqrt{g}}\right)^{2/5} \qquad \textbf{Eq. 2-14}$$

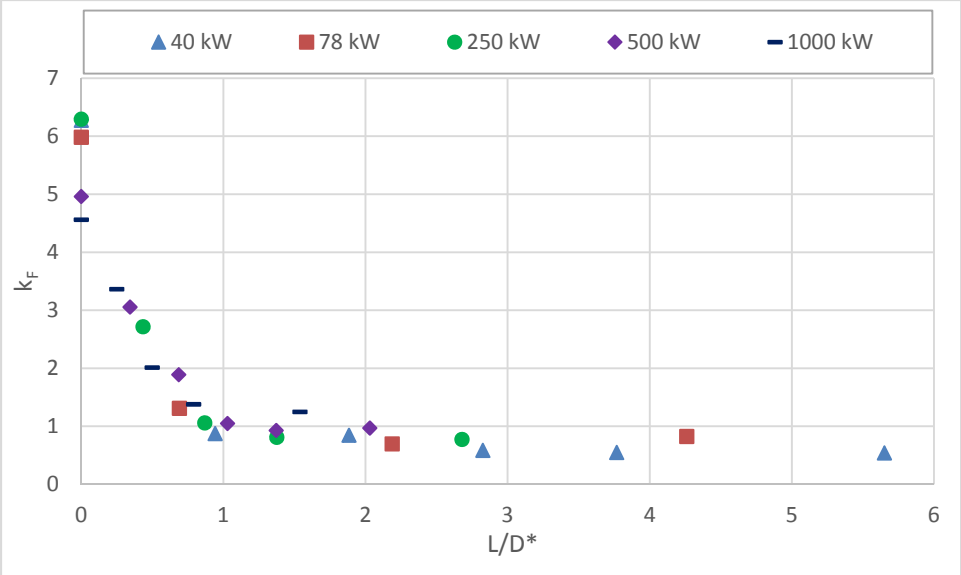


**Figure 2-26**
**$k_f$ vs. distance from corner/D***

Figure 2-26 shows that the distance from the corner is an influencing factor for the estimation of $k_F$.

### 2.4.7.2 Fuel Source Diameter, D

In the simulations used for this investigation, the HRR was used with the HRRPUA to determine the fuel source diameter. For many of the simulations, an HRRPUA of 1000 kW/m$^2$ was used. Therefore, the fuel source diameters are different for each HRR. A number of simulations were completed in which the HRR was kept constant, but the HRRPUA was prescribed as either 500, 1000, or 2000 kW/m$^2$. As a result, the diameter for the fuel source was varied for the same HRR. These results are presented in Figure 2-27, showing the largest estimated values of $k_F$ for each case.

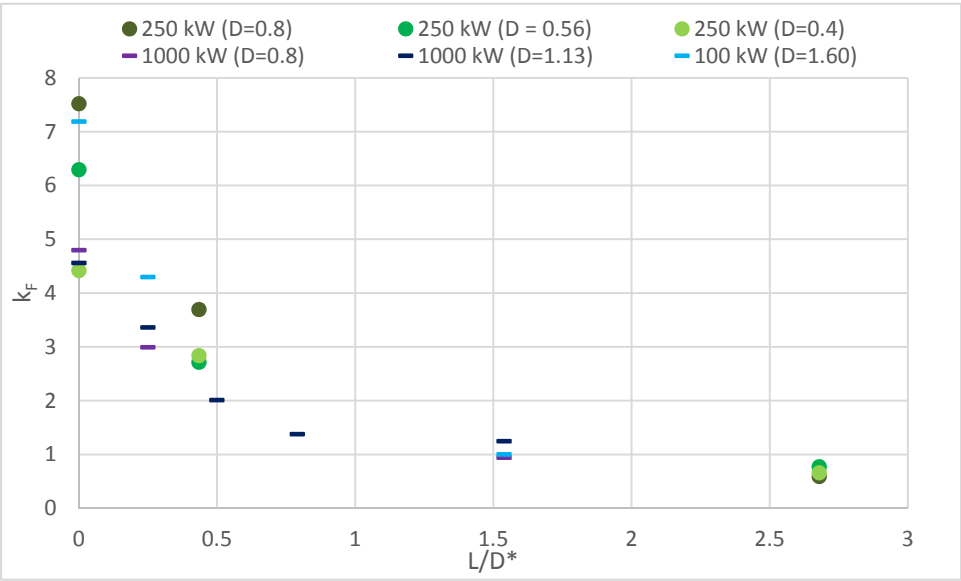


**Figure 2-27**
**Effect of fuel source diameter on $k_F$**

Figure 2-27 shows that the diameter is an influencing factor for the estimation of $k_F$. Following a similar trend seen in Figure 2-26, the most variation is observed near the corner; whereas, at a greater normalized distance, the effect of variation in the fuel source diameter becomes insignificant.

### 2.4.7.3 Height Above Fuel Source, H

For each simulation, the maximum plume temperature at multiple elevations was used to estimate $k_F$. Examples of different values of $k_F$ at various heights, normalized by D*, are presented in Figure 2-28. As observed in Figure 2-20, the 40 kW fire data cannot be taken at lower heights because of the lower estimated mean flame height. As discussed with Figure 2-25, at lower temperatures the values of $k_F$ estimated become less meaningful for NPP fire PRA. This becomes more apparent when plotting the estimated values of $k_F$ against the temperatures measured at different heights (see Figure 2-25). As the temperature is measured at increasing height above the 40 kW fire, the location factor continually increases.

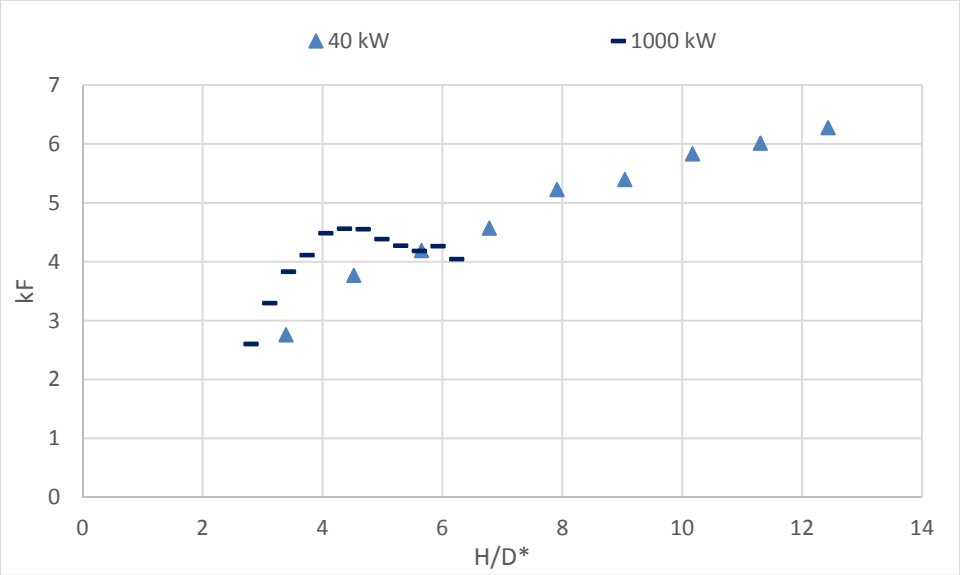


**Figure 2-28**
**$k_F$ vs. height above surface**

The results presented in Figure 2-28 show that the $k_F$ values increase as the distance above the fuel source increases. This trend is clear for the 40 kW fire. For the 1000 kW fire, it appears that the difference in temperatures between FDS and the Heskestad equation does not vary significantly, and the resulting values are close to the historically accepted value of 4 for corner configurations.

## 2.5 References


1. *Nuclear Power Plant Fire Modeling Analysis Guidelines (NPP FIRE MAG*). NUREG-1934 and EPRI 1023259. U.S. Nuclear Regulatory Commission, Office of Nuclear Regulatory Research (RES), Washington, DC and Electric Power Research Institute (EPRI), Palo Alto, CA: 2012.
2. Williamson, R. B., A. Revenaugh, and F. W. Mowrer. "Ignition Sources in Room Fire Tests and Some Implications for Flame Spread Evaluation," *Proceedings of the Third International Symposium on Fire Safety Science.* 1991.
3. Karlsson, B., and J. Quintere. *Enclosure Fire Dynamics*. CRC press, 2002.
4. *Fire PRA Methodology for Nuclear Power Facilities, Volume 2: Detailed Methodology*, NUREG/CR-6850 and EPRI 1011989. U.S. Nuclear Regulatory Commission, Office of Nuclear Regulatory Research (RES), Washington, DC and Electric Power Research Institute (EPRI), Palo Alto, CA: 2005.
5. *Technical Basis for Fire Protection Significance Determination Process (IMC 0609, Appendix F) at Power Operations*, U.S. Nuclear Regulatory Commission. February 2005.
6. Not Used.
7. Alpert, R. L., and E. J. Ward. "Evaluation of Unsprinklered Fire Hazards," *Fire Safety Journal.* Volume 7.2, pp. 127–143 (1984).
8. McGrattan, K.B., et al. *Fire Dynamics Simulator User's Guide*. National Institute of Standards and Technology, Gaithersburg, MD, USA and VTT Technical Research Centre of Finland, Espoo, Finland, Sixth edition, November 2013.
9. McGrattan, K. B., et al. *Fire Dynamics Simulator, Technical Reference Guide, Volume 1: Mathematical Model*. National Institute of Standards and Technology, Gaithersburg, Maryland, USA, and VTT Technical Research Centre of Finland, Espoo, Finland, Sixth edition, April 2013.
10. McGrattan, K. B., et al. Fire Dynamics Simulator, *Technical Reference Guide, Volume 2: Verification Guide.* National Institute of Standards and Technology, Gaithersburg, Maryland, USA, and VTT Technical Research Centre of Finland, Espoo, Finland, Sixth edition, November 2013.
11. McGrattan, K. B., et al. Fire Dynamics Simulator, *Technical Reference Guide, Volume 3: Validation.* National Institute of Standards and Technology, Gaithersburg, Maryland, USA, and VTT Technical Research Centre of Finland, Espoo, Finland, sixth edition, November 2013.
12. *Verification and Validation of Selected Fire Models for Nuclear Power Plant Applications, Volume 1: Main Report*, NUREG-1824 and EPRI 1011999.U.S. Nuclear Regulatory Commission, Office of Nuclear Regulatory Research (RES), Rockville, MD, and Electric Power Research Institute (EPRI), Palo Alto, CA: 2007.
13. Heskestad, G. "Engineering Relations for Fire Plumes," *Fire Safety Journal.* Volume 7.1, pp. 25–32 (1984).
14. Not Used.

15. Zukoski, E. E., T. Kubota, and B. Cetegen. "Entrainment in Fire Plumes," *Fire Safety Journal.* Volume 3.3, pp. 107–121 (1981).

16. Hasemi, Y., and T. Tokunaga. "Modeling of Turbulent Diffusion Flames and Fire Plumes for the Analysis of Fire Growth," 21st National Heat Transfer Conference, American Society of Mechanical Engineers, 1983.

17. Hasemi, Y., and T. Tokunaga. "Some Experimental Aspects of Turbulent Diffusion Flames and Buoyant Plumes from Fire Sources Against a Wall and in a Corner of Walls," *Combustion Science and Technology.* Volume 40.1-4, pp. 1–18 (1984).

18. Takahashi, W., et al. "Flame and Plume Behavior in and near a Corner of Walls." Fire Safety Science—Proceedings of the Fifth International Symposium. 1997.

19. Poreh, M., and G. Gordon. "A Study of Wall and Corner Fire Plumes," *Fire Safety Journal.* Volume 34.1, pp. 81–98 (2000).

20. Mowrer, F. W., and R. B., Williamson, "Estimating Room Temperatures from Fires Along Walls and in Corners," *Fire Technology.* Volume 23.2 pp. 133–145 (1987).

21. Beyler, C. L. "Fire Plumes and Ceiling Jets," *Fire Safety Journal.* Volume 11.1, pp. 53–75 (1986).

22. McCaffrey, B. J. *Purely Buoyant Diffusion Flames: Some Experimental Results*. 1979.

23. Nowlen, S. P. *Enclosure Environment Characterization Testing for the Base Line Validation of Computer Fire Simulation Codes*. Albuquerque, NM: Sandia National Laboratories, 1987.

24. Ypma, T. J. "Historical Development of the Newton-Raphson Method," *SIAM Review.* Volume 37.4, pp. 531–551 (1995).

25. Not Used.

26. Heskestad, G., "Fire Plumes, Flame Height, and Air Entrainment," Section 2–1, *The SFPE Handbook of Fire Protection Engineering, 4th Edition*, SFPE, Bethesda, MD, 2008.

27. Tewarson, A. "Generation of Heat and Chemical Compounds in Fires," *SFPE Handbook of Fire Protection Engineering*, National Fire Protection Association, Quincy, Massachusetts (2002).

28. *Refining and Characterizing Heat Release Rates from Electrical Enclosures During Fire (RACHELLE-FIRE), Volume 1: Peak Heat Release Rates and Effect of Obstructed Plume.* U.S. Nuclear Regulatory Commission, Office of Nuclear Regulatory Research (RES), Rockville, MD, and Electric Power Research Institute (EPRI), Palo Alto, CA: 2015. NUREG-2178, V1, and EPRI 3002005578.

# 3
# FIRE LOCATION FACTOR – RESULTS AND FIRE PRA IMPLEMENTATION

## 3.1 Results

Section 3 presents the results from the 51 FDS simulations exploring the wall and corner effects on fire plumes. The simulations explored a range of influencing factors from HRR, fire diameter, and distance from the wall. As discussed in Section 2.4.4, the FDS simulation results have been compared with the past FM/SNL experiments on wall and corner effects and show good agreement. The results are presented for both the wall and corner configurations. Table 3-3 presents the results that can be used in the support of fire PRAs. This investigation supports a realistic enhancement to current fire PRA methodology, including the treatment of uncertainty on the fire location factor parameter.

### *3.1.1 Corner Configuration Results*

Results from multiple simulations of fire scenarios (identified in Table 2-2 and Table 2-3) located in and near a corner are presented in Figure 3-1, showing the largest estimated value of $k_F$ for each simulation:

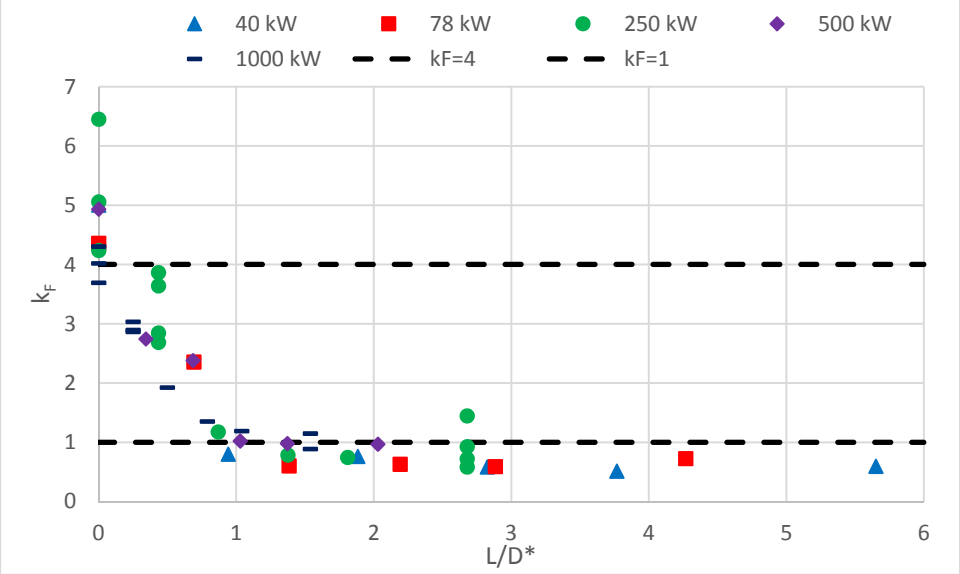


**Figure 3-1**
**Corner configuration results**

Figure 3-1 presents the results from multiple simulations for fires located in and near corners. . From the different simulations of fires located in and near corners, a single value of $k_F$, the largest estimated value at any height (excluding points in the flame as filtered per Section 2.4.6.4), was taken to represent that simulation. This shows the most conservative value of $k_F$ that can contribute to the analysis, while demonstrating the overall trend of the data.

From these results, a number of the trends discussed in reviewing the previous figures can be observed. The fire location factor is clearly a function of the distance from corner surfaces normalized by D* and varies with the HRR. Included in Figure 3-1 are lines identifying fire location factors of 4 (the historical value of $k_F$ for corners) and 1 (for fires located away from surfaces). With values of $k_F$ for fires directly adjacent to the corner ranging from 4.5–7.5, it appears that the historical fire location factor value of 4 for corners is not conservative, but this figure does not include all of the data that will be used in defining the recommended fire location factor through statistical analysis.

### *3.1.2 Wall Configuration Results*

Similar to the corner configuration, different parameters were reviewed to determine how they affect the estimation of $k_F$ in wall configurations. Figure 3-2 shows the largest estimated $k_F$ for wall configurations and the effect of different HRRs, distances from the wall, and changes in fuel source diameter.

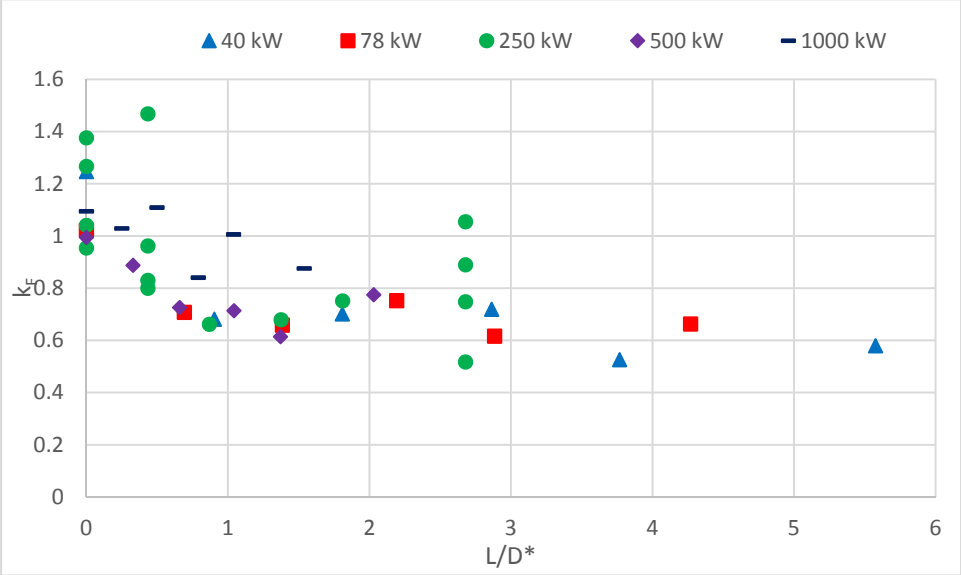


**Figure 3-2**
**$k_F$ vs. distance from wall – varied HRRs**

The wall configuration estimates of $k_F$ show different trends from those observed for the corner configuration. The estimated values of $k_F$ are all lower than the historical value of 2 used for fires located near walls [1]. This suggests that the value of fire location factor of 2 for walls is conservative when used with the Heskestad fire plume correlation. Another difference from the corner results is the observation that the values do not appear to have a consistent trend to lower values as the distance from the wall increases. In fact, the scatter in the results appears to remain relatively constant as the fuel source moves away from the wall.

### 3.1.3 Summary of Results

The results reported for the wall and corner configurations can be used to develop guidance for the use of the fire location factor for ZOI development. Furthermore, they can be useful as an expansive study of wall and corner effects, suitable for expanding applications in fundamental fire science.

Recall that in the discussion of plume scaling theory in Section 2.4.2.1, a proportionality constant, $A$, was defined as characterizing the ratio of plume temperature rise to a functional group made up of the HRR and the distance from the fire's virtual origin:

$$A \approx \frac{\Delta T_m}{\dot{Q}^{2/3}(z-z_0)^{-5/3}} \qquad \textbf{Eq. 3-1}$$

In Figure 3-3, results from the simulations conducted in this investigation are plotted to determine the proportionality constant (Equation 3-1) as the distance between the fire source and wall surfaces decreases.

For fires uninfluenced by any wall surface, the base configuration, an average proportionality constant of 25 is estimated. This is similar to the average value of 26 found in previous investigations for fires with a known convective HRR [2]. Trends for the corner and wall configurations can also be seen using the results presented in Figure 3-3. For the corner configuration, the proportionality increases as the distance between the fire source and the wall surfaces decrease. The average value for the corner configuration at a distance of zero, directly adjacent to the wall surfaces, is 61.7. This is approximately 2.7 times larger than the average value for the base configuration without any influence from wall surfaces. For fires directly next to a single wall surface, the average value is 24.7. This suggests that a single wall surface does not significantly increase the plume temperature.

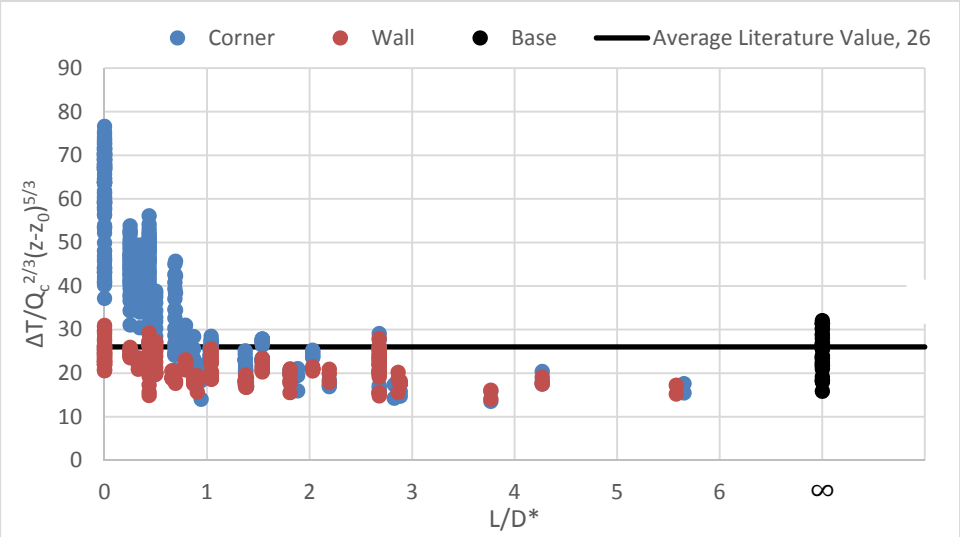


**Figure 3-3**
**Wall surface effect on plume proportionality constant**

A considerable amount of data is generated in this investigation. In previous figures, only the single largest estimated value of $k_F$ from each simulation was used in the analysis presented. This was done to demonstrate trends in the data without over-complication. As a result, multiple estimations of $k_F$ at different elevations were excluded. The full complement of $k_F$ estimates, with data filtering as described in Section 2.4.6.4, from simulations of fires located in corners are presented in Figure 3-4.

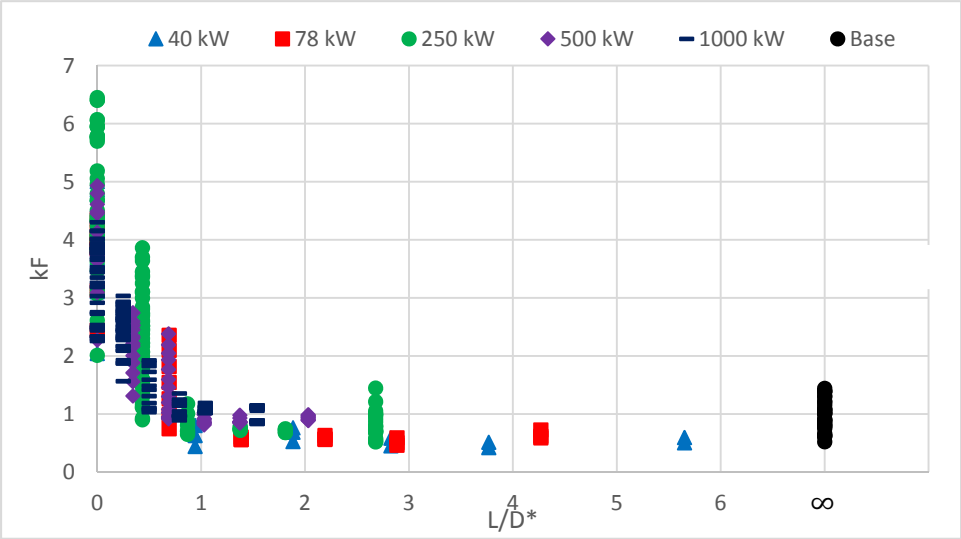


**Figure 3-4**
**Full corner configuration $k_F$ results**

The results in Figure 3-4 show the large variation in $k_F$ for fires directly adjacent to the corner that decrease as the normalized distance between the fire and the corner increases.

From these results, assuming a normal distribution, the mean estimate of $k_F$ for fires located directly adjacent to a corner is 4.03, which matches the value of 4 used in current guidance. The estimated values of $k_F$ for fires located in and near corners used in this investigation and presented in Figure 3-4 are reported in Appendix A.

Assuming normally distributed results, the mean, 2.5%, and 97.5% estimations of $k_F$ for each distance from the corner are presented in Table 3-1. Note that some values less than 1 are reported, but this should not be treated as a recommendation to use values less than 1 in any evaluation. There are a number of possible reasons for an estimated value lower than 1 for $k_F$. The normal variation in the plume temperatures predicted by the FDS simulations will result in some temperatures being greater and some temperatures being less than those predicted by the Heskestad fire plume correlation. This will result in estimated values of $k_F$ greater and less than one.

In Figure 3-5, temperature vectors obtained using slice files are used to visualize and compare the differences between an open and corner configuration. Temperatures shown are taken at an elevation of 3 m above the floor and at the end of the 30 second simulations. Both figures show results from simulations using 500 kW fires. Figure 3-5a shows the temperature profile for a fire located in the open away from any wall surfaces. In Figure 3-5b, the fire is located 1.48 m away from the corner. Figure 3-5b shows that the presence of the wall surfaces creates additional turbulence (identified by black arrows). This increased turbulence may increase entrainment of

air into the plume and result in lower predicted temperatures when compared to an open configuration. Lower predicted temperatures would also result in a lower estimated values of $k_F$ determined by the comparison to Heskestad's fire plume correlation used in this investigation. As previously stated, values of $k_F$ less than 1 are not recommended for use with any evaluation.

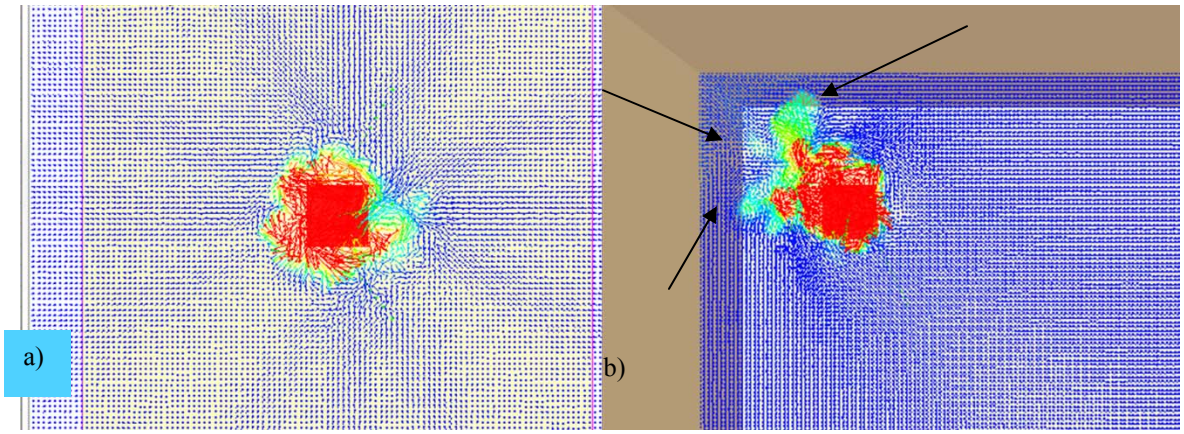


**Figure 3-5**
**a) Open configuration, 500 kW; b) corner configuration, L = 1.48 m, 500 kW**

The results from the open (control) configurations, simulations with no wall or corner effects, are included in Table 3-1 and are identified with the '∞' symbol. The results in Tables 3-1and 3-2 show that sufficiently far from wall and corner surfaces, a mean value for $k_F$ close to 1 is estimated.

**Table 3-1**
**Percentiles of kF using FDS simulations – corner configurations**

| Distance (m) | 2.50% | Mean | 97.50% |
|---|---|---|---|
| 0.00 | 1.96 | 4.03 | 6.12 |
| 0.24 | 0.88 | 2.24 | 3.61 |
| 0.48 | 0.19 | 1.23 | 2.29 |
| 0.76 | 0.43 | 0.88 | 1.33 |
| 1.00 | 0.39 | 0.87 | 1.33 |
| 1.48 | 0.48 | 0.89 | 1.31 |
| ∞ | 0.44 | 0.99 | 1.56 |

In Figure 3-6, all the estimated values of $k_F$ for the wall configuration simulations are presented.

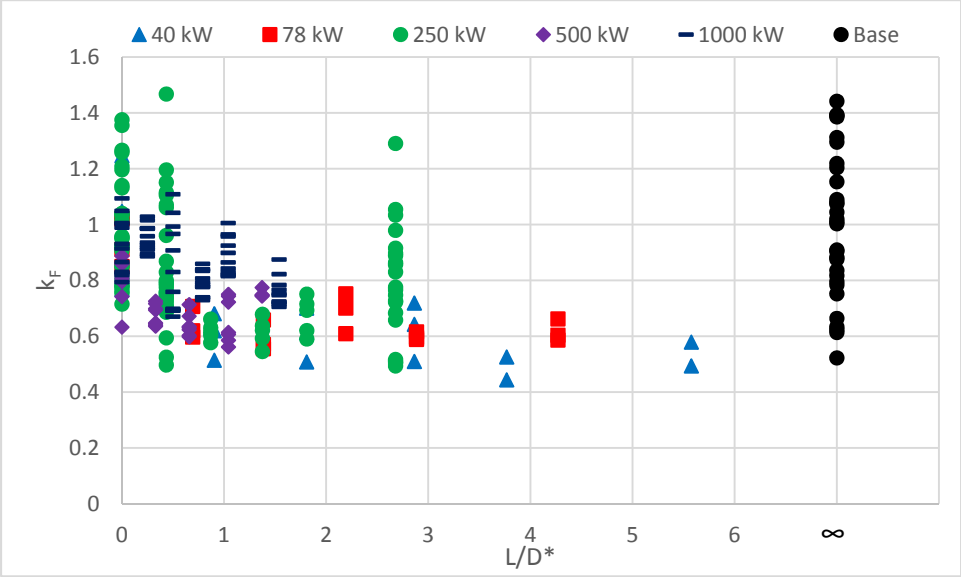


**Figure 3-6**
**Full wall configuration $k_F$ results**

The results for FDS simulations of fires located in wall configurations are presented in Figure 3-6. The estimated values of $k_F$ for fires located near a single wall surface used in this investigation and presented in Figure 3-6 are reported in Appendix A. Table 3-2 presents the mean, 2.5%, and 97.5% estimations of $k_F$ for fires located near walls.

**Table 3-2**
**Percentiles of kF using FDS simulations – wall configurations**

| Distance (m) | 2.50% | Mean | 97.50% |
|---|---|---|---|
| 0.00 | 0.65 | 0.95 | 1.26 |
| 0.24 | 0.52 | 0.87 | 1.22 |
| 0.48 | 0.40 | 0.71 | 1.03 |
| 0.76 | 0.52 | 0.70 | 0.89 |
| 1.00 | 0.38 | 0.72 | 1.06 |
| 1.48 | 0.43 | 0.75 | 1.08 |
| ∞ | 0.44 | 0.99 | 1.56 |

This information has been used to develop implementation guidance, and it can be used in future statistical analyses of the data to expand the application of location factors.

In Figure 3-7, the temperature predicted using the Heskestad fire plume correlation with a location factor of 4 is compared with a temperature predicted by FDS for a 40 kW fire located directly adjacent to a wall surface.

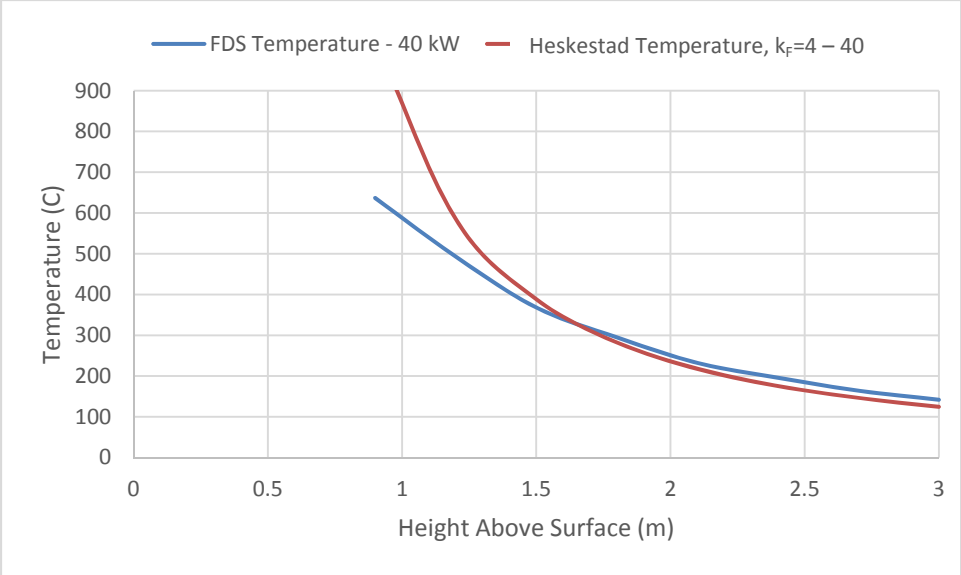


**Figure 3-7**
**Temperature vs. elevation above floor, corner configuration – 40 kW**

The results for the 1000 kW fire are similar to those seen with the 40 kW fire in Figure 3-8.

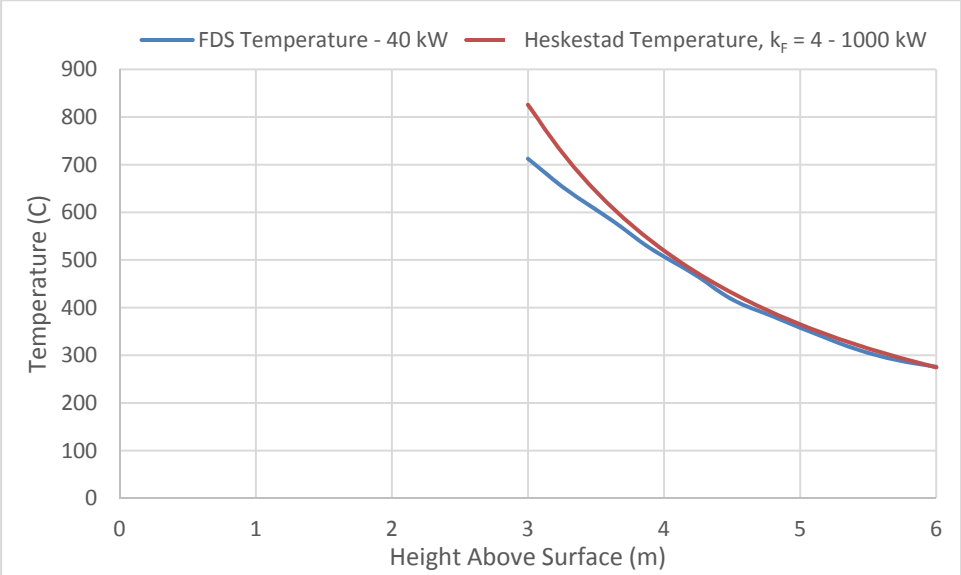


**Figure 3-8**
**Temperature vs. elevation above floor, corner configuration – 1000 kW**

In Figure 3-9, the Modified Heskestad fire plume correlation with a $k_F$ of 4 for a fire with a 60 kW HRR is compared with the measured plume temperatures provided by Hasemi and Tokunaga [3] for a fire located in a corner. The modified correlation results match closely with the measured data and start to deviate as the height above the surface approaches the flame height of 0.86 m predicted by Equation 2-6.

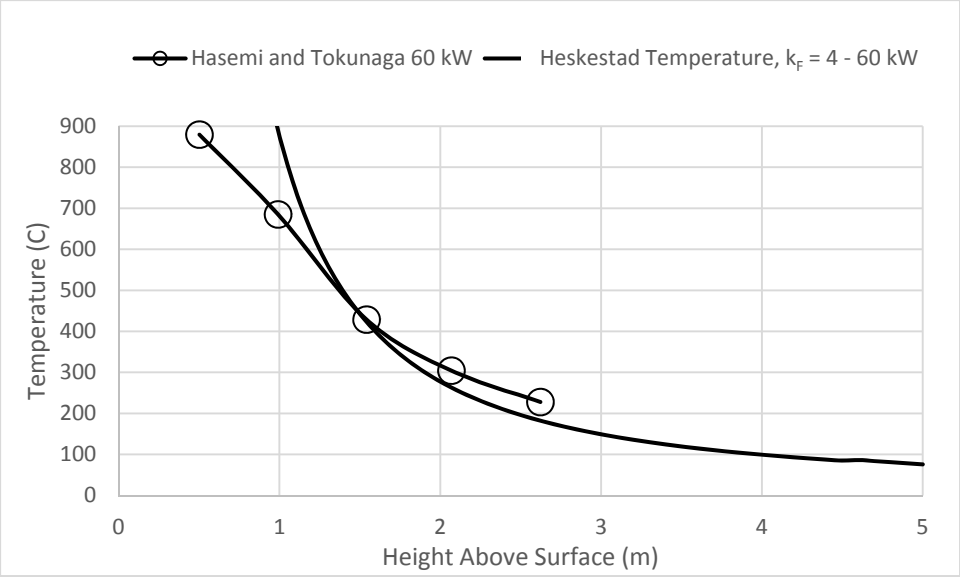


**Figure 3-9**
**Plume temperatures at different elevations, corner configuration – Hasemi and Tokunaga and modified Heskestad correlation**

A similar comparison can be made for a fire located near a single wall surface. This comparison is made in Figure 3-10. For the single wall surface configuration, the plume temperatures predicted by the modified Heskestad fire plume correlation are always greater than the experimentally measured plume temperatures provided by Hasemi and Tokunaga [3]. The results presented in Figure 3-10 continue to suggest that the current guidance for fires located near a single wall surface is conservative. These results coincide with the results observed as part of this investigation that the fire location factor value of 2 for wall configurations is conservative.

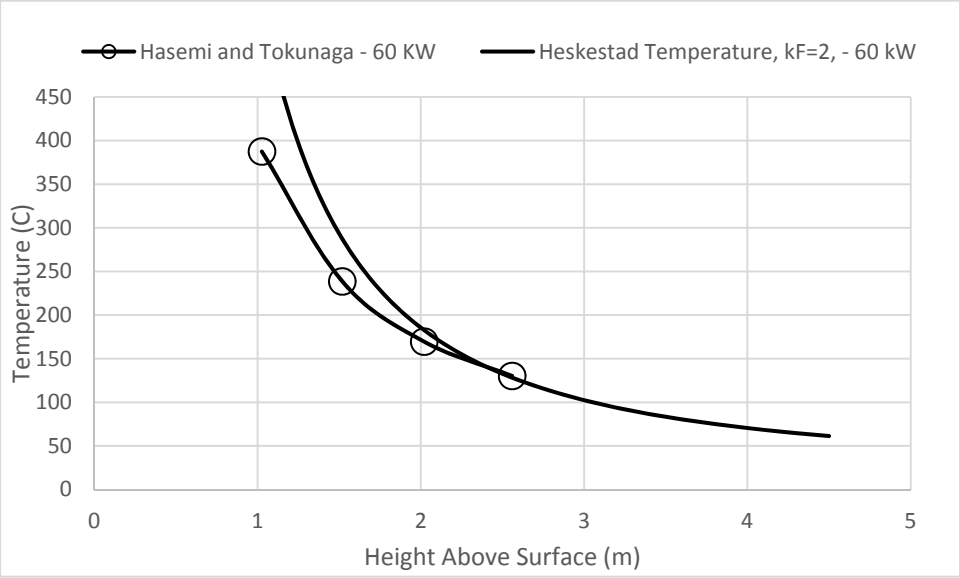


**Figure 3-10**
**Plume temperatures at different elevations, wall configuration – Hasemi and Tokunaga and modified Heskestad correlation**

In Section 3.2, the results of this investigation are used to modify the Heskestad fire plume correlation and provide guidance for the use of location factors for fires located near wall surfaces.

### *3.1.4 Sensitivity to Wall Surface Properties*

A number of simulations were completed using different wall surface characteristics. Different characteristics simulating gypsum, steel, and "cold" or inert wall surfaces were used to determine if the type of wall surface influences the guidance presented in this investigation. The results for these simulations are presented in Figure 3-11. The gypsum wall surface, assuming the paper has burned off, represents a ceramic fiber insulating surface. The steel surface is simulated to account for the thin steel coverings commonly seen in NPPs. A "cold" wall, in which the wall surface stays at a constant ambient temperature, is simulated using the inert property in the FDS simulations. An additional set of simulations using ambient wall surfaces was also completed. For the simulations with adiabatic walls, the plume temperatures did not decrease with increases in elevation at rates observed in the simulations with alternative wall properties. As a result, the location factor values are larger than those observed with concrete, steel, gypsum, and "inert" wall surface properties.

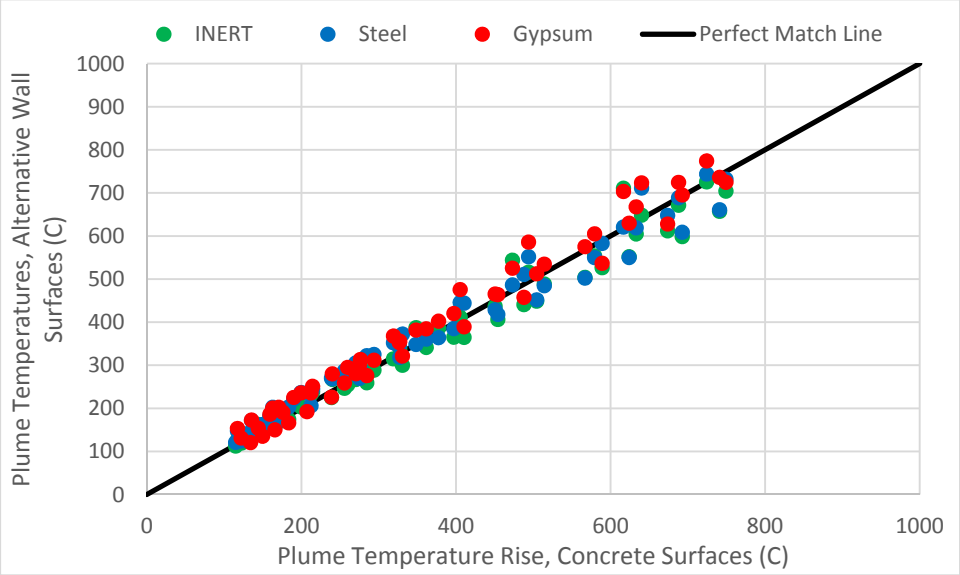


**Figure 3-11**
**Comparison of plume temperature rise with alternative wall surfaces – corner configuration**

In Figure 3-11, a comparison of the plume temperatures from simulations using alternative wall surfaces is presented. Simulations used to make this comparison were modeled with fires located directly adjacent to a corner surface. The results presented in Figure 3-11 suggest that the type of wall surface is not an influential characteristic in the determination of the location factor given the similarity of the simulated plume temperature rise. The biases calculated for each of the surfaces when compared to the results for the concrete walls used to develop the guidance in this investigation are all below 6%.

## 3.2 Fire PRA Implementation

Using the results of the FDS simulations, the $k_F$ values presented in Table 3-3 are suggested for fires located near corners or walls at various distances. The results have been presented in absolute distances since the *L/D** scaling would be difficult to apply directly in the field.

**Table 3-3**
**Fire location factors**

| Configuration | Location Factor 0 m–0.3 m (1 ft.) | Location Factor 0.3 m (1 ft.)–0.6 m (2 ft.) | Location Factor > 0.6 m (2 ft.) |
|---|---|---|---|
| Corner | 4 | 2 | 1 |
| Wall | 1 | 1 | 1 |

For ignition sources located along walls or within corners, the following guidance is provided for the determination of plume temperatures with ZOI analyses.

Equation 3-2, a modified version of Heskestad's fire plume correlation (also shown in Equation 2-7), should be used with the values of $k_F$ presented in Table 3-3:

$$T_{pl} = T_0 + 9.1\left[\frac{T_0}{(gc_p^2\rho_0^2)}\right]^{1/3}\left(k_F\dot{Q}_c\right)^{2/3}(z - z_0)^{-5/3} \qquad \textbf{Eq. 3-2}$$

Where:

$T_{pl}$ is the plume temperature (K).

$T_0$ is the ambient temperature (K).

$g$ is the acceleration due to gravity (m/s$^2$).

$c_p$ is the specific heat of air (kJ/kg·K).

$\rho$ is the density of air (kg/m$^3$).

$k_F$ is the fire location factor identified in Table 3-3.

$\dot{Q}_c$ is the convective HRR (kW).

$z$ is the distance above the fuel source (m).

$z_0$ is the virtual origin (m).

Equation 3-3, the virtual origin, $z_0$, (also shown as Equation 2-8) makes use of the HRR and must be modified as:

$$z_0 = -1.02D_F + 0.083\left(k_F\dot{Q}\right)^{2/5} \qquad \textbf{Eq. 3-3}$$

The effective diameter used in Equation 3-3 (also shown as Equation 2-9) includes the fire location factor and is determined as:

$$D_F = D\sqrt{k_F} = \sqrt{\frac{k_F\dot{Q}}{\dot{q}''}\cdot\frac{4}{\pi}} \qquad \textbf{Eq. 3-4}$$

Where $\dot{q}''$ is the HRRPUA (kW/m$^2$) for the fuel source.

When a fire ignition source is identified during walkdowns, the location is noted. Part of that identification is to determine the distance between the ignition source and walls or corners.

A value of 1 may be used at all distances for fires located near a single wall surface. For practical application in the commercial nuclear industry, the higher values of location factors observed are associated with low fire plume temperatures that are well below the damage threshold for cables. Therefore, the recommended guidance is appropriate for representing the hazards to cables due to fire plume temperatures.

In a case where two wall surfaces are located within a distance of 0.3 m (1 ft.), the corner configuration should be assumed, and a value of 4 should be used. If two wall surfaces are located within the range of 0.3–0.6 m (1–2 ft.) of the ignition source, it should be considered a transitional corner configuration, and a value of 2 may be used for $k_F$. A value of 1 should be used in all other cases where the separation distance from wall surfaces is greater than 0.6 m (2 ft.).

In the event that the location factors of $k_F$ shown in Table 3-3 do not provide the level of detail required for the analysis, the values in Tables 3-1 and 3-2 (percentiles of $k_F$ using FDS simulations—corner or wall configurations, respectively) may be used. In such cases, a functional relationship between each distance may be proposed and a value of $k_F$ interpolated. However, values less than 1.0 should not be used for $k_F$.

In Figures 3-12 and 3-13, a comparison between the location factors identified in Table 3-3, the upper and lower percentiles, and the mean values for the results presented in Tables 3-1 and 3-2, respectively, are shown for comparison. These figures illustrate the level of confidence that can be expected for the recommended values of $k_F$.

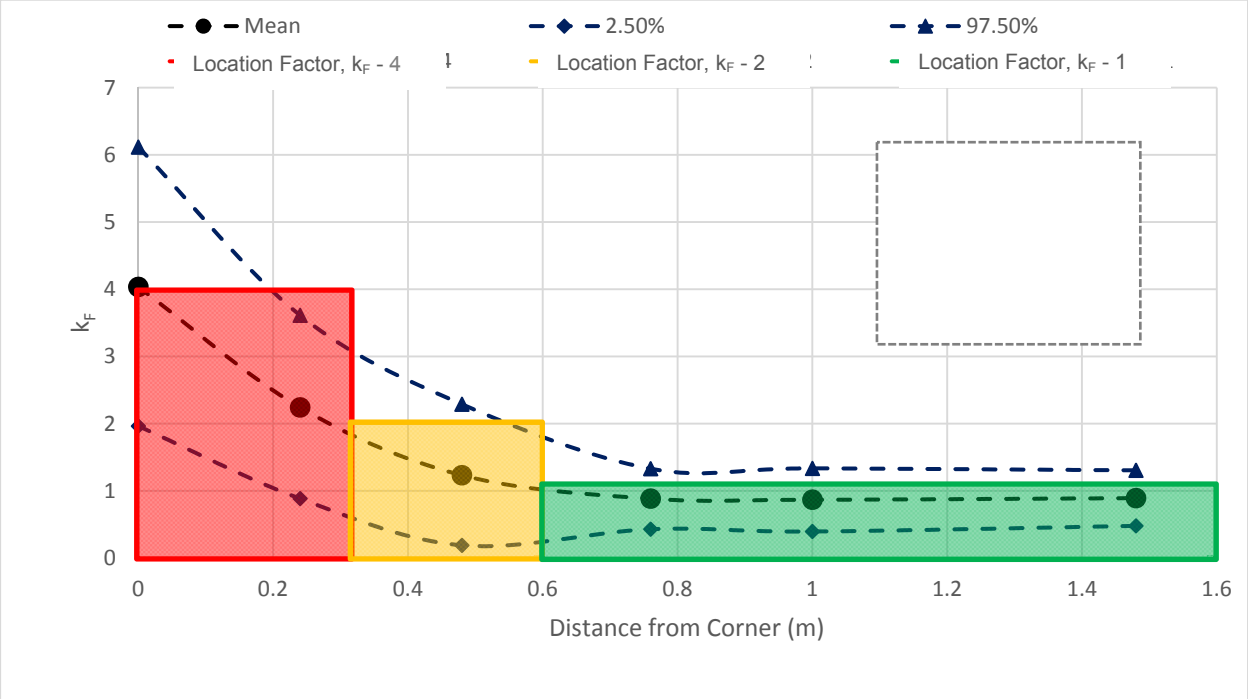


**Figure 3-12**
**Comparison of proposed $k_F$ location factors and percentile estimates – corner configuration**

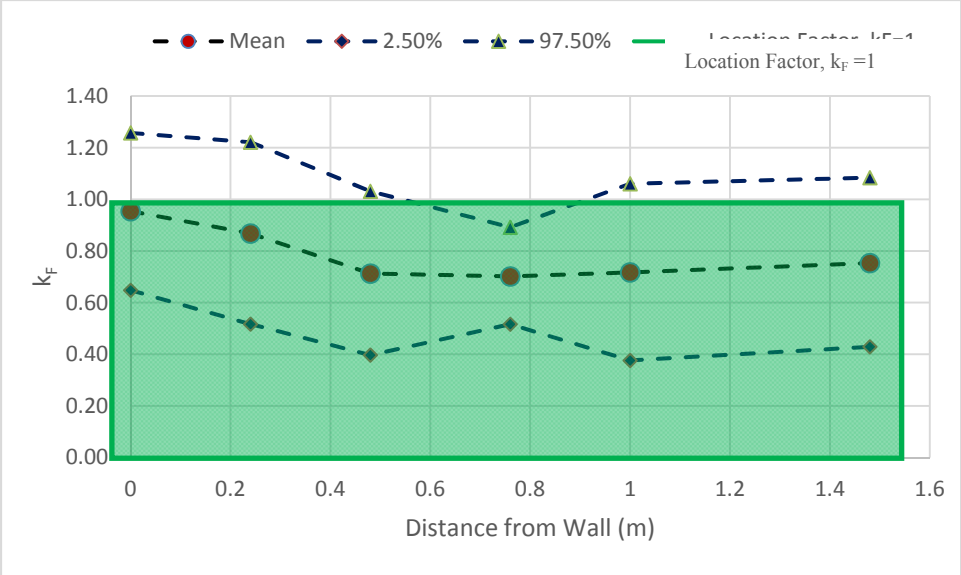


**Figure 3-13**
**Comparison of proposed $k_F$ location factor and percentile estimates – wall configuration**

The results presented in Figures 3-12 and 3-13 can be used to determine when the location factors are conservative with respect to the upper percentile estimates for $k_F$. It is also shown that the location factors proposed always encompass the mean estimates for $k_F$ at different distances from the wall and corner surfaces. The location factors in Table 3-3 are to be used with the modified Heskestad fire plume correlation and compared with FDS temperature predictions for fires located in corners and along walls.

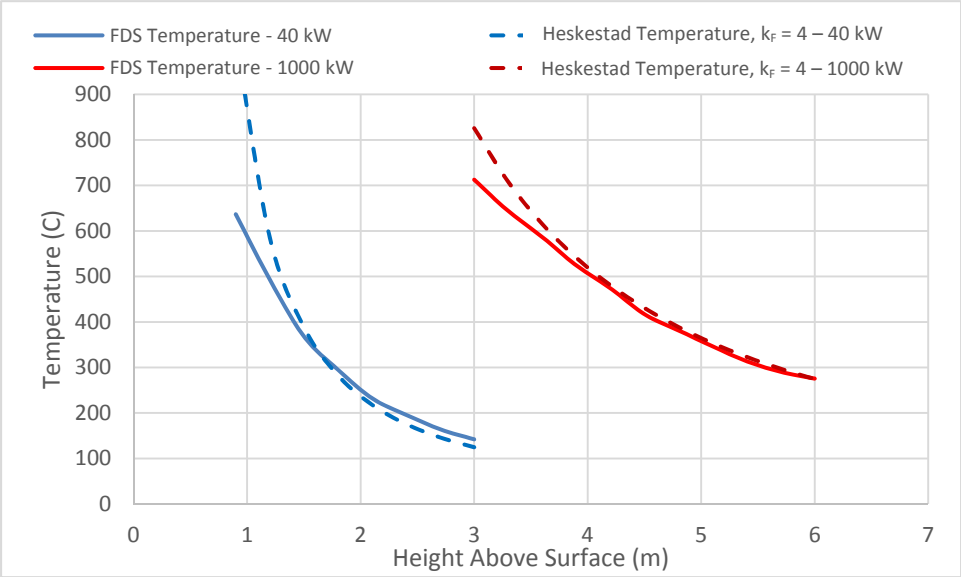


**Figure 3-14**
**Temperature vs. elevation above floor, direct corner configuration – 40 kW and 1000 kW with FDS and modified Heskestad results**

In Figure 3-14, FDS plume temperature predictions are shown for fires located directly in a corner with 40 kW and 1000 kW HRRs. Also shown are the temperature predictions made by the modified Heskestad fire plume correlation using a $k_F$ of 4. For both fires, the plume temperatures predicted by the modified Heskestad fire plume correlation are greater than those predicted by FDS. Recalling Figure 3-12, the value of 4 used for fires located up to 1 ft. from corners is conservative with respect to the mean estimates of $k_F$ for fires located near corners.

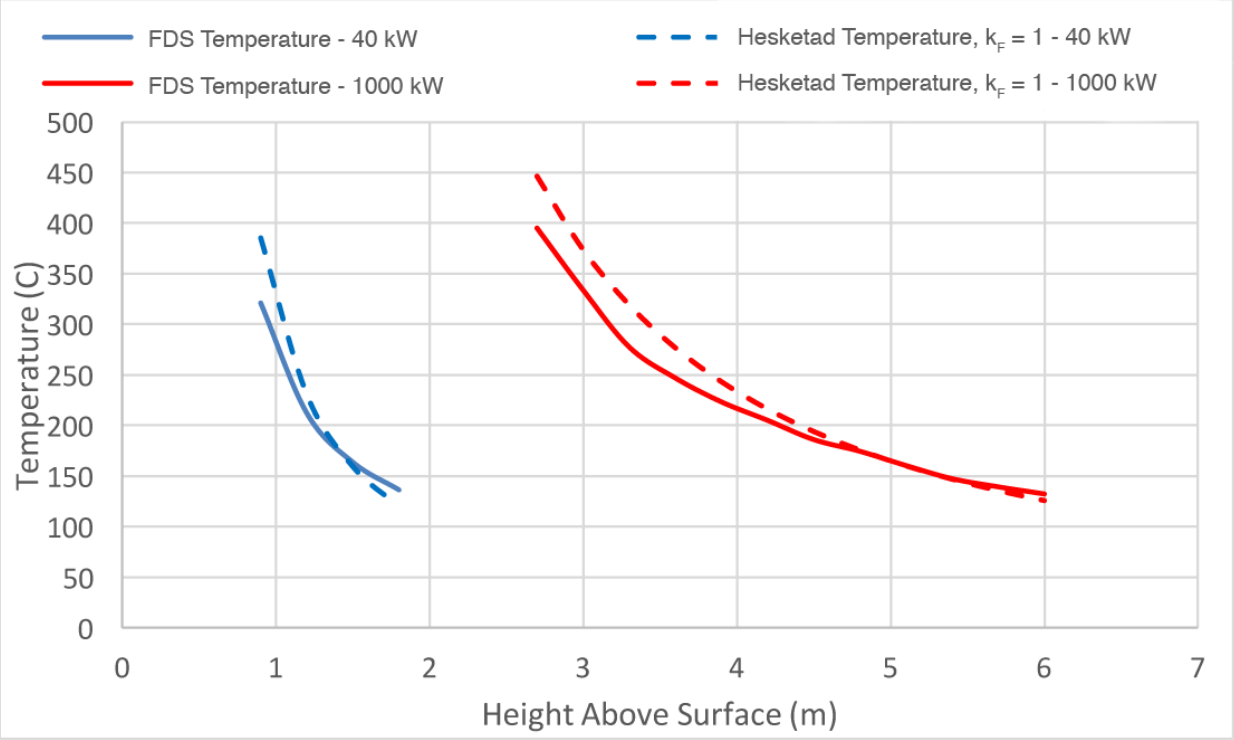


**Figure 3-15**
**Temperature vs. elevation above floor, wall configuration – 40 kW and 1000 kW with FDS and modified Heskestad results**

In Figure 3-15, FDS temperatures are compared with the unmodified Heskestad fire plume correlation ($k_F = 1$) for fires located adjacent to a single wall surface. The results of this investigation show that a single wall surface does not contribute significantly to an increased fire plume temperature and a fire location factor of 1 is conservative.

### 3.2.1 Evaluating Uncertainty of Recommended Fire Location Factors

The model bias and uncertainty statistics for the plume temperature rise are shown in Table 3-4. The statistics provided were determined following the methods outlined in the *FDS Technical Reference Guide* [4].

**Table 3-4**
**Bias and uncertainty of modified Heskestad fire plume correlation for wall and corner configurations**

| Configuration | Bias | Model Uncertainty | Experimental Uncertainty |
|---|---|---|---|
| Corner | 1.25 | 0.18 | 0.20 |
| Wall | 1.12 | 0.13 | 0.20 |

The bias for the model to consistently over-predict is made clear by comparing the plotted results to the Perfect Match Line in Figure 3-16. This line signifies where the temperatures predicted by FDS and the modified Heskestad fire plume correlation were equal, and any values above it represent instances where the modified Heskestad fire plume correlation predicted temperatures greater than the temperatures predicted by FDS and is conservative when applied.

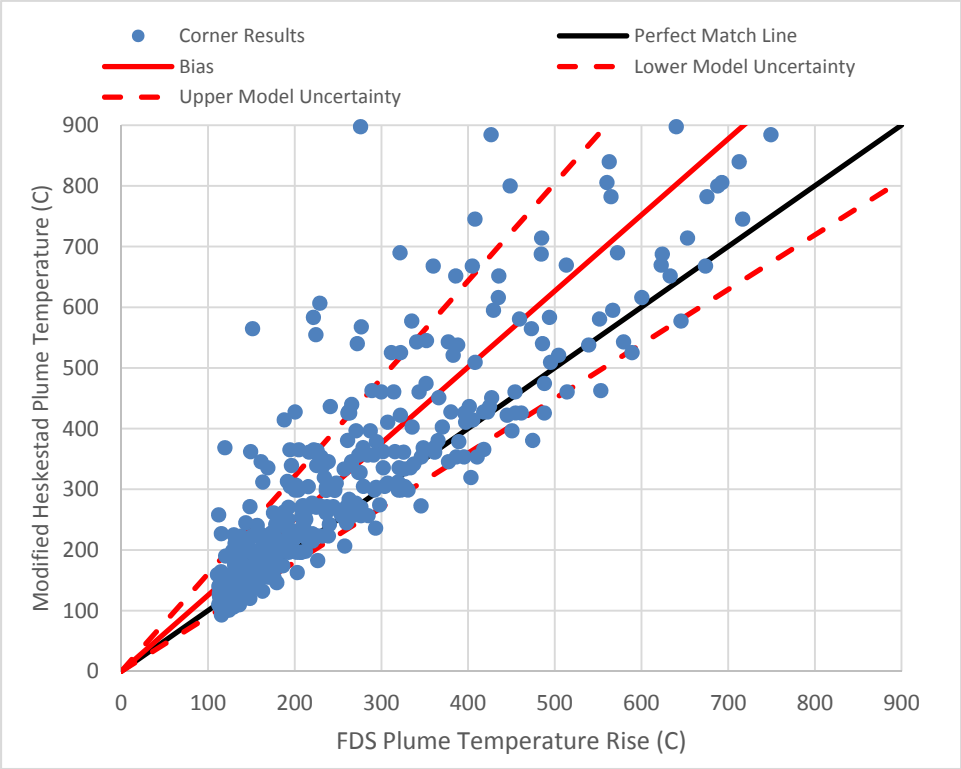


**Figure 3-16**
**Summary of plume temperature prediction for fires in corners**

The unmodified Heskestad fire plume correlation can be used for fires located near a single wall surface because the guidance provided by this investigation suggests that a fire location factor of 1 be used at all distances near a single wall surface. The value of 1 is still shown to be conservative (see Figure 3-13); therefore, the bias is still apparent when the FDS and Heskestad fire plume correlation temperatures are compared in Figure 3-17.

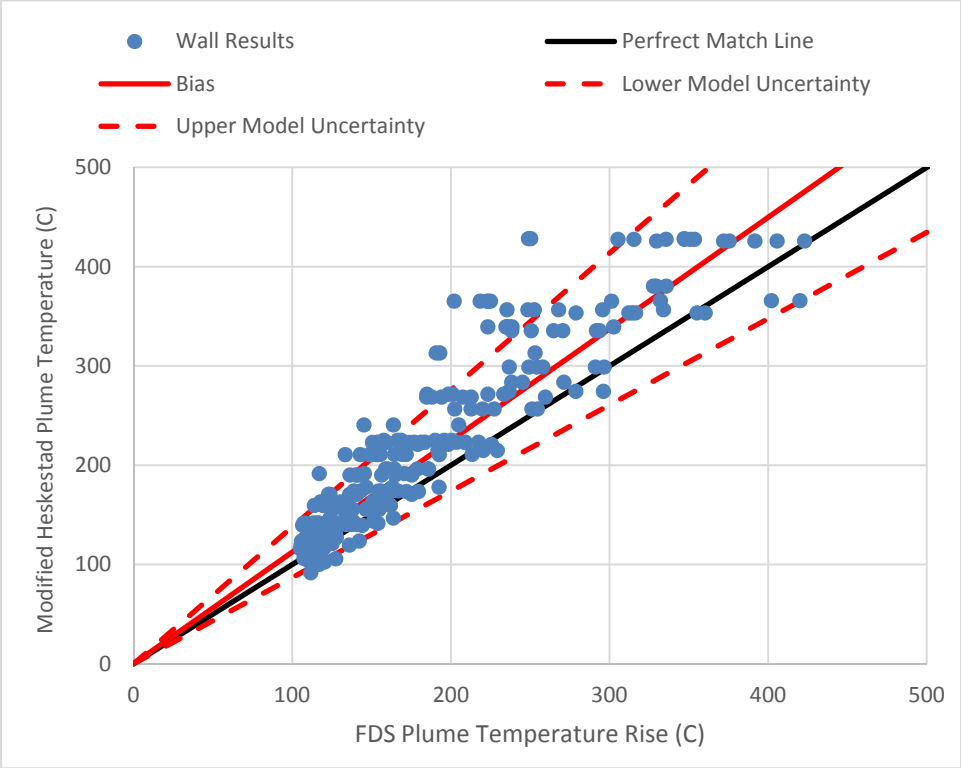


**Figure 3-17**
**Summary of plume temperature predictions for fires near walls**

### *3.2.2 Prediction of Temperature Correction*

#### 3.2.2.1 Fire Plume Temperature Rise (Example 1)

Using the values presented in Figure F-3 of NUREG/CR-6850 [5] (Appendix F, Page F-6), the exposure temperature for a fire located near a single wall surface and in a corner will be predicted using the guidance outlined above.

The required inputs from Figure F-3 of NUREG/CR-6850 are an HRR of 211 kW, fire diameter of 0.6 m, radiative fraction of 0.4, and assumed ambient temperature of 20°C. Equation 3-5 was used to predict the plume centerline temperature for a fire located in the open as specified in Figure F-3.

$$T_{pl} = T_0 + 9.1\left[\frac{T_0}{(gc_p^2\rho_0^2)}\right]^{1/3}\left(\dot{Q}_c\right)^{2/3}(z-z_0)^{-5/3} \qquad \textbf{Eq. 3-5}$$

Equations 3-2. 3-3, and 3-4 (shown again below) were used to predict the plume centerline temperature for a case where the fire source was located directly adjacent to a single wall surface.

$$T_{pl} = T_0 + 9.1\left[\frac{T_0}{(gc_p^2\rho_0^2)}\right]^{1/3}\left(k_F\dot{Q}_c\right)^{2/3}(z-z_0)^{-5/3} \qquad \textbf{Eq. 3-6}$$

$$z_0 = -1.02D_F + 0.083\left(k_F\dot{Q}\right)^{2/5} \qquad \textbf{Eq. 3-7}$$

$$D_F = D\sqrt{k_F} = \sqrt{\frac{k_F\dot{Q}}{\dot{q}''}\cdot\frac{4}{\pi}} \qquad \textbf{Eq. 3-8}$$

As presented in Table 3-3, the $k_F$ for a fire located near a single wall surface is equal to 1; therefore, the results for both predictions would be the same. However, if the fire were postulated to be located directly in a corner between two wall surfaces, the predictions would differ.

The results plotted with temperature predictions for a fire located in the open and in a corner versus the height above the fire base are illustrated in Figure 3-18, demonstrating the increase in plume temperature centerline temperature predictions for the fire located in the corner relative to the open case.

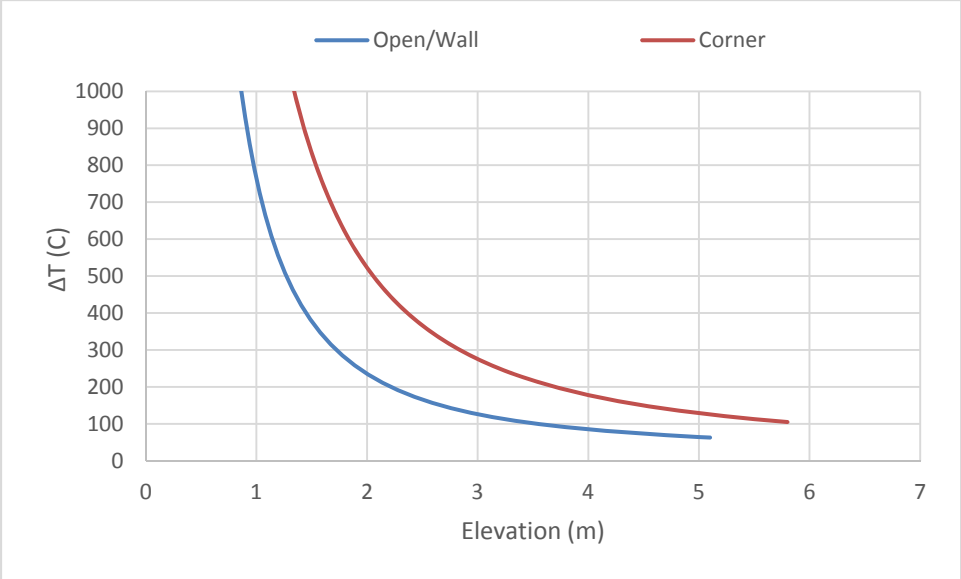


**Figure 3-18**
**Open and corner temperature predictions**

### 3.2.2.2 Zone of Influence (Example 2)

Once again, the values presented in Figure F-3 of NUREG/CR-6850 (Appendix F, page F-6), are used to predict the maximum thermal plume ZOI height for a fire using the existing information for a fire located in the open and the updated information for a fire located near wall surfaces. If Equation 3-2 is modified, the elevation at which a certain temperature is predicted to be reached can be determined as:

$$z = \left( \frac{9.1\left[\frac{T_0}{\left(g c_p^2 \rho_0^2\right)}\right]^{1/3} (k_F \dot{Q}_c)^{2/3}}{\Delta T} \right)^{3/5} + z_0 \qquad \textbf{Eq. 3-9}$$

The required inputs from F-3 of NUREG/CR-6850 (Appendix F, Page F-6) are an HRR of 211 kW, fire diameter of 0.6 m, radiative fraction of 0.4, and assumed ambient temperature of 20°C. No information is provided for the target failure properties; therefore, both TS (330°C) and TP (205°C) cables are evaluated.

Once again, for a single wall surface, no change will result in the predicted ZOI as a value of 1 is used with fires located near a single wall surface. However, for a fire located in a corner, the results will differ.

Use Equation 3-6 with a $k_F$ of 4 for a fire located in a corner to evaluate the vertical plume ZOI elevation. Use the same HRR, fire diameter, radiative fraction, and assumed ambient temperature to evaluate the vertical plume ZOI elevation for a corner fire. The results of this analysis are provided in Table 3-5, demonstrating the increase in the plume centerline temperature predictions. Visual representations of the changes in the vertical ZOI for corner fires are presented in Figure 3-19.

**Table 3-5**
**Example 2, ZOI calculations**

| Target Type | Configuration | kF | Heat Release Rate (kW) | Fire Diameter (m) | Radiative Fraction | Ambient Temperature (°C) | Vertical ZOI Height (m) |
|---|---|---|---|---|---|---|---|
| Thermoplastic (205°C) | Open/Wall | 1 | 211 | 0.6 | 0.4 | 20 | 2.2 |
| | Corner | 4 | 211 | 0.6 | 0.4 | 20 | 3.6 |
| Thermoset (330°C) | Open/Wall | 1 | 211 | 0.6 | 0.4 | 20 | 1.6 |
| | Corner | 4 | 211 | 0.6 | 0.4 | 20 | 2.7 |

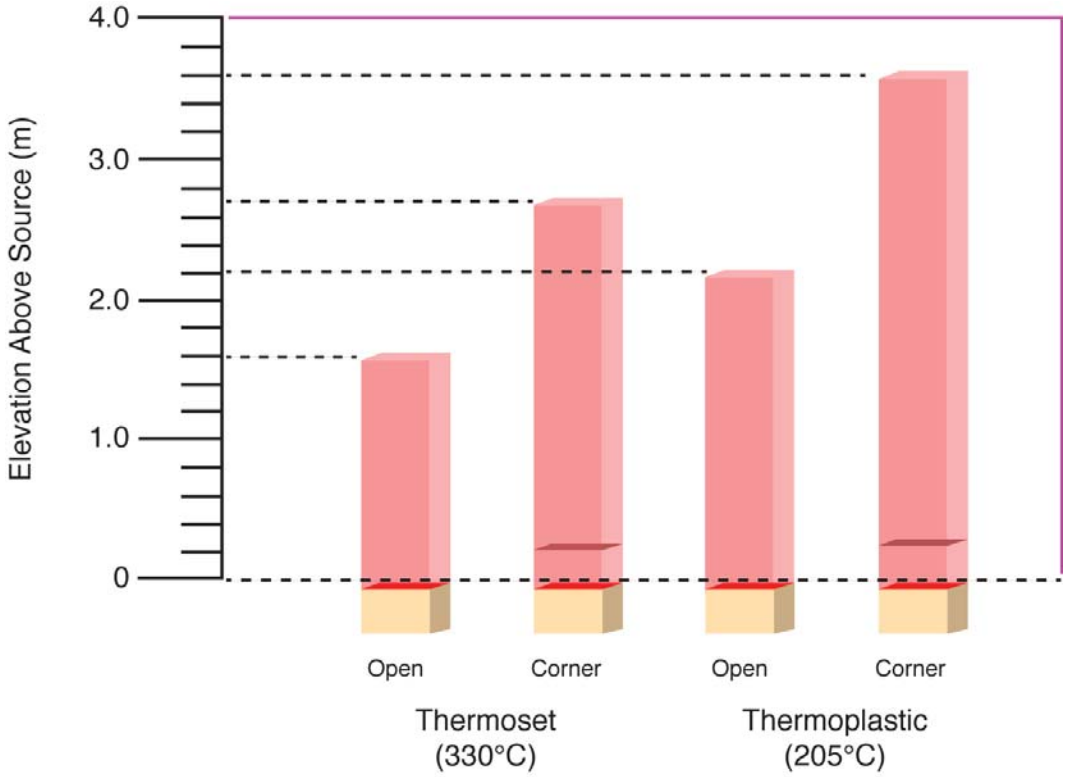


**Figure 3-19**
**Vertical plume ZOI**

### 3.2.2.3 Fire Protection SDP (Example 3)

During an inspection, it was noted that a section of cable tray fire-wrap was not properly maintained. This section of cable tray was noted to be within the plume ZOI of an electrical cabinet that was previously screened from the fire PRA.

The electrical cabinet had a height of 2.3 m and width (diameter) of 0.9 m (3 ft), and the fire base height was specified as 2.0 m. The electrical cabinet was located 0.46 m (1.5 ft.) from a corner. The cabinet was located in a compartment with a very high ceiling, and the development of an HGL was screened based on detailed fire modeling of the worst configuration in the compartment. The cabinet contained non-qualified, TP cables and was assigned an HRR of 464 kW. The ambient temperature in the compartment was 20°C, and a radiative fraction of 0.3 was used. The cable tray contained TP cables and was located at an elevation of 7 m above the floor. The separation between the fire base and the cable tray was 5 m. A diagram of the configuration evaluated is in Figure 3-20.

Since the electrical cabinet was located 0.46 m (1.5 ft.) away from the corner, the analysis was performed using the values in Table 3-3. Using Equation 3-6 and with a $k_F$ of 2, the total vertical ZOI was reduced to 4.6 m from the fire base height. Therefore, the cable tray was outside the ZOI, and only the cabinet would fail. This configuration is identical to the original analysis included in the PRA.

If the historical route had been taken for the application of the fire location factor and if a value of $k_F$=4 were used because the electrical cabinet was located within 2 ft. of a corner, then the total vertical ZOI would have been estimated as 9.3 m from the floor, and the cable tray would have been damaged.

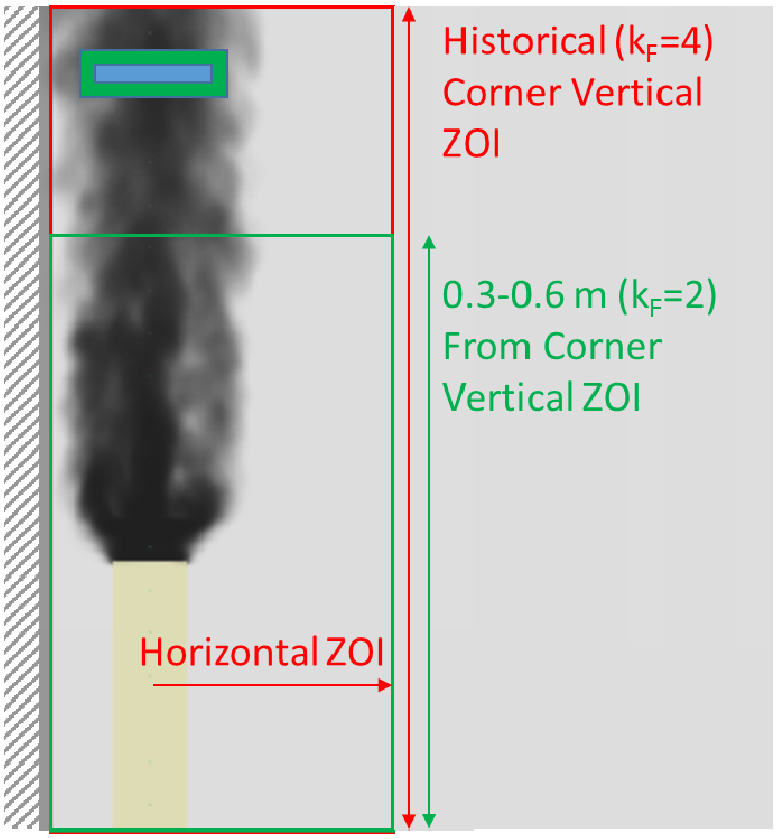


**Figure 3-20**
**Example 3, Reduction in vertical ZOI due to location factor reduction**

### 3.2.2.4 Fire PRA Application (Example 4)

Fire PRA targets are located in a simple 3 x 3 m square compartment (See Figure 3-21). Consideration of transient ignition sources (TISs) must be made to determine the risk associated with targets in this room. Some TISs may be located near wall and corner surfaces. A determination of the fraction of floor area for the appropriate location factor that should be used with a TIS can be determined as follows.

From the results presented in Table 3-3, no special consideration must be made for a TIS located near single wall surfaces; however, that is not the case for a TIS postulated near a corner.

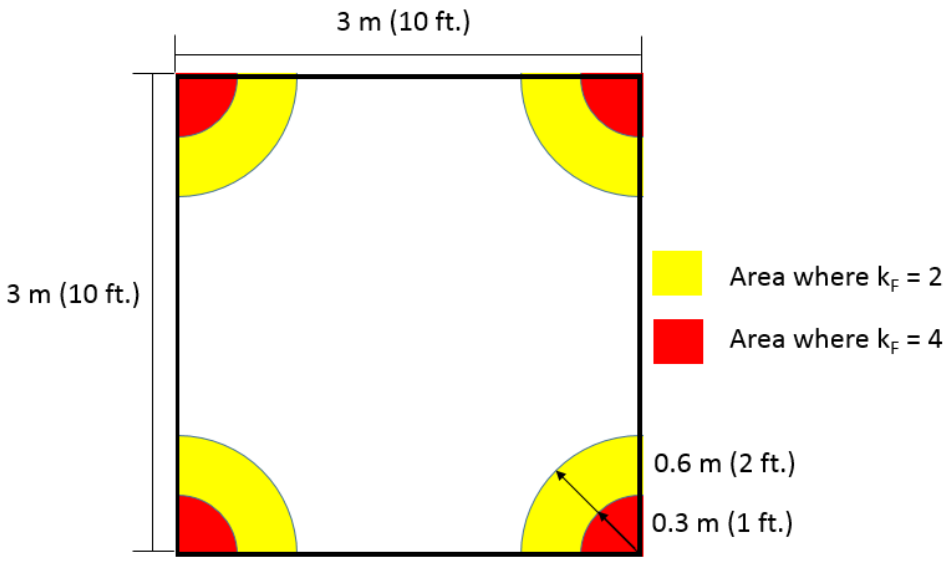


**Figure 3-21**
**Transient area associated with corner fire location factors**

To estimate fraction of area, $F_A$, for which a TIS would be required to use a $k_F$ of 4, the area associated with a radius of 0.3 m (1 ft.) from all corners must be estimated. The area of a circle is calculated as:

$$A = \pi R^2 \qquad \textbf{Eq. 3-10}$$

A $k_F$ of 4 is associated with an ignition source located a radius between 0 and 0.3 m (1 ft.) away from the nexus of a corner. Therefore, for this compartment, the area, $A$, associated with the $k_F$ of 4 would be calculated as one-fourth the area of a circle, for four corners as:

$$A_{k_F=4} = \frac{n_c \pi R^2}{4} = \frac{4 \cdot (\pi (0.3)^2)}{4} = 0.28\ m^2 \qquad \textbf{Eq. 3-11}$$

where $n_c$ is the number of corners of approximately 90° in a compartment.

And the fraction of area can be calculated as:

$$F_{A_{k_F=4}} = \frac{A_{k_F=4}}{A_T} = \frac{0.28}{9.0} = 0.03 \rightarrow 3\% \qquad \textbf{Eq. 3-12}$$

where $A_T$ is the total floor area.

The area associated with a $k_F$ of 2 would be estimated using Equations 3-8 and 3-9 as:

$$A_{k_F=2} = \frac{4 \cdot (\pi (0.6)^2) - (\pi (0.3)^2)}{4} = 0.85\ m^2,$$

And an area fraction of:

$$F_{A_{k_F=2}} = \frac{A_{k_F=2}}{A_T} = \frac{0.85}{9.0} = 0.09 \rightarrow 9\%,$$

For English units, if all corners are approximately 90°, then the area fraction, $F_A$, for each value of $k_F$ can be calculated as:

$$F_{A_{k_F=4}} = \frac{n_c \frac{\pi}{4}}{A_T} \quad \text{Eq. 3-13}$$

$$F_{A_{k_F=2}} = \frac{n_c \frac{3\pi}{4}}{A_T} \quad \text{Eq. 3-14}$$

$$F_{A_{k_F=1}} = \frac{A_T - \pi n_c}{A_T} \quad \text{Eq. 3-15}$$

where $n_c$ is the number of corners of approximately 90° in a compartment.

Special care must be taken when calculating the fraction of area associated with various fire location factors, especially when the room has a unique geometry.

### *3.2.3 Plume Temperature Calculations*

In the FDS simulations, an area of limited information for estimating the vertical damage ZOI for fire plumes near wall surfaces was explored. Data for exploration into this phenomenon were developed using FDS Version 6.0.1 to produce a series of simulations in support of this analysis. Results of these simulations were used to justify correction to the Heskestad fire plume correlation to estimate the change in the fire plume temperatures. A number of different parameters, including the HRR, the fire source diameter and HRRPUA are varied to determine their influence on the fire plume temperature rise.

The information provided for estimating the prescribed fire location factor for use with the Heskestad fire plume correlation is observed to be independent of and applicable over varying ranges of HRR, fire source diameter, and HRRPUA. Therefore, the provided information is appropriate for representing the hazards to cables due to fire plume temperatures for practical applications in the commercial nuclear power industry.

Results suggest that, for wall configurations, a $k_F$ value of 1 may be used at all distance separations between the fire source and a wall. Where two wall surfaces are located within a distance of 0.3 m (1 ft.), the corner configuration should be assumed, and a conservative value of 4 should be used. If two wall surfaces are located within the range of 0.3–0.6 m (1–2 ft.) of the ignition source, it should be considered a transitional corner configuration, and a value of 2 may be used for $k_F$. A value of 1 should be used in all other cases where the separation distance from wall surfaces is greater than 0.6 m (2 ft.).

### 3.2.4 Application of the Fire Location Factor

The fire location factor analysis was subjected to a limited peer review. Through analysis of the results and the assumptions and limitations stated in Section 2.3, the following limits are provided for implementation of the fire location factor:

- Fire location factors of less than 1 should not be used.
- The new fire location factors should be used for fire sources located near wall surfaces in which the wall surface extends horizontally past the fire source for a distance of at least two source diameters and vertically for the entire distance between the source and target as described in Section 2.4.3.
- The new fire location factor may be used with all wall types of wall surfaces. As presented in Section 3.1.4, concrete, gypsum, steel, and inert wall surface properties were studied as part of this investigation, and no significant differences were observed in the estimated fire location factors.
- The new fire location factor does not apply to configurations that include burning of secondary combustible materials. The modified Heskestad fire plume correlation, however, may be used to establish the likelihood that secondary combustibles may be ignited through the definition of the primary ignition source ZOI. The modified Heskestad fire plume correlation is limited to the ignition source only. That is, in the case of secondary combustible ignition (that is, cable trays), the subsequent analysis should follow existing information and modeling techniques.
- The new fire location factor does not apply to analysis that determines the HGL damage. The plume correlation may be used only for the duration of time in which thermal plume exposure is postulated but the HGL temperature has not yet reached the damage criteria. Existing information and modeling techniques should be used to evaluate the likelihood and timing of HGL damage. Modeling technique exits can combine the effects of a thermal plume immersed in an HGL, although these techniques may be applied only to exposures within the thermal plume prior to the HGL damage state.
- The new fire location factor does not apply to analyses that determine the visibility reduction due to smoke accumulation. Smoke accumulation has not been evaluated directly in this report, and the findings of this report do not invalidate existing guidelines for the evaluation of visibility.
- The new fire location factor does not apply to the evaluation of the ceiling jet damage ZOI. The ceiling jet has not been evaluated in this report, and the findings of this report do not invalidate existing guidelines for the evaluation of the ceiling jet.
- The new fire location factor does not apply to the evaluation of the horizontal thermal flame radiation ZOI. Existing information and modeling techniques should be used to evaluate the extent of the horizontal ZOI.

- The new location factor values prescribed in this report are not be applied to FDS predictions of fire plume temperatures. The new location factor does not apply to FDS results and is intended for use only with the Heskestad fire plume correlation. A qualified user of FDS should develop an appropriate set of inputs to address the effects of wall surfaces but not by adjusting the output data with a bias correction.
- The new fire location factor has not been studied in conjunction with forced or augmented ventilation. In the presence of non-ambient air flow conditions, a historically acceptable means of estimating fire plume temperatures should be used in lieu of this new fire location factor.

## 3.3 Conclusions

In this investigation, two specific areas of guidance for use of fire location factors with fire plume temperature analysis of ZOI applications in NPPs were explored. These two areas are identified as:

- When to use the fire location factor
- What value of the location factor to use

Evidence for this investigation was developed using FDS Version 6.0.1. Results from these simulations were used in a modified version of the Heskestad fire plume correlation to estimate values of the fire location factor, $k_F$, for fires located in wall and corner configurations. A number of different parameters, including HRR, distance from the wall surfaces, fire source diameter, the elevation above the fire source were varied to determine their influence on the estimation of $k_F$.

Using these estimated values of $k_F$, recommendations for the implementation of the fire location factor based on varying distances from wall surfaces are presented. Guidance on what values of the location factor to use is provided in the form of location factors for fires located at various distances away from wall and corner surfaces. The results of this investigation were compared with observations from previous studies showing that the wall surfaces influence fire plume temperatures.

While other researchers have reported that the mirror method is not always conservative, this investigation developed an implementation and showed that the implementation is, on average, conservative. For practical application in the commercial nuclear industry, the higher values of location factors observed are associated with low fire plume temperatures that are well below the damage threshold for cables. Therefore, the recommended guidance is appropriate for representing the hazards to cables due to fire plume temperatures.

Guidance provided from this investigation was developed using industry-accepted tools and statistical practices in a manner that combined aspects of a fire PRA and fire hazard analysis. Implementation of the guidance provided was done with an understanding and presentation of the bias and uncertainty of the results obtained during this investigation while applying fundamental fire science.

Evidence suggests that for fires located adjacent to corners, the current guidance to use a $k_F$ of 4 may be overestimated. At distances greater than 0.3 m (1 ft.), the current guidance for a $k_F$ of 4 is overly conservative and may be reduced for fires with greater than a 0.3 m (1 ft.) separation from the corner. For fires located along a single wall surface, the current guidance to use a $k_F$ of 2 has been shown to be more conservative than necessary, and a value of 1 is appropriate for all wall configurations, particularly when the plume temperature is greater than the cable damage threshold.

## 3.4 References


1. Alpert, R. L., and E. J. Ward, "Evaluation of Unsprinklered Fire Hazards," *Fire Safety Journal*. Volume 7.2, pp. 127–143 (1984).
2. Beyler, C. L, "Fire Plumes and Ceiling Jets," *Fire Safety Journal.* Volume 11.1, pp. 53–75 (1986).
3. Hasemi, Y., and T. Tokunaga, "Some Experimental Aspects of Turbulent Diffusion Flames and Buoyant Plumes from Fire Sources Against a Wall and in a Corner of Walls," *Combustion Science and Technology.* 40.1-4, pp. 1–18 (1984).
4. McGrattan, K. B., et al. *Fire Dynamics Simulator, Technical Reference Guide, Volume 3: Validation.* National Institute of Standards and Technology, Gaithersburg, Maryland, USA, and VTT Technical Research Centre of Finland, Espoo, Finland, sixth edition, November 2013.
5. *Fire PRA Methodology for Nuclear Power Facilities, Volume 2: Detailed Methodology*, NUREG/CR-6850 and EPRI 1011989. U.S. Nuclear Regulatory Commission, Office of Nuclear Regulatory Research (RES), Washington, DC and Electric Power Research Institute (EPRI), Palo Alto, CA: 2005.

# 4
# PROBABILITY OF PROPAGATION FOR TRANSIENT FIRES

## 4.1 Introduction

Risk analysts in the commercial nuclear industry have been modeling transient combustible fires in fire PRAs for a number of years. A review of the latest transient fire event data strongly suggests that the current transient fire scenario frequency calculations are missing an opportunity to reduce conservatism by accounting for the probability that a transient combustible package is present near the ignition source. Typically, the scenario frequency considers only the likelihood of an ignition source (for example, temporary electrical wiring, portable equipment, pinched extension cords, and so on), but does not consider the probability that the ignition source (1) would contain sufficient combustible material on its own to sustain a significant fire, or (2) would be close enough to a transient combustible package to ignite a significant transient fire. To capture the propagation probability, a term to represent the probability of a transient fire propagating from an ignition source to a significant transient combustible package may be introduced into the equation for the ignition source frequency for general transient fire scenarios.

## 4.2 Purpose and Scope

The purpose of this chapter is to refine the current approach for calculating the ignition frequency for general transients presented in NUREG/CR-6850 to include a term representing the probability that a transient fire develops into a significant fire event.

The scope of this effort includes general transients. This includes fire ignition frequency bins 7 (control/aux/reactor building), 25 (plant-wide), and 37 (turbine building). Fire event data are collected for all operating modes; however, the calculation of ignition frequencies is dependent on operating mode. Likewise, this review differentiates between at power and LPSD transient fire events.

## 4.3 Assumptions and Limitations

The following assumptions were used in the calculation:

- **Ignition source characteristics**. For a transient combustible fire that consists of an ignition source that is separate from a transient combustible package, the ignition source is described by a gamma distribution with a 98$^{th}$ percentile of 317 kW, as specified for general transient fires in NUREG/CR-6850. To further characterize the ignition source, a representative radiative fraction of 0.4 is used in the calculations to model combustible packages. The value of $\chi_r$ typically lies between 0.3 and 0.4 for natural materials (paper and wood) and between

0.2 and 0.6 for synthetic materials and electrical cables as published in *Generation of Heat and Gaseous Liquid, and Solid Products in Fires,* Table 3-4.16, p. 3-143 and p. 3-145, $\chi_r = \nabla H_{\mathrm{rad}}/\nabla H_{\mathrm{ch}}$ [10]. This assumption conservatively represents the ability of the ignition source to propagate to the combustible package.

- **Distance range for correlated ignition source and combustible**. For a transient combustible fire in which the location of the ignition source is separate from the location of the transient combustible package, but for which the locations of the two are correlated (that is, located close together due to being a part of the same work activity), the distance from the center of the ignition source to the edge of the transient combustible package for propagation purposes is assumed to be 1 m or less. A distance of 1 m or less is chosen as a reasonable distance for keeping material nearby for a work activity.
- **Critical heat flux distribution**. The critical heat flux to ignite the combustible package is probabilistically represented in the calculation as a uniform distribution between 6 and 20 kW/m$^2$. The lower and upper limits are justified in Section 4.5.5, based on literature values of critical heat flux for typical transient materials.
- **Precision of the Monte Carlo results**. The precision of the Monte Carlo results is determined by the number of realizations. With 100,000 realizations, the estimated standard error (or standard deviation of the average) is $s/\sqrt{100{,}000} = 0.003s$, where $s$ is the sample standard deviation of the 100,000 probability realizations as published in Equations 5A and 40 [2]. As the footnote to Table 4-3 shows, the standard deviation of the average probability of fire propagation was calculated to be less than about 2%. The statistical fluctuations can be made arbitrarily small by increasing the number of realizations at the cost of increased computing time. The choice of 100,000 realizations reduces the statistical fluctuations to below the precision of the reported results.

## 4.4 Methodology

### *4.4.1 Calculating Transient Ignition Frequency*

NUREG/CR-6850 (Section 6.3.1) [7] describes the process for calculating the scenario frequency for the general transient fire scenario, $\lambda_{GT}$, as follows:

$$\lambda_{GT} = \lambda_g \cdot W_L \cdot W_{IS} \cdot W_g \qquad \textbf{Eq. 4-1}$$

Where:

$\lambda_g$ is a plant-level fire frequency for general transient combustibles from EPRI 3002002936 / NUREG-2169 (for example, Bins 7, 25, or 37) [11].

$W_L$ is the location weighting factor.

$W_{IS}$ is the weighting factor for the general transient ignition source.

$W_g$ is the floor area ratio for the general transient fire.

The generic frequency, $\lambda_g$, for general transients was calculated using EPRI's updated fire events database, including potentially challenging events (a fire event that either did or could have presented a threat to nuclear safety) and undetermined events (an event with insufficient information to determine the classification). Fire frequencies for both at-power and LPSD conditions are published in EPRI 3002002936 and NUREG-2169 [11]. Included events were those that occurred during power operations or low-power operations, such as plant startup. Non-challenging fires and fires that occurred off site or on site in areas that are not associated with either the nuclear or power generation blocks of the plant were screened out (NUREG/CR-6850, App. C).

The location weighting factor, $W_L$, adjusts the frequencies for those situations where a common location is shared between multiple units. For example, if one turbine building serves two units, then 2.0 will be used for the location weighting factor (NUREG/CR-6850, Section 6.3.1) [7].

The term $W_{IS}$ is a weighting factor that distributes the generic frequency for general transient fires among the compartments within the particular general transient bin. The weighting factor is based on relative values of influence factors for maintenance, occupancy, and storage attributed to each fire compartment.

The floor area ratio for general transient scenario, $W_g$, is the floor area considered in the scenario, divided by the floor area of the fire compartment. The ratio apportions the frequency within the fire zone to a specific portion of the floor area.

Review of the latest transient fire events data strongly suggests that the current transient fire scenario frequency calculations are missing an opportunity to reduce conservatism by accounting for the probability that a transient combustible package is present near the ignition source. In order to capture the probability, a term, $\overline{W_p}$, is added to the equation for the ignition source frequency for a general transient fire scenario as follows:

$$\lambda_{GT} = \lambda_g \cdot W_L \cdot W_{IS} \cdot W_g \cdot \overline{W_p} \qquad \textbf{Eq. 4-2}$$

Where, $\overline{W_p}$ is the probability of a transient fire propagating from the ignition source to a transient combustible package capable of causing a significant fire event.

### 4.4.2 Definition of Probability of Propagation: $\overline{W_p}$

A general transient fire is defined with a gamma distribution with the 98$^{th}$ percentile of 317 kW [7]. One way for a significant transient fire to occur is for an ignition source to contain sufficient combustible material on its own to sustain the transient fire; in other words, the combustible material is integral to the ignition source. Another way is for an ignition source to be in close proximity to a transient combustible package so that the radiant heat flux from the ignition source ignites the combustible package. If an ignition source and a combustible package are brought into a fire compartment during a work activity, it is likely that they are placed near each other on the floor, and the relative locations of the ignition source and the combustible package can be described as correlated. If an ignition source and a combustible package are brought into a fire compartment at different times, as a part of different activities, the location of the ignition

source is not considered dependent on the placement of the combustible package. In this case, the relative locations of the ignition source and the combustible package are described as uncorrelated. Therefore, three types of transient fires, which are used in the development of $\overline{W_p}$, are defined as follows:

- **Integral**. The ignition source contains sufficient combustible material integral to the source (that is, combined ignition source and combustible material) to cause a significant fire event.
- **Correlated**. The ignition source does not contain sufficient combustible material to cause a significant fire event by itself, but the location of a separate transient combustible package is likely to be correlated to the location of the ignition source, since the placement of both is associated with a single work activity.
- **Uncorrelated**. The ignition source does not contain sufficient combustible material to cause a significant fire event by itself, and the location of a separate transient combustible package is likely to be uncorrelated to the location of the ignition source, since the placement of both is not associated with a single work activity.

Considering these three types of transient fires, the average probability of propagation for a transient fire, $\overline{W_p}$, can be defined as

$$\overline{W_p} = x_{int} W_{p,int} + x_{corr} W_{p,corr} + x_{uncorr} W_{p,uncorr} \quad \textbf{Eq. 4-3}$$

Where:

$x_{int}$ is the fraction of transient fires characterized as *integral.*

$x_{corr}$ is the fraction of transient fires characterized as *correlated.*

$x_{uncorr}$ is the fraction of transient fires characterized as *uncorrelated.*

$W_{p,int}$ is the probability of fire propagation for an *integral source.*

$W_{p,corr}$ is the probability of fire propagation for a *correlated source.*

$W_{p,uncorr}$ is the probability of fire propagation for an *uncorrelated source.*

The values of $x_{int}$, $x_{corr}$, and $x_{uncorr}$, are determined by analyzing the transient combustible fires in the EPRI *Updated Fire Events Database* [3], as described in Section 4.4.3. Note that:

$$x_{int} + x_{corr} + x_{uncorr} = 1 \quad \textbf{Eq. 4-4}$$

The value of $W_{p,int}$ is 1, by definition, since the combustible material is integral to the ignition source.

The values of $W_{p,corr}$ and $W_{p,uncorr}$ are calculated in Section 4.4.4, based on the following premises:

- The ignition source is separate from the transient combustible package.
- The transient combustible package will ignite when the ignition source produces a critical heat flux on the surface of the combustible package, as described in Section 4.4.5.

- The ignition source is described by a gamma distribution with a 98$^{th}$ percentile of 317 kW (Assumption 1). This is a conservative input, since the bulk of the combustible material is separate from the ignition source for a non-integral ignition source.
- The ignition source can be located anywhere within the floor area under consideration for a transient fire.
- For the correlated case, the transient combustible package is assumed to be located at a maximum distance of 1 m from the ignition source (Assumption 2).
- For the uncorrelated case, the transient combustible package can be located anywhere within the floor area under consideration for a transient fire.

### *4.4.3 Characterizing Transient Fires in EPRI Updated Fire Events Database*

A detailed review of the transient fires (~50 events) in the EPRI *Updated Fire Events Database* [3] from the 1990s and 2000s results in the following characterization of transient fires for three groupings based on the plant power levels at the time of the transient fire—all power levels, at power, and low power:

#### 4.4.3.1 All Power Levels (54 Events)

- 19% of ignition sources can be described as *integral* ($x_{int}$ = 0.19), for which the ignition sources contain significant combustibles (integral to the source), any of which can cause a significant fire by itself.
  - Example: A vacuum cleaner with a bag containing combustible material.
- 47% of ignition sources can be described as *correlated* ($x_{corr}$ =0.47), for which the ignition sources do not contain significant combustibles and the location of the separate transient combustible package is likely to be correlated to the location of the ignition source.
  - Example: Ignition of extension cord during maintenance; other combustibles could be nearby due to same activity.
- 34% of ignition sources can be described as *uncorrelated* ($x_{uncorr}$ =0.34), for which the ignition sources do not contain significant combustibles and the location of the separate transient combustible package is likely to be uncorrelated to the location of the ignition source.
  - Example: Electrical outlet for freeze protection overheated and caught fire; this would not involve a collection of significant combustible materials

#### 4.4.3.2 At Power (23 out of 54 Events)

- 24% of ignition sources can be described as *integral* ($x_{int}$ = 0.24).
- 50% of ignition sources can be described as *correlated* ($x_{corr}$ =0.50).
- 26% of ignition sources can be described as *uncorrelated* ($x_{uncorr}$ =0.26).

#### 4.4.3.3 Low Power (31 out of 54 Events)

- 15% of ignition sources can be described as *integral* ($x_{int}$ = 0.15).
- 45% of ignition sources can be described as *correlated* ($x_{corr}$ =0.45).
- 40% of ignition sources can be described as *uncorrelated* ($x_{uncorr}$ =0.40).

Appendix B contains a list of all the transient fires and the categorization details.

### *4.4.4 Calculation of Probability of Propagation for Transient Combustible Packages That Are Separate from Ignition Sources: $W_{p,corr}$ and $W_{p,uncorr}$*

Consider a typical fire compartment depicted in Figure 4-1 with a transient fire postulated on the floor area marked as "Transient Zone." The distance, *r*, represents the distance between the transient ignition source (red box) and the transient combustible package (yellow box). The probability of propagation for a transient fire is dependent on *r*, since a significant fire will occur only if the transient combustible package is close enough to the ignition source to receive a critical heat flux to cause ignition, as explained in Section 4.4.5.

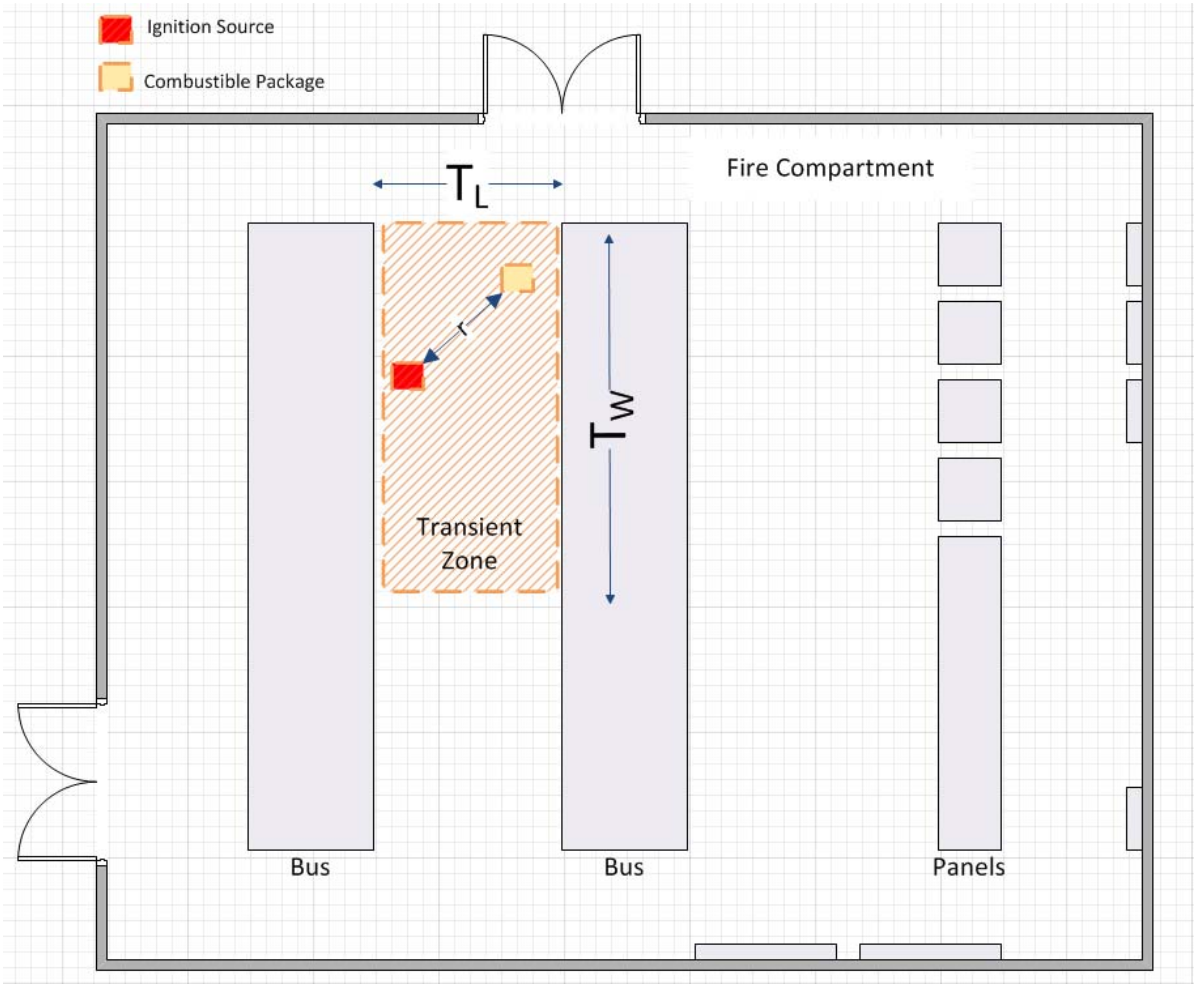


**Figure 4-1**
**Location of transient combustible package in relation to separate ignition source**

The HRR for the transient ignition source is characterized by a gamma probability distribution as defined in Appendix G of NUREG/CR-6850 (Assumption 1). The probability density function can be written as follows:

$$f(\dot{Q}) = \frac{\dot{Q}^{\alpha-1} e^{\frac{-\dot{Q}}{\beta}}}{\beta^{\alpha}\Gamma(\alpha)} \quad \textbf{Eq. 4-5}$$

Where:

$\dot{Q}$ is the random variable for the HRR.

$\alpha$ and $\beta$ are the scale and shape parameters for the gamma distribution, respectively.

From Appendix G of NUREG/CR-6850 [7], the values for $\alpha$ and $\beta$ are 1.8 and 57.4, respectively.

The incident heat flux generated by the ignition source can be estimated using the point source flame radiation model (See Chapter 5 of Reference 6). The point source flame radiation model has the following mathematical structure:

$$\dot{q}'' = \frac{\chi_r \dot{Q}}{4\pi r^2} \quad \textbf{Eq. 4-6}$$

Where:

$\dot{q}''$ is the radiant heat flux in units of kW/m$^2$.

$\chi_r$ is the radiative fraction.

*r* is the distance from the centerline of the fire to the surface of the transient combustible package receiving the flame radiation.

A representative value of 0.4 is used in the calculations to model combustible packages (Assumption 1).

Since the HRR parameter $\dot{Q}$ is a random variable governed by a gamma distribution, the parameter uncertainty can be propagated to the heat flux term $\dot{q}''$ using the transformation method as follows:

$$f(\dot{q}'') = \frac{f(\dot{Q})}{|g'(\dot{Q})|} \quad \textbf{Eq. 4-7}$$

The left side of the equation is the probability distribution for $\dot{q}''$, the numerator is the probability distribution for $\dot{Q}$ (which is the gamma distribution for the transient HRR), and the denominator is the absolute value of the derivative for the equation for $\dot{q}''$ (that is, the point source flame radiation model) described earlier. The derivative is:

$$\frac{d\,\dot{q}''}{d\dot{Q}} = \frac{\chi_r}{4\pi r^2} \quad \textbf{Eq. 4-8}$$

The point source flame radiation equation is solved for $\dot{Q}$, resulting in:

$$\dot{Q} = \frac{4\dot{q}''\pi r^2}{\chi_r} \quad \textbf{Eq. 4-9}$$

The last three equations are joined to produce the resulting probability distribution:

$$f(\dot{q}",r) = \frac{4\pi r^2 f\left(\frac{4\dot{q}"\pi r^2}{\chi_r}\right)}{\chi_r} = \frac{4\pi r^2}{\chi_r}\frac{\left(\frac{4\dot{q}"\pi r^2}{\chi_r}\right)^{\alpha-1} e^{\frac{-\left(\frac{4\dot{q}"\pi r^2}{\chi_r}\right)}{\beta}}}{\beta^{\alpha}\Gamma(\alpha)} \quad \text{Eq. 4-10}$$

The probability distribution is a function of *r*.

The probability distribution $f(\dot{q}",r)$ can be integrated for a given value of *r* to determine the probability of a heat flux exceeding the critical value assumed for ignition. Mathematically, this is expressed as:

$$W_p(r) = 1 - \int_0^{qcrit} f(\dot{q}",r)dq \quad \text{Eq. 4-11}$$

Given a value of *qcrit* and a value of *r*, the result is the probability of ignition of the combustible package.

### 4.4.5 Critical Heat Flux for Typical Transient Combustibles

For this analysis, the fire starts in an ignition source and potentially generates enough radiant heat flux to ignite a separate transient combustible package. The critical heat flux is defined as the heat flux below which ignition under practical conditions (in bench-scale test or a real fire) cannot occur. Therefore, for fire initiation, a material must be heated above its critical heat flux value. Literature values of critical heat flux for typical transient materials are presented in Table 4-1.

Based on NUREG/CR-6850 (Tables G-7 and G-8), typical transient combustibles are composed of paper, cardboard, plastics (such as polyethylene, polypropylene, polyurethane, polyvinyl chloride, and polystyrene), natural and synthetic fibers, wood, and yard waste [7]. The values of critical heat flux in Table 4-1 were measured using the ASTM E2058 fire propagation apparatus (FPA) designed by the Factory Mutual Research Corporation. In this method, the horizontal sample (approximately 100 mm × 100 mm square and up to about 25 mm in thickness) is exposed to a small pilot flame and various external heat flux values until a value is found at which there is no ignition for about 15 m [1]. This scenario represents what is called “piloted ignition,” which is when a material is heated in the presence of an ignition source, that is, a small flame, electric arc, burning ember, and so on. As the transient combustible material is heated, the solid transforms into gas-phase fuel, which is called *pyrolysis*. Once pyrolysis starts, gas emerges from the fuel surface, mixes with the ambient oxygen, and produces a flammable mixture. This flammable mixture is assumed to ignite immediately upon formation, due to the nearby ignition source.

The Society of Fire Protection Engineers (SFPE) Engineering Guide—*Piloted Ignition of Solids Materials Under Radiant Exposure* indicates that the values measured using the ASTM E2058 FPA method are conservative because the surface is blackened to maximize the surface absorptivity, thus minimizing the ignition temperature and minimizing the heat flux for ignition [9]. A further conservatism applies to this analysis due to the use of data from piloted ignition tests to represent unpiloted scenarios (spatial separation of the ignition source and combustible package).

Based on the critical heat flux values listed in Table 4-1, the range of 6–20 kW/m2 for typical transients was chosen as a conservative input for the analysis.

**Table 4-1**
**Critical heat flux values for potential transient combustible materials**

| Material | Critical Heat Flux ($kW/m^2$) | Source |
|---|---|---|
| Thermoplastic cables | 6 | NUREG/CR-6850, Section H.1.1 |
| Thermoset cables | 11 | NUREG/CR-6850, Section H.1.1 |
| Tissue paper, newspaper, corrugated paper | 10-15 | Tewarson 2008 |
| Wood | 10 | Tewarson 2008 |
| Plywood | 16 | SFPE 2002 (Table 4) |
| Polystyrene | 13 | Tewarson 2008 |
| Polypropylene | 8-15 | Tewarson 2008 |
| Polyethylene | 15 | Tewarson 2008 |
| Polystyrene foams | 10-15 | Tewarson 2008 |
| Polyurethane foams | 13-40 | Tewarson 2008 |
| Polyester | 8-18 | Tewarson 2008 |
| Rayon | 14-17 | Tewarson 2008 |
| Wool-nylon | 15 | Tewarson 2008 |
| Yard waste (pine needles, oak leaves) | 12-18<br>13 | Mindykowski et al. 2011 [4]<br>SFPE 2002 (Table 2) |

## 4.5 Results

The computer software MATLAB was used to calculate the value of $W_p(r)$ in Equation 4-11. As an example, the equation for $W_p(r)$ was solved numerically for values of $r$ = 0 to $r$ = 1.5 m, in increments of 0.05 m (Appendix B.2, MATLAB file: Trans_q_r_set.m) and a *qcrit* of 6, 10, and 20 $kW/m^2$. The plot of $W_p(r)$ versus $r$ is shown in Figure 4-2. In this example, if a transient combustible has a critical heat flux of 10 $kW/m^2$ and is located 0.6 m away from the ignition source, the probability of propagation is about 0.4.

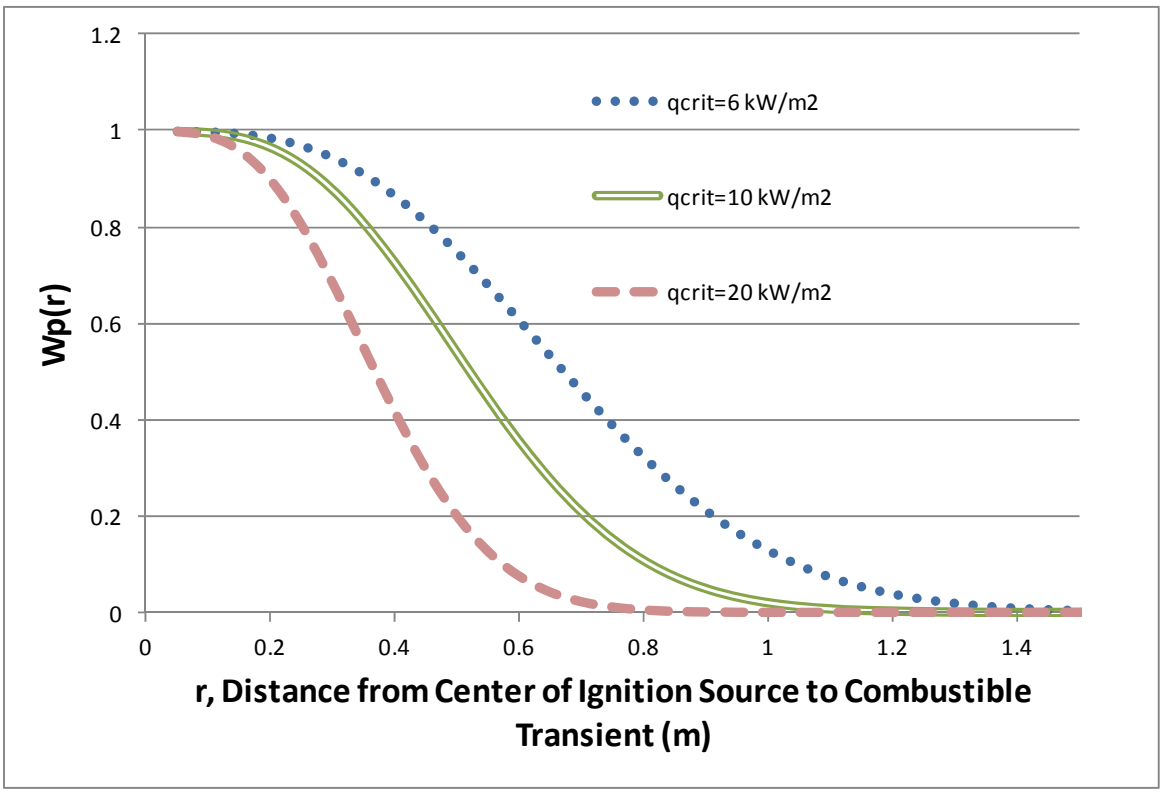


**Figure 4-2**
**Probability of propagation $W_p(r)$ versus distance**

The results in Figure 4-2 do not take into account the size of the transient zone area where the fire can occur, which is important for uncorrelated transient fires where the location of the ignition source is independent of the location of the transient combustible package. Fire PRAs typically assume that the ignition source can be located anywhere in the transient zone with dimensions $T_L$ x $T_W$, as shown in Figure 4-1. This research aims to generate an average probability value, $\overline{W_p}(L)$, resulting from averaging the function $W_p(r)$ over a range of achievable distances between the ignition source and combustible and over a range of *qcrit* from 6 to 20 kW/m$^2$. The value of $\overline{W_p}(L)$ as a function of transient zone size is calculated using a Monte Carlo simulation using MATLAB (Appendix B.2) as follows:

1. For a range of transient zone sizes, with characteristic length defined as, $L = \sqrt{T_L \times T_W}$, choose a value of $L$, starting with 0.1 m and increasing by 0.1 m each time this step is repeated.
2. Calculate a randomly generated value of $x_1$ and $y_1$ between 0 and $L$ to represent the location of the ignition source within the transient zone.
3. Calculate a randomly generated value of $x_2$ and $y_2$ between 0 and $L$ to represent the location of the combustible package within the transient zone.
4. Calculate the distance between the ignition source and the combustible package:

$$r = \sqrt{(y_2 - y_1)^2 + (x_2 - x_1)^2} \qquad \textbf{Eq. 4-12}$$

5. Choose a randomly generated *qcrit* between 6 and 20 kW/m$^2$, assuming a uniform distribution (Assumption 3).
6. Calculate $W_p$ using Equation 4-11 for the calculated value of *r* and *qcrit*.
7. Repeat steps 2 through 6 for 100,000 samples
8. Calculate $\overline{W_p}(L)$ for the chosen value of *L*
9. Repeat steps 1 through 8, each time increasing the value of *L* until *L* = 8 m.

The results of $\overline{W_p}(L)$ versus *L* are plotted in Figure 4-3. This plot applies to an uncorrelated transient fire in which the location of the ignition source is independent of the location of the transient combustible package and can be located anywhere within the transient area; therefore the value of $\overline{W_p}(L)$ in Figure 4-3 is equivalent to $W_{p,uncorr}$ from Equation 4-3. This shows that, for example, in a transient area equal to 9 m$^2$, with *L* = 3, when an ignition source and combustible package are separate from each other and not part of the same activity (that is, locations are uncorrelated), the probability that the transient combustible package is close enough to the ignition source to be ignited due to radiant heat flux, ranging from 6 to 20 kW/m$^2$, is 8%.

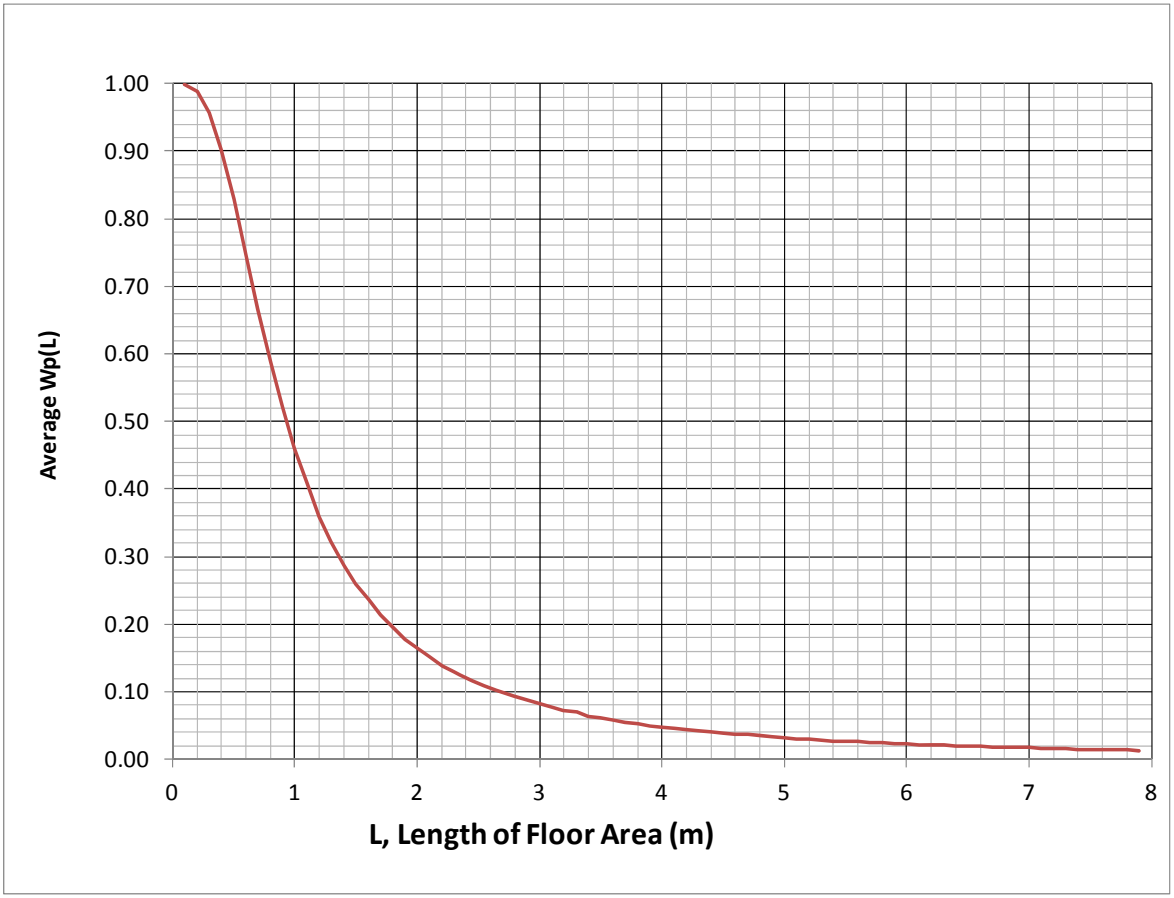


**Figure 4-3**
**Average probability of propagation for uncorrelated transient types**

For correlated transient fires, the distance between the center of the ignition source and the edge of the transient combustible package is limited to 1 m or less (Assumption 2). This is equivalent to restricting the transient zone size to $L$ = 1 m. This assumes that a worker entering a work area will place the ignition source and transient combustible package within 1 m or less of each other. Using a value of $L$ = 1, from Figure 4-3, the value of $\overline{W_{p,corr}}$ = 0.46 is obtained. In other words, when an ignition source and combustible package are separate from each other and both are part of the same activity (that is, locations are correlated), the probability that the transient combustible package is close enough to the ignition source to be ignited due to radiant heat flux, ranging from 6 to 20 kW/m$^2$, is 46%.

For transient combustibles in which the combustible material is integral to the ignition source, the distance between the ignition source and the combustible package, by definition is 0, $L$ = 0. From Figure 4-3, the value of $W_{p,int}$ is 1. In other words, for integral transient combustibles, probability of propagation by the ignition source to the combustible material is 100%, and a Monte Carlo calculation is not required.

All of the terms for calculating $\overline{W_p}$ in Equation 4-3 have been defined and calculated and are presented in Tables 4-2 and 4-3 for all power levels, at power, and low power. Table 4-3 contains the probability of propagation for a transient fire. These values are intended to be used in calculating scenario frequencies for transient fires. The results are plotted in Figure 4-4.

**Table 4-2**
**Inputs for calculating the probability of propagation for transient fires**

| Power Level | Fraction of Ignition Sources | | | $W_{p,int}$ | $W_{p,corr}$ (Equivalent to $W_{p,uncorr}$ at $L$ =1 m) |
|---|---|---|---|---|---|
| | Integral $x_{int}$ | Correlated $x_{corr}$ | Uncorrelated $x_{uncorr}$ | | |
| All levels | 0.19 | 0.47 | 0.34 | 1 | 0.461 |
| At power | 0.24 | 0.50 | 0.26 | | |
| Low power | 0.15 | 0.45 | 0.40 | | |

**Table 4-3**
**Probability of propagation for transient fires**

| $L$ (m) | $W_{p,uncorr}$ (Equivalent to $\overline{W_p}(L)$* | $\overline{W_p} = x_{int}W_{p,int} + x_{corr}W_{p,corr} + x_{uncorr}W_{p,uncorr}$ | | |
|---|---|---|---|---|
| | | All Power Levels | At Power | Low Power |
| 1.0 | 0.461 | 0.56 | 0.59 | 0.54 |
| 1.1 | 0.407 | 0.54 | 0.58 | 0.52 |
| 1.2 | 0.359 | 0.53 | 0.56 | 0.50 |
| 1.3 | 0.322 | 0.52 | 0.55 | 0.49 |
| 1.4 | 0.287 | 0.50 | 0.54 | 0.47 |
| 1.5 | 0.259 | 0.49 | 0.54 | 0.46 |
| 1.6 | 0.237 | 0.49 | 0.53 | 0.45 |

**Table 4-3 (continued)**
**Probability of propagation for transient fires**

| $L$ (m) | $W_{p,uncorr}$ (Equivalent to $\overline{W_p}(L)$* | $\overline{W_p} = x_{int}W_{p,int} + x_{corr}W_{p,corr} + x_{uncorr}W_{p,uncorr}$ | | |
|---|---|---|---|---|
| | | **All Power Levels** | **At Power** | **Low Power** |
| 1.7 | 0.213 | 0.48 | 0.53 | 0.44 |
| 1.8 | 0.196 | 0.47 | 0.52 | 0.44 |
| 1.9 | 0.177 | 0.47 | 0.52 | 0.43 |
| 2.0 | 0.165 | 0.46 | 0.51 | 0.42 |
| 2.1 | 0.153 | 0.46 | 0.51 | 0.42 |
| 2.2 | 0.139 | 0.45 | 0.51 | 0.41 |
| 2.3 | 0.130 | 0.45 | 0.50 | 0.41 |
| 2.4 | 0.121 | 0.45 | 0.50 | 0.41 |
| 2.5 | 0.112 | 0.44 | 0.50 | 0.40 |
| 2.6 | 0.105 | 0.44 | 0.50 | 0.40 |
| 2.7 | 0.0988 | 0.44 | 0.50 | 0.40 |
| 2.8 | 0.0922 | 0.44 | 0.49 | 0.39 |
| 2.9 | 0.0876 | 0.44 | 0.49 | 0.39 |
| 3.0 | 0.0821 | 0.43 | 0.49 | 0.39 |
| 3.1 | 0.0766 | 0.43 | 0.49 | 0.39 |
| 3.2 | 0.0716 | 0.43 | 0.49 | 0.39 |
| 3.3 | 0.0698 | 0.43 | 0.49 | 0.39 |
| 3.4 | 0.0640 | 0.43 | 0.49 | 0.38 |
| 3.5 | 0.0616 | 0.43 | 0.49 | 0.38 |
| 3.6 | 0.0577 | 0.43 | 0.49 | 0.38 |
| 3.7 | 0.0543 | 0.43 | 0.48 | 0.38 |
| 3.8 | 0.0536 | 0.42 | 0.48 | 0.38 |
| 3.9 | 0.0497 | 0.42 | 0.48 | 0.38 |
| 4.0 | 0.0478 | 0.42 | 0.48 | 0.38 |
| 4.1 | 0.0459 | 0.42 | 0.48 | 0.38 |
| 4.2 | 0.0437 | 0.42 | 0.48 | 0.37 |
| 4.3 | 0.0420 | 0.42 | 0.48 | 0.37 |
| 4.4 | 0.0397 | 0.42 | 0.48 | 0.37 |

**Table 4-3 (continued)**
**Probability of propagation for transient fires**

| $L$ (m) | $W_{p,uncorr}$ (Equivalent to $\overline{W_p}(L)$* | $\overline{W_p} = x_{int}W_{p,int} + x_{corr}W_{p,corr} + x_{uncorr}W_{p,uncorr}$ | | |
|---|---|---|---|---|
| | | All Power Levels | At Power | Low Power |
| 4.5 | 0.0394 | 0.42 | 0.48 | 0.37 |
| 4.6 | 0.0372 | 0.42 | 0.48 | 0.37 |
| 4.7 | 0.0364 | 0.42 | 0.48 | 0.37 |
| 4.8 | 0.0352 | 0.42 | 0.48 | 0.37 |
| 4.9 | 0.0329 | 0.42 | 0.48 | 0.37 |
| 5.0 | 0.0322 | 0.42 | 0.48 | 0.37 |
| 5.1 | 0.0307 | 0.42 | 0.48 | 0.37 |
| 5.2 | 0.0294 | 0.42 | 0.48 | 0.37 |
| 5.3 | 0.0276 | 0.42 | 0.48 | 0.37 |
| 5.4 | 0.0271 | 0.42 | 0.48 | 0.37 |
| 5.5 | 0.0259 | 0.42 | 0.48 | 0.37 |
| 5.6 | 0.0257 | 0.42 | 0.48 | 0.37 |
| 5.7 | 0.0241 | 0.41 | 0.48 | 0.37 |
| 5.8 | 0.0241 | 0.41 | 0.48 | 0.37 |
| 5.9 | 0.0231 | 0.41 | 0.48 | 0.37 |
| 6.0 | 0.0229 | 0.41 | 0.48 | 0.37 |
| 6.1 | 0.0215 | 0.41 | 0.48 | 0.37 |
| 6.2 | 0.0208 | 0.41 | 0.48 | 0.37 |
| 6.3 | 0.0206 | 0.41 | 0.48 | 0.37 |
| 6.4 | 0.0197 | 0.41 | 0.48 | 0.37 |
| 6.5 | 0.0196 | 0.41 | 0.48 | 0.37 |
| 6.6 | 0.0188 | 0.41 | 0.48 | 0.36 |
| 6.7 | 0.0181 | 0.41 | 0.48 | 0.36 |
| 6.8 | 0.0177 | 0.41 | 0.47 | 0.36 |
| 6.9 | 0.0173 | 0.41 | 0.47 | 0.36 |
| 7.0 | 0.0170 | 0.41 | 0.47 | 0.36 |
| 7.1 | 0.0163 | 0.41 | 0.47 | 0.36 |
| 7.2 | 0.0162 | 0.41 | 0.47 | 0.36 |

**Table 4-3 (continued)**
**Probability of propagation for transient fires**

| $L$ (m) | $W_{p,uncorr}$ (Equivalent to $\overline{W_p}(L)$* | $\overline{W_p} = x_{int}W_{p,int} + x_{corr}W_{p,corr} + x_{uncorr}W_{p,uncorr}$ | | |
|---|---|---|---|---|
| | | All Power Levels | At Power | Low Power |
| 7.3 | 0.0158 | 0.41 | 0.47 | 0.36 |
| 7.4 | 0.0149 | 0.41 | 0.47 | 0.36 |
| 7.5 | 0.0146 | 0.41 | 0.47 | 0.36 |
| 7.6 | 0.0143 | 0.41 | 0.47 | 0.36 |
| 7.7 | 0.0139 | 0.41 | 0.47 | 0.36 |
| 7.8 | 0.0136 | 0.41 | 0.47 | 0.36 |
| 7.9 | 0.0133 | 0.41 | 0.47 | 0.36 |

***Note**: The standard deviation of $W_{p,uncorr}$ ranges from <0.001% at L=0.1 m to 2.1% at L=7.9 m (Reference 2, Equations 5A and 40).

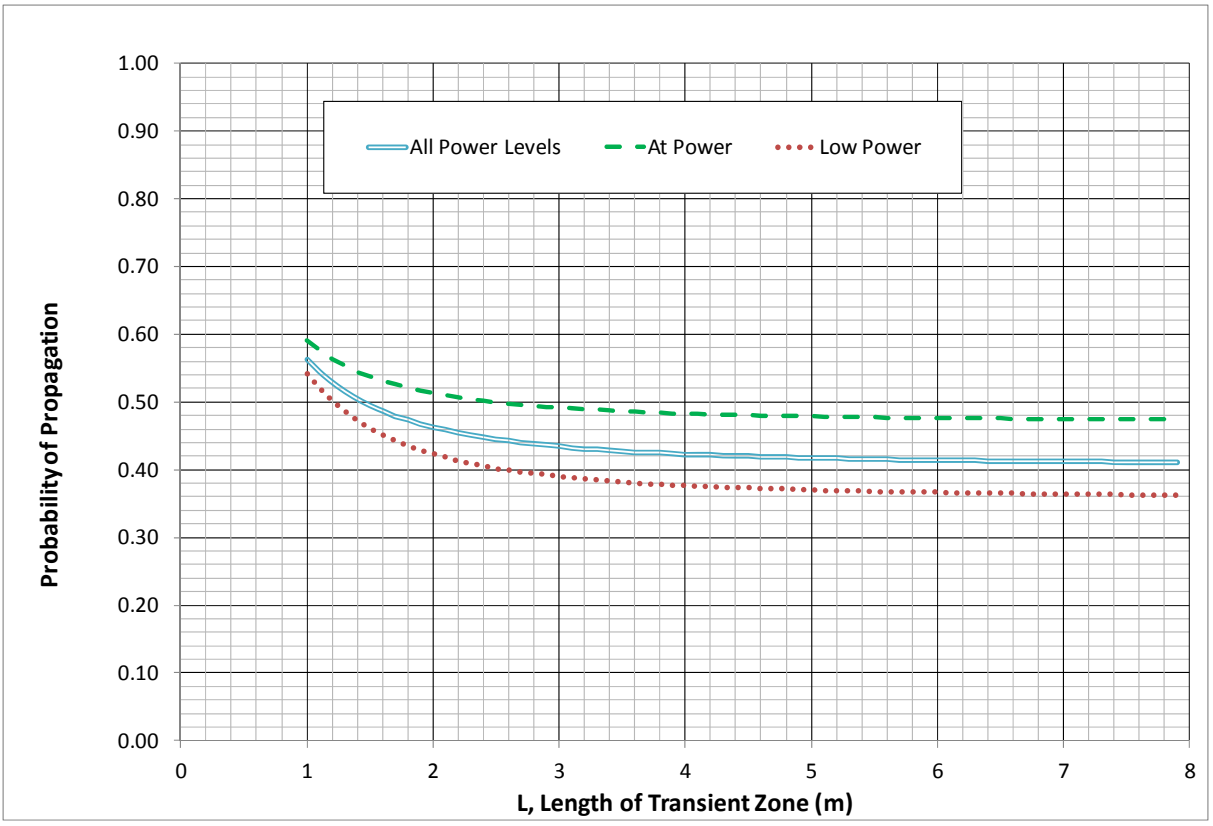


**Figure 4-4**
**Average probability of propagation for a transient fire for scenario frequency calculations**

The value of $\overline{W_p}$ for transient zone lengths larger than 7 m is 0.47 for at power and 0.36 for LPSD. The difference is due to the higher fraction of uncorrelated transient fires for low power (0.40) compared to the at power level (0.26), as shown in Tables B-3 and B-4 and discussed in Appendix B.

## 4.6 Conclusions and Recommendations

The average probability of propagation of a transient fire, $\overline{W_p}$, has been calculated using a Monte Carlo analysis and is plotted in Figure 4-4 and tabulated in Table 4-3. The value $\overline{W_p}$ is intended for use in calculating the scenario frequency for a general transient fire, when a transient fire is postulated in a subsection of a fire compartment, referred to as a *transient zone*, as follows:

$$\lambda_{GT} = \lambda_g \cdot W_L \cdot W_{IS} \cdot W_g \cdot \overline{W_p} \qquad \textbf{Eq. 4-13}$$

The calculated values of $\overline{W_p}$ include the characteristics of three types of transient fires, based on observations in EPRI's *Updated Fire Events Database*:

- Integral (combustible material is integral to the ignition source)
- Correlated (combustible material is located within 1 m of the ignition source)
- Uncorrelated (combustible material is located more than 1 m from the ignition source)

The results are based on literature values of critical heat flux for common transient materials, ranging from 6 to 20 kW/m$^2$ (Section 4.4.5). The heat flux for the transient ignition source is characterized by a gamma probability distribution, based on the HRR probability distribution for general transients, as defined in Appendix G of NUREG/CR-6850, rewritten in terms of heat flux rather than HRR, using the point source radiation model. The characteristic length, $L$, of the transient zone (the square root of the floor area of the transient zone) is the only input necessary to calculate $\overline{W_p}$ from the results presented. The recommended values of $\overline{W_p}$ range from 0.59 for small transient zones ($L$ =1 m) to 0.47 for large transient zones ($L \geq 8$ m) for full power conditions and range from 0.54 ($L$ =1 m) to 0.36 ($L \geq 8$ m) for low power conditions.

**Fire PRA Implementation**

To implement this method in a fire PRA, the following steps should be taken:

1. Identify the location of a transient fire area, such as the area marked as "Transient Zone" in Figure 4-1.
2. Calculate the characteristic length of the transient zone from $L = \sqrt{T_L \times T_W}$.
3. Determine the average probability of propagation, $\overline{W_p}$, for the value of $L$ at the applicable power level, using Figure 4-4 or Table 4-3.
4. Use Equation 4-13, along with the value of $\overline{W_p}$, to calculate the scenario frequency for the general transient fire.

For example, if a transient zone has dimensions $T_L \times T_W$ = 7 × 4 m. The characteristic length is $L = \sqrt{7 \times 4} = 5.3$ m. From Table 4-3, for all power levels, $\overline{W_p} = 0.42$. Once multiplied in Equation 4-13, the result is a scenario frequency that is reduced by a factor of 0.42.

## 4.7 References


1. ASTM E2058-00, Standard Test Methods for Measurement of Synthetic Polymer Material Flammability Using a Fire Propagation Apparatus (FPA), 2000.
2. Beers, Y., *Introduction to the Theory of Error*. Addison-Wesley Publishing Company, Inc., Reading, Mass.: 1957
3. *The Updated Fire Events Database: Description of Content and Fire Event Classification Guidance.* EPRI, Palo Alto, CA: 2013. 1025284.
4. Mindykowski, P., A. Fuentes, J. Consalvi, and B. Porterie, "Piloted Ignition of Wildland Fuels," *Fire Safety Journal.* Volume 46, pp. 34–40 (2011).
5. Not Used.
6. NUREG-1805, *Fire Dynamic Tools (FDT$^s$) Quantitative Fire Hazard Analysis Methods for the U.S. Nuclear Regulatory Commission Fire Protection Inspection Program*, U.S. Nuclear Regulatory Commission (NRC), Office of Nuclear Reactor Regulation, Washington, DC, 2004.
7. *Fire PRA Methodology for Nuclear Power Facilities,* NUREG/CR-6850 and EPRI 1011989. U.S. Nuclear Regulatory Commission, Office of Nuclear Regulatory Research (RES), Rockville, MD, and Electric Power Research Institute (EPRI), Palo Alto, CA, 2005.
8. Not Used.
9. Society of Fire Protection Engineers (SFPE), "Engineering Guide – Piloted Ignition of Solid Materials Under Radiant Exposure," 2002.
10. Tewarson, A., "Generation of Heat and Gaseous, Liquid, and Solid Products in Fires," Section 3, Chapter 4, *The SFPE Handbook of Fire Protection Engineering*, 4th Edition, P. J. DiNenno, Editor-in-Chief, National Fire Protection Association, Quincy, MA, 2008.
11. EPRI 3002002936 and NUREG-2169, *Nuclear Power Plant Fire Ignition Frequency and Non-Suppression Probability Estimation Using the Updated Fire Events Database,* EPRI, Palo Alto, CA and U.S. Nuclear Regulatory Commission, Office of Nuclear Regulatory Research, Rockville, MD: 2014.

# 5
# DETERMINATION OF LIQUID SPILL FIRE HEAT RELEASE RATES

Combustible and flammable liquid spill fire scenarios are an important class of fires considered at NPPs due to their potential to generate high HRRs over a short time interval, which can result in a severe fire hazard to critical components, raceways, and structural elements. Combustible and flammable liquids are present in many types of equipment at nuclear facilities, including transformers, chillers, pumps, motors, and diesel generators. The fuels may be contained within equipment, stored in tanks, or contained in drums and are often in close proximity to an ignition source, which may include the equipment containing the combustible or flammable liquids.

Current methods of predicting the HRR profiles in combustible and flammable liquid spill fires are based on a mix of data applicable to fires involving deep liquid pools and thin spills. The failure to consider the HRR data selectively, accounting for the depth of the liquid, results in significant over-predictions of the HRR and significant under-predictions of the fire durations for thin spills. The resulting errors in many cases may exceed a factor of 5.

It is natural to assume that an over-prediction of the HRR will universally yield a conservative result when considering the effects of a fire; however, several examples are identified in which the reverse is true. In these cases, fire duration plays a key role in the determination of the fire hazard associated with the liquid fuel fire, and a significant under-prediction of the fire duration results in a non-conservative assessment of the particular fire effect.

A large number of liquid fuel fire tests conducted in support of the United States National Institute of Justice (NIJ) [1] provide a unique opportunity to assess and improve existing HRR models for liquid fuel fires. The overall goal of this effort was to incorporate the spill fire test data developed in *Fire Dynamics and Forensic Analysis of Liquid Fuel Fires* [1] into an empirical model that can be applied to liquid fuel spills at commercial NPPs when predicting the HRR profile. Overall, the expectation is that an improved empirical treatment of liquid pool fires will produce more realistic HRR profiles. This will be especially useful for modeling the response of a target to fire exposure. Improved empirical treatment will also reduce conservatism in predicting HRR for thin-spill fire scenarios that had previously been treated using deep pool data. Useful applications of the improved empirical treatment include determining a ZOI and using an HRR as an input into a zone or field-based fire model.

Four liquid fuel fire empirical HRR models are considered in this report:

- Method 1 is based on guidance published in NUREG/CR-6850 [2]. This method is a very simplified model that is useful for predicting the maximum possible HRR of a liquid fuel fire. It does not account for fire growth or decay, or for reduced mass loss rates in thin and/or small diameter pools, resulting in the shortest burning durations and highest HRRs of all the methods considered in this report.

- Method 2 is described and implemented in NUREG-1805 [7]. This method is also a simplified model that is useful for predicting peak HRRs for pool fires where pool diameter is taken into account as an influence on the burning rate. It does not account for fire growth or decay or for reduced mass loss rates in thin pools, resulting in very short burning durations with very high HRRs.
- Method 3 is described by Gottuk and White [3]. This method is a simplified model that improves upon Method 2 by adding the effect of fuel depth and substrate cooling on reducing the burning rate of the spill fire. It does not account for fire growth or decay, resulting in short burning durations with high HRRs, although the accuracy is improved for thin pool fires as compared to Methods 1 and 2.
- Method 4, which is developed in this report, is an updated model that addresses the growth stage of the HRR in liquid fuel fires using observations of the behavior reported in Reference 1. A simple decay stage is included that is directly related to the surface flame spread rate on the liquid fuel and the localized mass burning rate. This method is shown to produce good agreement with the simple methods based on previous pool fire and spill fire data for deep pool data, but is significantly improved for liquid spill fires, in which the growth phase is a significant fraction of the overall HRR profile.

An analysis procedure was developed for implementing the empirical HRR models. The procedure is applicable to liquid fuel spills involving kerosene, gasoline, heptane, ethanol, or lubricating oils when substrate (that is, floor) temperatures are less than 40°C. Fuels that have burning characteristics similar to those listed above may be evaluated using this approach provided the empirical constants for the fuels are known or are bound by the selected values. Additionally, the analysis is not applicable to continuously fed spill fires. For applications that do not meet the applicability requirements, an alternative approach is recommended for determining the HRR profiles, with deference to the existing conservative guidance for deep pool fires. Appendix C provides graphical and tabular solutions to the updated or integral model presented in this report for different volumes of common flammable and combustible liquids. The data in the appendix may be used for applicable fuels and fuel volumes in place of solving the integral model.

Because the proposed updated model (Method 4) contains several variable input parameters that may be uncertain, the model sensitivity to variations in these parameters is evaluated and quantified. The uncertainty of the results may be quantitatively addressed through known uncertainty ranges for empirical parameters associated with each method. In particular, uncertainty ranges for the spill depth, the maximum mass burning rate, the depth coefficient, and the fire diameter empirical constant are provided in this report with guidance for the types of scenarios to which they apply and their general effect on the predicted HRR and burning duration.

The empirical HRR models considered in this report can readily be incorporated into an analytical model for ease of implementation. They are well suited for inclusion in spreadsheet-type calculations.

The empirical model described in this report accomplishes the primary goals for an improved method, namely improving the prediction of the peak HRR, fire duration, and growth stage of the fire.

## 5.1 Introduction

The overall goal of this effort is to incorporate the spill fire test data developed in Reference 1 into an empirical model that can be applied to liquid fuel spills at commercial NPPs when determining the HRR profile. Overall, the expectation is that an improved empirical treatment of liquid pool fires will produce more realistic HRR profiles. Improved empirical treatment will also reduce conservatism in predicting HRRs for thin-spill fire scenarios that had previously been treated using deep pool data. Useful applications of the improved empirical treatment include determining a ZOI and using a HRR as an input into a zone- or field-based computer fire model.

Fire scenarios involving combustible or flammable liquid spills can be categorized based on the presence or absence of confining structures (curbs, berms, or physical obstructions) and on the type of spill (fixed quantity or continuously fed) [1]. There are four categories of spill fire scenarios when grouped using the aforementioned parameters [1]:

- Fixed quantity, confined area
- Fixed quantity, unconfined area
- Continuously fed, confined area
- Continuously fed, unconfined area

Fixed quantity spill fire scenarios are most commonly postulated in commercial NPPs because the fire compartment and HRR tend to be greater than they would be for continuously fed scenarios, which in turn produces a conservative input for evaluating the effects on critical targets. Continuously fed spill fire scenarios ultimately involve a fixed quantity of flammable or combustible liquids; however, the fixed quantity is released during the combustion process at a known or assumed rate. This tends to produce a lower-hazard fire scenario as compared to one in which the entire volume is assumed to spill prior to ignition, although the duration of burning may be extended.

The HRR as a function of time from a combustible or flammable liquid fuel spill fire is the primary determinant of the fire hazard of a fuel spill fire. The recommended method for determining the HRR for spill fires, provided in EPRI 1011989 and NUREG/CR-6850 [2], is largely based on data applicable to confined-area deep pool fires coupled with the spill depth data recommended for unconfined spills in Chapter 2-15 of the *SFPE Handbook of Fire Protection Engineering* [3]. A *deep pool* is one in which the substrate effects are not significant, and the burning rate is essentially independent of the pool depth. The treatment provides a reasonable assessment of fixed quantity, confined area spill fires, provided that the liquid is sufficiently deep, but significantly over-predicts the HRR and under-predicts the fire duration for thin spills, whether unconfined or confined [1]. Although it is usually conservative to over-predict the HRR of a source fire when determining the damage potential to critical targets, brief fire durations coupled with a detailed evaluation of the target response can yield non-conservative results.

The use of confined-area deep pool fire data to determine the HRR from a thin spill fire in NUREG/CR-6850 [2] was reflective of the general lack of full-scale test data applicable to thin spill fires. Spill fires were investigated by Gottuk et al. [4, 5] and Putori et al. [6] and some guidelines for computing the HRR from spill fires were presented in Chapter 2-15 of the

*SFPE Handbook of Fire Protection Engineering* [3]. Both Gottuk et al. [4, 5] and Putori et al. [6] noted that the HRRPUA for thin liquid spills is significantly lower than the HRRPUA for the same fuel confined in a deep pool with the same area, which implies that the predicted fire duration is significantly under-predicted when applying deep pool HRR data to thin pools.

Recent work performed under Grant No. 2008-DN-BX-K168 for the National Institute of Justice (NIJ) has greatly expanded the available test data applicable to liquid spill fires [1]. These data consist of over 500 individual tests involving six liquid fuels and two nonfuel liquid surrogates. Tests included variations in the spill substrate, liquid volume, spill rate, ignition delay, substrate temperature, and type of confinement. The data developed in Reference 1 support the observations by Gottuk et al. [4, 5] and Putori et al. [6] that the HRR is significantly reduced for thin pools. Mealy et al. [1] also observed other aspects of spill fires that were not previously identified and present framework for an empirical analysis that addresses the fire development in spill fires. The data provide a means to substantially improve the current empirical treatments of liquid spill fires by incorporating the effects of the liquid depth as well as other key factors identified in Reference 1.

## 5.2 Purpose and Scope

### *5.2.1 Purpose*

This study provides an improved empirical model for predicting the HRR for a combustible or flammable liquid spill fire as a function of time. The empirical model developed is based on the spill fire test data provided in Reference 1. The two element study includes:

- A description of recent research providing a technical basis for the determination of liquid spill fire HRRs.
- A description of the recommended methodology for determining the HRRs of liquid spill fires in typical commercial NPP fire scenarios. Specifically, this report provides an empirical calculation methodology for determining the HRR profile for liquid spill fires using available spill fire test data.

### *5.2.2 Scope*

The scope of the research includes a description of the spill fire test data provided in Reference 1 that are applicable to NPP applications, including an assessment of the key parameters that affect HRR development and a recommended empirical methodology that incorporates the findings presented in Reference 1 regarding spill fires.

The focus of this analysis is on thin unconfined spill fires; however, some assessment of the limits of the recommended calculation as the depth increases is presented. Continuously fed spill fires are not considered in this evaluation, given that they are rarely postulated in NPPs. Nevertheless, the methods presented in this research are readily extended to continuously fed spill fire scenarios. Finally, a sample application of the recommended methodology is developed and discussed.

## 5.3 Assumptions and Limitations

The assumptions and limitations applicable to this research are described in this section. Several of the listed assumptions and limitations will be used to define limits on the implementation of the spill fire models as described in Section 6.2.

### *5.3.1 Fixed Quantity Liquid Spill Fires*

This analysis considers fixed quantity liquid spill fires, with a particular focus on determining the HRR profile in a thin, unconfined liquid pool of combustible or flammable liquids. The evaluation of deep pool liquid spill HRRs is well established (see References 2 and 7, for example) and does not require refinement. Deep pool liquid spill fires will be considered to the extent that they represent a limit of the thin pool model approach.

Continuously fed spill fire scenarios are not considered in this report largely because they are not frequently postulated in NPP applications. Continuously fed spill fire scenarios ultimately involve a fixed quantity of flammable or combustible liquid, and it is conservative to evaluate a known fixed quantity of flammable or combustible liquid as a complete spill. Nevertheless, the methods presented in this research are readily extended to continuously fed spill fire scenarios.

### *5.3.2 Concrete Substrate*

The substrate is assumed to be flat, level, thermally thick concrete at approximately normal ambient temperature. This is by far the most common substrate surface at commercial NPPs and is, therefore, of particular interest. Consideration of a single substrate reduces the complexity of an empirical approach, especially for substrates that may themselves contribute to the HRR of the source fire. The data provided in Reference 1 for recommended spill thickness are averaged over multiple substrate types, and standard deviations are provided. These data are used directly in this report owing to the uncertainty in the substrate finish characteristics and permeability.

The substrate must also be flat and level such that the spill location can be easily defined. Graded floors and floor drains are not considered in this analysis, and any scenario that credits these features must be accompanied with a defensible engineering analysis.

The normal substrate temperature for the spill fire tests in Reference 1 is between 20°C and 25°C; thus, the results and subsequent model development are limited to applications with a substrate temperature in this range for low flashpoint fuels. A safety factor of 25%–50% may be applied by increasing the HRR of the fire to substrate temperatures up to about 40°C for low flashpoint fuels. This limitation does not apply to high flashpoint fuels such as lubricating oil, although a limiting temperature of 40°C is reasonable to ensure that the substrate temperature remains significantly below the fuel flashpoint temperature. Similarly, a cold substrate may be considered to have an opposite effect; however, it is not recommended to credit a cold substrate for reducing the HRR of the fire.

### 5.3.3 Applicable Fuels

The empirical approach is limited to the fuels considered in Reference 1:

- Gasoline
- Kerosene
- Diesel fuel
- Lubricating oil
- Denatured alcohol (ethanol)
- Heptane

HRR data are primarily reported for gasoline, kerosene, diesel, and denatured alcohol. Heptane is used to confirm the deep pool calculations, and lubricating oil is used primarily for determining spill depths for high viscosity fluids. Because lubricating oil is a common combustible liquid at NPPs, the methodology is extended to this fuel using insights obtained in Reference 1 and mass burning rate data provided in References 7, 8, 9, and 10, for example.

### 5.3.4 Fire Effects

Fire effects from the spill fires are not modified in this analysis. Fire effects include the thermal plume temperature, the radiant heat flux to targets adjacent to the spill fire, the compartment temperature within an enclosure in which a spill fire is postulated, and the thermal response of a target to a heat flux exposure. Calculations of fire effects are provided to illustrate key points, namely, to demonstrate the potential effects of over-predicting the HRR and under-predicting the fire duration. However, the general application of the HRR to determine the fire effect on a target is case specific and could involve the use of any number of fire modeling tools available to the analyst. EPRI 1023259/NUREG-1934 [11] provides a description of the use of the HRR parameter to determine the effect of a fire on NPP targets. This analysis will provide guidance only on the definition of the spill fire HRR, and all other tools for evaluating fire effects will remain unchanged.

### 5.3.5 Enclosure Effects

Enclosure effects consist primarily of the development of a hot gas layer that can radiate a sufficient amount of energy to the pool fire so that the mass burning rate is affected. Given that the radiant heat flux from the fire to the fuel surface is on the order of 30–77 kW/m² [14] for liquid fuels and that the burning rate is nominally a linear function of the incident heat flux, a reasonable heat flux threshold for identifying a significant enclosure effect would be 4.5 kW/m², which is about 15% of the source fire heat flux. This is within the experimental uncertainty of calorimeter HRR measurements according to Reference 15. A simple black body radiation calculation indicates that a temperature of 257°C produces a heat flux of 4.5 kW/m² and is thus an upper limit for the applicability of the pool fire HRR methods considered in this calculation.

### 5.3.6 Calculation Tools

This report provides a recommended methodology for computing the HRR of a combustible or flammable liquid spill fire. The computations are suitable for use in a spreadsheet tool, such as Microsoft Excel. However, a spreadsheet tool was not specifically developed as part of this report. It is expected that the methodologies presented in this report can be incorporated into an existing suite of spreadsheets, such as the Fire Induced Vulnerability Evaluation (FIVE) [12] or the NUREG-1805, Fire Dynamics Tools, FDT$^S$ [13].

### 5.3.7 Summary of Limitations

Table 5-1 contains a summary of the primary limitations of use for the selected spill fire models.

**Table 5-1**
**Summary of liquid fuel fire HRR model limitations**

| Parameter | Limitation | | | |
|---|---|---|---|---|
| | **Method 1** | **Method 2** | **Method 3** | **Method 4** |
| **Fuel** | **Fuels identified in Table G-4 of Ref. 2.** | **Fuels identified in Table 3-4 of Ref. 7.** | **Gasoline, Kerosene, Diesel Fuel, Lubricating Oil, Ethanol, Heptane** | **Gasoline, Kerosene, Diesel Fuel, Lubricating Oil, Ethanol, Heptane** |
| Substrate temperature | < 40°C | < 40°C | < 40°C | < 40°C |
| Fuel temperature | < 40°C | < 40°C | < 40°C | < 40°C |
| Fuel volume | No limit | No limit | No limit | No limit |
| Maximum depth | No limit | No limit | No limit | No limit |
| Substrate type | Solid, flat | Solid, flat | Solid, flat | Solid, flat |
| Pool type | Deep | Deep | Deep or thin | Deep or thin |
| Maximum enclosure temperature | < 257°C | < 257°C | < 257°C | < 257°C |
| Liquid fuel fire scenario(s) | Fixed quantity, confined† | Fixed quantity, confined† | Fixed quantity, confined or unconfined† | Fixed quantity, confined or unconfined† |
| Pressurized fuel spills | No | No | No | No |

**Table 5-1 (continued)**
**Summary of liquid fuel fire HRR model limitations**

| Parameter | Limitation | | | |
|---|---|---|---|---|
| | **Method 1** | **Method 2** | **Method 3** | **Method 4** |
| **Fuel** | **Fuels identified in Table G-4 of Ref. 2.** | **Fuels identified in Table 3-4 of Ref. 7.** | **Gasoline, Kerosene, Diesel Fuel, Lubricating Oil, Ethanol, Heptane** | **Gasoline, Kerosene, Diesel Fuel, Lubricating Oil, Ethanol, Heptane** |
| Obstructions in pool area | Acceptable, provided obstruction area removed from calculations‡ | Acceptable, provided obstruction area removed from calculations‡ | Acceptable, provided obstruction area removed from calculations‡ | Acceptable, provided obstruction area removed from calculations‡ |

†These methods are applicable to continuously fed liquid fuel fires; however, the modifications to the input parameters to account for this effect are not described in this document.
‡Although it is acceptable to determine the HRR with obstructions in the pool area (for example, pedestals, equipment, and so on), caution is necessary when using the HRR to determine flame heights, radiant heat fluxes, and thermal plume temperatures. It is generally conservative to consolidate the pool into an equivalent circular plan area and to apply the results at the pool boundary.

## 5.4 Summary of Experimental Results

This section presents the spill fire test data obtained under Grant No. 2008-DN-BX-K168 for the NIJ [1]. The focus of this summary is on unconfined spill fires since this is an area where an improved treatment can lead to tangible benefits in fire effects calculations. However, because confined and deep pool burning behaviors are coupled with the unconfined spill fire empirical model, data for such fires are presented, and elements of the empirical models that apply to deep pool scenarios are assessed in this context. Continuously fed spill fires, whether confined or unconfined, are not addressed in this effort because they are not frequently postulated in commercial NPP fire scenarios. This simplifies the overall analysis methodology, which is a desirable attribute for the empirical model approach. Nevertheless, the continuously fed spill fires are an extension of the methods presented in this section and could readily be developed using the empirical models.

### *5.4.1 Liquid Fuel Fire Test Results*

#### 5.4.1.1 Liquid Spill Dynamics

Liquid spill dynamic tests were performed to determine the spill growth (spread) and maximum spill area over various substrates. A total of 98 spill dynamics tests were performed in the NIJ test series [1] with three liquids. Twenty-one of the tests were performed using impermeable substrates and are of most interest in this effort. Two of the liquids were noncombustible surrogates with surface tensions that bracketed (higher and lower) surface tensions compared to the combustible fuels considered in the spill fire tests. The third liquid was lubricating oil, which has a higher viscosity and surface tension than the combustible and flammable liquids considered in the spill fire tests. The use of a surrogate liquid is based on an assessment of spill models and the identification of the surface tension as the governing parameter for characterizing the spill

behavior of different liquids [1, 3]. Overall, the two surrogate liquids have similar fluid properties when compared to the combustible fuels and were considered to produce representative spill characteristics without the safety issues associated with testing combustible fuels. The specific liquids used in the spill dynamics tests were as follows [1]:

1. Buckey BFC-3.1 3% aqueous film forming foam (AFFF) concentrate
2. Ansul 3% fluoroprotein (FP) foam concentrate
3. BP Turbinol Select AS lubricating oil

A summary of the liquid properties for the liquids used in the spill dynamics tests is provided in Table 5-2. Table 5-2 also shows the relevant properties for the fuels used in the spill fire tests for comparison [1]. Table 5-2 indicates that the surface tension of the surrogate liquids brackets the surface tension of the spill fire fuels. The viscosity of the lubricating oil is also seen to be an order of magnitude greater than any of the surrogate liquids or the spill fire fuels.

**Table 5-2**
**Summary of liquid properties used in spill dynamics tests and spill fire tests [1]**

| Liquid | Test Purpose | Surface Tension (mN/m) | Viscosity (cp) | Density (kg/m³) |
|---|---|---|---|---|
| AFFF | Spill dynamics | 17.2 | 1.2 | 990 |
| FP | Spill dynamics | 27.0 | 1.1 | 1,000 |
| Lube oil | Spill dynamics | 29.2 | 43.0 | 844 |
| Gasoline | Spill fire | 21.9 | 0.6 | 742 |
| Kerosene | Spill fire | 26.1 | 2.4 | 798 |
| Diesel | Spill fire | 27.2 | 2.8 | 823 |
| Ethanol | Spill fire | 22.3 | 1.1 | 790 |
| Heptane | Spill fire | 19.9 | 0.4 | 671 |

#### *5.4.1.1.1 Liquid Spill Testing Results*

The liquid spill testing involved the determination of the maximum spill area and minimum spill depths for the various liquids considered. The maximum spill area and minimum spill depth results for the 21 tests on impermeable surfaces are summarized in Table 5-3. Note that the data for repeat tests are averaged. The spill area and depth generally correspond to a spread time of 300 seconds, although some tests were permitted to spread for longer durations to verify that the spill area and spill depths had achieved their limiting values [1].

**Table 5-3**
**Summary of spill dynamics results for impermeable substrates [1]**

| Test | Liquid | Substrate | Spill Volume (L) | Maximum Spill Area (m²) | Minimum Spill Depth (mm) |
|---|---|---|---|---|---|
| SD28, SD29, SD30 | AFFF | Coated concrete | 0.5 | 1.47 | 0.34 |
| SD31, SD32, SD33 | FP | Coated concrete | 0.5 | 0.57 | 0.88 |
| SD34, SD35, SD36 | Lube oil | Coated concrete | 0.5 | 0.22 | 2.30 |
| SD04, SD05, SD06 | FP | Vinyl | 0.25 | 0.35 | 0.71 |
| SD01B, SD02, SD03 | AFFF | Vinyl | 0.1 | 0.42 | 0.25 |
| SD07, SD08, SD09 | Lube oil | Vinyl | 0.5 | 0.35 | 1.42 |
| SD61, SD62, SD63 | AFFF | Vinyl | 0.5 | 1.71 | 0.30 |

The results in Table 5-3 and additional testing reported in Reference 2 indicate that the recommended spill depth of 0.7 mm for spills involving liquid volumes under 95 L [2, 3] is reasonable for liquids having characteristics similar to fluoroprotein (for example, kerosene and diesel), but it may be high by a factor of 2–3 for liquids with lower surface tensions (for example, gasoline and ethanol) and low by a factor of 2–3 for lubricating oils.

Transient spill area data were obtained from the spill tests to determine the time frame over which the liquids spread and are used as a basis for establishing the ignition-delay times in the spill fire tests. These results are shown in Figures 5-1 through 5-4 for the impermeable liquid substrates. The parameter $\sigma$ is the surface tension of the liquid (mN/m). The spill areas are averaged among repeat tests as well as among different spill volumes. Also shown in these figures are the temporal spill area data for the corresponding gasoline and kerosene spill fire tests.

Figures 5-1 through 5-4 show that the spill area rapidly increased over the first 30 seconds and reached about 50%–70% of the maximum spread area over this time. A transition to a slower spread regime occurs over the next several hundred seconds, and the spill areas reached 90% of the maximum value by 300 seconds [1]. According to Reference 1, this is consistent with the underlying theory of liquid spreads on impermeable substrates and represents a transition from a flow dominated by gravity and inertia forces to one that is dominated by viscous and surface tension forces. The lubricating oil spills exhibit somewhat different spreading behavior—in the first 30 seconds, the spill areas reach approximately 75%–90% of the maximum value, and after 300 seconds, the liquid areas are near their maximum values. Figures 5-1, 5-2, and 5-4 also show that the surrogate liquids provide good representation of the spill behavior of kerosene, gasoline, and ethanol fuels, suggesting that the surface tension is a governing parameter for the spill behavior of these liquids. The behavior of the lubricating oil is clearly dominated by the high viscosity of the liquid.

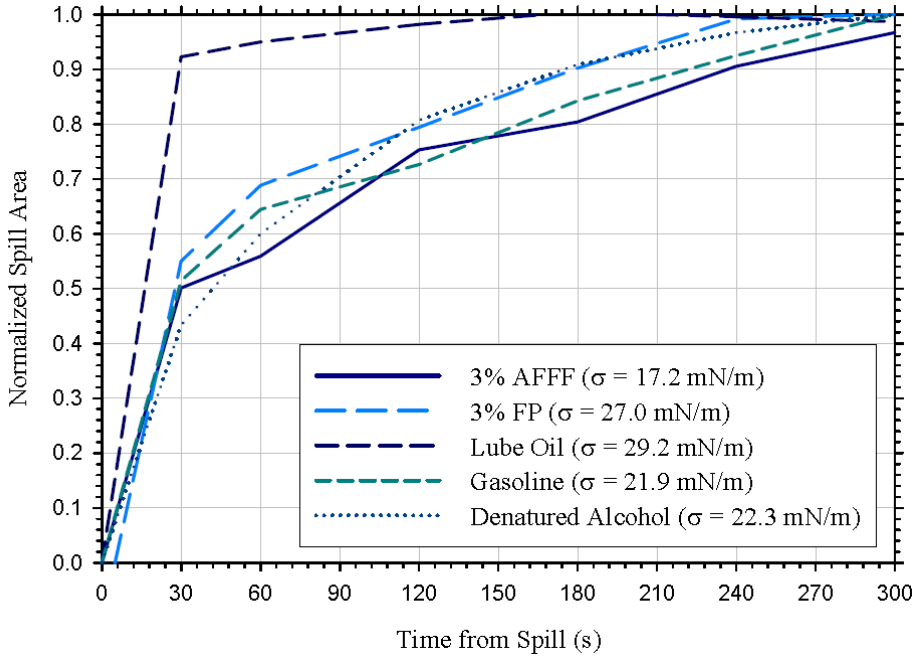


**Figure 5-1**
**Liquid spill area on a coated concrete substrate as a function of time for various liquid fuels and liquid fuel surrogate spill volumes [1]**

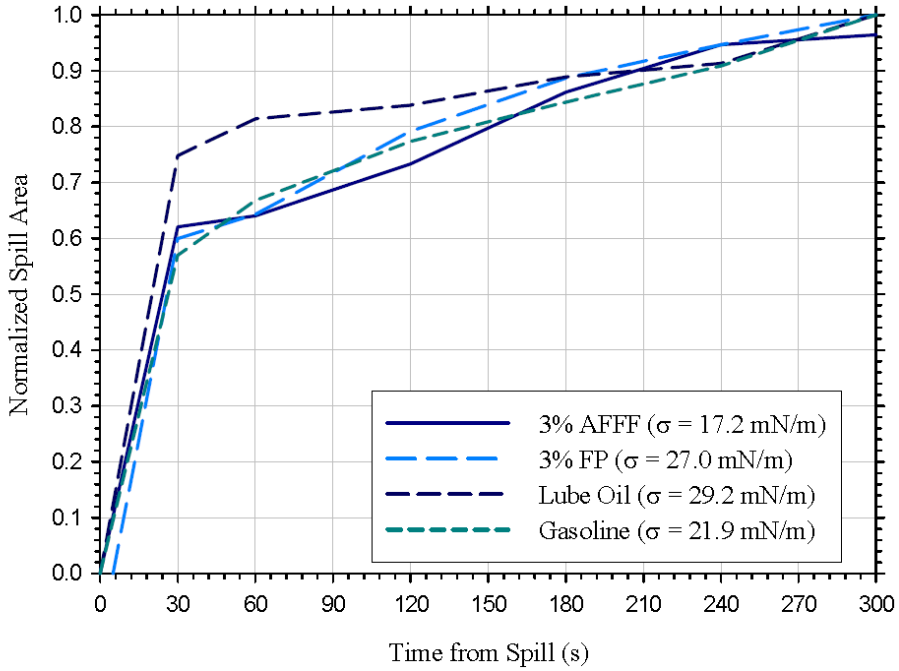


**Figure 5-2**
**Liquid spill area on a smooth (uncoated) concrete substrate as a function of time for various liquid fuels and liquid fuel surrogate spill volume [1]**

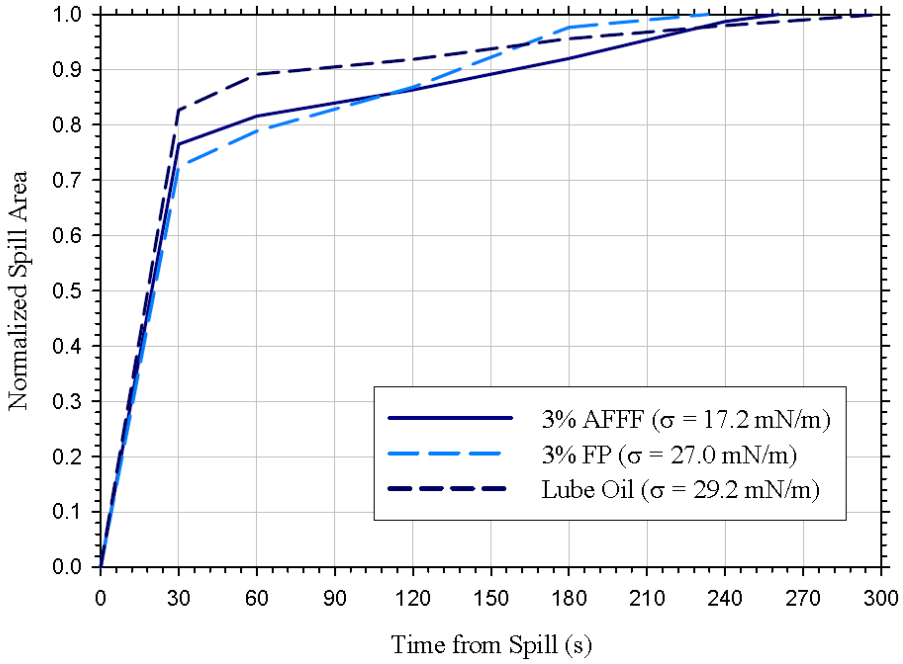


**Figure 5-3**
**Liquid spill area on a brushed (rough) concrete substrate as a function of time for various liquid fuels and liquid fuel surrogate spill volumes [1]**

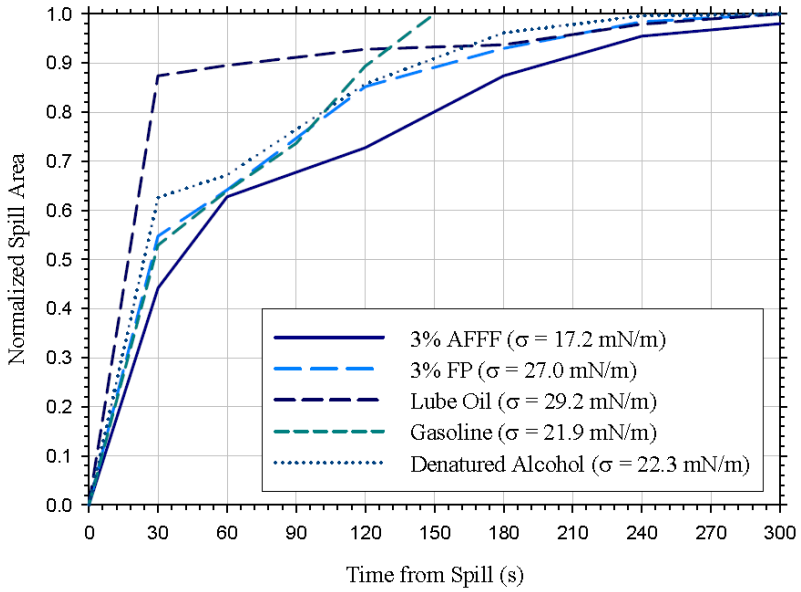


**Figure 5-4**
**Liquid spill area on a vinyl substrate as a function of time for various liquid fuels and liquid fuel surrogate spill volumes [1]**

Figure 5-5 depicts the minimum spill thickness for all liquids considered over all substrates. The data include thickness measurements for spill fire tests and provide an indication of the average and range of values for a particular liquid. The figure shows that the liquid fuels considered in the spill fire tests and the AFFF liquid surrogate have spill thicknesses between 0.5 and 1.0 mm and have a relatively consistent range. The FP fuel surrogate also has a value between 0.5 and 1 mm, but the range is over 1 mm. The lubricating oil has an average value close to 1.5 mm and a range somewhat larger than 1 mm.

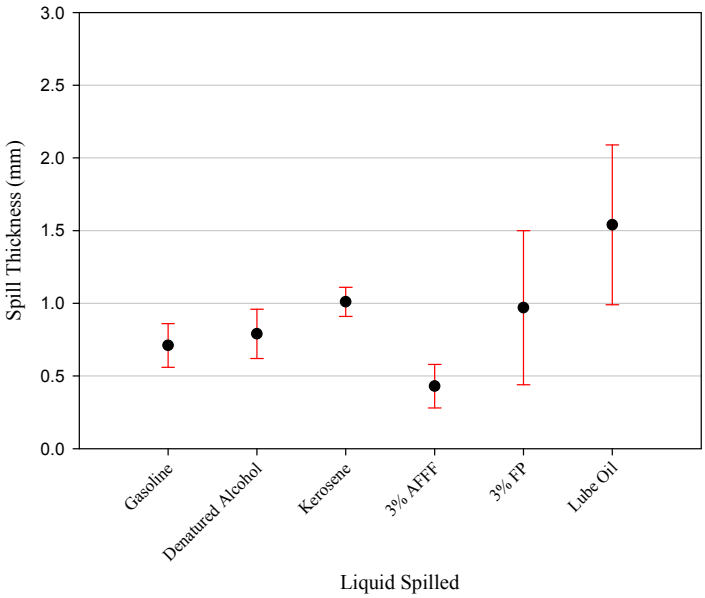


**Figure 5-5**
**Minimum liquid spill depths as a function of liquid – all liquid volumes and all substrates [1]**

A simple statistical assessment of the minimum spill depth of all liquids on all substrates was performed in Reference 1 and is summarized in Table 5-4. The table indicates that the average spill depth for all liquids, except the lubricating oil, is 0.72 mm. This is nearly equal to the value of 0.7 mm recommended in NUREG/CR-6850 [2], but the range is 0.22–2.4 mm, and the standard deviation is 0.34 mm. Gasoline and kerosene are closest to the overall average for all liquids, the fuels, and the surrogate liquids, whereas the lubricating oil deviates the most.

**Table 5-4**
**Summary of spill dynamics results for impermeable substrates [1]**

| Liquid | Substrate | Average Depth (mm) | Minimum Depth (mm) | Maximum Depth (mm) | Standard Deviation (mm) |
|---|---|---|---|---|---|
| All† | All | 0.72 | 0.22 | 2.4 | 0.34 |
| Fuels | All | 0.74 | 0.45 | 1.2 | 0.19 |
| Surrogates | All | 0.69 | 0.22 | 2.4 | 0.49 |
| Gasoline | All | 0.71 | 0.48 | 1.1 | 0.15 |
| Ethanol | All | 0.79 | 0.56 | 1.1 | 0.17 |
| Kerosene | All | 1.01 | 0.91 | 1.2 | 0.10 |
| AFFF | All | 0.43 | 0.22 | 0.7 | 0.15 |
| FP | All | 0.97 | 0.37 | 2.4 | 0.53 |
| Lubricant oil | All | 1.54 | 0.86 | 2.4 | 0.55 |

†Except lubricant oil

#### *5.4.1.1.2 Discussion*

The spill dynamics tests provide an indication of the rate at which a liquid fuel spills over a substrate surface, which provides a basis for the ignition-delay times used in the spill fire tests. It is shown that after 30 seconds, most combustible and flammable liquid fuels will spread to about 50%–75% of the maximum spill area, and lubricating oils will spread to about 75%–90% of the maximum spill area. After 300 seconds, most combustible and flammable liquid fuels will spread to about 90% of the maximum spill area, and lubricating oils will spread to nearly 100% of the maximum spread area.

The spill dynamics tests indicate that the overall average spill depth for flammable and combustible liquids is about 0.72 mm, with a standard deviation of 0.34 mm. The average spill depth is nearly equal to the value recommended in NUREG/CR-6850 [2] and provides a verification of this value. However, the range of spill depths is large (0.2–2.4 mm), indicating the need to consider the uncertainty in this parameter when calculating the fire effects of a spill fire. Detailed information was obtained for specific fuels, including gasoline, kerosene, ethanol, and lubricating oil. This information includes the average spill depth and the standard deviation and can be used to predict the spill areas for spills involving these specific liquids.

### 5.4.1.2 Confined Liquid Spill Fires

Confined liquid spill fire tests were performed to determine the influence of the liquid depth on the HRR and to provide validation of the burning rate model for small diameter pool fires [1]. The confined liquid spill fires were conducted in square steel pans with length dimensions of 0.3 m, 0.6 m, and 1.2 m [1]. Confined liquid spill fires were also evaluated in curbed areas over coated concrete and vinyl substrates and on water substrates within the steel pans. Initial fuel spill depths ranging from 1 mm to 20 mm were evaluated for kerosene, gasoline, heptane, and denatured alcohol.

#### *5.4.1.2.1 Fire Diameter Effects on the Mass Burning Rate*

The burning mode of a liquid fuel fire is a function of diameter and is generally characterized as follows [1, 17]:

- Convectively dominated heat transfer with laminar flames: diameter less than 0.05 m
- Convectively dominated heat transfer, turbulent flames: diameter between 0.05–0.2 m
- Thermal radiation dominated heat transfer, optically thin flames: diameter between 0.2–1.0 m
- Thermal radiation dominated heat transfer, optically thick flames: diameter greater than 1.0 m

Fires dominated by thermal radiation heat transfer are of most interest because the pool diameters associated with this burning regime can produce challenging fires for NPP targets. The burning rate model for the thermal radiation dominated liquid fuel fires is described using the following equation [1, 7, 8]:

$$\dot{m}'' = \dot{m}''_{\infty}\left(1 - \exp(-k\beta D_e)\right) \qquad \textbf{Eq. 5-1}$$

Where:

$\dot{m}''_{\infty}$ is the ideal or maximum mass burning rate per unit area of the combustible or flammable liquid (kg/s-m²).

$k$ and $\beta$ are empirical parameters that are normally treated as a single entity having units of 1/m [7, 8, 10].

$D_e$ is the effective fire diameter (m).

The maximum burning rate, $\dot{m}''_{\infty}$, corresponds to the mass burning rate for spill fires in which thermal radiation is the dominant heat transfer mode and the flames are optically thick. The exponential diameter function modifies the maximum burning rate for optically thin flames. The maximum burning rate and the empirical parameters are experimentally determined. The average value and the uncertainty range for these values are reported in Reference 8 for various fuels including those considered in this analysis. They are summarized in Table 5-5. It is noted in Reference 8 that the burning behavior of alcohols does not follow the same form as other hydrocarbon liquids due to the low radiative heat fluxes produced by the flames. As such, a burning rate is provided for diameter ranges that nominally correlate with an increasing radiant heat flux from the flames to the fuel [8].

**Table 5-5**
**Liquid fuel fire mass burning rate model parameter [8]**

| Fuel | Maximum Mass Burning Rate (kg/m²-s) | Empirical Constant, $k\beta$ ($m^{-1}$) |
|---|---|---|
| Gasoline | 0.055 ± 0.002 | 2.1 ± 0.3 |
| Kerosene | 0.039 ± 0.003 | 3.5 ± 0.8 |
| Heptane | 0.101 ± 0.009 | 1.1 ± 0.3 |
| Ethanol | 0.015 (Diameter less than 0.6 m)<br>0.022 (Diameter between 0.6–3.0 m)<br>0.029 (Diameter greater than 3.0 m) | ∞† |
| Fuel oil | 0.035 ± 0.003 | 1.7 ± 0.6 |
| Transformer oil | 0.039 | 0.7 |

†No diameter dependence noted.

The NIJ test results confirm the functionality of the diameter on the mass burning rate and the empirical constants provided in Reference 8. This is shown in Figures 5-6 through 5-8 for heptane, gasoline, and kerosene.

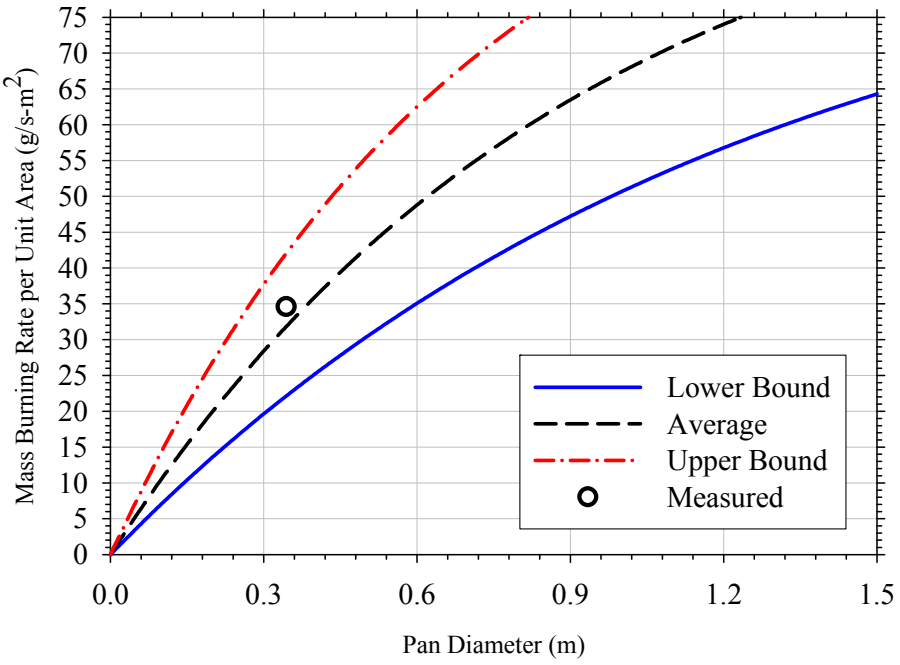


**Figure 5-6**
**Measured and predicted burning rate for heptane pan fire tests with a 20 mm fuel depth [1]**

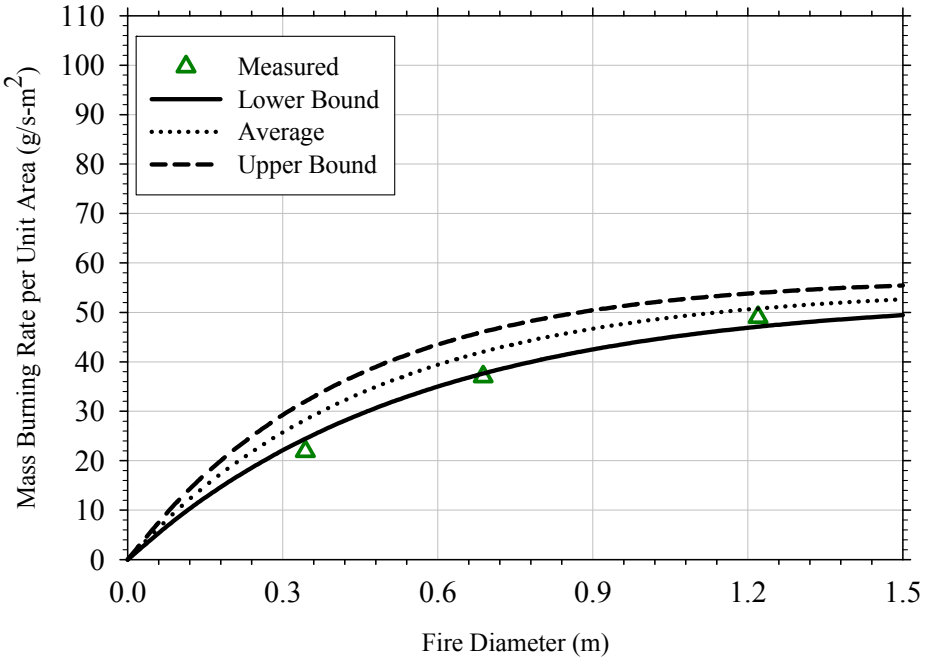


**Figure 5-7**
**Measured and predicted burning rate for gasoline pan fire tests with a 20 mm fuel depth [1]**

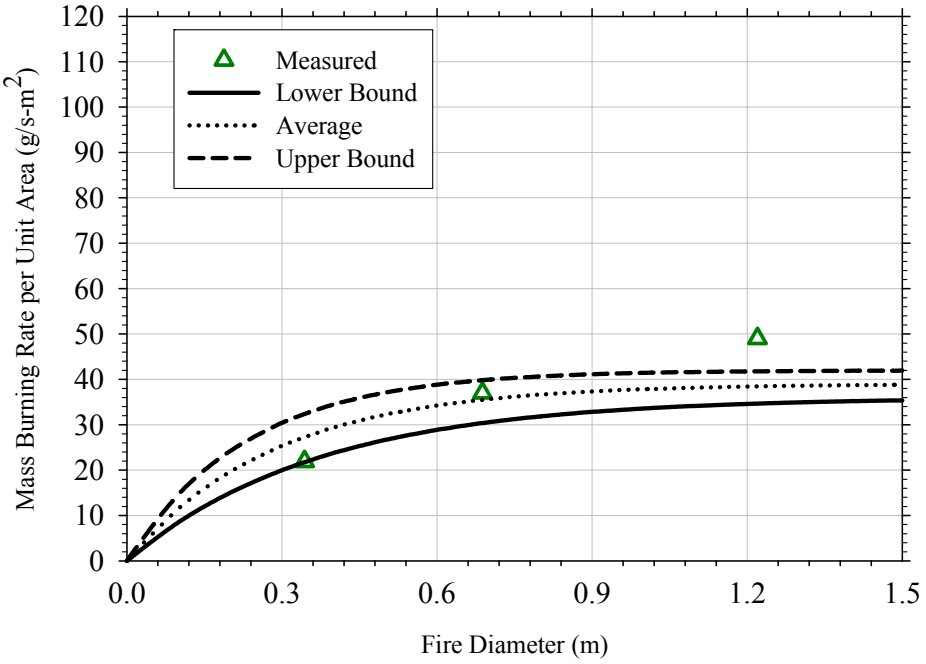


**Figure 5-8**
**Measured and predicted burning rate for kerosene pan fire tests with a 20 mm fuel depth [1]**

Figure 5-6 indicates that the measured burning rate for the heptane fuel is nearly equal to the average value as determined using Equation 5-1. Figures 5-7 and 5-8 indicate that the measured values for gasoline and kerosene are generally within the uncertainty range as determined using Equation 5-1 and the data provided in Table 5-6; although the results for gasoline are on the lower end of the range, and the values for kerosene range from the lower end for small diameter fires to the upper end for larger diameter fires. Reference 1 suggests that the variations in the gasoline kerosene formulations are a likely cause for the differences in the predicted and measured results. The NIJ tests, therefore, confirm the functionality of the burning rate on the fire diameter and indicate that the recommended parameters provided by Babrauskas [8] provide a reasonable prediction of the mass burning rate of deep liquid pools in terms when applied to Equation 5-1. In addition, the uncertainty range provided by Babrauskas [8] for the recommended parameters provides a reasonable approximation of the mass burning rate range for a given fire diameter.

#### *5.4.1.2.2 Fuel Depth Effects on the Mass Burning Rate*

The fuel depth is known to affect the mass burning rate as reported by Gottuk [3] and Putori [6]. The original hypothesis developed to explain this effect was that thermal losses to the substrate reduced the available energy for pyrolysis, thereby resulting in a lower mass loss rate. Recent work provided by Reference 1 indicates that reduced burning rates for thin liquid fuel fires is partially attributed to thermal losses to the substrate, but that other factors may play an equal or greater role in reducing the burning rate. These factors include a threshold fuel depth for fire growth and a finite time over which the burning rate becomes established and taken together can result in a reduced burning rate as the fuel regresses. Essentially, the fuel is consumed before the maximum burning rate can be achieved. This conclusion was based in part on continuously fed fuel fires with very thin depths. In these situations, the peak HRR corresponded to a deeper pool and indicates that the heat losses to the substrate were not always the dominant factor in limiting the burning rate of the liquid fuel fires [1].

The HRRPUA data for gasoline and kerosene pan fire tests are shown in Figures 5-9 and 5-10 for initial spill depths ranging from 1 to 20 mm on various substrate materials for the 0.3 m and 0.6 m pan fire tests (refer to Appendix C.1 for a description of the NIJ test naming convention). The corresponding peak mass burning rate is summarized in Tables 5-6 and 5-7 for gasoline and kerosene. Figures 5-11 and 5-12 show the HRRPUA for initial spill depths ranging from 1 to 18 mm for gasoline and ethanol in 1.2 m pans. These tests include additional depth increments between 1 and 5 mm to determine the transition from thin pool burning to deep pool burning. The corresponding peak mass loss rate data are summarized in Table 5-8.

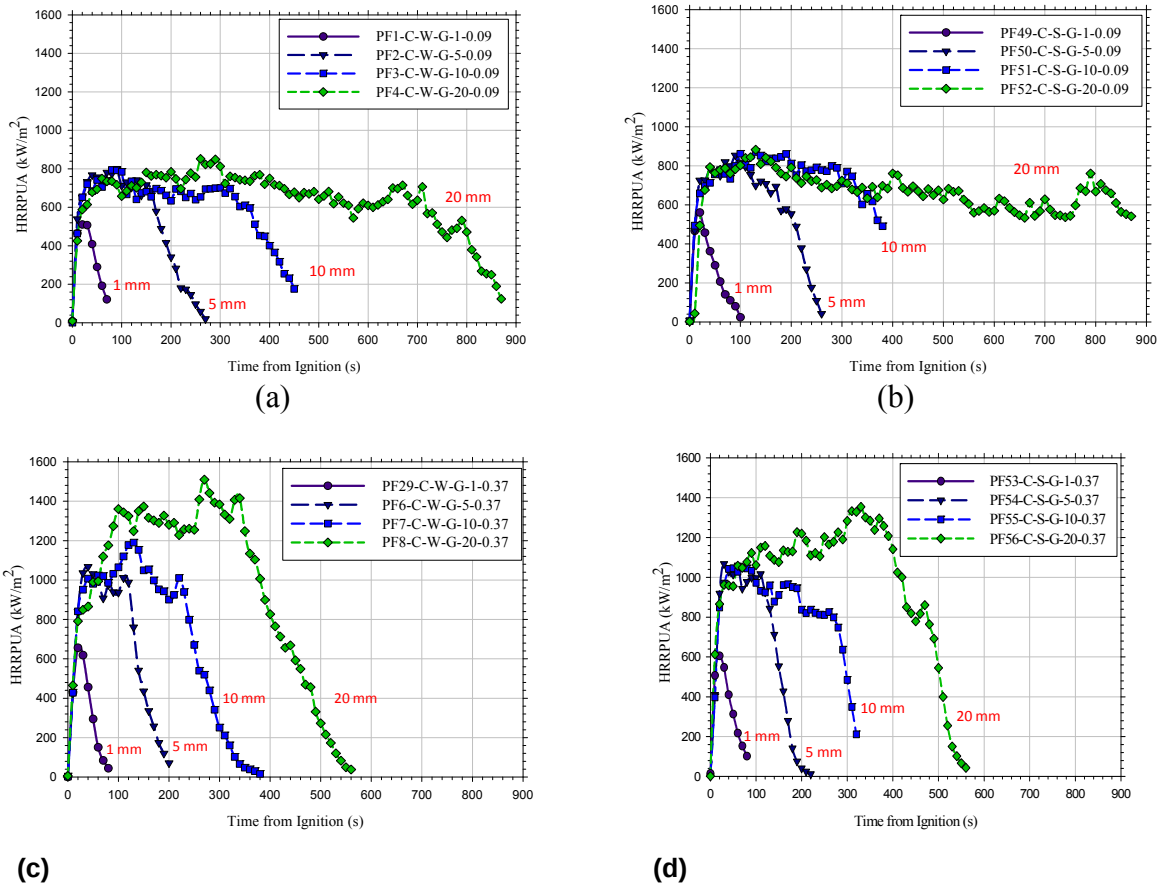


**Figure 5-9**
**(a) HRR per unit area (HRRPUA) for 0.3 m gasoline pan fires on water substrate [1], (b) HRRPUA for 0.3 m gasoline pan fires on steel substrate [1], (c) HRRPUA for 0.6 m gasoline pan fires on water substrate [1], (d) HRRPUA for 0.6 m gasoline pan fires on steel substrate [1]**

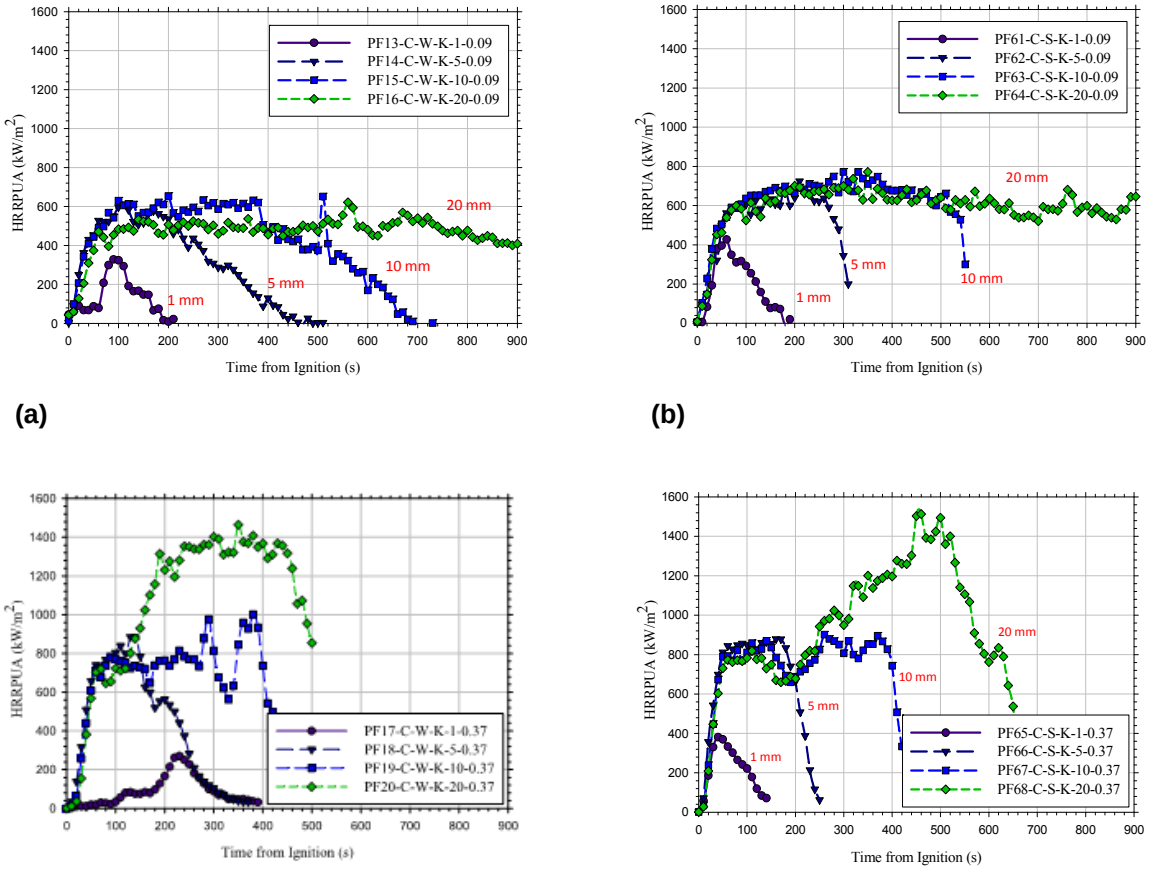


**Figure 5-10**
**(a) HRRPUA for 0.3 m kerosene pan fires on water substrate [1], b) HRRPUA for 0.3 m kerosene pan fires on steel substrate [1], (c) HRRPUA for 0.6 m kerosene pan fires on water substrate [1], (d) HRRPUA for 0.6 m kerosene pan fires on steel substrate [1]**

**Table 5-6**
**Peak mass burning rate for liquid fuels as a function of the initial fuel depth – 0.3 m pan fire tests [1]**

| Fuel | Substrate | Fuel Thickness (mm) | Peak Mass Burning Rate (kg/s-m²) |
|---|---|---|---|
| Gasoline | Water | 1 | 0.0129 |
| | | 5 | 0.0205 |
| | | 10 | 0.0205 |
| | | 20 | 0.0215 |
| | Steel | 1 | 0.0135 |
| | | 5 | 0.0221 |
| | | 10 | 0.0227 |
| | | 20 | 0.0220 |
| Kerosene | Water | 1 | 0.0072 |
| | | 5 | 0.0139 |
| | | 10 | 0.0154 |
| | | 20 | 0.0144 |
| | Steel | 1 | 0.0094 |
| | | 5 | 0.0165 |
| | | 10 | 0.0177 |
| | | 20 | 0.0174 |

**Table 5-7**
**Peak mass burning rate for liquid fuels as a function of the initial fuel depth – 0.6 m pan fire tests [1]**

| Fuel Type | Substrate | Fuel Thickness (mm) | Peak Mass Burning Rate (kg/s-m²) |
|---|---|---|---|
| Gasoline | Water | 1 | 0.01168 |
| | | 5 | 0.01941 |
| | | 10 | 0.02147 |
| | | 20 | 0.02699 |
| | Steel | 1 | 0.01047 |
| | | 5 | 0.02000 |
| | | 10 | 0.02213 |
| | | 20 | 0.02685 |
| Kerosene | Water | 1 | 0.00537 |
| | | 5 | 0.01371 |
| | | 10 | 0.01677 |
| | | 20 | 0.02572 |
| | Steel | 1 | 0.00647 |
| | | 5 | 0.01673 |
| | | 10 | 0.01818 |
| | | 20 | 0.02334 |

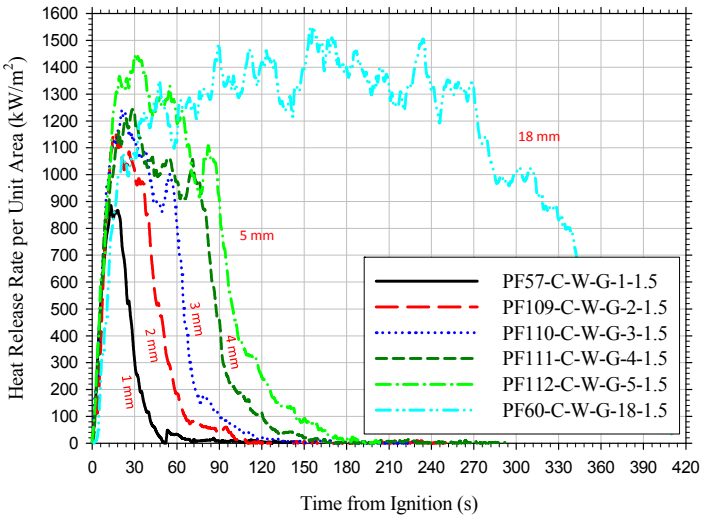


**Figure 5-11**
**HRRPUA for 1.2 m gasoline pan fires on water substrate [1]**

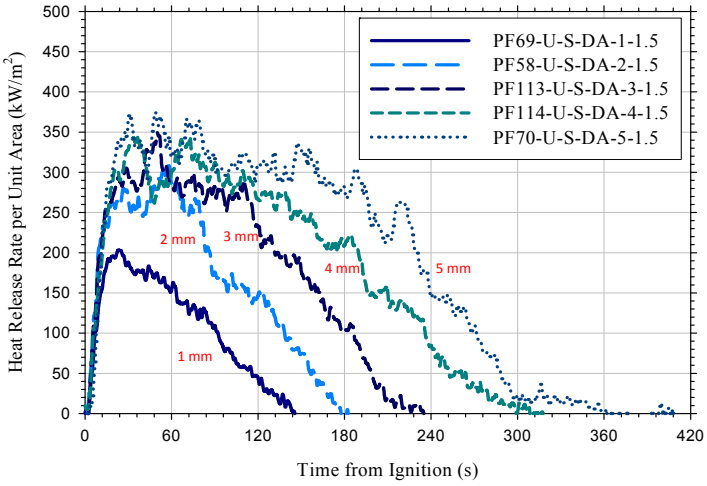


**Figure 5-12**
**HRRPUA for 1.2 m ethanol pan fires on water substrate [1]**

**Table 5-8**
**Peak mass burning rate for liquid fuels as a function of the initial fuel depth – 0.6 m pan fire tests [1]**

| Fuel Type | Substrate | Fuel Thickness (mm) | Peak Mass Burning Rate (kg/s-m²) |
|---|---|---|---|
| Gasoline | Steel | 1 | 0.00844 |
| | | 5 | 0.03020 |
| | Water | 1 | 0.01098 |
| | | 2 | 0.01435 |
| | | 3 | 0.03312 |
| | | 4 | 0.03518 |
| | | 5 | 0.03177 |
| | | 18 | 0.03245 |
| Ethanol | Steel | 1 | 0.00567 |
| | | 2 | 0.00815 |
| | | 3 | 0.00927 |
| | | 4 | 0.01013 |
| | | 5 | 0.01111 |

Figures 5-9 through 5-12 and Tables 5-6 through 5-8 show that the HRR growth is independent of the liquid depth but that the peak burning rate is clearly a function of the liquid depth up to spill depths of about 5 mm. The burning rate and HRRPUA do not significantly change with increasing liquid depths above 5 mm, which suggests a 5 mm spill depth is a reasonable spill depth above which deep pool burning rate data are applicable [1].

An empirical model that accounts for the liquid depth having the following form is presented in Reference 1:

$$\dot{m}''(D,\delta) = C_\delta\left(1 - e^{-k\beta D}\right)\dot{m}''_\infty \qquad \textbf{Eq. 5-2}$$

Where:

$\dot{m}''(D,\delta)$ is the mass burning rate (kg/s-m²) as a function of the pool diameter, $D$ (m), and the pool depth, $\delta$ (m).

$C_\delta$ is an empirical constant that is a function of the fuel and the fuel depth.

$k$ and $\beta$ are empirical constants that are treated as a single entity with units of 1/m and account for different burning regimes (see Section 5.4.1.2).

$\dot{m}''_\infty$ is the deep pool burning rate (kg/s-m²) (see Table 5-5).

The empirical constant is given as follows for gasoline and kerosene [1]:

$$C_\delta = 0.95\left(1 - e^{-0.71\delta}\right) \text{ (Gasoline)} \qquad \textbf{Eq. 5-3a}$$

$$C_\delta = 0.91\left(1 - e^{-0.58\delta}\right) \text{ (Kerosene)} \qquad \textbf{Eq. 5-3b}$$

where $\delta$ is the liquid depth (mm) and all other terms have been defined.

The predicted burning rate for gasoline and kerosene fires as computed using Equations 5-2 and 5-3a are compared against the measured data in Figures 5-13 and 5-14. The empirical constant determined by Equations 5-3a and 5-3b are based on an average fit of the available data. Figures 5-13 and 5-14 also depict upper- and lower-bound correlations for the same data set. As will be shown in Section 5.4.2, Equation 5-3a provides a reasonable assessment of the burning rate for ethanol and heptane and is thus recommended in this analysis for use with ethanol and heptane.

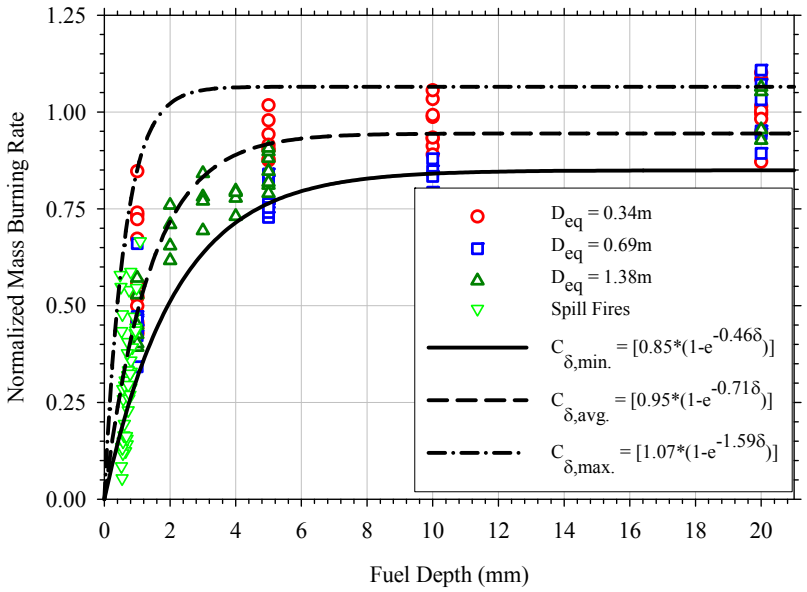


**Figure 5-13**
**Measured and predicted mass burning rate for gasoline pan and spill fires – predicted values determined using recommended liquid depth correlation [1]**

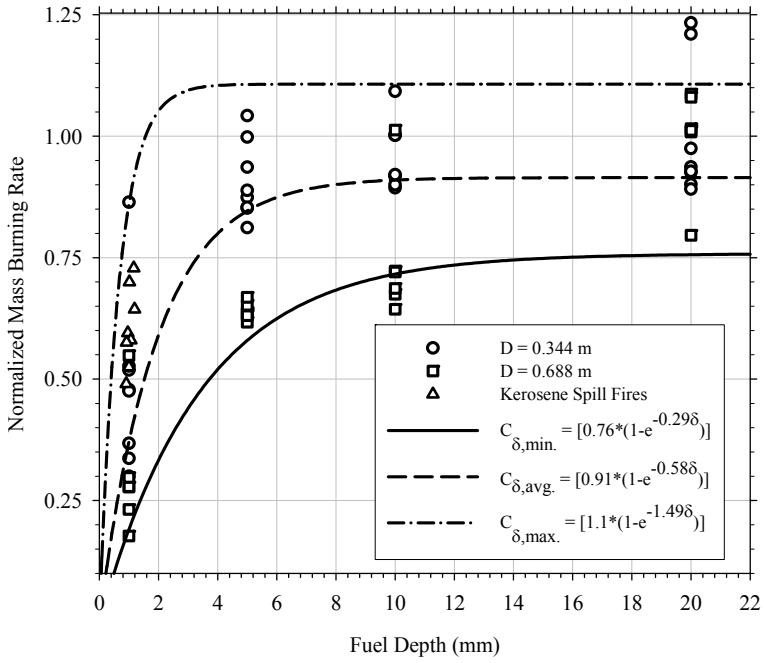


**Figure 5-14**
**Measured and predicted mass burning rate for gasoline pan and spill fires – predicted values determined using recommended liquid depth correlation [1]**

A value of 0.2 is recommended in Reference 1 for the fuel depth empirical constant for spilled fuel depths less than 5 mm for fuels other than gasoline and kerosene; however, based on the results presented in Figures 5-11 and 5-12, a value of 1.0 would be reasonable for spill fire depths greater than 2 mm, and a value of 0.2 would be applicable to spill depths of 1 mm or less. Intermediate spill depths for fuels other than gasoline and kerosene, such as lubricating oil, would need to postulate constants of 0.2 and 1.0 to determine the most adverse scenario.

#### 5.4.1.3 Unconfined Liquid Spill Fires

Unconfined liquid spill fires, or spill fire dynamics fire tests, were conducted to determine the HRR profile in liquid spill fires on various substrates. Two parameters were initially considered in addition to the fuel and the substrate—the fuel volume and the ignition delay. The fuel volume clearly correlates to the HRR profile. However, as was determined in the spill thickness evaluations, the ignition delay can also influence the HRR profile. The ignition delay is simply the time difference between the initiation of the liquid spill time and the time the fuel surface is ignited [1].

The ignition delay can affect the HRR profile of a liquid fuel fire in two ways. First, the liquid will spread further from the spill point when provided with a longer ignition delay. This, in turn, results in a pool with a larger surface area and a thinner depth when compared to one provided with a shorter ignition delay. Spill thickness results indicate that most fuels achieve approximately 75% of the maximum spill area after 30 seconds and 90% of the maximum spill area after 300 seconds. Lubricating oil is an exception and was found to achieve about 90% of the maximum spill area after 30 seconds [1].

The second way in which the ignition delay can affect the HRR profile is via an alteration in the fuel mass and composition. Fuels such as gasoline consist of a mix of low- and high-volatility components. Longer ignition delays allows for a greater fraction of the highly volatile constituents to evaporate from the fuel pool, thereby changing the composition of the fuel that remains. If the fuel spreads over a permeable surface such as wood, a longer ignition delay allows for a greater fraction of the fuel to become absorbed by the substrate, which further reduces the fuel spill thickness. Permeable substrates are not considered in this evaluation since they are not a commonly encountered substrate at commercial NPPs.

During the initial spill fire testing, the substrate temperature was allowed to vary over a 10°C–19°C range. Essentially, the average substrate temperature tended to increase with each additional test. Because up to four tests were conducted for a single spill configuration as defined by a fuel type, spill volume, substrate, and ignition delay, it became apparent that the substrate temperature was having an effect on the HRR development [1]. Because this was not a parameter that was considered when the test plan was developed, spill fire tests were not conducted to quantify the impact of the substrate temperature on the HRR development. However, subsequent testing was performed with a substrate temperature maintained at about 20°C to eliminate the effect of this parameter on the test results.

The substrate temperature is expected to have a greater effect on the burning behavior of highly volatile fuels with a low flashpoint temperature such as gasoline and ethanol and a minimal effect on the low volatility fuels with a high flashpoint temperature such as lubricating oil. An approximate effect may be estimated from the initial tests in which the substrate temperature

varied. This is because the high volatility fuels are closer to their flashpoint and will thus be more sensitive to smaller temperature variations. These variations affect the mass flow of highly volatile fuel components and the localized fuel-air concentration above the liquid pool. An approximate effect can be estimated from the initial tests in which the substrate temperature varied.

The spill fire test results presented in this section are as reported in Reference 1. They are grouped by substrate; only the non-permeable substrate data are shown. The results for permeable surfaces are not used in the development of the HRR model for spill fires in this report because consideration of these types of surfaces would add unnecessary complexity to the model since they are not frequently encountered in commercial NPPs. Note that the spill fire tests were performed with three fuels: gasoline, heptane, and ethanol. Kerosene was found to be difficult to ignite as a spill fire and generally did not sustain a fire with the ignition process used [1]. There were no spill fire tests on non-permeable substrates performed with the lubricating oil; however, based on the flashpoint of the lubricating oil, it is reasonable to conclude it would be at least as difficult to ignite as the kerosene.

#### *5.4.1.3.1 Coated Concrete*

The coated concrete substrate is fully cured and smoothed, and has an epoxy coating. This type of surface is typical of finished concrete floors at commercial NPPs. Figures 5-15 through 5-23 depict the spill fire HRR test data on coated concrete (refer to Appendix C.1 for a description of the NIJ test naming convention). Three fuels were evaluated on the coated concrete substrate: gasoline, heptane, and ethanol.

Figures 5-15 and 5-16 depict the results for 0.5 L gasoline spill fires with 30 second and 300 second ignition delays, respectively. Each figure consists of four identical tests. The tests shown in Figure 5-15 were performed with a roughly constant substrate temperature (22°C–24°C) and show that the tests are highly repeatable. The tests shown in Figure 5-16 were performed at variable substrate temperatures, ranging from 22°C–28°C. The tests with the warmest substrates (SFD21 and SFD21A) resulted in a peak HRR that was 50% larger than the cooler substrate tests and a significantly shorter fire duration. The effect of the ignition delay is also evident through comparison of Figures 5-15 and 5-16. For comparable substrate temperatures, a 300 second ignition delay results in a peak HRR that is about one-half that of the 30 second ignition-delay fire tests. The fire durations are approximately the same, which suggests that fuel loss during the ignition delay is a significant mitigating factor.

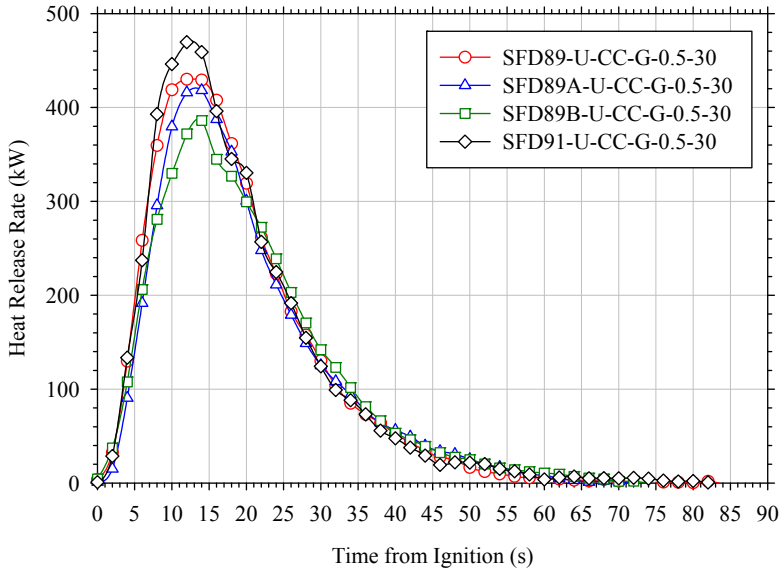


**Figure 5-15**
**Heat release rate (HRR) profiles for 0.5 L gasoline spill fires on coated concrete – 30 second ignition delay [1]**

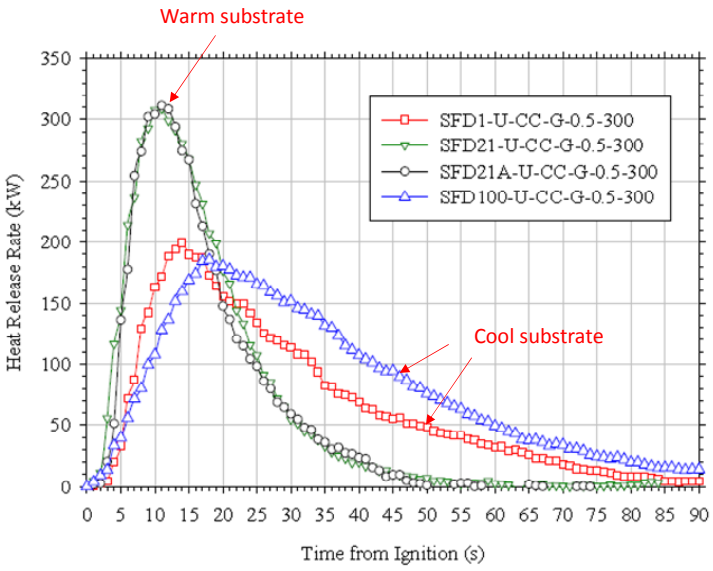


**Figure 5-16**
**HRR profiles for 0.5 L gasoline spill fires on coated concrete – 300 second ignition delay [1]**

Figures 5-17 and 5-18 depict the results for 1.0 L gasoline spill fires with 30 second and 150–300 second ignition delays, respectively. Each figure consists of four identical tests. The tests shown in Figures 5-17 and 5-18 were performed with a roughly constant substrate temperature (19°C–22°C) and show that the tests are highly repeatable. The peak HRR for the 300 second ignition delay is about one-half the peak HRR of the 30 second ignition-delay fire tests, although the fire durations are comparable. This is consistent with the 0.5 L fire test data shown in Figures 5-15 and 5-16.

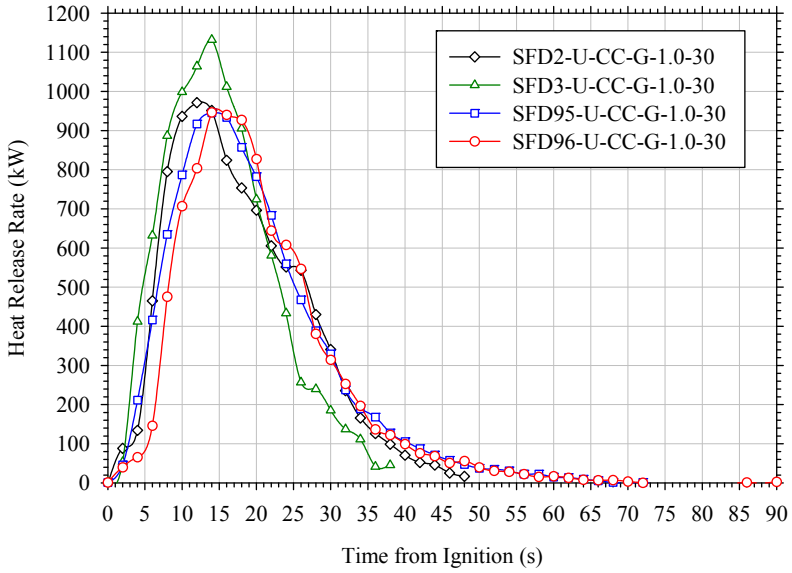


**Figure 5-17**
**HRR profiles for 1.0 L gasoline spill fires on coated concrete – 30 second ignition delay [1]**

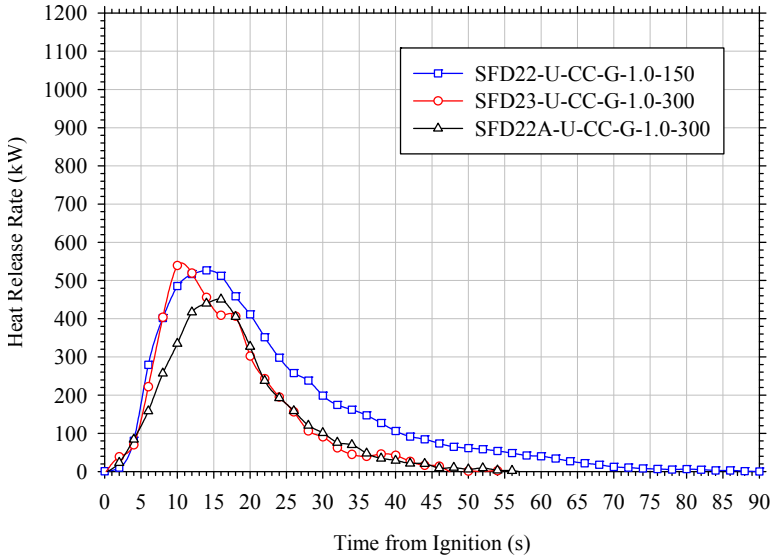


**Figure 5-18**
**HRR profiles for 1.0 L gasoline spill fires on coated concrete – 150 to 300 second ignition delay [1]**

Figures 5-19 through 5-21 depict the results for 0.5 and 1.0 L ethanol spill fires with 30 second and 300 second ignition delays. The trends are similar to those noted for the gasoline spill fires, though the reduction in the heat peak HRR is about 30% rather than 50% for 300 second ignition delays as compared to the 30 second ignition delays. The fire duration and the peak HRR is significantly smaller for the 300 second ignition delay, 1.0 L fire scenarios (see Figure 5-21) suggesting that a substantial fuel mass is lost during the delay period.

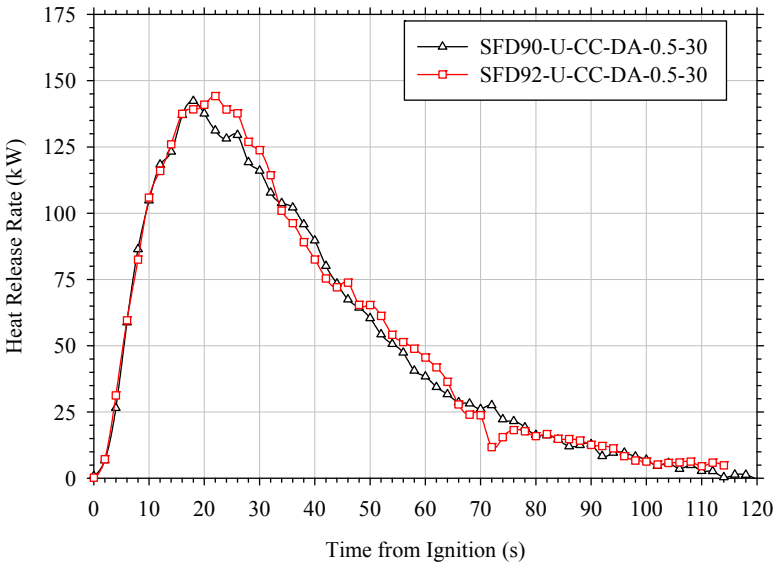


**Figure 5-19**
**HRR profiles for 0.5 L ethanol spill fires on coated concrete –30 second ignition delay [1]**

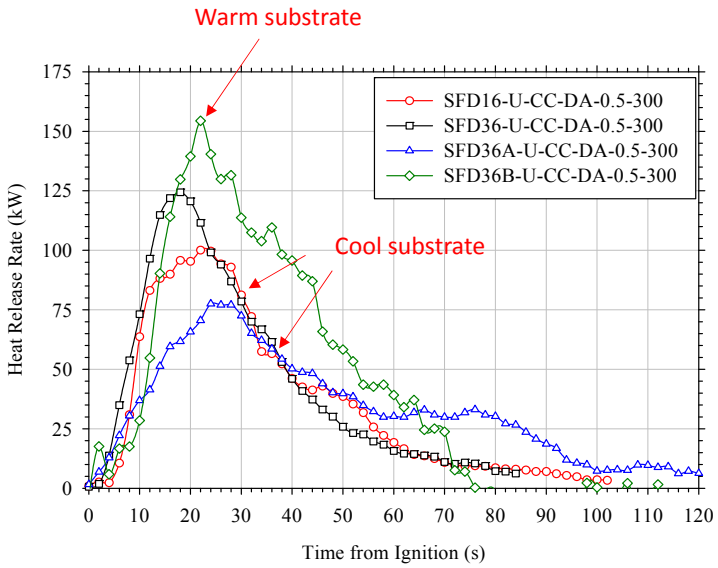


**Figure 5-20**
**HRR profiles for 0.5 L ethanol spill fires on coated concrete – 300 second ignition delay [1]**

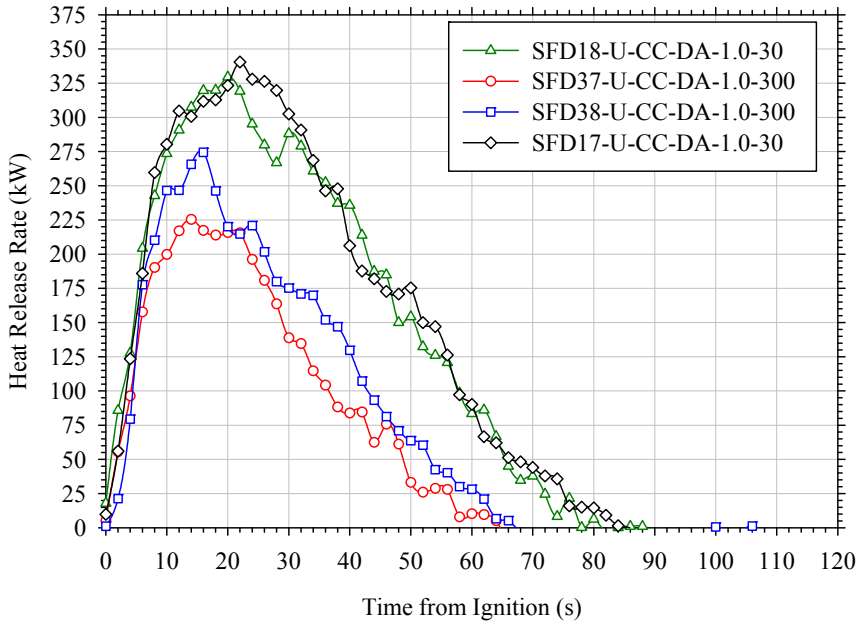


**Figure 5-21**
**HRR profiles for 1.0 L ethanol spill fires on coated concrete – 30 and 300 second ignition delays [1]**

Figures 5-22 and 5-23 depict the results for 0.5 and 1.0 L heptane spill fires with 30 second and 300 second ignition delays. The 0.5 L spill fire tests were conducted on substrates with an initial temperature ranging from 19°C to 38°C, whereas the 1.0 L heptane spill fire tests were conducted on substrates that were relatively constant, ranging from 19°C to 1°C. The trends are similar to those noted for the gasoline spill fires, although the effect of the substrate temperature on the HRR is not as strong for heptanes relative to gasoline. There is also a larger variation in the HRR profiles for constant substrate temperatures and constant ignition delays than was observed for the gasoline and ethanol spill fire scenarios.

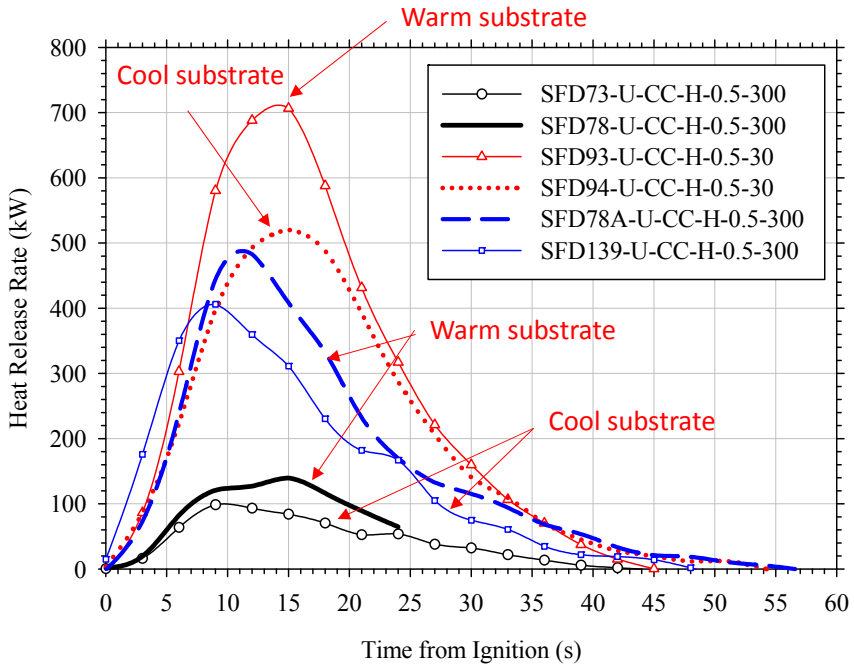


**Figure 5-22**
**HRR profiles for 0.5 L heptane spill fires on coated concrete – 30 and 300 second ignition delays [1]**

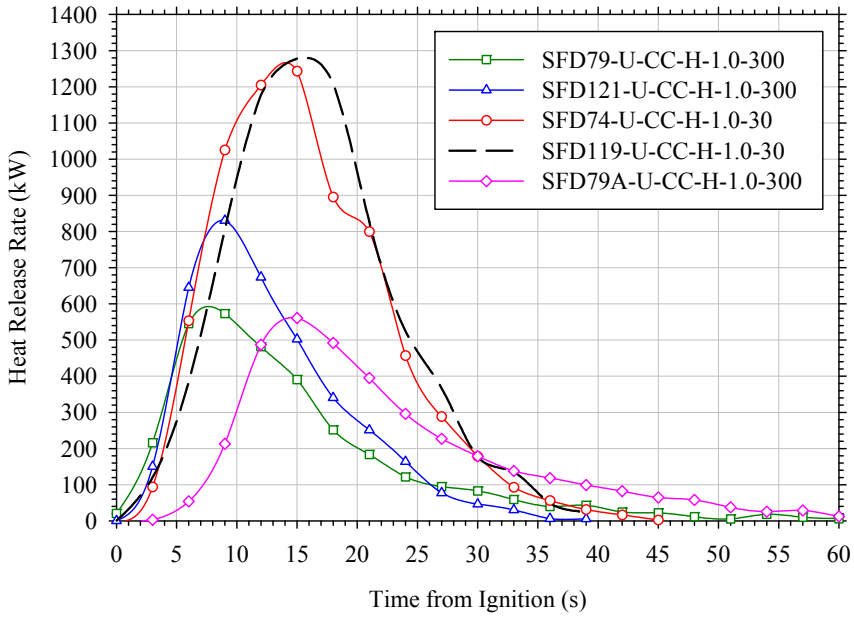


**Figure 5-23**
**HRR profiles for 1.0 L heptane spill fires on coated concrete – 30 and 300 second ignition delays [1]**

#### *5.4.1.3.2 Smooth Concrete*

The smooth concrete substrate is fully cured and smoothed, but lacks the epoxy coating. This type of substrate is typically seen on concrete pedestals and unfinished concrete surfaces. Figures 5-24 and 5-25 depict the spill fire HRR test data on smooth concrete (refer to Appendix C.1 for a description of the NIJ test naming convention). Only gasoline fuel spills were evaluated on the smooth concrete substrate. The substrate temperature for these tests was maintained at about 20°C–25°C.

Figures 5-24 and 5-25 indicate that the trends are similar to those noted for the gasoline spill fires (see Figures 5-15 through 5-18). The peak HRRs and fire durations are approximately the same as those observed for coated concrete. In addition, the peak HRR for fire scenarios with a 300 second ignition delay is about one-half the peak HRR of the 30 second ignition-delay fire scenarios.

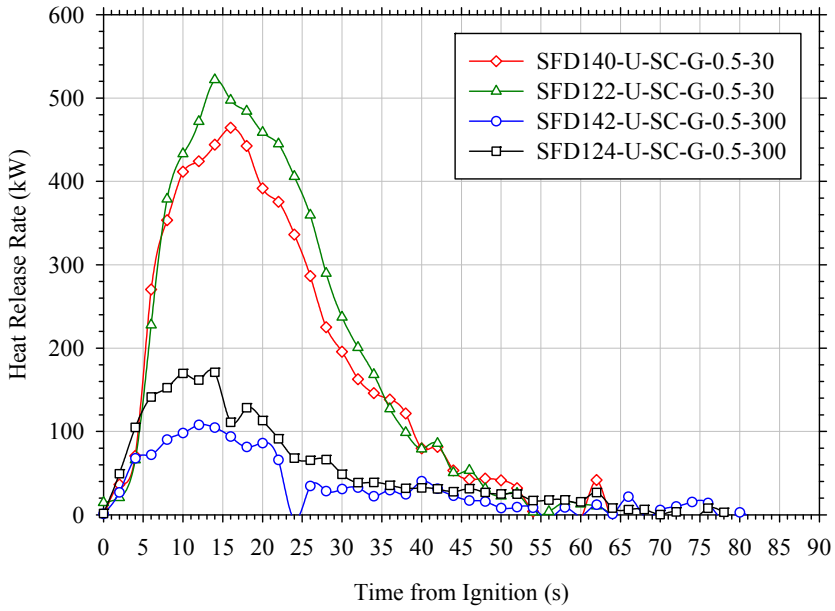


**Figure 5-24**
**HRR profiles for 0.5 L gasoline spill fires on smooth concrete – 30 and 300 second ignition delays [1]**

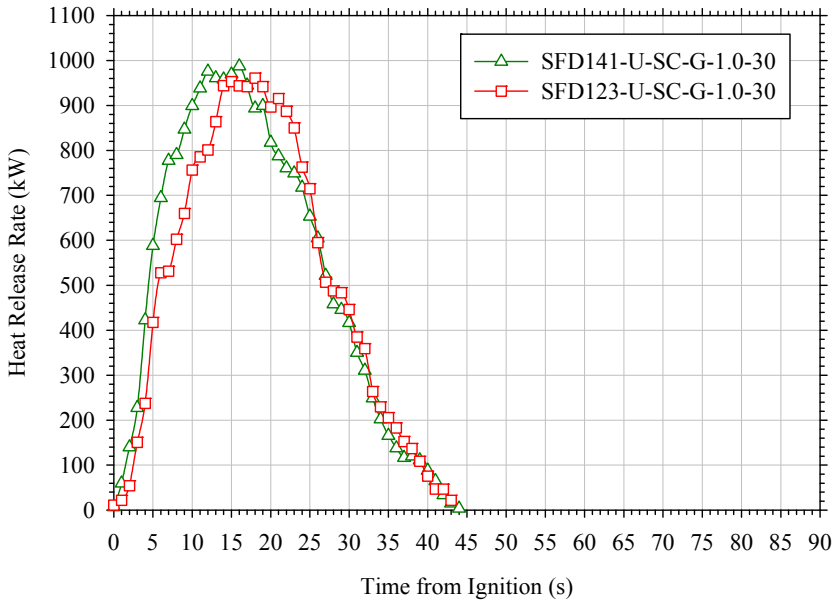


**Figure 5-25**
**HRR profiles for 1.0 L gasoline spill fires on smooth concrete – 30 and 300 second ignition delays [1]**

#### *5.4.1.3.3 Brushed Concrete*

The brushed concrete substrate is fully cured and smoothed, but it is roughened with a wire brush. The brushed concrete surface has a greater variation in the surface elevation relative to a fixed datum and, therefore, provides a greater flow resistance when compared to smooth concrete and coated concrete substrates. This type of substrate may be representative of weathered concrete surfaces located outside or roughly finished concrete pedestals.

Figures 5-26 and 5-27 depict the spill fire HRR test data on brushed concrete (refer to Appendix C.1 for a description of the NIJ test naming convention). Only gasoline fuel spills were evaluated on the brushed concrete substrate. The substrate temperature for these tests was maintained at about 20°C–25°C.

Figures 5-26 and 5-27 indicate that the trends are similar to those noted for the gasoline spill fires (see Figures 5-15 through 5-18 and Figures 5-24 and 5-25), though the HRRs are somewhat lower for brushed concrete. In addition, the peak HRR for fire scenarios with a 300 second ignition delay is about one-third the peak HRR of the 30 second ignition-delay fire scenarios rather than one-half.

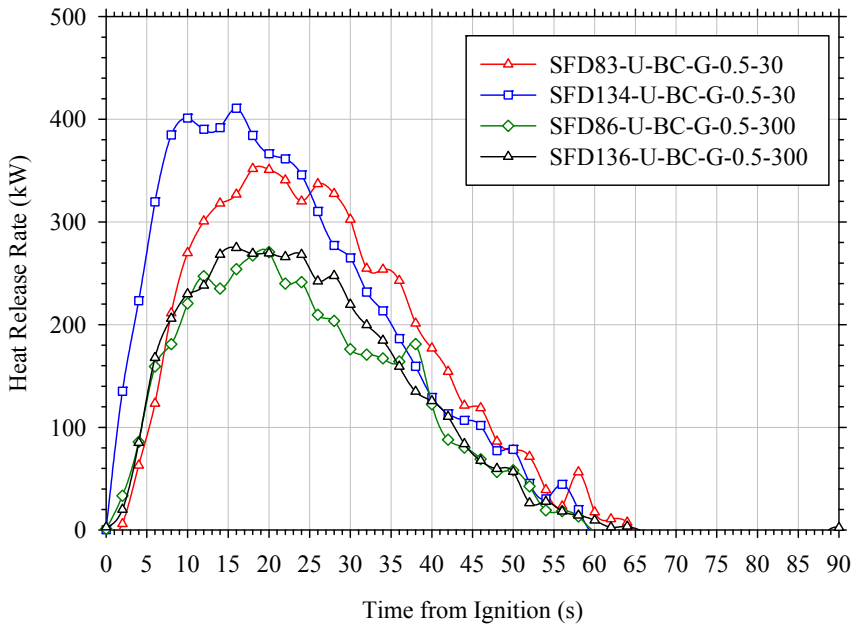


**Figure 5-26**
**HRR profiles for 0.5 L gasoline spill fires on brushed concrete – 30 and 300 second ignition delays [1]**

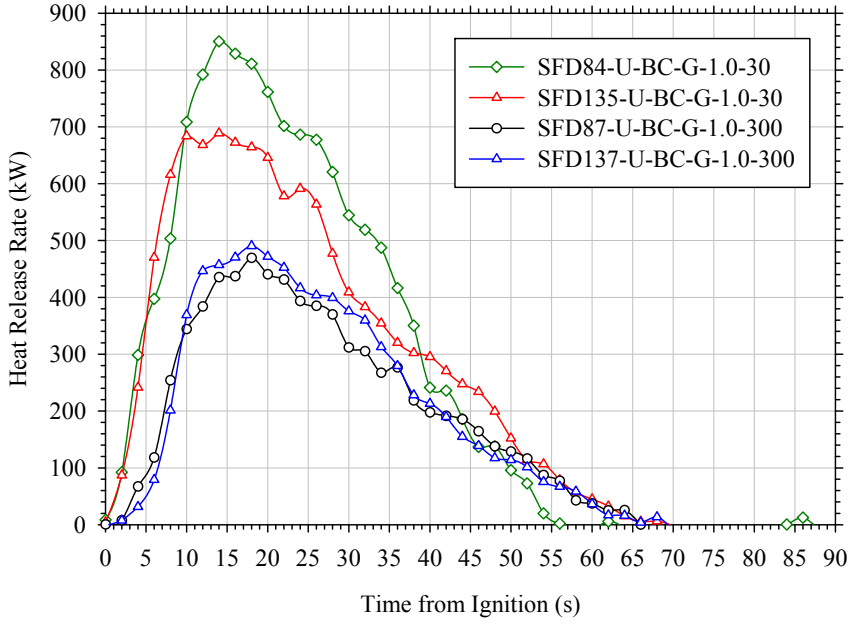


**Figure 5-27**
**HRR profiles for 1.0 L gasoline spill fires on brushed concrete – 30 and 300 second ignition delays [1]**

#### 5.4.1.4 Discussion of Liquid Spill Fire Testing Results

The spill fire tests described in Reference 1 reveal a number of features that may be addressed in an improved HRR model. The most notable feature that is common to all spill fire tests is that there is a finite ramping stage that ranges from 15 to 20 seconds over which the fire size grows from zero to its peak value. After the peak value is reached, a decay stage follows that persists for about 30–60 seconds. Most of the tests indicate a decay stage that is similar to the growth stage but reversed and extended by a factor of about 2–3. There was no steady-state period observed for the spill fires considered.

The spill dynamics tests in Reference 1 provide an indication of the rate at which a liquid fuel spills over a substrate surface and their ultimate spill depths. It is shown that after about 30 seconds, a liquid fuel will spread to 50%–75% of the maximum spill area, and lubricating oils will spread to about 75%–90% of their maximum spill area. After 300 seconds, most combustible and flammable liquid fuels will spread to about 90% of the maximum spill area, and lubricating oils will spread to nearly 100% of the maximum spread area. However, it is also shown in the spill fire HRR tests that the fuels with a 30 second ignition delay achieve a higher peak HRR and have a similar burning duration as a comparable scenario with a 300 second ignition delay. This is applicable to highly volatile fuels such as gasoline, heptane, and ethanol, and, as such, it is always conservative to assume a 30 second ignition delay.

It may be concluded that a 30 second ignition delay will always bound a 300 second ignition delay when evaluating the effects of a fire in an enclosure or the response of a target to a fire exposure boundary condition. Nevertheless, it is expected that the ignition-delay effects would be less significant for low volatility fuels such as lubricating oil since it has been shown that the lubricating oil spills achieve approximately 90% of their maximum spread area within 30 seconds, and the mass of fuel that would evaporate over a longer ignition delay would be minimal as compared to a high volatility fuel.

The spill dynamics tests indicate that the overall average spill depth for flammable and combustible liquids is about 0.72 mm, with a standard deviation of 0.34 mm. The average spill depth is nearly equal to the value recommended in NUREG/CR-6850 [2] and provides a verification of this value. However, the range of spill depths is large (0.2–2.4 mm) indicating the need to consider the uncertainty in this parameter when calculating the fire effects of a spill fire. Detailed information was obtained for specific fuels, including gasoline, kerosene, ethanol, and lubricating oil. This information includes the average spill depth and the standard deviation and may be used to predict the spill areas for spills involving these specific liquids

The pan fire tests, which were conducted with a known initial fuel depth and a fixed fuel surface area, demonstrate that the fire diameter empirical constant provides an accurate description of the deep pool burning behavior for small diameter fires. In addition, the pan fire data was used to develop depth coefficients that correlate the burning rate of the fuel to the liquid depth. Depth coefficients were developed for gasoline and kerosene, but they are shown in Section 6.2.3 to be applicable to heptane and ethanol as well. Depth coefficients for other fuels, including lubricating oil are recommended to be 0.2 for thin spills (1 mm or less) and 1.0 for deep pools (2 mm or greater).

The spill fire tests were initially conducted on a variable temperature substrate, which revealed a significant sensitivity of the HRR profile to the substrate temperature. The effect of this parameter was not initially considered, and a systematic assessment of its effect was not performed in Reference 1. However, for temperature variations up to about 20°C, the peak HRR can increase by 25%–50% with a proportionate decrease in the fire duration. The effect is expected to be significant for high volatility fuels that are relatively close to their flashpoint and less so for low volatility fuels with a high flashpoint. The target substrate temperature for the spill fire tests is between 20°C and 25°C; therefore, the results and subsequent model development are limited to applications with a substrate temperature in this range for low flashpoint fuels. A safety factor of 25%–50% may be applied to substrate temperatures up to about 40°C. This limitation does not apply to high flashpoint fuels such as lubricating oil, although a limiting temperature of 40°C is reasonable to ensure that the fuel temperature remains significantly below the flashpoint temperature. The spill fire tests were conducted on various non-permeable substrates indicating that the peak HRR and fire duration are not overly sensitive to the substrate itself and that individual tests are highly repeatable when the initial substrate temperature is maintained within a narrow range.

The growth stage of the HRR profiles is an important feature and may be considered to consist of two factors. The first factor involves the physical spread of the fire from the ignition point, which is generally rapid, but not instantaneous. The range of fire diameters for the 0.5 L and 1 L spill fires is 0.8–1.5 m, and the surface flame spread speed for low flashpoint liquids is on the order of 10 cm/s [3]. This suggests that the flames require between 8 and 15 seconds to spread across the liquid surface. This does not fully account for the growth stage duration and, therefore, suggests that there is also a localized HRR development function on the liquid surface as the pyrolysis mass rate increases from zero to its peak value. This is analogous to the localized HRR development stage postulated for cable fires in the Flame Spread over Horizontal Cable Trays (FLASH-CAT) calculation method described in NUREG/CR-7010, Volume 1 [16], although the ramping stage is much shorter for liquid fuel fires. Based on the time to reach the peak HRR shown in Figures 5-15 through 5-27, the localized HRR ramping time is on the order of 10–30 seconds.

The spill fire tests described in Reference 1 reveal a number of features that may be addressed in an improved HRR. Most of the tests indicate a decay stage that is similar to the growth stage, but reversed and extended by a factor of about 2–3. There was no steady-state period observed for the spill fires considered. An assessment of the fuel depth at the time the peak HRR was reached is provided in Reference 1. It is estimated that the decay stage occurs when the fuel depth is between 0.2 mm and 0.85 mm, with an average value of 0.55 mm.

## 5.5 References

1. Grant No. 2008-DN-BX-K168, *Fire Dynamics and Forensic Analysis of Liquid Fuel Fires, Final Report,* Mealy, C., Benfer, M., and Gottuk, D., Hughes Associates, Inc., Baltimore, MD, February 18, 2011.
2. *Fire PRA Methodology for Nuclear Power Facilities, Volume 2: Detailed Methodology*, NUREG/CR-6850 and EPRI 1011989. U.S. Nuclear Regulatory Commission (NRC), Office of Nuclear Regulatory Research (RES), Washington, DC and Electric Power Research Institute (EPRI), Palo Alto, CA: 2005.

3. Gottuk, D. T. and White, D. A., "Liquid Fuel Fires," Section 3, Chapter 10, *The SFPE Handbook of Fire Protection Engineering,* 4th Edition, Society of Fire Protection Engineers, Bethesda, MD, 2008.
4. Gottuk, D., Gott, J., and Williams, F., "Fire Dynamics of Spill Fires: an Experimental Study," *Proceedings of the Sixth International Symposium on Fire Safety Science*, France, July 1999.
5. NRL/M6180—00-8457, "Optical Fire Detection (OFD) for Military Aircraft Hangars: Final Report on OFD Performance to Fuel Spill Fires and Optical Stresses," Gottuk, D. T., Scheffey, J. L., Williams, F. W., Gott, J. E., and Tabet, R. J., Naval Research Laboratory, Washington, DC, May 22, 2000.
6. Putori, A. D., McElroy, J. A., and Madrzykowski, D., "Flammable and Combustible Liquid Spill/Burn Patterns," NIJ Report 604-00, National Institute of Justice (NIJ), Washington, DC, 2001.
7. NUREG-1805, *Fire Dynamics Tools (FDTS) Quantitative Fire Hazard Analysis Methods for the U. S. Nuclear Regulatory Commission Fire Protection Inspection Program*, Iqbal, N. and Salley, M. H., U.S. Nuclear Regulatory Commission (NRC), Office of Nuclear Reactor Regulation, Washington, D C, 2004.
8. Babrauskas, V., "Heat Release Rates," Section 3, Chapter 1, *The SFPE Handbook of Fire Protection Engineering*, 4th Edition, Society of Fire Protection Engineers, Bethesda, MD, 2008.
9. Babrauskas, V., "Pool Fires: Burning Rates and Heat Fluxes," Section 21, Chapter 6, *Fire Protection Handbook*, Sixteenth Edition, National Fire Protection Association (NFPA), Quincy, MA, 1986.
10. Blinov, V. and Khudiakov, G., "Diffusion Burning of Liquids," U.S. Army Translation, NTIS No. AD296762, 1961.
11. *Nuclear Power Plant Fire Modeling Analysis Guidelines (NPP FIRE MAG*). NUREG-1934 and EPRI 1023259. U.S. Nuclear Regulatory Commission, Office of Nuclear Regulatory Research (RES), Washington, DC and Electric Power Research Institute (EPRI), Palo Alto, CA: 2012.
12. *Fire-Induced Vulnerability Evaluation (FIVE) User's Guide: Revision 2*. EPRI, Palo Alto, CA: 2014. 3002000830.
13. NUREG-1805, Supplement 1, *Fire Dynamics Tools (FDT$^S$) Quantitative Fire Hazard Analysis Methods for the U. S. Nuclear Regulatory Commission Fire Protection Inspection Program*, Stroup, D., Taylor, G., Hausman, G., and Salley, M. H., Final Report, U.S. Nuclear Regulatory Commission, Office of Nuclear Reactor Regulation, Washington, D C, July 2013.
14. Tewarson, A., "Generation of Heat and Gaseous, Liquid, and Solid Products in Fires," Section 3, Chapter 4, *The SFPE Handbook of Fire Protection Engineering*, 4th Edition, Society of Fire Protection Engineers, Bethesda, MD, 2008.
15. Janssens, M., "Calorimetry," Section 3-2. *The SFPE Handbook of Fire Protection Engineering*, 4th Edition, Society of Fire Protection Engineers, Bethesda, MD, 2008.

16. NUREG/CR-7010, *Cable Heat Release, Ignition, and Spread in Tray Installations During Fire (CHRISTIFIRE), Volume 1: Horizontal Trays,* Final Report, McGrattan, K., U.S. Nuclear Regulatory Commission, Office of Nuclear Regulatory Research, NRC, Washington, DC, July 2012.

17. Babrauskas, V., "Estimating Large Pool Fire Burning Rates," *Fire Technology*, Vol. 19, 1983, p. 251.

# 6
# RESULTS AND IMPLEMENTATION GUIDANCE FOR LIQUID SPILL HEAT RELEASE RATES

## 6.1 Technical Approach

There are several situations in fire modeling work performed at NPPs when the HRR for a spill fire is over-predicted and the fire duration is under-predicted. Such situations are often found in the following types of fire modeling computations:

- The determination of a ZOI around an ignition source
- The determination of the target response to an input boundary condition
- The determination of the HGL temperature and HGL descent time (for target immersion and exposure)

The following sections discuss the impacts of different spill fire HRR models on the above-listed computations and the resulting impacts on typical risk evaluations.

### *6.1.1 Background*

Four liquid fuel fire empirical HRR models are considered in this report.

Method 1 is based on guidance published in NUREG/CR-6850 [2]. It is a very simplified model that is useful for predicting the maximum possible HRR of a liquid fuel fire. It does not account for fire growth or decay or for reduced mass loss rates in thin and/or small diameter pools, resulting in the shortest burning durations and highest HRRs of all the methods considered in this report.

Method 2 is described and implemented in NUREG-1805 [7]. It is also a simplified model that is useful for predicting peak HRRs for pool fires where pool diameter is taken into account as an influence on the burning rate. It does not account for fire growth or decay or for reduced mass loss rates in thin pools, resulting in very short burning durations with very high HRRs.

Method 3 is described by Gottuk et al. [3]. It is a simplified model that improves upon Method 2 by adding the effect of fuel depth and substrate cooling on reducing the burning rate of the spill fire. It does not account for fire growth or decay, resulting in short burning durations with high HRRs, although the accuracy is improved for thin pool fires when compared to Methods 1 and 2.

Method 4, which is developed in this report, addresses the growth stage of the HRR in liquid fuel fires using observations of the behavior reported in Reference 1. A simple decay stage is included that is directly related to the surface flame spread rate on the liquid fuel and the localized mass burning rate. This method is shown to produce good agreement with the simple methods based on previous pool fire and spill fire data for deep pool data, but it is significantly improved for liquid spill fires in which the growth phase is a significant fraction of the overall HRR profile.

#### 6.1.1.1 Method 1 – NUREG/CR-6850

The currently recommended method for calculating the HRR profile of a combustible or flammable liquid spill fire in a commercial NPP is described in Section G.4 of NUREG/CR-6850 [2]. The approach uses pool fire mass loss rate data associated with optically thick, deep pool fires and liquid spread data for unconfined, thin liquid pools to determine a constant peak HRR. The peak HRR is determined using the following equation [2]:

$$\dot{Q}_p = \dot{m}''_\infty \Delta H_c A \qquad \textbf{Eq. 6-1}$$

Where:

$\dot{Q}_p$ is the peak HRR of the liquid spill fire (kW).

$\dot{m}''_\infty$ is the ideal or maximum burning rate per unit area of the combustible or flammable liquid (kg/s-m²).

$\Delta H_c$ is the fuel heat of combustion (kJ/kg).

$A$ is the area of the liquid spill (m²).

The maximum burning rate is based on data provided in NUREG-1805 [7], which is derived from deep pool fire data [9, 10].

The area for a confined liquid spill is equal to the area of confinement; a typical example is the area enclosed by curbing less the area occupied by solid obstructions such as a concrete pedestal. The area for unconfined liquid spills is determined using guidance provided in Reference 3 and is a function of the volume of liquid involved. Specifically, for fuel volumes of 95 L or less, the liquid depth is assumed to be 0.7 mm, which is equivalent to a spill area of 1.4 m²/L. For fuel volumes greater than 95 L, the liquid depth is assumed to be 2.8 mm, which is equivalent to a spill area of 0.36 m²/L [2, 3]. It is significant to note that the peak HRR computed using Equation 6-1 is independent of both the fire diameter and the fuel depth, both of which have been shown to have a significant effect on the HRR of a liquid spill fire [1, 3, 8].

The HRR in liquid spill fires, whether constrained or unconstrained, is postulated to reach its peak value nearly instantly and remain at the peak HRR until all fuel is consumed [2, 3, 7, 8]. The fire duration is determined using the fixed spill volume, the fuel density, and the mass burning rate [2, 3, 7, 8]:

$$t_d = \frac{V\rho}{A\dot{m}''_\infty} \qquad \textbf{Eq. 6-2}$$

Where:

$t_d$ is the spill fire duration (s).

$V$ is the volume of liquid fuel involved in the spill (m³).

$\rho$ is the liquid fuel density (kg/m³).

All other terms have been defined.

The ratio of the fuel volume to the spill area in Equation 6-2 is constant and fuel independent, although it does take on one of two values depending on the volume of fuel involved. Accordingly, the fire duration is essentially a function only of the fuel density and the burning rate. Table 6-1 lists the fire durations for liquid spill fires for the fuels listed in Table G-4 of NUREG/CR-6850 [2]. The range of fire durations for fuel spills involving 95 L or less is from about 5–37 seconds. The range of durations for fuel spills involving more than 95 L differs from the lower volume spills by the ratio of the assumed spill depth (4) and is from 19–148 seconds.

**Table 6-1**
**Spill fire duration for common liquid fuels as calculated using the method and data provided in Appendix G of NUREG/CR-6850 [2]**

| Fuel | Mass Loss Rate ($kg/m^2$-s) | Density ($kg/m^3$) | Heat of Combustion (kJ/kg) | Duration for Spill Involving 95 L or Less (s) | Duration for Spill Involving More than 95 L (s) |
|---|---|---|---|---|---|
| Acetone | 0.041 | 791 | 25,800 | 13.5 | 54.0 |
| Benzene | 0.085 | 874 | 40,100 | 7.2 | 28.7 |
| Ethanol | 0.015[†] | 794 | 26,800 | 37.1 | 148.2 |
| Fuel oil, heavy | 0.035 | 940 – 1,000 | 39,700 | 18.8 – 20.0 | 75.2 – 80.0 |
| Gasoline | 0.055 | 740 | 43,700 | 9.4 | 37.7 |
| Heptane | 0.101 | 675 | 44,600 | 4.7 | 18.7 |
| Hexane | 0.074 | 650 | 44,700 | 6.1 | 24.6 |
| JP-4 | 0.051 | 760 | 43,500 | 10.4 | 41.7 |
| JP-5 | 0.054 | 810 | 43,000 | 10.5 | 42.0 |
| Kerosene | 0.039 | 820 | 32,200 | 14.7 | 58.9 |
| Methanol | 0.017 | 796 | 20,000 | 32.8 | 131.1 |
| Transformer oil | 0.039 | 760 | 46,400 | 13.6 | 54.6 |
| Xylene | 0.09 | 870 | 40,800 | 6.8 | 27.1 |

[†]These data have been updated to 0.015 kg/s-$m^2$ for fire diameters less than 0.6 m; 0.022 kg/s-$m^2$ for fire diameters between 0.6 m and 3.0 m; 0.029 for fire diameters greater than 3.0 m kg/s-$m^2$ per Reference 3. This distinction is not made in NUREG/CR-6850 [2].

Scenarios involving kerosene, which is often used as a surrogate for diesel fuel, and transformer oil are of particular interest in commercial NPP applications. Table 6-1 indicates that for spill volumes with less than 95 L, the fire duration is on the order of 14 seconds. This is far shorter than the fire durations of 1–2 minutes for diesel fuel and kerosene as reported in Reference 1 and suggest that the method significantly under-predicts the fire duration for a spill fire. This is directly attributed to the use of the deep pool mass loss rate data for thin spill fires as may be seen by combining Equations 6-1 and 6-2:

$$t_d = \frac{V\rho\Delta H_c}{\dot{Q}_p \dot{m}''_\infty} \quad \text{Eq. 6-3}$$

where all terms have been previously defined.

Thus, for a given fuel, if the peak HRR is over-predicted, the fire duration will be proportionately under-predicted. Note that the fire durations for the larger volumes are closer to the observed fire durations of 1–2 minutes as reported in Reference 1. The assumed spill depth of 2.8 mm is closer to the pool depth of 5 mm at which deep pool burning behavior is observed according to Reference 1.

#### 6.1.1.2 Method 2 – NUREG-1805

NUREG-1805 [7] provides a slight modification to the pool fire HRR calculation described by Equations 6-1 and 6-2 using the methods originally presented in Blinov et al. [10]. The modification adjusts the mass burning rate for small diameter pools using the following equation:

$$\dot{Q}_p = \dot{m}''_\infty\left(1 - \exp(-k\beta D_e)\right)\Delta H_c A \quad \text{Eq. 6-4}$$

Where:

$k$ and $\beta$ are empirical parameters, the product of which is normally treated as a single entity having units of 1/m [7, 8, 10].

$D_e$ is the effective fire diameter (m).

The exponential term in Equation 6-4 accounts for the reduced mass loss rate per unit area observed for small diameter fires due to the transition between convective and radiant burning regimes [8]. The exponential term typically vanishes for diameters greater than 1–2 m, although the diameter at which the transition is made to turbulent radiant burning is fuel specific.

Including the diameter dependence in the HRR computation provides some improvement in the predicted peak HRR relative to the measured data; however, Equation 6-4 uses deep pool mass loss rate data and tends to over-predict the HRR and under-predict the fire duration for flammable or combustible liquid spill fires. This is illustrated in Figures 6-1a through 6-3b, which compare the measured HRR from the NIJ tests to the predicted HRR for spill fires using the NUREG/CR-6850 [2] approach described in Section 6.1.1.1 and the NUREG-1805 [7] approach for three fuels (gasoline, heptane, and denatured alcohol) and two fuel volumes (0.5 L and 1 L) on coated concrete. Note that the test naming convention describes the fuel, the substrate, the type of test, and the fuel volume. Appendix C.1 provides a description of the NIJ test nomenclature [1].

A more detailed description of the test result is provided in Section 5.4 of this report. The data shown in Figures 6-1a through 6-3b are provided to illustrate the effect of inaccurate predictions of the HRRs. Note that the heats of combustion, the mass loss rates, and the densities for the three fuels used to compute the HRRs with Equations 6-1 through 6-4 are as shown in Table 6-1. The product of the empirical constants $k$ and $\beta$ for each of the three fuels are as listed in NUREG-1805 [7] and are as follows:

- Gasoline: 2.1 $m^{-1}$
- Heptane: 1.1 $m^{-1}$
- Denatured alcohol (ethanol): 100 $m^{-1}$

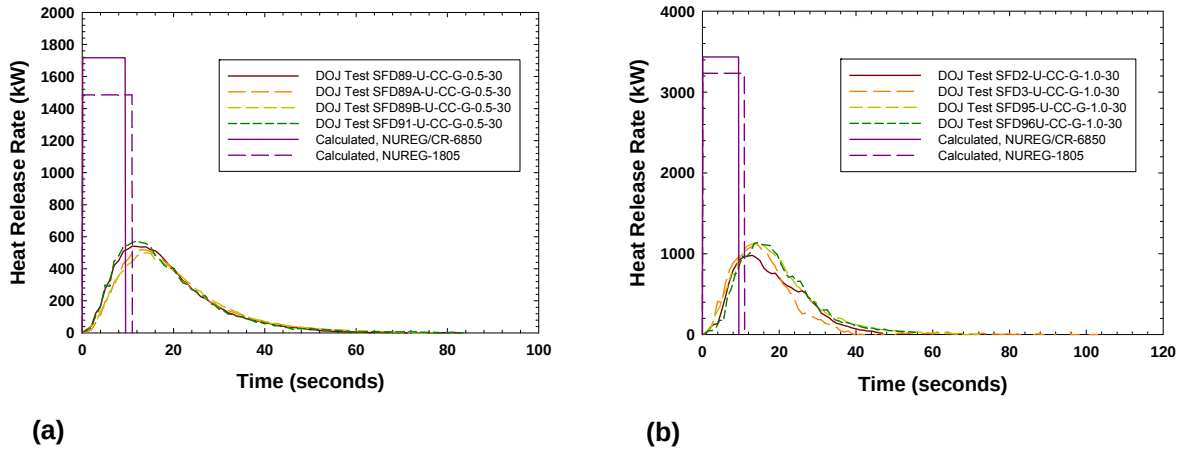


**Figure 6-1**
**(a) Measured and calculated HRRs for a 0.5 L gasoline spill fire on coated concrete – 30 second ignition delay, (b) Measured and calculated HRRs for a 1.0 L gasoline spill fire on coated concrete – 30 second ignition delay**

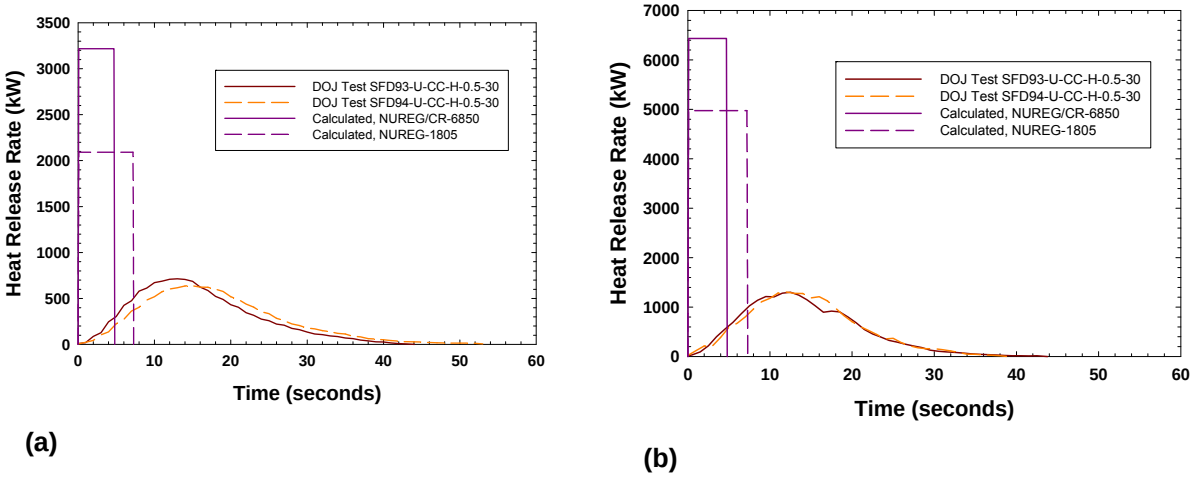


**Figure 6-2**
**(a) Measured and calculated HRRs for a 0.5 L heptane spill fire on coated concrete – 30 second ignition delay, (b) Measured and calculated HRRs for a 1.0 L heptane spill fire on coated concrete – 30 second ignition delay**

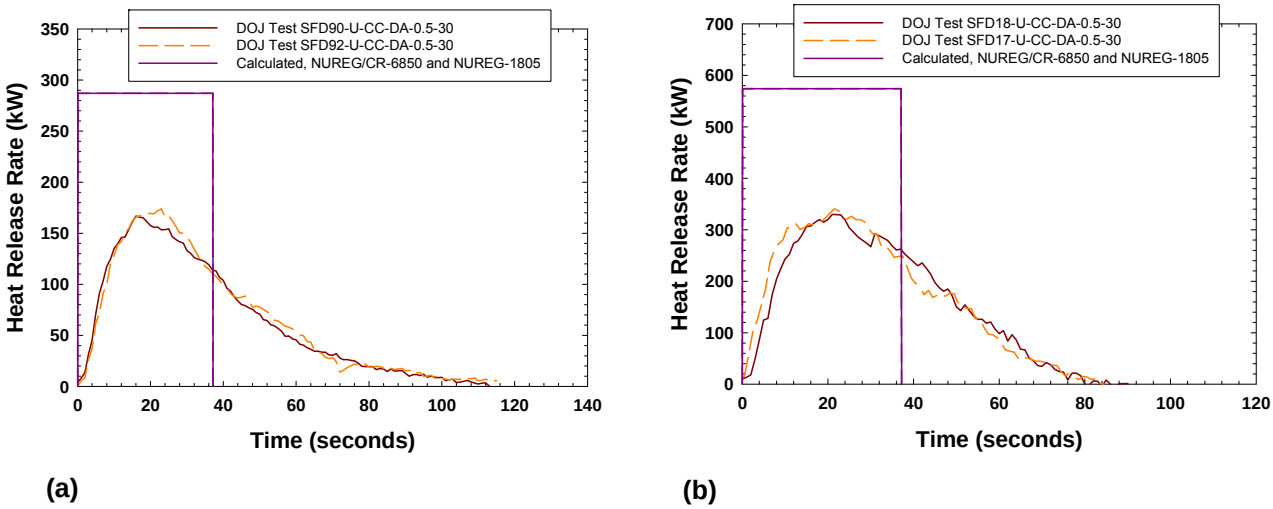


**Figure 6-3**
**(a) Measured and calculated HRRs for a 0.5 L ethanol spill fire on coated concrete – 30 second ignition delay, (b) Measured and calculated HRRs for a 1.0 L ethanol spill fire on coated concrete – 30 second ignition delay**

Figures 6-1 and 6-2 indicate that both the NUREG/CR-6850 [2] and NUREG-1805 [7] calculation approaches over-predict the peak HRR by a factor of 3–5 and under-predict the fire duration by a comparable factor for low volatility hydrocarbon fuels. Figure 6-3 shows that the NUREG/CR-6850 [2] and NUREG-1805 [7] calculation approaches are identical and over-predict the peak HRR by a factor of 2 and under-predict the fire duration by a comparable factor. Figures 6-1 through 6-3 use spill data from Reference 1 for coated concrete with an ignition

delay of 30 seconds. Spill fires involving low volatility fuels have a lower HRR and a comparable burning duration when the ignition delay is increased due to evaporation losses [1] and would thus diverge further from the HRR models described in NUREG/CR-6850 [2] and NUREG-1805 [7] than shown in Figures 6-1a through 6-3b.

#### 6.1.1.3 Method 3 – Gottuk et al.

Method 3 [1, 3] is an extension of the deep pool model that is applicable to thin liquid spills. The HRR is constant and is determined using the following equation [1, 3]:

$$\dot{Q}_p = C_\delta \dot{m}''_\infty \left(1 - \exp(-k\beta D_e)\right) \Delta H_c A \qquad \textbf{Eq. 6-5}$$

Where:

$\dot{Q}_p$ is the HRR of the spill fire.

$C_\delta$ is an empirical constant that is a function of the spill depth.

$\dot{m}''_\infty$ is the ideal or deep pool mass burning rate (kg/s-m²).

$k$ and $\beta$ are empirical constants whose product is treated as a single entity with units of 1/m.

$D_e$ is the effective fire diameter (m).

$H_c$ is the fuel heat of combustion (kJ/kg).

$A$ is the spill area (m²).

The deep pool mass burning rate and the product of $k$ and $\beta$ are empirical parameters and are tabulated in Table 5-5 for the fuels of interest in this report. The depth coefficient for gasoline and kerosene is an empirical constant or function. The functions for gasoline and kerosene have been correlated to the data in Reference 1 and are provided by Equations 5-3a and 5-3b, respectively. The spill constant is equal to 0.2 for other fuels when the spill depth is less than 1 mm and 1.0 when the spill depth is greater than 2 mm. A spill constant of 0.2 or 1.0 should be considered for spill depths between 1 and 2 mm (see Section 5.4.1.2.2). The recommended spill depth is 0.72 mm for gasoline, kerosene, ethanol, and heptane and 1.54 mm for lubricating oil according to Reference 1 (see Table 5-4). Table 6-3 provides the standard deviation for the spill depth for use in parameter uncertainty evaluations.

The spill fire diameter is related to the spill area via the following equation [1, 3]:

$$D_e = \sqrt{\frac{4A}{\pi}} \qquad \textbf{Eq. 6-6}$$

where all terms have been defined. The spill area is related to the initial fuel volume and the spill depth [1, 3]:

$$A = \frac{V}{\delta} \qquad \textbf{Eq. 6-7}$$

Where:

$V$ is the fuel spill volume (m³).

$\delta$ is the spill depth (m).

The fire duration is computed using total available energy and the HRR as follows [1, 3]:

$$t_d = \frac{V\rho\Delta H_c}{\dot{Q}} \qquad \textbf{Eq. 6-8}$$

Where:

$t_d$ is the fire duration (s).

$\rho$ is the fuel density (kg/m³).

All other terms have been defined.

The fuel density and heat of combustion are documented for a large number of fuels. Table 6-1, for example, provides values for these parameters for the fuels considered in this analysis. The method recommended by Gottuk et al. [3] produces a constant HRR profile with a duration equal to $t_d$. Typical HRR profiles are shown in Figure 6-4 for 0.5 L and 1 L gasoline spill fires with a spill depth of 0.72 mm. The model parameters listed in Table 6-1 and Table 5-5 in combination with Equations 6-5 through 6-8 are used to generate the HRR data.

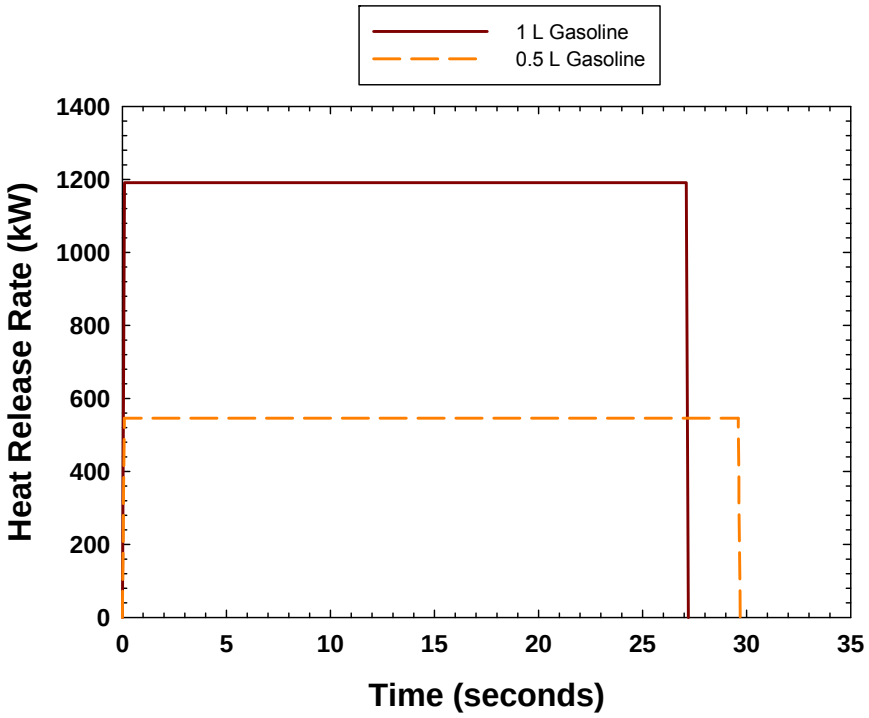


**Figure 6-4**
**Typical HRR profiles generated using Method 3 [3]**

### 6.1.1.4 Method 4 – Updated NIJ

Method 4 is an updated method that incorporates several features observed in the NIJ spill fire tests. Specifically, an improved prediction of the HRR profile is possible if a finite flame spread rate is modeled over the liquid surface and a finite HRR development time is modeled at each location. In this treatment, the flame front is postulated to travel across the burning liquid as shown in Figure 6-5.

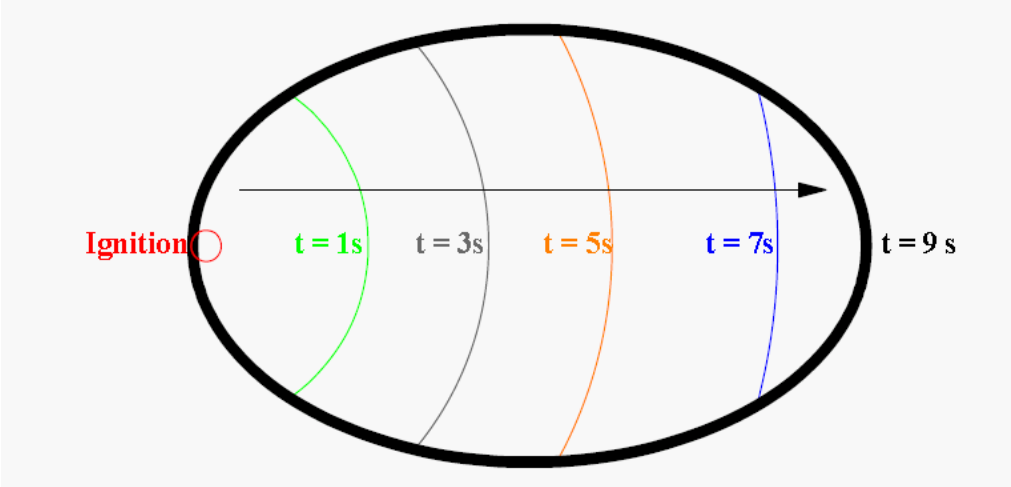


**Figure 6-5**
**Flame propagation over a generalized liquid spill surface [1]**

It is postulated that the burning behavior at any fixed location within the liquid pool is independent of other areas during the HRR development stage (that is, the flow of liquid away from a point due to fuel consumption elsewhere in the pool is slow enough that the time required to achieve the peak burning rate at that point is not affected). Therefore, the burning rate at any point may be represented using a time-lag growth rate parameter:

$$\dot{m}"(t) = \left(\frac{t}{t_{lag}}\right) C_\delta \left(1 - e^{-k\beta D_e}\right) \dot{m}"_\infty \; t \le t_{lag} \qquad \textbf{Eq. 6-9a}$$

$$\dot{m}"(t) = C_\delta \left(1 - e^{-k\beta D_e}\right) \dot{m}"_\infty \; t > t_{lag} \qquad \textbf{Eq. 6-9b}$$

Where:

$\dot{m}"(t)$ is the burning rate at a particular location within the liquid pool (kg/s-m²).

$t$ is the time from ignition at the particular point (s).

$t_{lag}$ is the HRR development time at a fixed location (s).

$C_\delta$ is the depth coefficient or function.

$\dot{m}"_\infty$ is the ideal or deep pool mass burning rate (kg/s-m²).

$k$ and $\beta$ are empirical constants whose product is treated as a single entity with units of 1/m.

$D_e$ is the effective fire diameter (m).

It is conservatively postulated that the ignition point is at the center of the spill fire. Therefore, the total mass consumed per unit area is given by the following equation [1]:

$$M" = \int_0^t \dot{m}"(t)\, dt \; t \le t_{lag} \quad \textbf{Eq. 6-10a}$$

$$M" = \int_0^{t_{lag}} \dot{m}"(t) dt + \int_{t_{lag}}^{t} C_\delta \left(1 - e^{-k\beta D_e}\right) \dot{m}"_\infty dt \;\; t > t_{lag} \quad \textbf{Eq. 6-10b}$$

Where:

$M"$ is the mass consumption rate at a fixed location in the liquid pool (kg/m²).

All other terms have been defined.

The HRR is then determined by integrating Equation 6-10 over the burning surface of the fuel:

$$\dot{Q} = \int M" \, dA = \int_0^{2\pi} \int_0^r M" r dr d\theta \;\; t \le t_{lag} \quad \textbf{Eq. 6-11}$$

The fire duration at any fixed location may then be determined using the following equation:

$$t_b = \frac{V\rho}{AC_\delta \left(1 - e^{-k\beta D_e}\right) \dot{m}"_\infty} + \frac{t_{lag}}{2} \quad \textbf{Eq. 6-12}$$

Where:

$t_b$ is the fire burning duration at a particular location.

All other terms have been defined.

The time at which the flame has spread to the edge of the pool is determined as:

$$t_v = \frac{D_e}{2v} \quad \textbf{Eq. 6-13}$$

Where:

$v$ is the flame spread rate over the surface of the liquid pool (m/s).

$t_v$ is the time required for fire to propagate to reach the outer edge of the liquid pool (s).

All other terms have been defined.

The characteristic times in Equations 6-12 and 6-13 plus the lag time ($t_{lag}$), and the total time required to consume all the fuel ($t_b + t_v$) can be used to define the integral solutions.

The closed form solutions to the integral are provided in Table 6-2 where all the characteristic times are provided between the ignition time ($t = 0$) and the total time required to consume all the fuel ($t_b + t_v$) [1].

The cases indicated in Table 6-2 correspond to different overall pool burn evolutions. The character of a burn evolution depends on the relative sizes of input parameters as noted in the Case column and the Case Description column. A diagrammatic representation of the relative timescales is provided in Figure 6-6, corresponding to the Case 3 closed form solution. The Note column provides a description of the burning behavior during each time period. The following simplified algorithm roughly illustrates a calculation of the HRR as a function of time for a thin pool fire based on Table 6-2:

1. Test the timescale parameters listed in the case descriptions to decide which case applies.
2. Define a time increment (step) for the simulation that is adequate to resolve the relevant timescale parameters.
3. Begin a program loop for cases and the time periods, beginning with the first time period.
   a. For a given time step during the current time period, calculate the HRR using the equation applicable to the selected case and time period as provided in the HRR equation column. Increase the simulation time by adding one time increment, and repeat the HRR calculation for the next time step.
   b. When the simulation time reaches the end of the current time period, increment the time period, and repeat Step 3a until all of the time periods for the selected case have been covered.
4. Display the HRR as a function of time.

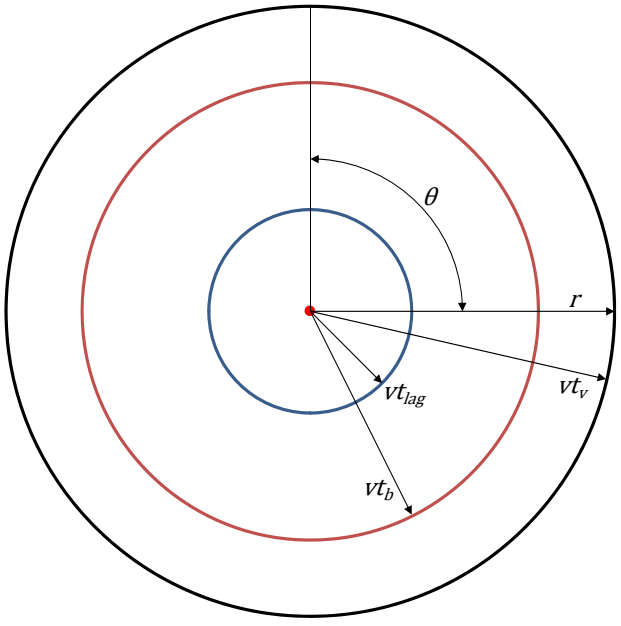


**Figure 6-6**
**Flame spread geometry over a liquid fuel surface (Case 3)**

**Table 6-2**
**HRR solutions for Method 4 from Equation 6-11**

| Case | Time Period | HRR Equation, $\dot{Q}(t)$ (kW) | Note | Case Description |
|---|---|---|---|---|
| Case 1 $\begin{pmatrix} t_b \le t_{lag} \\ AND \\ t_b \le t_v \end{pmatrix}$ | $t \le t_b$ | $\Delta H_c \frac{2\pi C_\delta \left(1 - e^{-k\beta D_e}\right) \dot{m}''_\infty v^2}{t_{lag}} \left[\frac{t^3}{6}\right]$ | Combined flame spread and lag growth | Because the lag time exceeds the burn duration, the fire never reaches a steady-state burn rate locally. Because the time required for flames to reach the edge exceeds the burn duration, the fuel is consumed at the center of the pool before the flames spread to the edge. |
| | $t_b < t \le t_v$ | $\Delta H_c \frac{2\pi C_\delta \left(1 - e^{-k\beta D_e}\right) \dot{m}''_\infty v^2}{t_{lag}} \left[\frac{t^3}{6} - \frac{t(t-t_b)^2}{2} + \frac{(t-t_b)^3}{3}\right]$ | Flame spread growth | |
| | $t_v < t \le t_v + t_b$ | $\Delta H_c \frac{2\pi C_\delta \left(1 - e^{-k\beta D_e}\right) \dot{m}''_\infty v^2}{t_{lag}} \left[\frac{t t_v^2}{2} - \frac{{t_v}^3}{3} - \frac{t(t-t_b)^2}{2} + \frac{(t-t_b)^3}{3}\right]$ | Decay | |
| Case 2 $\begin{pmatrix} t_b \le t_{lag} \\ AND \\ t_b > t_v \end{pmatrix}$ | $t \le t_v$ | $\Delta H_c \frac{2\pi C_\delta \left(1 - e^{-k\beta D_e}\right) \dot{m}''_\infty v^2}{t_{lag}} \left[\frac{t^3}{6}\right]$ | Combined flame spread and lag growth | Because the lag time exceeds the burn duration, the fire never reaches a steady-state burn rate locally. Because the burn duration exceeds the time required for flames to reach the edge, the center of the pool continues to burn after the entire surface is on fire. |
| | $t_v < t \le t_b$ | $\Delta H_c \frac{2\pi C_\delta \left(1 - e^{-k\beta D_e}\right) \dot{m}''_\infty v^2}{t_{lag}} \left[\frac{t t_v^2}{2} - \frac{t_v^3}{3}\right]$ | Lag growth | |
| | $t_b < t \le t_v + t_b$ | $\Delta H_c \frac{2\pi C_\delta \left(1 - e^{-k\beta D_e}\right) \dot{m}''_\infty v^2}{t_{lag}} \left[\frac{t t_v^2}{2} - \frac{t_v^3}{3} - \frac{t(t-t_b)^2}{2} + \frac{(t-t_b)^3}{3}\right]$ | Decay | |

**Table 6-2 (continued)**
**HRR solutions for Method 4 from Equation 6-11**

| Case | Time Period | HRR Equation, $\dot{Q}(t)$ (kW) | Note | Case Description |
|---|---|---|---|---|
| Case 3 $\begin{pmatrix} t_b > t_{lag} \\ AND \\ t_b < t_v \\ AND \\ t_{lag} < t_v \end{pmatrix}$ | $t \le t_{lag}$ | $\Delta H_c \frac{2\pi C_\delta \left(1 - e^{-k\beta D_e}\right) \dot{m}''_\infty v^2}{t_{lag}} \left[\frac{t^3}{6}\right]$ | Combined flame spread and lag growth | Because the burn duration exceeds the lag time, the burn rate reaches steady state locally before the fuel is consumed there. Because the time to reach the edge exceeds the burn duration, the fuel is consumed at the center of the pool before the flames reach the edge. Because the time to reach the edge exceeds the lag time, the local burn rate continues to grow after the fire spreads to the edge. |
| | $t_{lag} < t \le t_b$ | $\Delta H_c \frac{2\pi C_\delta \left(1 - e^{-k\beta D_e}\right) \dot{m}''_\infty v^2}{t_{lag}} \left[\frac{t^3}{6} - \frac{t\left(t - t_{lag}\right)^2}{2} + \frac{\left(t - t_{lag}\right)^3}{3}\right]$ $+\Delta H_c \pi C_\delta \left(1 - e^{-k\beta D_e}\right) \dot{m}''_\infty v^2 \left(t - t_{lag}\right)^2$ | Lag growth | |
| | $t_b < t \le t_v$ | $\Delta H_c \frac{2\pi C_\delta \left(1 - e^{-k\beta D_e}\right) \dot{m}''_\infty v^2}{t_{lag}} \left[\frac{t^3}{6} - \frac{t\left(t - t_{lag}\right)^2}{2} + \frac{\left(t - t_{lag}\right)^3}{3}\right]$ $+\Delta H_c \pi C_\delta \left(1 - e^{-k\beta D_e}\right) \dot{m}''_\infty v^2 \left[\left(t - t_{lag}\right)^2 - (t - t_v)^2\right]$ | Flame spread growth | |
| | $t_v < t \le t_v + t_{lag}$ | $\Delta H_c \frac{2\pi C_\delta \left(1 - e^{-k\beta D_e}\right) \dot{m}''_\infty v^2}{t_{lag}} \left[\frac{t t_v^2}{2} - \frac{t_v^3}{3} - \frac{t\left(t - t_{lag}\right)^2}{2} + \frac{\left(t - t_{lag}\right)^3}{3}\right]$ $+\Delta H_c \pi C_\delta \left(1 - e^{-k\beta D_e}\right) \dot{m}''_\infty v^2 \left[\left(t - t_{lag}\right)^2 - (t - t_v)^2\right]$ | Lag decay | |
| | $t_v + t_{lag} < t \le t_v + t_b$ | $\Delta H_c \pi C_\delta \left(1 - e^{-k\beta D_e}\right) \dot{m}''_\infty v^2 [t_v^2 - (t - t_b)^2]$ | Decay | |

**Table 6-2 (continued)**
**HRR solutions for Method 4 from Equation 6-11**

| Case | Time Period | HRR Equation, $\dot{Q}(t)$ (kW) | Note | Case Description |
|---|---|---|---|---|
| Case 4 $\left(\begin{array}{c} t_b > t_{lag} \\ AND \\ t_b \le t_v + t_{lag} \\ AND \\ t_b > t_v \\ AND \\ t_{lag} < t_v \end{array}\right)$ | $t \le t_{lag}$ | $\Delta H_c \frac{2\pi C_\delta \left(1 - e^{-k\beta D_e}\right) \dot{m}''_\infty v^2}{t_{lag}} \left[\frac{t^3}{6}\right]$ | Combined flame spread and lag growth | Because the burn duration exceeds the lag time, the burn rate reaches steady state locally before the fuel is consumed there. Because the time to reach the edge exceeds the lag time, the local burn rate continues to grow until after the fire spreads to the edge. Because the burn duration is not greater than the time to reach the edge plus the lag time, the fuel is consumed at the center of the pool before the flames reach their maximum burn rate at the edge of the pool. |
| | $t_{lag} < t \le t_v$ | $\Delta H_c \frac{2\pi C_\delta \left(1 - e^{-k\beta D_e}\right) \dot{m}''_\infty v^2}{t_{lag}} \left[\frac{t^3}{6} - \frac{t\left(t - t_{lag}\right)^2}{2} + \frac{\left(t - t_{lag}\right)^3}{3}\right]$ $+\Delta H_c \pi C_\delta \left(1 - e^{-k\beta D_e}\right) \dot{m}''_\infty v^2 \left(t - t_{lag}\right)^2$ | Flame spread growth | |
| | $t_v < t \le t_b$ | $\Delta H_c \frac{2\pi C_\delta \left(1 - e^{-k\beta D_e}\right) \dot{m}''_\infty v^2}{t_{lag}} \left[\frac{t t_v^2}{2} - \frac{t_v^3}{3} - \frac{t\left(t - t_{lag}\right)^2}{2} + \frac{\left(t - t_{lag}\right)^3}{3}\right]$ $+\Delta H_c \pi C_\delta \left(1 - e^{-k\beta D_e}\right) \dot{m}''_\infty v^2 \left(t - t_{lag}\right)^2$ | Lag growth | |
| | $t_b < t \le t_b + t_{lag}$ | $\Delta H_c \frac{2\pi C_\delta \left(1 - e^{-k\beta D_e}\right) \dot{m}''_\infty v^2}{t_{lag}} \left[\frac{t t_v^2}{2} - \frac{t_v^3}{3} - \frac{t\left(t - t_{lag}\right)^2}{2} + \frac{\left(t - t_{lag}\right)^3}{3}\right]$ $+\Delta H_c \pi C_\delta \left(1 - e^{-k\beta D_e}\right) \dot{m}''_\infty v^2 \left[\left(t - t_{lag}\right)^2 - (t - t_b)^2\right]$ | Lag decay | |
| | $t_b + t_{lag} < t \le t_v + t_b$ | $\Delta H_c \pi C_\delta \left(1 - e^{-k\beta D_e}\right) \dot{m}''_\infty v^2 [t_v^2 - (t - t_b)^2]$ | Decay | |

**Table 6-2 (continued)**
**HRR solutions for Method 4 from Equation 6-11**

| Case | Time Period | HRR Equation, $\dot{Q}(t)$ (kW) | Note | Case Description |
|---|---|---|---|---|
| Case 5 ($t_b > t_{lag}$ AND $t_b \le t_v + t_{lag}$ AND $t_b > t_v$ AND $t_{lag} > t_v$) | $t \le t_v$ | $\Delta H_c \frac{2\pi C_\delta \left(1 - e^{-k\beta D_e}\right) \dot{m}''_\infty v^2}{t_{lag}} \left[\frac{t^3}{6}\right]$ | Combined flame spread and lag growth | Because the burn duration exceeds the lag time, the burn rate reaches steady state locally before the fuel is consumed there. Because the time to reach the edge exceeds the lag time, the local burn rate continues to grow until after the fire spreads to the edge. Because the burn duration is not greater than the time to reach the edge plus the lag time, the fuel is consumed at the center of the pool before the flames reach their maximum burn rate at the edge of the pool. Because the lag time exceeds the time to reach the edge, the fire reaches its maximum burn rate at the center before the flames reach the edge. |
| | $t_v < t \le t_{lag}$ | $\Delta H_c \frac{2\pi C_\delta \left(1 - e^{-k\beta D_e}\right) \dot{m}''_\infty v^2}{t_{lag}} \left[\frac{t t_v^2}{2} - \frac{t_v^3}{3}\right]$ | Lag growth | |
| | $t_{lag} < t \le t_b$ | $\Delta H_c \frac{2\pi C_\delta \left(1 - e^{-k\beta D_e}\right) \dot{m}''_\infty v^2}{t_{lag}} \left[\frac{t t_v^2}{2} - \frac{t_v^3}{3} - \frac{t\left(t - t_{lag}\right)^2}{2} + \frac{\left(t - t_{lag}\right)^3}{3}\right]$ $+\Delta H_c \pi C_\delta \left(1 - e^{-k\beta D_e}\right) \dot{m}''_\infty v^2 \left(t - t_{lag}\right)^2$ | Transition | |
| | $t_b < t \le t_v + t_{lag}$ | $\Delta H_c \frac{2\pi C_\delta \left(1 - e^{-k\beta D_e}\right) \dot{m}''_\infty v^2}{t_{lag}} \left[\frac{t t_v^2}{2} - \frac{t_v^3}{3} - \frac{t\left(t - t_{lag}\right)^2}{2} + \frac{\left(t - t_{lag}\right)^3}{3}\right]$ $+\Delta H_c \pi C_\delta \left(1 - e^{-k\beta D_e}\right) \dot{m}''_\infty v^2 \left[\left(t - t_{lag}\right)^2 - (t - t_b)^2\right]$ | Lag decay | |
| | $t_v + t_{lag} < t \le t_v + t_b$ | $\Delta H_c \pi C_\delta \left(1 - e^{-k\beta D_e}\right) \dot{m}''_\infty v^2 [t_v^2 - (t - t_b)^2]$ | Decay | |

**Table 6-2 (continued)**
**HRR solutions for Method 4 from Equation 6-11**

| Case | Time Period | HRR Equation, $\dot{Q}(t)$ (kW) | Note | Case Description |
|---|---|---|---|---|
| Case 6 $\left(\begin{array}{c} t_b > t_{lag} \\ AND \\ t_b > t_v + t_{lag} \\ AND \\ t_b > t_v \\ AND \\ t_{lag} \geq t_v \end{array}\right)$ | $t \leq t_{lag}$ | $\Delta H_c \frac{2\pi C_\delta \left(1 - e^{-k\beta D_e}\right) \dot{m}''_\infty v^2}{t_{lag}} \left[\frac{t^3}{6}\right]$ | Combined flame spread and lag growth | Because the burn duration exceeds the lag time, the burn rate reaches steady state locally before the fuel is consumed there. Because the time to reach the edge exceeds the lag time, the local burn rate continues to grow until after the fire spreads to the edge. Because the burn duration is greater than the time to reach the edge plus the lag time, the fuel is consumed at the center of the pool before the maximum burn rate occurs at the edge of the pool. Because the lag time exceeds the time to reach the edge, the fire does not reach its maximum burn rate at the center before the flames reach the edge. |
| | $t_{lag} < t \leq t_v$ | $\Delta H_c \frac{2\pi C_\delta \left(1 - e^{-k\beta D_e}\right) \dot{m}''_\infty v^2}{t_{lag}} \left[\frac{t^3}{6} - \frac{t\left(t - t_{lag}\right)^2}{2} + \frac{\left(t - t_{lag}\right)^3}{3}\right] + \Delta H_c \pi C_\delta \left(1 - e^{-k\beta D_e}\right) \dot{m}''_\infty v^2 \left(t - t_{lag}\right)^2$ | Flame spread growth | |
| | $t_v < t \leq t_v + t_{lag}$ | $\Delta H_c \frac{2\pi C_\delta \left(1 - e^{-k\beta D_e}\right) \dot{m}''_\infty v^2}{t_{lag}} \left[\frac{t t_v^2}{2} - \frac{t_v^3}{3} - \frac{t\left(t - t_{lag}\right)^2}{2} + \frac{\left(t - t_{lag}\right)^3}{3}\right] + \Delta H_c \pi C_\delta \left(1 - e^{-k\beta D_e}\right) \dot{m}''_\infty v^2 \left(t - t_{lag}\right)^2$ | Transition | |
| | $t_v + t_{lag} < t \leq t_b$ | $\Delta H_c \pi C_\delta \left(1 - e^{-k\beta D_e}\right) \dot{m}''_\infty v^2 (t_v^2)$ | Steady burning | |
| | $t_b < t \leq t_v + t_b$ | $\Delta H_c \pi C_\delta \left(1 - e^{-k\beta D_e}\right) \dot{m}''_\infty v^2 [t_v^2 - (t - t_b)^2]$ | Decay | |

**Table 6-2 (continued)**
**HRR solutions for Method 4 from Equation 6-11**

| Case | Time Period | HRR Equation, $\dot{Q}(t)$ (kW) | Note | Case Description |
|---|---|---|---|---|
| Case 7 $\left(\begin{array}{c} t_b > t_{lag} \\ AND \\ t_b > t_v + t_{lag} \\ AND \\ t_b > t_v \\ AND \\ t_{lag} < t_v \end{array}\right)$ | $t \le t_v$ | $\Delta H_c \frac{2\pi C_\delta \left(1 - e^{-k\beta D_e}\right) \dot{m}''_\infty v^2}{t_{lag}} \left[\frac{t^3}{6}\right]$ | Combined flame spread and lag growth | Because the burn duration exceeds the lag time, the burn rate reaches steady state locally before the fuel is consumed there. Because the time to reach the edge exceeds the lag time, the local burn rate continues to grow until after the fire spreads to the edge. Because the burn duration is greater than the time to reach the edge plus the lag time, there is a period of time after the flames reach the edge that the entire surface of the pool is burning steadily at its maximum rate. Because the time to reach the edge exceeds the lag time, the fire reaches its maximum burn rate at the center before the flames reach the edge. |
| | $t_v < t \le t_{lag}$ | $\Delta H_c \frac{2\pi C_\delta \left(1 - e^{-k\beta D_e}\right) \dot{m}''_\infty v^2}{t_{lag}} \left[\frac{t t_v^2}{2} - \frac{t_v^3}{3}\right]$ | Lag growth | |
| | $t_{lag} < t \le t_v + t_{lag}$ | $\Delta H_c \frac{2\pi C_\delta \left(1 - e^{-k\beta D_e}\right) \dot{m}''_\infty v^2}{t_{lag}} \left[\frac{t t_v^2}{2} - \frac{t_v^3}{3} - \frac{t\left(t - t_{lag}\right)^2}{2} + \frac{\left(t - t_{lag}\right)^3}{3}\right]$ $+\Delta H_c \pi C_\delta \left(1 - e^{-k\beta D_e}\right) \dot{m}''_\infty v^2 \left(t - t_{lag}\right)^2$ | Transition | |
| | $t_v + t_{lag} < t \le t_b$ | $\Delta H_c \pi C_\delta \left(1 - e^{-k\beta D_e}\right) \dot{m}''_\infty v^2 (t_v^2)$ | Steady burning | |
| | $t_b < t \le t_v + t_b$ | $\Delta H_c \pi C_\delta \left(1 - e^{-k\beta D_e}\right) \dot{m}''_\infty v^2 [t_v^2 - (t - t_b)^2]$ | Decay | |

The parameters in Equations 6-10 through 6-13 are the same as those used by Method 3 [3], except for the surface flame spread rate and the HRR development time or the lag time. The surface flame spread rate for combustible and flammable liquids is typically between 5 and 10 cm/s, with the faster spread rates associated with the lower flashpoint fuels [3]. Flame spread rates can approach 100 cm/s for flammable liquids that are heated to nearly the flashpoint temperature [3]. In the cases considered in this report, which are typical of those postulated in NPPs, the flame spread rates are expected to be within the 5–10 cm/s range. As noted in Section 5.4.1.4, the HRR development time is on the order of 10–30 seconds.

Method 4 produces a HRR profile that varies with time, with a pronounced growth stage and a short, but finite, decay stage. Typical HRR profiles are shown in Figure 6-7 for 0.5 L and 1 L gasoline spill fires having a spill depth of 0.72 mm. The model parameters listed in Tables 6-1 and 5-5 in combination with Equation 5-3a and 5-3b are used to generate the HRR data. The flame spread rate is assumed to be 10 cm/s, and the HRR development time is assumed to be 10 seconds in this example.

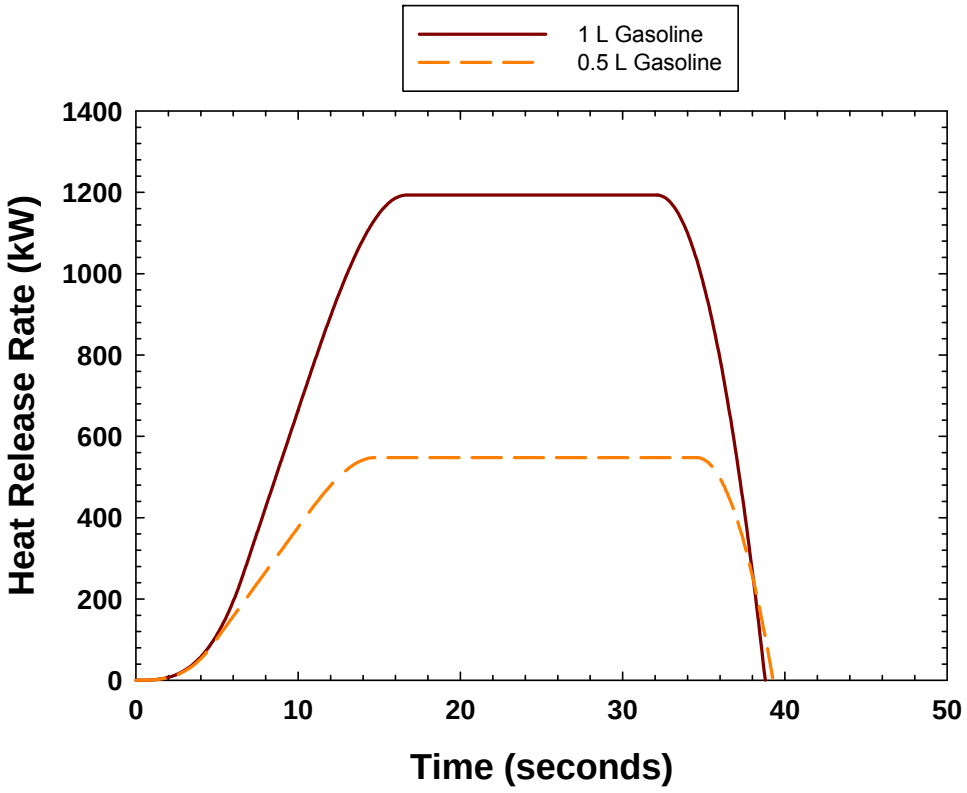


**Figure 6-7**
**Typical HRR profiles generated using Method 4**

### 6.1.2 Spill Fire Heat Release Rate Applications

#### 6.1.2.1 ZOI Calculations

ZOIs are regions around a fire inside which all susceptible targets are postulated to be damaged by the fire. ZOIs are normally determined using a fixed exposure temperature or heat flux threshold for target damage and the peak HRR of the postulated fire. The ZOI evaluation requires a heat flux calculation and a thermal plume temperature calculation. Over-prediction of the peak fire HRR of a spill fire will, therefore, result in a conservative ZOI that does not accurately reflect the effects of the spill fire scenario.

An approximate method of evaluating the effect of an over-predicted HRR on the ZOI is provided in NUREG-1934 [11]. The approach uses differentials to extrapolate the variation in an output parameter quantity given a variation in an input parameter. In this case, the input parameter is the HRR, and the output parameter is the heat flux or the plume temperature. The variation is performed using the power dependence of the output parameter on the input parameter. According to Table 6-1 in NUREG-1934 [11], the power dependence of the heat flux on the HRR is 4/3, and the power dependence of the plume temperature on the HRR is 2/3.

The heat flux damage threshold implied in a model in which an over-predicted HRR is used may be computed using the power dependence of the heat flux on the HRR as follows [11]:

$$\frac{\dot{q}''_{act}}{\dot{q}''_{cr}} \cong 1 + P\left(\frac{\dot{Q}_{act}}{\dot{Q}_{pred}} - 1\right) \qquad \textbf{Eq. 6-14}$$

Where:

$\dot{q}''_{act}$ is the actual heat flux used to define the ZOI dimension (kW/m²).

$\dot{q}''_{cr}$ is the target damage heat flux threshold (kW/m²).

$\dot{Q}_{pred}$ is the predicted peak HRR for the spill fire (kW).

$\dot{Q}_{act}$ is the actual peak HRR for the spill fire (kW).

$P$ is the power dependence of the heat flux on the HRR.

Given a $\frac{\dot{Q}_{act}}{\dot{Q}_{pred}}$ ratio that ranges from approximately 0.2 to 0.5 (see Figures 6-1a through 6-3b) and a power dependence of 4/3 for a heat flux calculation [11], the ratio $\frac{\dot{q}''_{act}}{\dot{q}''_{cr}}$ ranges from approximately 0.0 to 0.33.

The actual heat flux at the ZOI boundary would thus be approximately ~0 – 0.33 × 5.7, or 0.0 to 1.88 kW/m². This means that the ZOI for TP cable targets would be based on a heat flux of approximately 0.0–1.88 kW/m² rather than 5.7 kW/m² if the HRR for a spill fire is computed using the methods described in NUREG/CR-6850 [2] or NUREG-1805 [7]. A similar result is observed for ZOIs determined using heat flux calculations for TS cable targets.

The temperature damage threshold implied in a model in which an over-predicted HRR is used may be computed using the power dependence of the thermal plume temperature on the HRR as follows [11]:

$$T_{cr} - T_{act} \cong P(T_{cr} - T_{\infty})\left(\frac{\dot{Q}_{act}}{\dot{Q}_{pred}} - 1\right) \quad \textbf{Eq. 6-15}$$

Where:

$T_{cr}$ is the predicted temperature at the target in the thermal plume (°C).

$T_{act}$ is the actual temperature at the target in the thermal plume (°C).

$T_{\infty}$ is the ambient temperature (°C).

All other terms have been defined.

Assuming an ambient temperature of 20 (°C) and given a $\frac{\dot{Q}_{pred}}{\dot{Q}_{act}}$ ratio that ranges from 0.2 to 0.5 based on Figures 6-1a through 6-3b, and given a power dependence of 2/3 for a plume temperature calculation, the temperature differential $T_{cr} - T_{act}$ ranges from about 62°C to 98°C at the ZOI boundary for TP cables with a critical temperature of 205°C according to Equation 6-15. This means that the ZOI for TP cable targets would be based on a critical temperature of approximately 107°C–143°C rather than 205°C if the HRR for a spill fire is computed using the methods described in NUREG/CR-6850 [2] or NUREG-1805 [7]. A similar result is observed for ZOIs determined using thermal plume calculations for TS cable targets.

#### 6.1.2.2 Target Response to the Predicted Thermal Exposures

The target response to a calculated boundary condition determined with an HRR profile with a significantly larger peak HRR and significantly shorter fire duration will not be correct and may potentially be non-conservative. A simple illustration of this is provided by noting the predicted and observed fire durations for the ethanol spill fires shown in Figures 6-3a and 6-3b. The predicted fire duration using Methods 1 or 2 for the spill fire is approximately 40 seconds, whereas the observed fire durations are on the order of 1.5 minutes. Tables H-5 through H-8 in Appendix H of NUREG/CR-6850 [2] indicate that cable target damage times would not be predicted for exposures that are shorter than 1 minute. This means that for a target within the ZOI, it could be concluded that damage would not occur if the HRR profile is predicted to have a duration less than 1 minute as computed using the methods of NUREG/CR-6850 [2] or NUREG-1805 [7]. Conversely, if the actual fire duration of 1.5 minutes is assumed, then the same target could be exposed to a temperature or a heat flux boundary condition that leads to damage, following the guidance in Tables H-5 through H-8 of NUREG/CR-6850, Appendix H [2].

A more complex example may be generated using the Thermally Induced Electrical Failure (THIEF) model as contained in NUREG-1805, Supplement 1 [13] to illustrate the same point. A TS cable that is 22.13 mm in diameter, has a jacket thickness of 2.03 mm, and has a mass per unit length of 1.22 kg/m is assumed to be exposed to a 0.5 L gasoline spill fire plume (see Figure 6-1a). The cable target is positioned 1 m above the base of the fire, and the exposure heat flux is determined using the ‘Within Fire Plume’ sub-calculation in NUREG-1805, Supplement 1 [13] 19_THIEF_of_Cables_Calculations_Sup1_SI.xls spreadsheet.

The temperature exposure for the spill fire is shown in Figure 6-8 for spill fire HRR profiles calculated using the NUREG/CR-6850 [2] and NUREG-1805 [7] methods as well as the temperature exposure that would result from the measured HRR profile for a 0.5 L gasoline spill fire (see Figure 6-1a). The resulting cable temperatures for each exposure are shown in Figure 6-9. Figure 6-9 shows that the maximum predicted cable temperature is between 60°C and 65°C for spill fire exposures characterized using the methods described in NUREG/CR-6850 [2] and NUREG-1805 [7] but that the maximum cable temperature is about 100°C for a spill fire exposure characterized using the HRR profile measured in the NIJ tests [1]. Although the cable is not predicted to fail for any of the three exposures, Figure 6-9 demonstrates that the actual target temperature response could be much greater than that predicted using a short-duration, high-HRR characterization of a spill fire. There will clearly be target types and target elevations that would result in a different conclusion regarding its failure, depending on the method used to characterize the spill fire HRR.

A related application involving target response modeling involves the determination of an acceptable fuel load threshold. Based on the results shown in Figure 6-9, it is apparent that an incorrect and non-conservative fuel load limitation could be derived if the spill fire is characterized using either the methods described in NUREG/CR-6850 [2] or NUREG-1805 [7].

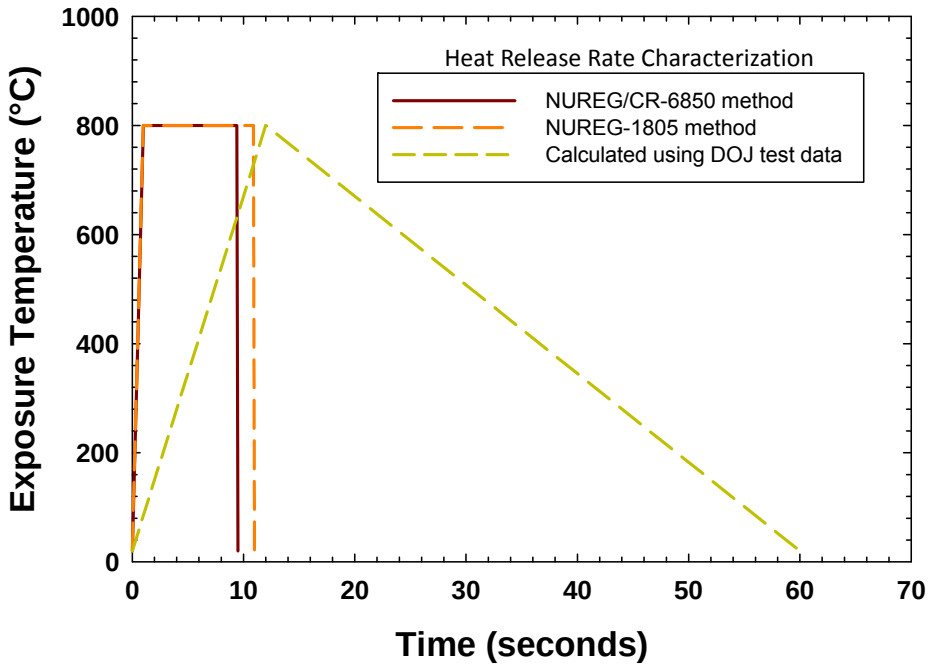


**Figure 6-8**
**Exposure temperatures to a generic TS cable target as calculated using NUREG-1805, Supplement 1 [13] for a 0.5 L gasoline spill fire**

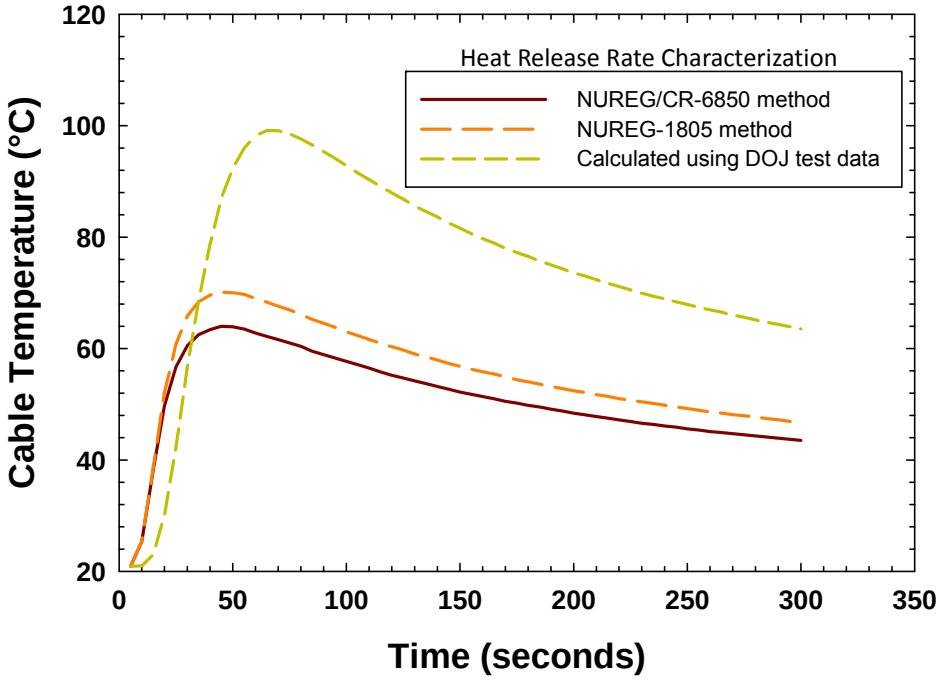


**Figure 6-9**
**Generic TS cable target temperature exposed to liquid spill fires as calculated using NUREG-1805, Supplement 1 [13]**

### 6.1.2.3 Hot Gas Layer Calculations

HGL calculations involve the solution of equations describing coupled fire effects, including the HRR, the air entrainment rate in a thermal plume, the mass flows across enclosure boundaries, and the thermal losses to the boundaries. If the HRR profile for a spill fire is characterized with a significantly over-predicted peak value and a significantly under-predicted duration, the thermal losses to the boundary would tend to be under-predicted and the temperature and hot gas layer temperature over-predicted, leading to an initially conservative result. However, over a longer time scale, the results may be less conservative, especially if the HGL temperatures are used as input into a target thermal response model such as THIEF [13, 14].

An illustration of the effect of an incorrect characterization of a spill fire HRR profile may be generated using the zone computer model Consolidated Fire and Smoke Transport (CFAST), Version 6.1.1 [15, 16]. A simple concrete enclosure that is 6.1 m tall and has plan dimensions of 6.1 × 6.1 m is assumed. A single door is included to provide pressure relief and ventilation for the fire. Figure 6-10 depicts the geometry used for this illustration. Three separate 1 L gasoline spill fire scenarios are postulated in the center of the test enclosure: one with an HRR profile characterized using the NUREG/CR-6850 [2] method, one with an HRR profile characterized using the NUREG-1805 [7] method, and one that uses the HRR profile measured for NIJ Test SFD96-U-CC-G-1.0-30 [1] (see Figure 6-1b). The results for typical CFAST output parameter used to assess target damage or habitability are shown in Figures 6-11 through 6-13. Figure 6-11 depicts the temperature of the HGL as a function of time and shows that the NUREG/CR-6850 [2] method and the NUREG-1805 [7] method of characterizing the spill fire HRR produce

significantly higher enclosure temperatures than the actual test data. The most conservative result is achieved by the NUREG-1805 [7] HRR characterization. If the enclosure contained TP cable targets with a damage threshold of 205°C, three different conclusions could be reached for each spill fire HRR characterization method:

- Method 1 – NUREG/CR-6850 [2] method: a damaging HGL would not be predicted, but there would be no safety margin.
- Method 2 – NUREG-1805 [7] method: a damaging HGL would be predicted.
- Direct application of NIJ Test SFD96-U-CC-G-1.0-30 data [1]: a damaging HGL would not be predicted, and the safety margin would be approximately 2, based on peak temperature rise.

Figure 6-12 depicts the HGL elevation as a function of time in the enclosure predicted for each of the three spill fire HRR characterizations. The NUREG/CR-6850 [2] and NUREG-1805 [7] methods for characterizing the spill fire HRR produce the fastest developing hot gas layers, but the NIJ Test SFD96-U-CC-G-1.0-30 data [1] result in the lowest HGL position. When habitability calculations are performed for assessing the feasibility of an operator manual action (OMA), for example, one of the thresholds for causing control room abandonment is the position of the HGL.

Figure 6-12 therefore suggests that the use of actual test data (or a method that characterizes the HRR comparable to the test results) could generate a more conservative result than the NUREG/CR-6850 [2] and NUREG-1805 [7] methods. Due to the different performance metrics (HGL position versus HGL temperature), the selected HRR profile can produce dramatic differences in modeling conclusions.

Figure 6-13 depicts the HGL optical density, a measure of the smoke visibility, as a function of time in the enclosure predicted for each of the three spill fire HRR characterizations. The NUREG/CR-6850 [2] and NUREG-1805 [7] methods for characterizing the spill fire HRR produce the most adverse visibility conditions and exceed the visibility predicted using the NIJ Test SFD96-U-CC-G-1.0-30 data by a factor of 2. The visibility parameter is related to the fuel mass burning rate by the rate of production of smoke by the fire and does not have a decay factor in CFAST [15, 16] other than through mass loss across the door opening.

Accordingly, Figure 6-13 suggests that the fuel mass burning rate in the NUREG/CR-6850 [2] and NUREG-1805 [7] burning rate characterizations exceed the burning rate observed in NIJ Test SFD96-U-CC-G-1.0-30 [1]. The result is that more optically dense smoke remains within the room, and the use of actual test data (or a method that characterizes the HRR comparable to the test results) could generate a less conservative result than the NUREG/CR-6850 [2] and NUREG-1805 [7] methods.

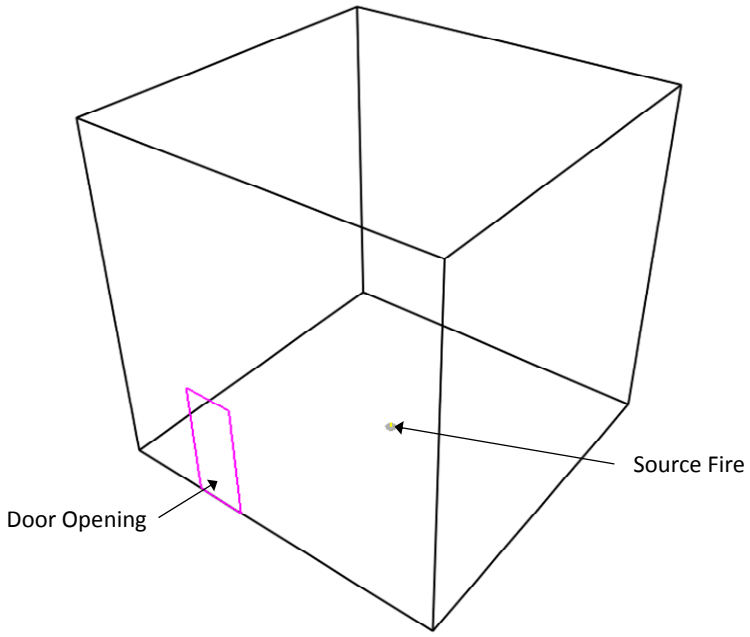


**Figure 6-10**
**CFAST geometry used to compare the effect of the spill fire HRR characterization**

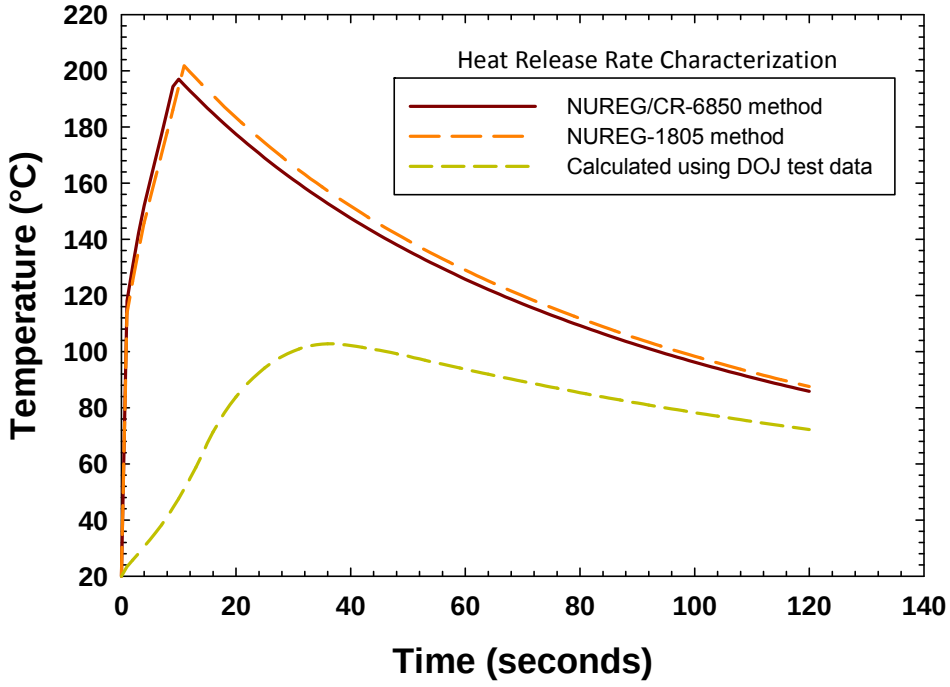


**Figure 6-11**
**HGL temperature in CFAST geometry for different spill fire HRR Characterizations – 1 L gasoline on coated concrete**

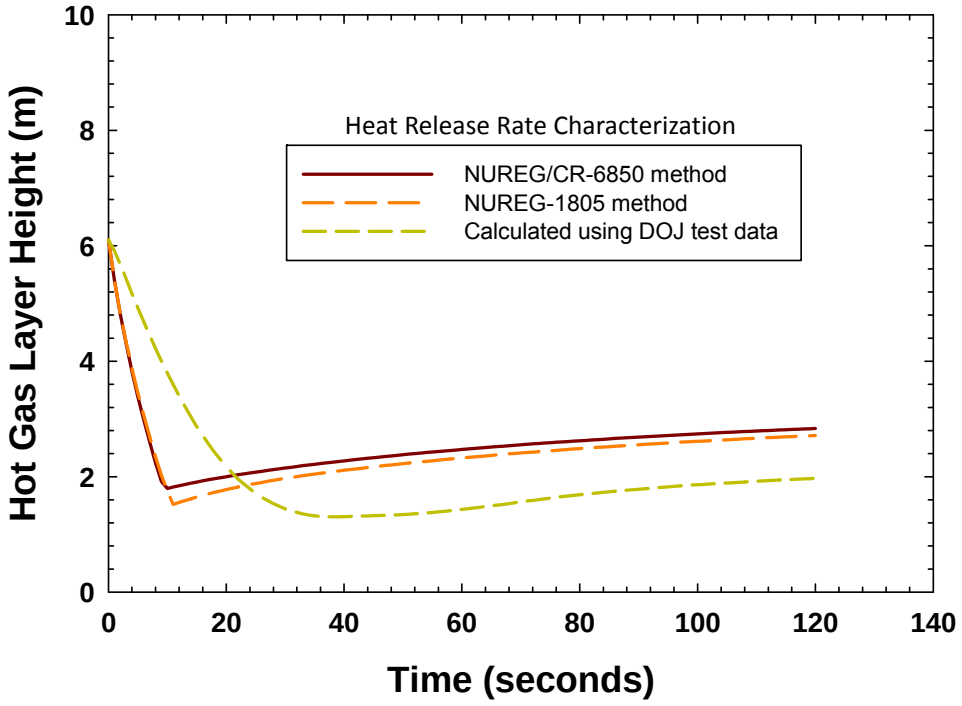


**Figure 6-12**
**HGL elevation in CFAST geometry for different spill fire HRR characterizations – 1 L gasoline on coated concrete**

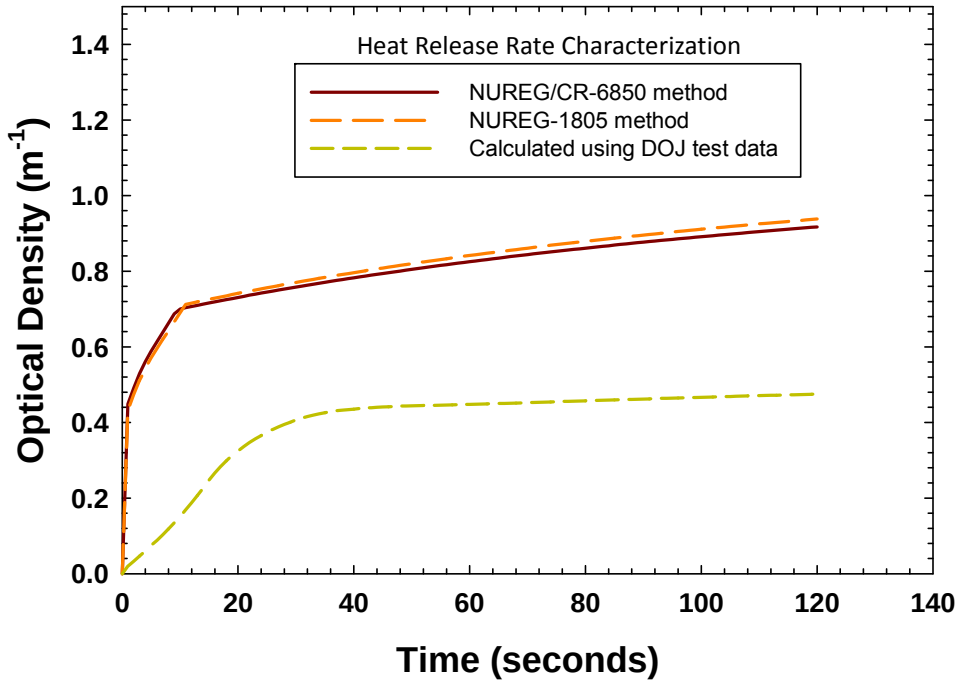


**Figure 6-13**
**HGL visibility in CFAST geometry for different spill fire HRR characterizations – 1 L gasoline on coated concrete**

#### 6.1.2.4 Summary

The consequences of using a spill fire HRR model that significantly over-predicts the peak HRR and significantly under-predicts the fire duration suggests the need for an improved treatment. The improved treatment developed in this report provides a more realistic assessment of the fire effects and could eliminate potentially non-conservative conclusions regarding the response of a target to a thermal boundary condition or the position of an HGL in an enclosure fire model. The improved treatment predicts the peak HRRs more accurately and provides better predictions of fire durations. Improved treatment of HRR growth and decay stages provides further refinement on the HRR characterization and leads to further improvements in predictions made by calculations that use the HRR as an input parameter.

The recent work performed under Grant No. 2008-DN-BX-K168 for the NIJ has greatly expanded the available test data applicable to liquid spill fires [1]. These data consist of over 500 individual tests involving six liquid fuels and two nonfuel liquid surrogates. The tests evaluated a number of aspects of liquid spill fires, many of which are relevant to the goals of this analysis. These include [1]:

- Evaluation of the spill depth for various fuels and fuel volumes on different substrates
- Evaluation of the HRR profile for confined liquid spill fires with different initial depths
- Evaluation of the HRR profile for unconfined liquid spill fires over different substrates for different fuels and fuel volumes

Several secondary parameters are evaluated that are postulated to have an effect on the fire development in liquid fuel fires. These include [1]:

- Evaluation of the ignition-delay time
- The evaluation of the substrate temperature

The ignition-delay time affects the development of an unconfined spill fire in two general ways. First, a longer ignition-delay time permits the fuel to spread out further and approach its asymptotic limit. Second, a longer ignition-delay time permits the high-volatility components of a fuel to evaporate, which affects the fuel composition and, thus, its combustion properties.

Given the comprehensive nature of the NIJ test series, they provide a unique opportunity to refine the empirical methods used to calculate the HRR profile in an unconfined spill fire and to provide verification for the methods used to calculate the deep pool burning behavior.

### *6.1.3 Updated Spill Fire Heat Release Rate Calculation Approach*

Two empirical models will be presented that improve the HRR predictive capability for spill fires. The first model (Method 3) is a simple enhancement to the NUREG-1805 approach that accounts for liquid fuels burning in thin layers. This model is currently reported in Section 3–10 of the 4$^{th}$ Edition of the *SFPE Handbook of Fire Protection Engineering* [3]. A second model (Method 4) will be presented that expands on Method 3 to incorporate the growth and decay stages of liquid pool fires. These models will be compared against applicable data for spill fires as reported in Reference 1. The comparison will include confined spills to demonstrate the

prediction as the pools transition to deep pool burning rates. In addition, aspects of the deep pool burning rate model will be compared with test data obtained in the NIJ test series to verify the input parameters and the diameter based sub-model used in the NUREG-1805 method and the two enhanced methods presented in this report.

A simple analysis methodology will be presented that guides the user through the necessary steps for evaluating spill fires and confined liquid fuel fires. The methodology will provide decision points and identify the equations and parameter data that should be used for the particular analysis path selected. The methodology will be demonstrated using several examples.

Model uncertainty will be discussed and uncertainty bands or standard deviations will be provided for key model input parameters. The uncertainty bands and standard deviations may be used to assess the model uncertainty when they are applied in support of probabilistic risk assessments.

Finally, a discussion on the development of a spreadsheet tool will be provided.

#### 6.1.3.1 Application for Deep Pools

The HRR predictive capability of Method 3 [3] and Method 4 is compared against the measured pan fire HRR data provided in Section 5.4.1.2. Given the similarity of the test results for the water and steel substrates, only the steel substrate data are used in this validation study where data for both substrates is available. The following tests are selected for comparison against the HRR models:

- 0.3 m pan fires with gasoline (steel substrate)
- 0.6 m pan fires with gasoline (steel substrate)
- 0.3 m pan fires with kerosene (steel substrate)
- 0.6 m pan fires with kerosene (steel substrate)
- 1.2 m pan fires with gasoline (water substrate)
- 1.2 m pan fires with ethanol (water substrate)

The validation results for each model using these tests are shown in Figures 6-14 through 6-19. The model parameters listed in Tables 6-1 and 5-5 in combination with Equations 6-5 through 6-12 and are used to generate the HRR data. The flame spread rate over the liquid surface is assumed to be 10 cm/s for gasoline and ethanol and 5 cm/s for kerosene due to the higher flashpoint. The HRR development time is assumed to be ten seconds for gasoline and ethanol and fifteen seconds for kerosene, consistent with the data and observations provided in Section 5.4. Note that Equation 5-3a is used to determine the depth coefficient for the ethanol pan fires shown in Figures 6-19a and 6-19b.

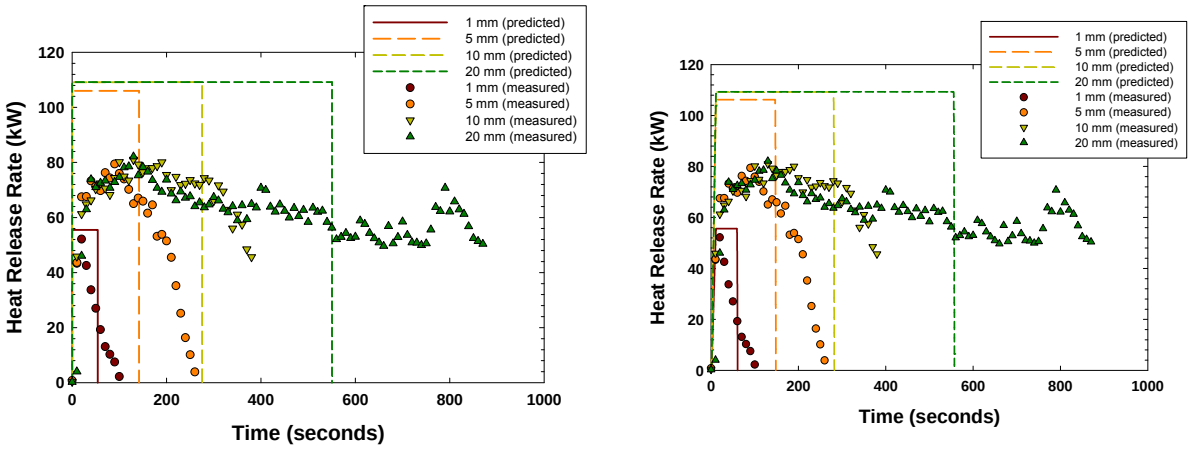


(a) (b)

**Figure 6-14**
**(a) 0.3 m pan fire with gasoline – comparison of test data with Method 3 (steel substrate),**
**(b) 0.3 m pan fire with gasoline – comparison of test data with Method 4 (steel substrate)**

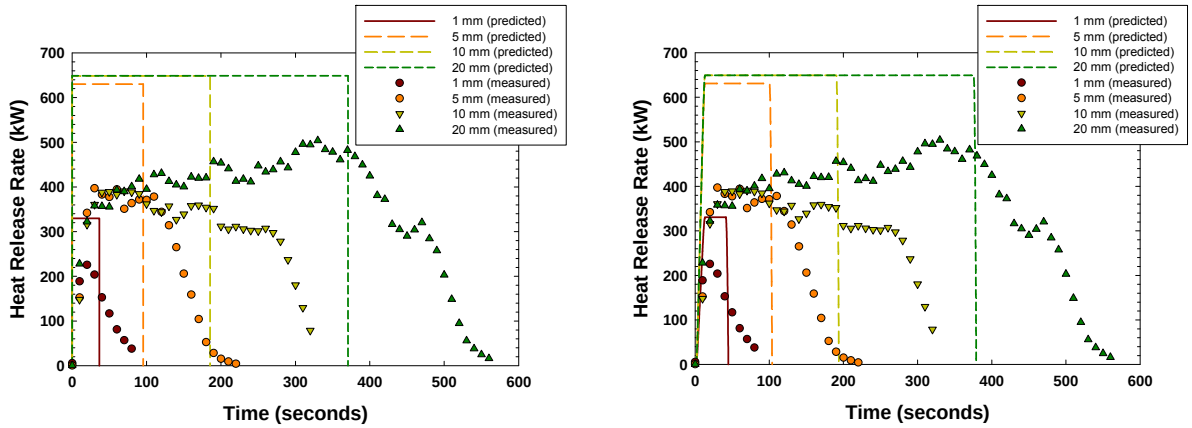


(a) (b)

**Figure 6-15**
**(a) 0.6 m pan fire with gasoline – comparison of test data with Method 3 (steel substrate),**
**(b) 0.6 m pan fire with gasoline – comparison of test data with Method 4 (steel substrate)**

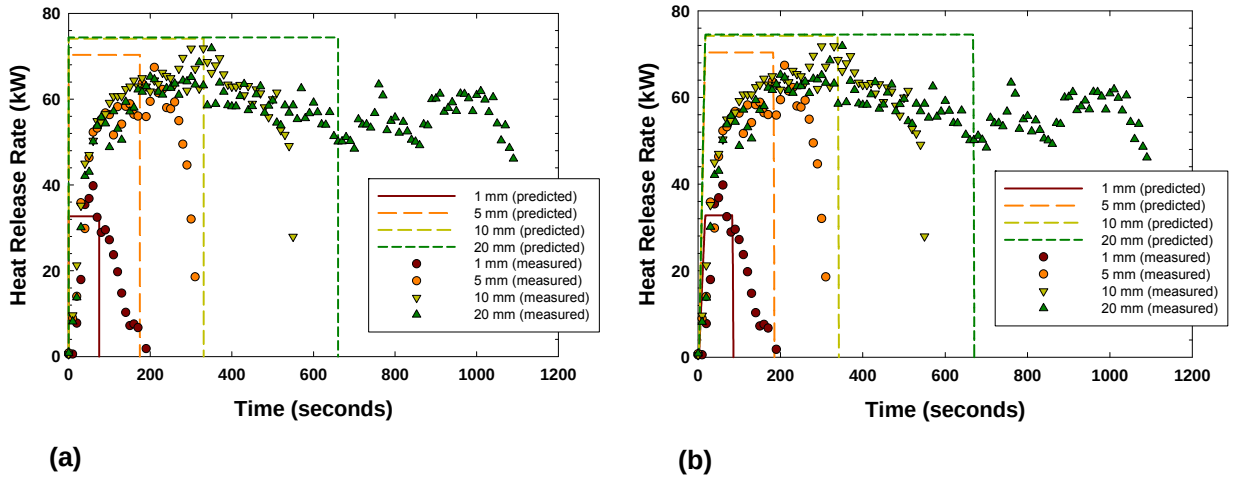


**Figure 6-16**
**(a) 0.3 m pan fire with kerosene – comparison of test data with Method 3 (steel substrate),**
**(b) 0.3 m pan fire with kerosene – comparison of test data with Method 4 (steel substrate)**

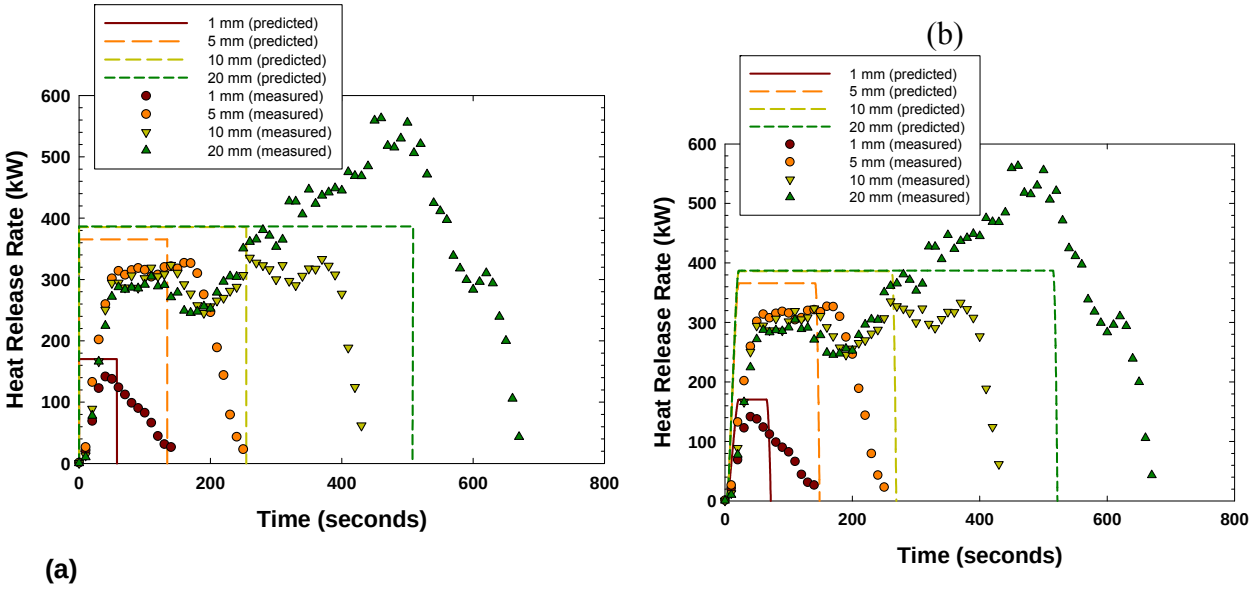


**Figure 6-17**
**(a) 0.6 m pan fire with kerosene – comparison of test data with Method 3 (steel substrate),**
**(b) 0.6 m pan fire with kerosene – comparison of test data with Method 4 (steel substrate)**

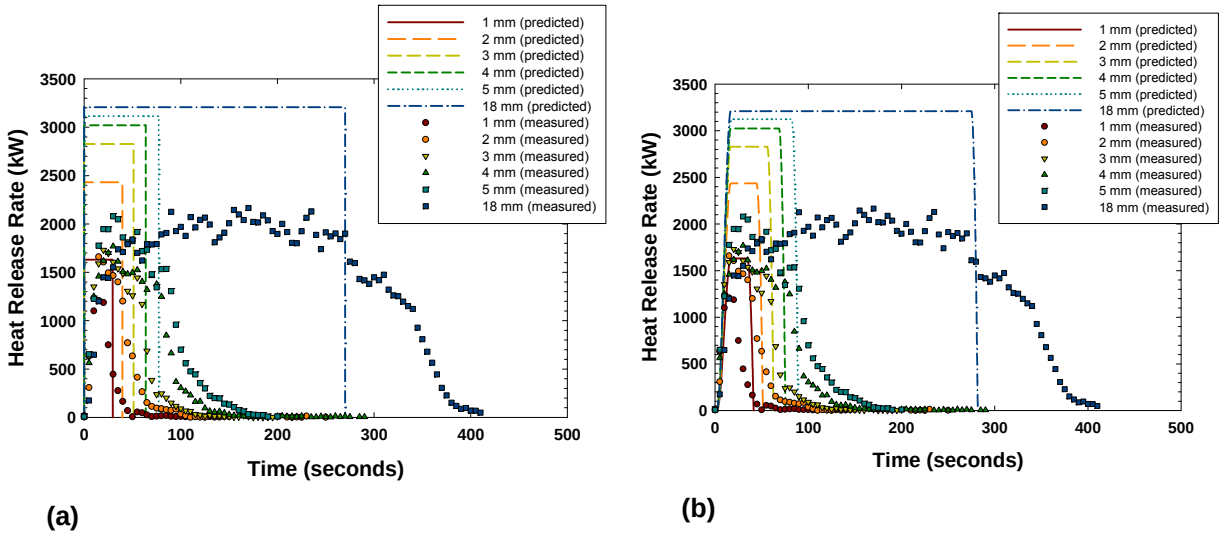


**Figure 6-18**
**(a) 1. 2 m pan fire with gasoline – comparison of test data with Method 3 (water substrate),**
**(b) 1.2 m pan fire with gasoline – comparison of test data with Method 4 (water substrate)**

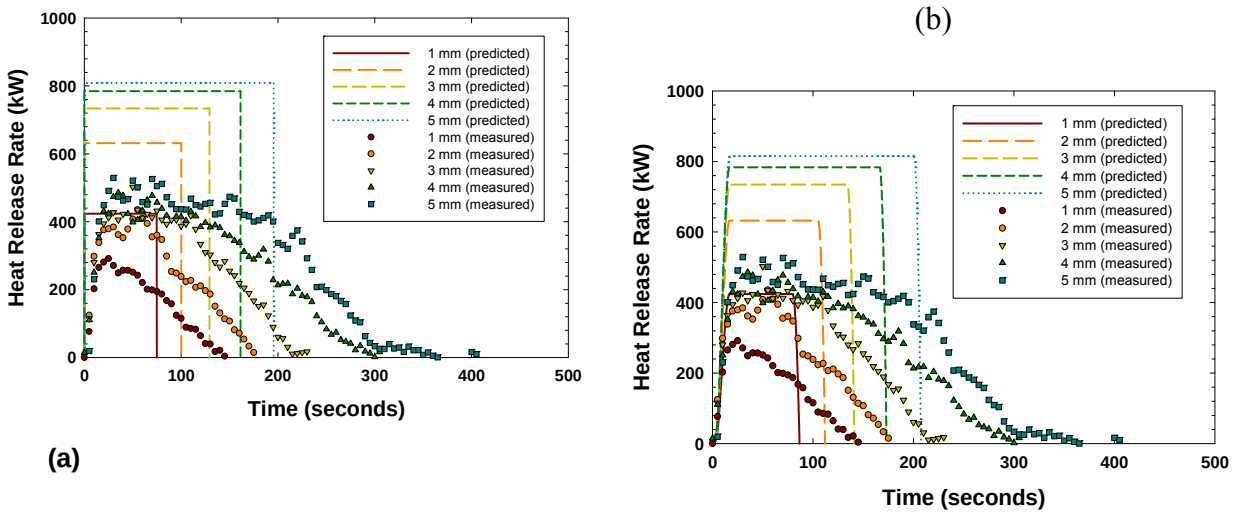


**Figure 6-19**
**(a) 1.2 m pan fire with ethanol – comparison of test data with Method 3 (water substrate),**
**(b) 1.2 m pan fire with ethanol – comparison of test data with Method 4 (water substrate)**

Figures 6-14 through 6-19 indicate that both Methods 3 and 4 produce similar results for pool depths of 2 mm or greater. This confirms that Method 4 transitions to a deep pool model as the fuel depth increases.

The results for gasoline pan fires are presented in Figures 6-14, 6-15, and 6-18. The figures indicate that both models systematically over-predict the HRR by about 30%–50% and under-predict the fire duration by a similar factor. The maximum burning rate parameter assumed for gasoline is based on data provided by Babrauskas [8], which is based on data collected by Blinov et al. [10] over 50 years ago. Because the formulation of gasoline has changed over time, it is likely that the data is not representative of the gasoline used in the NIJ tests. A comparison of the measured and predicted burning rate for gasoline using the empirical parameters provided by Babrauskas [8] in Reference 1 indicates that the maximum burning rate for the gasoline formation used in the NIJ tests may be about 20%–30% lower than the gasoline formulation on which the empirical constants are based. Nevertheless, the HRR profiles generated for the gasoline pan fires using Method 3 or 4 represent a significant improvement over Methods 1 and 2, and are expected to provide a conservative prediction of the effects of deep pool gasoline fires.

The results for kerosene pan fires are presented in Figures 6-16 and 6-17. Both methods provide goods predictions of the peak burning rate but under-predict the burning duration by about 20%. This is primarily due to the manner in which the predicted HRR profiles treat the decay stage of the fire. Method 3 has no decay stage and the HRR abruptly terminates when all fuel is consumed. Method 4 has a short decay stage that is related to the flame spread rate over the surface of the liquid spill. As described in Section 5.4.1.4, spill fires tend to begin the decay stage when the depth reaches 0.55 mm and exhibit a more gradual decrease in the HRR than either method predicts. This is one area of improvement for the methods presented in this report, but it is considered conservative to over-predict the HRR during the decay stage given the exposure boundary conditions to a target are decreasing during this stage of the fire.

Figure 6-19 presents the results for the ethanol pan fire tests. The predicted results apply the depth coefficient function generated for gasoline fires and are shown to over-predict the HRR for thin pools by about 50%, with a comparable under-prediction of the burning duration. Nevertheless, if a coefficient of 0.2 is assumed for the 1 mm spill fires as recommended in Ref. 1, the HRR would be under-predicted by about 30% and the burning duration would be over-predicted by a factor of about 30%. Similar to the gasoline fires, an over-prediction of the HRR for deep pool fire is generally a conservative attribute provided the burning duration is predicted reasonably well. In this case, the under-predicted portion of the burning rate is in the decay stage.

The model predictions and experimental results provided in Figures 6-14 through 6-19 can be compared following the statistical guidance provided in NUREG-1934 [11]. Using this approach, the model bias indicates the ratio that the model will over or under-predict the observed experimental result (See Appendix C.3). The model bias for each of the four models discussed in the beginning of Section 5 is provided in Figure 6-20. A model bias of 1.0 would indicate perfect agreement between the model and the experiment on average as indicated by the solid black line in Figure 6-20. Note that Methods 1 and 2 demonstrate considerable over-prediction of the peak HRR (by a factor of approximately two on average), and commensurate under-prediction of the burning duration, as previously discussed. Methods 3 and 4 produce improved predictions, where the peak HRR is approximately 31% over-predicted, and the burning duration predictions are improved, with Method 3 producing the closest prediction to the perfect match line. The results

of the evaluation are provided in Table 6-3, which also demonstrate that the model relative standard deviation for Method 3 to be the lowest. This indicates that Method 3 will provide the most accurate and reliable prediction of the fire behavior for the deep pools, followed by Method 4, which demonstrates very good performance.

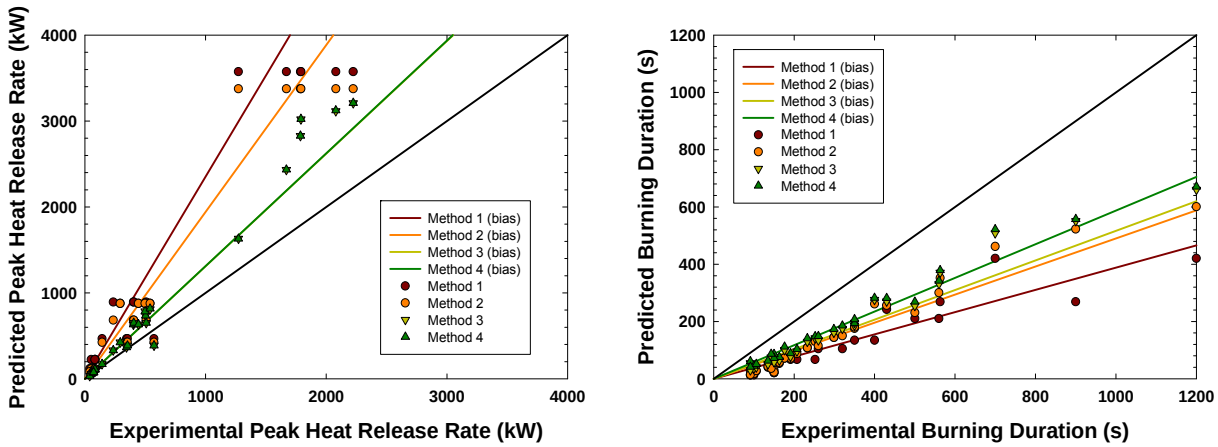


**Figure 6-20**
**(a) Model bias evaluation of the predicted peak HRR for confined spill fires in Figures 6-14 through 6-19, (b) Model bias evaluation of the predicted burning duration for confined spill fires in Figures 6-14 through 6-19**

**Table 6-3**
**Model bias and uncertainty for confined spill fires in Figures 6-14 through 6-19 evaluated using guidance in NUREG-1934 [11]**

| Model Output | Statistic | Method 1 | Method 2 | Method 3 | Method 4 |
|---|---|---|---|---|---|
| Peak HRR | Model bias, $\delta$ | 2.352 | 1.942 | 1.310 | 1.312 |
| | Model relative standard deviation, $\tilde{\sigma}_M$ | 0.517 | 0.566 | 0.263 | 0.264 |
| Burning duration | Model bias, $\delta$ | 0.388 | 0.490 | 0.517 | 0.588 |
| | Model relative standard deviation, $\tilde{\sigma}_M$ | 0.663 | 0.686 | 0.197 | 0.292 |

#### 6.1.3.2 Spill Fires

The HRR predictive capability of Methods 3 and 4 are compared against the measured spill fire HRR data provided in Section 5.4.1.3. Given the similarity of the test results for the coated concrete, smooth concrete, and brushed concrete results, only the coated concrete data are used in this validation study where data for both substrates is available. In addition, as noted in Section 5.4.1.3, a 30 second ignition delay produces a more conservative result than a 300 second ignition delay given the fire durations are approximately equal, but the HRR of the 30 second ignition-delay tests is greater. As such, only the 30 second ignition-delay tests are considered in this section. The following tests are selected for comparison against the HRR models:

- 0.5 L gasoline spill fire tests with a 30 second delay (coated concrete substrate)
- 1.0 L gasoline spill fire tests with a 30 second delay (coated concrete substrate)
- 0.5 L ethanol spill fire tests with a 30 second delay (coated concrete substrate)
- 1.0 L ethanol spill fire tests with a 30 second delay (coated concrete substrate)
- 0.5 L heptane spill fire tests with a 30 second delay (coated concrete substrate)
- 1.0 L heptane spill fire tests with a 30 second delay (coated concrete substrate)

The validation results for each model using these tests are shown in Figures 6-21 through 6-26. The model parameters listed in Tables 6-1 and 5-5 in combination with Equations 6-5 through 6-12 and are used to generate the HRR data. The flame spread rate over the liquid surface is assumed to be 10 cm/s and the HRR development time is assumed to be ten seconds, consistent with the data and observations provided in Section 5.4.1.3. Note that Equation 5-3a is used to determine the depth coefficient for the ethanol pan fires shown in Figures 6-23 and 6-24 and the heptane pan fires shown in Figures 6-25 and 6-26.

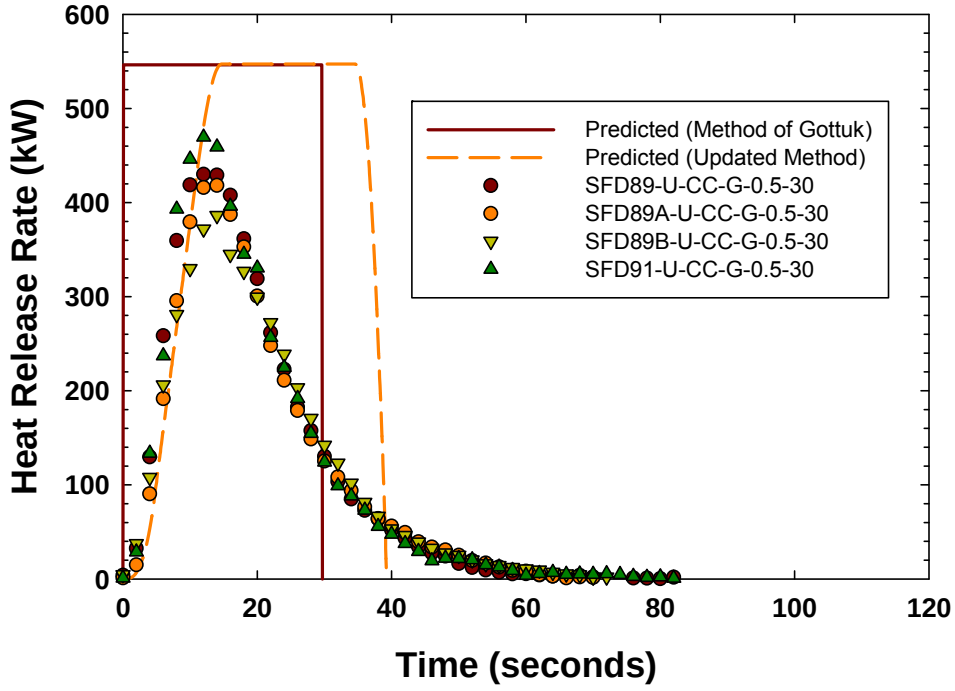


**Figure 6-21**
**0.5 L gasoline spill fires with a 30 second ignition delay – comparison of test data with the HRR prediction methods 3 and 4 (coated concrete substrate)**

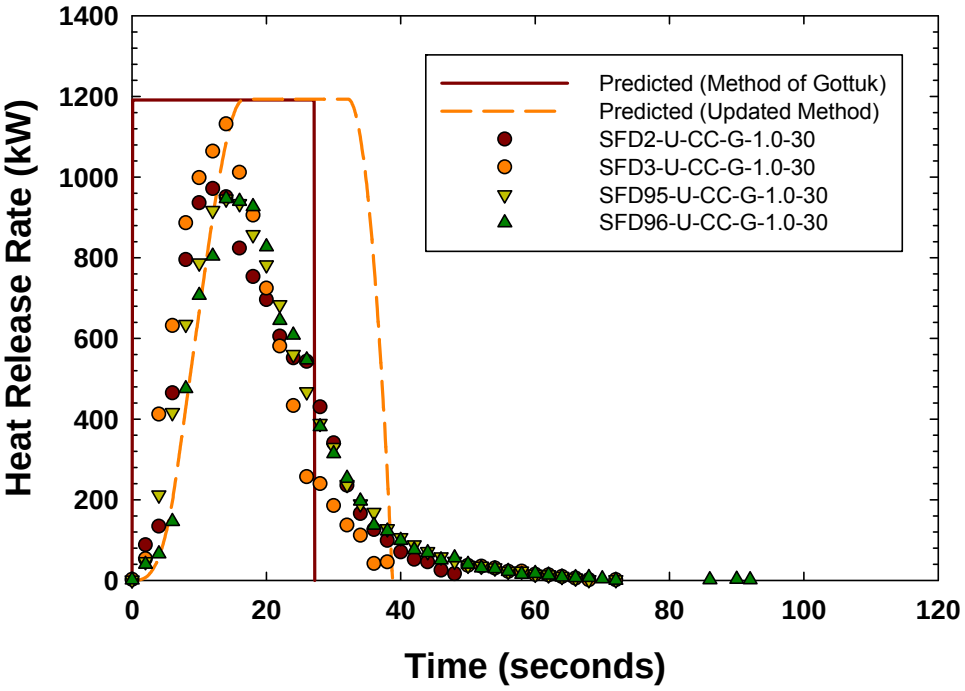


**Figure 6-22**
**1.0 L gasoline spill fires with a 30 second ignition delay – comparison of test data with the HRR Prediction Methods 3 and 4 (coated concrete substrate)**

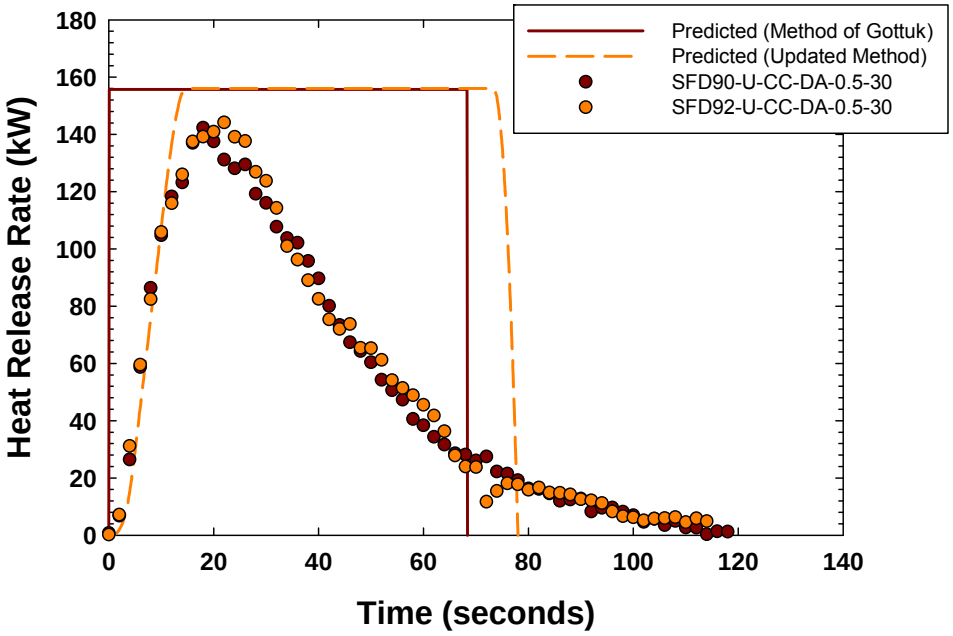


**Figure 6-23**
**0.5 L ethanol spill fires with a 30 second ignition delay – comparison of test data with the HRR prediction Methods 3 and 4 (coated concrete substrate)**

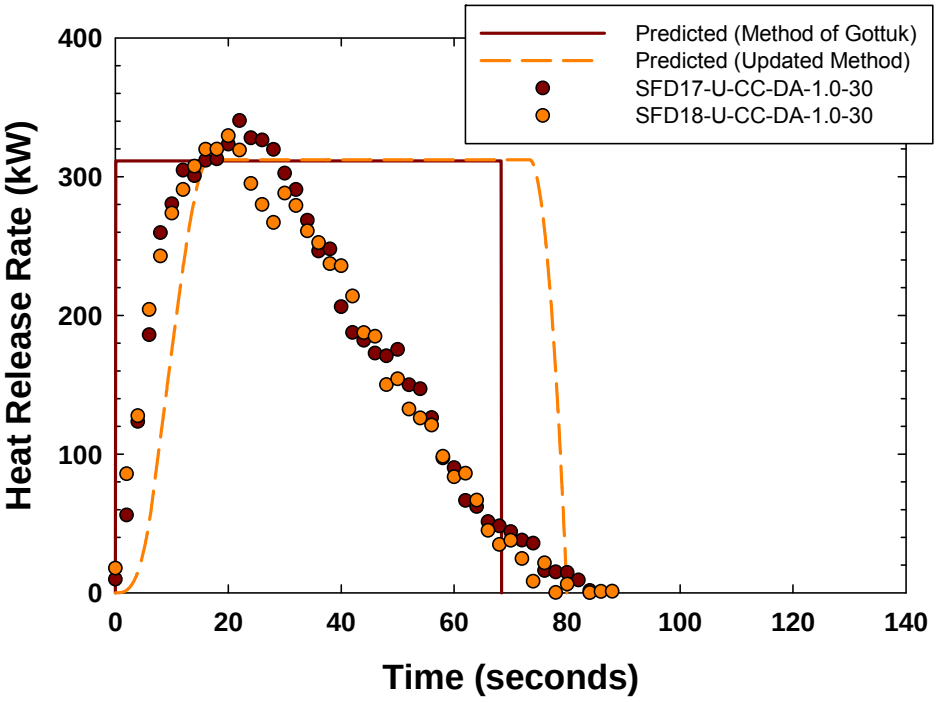


**Figure 6-24**
**1.0 L ethanol spill fires with a 30 second ignition delay – comparison of test data with the HRR prediction Methods 3 and 4 (coated concrete substrate)**

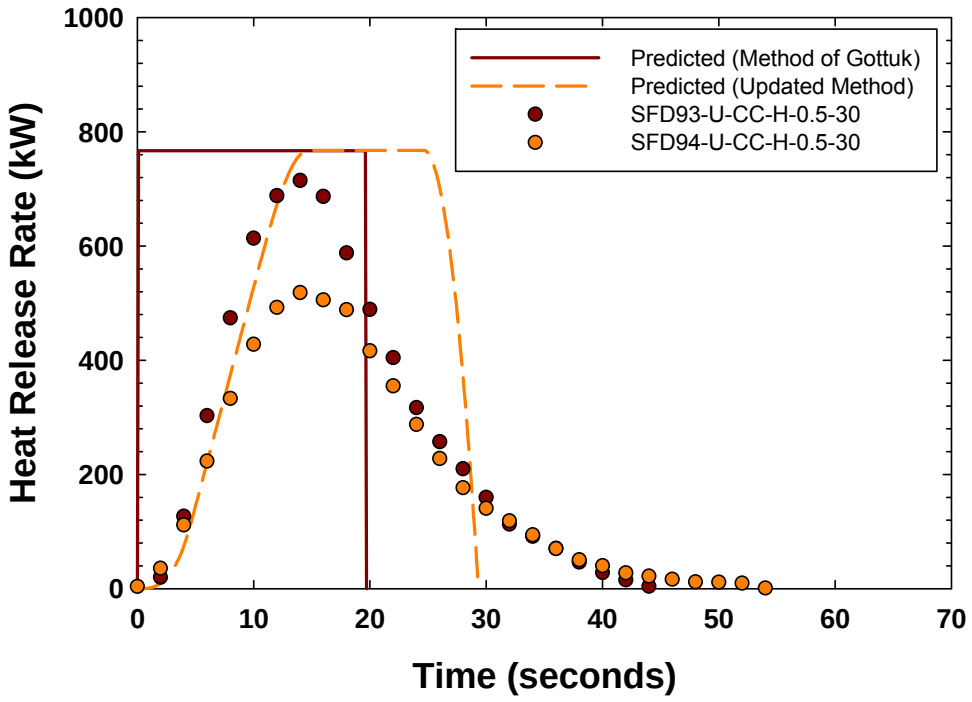


**Figure 6-25**
**0.5 L heptane spill fires with a 30 second ignition delay – comparison of test data with the HRR prediction Methods 3 and 4 (coated concrete substrate)**

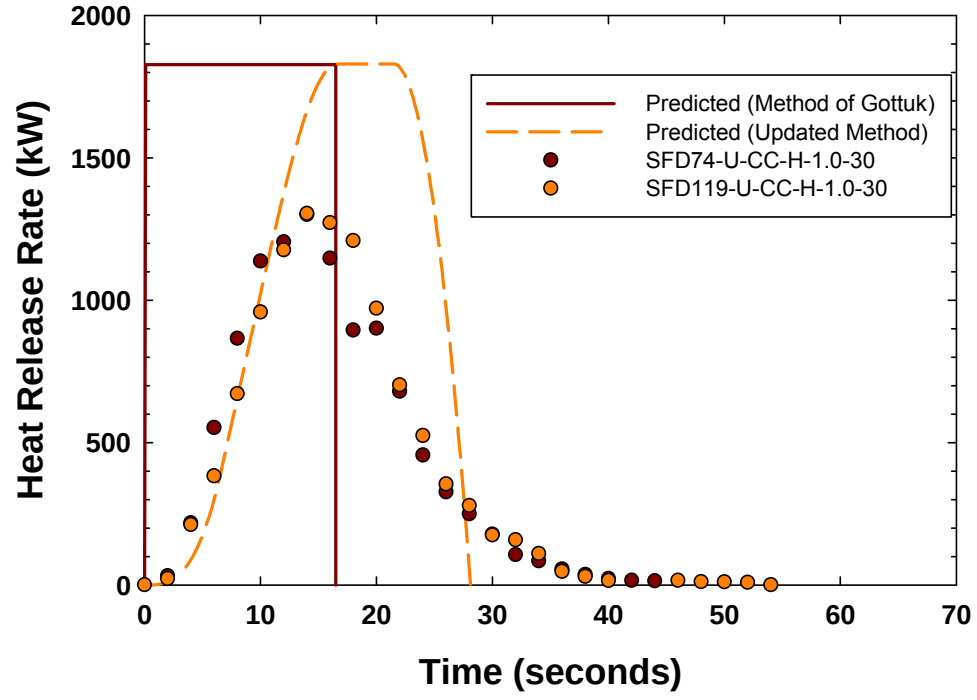


**Figure 6-26**
**1.0 L heptane spill fires with a 30 second ignition delay – comparison of test data with the HRR prediction Methods 3 and 4 (coated concrete substrate)**

Figures 6-21 through 6-26 indicate that the predicted peak HRR is similar for both Methods 3 and 4. However, the updated HRR model is shown to predict the growth stage of the fire accurately for the three fuels considered. The predicted peak HRRs are within 20% of the measured values for all tests except the 1 L heptane spill fires, which indicate the predicted values are about 35% greater than the measure values. Although the predicted peak HRR for the 0.5 L heptane spill fires is within 10% of the measured value, one of the tests presented in Figure 6-24 for the heptane had a warm substrate (see Figure 5-22). The test with the cool substrate data in Figure 6-25 shows a similar over-predicted HRR percentage as the 1.0 L spill fire comparisons shown in Figure 6-26.

It is clear, however, that under-predicted portions of the fire duration are at the end of the decay stage in all cases, indicating that the method as applied to these fuels will yield a conservative result when applied to a target thermal response or an enclosure temperature model. In addition, in situations where the HRR growth stage is an integral aspect of the analysis, the updated model will yield an accurate representation of HRR development on the spill fire.

The model predictions and experimental results provided in Figures 6-21 through 6-26 can be compared following the statistical guidance provided in NUREG-1934 [11]. Using this approach, the model bias indicates the ratio that the model will over- or under-predict the observed experimental result (see Appendix C.3) [11]. The model bias for each of the four models is provided in Figure 6-27. A model bias of 1.0 would indicate perfect agreement between the model and the experiment on average as indicated by the solid black line in Figure 6-27.

Note that Methods 1 and 2 demonstrate considerable over-prediction of the peak HRR (by a factor of approximately 3 on average) and considerable under-prediction of the burning duration, as previously discussed. Methods 3 and 4 produce improved predictions, where the peak HRR is approximately 7% over-predicted, and the burning duration predictions are considerably improved, with Method 4 producing the best predictions. The results of the evaluation are provided in Table 6-4, which also demonstrate that the model relative standard deviation for Method 4 to be the lowest. This indicates that Method 4 will provide the most accurate and reliable prediction of the thin spill fire behavior, followed by Method 3, which demonstrates very good performance.

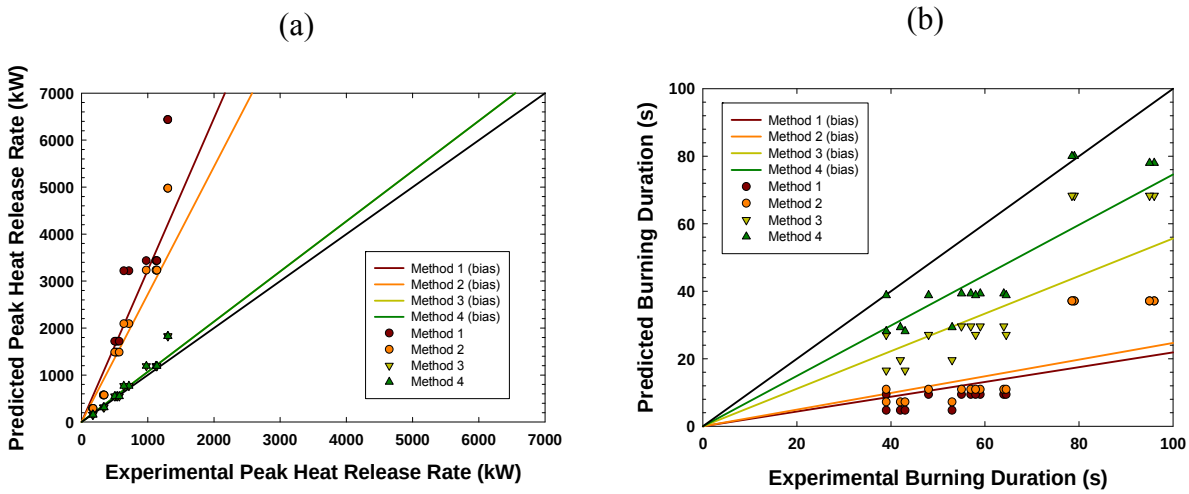


**Figure 6-27**
**(a) Model bias evaluation of the predicted peak HRR for liquid spill fires in Figures 6-21 through 6-26, (b) Model bias evaluation of the predicted burning duration for liquid spill fires in Figures 6-21 through 6-26**

**Table 6-4**
**Model bias and uncertainty for liquid spill fires in Figures 6-21 through 6-26 evaluated using guidance in NUREG-1934 [11]**

| Model Output | Statistic | Method 1 | Method 2 | Method 3 | Method 4 |
|---|---|---|---|---|---|
| Peak HRR | Model bias, $\delta$ | 3.232 | 2.717 | 1.068 | 1.068 |
| | Model relative standard deviation, $\tilde{\sigma}_M$ | 0.377 | 0.264 | 0.095 | 0.095 |
| Burning duration | Model bias, $\delta$ | 0.219 | 0.246 | 0.556 | 0.746 |
| | Model relative standard deviation, $\tilde{\sigma}_M$ | 0.528 | 0.392 | 0.255 | 0.158 |

### 6.1.3.3 Model Parameter Uncertainty

The input parameter uncertainty associated with Methods 3 and 4 may be quantified using the observed experimental uncertainty for the liquid spill depth, the mass burning rate, the depth empirical constant ($C_\delta$), and the fire diameter empirical constant ($k\beta$). The parameter uncertainty will be evaluated using the techniques described in NUREG-1934 (Reference 11 and Appendix C.3) for the impact on the model bias and standard deviation. A baseline input parameter is selected as the recommended values reported in Reference 1, and the minimum and maximum observed parameters will be evaluated to quantify the model uncertainty.

#### *6.1.3.3.1 Spill Depth Uncertainty*

The uncertainty in the spill depth of a particular fuel is provided in Table 5-4. In particular:

- A generic fuel has a spill depth of 0.72 mm with a standard deviation of 0.34 mm and an absolute range of 0.22–2.4 mm.
- Lubricating oil has a spill depth of 1.54 mm with a standard deviation of 0.55 mm and an absolute range of 0.86–2.4 mm.

The distribution of the spill depths is expected to be somewhat asymmetric about the average value, indicating that the standard deviation based on a normal distribution is not the ideal statistical metric. This is apparent when considering the 97$^{th}$ percentile range of spill fires (that is, two standard deviations) for the generic fuel, which yields a value of 0.04–1.4 mm. When considering more than one standard deviation, it is most practical to consider the entire range measured, or 0.22–2.4 mm. This produces a family of HRR profiles: one for the minimum depth, one for the average depth, and one for the maximum depth.

A smaller spill thickness produces a large fire surface area, which tends to increase the HRR and decrease the fire duration. However, for thin spills, decreasing the spill thickness results in a smaller depth coefficient, which has the opposite effect. As such, the overall effect on the HRR and fire duration is not obvious. In addition, the most adverse or limiting case is not necessarily the scenario that generates the highest peak HRR. As shown in Section 6.1.2, lower HRR fires with a longer duration may be more severe. As such, the fire effects will need to be explicitly computed in order to determine which scenario is limiting.

Since this parameter uncertainty is the spill depth directly, it will be evaluated against the spill fires from Section 5.4.1.3 only. The model predictions and experimental results provided in Figures 6-21 through 6-26 can be compared following the statistical guidance provided in NUREG-1934 [11]. Using this approach, the model bias indicates the ratio that the model will over- or under-predict the observed experimental result, on average (see Appendix C.3). The model bias for the baseline parameter, and the two bounding sensitivity parameters is provided in Figures 6-28 and 6-29. A model bias of 1.0 would indicate perfect agreement between the model and the experiment on average as indicated by the solid black line in the figures.

Figure 6-28 evaluates the sensitivity for Method 3, which shows that the baseline assumption produces the most accurate peak HRR prediction, but increased spill depth may improve the results for both HRR and duration. Figure 6-29 evaluates the sensitivity for Method 4, which also shows that the baseline assumption produces the most accurate peak HRR prediction, but increased spill depth may improve the results for both HRR and duration. The results of the evaluation are provided in Table 6-5.

Note that these results show that there is significant overlap between the confidence interval of the baseline evaluation and the two extreme sensitivity cases. This indicates that the selected input parameter is appropriate, although increasing the assumed spill depth may marginally improve the result. Given that the baseline parameter selection is slightly conservative, it is likely the most appropriate choice.

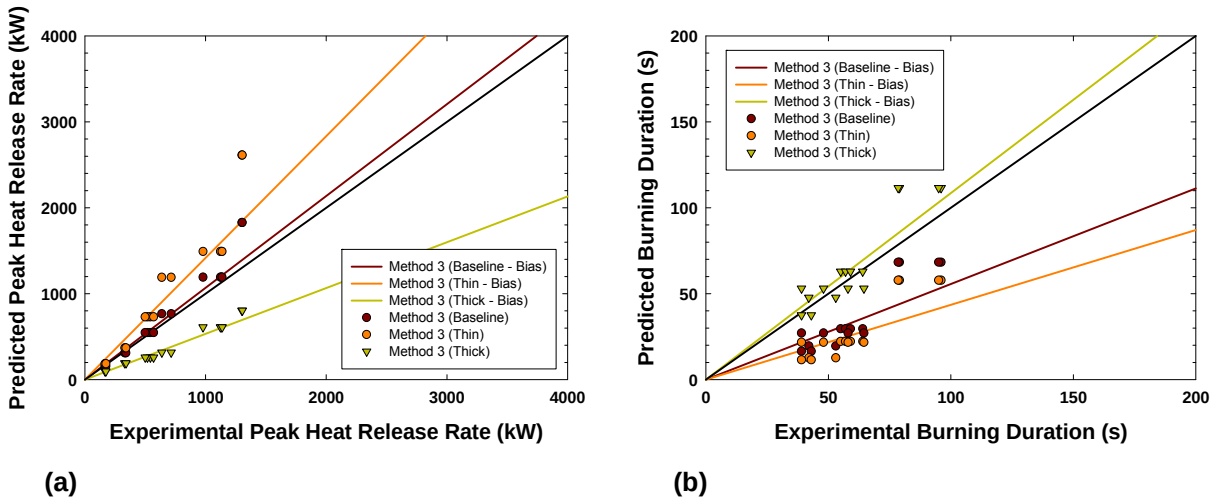


**Figure 6-28**
**(a) Model spill depth uncertainty evaluation of the predicted peak HRR for liquid spill fires in Figures 6-21 through 6-26 (Method 3), (b) Model spill depth uncertainty evaluation of the predicted burning duration for liquid spill fires in Figures 6-21 through 6-26 (Method 3)**

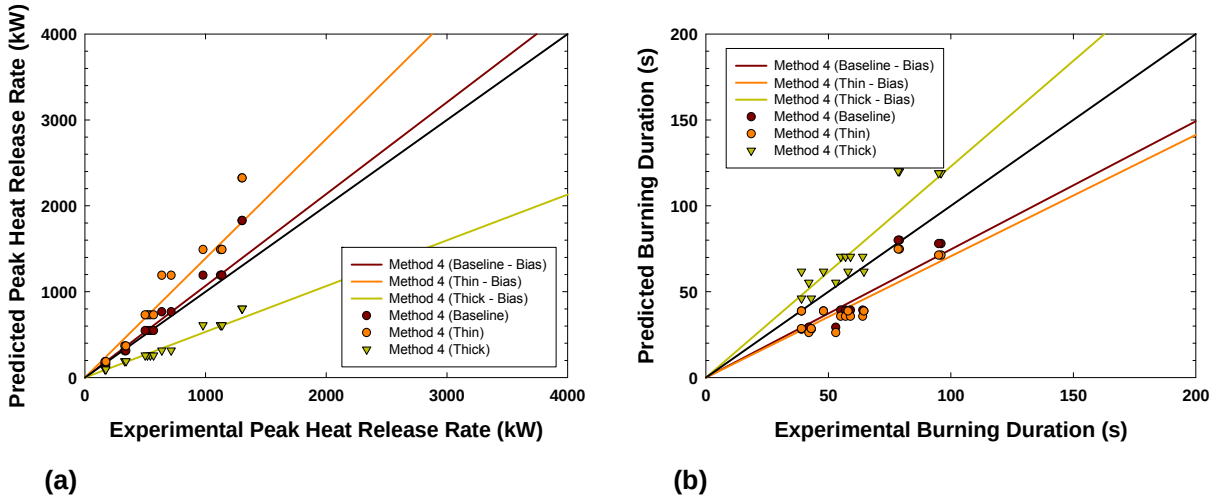


**Figure 6-29**
**(a) Model spill depth uncertainty evaluation of the predicted peak HRR for liquid spill fires in Figures 6-21 through 6-26 (Method 4), (b) Model spill depth uncertainty evaluation of the predicted burning duration for liquid spill fires in Figures 6-21 through 6-26 (Method 4)**

**Table 6-5**
**Model bias and uncertainty for spill depth evaluated using guidance in NUREG-1934 [11]**

| Model Output | Statistic | Method 3 | Method 4 |
|---|---|---|---|
| Peak HRR (0.72 mm baseline) | Model bias, $\delta$ | 1.068 | 1.068 |
| | Model relative standard deviation, $\tilde{\sigma}_M$ | 0.095 | 0.095 |
| Peak HRR (0.22 mm thin) | Model bias, $\delta$ | 1.417 | 1.389 |
| Peak HRR (2.4 mm thick) | Model bias, $\delta$ | 0.533 | 0.533 |
| Burning duration (0.72 mm baseline) | Model bias, $\delta$ | 0.556 | 0.746 |
| | Model relative standard deviation, $\tilde{\sigma}_M$ | 0.255 | 0.158 |
| Burning duration (0.22 mm thin) | Model bias, $\delta$ | 0.435 | 0.707 |
| Burning duration (2.4 mm thick) | Model bias, $\delta$ | 1.086 | 1.229 |

#### *6.1.3.3.2 Depth Coefficient Uncertainty*

The depth coefficient for gasoline, kerosene, heptane, and ethanol given by Equations 5-3a and b are based on an empirical curve fit that captures the average burning rate. Maximum and minimum bound correlations are provided in Figures 5-13 and 5-14 of this report and are as follows for gasoline, heptane, and ethanol [1]:

- $C_\delta = 0.85\left(1 - e^{-0.46\delta}\right)$ (minimum)
- $C_\delta = 0.95\left(1 - e^{-0.71\delta}\right)$ (average or baseline)
- $C_\delta = 1.07\left(1 - e^{-1.59\delta}\right)$ (maximum)

where all terms have been defined.

Similarly, the correlation range for kerosene is given as follows [1]:

- $C_\delta = 0.76\left(1 - e^{-0.29\delta}\right)$ (minimum)
- $C_\delta = 0.91\left(1 - e^{-0.58\delta}\right)$ (average or baseline)
- $C_\delta = 1.1\left(1 - e^{-1.49\delta}\right)$ (maximum)

where all terms have been defined.

The depth coefficient primarily affects the predicted burning behavior of thin spill fires, that is, spill depths less than about 2 mm. When the depth coefficient is increased, both the predicted HRR and the fire duration decrease and vice versa. Because the correlations span the test data range, they may be viewed as providing 98$^{th}$ percentile limits on this parameter.

The parameter uncertainty will be evaluated against the pan fires from Section 5.4.1.2 and the spill fires from Section 5.4.1.3. The model predictions and experimental results provided in Figures 6-14 through 6-26 can be compared following the statistical guidance provided in NUREG-1934 [11]. Using this approach, the model bias indicates the ratio that the model will over- or under-predict the observed experimental result (See Appendix C.3). The model bias for the baseline parameter and the two bounding sensitivity parameters is provided in Figures 6-30 and 6-31. A model bias of 1.0 would indicate perfect agreement between the model and the experiment on average as indicated by the solid black line in the figures.

Figure 6-30 evaluates the sensitivity for Method 3, which shows that the minimum depth coefficient assumption produces the most accurate peak HRR prediction; however, the line is still within the scatter of the baseline evaluation. Figure 6-31 evaluates the sensitivity for Method 4, which also shows that the minimum depth coefficient assumption produces the most accurate peak HRR prediction, but also within the scatter of the baseline evaluation. The results of the evaluation are provided in Table 6-6.

Note that these results show that there is significant overlap between the confidence interval of the baseline evaluation and the two extreme sensitivity cases. This indicates that the selected input parameter is appropriate, although selecting the minimum depth coefficient may marginally improve the result. Given that the baseline parameter selection is slightly conservative, it is likely the most appropriate choice.

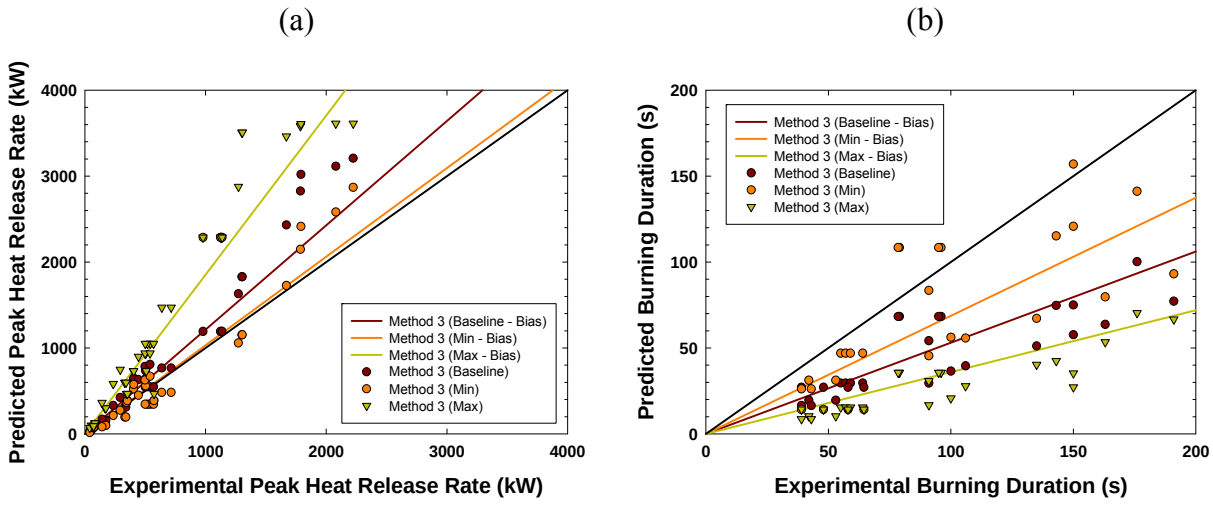


**Figure 6-30**
**(a) Model depth coefficient uncertainty evaluation of the predicted peak HRR for liquid spill fires in Figures 6-14 through 6-26 (Method 3), (b) Model depth coefficient uncertainty evaluation of the predicted burning duration for liquid spill fires in Figures 6-14 through 6-26 (Method 3)**

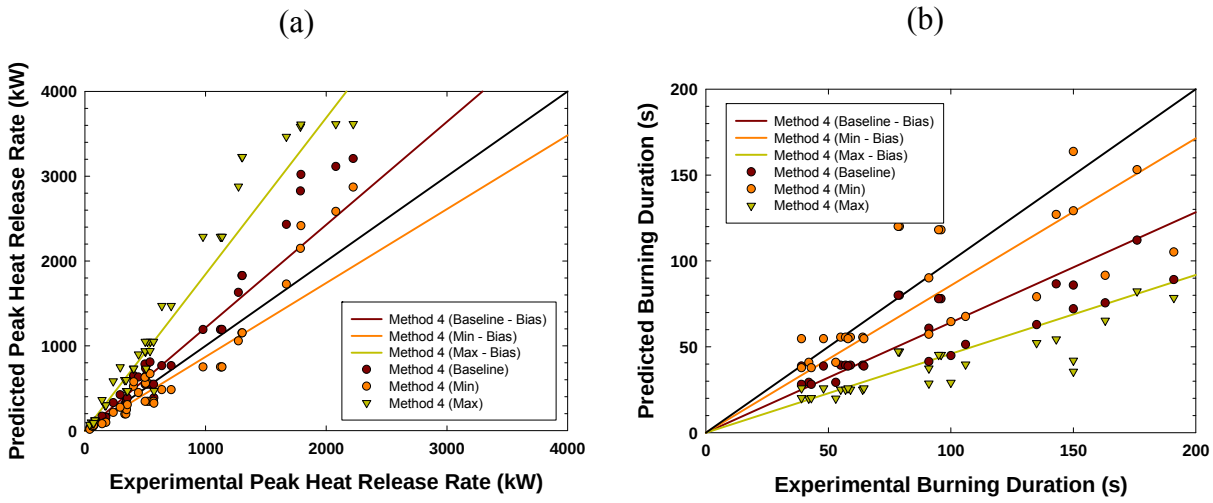


**Figure 6-31**
**(a) Model depth coefficient uncertainty evaluation of the predicted peak HRR for liquid spill fires in Figures 6-14 through 6-26 (Method 4), (b) Model depth coefficient uncertainty evaluation of the predicted burning duration for liquid spill fires in Figures 6-14 through 6-26 (Method 4)**

**Table 6-6**
**Model bias and uncertainty for depth coefficient evaluated using guidance in NUREG-1934 [11]**

| Model Output | Statistic | Method 3 | Method 4 |
|---|---|---|---|
| Peak HRR ($C_\delta$ baseline) | Model bias, $\delta$ | 1.214 | 1.215 |
| | Model relative standard deviation, $\tilde{\sigma}_M$ | 0.214 | 0.215 |
| Peak HRR ($C_\delta$ minimum) | Model bias, $\delta$ | 1.031 | 0.870 |
| Peak HRR ($C_\delta$ maximum) | Model bias, $\delta$ | 1.853 | 1.844 |
| Burning duration ($C_\delta$ baseline) | Model bias, $\delta$ | 0.556 | 0.746 |
| | Model relative standard deviation, $\tilde{\sigma}_M$ | 0.255 | 0.158 |
| Burning duration ($C_\delta$ Minimum) | Model bias, $\delta$ | 0.687 | 0.857 |
| Burning duration ($C_\delta$ Maximum) | Model bias, $\delta$ | 0.360 | 0.459 |

#### 6.1.3.3.3 Maximum Mass Burning Rate Uncertainty

The maximum mass burning rate, $\dot{m}''_{\infty}$, is based on an average value among various test data. The range for this parameter is provided in Table 5-5 for the fuels considered in this report. They are summarized as follows:

- Gasoline (baseline 0.055 kg/m²-s): 0.053–0.057 kg/m²-s (±3.6%)
- Kerosene (baseline 0.039 kg/m²-s): 0.036–0.042 kg/m²-s (±7.7%)
- Heptane (baseline 0.101 kg/m²-s): 0.092–0.119 kg/m²-s (-8.9%–17.8%)
- Fuel oil (lubricating oil) (baseline 0.035 kg/m²-s): 0.032–0.038 kg/m²-s (±8.6%)

When the maximum mass burning rate is increased, the predicted HRR increases and the burning duration decreases. The reverse is true when the maximum mass burning rate is decreased. Because the value range represents the observed test data range, it may be viewed as a 98$^{th}$ percentile range for the parameter. Note that the relative change of the burning rate parameter, relative to the baseline, is only approximately ±5%–10%, with the exception of heptane. Changing this parameter in the HRR models will have an equivalent and proportional effect of approximately ±5%–10%. Given the existing model standard deviation of 10%–15% for HRR and burning duration, it is clear that the variation in the maximum burning rate parameter is well within the existing uncertainty of the model. This indicates that the selected input parameter is appropriate, and no further analysis of the model sensitivity is required.

#### 6.1.3.3.4 Fire Diameter Empirical Constant Uncertainty

The fire diameter empirical constant, $k\beta$, is based on an average value among various test data. The range for this parameter is provided in Table 5-5 for the fuels considered in this report. They are summarized as follows:

- Gasoline (baseline 2.1 m$^{-1}$): 1.8–2.4 m$^{-1}$
- Kerosene (baseline 3.5 m$^{-1}$): 2.7–4.3 m$^{-1}$
- Heptane (baseline 1.1 m$^{-1}$): 0.8–1.4 m$^{-1}$
- Fuel oil (lubricating oil) (baseline 1.7 m$^{-1}$): 1.1–2.3 m$^{-1}$

When the fire diameter depth constant is increased, the mass burning rate increases. The effect is most pronounced for small diameter fires and diminishes to nearly zero for liquid fuel fires with diameters greater than 1–3 m. The reverse is true when the fire diameter depth constant is increased. Because the value range represents the observed test data range, it may be viewed as a 98$^{th}$ percentile range for the parameter.

The parameter uncertainty will be evaluated against the pan fires from Section 5.4.1.2 and the spill fires from Section 5.4.1.3, although the ethanol results have been excluded because there is no observed diameter dependence on the mass burning rate. The model predictions and experimental results provided in Figures 6-14 through 6-26 can be compared following the statistical guidance provided in NUREG-1934 [11]. Using this approach, the model bias indicates the ratio that the model will over- or under-predict on average the observed experimental result

(see Appendix C.3). The model bias for the baseline parameter and the two bounding sensitivity parameters is provided in Figures 6-32 and 6-33. A model bias of 1.0 would indicate perfect agreement between the model and the experiment on average as indicated by the solid black line in the figures.

Figure 6-32 evaluates the sensitivity for Method 3, which shows that the minimum diameter empirical constant assumption produces the most accurate peak HRR prediction; however, the line is still within the scatter of the baseline evaluation. Figure 6-33 evaluates the sensitivity for Method 4, which also shows that the minimum depth coefficient assumption produces the most accurate peak HRR prediction, but also within the scatter of the baseline evaluation. The results of the evaluation are provided in Table 6-7.

Note that these results show that there is significant overlap between the confidence interval of the baseline evaluation and the two extreme sensitivity cases. This indicates that the selected input parameter is appropriate, although selecting the minimum diameter empirical constant may marginally improve the result. Given that the baseline parameter selection is slightly conservative, it is likely the most appropriate choice.

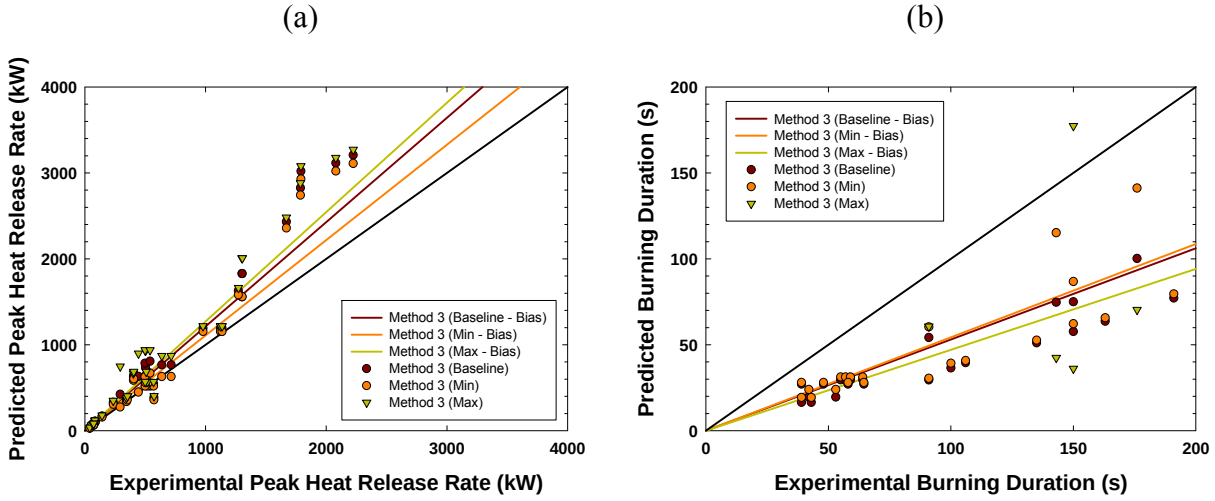


**Figure 6-32**
**(a) Model diameter empirical constant uncertainty evaluation of the predicted peak HRR for liquid spill fires in Figures 6-14 through 6-26 (Method 3), (b) Model diameter empirical constant uncertainty evaluation of the predicted burning duration for liquid spill fires in Figures 6-14 through 6-26 (Method 3)**

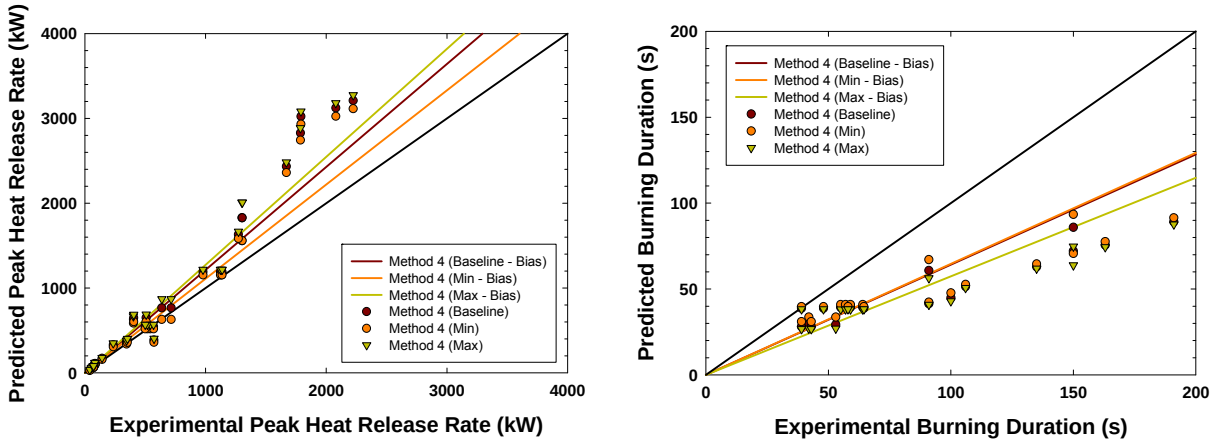


**Figure 6-33**
**(a) Model diameter empirical constant uncertainty evaluation of the predicted peak HRR for liquid spill fires in Figures 6-14 through 6-26 (Method 4), (b) Model diameter empirical constant uncertainty evaluation of the predicted burning duration for liquid spill fires in Figures 6-14 through 6-26 (Method 4)**

**Table 6-7**
**Model bias and uncertainty for diameter empirical constant evaluated using guidance in NUREG-1934 [11]**

| Model Output | Statistic | Method 3 | Method 4 |
|---|---|---|---|
| Peak HRR ($k\beta$ baseline) | Model bias, $\delta$ | 1.214 | 1.215 |
| | Model relative standard deviation, $\tilde{\sigma}_M$ | 0.214 | 0.215 |
| Peak HRR ($k\beta$ minimum) | Model bias, $\delta$ | 1.109 | 1.110 |
| Peak HRR ($k\beta$ maximum) | Model bias, $\delta$ | 1.272 | 1.273 |
| Burning duration ($k\beta$ baseline) | Model bias, $\delta$ | 0.531 | 0.642 |
| | Model relative standard deviation, $\tilde{\sigma}_M$ | 0.217 | 0.248 |
| Burning duration ($k\beta$ minimum) | Model bias, $\delta$ | 0.543 | 0.646 |
| Burning duration ($k\beta$ maximum) | Model bias, $\delta$ | 0.471 | 0.574 |

#### 6.1.3.3.5 Flame Spread Velocity

The flame spread velocity, $v$, is based on a characteristic value observed among various test data. The range for this parameter is discussed in Section 6.1.1.4 for the fuels considered in this report. The surface flame spread rate for combustible and flammable liquids is typically between 5 and 10 cm/s, with the faster spread rates associated with the lower flashpoint fuels [3]. Flame spread rates can approach 100 cm/s for flammable liquids that are heated to nearly the flashpoint temperature [3]. In the cases considered in this report, which are typical of those postulated in NPPs, the flame spread rates are expected to be within the 5–10 cm/s range. The recommended values and sensitivity range are summarized as follows:

- Gasoline (baseline 10 cm/s): 5–100 cm/s
- Ethanol (baseline 10 cm/s): 5–100 cm/s
- Kerosene (baseline 5 cm/s): 5–100 cm/s
- Heptane (baseline 10 cm/s): 5–100 cm/s
- Fuel oil (lubricating oil) (baseline 5 cm/s): 5–100 cm/s

When the flame spread velocity is increased, the fire growth rate increases. The result is that the fire will reach its peak burning rate quickly and consume the fuel faster. When the flame spread velocity is decreased, the opposite may be true, depending on the relative timescales discussed in Section 6.1.1.4. In many cases, the peak HRR of the fire will be unchanged by this parameter, and only the burning duration will be affected by this sensitivity.

This parameter uncertainty applies only to Method 4. The model predictions and experimental results provided in Figures 6-14 through 6-26 can be compared following the statistical guidance provided in NUREG-1934 [11]. Using this approach, the model bias indicates the ratio that the model will over- or under-predict the observed experimental result. The model bias for the baseline parameter and the two bounding sensitivity parameters is provided in Figure 6-34. A model bias of 1.0 would indicate perfect agreement between the model and the experiment on average as indicated by the solid black line in the figures (see Appendix C.3).

Figure 6-34 evaluates the sensitivity for Method 4, which shows that the peak HRR prediction is very insensitive to the assumed flame spread velocity. The burning duration is similarly insensitive to the flame spread velocity, but the slower flame speed produces marginally better predictions. The results of the evaluation are provided in Table 6-8. Note that these results show that there is significant overlap between the confidence interval of the baseline evaluation and the two extreme sensitivity cases. This indicates that the selected input parameter is appropriate, although selecting the minimum flame spread velocity may marginally improve the result. Given that the baseline parameter was selected to accurately match the observed fire growth behavior, it is considered the most appropriate input value. However, a default value of 10 cm/s is an appropriate starting point for fuels with unknown characteristics because the model is largely insensitive to this input parameter.

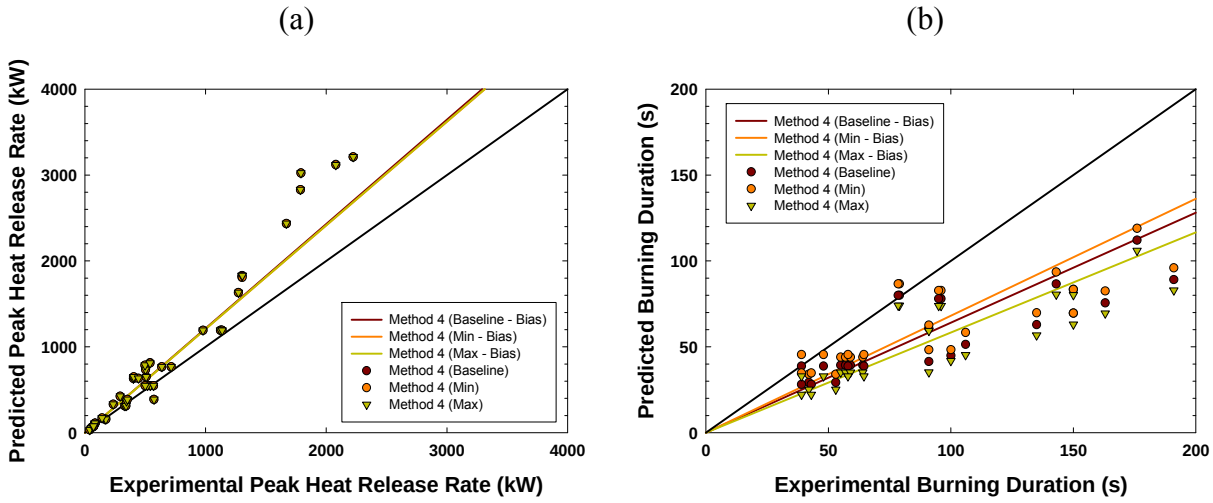


**Figure 6-34**
**(a) Model flame spread velocity uncertainty evaluation of the predicted peak HRR for liquid spill fires in Figures 6-14 through 6-26 (Method 4), (b) Model flame spread velocity uncertainty evaluation of the predicted burning duration for liquid spill fires in Figures 6-14 through 6-26 (Method 4)**

**Table 6-8**
**Model bias and uncertainty for flame spread velocity evaluated using guidance in NUREG-1934 [11]**

| Model Output | Statistic | Method 4 |
|---|---|---|
| Peak HRR ($v$ baseline) | Model bias, $\delta$ | 1.215 |
| | Model relative standard deviation, $\tilde{\sigma}_M$ | 0.215 |
| Peak HRR ($v$ minimum) | Model bias, $\delta$ | 1.207 |
| Peak HRR ($v$ maximum) | Model bias, $\delta$ | 1.207 |
| Burning duration ($v$ baseline) | Model bias, $\delta$ | 0.642 |
| | Model relative standard deviation, $\tilde{\sigma}_M$ | 0.248 |
| Burning duration ($v$ minimum) | Model bias, $\delta$ | 0.681 |
| Burning duration ($v$ maximum) | Model bias, $\delta$ | 0.583 |

#### 6.1.3.3.6 Fire Growth Lag Time

The fire growth lag time, $t_{lag}$, is based on a characteristic value observed among various test data. The range for this parameter is discussed in Section 6.1.1.4 for the fuels considered in this report. Based on the time to reach the peak HRR shown in Figures 5-15 through 5-27, the localized HRR ramping time is on the order of 10–30 seconds. The recommended values and sensitivity range are summarized as follows:

- Gasoline (baseline 10 s): 5–30 s
- Ethanol (baseline 10 s): 5–30 s
- Kerosene (baseline 10 s): 5–30 s
- Heptane (baseline 10 s): 5–30 s
- Fuel oil (lubricating oil) (baseline 10 s): 5–30 s

Note that a 5 second minimum is assumed in order to capture a faster ramp up time than observed. When the fire growth lag time is decreased, the fire growth rate increases. The result is that the fire will reach its peak burning rate quickly and consume the fuel faster. When the fire growth lag time is increased, the opposite may be true, depending on the relative timescales discussed in Section 6.1.1.1. In many cases, the peak HRR of the fire will be unchanged by this parameter, and only the burning duration will be affected by this sensitivity. Because the value range represents the observed test data range, it may be viewed as a 98$^{th}$ percentile range for the parameter.

This parameter uncertainty applies only to Method 4. The model predictions and experimental results provided in Figures 6-14 through 6-26 can be compared following the statistical guidance provided in NUREG-1934 [11]. Using this approach, the model bias indicates the ratio that the model will over- or under-predict the observed experimental result. The model bias for the baseline parameter and the two bounding sensitivity parameters is provided in Figure 6-35. A model bias of 1.0 would indicate perfect agreement between the model and the experiment on average as indicated by the solid black line in the figures (see Appendix C.3).

Figure 6-35 evaluates the sensitivity for Method 4, which shows that the peak HRR prediction is very insensitive to the assumed fire growth lag time. The burning duration is similarly insensitive to the fire growth lag time, but the longer fire growth lag time produces marginally better predictions. The results of the evaluation are provided in Table 6-9. Note that these results show that there is significant overlap between the confidence interval of the baseline evaluation and the two extreme sensitivity cases. This indicates that the selected baseline input parameter is appropriate, although selecting the longest fire growth lag time may marginally improve the result. However, the baseline default value of 10 seconds is an appropriate starting point for fuels with unknown characteristics because the model is largely insensitive to this input parameter.

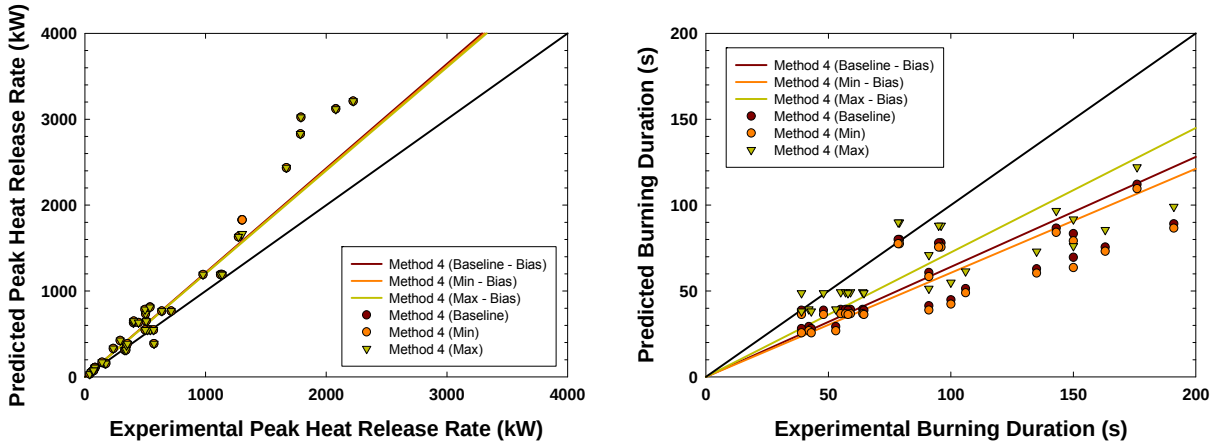


**Figure 6-35**
**(a) Model fire growth lag time uncertainty evaluation of the predicted peak HRR for liquid spill fires in figures 6-14 through 6-26 (Method 4), (b) Model fire growth lag time uncertainty evaluation of the predicted burning duration for liquid spill fires in Figures 6-14 through 6-26 (Method 4)**

**Table 6-9**
**Model bias and uncertainty for fire growth lag time evaluated using guidance in NUREG-1934 [11]**

| Model Output | Statistic | Method 4 |
|---|---|---|
| Peak HRR ($t_{lag}$ baseline) | Model bias, $\delta$ | 1.215 |
| | Model relative standard deviation, $\tilde{\sigma}_M$ | 0.215 |
| Peak HRR ($t_{lag}$ minimum) | Model bias, $\delta$ | 1.207 |
| Peak HRR ($t_{lag}$ maximum) | Model bias, $\delta$ | 1.201 |
| Burning duration ($t_{lag}$ baseline) | Model bias, $\delta$ | 0.642 |
| | Model relative standard deviation, $\tilde{\sigma}_M$ | 0.248 |
| Burning duration ($t_{lag}$ minimum) | Model bias, $\delta$ | 0.606 |
| Burning duration ($t_{lag}$ maximum) | Model bias, $\delta$ | 0.725 |

#### *6.1.3.3.7 Experimental Uncertainty*

The uncertainty associated with HRR measurements obtained using calorimeters is on the order of 7%–12% with a total uncertainty in the HRR measurement of up to 23% according to Reference 19. When viewed as a random variable, the general impact of this uncertainty should be reflected in the repeated tests with the same spill or pool configuration. The experimental uncertainty is considered in the NUREG-1934 approach detailed above, by assuming that the normalized experimental standard deviation is 10 %.

#### *6.1.3.3.8 Overall Treatment of Uncertainty*

The overall treatment of the uncertainty involves the variation of several parameters in order to identify the uncertainty range of the predicted HRR profile. The effort is further complicated by the fact that increasing the peak fire size decreases the fire duration, which means that the most conservative case is not intuitively obvious unless a maximum exposure time or HRR is known to be the limiting factor.

There are simplifications that may be made to the process of identifying a limiting HRR profile within the range of uncertainty. For example, a deep liquid pool fire that is confined and has a diameter greater than 3 m needs to consider only the uncertainty in the mass burning rate. Table 6-10 summarizes the uncertainty parameters that affect various liquid fuel fire scenarios. Table 6-11 summarizes the effect of the uncertainty variation in the parameters. Tables 6-10 and 6-11 may be used to identify the uncertainty parameters and the uncertainty direction that should be postulated to maximize or minimize the HRR and fire duration.

**Table 6-10**
**Uncertainty parameters applicable to various liquid fuel fire scenarios**

| Scenario Type | Spill Depth | Fire Diameter | Applicable Uncertainty Parameters |
|---|---|---|---|
| Confined | Deep (over ~2 mm) | Large (Over ~3 m) | Mass burning rate |
| | Deep (over ~2 mm) | Small (Under ~3 m) | Mass burning rate, fire diameter empirical constant |
| | Thin (under ~2 mm) | Large (Over ~3 m) | Mass burning rate<br>Depth constant |
| | Thin (Under ~2 mm) | Small (Under ~3 m) | Mass burning rate<br>Depth constant, fire diameter empirical constant |
| Unconfined | Deep (over ~2 mm) | Large (Over ~3 m) | Spill depth, mass burning rate |
| | Deep (over ~2 mm) | Small (Under ~3 m) | Spill depth, mass burning rate, fire diameter empirical constant |

**Table 6-10 (continued)**
**Uncertainty parameters applicable to various liquid fuel fire scenarios**

| Scenario Type | Spill Depth | Fire Diameter | Applicable Uncertainty Parameters |
|---|---|---|---|
| Unconfined (continued) | Thin (under ~2 mm) | Large (Over ~3 m) | Spill depth, mass burning rate<br>Depth constant |
| | Thin (Under ~2 mm) | Small (Under ~3 m) | Spill depth, mass burning rate<br>Depth constant, fire diameter empirical constant |

**Table 6-11**
**Uncertainty parameters applicable to various liquid fuel fire scenarios**

| Uncertainty Parameter | Parameter Variation | Effect on Peak HRR | Effect on Fire Duration |
|---|---|---|---|
| Spill depth | Increase | Indeterminate† | Indeterminate† |
| | Decrease | Indeterminate† | Indeterminate† |
| Mass burning rate | Increase | Increase | Decrease |
| | Decrease | Decrease | Increase |
| Fire diameter empirical constant | Increase | Increase | Decrease |
| | Decrease | Decrease | Increase |
| Depth constant | Increase | Increase | Decrease |
| | Decrease | Decrease | Increase |

†Increasing the spill depth decreases the surface area, which tends to decrease the HRR of the fire and decrease the fire duration, but it may also increase the value of the depth constant, which has the opposite effect.

The overall uncertainty of Methods 3 and 4 can be quantified using the method of addition of variances. This analysis assumes that any covariance is negligible; that is, the output quantity can be expressed as a system of independent variables. Following this assumption, a quantity $Q$ is expressed as a function of independent variables, $w_i$, written as:

$$Q = Q(w_1, w_2, \ldots, w_n) \qquad \textbf{Eq. 6-16}$$

The overall change in $Q$ associated with a change in all $w_i$ is expressed as a function of uncertainties, $\Delta w_i$, resulting in:

$$\Delta Q_{tot} = \sqrt{\sum_{i=1}^{n} \left(\frac{\partial Q_i}{\partial w_i} \Delta w_i\right)^2} \qquad \textbf{Eq. 6-17}$$

or approximated using the bias predictions as:

$$\frac{\Delta Q_{tot}}{Q} = \sqrt{\sum_{i=1}^{n} \left(\frac{\Delta \delta_i}{\delta}\frac{\Delta w_i}{w}\right)^2} \qquad \textbf{Eq. 6-18}$$

where the functional changes of the output parameters have been evaluated in Sections 6.1.3.3.1 through 6.1.3.3.7. Using this approach, the cumulative uncertainty of the predicted quantity can be approximated from the piecewise uncertainty of each input parameter. The result for the predicted peak HRR is that Method 3 is approximately ±57% and Method 4 is approximately ±57%. While these may seem high, they are comparable to the 98% confidence interval of $2\tilde{\sigma}_M$ from Tables 6-3 and 6-4. This can be interpreted as the model input parameter uncertainty being approximately equivalent to the observed experimental uncertainty.

The result for the predicted burning duration is considerably higher, since all models systematically under-predict the quantity, thus producing high uncertainty on the order of 88% for Method 3 and 62% for Method 4. This is due to the extended burning decay period observed experimentally that is not modeled in favor of a longer peak burning duration. Since this is conservatively bounding, the uncertainty in burning duration is considered acceptable.

### 6.1.3.4 Solution Results and Spreadsheet Development

The empirical HRR models described in Sections 6.1.1.3 and 6.1.1.4 may readily be incorporated into an analytical model for ease of implementation. They are well suited for inclusion in spreadsheet-type calculations, such as the FIVE calculation suite [12]. A spreadsheet-type model has not specifically been developed with this report, but it is expected that subsequent efforts with this approach will lead to a model that will be available for general use within the commercial nuclear industry.

The calculation of the HRR profile using Method 3 presented in Section 6.1.1.3 is straightforward and, thus, may be implemented in any spreadsheet as the calculation need arises. This is not the case with Method 4 presented in Section 6.1.1.4. The solution of the integral equation is best implemented in a spreadsheet using a macro construct involving various Visual Basic subroutines. Alternatively, the solution may be calculated using a computer language such as FORTRAN with a text input file to provide the empirical constants and initial conditions such as the fuel volume and spill depth. Because of the difficultly in solving the integral model,

Appendix C.2 of this report provides the full HRR profiles for different volumes of liquid fuels commonly found in commercial NPPs. The HRR profiles in Appendix C.2 are expected to encompass a significant portion of unconfined liquid fuel fire scenarios that may be postulated in commercial NPPs.

### 6.1.3.5 Summary

The pan fire HRR data and the spill fire HRR data provided in Reference 1 have been used to provide a validation basis for predicting the HRR profiles in liquid fuel fires using both the method of Gottuk et al. [1, 3] (Method 3) and the updated method that accounts for flame spread and fire growth (Method 4). The pan fire HRR data primarily consist of deep pool fires and are used to test the heat limiting behavior of the empirical HRR models. The characteristic dimension of the pans considered ranges from 0.3–1.2 m and the peak HRRs range from about

60–2,000 kW. It is shown that both methods predict similar results for deep pool burning, which is expected given that the transient growth stage is a short fraction of the overall fire scenario duration. The methods tend to over-predict the HRR for gasoline and ethanol fires and provide good predictions of the peak HRR for kerosene fires. The accuracy of the predictions in these cases is a function of the quality of the empirical burning rate parameters. The uncertainty range for these parameters is expected to account for a significant fraction of the over-predicted HRRs (see Table 5-5). Both models tend to under-predict the burning duration, in particular during the decay stage of the fire. Neither model was developed to accurately capture the decay stage of the fires and under-predict the duration of this stage of the fire. Nevertheless, for deep pool burning, it is considered conservative to slightly over-predict the HRR and under-predict the burning duration, especially during the decay stage of the fire. Because Method 3 [1, 3] is simpler and has fewer parameters, it is an adequate model for evaluating the HRR profile in deep pools, which are defined as those with a spill depth greater than 2 mm.

The spill fire HRR data consists of heptane, ethanol, and gasoline spill fires involving 0.5–1.0 L of fuel. The HRRs range from about 150 – 1,300 kW, and the fire durations are between 40–120 seconds. It is shown that both methods predict similar peak HRRs but that Method 4 accurately predicts the growth stage of the HRR profile, whereas Method 3 [1, 3] assumes an instantaneous growth stage. Both models under-predict the fire duration; however, Method 4 is significantly closer to the observed duration and misses only a small portion of the decay stage. The predictions of the peak HRR are within 20% of the measured values for all fuels considered, except heptane. In this case, the methods over-predict the peak HRR of heptane by about 35%. Because Method 4 accurately captures the growth stage of the fire and misses only a small portion of the decay stage, it is a conservative method to apply for spill fires. Spill fires are defined in this analysis as those with a depth less than 2 mm. Overall, both methods represent a significant improvement over the methods currently used in NUREG-1805 [7] and NUREG/CR-6850 [2] for thin liquid spill fires.

## 6.2 Implementation Guidance

### *6.2.1 Detailed Analysis Procedure*

Method 3 [1, 3] and Method 4 presented in this report may be used to determine the HRR profile in both deep pools and spill fires involving flammable liquids. The recommended approach for applying these methods is described using a number of simple steps:

**Step 1**. Determine the applicability of the analysis. The analysis is applicable to liquid fuel spills involving kerosene (diesel), gasoline, heptane, ethanol, and lubricating oils and substrate (that is, floor) temperatures less than 40°C. Fuels that have burning characteristics similar to those identified above may be evaluated using this approach provided the empirical constants for the fuels are known or are bound by the selected values. Additionally, the analysis is not applicable to continuously fed spill fires. If the application does not meet the applicability requirements, an alternative approach is recommended for determining the HRR profiles.

**Step 2**. Determine whether the fire is confined or unconfined. A confined spill fire is one that is postulated to occur within a curbed region around the spill source or within a well-defined cavity in a floor or the ground.

**Step 3a**. Determine the liquid spill depth.

If the liquid is confined, the spill depth is given using the following equation:

$$\delta = \frac{V}{A} \qquad \textbf{Eq. 6-19}$$

Where:

$\delta$ is the spill depth (m).

$V$ is the liquid volume ($m^3$).

$A$ is the area in which the liquid is confined ($m^2$).

Note that the confined area is equal to the area into which the fuel may accumulate. If fuel is spilled into a curbed region, this is equal to the area within the curbs minus the volume of obstructions such as a pedestal.

If the liquid is unconfined, the spill depth is 0.72 mm for kerosene, gasoline, heptane, and ethanol and 1.54 mm for lubricating oils. Note that the spill depth associated with a particular fuel may be selected in lieu of the generic value. Fuel-specific values are provided in Table 5-4 of this report.

**Step 3b**. Determine the liquid surface area.

If the liquid is confined, the spill area is equal to the confined area defined in Equation 6-19.

If the liquid spill is unconfined, the spill area is determined using the following equation:

$$A = \frac{V}{\delta} \qquad \textbf{Eq. 6-20}$$

where all terms have been defined.

**Step 4**. Determine the effective fire diameter. The fire diameter is determined using the following equation:

$$D_e = \sqrt{\frac{4A}{\pi}} \qquad \textbf{Eq. 6-21}$$

Where:

$D_e$ is the effective fire diameter (m).

$A$ is the liquid fuel surface area ($m^2$) as defined in Steps 3a and 3b.

**Step 5**. Select empirical model.

If the spill depth is greater than 2 mm, select Method 3 [1, 3], as defined using Equations 6-5 through 6-8.

If the spill depth is less than 2 mm, select Method 4 using Equations 6-9 through 6-13, with specific solutions provided in Table 6-2.

**Step 6**. Determine the number of HRR scenarios to consider.

If the fuel is gasoline, kerosene, heptane, or ethanol of any spill depth, then a single HRR scenario is required.

If the fuel is lubricating oil with a depth less than 1 mm or a depth greater than 2 mm, then a single HRR scenario is required.

If the fuel is lubricating oil with a depth between 1 mm and 2 mm, two HRR scenarios are suggested for analysis. Two HRR scenarios for lubricating oil spill fires with a depth between 1 and 2 mm are recommended because there is insufficient data to quantify the effect of the depth on the HRR. The two HRR scenarios, therefore, correspond to the minimum HRR as determined using a depth coefficient of 0.2 and to the maximum HRR as determined using a depth coefficient of 1.0 (see Step 8).

**Step 7**. Select the empirical parameters. The applicable empirical parameters are the heat of combustion, the maximum mass burning rate, the diameter constant, and the fuel density. These parameters are provided in Tables 6-1 and 5-5 for the fuels considered in this analysis.

**Step 8**. Determine the depth coefficient.

If the fuel is gasoline, heptane, or ethanol, the depth coefficient is determined using Equation 5-3a.

If the fuel is kerosene or diesel, the depth coefficient is determined using Equation 5-3b.

If the fuel is lubricating oil, the depth coefficient is 0.2 for spill depths less than 1 mm and 1.0 for depths greater than 2 mm.

If the lubricating oil spill depth is between 1 and 2 mm, one scenario should be postulated with a depth coefficient of 0.2, and one should be postulated with a depth coefficient of 1.0 as specified in Step 5.

**Step 9**. Determine the HRR profile for the single HRR scenario or both HRR scenarios, depending on the number required. If two HRR scenarios are defined, the most adverse scenario should be determined based on the evaluation of each scenario relative to the performance criteria of interest and selected as the basis for the particular application. If the empirical model selected is Method 3, then the peak HRR is constant and is determined using Equation 6-5. The fire duration is determined using Equation 6-8. If Method 4 is selected, the HRR and mass burning rate are time dependent and are determined through the solution of Equations 6-9 through 6-13 (see Table 6-2). Because this is not a simple model to implement, solutions for different volumes of common combustible and flammable liquids are provided in Appendix C.2

### *6.2.2 Example Calculations*

Two example applications are provided to illustrate the implementation of the analysis procedure steps. The examples involve both confined and unconfined spill fire scenarios using Methods 3 and 4.

### 6.2.2.1 Example 1

Example 1 provides a simple illustration of the HRR determination using Method 3.

#### *6.2.2.1.1 Scenario Background*

An evaluation is required to postulate a potential diesel spill fire to generate an HGL in a diesel generator room. As part of this evaluation, the HRR profile for a diesel spill fire, as characterized using kerosene, is a required input parameter.

The diesel generator room contains a single source of non-pressurized diesel fuel associated with a standby diesel generator. The maximum volume of diesel fuel that could spill is contained in a day tank having a capacity of 756 L. There is a curbed region surrounding the diesel generator that is capable of containing the maximum quantity of diesel fuel that could spill. The curbed area is approximately 6 × 4 m. The diesel generator is located in the center of the curbed area on a concrete pedestal that is approximately 2 × 1.5 m. The floor is flat and is constructed of concrete with an epoxy coating (that is, coated concrete). The ambient temperature in the area is 30°C, and the maximum temperature of the diesel fuel is expected to be less than 30°C. There are no floor drains in the general area, and the lubricating oil is unpressurized.

#### *6.2.2.1.2 Analysis*

**Step 1**. (Determine the analysis applicability.) The analysis is applicable because the floor temperature, assumed to be equal to the ambient temperature of the enclosure, and the diesel fuel temperature are both less than 40°C. In addition, the fuel is characterized as kerosene, which is one of the fuels for which this report provides data. Finally, a continuously fed spill fire is not postulated because a complete fuel spill is bounding.

**Step 2**. (Determine the type of liquid fuel fire.) A confined spill fire is postulated.

**Step 3a**. (Determine the spill depth.) The spill depth for the confined kerosene spill fire is determined using Equation 6-19. In this case, the spill area is equal to the area enclosed by the curbing (6 × 4 m or 24 m²) minus the area of the diesel generator pedestal (2 × 1.5 m or 3 m²), which is equal to 21 m². The fuel volume is 756 L or 0.756 m³, and the resulting spill depth for the confined kerosene fuel is 0.036 m or 36 mm.

**Step 3b**. (Determine the fuel surface area.) The fuel surface area of the confined kerosene spill is as determined in Step 3a, or 21 m².

**Step 4**. (Determine the effective fire diameter.) The effective fire diameter is determined using Equation 6-21 with the fire areas as determined in Step 3b. The liquid fuel surface area for the confined kerosene spill is 21 m² so that the effective fire diameter is 5.17 m.

**Step 5**. (Select the empirical model.) The spill depth for the confined kerosene spill fire is 36 mm, which is greater than 2 mm. As such, Method 3 is the applicable model for determining the HRR of the confined kerosene spill fire.

**Step 6**. (Determine the number of HRR scenarios.) The confined kerosene spill depth is 36 mm, which is greater than 2 mm. Only a single HRR scenario is needed to characterize the confined kerosene spill fire.

**Step 7**. (Select the empirical parameters.) The empirical diameter constant for kerosene fuel is 3.5 $m^{-1}$ for fuel oil as shown in Table 5-5. The maximum mass burning rate is 0.039 kg/m²-s as shown in Table 6-1. The fuel density is 820 kg/m³ as shown in Table 6-1, which is the average value of the reported range, and the fuel heat of combustion is 32,200 kJ/kg from Table 6-1.

**Step 8**. (Select the depth coefficients.) The depth coefficient for the confined kerosene spill fire HRR scenario is 1.0 (maximum value) since the depth is greater than 2 mm (see Section 5.4.1.2.2).

**Step 9**. (Determine the HRR profile.) The HRR profile for the confined kerosene spill fire is determined using Method 3 as described in Section 6.1.1.3, with a surface area as determined in Step 3b, the fire diameter as determined in Step 4, the empirical parameters selected in Step 7, and the depth coefficient set to 1.0 as shown in Step 8. The HRR profile for the confined kerosene spill fire is shown in Figure 6-36. The peak HRR is 26,400 kW, and the fire duration is about 757 seconds or 12.6 minutes.

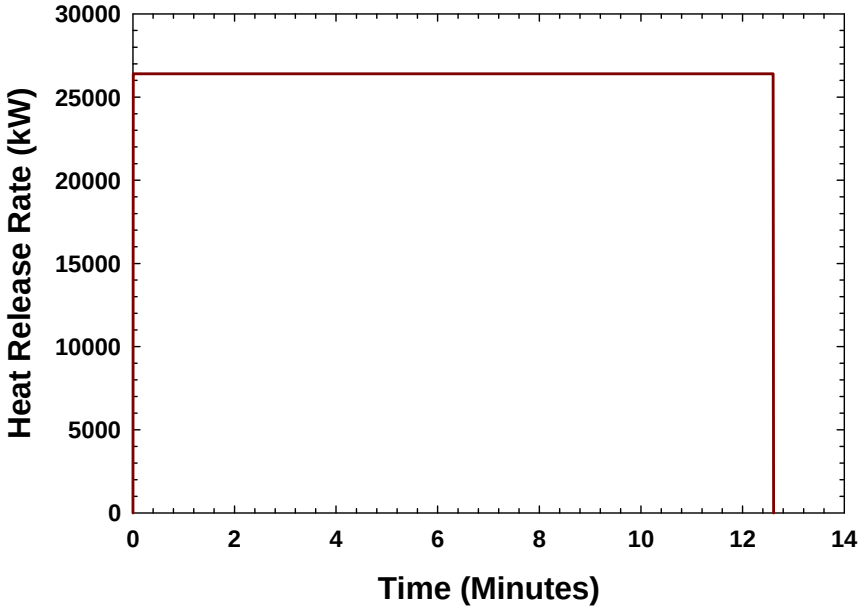


**Figure 6-36**
**HRR profiles for confined kerosene spill fires involving 756 L of fuel (Example 1)**

### 6.2.2.2 Example 2

Example 2 provides a more complex illustration of the HRR determination of an unconfined fuel spill and the potential mitigating effect provided by curbing. This represents a typical fuel spill fire analysis for a NPP application and involves the use of both Methods 3 and 4.

#### *6.2.2.2.1 Scenario Background*

An evaluation of the combustible inventory of a plant area identified a pump containing 37.8 L of lubricating oil. The area around the pump is not curbed and is free of obstructions, with the exception of a 0.6 × 0.9 m concrete pedestal beneath the pump. The floor is flat concrete and is constructed of concrete with an epoxy coating (that is, coated concrete). The ambient temperature

in the area is 25°C, and the maximum temperature of the lubricating oil is expected to be less than 30°C. There are no floor drains in the general area, and the lubricating oil is unpressurized. Several risk-significant raceway targets have been identified in the general area of the pump.

In order to quantify the contribution to plant risk posed by the lubricating oil, a pump fire scenario is required for analysis in the fire PRA. A preliminary assessment suggests that the risk contribution is likely to be significant; as such, a potential risk mitigating strategy has been proposed that involves providing a curb system around the pump to limit the spread of a lubricating oil fire and the total HRR that could be achieved. The proposed curb system fully encloses the pump and the pedestal and the dimensions are 1.83 × 1.83 m. Based on the preliminary assessment, the HRR profiles for an unconfined lubricant spill around the pump and a confined lubricant fire in the curbed area are needed to quantify the effects of a lubricant fire on plant risk as well as to determine the potential benefits of the proposed curb modification.

#### *6.2.2.2.2 Analysis*

**Step 1**. (Determine the analysis applicability.) The analysis is applicable because the floor temperature, assumed to be equal to the ambient temperature of the enclosure, and the oil temperature are both less than 40°C. In addition, the fuel is lubricating oil, which is one of the fuels for which this report provides data. Finally, a continuously fed spill fire is not postulated because a complete fuel spill is bounding.

**Step 2**. (Determine the type of liquid fuel fire.) Both unconfined and confined spill fires are postulated.

**Step 3a**. (Determine the spill depth.) The spill depth for the unconfined lubricating oil fire is 1.54 mm. The spill depth for the confined lubricating spill fire is determined using Equation 6-19. In this case, the spill area is equal to the area enclosed by the curbing (1.83 × 1.83 m or 3.35 m²) minus the area of the pedestal (0.6 × 0.9 m or 0.54 m²), which is equal to 2.81 m². The fuel volume is 37.8 L or 0.0378 m³, and the resulting spill depth for the confined lubricating fuel is 0.0135 m or 13.5 mm.

**Step 3b**. (Determine the fuel surface area.) The fuel surface area of the confined fuel spill is as determined in Step 3a, or 2.81 m². The fuel surface area of the unconfined fuel spill is determined using Equation 6-20. In this case, the spill depth is 1.54 mm, or 0.00154 m, and the fuel volume is 37.8 L or 0.0378 m³. The resulting fuel surface area of the unconfined lubricant spill is, thus, 24.5 m².

**Step 4**. (Determine the effective fire diameter.) The effective fire diameter is determined using Equation 6-21 with the fire area as determined in Step 3b. The liquid fuel surface area for the unconfined lubricant spill is 24.5 m² so that the effective fire diameter is 5.6 m. The liquid fuel surface area for the confined lubricant spill is 2.81 m² so that the effective fire diameter is 1.89 m.

**Step 5**. (Select the empirical model.) The spill depth for the unconfined lubricant spill is 1.54 mm, which is less than 2 mm. As such, Method 4 is the applicable HRR model. The spill depth for the confined lubricant spill fire is 13.5 mm, which is greater than 2 mm. As such, Method 3 is the applicable model for determining the HRR of the confined lubricant spill fire.

**Step 6**. (Determine the number of HRR scenarios.) The unconfined lubricant spill depth is 1.54 mm, which is between 1 and 2 mm. As such, two HRR scenarios are needed to characterize the HRR profile. One corresponds to the minimum depth coefficient, and one corresponds to the maximum depth coefficient.

The confined lubricant spill depth is 13.5 mm, which is greater than 2 mm. Only a single HRR scenario is needed to characterize the confined lubricant spill fire.

**Step 7**. (Select the empirical parameters.) The empirical diameter constant for lubricating oil is 1.7 $m^{-1}$ for fuel oil as shown in Table 5-5. The maximum mass burning rate is 0.035 kg/m²-s as shown in Table 6-1. The fuel density is 970 kg/m³ as shown in Table 6-1, which is the average value of the reported range, and the fuel heat of combustion is 39,700 kJ/kg as shown in Table 6-1.

**Step 8**. (Select the depth coefficients.) As shown in Section 5.4.1.2.2, the depth coefficient for lubricating oil is 1.0 for spill depths greater than 2 mm, 0.2 for spill depths less than 1 mm, and either 0.2 or 1.0 for spill depths between 1 and 2 mm.

Accordingly, the depth coefficient for the confined lubricant spill fire scenario is 1.0 based on the calculated confined spill depth of 13.5 mm from Step 3a. The unconfined spill depth is 1.54 mm, and the depth coefficient for the first unconfined spill fire HRR scenario is 1.0 (maximum value) and 0.2 for the second HRR scenario (minimum value).

**Step 9**. (Determine the HRR profile.) The HRR profile for the unconfined lubricant spill fire is determined using the integral model described in Section 6.1.1.4 with a surface area as determined in Step 3b, the fire diameter as determined in Step 4, the empirical parameters selected in Step 7, and the depth coefficients selected in Step 8.

Appendix C.2 provides solutions to the integral model for different volumes of common combustible and flammable liquids. The solution provided in Figure C-45 for 37.8 L of lubricating oil with a spill depth of 1.54 mm and a depth coefficient of 1.0 is directly applicable to this example and is the solution for the maximum HRR scenario.

The solution provided in Figure C-34 for 37.8 L of lubricating oil with a spill depth of 1.54 mm and a depth coefficient of 0.2 is directly applicable to this example and is the solution for the minimum HRR scenario. The two HRR profiles are shown in Figure 6-37.

The fire PRA must consider the effects of each scenario separately to determine the limiting HRR scenario. The peak HRR for the larger HRR scenario is 30.4 MW, and the fire duration is about 106 seconds. Similarly, the peak HRR for the smaller HRR scenario is 6,830 kW, and the fire duration is about 277 seconds. Because the scenario with the maximum depth coefficient has a significantly higher HRR and has a burning duration longer than 1 minute, it is likely that this will be the limiting scenario.

The HRR profile for the confined lubricant spill fire is determined using Method 3 as described in Section 6.1.1.3 with a surface area as determined in Step 3b, the fire diameter as determined in Step 4, the empirical parameters selected in Step 7, and the depth coefficient set to unity per Step 8. The HRR profile for the confined lubricant spill fire is shown in Figure 6-37 alongside the two HRR profiles for the unconfined lubricant spill fire HRR scenarios. The peak HRR is 3,747 kW, and the fire duration is about 304 seconds. The figure indicates that the curbing provides a significant reduction in the HRR, but that the fire duration is extended proportionately.

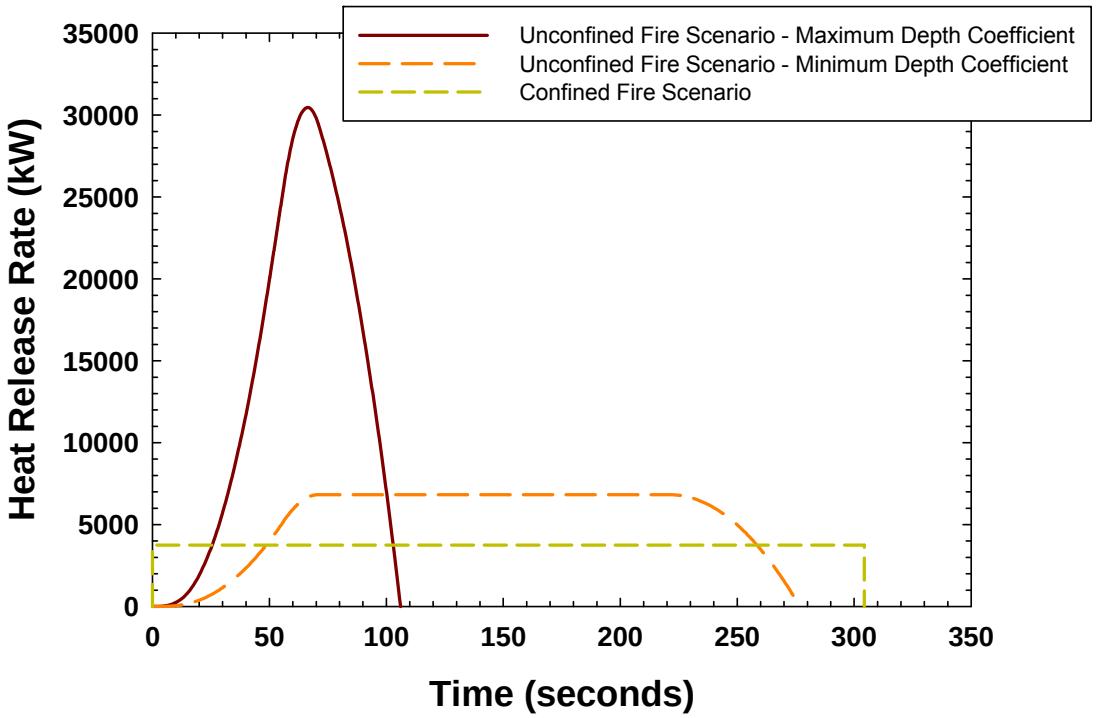


**Figure 6-37**
**HRR profiles for confined and unconfined lubricant spill fires involving 37.8 L of fuel (Example 2)**

### *6.2.3 Limitations on Model Implementation*

Table 6-12 contains a summary of the primary limitations of use for the selected spill fire models. Any condition that falls outside the listed limitations should be evaluated for appropriateness by carefully considering the assumptions listed in Section 5.3 of this report.

**Table 6-12**
**Summary of liquid fuel fire HRR model limitations**

| Parameter | Limitation | | | |
|---|---|---|---|---|
| | **Method 1** | **Method 2** | **Method 3** | **Method 4** |
| **Fuel** | **Fuels identified in Table G-4 of Ref. 2.** | **Fuels identified in Table 3-4 of Ref. 7.** | **Gasoline, kerosene, diesel fuel, lubricating oil, ethanol, heptane** | **Gasoline, kerosene, diesel fuel, lubricating oil, ethanol, heptane** |
| Substrate temperature | < 40°C | < 40°C | < 40°C | < 40°C |
| Fuel temperature | < 40°C | < 40°C | < 40°C | < 40°C |
| Fuel volume | No limit | No limit | No limit | No limit |
| Maximum depth | No limit | No limit | No limit | No limit |
| Substrate type | Solid, flat | Solid, Flat | Solid, flat | Solid, flat |

**Table 6-12 (continued)**
**Summary of liquid fuel fire HRR model limitations**

| Parameter | Limitation | | | |
|---|---|---|---|---|
| | **Method 1** | **Method 2** | **Method 3** | **Method 4** |
| **Fuel** | **Fuels identified in Table G-4 of Ref. 2.** | **Fuels identified in Table 3-4 of Ref. 7.** | **Gasoline, kerosene, diesel fuel, lubricating oil, ethanol, heptane** | **Gasoline, kerosene, diesel fuel, lubricating oil, ethanol, heptane** |
| Pool type | Deep | Deep | Deep or thin | Deep or thin |
| Maximum enclosure temperature | < 257°C | < 257°C | < 257°C | < 257°C |
| Liquid fuel fire scenario(s) | Fixed quantity, confined† | Fixed quantity, confined† | Fixed quantity, confined or unconfined† | Fixed quantity, confined or unconfined† |
| Pressurized fuel spills | No | No | No | No |
| Obstructions in pool area | Acceptable, provided the obstruction area is removed from calculations‡ | Acceptable, provided the obstruction area is removed from calculations‡ | Acceptable, provided the obstruction area is removed from calculations‡ | Acceptable, provided the obstruction area is removed from calculations‡ |

†The methods are applicable to continuously fed liquid fuel fires; however, the modifications to the input parameters to account for this effect are not described in this document.
‡Although it is acceptable to determine the HRR with obstructions in the pool area (for example, pedestals, equipment, and so on), caution is necessary when using the HRR to determine flame heights, radiant heat fluxes, and thermal plume temperatures. It is generally conservative to consolidate the pool into an equivalent circular plan area and to apply the results at the pool boundary.

## 6.3 Conclusions and Recommendations

Combustible and flammable liquid spill fire scenarios are an important class of fires considered at NPPs due to their potential to generate high HRRs over a short time, which can result in a severe fire hazard to critical components, raceways, and structural elements. Current treatments for determining the HRR profiles in combustible and flammable liquid spill fires are based on a mix of data applicable to deep liquid pools and spill fires. This results in a significant over-prediction of the HRR and a significant under-prediction of the fire duration, in many cases by a factor of 5 or greater. It is natural to assume that an over-prediction of the HRR will universally yield a conservative result when considering the effects of a fire; however, several examples are identified in Section 6.1.1.4 in which the reverse is true. In these cases, the fire duration plays a key role in the determination of the fire hazard associated with the liquid fuel fire, and a significant under-prediction of the fire duration results in a non-conservative assessment of the particular fire effect.

A large number of liquid fuel fire tests conducted in support of the NIJ [1] provide a unique opportunity to assess and improve existing HRR prediction models for liquid fuel fires. Overall, the expectation is that an improved empirical treatment of liquid pool fires will produce a more realistic HRR profile. This will be especially useful for input into an analysis of a target response to a source fire exposure. It will also reduce conservatism in predicting the HRR for thin spill fire scenarios that are treated using deep pool data, which will be particularly useful when determining a ZOI or when using the HRR as an input into a zone or field computer fire model.

Two liquid fuel fire empirical HRR models are considered in this report. The first is a simple method described in Gottuk et al. [3] and updated with empirical data obtained in Reference 1. This method does not attempt to simulate the growth or decay stages and is shown to provide reasonable HRR predictions for deep pools with large or small diameters. The second method is an updated model that addresses the growth stage of the HRR in liquid fuel fires using observations of the behavior reported in Reference 1. A simple decay stage is included that is directly related to the surface flame spread rate on the liquid fuel and the localized mass burning rate. This method is shown to produce good agreement with Method 3 [1, 3] for deep pool data, but is significantly improved for liquid spill fires in which the growth phase is a significant fraction of the overall HRR profile.

An analysis procedure for implementing the empirical HRR prediction models is provided in Section 6.2.1. The procedure is applicable to liquid fuel spills involving kerosene, gasoline, heptane, ethanol, and lubricating oils and substrate (that is, floor) temperatures less than 40°C. Fuels that have burning characteristics similar to those identified above may be evaluated using this approach if the empirical constants for the fuels are known or are bound by the selected values. Additionally, the analysis is not applicable to continuously fed spill fires. If the application does not meet the applicability requirements, an alternative approach is recommended for determining the HRR profiles. Appendix C.2 provides graphical and tabular solutions to the updated or integral model presented in Section 6.2.2 for different volumes of common flammable and combustible liquids. The data in the appendix may be used for applicable fuels and fuel volumes in place of solving the integral model.

The uncertainty of the methods may be quantitatively addressed through known uncertainty ranges for empirical parameters associated with each method. In particular, uncertainty ranges for the spill depth, the maximum mass burning rate, the depth coefficient, and the fire diameter empirical constant are provided in Section 6.1.3.3 along with guidance for the types of scenarios for which they apply and their general effect on the predicted HRR and burning duration.

The empirical HRR models described in Section 6.1.1 may readily be incorporated into an analytical model for ease of implementation. They are well suited for inclusion in spreadsheet-type calculations such as the FIVE calculation suite [12]. A spreadsheet-type model has not specifically been developed with this report, but it is expected that subsequent efforts with this approach will lead to a model that will be available for general use within the commercial nuclear industry.

There are several features or improvements to the updated model that may be considered and assessed against the test data provided in Reference 1. These additional features include:

- Inclusion of an empirical treatment for the decay stage. Data provided in Reference 1 provide a framework for imposing a decay stage, that is, a fuel depth at which the HRR begins to decay.
- Inclusion of the empirical diameter function within the integral may provide a more explicit treatment of the burning rate development time and reduce the need for including this as a parameter.

Because the models considered accomplished the primary goals for an improved prediction method, namely, improving the prediction of the peak HRR, fire duration, and the growth stage of the fire, these features are not considered essential for most method applications.

## 6.4 References

1. Grant No. 2008-DN-BX-K168, *Fire Dynamics and Forensic Analysis of Liquid Fuel Fires, Final Report,* Mealy, C., Benfer, M., and Gottuk, D., Hughes Associates, Inc., Baltimore, MD, February 18, 2011.
2. *Fire PRA Methodology for Nuclear Power Facilities, Volume 2: Detailed Methodology,* NUREG-6850 and EPRI/NRC-RES 1008239. Nuclear Regulatory Commission (NRC), Office of Nuclear Regulatory Research (RES), Washington, DC and Electric Power Research Institute (EPRI), Palo Alto, CA: September 2005.
3. Gottuk, D. T. and White, D. A., "Liquid Fuel Fires," Section 3, Chapter 10, *The SFPE Handbook of Fire Protection Engineering,* 4th Edition, Society of Fire Protection Engineers, Bethesda, MD, 2008.
4. Gottuk, D., Gott, J., and Williams, F., "Fire Dynamics of Spill Fires: An Experimental Study," *Proceedings of the Sixth International Symposium on Fire Safety Science,* France, July 1999.
5. Not Used.
6. Not Used.
7. NUREG-1805, *Fire Dynamics Tools (FDTS) Quantitative Fire Hazard Analysis Methods for the U. S. Nuclear Regulatory Commission Fire Protection Inspection Program,* Iqbal, N. and Salley, M. H. , U.S. Nuclear Regulatory Commission (NRC), Office of Nuclear Reactor Regulation, Washington, DC, December 2004.
8. Babrauskas, V., "Heat Release Rates," Section 3, Chapter 1, *The SFPE Handbook of Fire Protection Engineering,* 4th Edition, Society of Fire Protection Engineers, Bethesda, MD, 2008.
9. Babrauskas, V., "Pool Fires: Burning Rates and Heat Fluxes," Section 21, Chapter 6, *Fire Protection Handbook,* Sixteenth Edition, National Fire Protection Association (NFPA), Quincy, MA, 1986.
10. Blinov, V. and Khudiakov, G., "Diffusion Burning of Liquids," U.S. Army Translation, NTIS No. AD296762, 1961.

11. *Nuclear Power Plant Fire Modeling Analysis Guidelines (NPP FIRE MAG*). NUREG-1934 and EPRI 1023259, U.S. Nuclear Regulatory Commission, Office of Nuclear Regulatory Research (RES), Washington, DC and Electric Power Research Institute (EPRI), Palo Alto, CA: 2012.
12. *Fire Modeling Guide for Nuclear Power Plant Applications*. EPRI, Palo Alto, CA, August, 2002. TR-1002981.
13. NUREG-1805, Supplement 1, *Fire Dynamics Tools (FDTS) Quantitative Fire Hazard Analysis Methods for the U. S. Nuclear Regulatory Commission Fire Protection Inspection Program*, Stroup, D., Taylor, G., Hausman, G., and Salley, M. H., Final Report, U.S. Nuclear Regulatory Commission, Office of Nuclear Reactor Regulation, Washington, DC, July 2013.
14. NUREG/CR-6931, *Cable Response to Live Fire (CAROLFIRE) Volume 3; Thermally-Induced Electrical Failure (THIEF) Model*, McGrattan, K., NRC, Washington, DC, January, 2008.
15. NIST Special Publication (SP) 1026, *CFAST – Consolidated Model of Fire Growth and Smoke Transport (Version 6) Technical Reference Guide*, Jones, W. W., Peacock, R. D., Forney, G. P., and Reneke, P. A., National Institute of Standards and Technology (NIST), Gaithersburg, MD, April 2009.
16. NIST SP 1041, *CFAST – Consolidated Model of Fire Growth and Smoke Transport (Version 6) User's Guide*, Peacock, R. D., Jones, W. W., Reneke, P. A., and Forney, G. P., National Institute of Standards and Technology (NIST), Gaithersburg, MD, December 2008.
17. Not Used.
18. Not Used.
19. Janssens, M., "Calorimetry," Section 3, Chapter 2, *The SFPE Handbook of Fire Protection Engineering,* 4th Edition, Society of Fire Protection Engineers, Bethesda, MD, 2008.

# A
# FIRE LOCATION FACTOR – WALL AND CORNER CONFIGURATION RESULTS

This appendix presents the results of the FDS simulations for fires postulated in or near corner configurations. The contents of each table are summarized below:

- Table A-1 contains results for simulations with a corner configuration used in this investigation. It includes the simulation Test ID, the distance of the fire source from the corner, the HRR used in the simulation, the Fire Froude number for the simulation, the HRRPUA of the source used in the simulation, the fire source diameter, the characteristic fire diameter for each simulation, the elevation of the temperature prediction, the maximum time averaged plume temperature rise, and the estimated value of $k_F$ for the simulation.
- Table A-2 contains results for simulations with a wall configuration used in this investigation. It includes the simulation Test ID, the distance of the fire source from the corner, the HRR used in the simulation, the Fire Froude number for the simulation, the HRRPUA of the source used in the simulation, the fire source diameter, the characteristic fire diameter for each simulation, the elevation of the temperature prediction, the maximum time averaged plume temperature rise, and the estimated value of $k_F$ for the simulation.
- Table A-3 contains results for simulations with an open configuration used in this investigation. It includes the simulation Test ID, the distance of the fire source from the corner, the HRR used in the simulation, the Fire Froude number for the simulation, the HRRPUA of the source used in the simulation, the fire source diameter, the characteristic fire diameter for each simulation, the elevation of the temperature prediction, the maximum time averaged plume temperature rise, and the estimated value of $k_F$ for the simulation.
- Table A-4 contains results for simulations with a corner configuration used to determine the sensitivity of the wall surface properties. It includes the simulation Test ID, the distance of the fire source from the corner, the HRR used in the simulation, the Fire Froude number for the simulation, the HRRPUA of the source used in the simulation, the fire source diameter, the characteristic fire diameter for each simulation, the elevation of the temperature prediction, the maximum time averaged plume temperature rise, the estimated value of $k_F$ for the simulation, and the wall surface properties used in the simulation.

**Table A-1**
**FDS corner results**

| Case ID | Length (m) | HRR (kW) | Q* | HRRPUA | Diameter (m) | D* | $H_p$ (m) | Temperature Rise (°C) | $k_F$ |
|---|---|---|---|---|---|---|---|---|---|
| CORNER_100 | 0 | 40 | 1.43 | 1000 | 0.23 | 0.27 | 0.9 | 636.61 | 2.04 |
| CORNER_100 | 0 | 40 | 1.43 | 1000 | 0.23 | 0.27 | 1.2 | 492.93 | 3.11 |
| CORNER_100 | 0 | 40 | 1.43 | 1000 | 0.23 | 0.27 | 1.5 | 368.16 | 3.68 |
| CORNER_100 | 0 | 40 | 1.43 | 1000 | 0.23 | 0.27 | 1.8 | 294.93 | 4.27 |
| CORNER_100 | 0 | 40 | 1.43 | 1000 | 0.23 | 0.27 | 2.1 | 232.25 | 4.42 |
| CORNER_100 | 0 | 40 | 1.43 | 1000 | 0.23 | 0.27 | 2.4 | 195.86 | 4.78 |
| CORNER_100 | 0 | 40 | 1.43 | 1000 | 0.23 | 0.27 | 2.7 | 164.02 | 4.86 |
| CORNER_100 | 0 | 40 | 1.43 | 1000 | 0.23 | 0.27 | 3 | 141.82 | 5.00 |
| CORNER_101 | 0.25 | 40 | 1.50 | 1000 | 0.23 | 0.27 | 0.9 | 221.21 | 0.44 |
| CORNER_101 | 0.25 | 40 | 1.50 | 1000 | 0.23 | 0.27 | 1.2 | 171.3 | 0.63 |
| CORNER_101 | 0.25 | 40 | 1.50 | 1000 | 0.23 | 0.27 | 1.5 | 139.38 | 0.80 |
| CORNER_102 | 0.5 | 40 | 1.50 | 1000 | 0.23 | 0.27 | 0.9 | 248.87 | 0.53 |
| CORNER_102 | 0.5 | 40 | 1.50 | 1000 | 0.23 | 0.27 | 1.2 | 181.15 | 0.69 |
| CORNER_102 | 0.5 | 40 | 1.50 | 1000 | 0.23 | 0.27 | 1.5 | 135.29 | 0.76 |
| CORNER_103 | 0.75 | 40 | 1.50 | 1000 | 0.23 | 0.27 | 0.9 | 224.65 | 0.45 |
| CORNER_103 | 0.75 | 40 | 1.50 | 1000 | 0.23 | 0.27 | 1.2 | 163.67 | 0.58 |
| CORNER_104 | 1 | 40 | 1.50 | 1000 | 0.23 | 0.27 | 0.9 | 214.43 | 0.42 |
| CORNER_104 | 1 | 40 | 1.50 | 1000 | 0.23 | 0.27 | 1.2 | 151.15 | 0.51 |
| CORNER_105 | 1.5 | 40 | 1.50 | 1000 | 0.23 | 0.27 | 0.9 | 241.94 | 0.51 |
| CORNER_105 | 1.5 | 40 | 1.50 | 1000 | 0.23 | 0.27 | 1.2 | 165.81 | 0.60 |
| CORNER_106 | 0 | 78 | 1.26 | 1000 | 0.32 | 0.35 | 1.2 | 660 | 2.45 |
| CORNER_106 | 0 | 78 | 1.26 | 1000 | 0.32 | 0.35 | 1.5 | 513.79 | 3.13 |
| CORNER_106 | 0 | 78 | 1.26 | 1000 | 0.32 | 0.35 | 1.8 | 425.27 | 3.87 |
| CORNER_106 | 0 | 78 | 1.26 | 1000 | 0.32 | 0.35 | 2.1 | 338.99 | 4.13 |
| CORNER_106 | 0 | 78 | 1.26 | 1000 | 0.32 | 0.35 | 2.4 | 279.72 | 4.36 |
| CORNER_106 | 0 | 78 | 1.26 | 1000 | 0.32 | 0.35 | 2.7 | 219.4 | 4.03 |

**Table A-1 (continued)**
**FDS corner results**

| Case ID | Length (m) | HRR (kW) | Q* | HRRPUA | Diameter (m) | D* | $H_p$ (m) | Temperature Rise (°C) | $k_F$ |
|---|---|---|---|---|---|---|---|---|---|
| CORNER_106 | 0 | 78 | 1.26 | 1000 | 0.32 | 0.35 | 3 | 182.69 | 3.94 |
| CORNER_106 | 0 | 78 | 1.26 | 1000 | 0.32 | 0.35 | 3.3 | 155.27 | 3.84 |
| CORNER_106 | 0 | 78 | 1.26 | 1000 | 0.32 | 0.35 | 3.6 | 137.1 | 3.90 |
| CORNER_107 | 0.24 | 78 | 1.26 | 1000 | 0.32 | 0.35 | 1.2 | 295.86 | 0.75 |
| CORNER_107 | 0.24 | 78 | 1.26 | 1000 | 0.32 | 0.35 | 1.5 | 241.45 | 0.99 |
| CORNER_107 | 0.24 | 78 | 1.26 | 1000 | 0.32 | 0.35 | 1.8 | 207.81 | 1.26 |
| CORNER_107 | 0.24 | 78 | 1.26 | 1000 | 0.32 | 0.35 | 2.1 | 183.09 | 1.55 |
| CORNER_107 | 0.24 | 78 | 1.26 | 1000 | 0.32 | 0.35 | 2.4 | 163.45 | 1.82 |
| CORNER_107 | 0.24 | 78 | 1.26 | 1000 | 0.32 | 0.35 | 2.7 | 148.08 | 2.10 |
| CORNER_107 | 0.24 | 78 | 1.26 | 1000 | 0.32 | 0.35 | 3 | 134.98 | 2.36 |
| CORNER_108 | 0.48 | 78 | 1.26 | 1000 | 0.32 | 0.35 | 1.2 | 244.33 | 0.56 |
| CORNER_108 | 0.48 | 78 | 1.26 | 1000 | 0.32 | 0.35 | 1.5 | 169.08 | 0.56 |
| CORNER_108 | 0.48 | 78 | 1.26 | 1000 | 0.32 | 0.35 | 1.8 | 132.17 | 0.60 |
| CORNER_109 | 0.76 | 78 | 1.26 | 1000 | 0.32 | 0.35 | 1.2 | 245.29 | 0.56 |
| CORNER_109 | 0.76 | 78 | 1.26 | 1000 | 0.32 | 0.35 | 1.5 | 170.99 | 0.57 |
| CORNER_109 | 0.76 | 78 | 1.26 | 1000 | 0.32 | 0.35 | 1.8 | 135.76 | 0.63 |
| CORNER_110 | 1 | 78 | 1.26 | 1000 | 0.32 | 0.35 | 1.2 | 216.15 | 0.46 |
| CORNER_110 | 1 | 78 | 1.26 | 1000 | 0.32 | 0.35 | 1.5 | 158.15 | 0.51 |
| CORNER_110 | 1 | 78 | 1.26 | 1000 | 0.32 | 0.35 | 1.8 | 130.72 | 0.59 |
| CORNER_111 | 1.48 | 78 | 1.26 | 1000 | 0.32 | 0.35 | 1.2 | 252.78 | 0.59 |
| CORNER_111 | 1.48 | 78 | 1.26 | 1000 | 0.32 | 0.35 | 1.5 | 179.05 | 0.62 |
| CORNER_111 | 1.48 | 78 | 1.26 | 1000 | 0.32 | 0.35 | 1.8 | 147.74 | 0.73 |
| CORNER_112 | 0 | 250 | 0.95 | 1000 | 0.56 | 0.55 | 1.8 | 769.2 | 3.06 |
| CORNER_112 | 0 | 250 | 0.95 | 1000 | 0.56 | 0.55 | 2.1 | 693.73 | 4.05 |
| CORNER_112 | 0 | 250 | 0.95 | 1000 | 0.56 | 0.55 | 2.4 | 608.99 | 4.80 |
| CORNER_112 | 0 | 250 | 0.95 | 1000 | 0.56 | 0.55 | 2.7 | 507.81 | 4.96 |

**Table A-1 (continued)**
**FDS corner results**

| Case ID | Length (m) | HRR (kW) | Q* | HRRPUA | Diameter (m) | D* | $H_p$ (m) | Temperature Rise (°C) | $k_F$ |
|---|---|---|---|---|---|---|---|---|---|
| CORNER_112 | 0 | 250 | 0.95 | 1000 | 0.56 | 0.55 | 3 | 430.3 | 5.06 |
| CORNER_112 | 0 | 250 | 0.95 | 1000 | 0.56 | 0.55 | 3.3 | 350.58 | 4.68 |
| CORNER_112 | 0 | 250 | 0.95 | 1000 | 0.56 | 0.55 | 3.6 | 304.47 | 4.69 |
| CORNER_112 | 0 | 250 | 0.95 | 1000 | 0.56 | 0.55 | 3.9 | 258.72 | 4.43 |
| CORNER_112 | 0 | 250 | 0.95 | 1000 | 0.56 | 0.55 | 4.2 | 226.97 | 4.34 |
| CORNER_112 | 0 | 250 | 0.95 | 1000 | 0.56 | 0.55 | 4.5 | 203.29 | 4.32 |
| CORNER_112 | 0 | 250 | 0.95 | 1000 | 0.56 | 0.55 | 4.8 | 185.49 | 4.39 |
| CORNER_112 | 0 | 250 | 0.95 | 1000 | 0.56 | 0.55 | 5.1 | 169.54 | 4.41 |
| CORNER_112 | 0 | 250 | 0.95 | 1000 | 0.56 | 0.55 | 5.4 | 154.03 | 4.33 |
| CORNER_112 | 0 | 250 | 0.95 | 1000 | 0.56 | 0.55 | 5.7 | 142.63 | 4.36 |
| CORNER_112 | 0 | 250 | 0.95 | 1000 | 0.56 | 0.55 | 6 | 134.8 | 4.51 |
| CORNER_113 | 0.24 | 250 | 0.95 | 1000 | 0.56 | 0.55 | 1.8 | 446.41 | 1.30 |
| CORNER_113 | 0.24 | 250 | 0.95 | 1000 | 0.56 | 0.55 | 2.1 | 379.67 | 1.54 |
| CORNER_113 | 0.24 | 250 | 0.95 | 1000 | 0.56 | 0.55 | 2.4 | 331.41 | 1.78 |
| CORNER_113 | 0.24 | 250 | 0.95 | 1000 | 0.56 | 0.55 | 2.7 | 281.3 | 1.88 |
| CORNER_113 | 0.24 | 250 | 0.95 | 1000 | 0.56 | 0.55 | 3 | 250.26 | 2.07 |
| CORNER_113 | 0.24 | 250 | 0.95 | 1000 | 0.56 | 0.55 | 3.3 | 223.86 | 2.22 |
| CORNER_113 | 0.24 | 250 | 0.95 | 1000 | 0.56 | 0.55 | 3.6 | 203.09 | 2.38 |
| CORNER_113 | 0.24 | 250 | 0.95 | 1000 | 0.56 | 0.55 | 3.9 | 181.7 | 2.44 |
| CORNER_113 | 0.24 | 250 | 0.95 | 1000 | 0.56 | 0.55 | 4.2 | 165.26 | 2.52 |
| CORNER_113 | 0.24 | 250 | 0.95 | 1000 | 0.56 | 0.55 | 4.5 | 151.07 | 2.59 |
| CORNER_113 | 0.24 | 250 | 0.95 | 1000 | 0.56 | 0.55 | 4.8 | 141.05 | 2.72 |
| CORNER_113 | 0.24 | 250 | 0.95 | 1000 | 0.56 | 0.55 | 5.1 | 132.39 | 2.85 |
| CORNER_114 | 0.48 | 250 | 0.95 | 1000 | 0.56 | 0.55 | 1.8 | 296.69 | 0.69 |
| CORNER_114 | 0.48 | 250 | 0.95 | 1000 | 0.56 | 0.55 | 2.1 | 220.3 | 0.65 |
| CORNER_114 | 0.48 | 250 | 0.95 | 1000 | 0.56 | 0.55 | 2.4 | 188.89 | 0.72 |

**Table A-1 (continued)**
**FDS corner results**

| Case ID | Length (m) | HRR (kW) | Q* | HRRPUA | Diameter (m) | D* | $H_p$ (m) | Temperature Rise (°C) | $k_F$ |
|---|---|---|---|---|---|---|---|---|---|
| CORNER_114 | 0.48 | 250 | 0.95 | 1000 | 0.56 | 0.55 | 2.7 | 168.25 | 0.81 |
| CORNER_114 | 0.48 | 250 | 0.95 | 1000 | 0.56 | 0.55 | 3 | 149.71 | 0.88 |
| CORNER_114 | 0.48 | 250 | 0.95 | 1000 | 0.56 | 0.55 | 3.3 | 140.26 | 1.01 |
| CORNER_114 | 0.48 | 250 | 0.95 | 1000 | 0.56 | 0.55 | 3.6 | 134.55 | 1.18 |
| CORNER_115 | 0.76 | 250 | 0.95 | 1000 | 0.56 | 0.55 | 1.8 | 310.56 | 0.74 |
| CORNER_115 | 0.76 | 250 | 0.95 | 1000 | 0.56 | 0.55 | 2.1 | 234.94 | 0.72 |
| CORNER_115 | 0.76 | 250 | 0.95 | 1000 | 0.56 | 0.55 | 2.4 | 189.74 | 0.73 |
| CORNER_115 | 0.76 | 250 | 0.95 | 1000 | 0.56 | 0.55 | 2.7 | 160.31 | 0.75 |
| CORNER_115 | 0.76 | 250 | 0.95 | 1000 | 0.56 | 0.55 | 3 | 140.31 | 0.79 |
| CORNER_116 | 1 | 250 | 0.95 | 1000 | 0.56 | 0.55 | 1.8 | 293.83 | 0.68 |
| CORNER_116 | 1 | 250 | 0.95 | 1000 | 0.56 | 0.55 | 2.1 | 227.7 | 0.69 |
| CORNER_116 | 1 | 250 | 0.95 | 1000 | 0.56 | 0.55 | 2.4 | 188.88 | 0.72 |
| CORNER_116 | 1 | 250 | 0.95 | 1000 | 0.56 | 0.55 | 2.7 | 160.08 | 0.75 |
| CORNER_116 | 1 | 250 | 0.95 | 1000 | 0.56 | 0.55 | 3 | 134.63 | 0.73 |
| CORNER_117 | 1.48 | 250 | 0.95 | 1000 | 0.56 | 0.55 | 1.8 | 303.79 | 0.72 |
| CORNER_117 | 1.48 | 250 | 0.95 | 1000 | 0.56 | 0.55 | 2.1 | 229.94 | 0.70 |
| CORNER_117 | 1.48 | 250 | 0.95 | 1000 | 0.56 | 0.55 | 2.4 | 183.38 | 0.69 |
| CORNER_117 | 1.48 | 250 | 0.95 | 1000 | 0.56 | 0.55 | 2.7 | 154.43 | 0.70 |
| CORNER_117 | 1.48 | 250 | 0.95 | 1000 | 0.56 | 0.55 | 3 | 133.69 | 0.72 |
| CORNER_118 | 0 | 500 | 0.80 | 1000 | 0.80 | 0.73 | 2.1 | 744.18 | 2.27 |
| CORNER_118 | 0 | 500 | 0.80 | 1000 | 0.80 | 0.73 | 2.4 | 707.9 | 3.09 |
| CORNER_118 | 0 | 500 | 0.80 | 1000 | 0.80 | 0.73 | 2.7 | 653 | 3.80 |
| CORNER_118 | 0 | 500 | 0.80 | 1000 | 0.80 | 0.73 | 3 | 599.26 | 4.45 |
| CORNER_118 | 0 | 500 | 0.80 | 1000 | 0.80 | 0.73 | 3.3 | 534.12 | 4.80 |
| CORNER_118 | 0 | 500 | 0.80 | 1000 | 0.80 | 0.73 | 3.6 | 470.5 | 4.93 |
| CORNER_118 | 0 | 500 | 0.80 | 1000 | 0.80 | 0.73 | 3.9 | 397.32 | 4.61 |

**Table A-1 (continued)**
**FDS corner results**

| Case ID | Length (m) | HRR (kW) | Q* | HRRPUA | Diameter (m) | D* | $H_p$ (m) | Temperature Rise (°C) | $k_F$ |
|---|---|---|---|---|---|---|---|---|---|
| CORNER_118 | 0 | 500 | 0.80 | 1000 | 0.80 | 0.73 | 4.2 | 347.12 | 4.49 |
| CORNER_118 | 0 | 500 | 0.80 | 1000 | 0.80 | 0.73 | 4.5 | 296.23 | 4.13 |
| CORNER_118 | 0 | 500 | 0.80 | 1000 | 0.80 | 0.73 | 4.8 | 259.88 | 3.93 |
| CORNER_118 | 0 | 500 | 0.80 | 1000 | 0.80 | 0.73 | 5.1 | 234.29 | 3.87 |
| CORNER_118 | 0 | 500 | 0.80 | 1000 | 0.80 | 0.73 | 5.4 | 209.93 | 3.73 |
| CORNER_118 | 0 | 500 | 0.80 | 1000 | 0.80 | 0.73 | 5.7 | 190.47 | 3.64 |
| CORNER_118 | 0 | 500 | 0.80 | 1000 | 0.80 | 0.73 | 6 | 179.06 | 3.74 |
| CORNER_119 | 0.25 | 500 | 0.80 | 1000 | 0.80 | 0.73 | 2.1 | 531.2 | 1.31 |
| CORNER_119 | 0.25 | 500 | 0.80 | 1000 | 0.80 | 0.73 | 2.4 | 468.36 | 1.56 |
| CORNER_119 | 0.25 | 500 | 0.80 | 1000 | 0.80 | 0.73 | 2.7 | 405.68 | 1.71 |
| CORNER_119 | 0.25 | 500 | 0.80 | 1000 | 0.80 | 0.73 | 3 | 360.53 | 1.88 |
| CORNER_119 | 0.25 | 500 | 0.80 | 1000 | 0.80 | 0.73 | 3.3 | 319.78 | 2.01 |
| CORNER_119 | 0.25 | 500 | 0.80 | 1000 | 0.80 | 0.73 | 3.6 | 290.68 | 2.17 |
| CORNER_119 | 0.25 | 500 | 0.80 | 1000 | 0.80 | 0.73 | 3.9 | 258.56 | 2.21 |
| CORNER_119 | 0.25 | 500 | 0.80 | 1000 | 0.80 | 0.73 | 4.2 | 235.46 | 2.31 |
| CORNER_119 | 0.25 | 500 | 0.80 | 1000 | 0.80 | 0.73 | 4.5 | 212.73 | 2.34 |
| CORNER_119 | 0.25 | 500 | 0.80 | 1000 | 0.80 | 0.73 | 4.8 | 198.07 | 2.46 |
| CORNER_119 | 0.25 | 500 | 0.80 | 1000 | 0.80 | 0.73 | 5.1 | 183.09 | 2.52 |
| CORNER_119 | 0.25 | 500 | 0.80 | 1000 | 0.80 | 0.73 | 5.4 | 168.48 | 2.54 |
| CORNER_119 | 0.25 | 500 | 0.80 | 1000 | 0.80 | 0.73 | 5.7 | 157.21 | 2.59 |
| CORNER_119 | 0.25 | 500 | 0.80 | 1000 | 0.80 | 0.73 | 6 | 150.43 | 2.74 |
| CORNER_120 | 0.5 | 500 | 0.80 | 1000 | 0.80 | 0.73 | 2.1 | 424.75 | 0.92 |
| CORNER_120 | 0.5 | 500 | 0.80 | 1000 | 0.80 | 0.73 | 2.4 | 341.98 | 0.94 |
| CORNER_120 | 0.5 | 500 | 0.80 | 1000 | 0.80 | 0.73 | 2.7 | 283.34 | 0.95 |
| CORNER_120 | 0.5 | 500 | 0.80 | 1000 | 0.80 | 0.73 | 3 | 248.73 | 1.02 |
| CORNER_120 | 0.5 | 500 | 0.80 | 1000 | 0.80 | 0.73 | 3.3 | 220.27 | 1.08 |

**Table A-1 (continued)**
**FDS corner results**

| Case ID | Length (m) | HRR (kW) | Q* | HRRPUA | Diameter (m) | D* | $H_p$ (m) | Temperature Rise (°C) | $k_F$ |
|---|---|---|---|---|---|---|---|---|---|
| CORNER_120 | 0.5 | 500 | 0.80 | 1000 | 0.80 | 0.73 | 3.6 | 204.05 | 1.20 |
| CORNER_120 | 0.5 | 500 | 0.80 | 1000 | 0.80 | 0.73 | 3.9 | 188.88 | 1.30 |
| CORNER_120 | 0.5 | 500 | 0.80 | 1000 | 0.80 | 0.73 | 4.2 | 179.78 | 1.46 |
| CORNER_120 | 0.5 | 500 | 0.80 | 1000 | 0.80 | 0.73 | 4.5 | 170.47 | 1.60 |
| CORNER_120 | 0.5 | 500 | 0.80 | 1000 | 0.80 | 0.73 | 4.8 | 163.91 | 1.77 |
| CORNER_120 | 0.5 | 500 | 0.80 | 1000 | 0.80 | 0.73 | 5.1 | 157.48 | 1.94 |
| CORNER_120 | 0.5 | 500 | 0.80 | 1000 | 0.80 | 0.73 | 5.4 | 149.17 | 2.05 |
| CORNER_120 | 0.5 | 500 | 0.80 | 1000 | 0.80 | 0.73 | 5.7 | 143.1 | 2.19 |
| CORNER_120 | 0.5 | 500 | 0.80 | 1000 | 0.80 | 0.73 | 6 | 138.95 | 2.38 |
| CORNER_121 | 0.75 | 500 | 0.80 | 1000 | 0.80 | 0.73 | 2.1 | 400.09 | 0.84 |
| CORNER_121 | 0.75 | 500 | 0.80 | 1000 | 0.80 | 0.73 | 2.4 | 322.05 | 0.85 |
| CORNER_121 | 0.75 | 500 | 0.80 | 1000 | 0.80 | 0.73 | 2.7 | 257.06 | 0.81 |
| CORNER_121 | 0.75 | 500 | 0.80 | 1000 | 0.80 | 0.73 | 3 | 222.63 | 0.85 |
| CORNER_121 | 0.75 | 500 | 0.80 | 1000 | 0.80 | 0.73 | 3.3 | 194.84 | 0.88 |
| CORNER_121 | 0.75 | 500 | 0.80 | 1000 | 0.80 | 0.73 | 3.6 | 173.87 | 0.91 |
| CORNER_121 | 0.75 | 500 | 0.80 | 1000 | 0.80 | 0.73 | 3.9 | 154.34 | 0.92 |
| CORNER_121 | 0.75 | 500 | 0.80 | 1000 | 0.80 | 0.73 | 4.2 | 143.76 | 0.99 |
| CORNER_121 | 0.75 | 500 | 0.80 | 1000 | 0.80 | 0.73 | 4.5 | 132.28 | 1.02 |
| CORNER_122 | 1 | 500 | 0.80 | 1000 | 0.80 | 0.73 | 2.1 | 442.36 | 0.98 |
| CORNER_122 | 1 | 500 | 0.80 | 1000 | 0.80 | 0.73 | 2.4 | 340.28 | 0.93 |
| CORNER_122 | 1 | 500 | 0.80 | 1000 | 0.80 | 0.73 | 2.7 | 264.34 | 0.85 |
| CORNER_122 | 1 | 500 | 0.80 | 1000 | 0.80 | 0.73 | 3 | 224.45 | 0.86 |
| CORNER_122 | 1 | 500 | 0.80 | 1000 | 0.80 | 0.73 | 3.3 | 190.46 | 0.85 |
| CORNER_122 | 1 | 500 | 0.80 | 1000 | 0.80 | 0.73 | 3.6 | 168.89 | 0.87 |
| CORNER_122 | 1 | 500 | 0.80 | 1000 | 0.80 | 0.73 | 3.9 | 148.47 | 0.86 |
| CORNER_122 | 1 | 500 | 0.80 | 1000 | 0.80 | 0.73 | 4.2 | 133.09 | 0.86 |

**Table A-1 (continued)**
**FDS corner results**

| Case ID | Length (m) | HRR (kW) | Q* | HRRPUA | Diameter (m) | D* | $H_p$ (m) | Temperature Rise (°C) | $k_F$ |
|---|---|---|---|---|---|---|---|---|---|
| CORNER_123 | 1.48 | 500 | 0.80 | 1000 | 0.80 | 0.73 | 2.1 | 437.87 | 0.96 |
| CORNER_123 | 1.48 | 500 | 0.80 | 1000 | 0.80 | 0.73 | 2.4 | 353.31 | 0.99 |
| CORNER_123 | 1.48 | 500 | 0.80 | 1000 | 0.80 | 0.73 | 2.7 | 280.05 | 0.94 |
| CORNER_123 | 1.48 | 500 | 0.80 | 1000 | 0.80 | 0.73 | 3 | 228.28 | 0.89 |
| CORNER_123 | 1.48 | 500 | 0.80 | 1000 | 0.80 | 0.73 | 3.3 | 198.63 | 0.91 |
| CORNER_123 | 1.48 | 500 | 0.80 | 1000 | 0.80 | 0.73 | 3.6 | 179.95 | 0.97 |
| CORNER_123 | 1.48 | 500 | 0.80 | 1000 | 0.80 | 0.73 | 3.9 | 155.66 | 0.93 |
| CORNER_123 | 1.48 | 500 | 0.80 | 1000 | 0.80 | 0.73 | 4.2 | 135.99 | 0.90 |
| CORNER_124 | 0 | 1000 | 0.67 | 1000 | 1.13 | 0.96 | 2.7 | 760.97 | 2.49 |
| CORNER_124 | 0 | 1000 | 0.67 | 1000 | 1.13 | 0.96 | 3 | 712.65 | 3.03 |
| CORNER_124 | 0 | 1000 | 0.67 | 1000 | 1.13 | 0.96 | 3.3 | 643.88 | 3.35 |
| CORNER_124 | 0 | 1000 | 0.67 | 1000 | 1.13 | 0.96 | 3.6 | 586.73 | 3.66 |
| CORNER_124 | 0 | 1000 | 0.67 | 1000 | 1.13 | 0.96 | 3.9 | 524.28 | 3.77 |
| CORNER_124 | 0 | 1000 | 0.67 | 1000 | 1.13 | 0.96 | 4.2 | 474.03 | 3.89 |
| CORNER_124 | 0 | 1000 | 0.67 | 1000 | 1.13 | 0.96 | 4.5 | 417.11 | 3.77 |
| CORNER_124 | 0 | 1000 | 0.67 | 1000 | 1.13 | 0.96 | 4.8 | 381.34 | 3.85 |
| CORNER_124 | 0 | 1000 | 0.67 | 1000 | 1.13 | 0.96 | 5.1 | 346.42 | 3.85 |
| CORNER_124 | 0 | 1000 | 0.67 | 1000 | 1.13 | 0.96 | 5.4 | 313.75 | 3.79 |
| CORNER_124 | 0 | 1000 | 0.67 | 1000 | 1.13 | 0.96 | 5.7 | 290.33 | 3.83 |
| CORNER_124 | 0 | 1000 | 0.67 | 1000 | 1.13 | 0.96 | 6 | 275.5 | 4.02 |
| CORNER_125 | 0.24 | 1000 | 0.67 | 1000 | 1.13 | 0.96 | 2.7 | 648.5 | 1.88 |
| CORNER_125 | 0.24 | 1000 | 0.67 | 1000 | 1.13 | 0.96 | 3 | 580.06 | 2.10 |
| CORNER_125 | 0.24 | 1000 | 0.67 | 1000 | 1.13 | 0.96 | 3.3 | 504.27 | 2.17 |
| CORNER_125 | 0.24 | 1000 | 0.67 | 1000 | 1.13 | 0.96 | 3.6 | 449.15 | 2.28 |
| CORNER_125 | 0.24 | 1000 | 0.67 | 1000 | 1.13 | 0.96 | 3.9 | 402.7 | 2.36 |
| CORNER_125 | 0.24 | 1000 | 0.67 | 1000 | 1.13 | 0.96 | 4.2 | 363.35 | 2.43 |

**Table A-1 (continued)**
**FDS corner results**

| Case ID | Length (m) | HRR (kW) | Q* | HRRPUA | Diameter (m) | D* | $H_p$ (m) | Temperature Rise (°C) | $k_F$ |
|---|---|---|---|---|---|---|---|---|---|
| CORNER_125 | 0.24 | 1000 | 0.67 | 1000 | 1.13 | 0.96 | 4.5 | 327.15 | 2.45 |
| CORNER_125 | 0.24 | 1000 | 0.67 | 1000 | 1.13 | 0.96 | 4.8 | 298.76 | 2.50 |
| CORNER_125 | 0.24 | 1000 | 0.67 | 1000 | 1.13 | 0.96 | 5.1 | 276.91 | 2.59 |
| CORNER_125 | 0.24 | 1000 | 0.67 | 1000 | 1.13 | 0.96 | 5.4 | 256.41 | 2.65 |
| CORNER_125 | 0.24 | 1000 | 0.67 | 1000 | 1.13 | 0.96 | 5.7 | 239.96 | 2.73 |
| CORNER_125 | 0.24 | 1000 | 0.67 | 1000 | 1.13 | 0.96 | 6 | 227.81 | 2.87 |
| CORNER_127 | 0.48 | 1000 | 0.67 | 1000 | 1.13 | 0.96 | 2.7 | 455.34 | 1.03 |
| CORNER_127 | 0.48 | 1000 | 0.67 | 1000 | 1.13 | 0.96 | 3 | 397.06 | 1.11 |
| CORNER_127 | 0.48 | 1000 | 0.67 | 1000 | 1.13 | 0.96 | 3.3 | 334.15 | 1.08 |
| CORNER_127 | 0.48 | 1000 | 0.67 | 1000 | 1.13 | 0.96 | 3.6 | 307.01 | 1.19 |
| CORNER_127 | 0.48 | 1000 | 0.67 | 1000 | 1.13 | 0.96 | 3.9 | 285.48 | 1.31 |
| CORNER_127 | 0.48 | 1000 | 0.67 | 1000 | 1.13 | 0.96 | 4.2 | 265.72 | 1.42 |
| CORNER_127 | 0.48 | 1000 | 0.67 | 1000 | 1.13 | 0.96 | 4.5 | 244.75 | 1.49 |
| CORNER_127 | 0.48 | 1000 | 0.67 | 1000 | 1.13 | 0.96 | 4.8 | 230.15 | 1.59 |
| CORNER_127 | 0.48 | 1000 | 0.67 | 1000 | 1.13 | 0.96 | 5.1 | 219.39 | 1.73 |
| CORNER_127 | 0.48 | 1000 | 0.67 | 1000 | 1.13 | 0.96 | 5.4 | 207.35 | 1.83 |
| CORNER_127 | 0.48 | 1000 | 0.67 | 1000 | 1.13 | 0.96 | 5.7 | 194.42 | 1.89 |
| CORNER_127 | 0.48 | 1000 | 0.67 | 1000 | 1.13 | 0.96 | 6 | 181.96 | 1.93 |
| CORNER_128 | 0.76 | 1000 | 0.67 | 1000 | 1.13 | 0.96 | 2.7 | 416.01 | 0.89 |
| CORNER_128 | 0.76 | 1000 | 0.67 | 1000 | 1.13 | 0.96 | 3 | 365.87 | 0.97 |
| CORNER_128 | 0.76 | 1000 | 0.67 | 1000 | 1.13 | 0.96 | 3.3 | 311.89 | 0.96 |
| CORNER_128 | 0.76 | 1000 | 0.67 | 1000 | 1.13 | 0.96 | 3.6 | 274.28 | 0.98 |
| CORNER_128 | 0.76 | 1000 | 0.67 | 1000 | 1.13 | 0.96 | 3.9 | 235.33 | 0.94 |
| CORNER_128 | 0.76 | 1000 | 0.67 | 1000 | 1.13 | 0.96 | 4.2 | 212.9 | 0.97 |
| CORNER_128 | 0.76 | 1000 | 0.67 | 1000 | 1.13 | 0.96 | 4.5 | 199.42 | 1.05 |
| CORNER_128 | 0.76 | 1000 | 0.67 | 1000 | 1.13 | 0.96 | 4.8 | 189.85 | 1.14 |

**Table A-1 (continued)**
**FDS corner results**

| Case ID | Length (m) | HRR (kW) | Q* | HRRPUA | Diameter (m) | D* | $H_p$ (m) | Temperature Rise (°C) | $k_F$ |
|---|---|---|---|---|---|---|---|---|---|
| CORNER_128 | 0.76 | 1000 | 0.67 | 1000 | 1.13 | 0.96 | 5.1 | 175.8 | 1.17 |
| CORNER_128 | 0.76 | 1000 | 0.67 | 1000 | 1.13 | 0.96 | 5.4 | 163.9 | 1.21 |
| CORNER_128 | 0.76 | 1000 | 0.67 | 1000 | 1.13 | 0.96 | 5.7 | 154.07 | 1.25 |
| CORNER_128 | 0.76 | 1000 | 0.67 | 1000 | 1.13 | 0.96 | 6 | 149.28 | 1.35 |
| CORNER_129 | 1 | 1000 | 0.67 | 1000 | 1.13 | 0.96 | 2.7 | 481.18 | 1.13 |
| CORNER_129 | 1 | 1000 | 0.67 | 1000 | 1.13 | 0.96 | 3 | 415.2 | 1.19 |
| CORNER_129 | 1 | 1000 | 0.67 | 1000 | 1.13 | 0.96 | 3.3 | 342.64 | 1.13 |
| CORNER_129 | 1 | 1000 | 0.67 | 1000 | 1.13 | 0.96 | 3.6 | 286.48 | 1.06 |
| CORNER_129 | 1 | 1000 | 0.67 | 1000 | 1.13 | 0.96 | 3.9 | 246.11 | 1.02 |
| CORNER_129 | 1 | 1000 | 0.67 | 1000 | 1.13 | 0.96 | 4.2 | 222.17 | 1.05 |
| CORNER_129 | 1 | 1000 | 0.67 | 1000 | 1.13 | 0.96 | 4.5 | 196.53 | 1.02 |
| CORNER_129 | 1 | 1000 | 0.67 | 1000 | 1.13 | 0.96 | 4.8 | 178.86 | 1.03 |
| CORNER_129 | 1 | 1000 | 0.67 | 1000 | 1.13 | 0.96 | 5.1 | 165.09 | 1.05 |
| CORNER_129 | 1 | 1000 | 0.67 | 1000 | 1.13 | 0.96 | 5.4 | 153.9 | 1.08 |
| CORNER_129 | 1 | 1000 | 0.67 | 1000 | 1.13 | 0.96 | 5.7 | 140.25 | 1.06 |
| CORNER_129 | 1 | 1000 | 0.67 | 1000 | 1.13 | 0.96 | 6 | 133.94 | 1.11 |
| CORNER_130 | 1.48 | 1000 | 0.67 | 1000 | 1.13 | 0.96 | 2.7 | 474.65 | 1.11 |
| CORNER_130 | 1.48 | 1000 | 0.67 | 1000 | 1.13 | 0.96 | 3 | 406.26 | 1.15 |
| CORNER_130 | 1.48 | 1000 | 0.67 | 1000 | 1.13 | 0.96 | 3.3 | 339.41 | 1.11 |
| CORNER_130 | 1.48 | 1000 | 0.67 | 1000 | 1.13 | 0.96 | 3.6 | 296.31 | 1.12 |
| CORNER_130 | 1.48 | 1000 | 0.67 | 1000 | 1.13 | 0.96 | 3.9 | 251.66 | 1.06 |
| CORNER_130 | 1.48 | 1000 | 0.67 | 1000 | 1.13 | 0.96 | 4.2 | 227.1 | 1.09 |
| CORNER_130 | 1.48 | 1000 | 0.67 | 1000 | 1.13 | 0.96 | 4.5 | 206.18 | 1.11 |
| CORNER_130 | 1.48 | 1000 | 0.67 | 1000 | 1.13 | 0.96 | 4.8 | 190.53 | 1.15 |
| CORNER_130 | 1.48 | 1000 | 0.67 | 1000 | 1.13 | 0.96 | 5.1 | 173.27 | 1.14 |
| CORNER_130 | 1.48 | 1000 | 0.67 | 1000 | 1.13 | 0.96 | 5.4 | 155.46 | 1.10 |

**Table A-1 (continued)**
**FDS corner results**

| Case ID | Length (m) | HRR (kW) | Q* | HRRPUA | Diameter (m) | D* | $H_p$ (m) | Temperature Rise (°C) | $k_F$ |
|---|---|---|---|---|---|---|---|---|---|
| CORNER_130 | 1.48 | 1000 | 0.67 | 1000 | 1.13 | 0.96 | 5.7 | 143.9 | 1.11 |
| CORNER_130 | 1.48 | 1000 | 0.67 | 1000 | 1.13 | 0.96 | 6 | 135.58 | 1.14 |
| CORNER_131 | 0 | 250 | 2.26 | 2000 | 0.40 | 0.55 | 1.8 | 765.03 | 2.01 |
| CORNER_131 | 0 | 250 | 2.26 | 2000 | 0.40 | 0.55 | 2.1 | 677.98 | 2.61 |
| CORNER_131 | 0 | 250 | 2.26 | 2000 | 0.40 | 0.55 | 2.4 | 592.2 | 3.13 |
| CORNER_131 | 0 | 250 | 2.26 | 2000 | 0.40 | 0.55 | 2.7 | 505.73 | 3.47 |
| CORNER_131 | 0 | 250 | 2.26 | 2000 | 0.40 | 0.55 | 3 | 444.57 | 3.85 |
| CORNER_131 | 0 | 250 | 2.26 | 2000 | 0.40 | 0.55 | 3.3 | 381.34 | 4.00 |
| CORNER_131 | 0 | 250 | 2.26 | 2000 | 0.40 | 0.55 | 3.6 | 323.54 | 3.97 |
| CORNER_131 | 0 | 250 | 2.26 | 2000 | 0.40 | 0.55 | 3.9 | 272.55 | 3.81 |
| CORNER_131 | 0 | 250 | 2.26 | 2000 | 0.40 | 0.55 | 4.2 | 240.22 | 3.83 |
| CORNER_131 | 0 | 250 | 2.26 | 2000 | 0.40 | 0.55 | 4.5 | 215.87 | 3.90 |
| CORNER_131 | 0 | 250 | 2.26 | 2000 | 0.40 | 0.55 | 4.8 | 199.16 | 4.08 |
| CORNER_131 | 0 | 250 | 2.26 | 2000 | 0.40 | 0.55 | 5.1 | 180.6 | 4.09 |
| CORNER_131 | 0 | 250 | 2.26 | 2000 | 0.40 | 0.55 | 5.4 | 164.03 | 4.07 |
| CORNER_131 | 0 | 250 | 2.26 | 2000 | 0.40 | 0.55 | 5.7 | 152.1 | 4.15 |
| CORNER_131 | 0 | 250 | 2.26 | 2000 | 0.40 | 0.55 | 6 | 142.13 | 4.24 |
| CORNER_132 | 0.24 | 250 | 2.26 | 2000 | 0.40 | 0.55 | 1.8 | 508.97 | 1.18 |
| CORNER_132 | 0.24 | 250 | 2.26 | 2000 | 0.40 | 0.55 | 2.1 | 407.84 | 1.32 |
| CORNER_132 | 0.24 | 250 | 2.26 | 2000 | 0.40 | 0.55 | 2.4 | 341.37 | 1.47 |
| CORNER_132 | 0.24 | 250 | 2.26 | 2000 | 0.40 | 0.55 | 2.7 | 292.08 | 1.60 |
| CORNER_132 | 0.24 | 250 | 2.26 | 2000 | 0.40 | 0.55 | 3 | 260.96 | 1.79 |
| CORNER_132 | 0.24 | 250 | 2.26 | 2000 | 0.40 | 0.55 | 3.3 | 236.56 | 1.99 |
| CORNER_132 | 0.24 | 250 | 2.26 | 2000 | 0.40 | 0.55 | 3.6 | 214.86 | 2.16 |
| CORNER_132 | 0.24 | 250 | 2.26 | 2000 | 0.40 | 0.55 | 3.9 | 195.38 | 2.30 |
| CORNER_132 | 0.24 | 250 | 2.26 | 2000 | 0.40 | 0.55 | 4.2 | 179.85 | 2.45 |

**Table A-1 (continued)**
**FDS corner results**

| Case ID | Length (m) | HRR (kW) | Q* | HRRPUA | Diameter (m) | D* | $H_p$ (m) | Temperature Rise (°C) | $k_F$ |
|---|---|---|---|---|---|---|---|---|---|
| CORNER_132 | 0.24 | 250 | 2.26 | 2000 | 0.40 | 0.55 | 4.5 | 163.23 | 2.52 |
| CORNER_132 | 0.24 | 250 | 2.26 | 2000 | 0.40 | 0.55 | 4.8 | 150.56 | 2.61 |
| CORNER_132 | 0.24 | 250 | 2.26 | 2000 | 0.40 | 0.55 | 5.1 | 139.16 | 2.69 |
| CORNER_133 | 1.48 | 250 | 2.26 | 2000 | 0.40 | 0.55 | 1.8 | 282.31 | 0.53 |
| CORNER_133 | 1.48 | 250 | 2.26 | 2000 | 0.40 | 0.55 | 2.1 | 211.52 | 0.52 |
| CORNER_133 | 1.48 | 250 | 2.26 | 2000 | 0.40 | 0.55 | 2.4 | 176.58 | 0.56 |
| CORNER_133 | 1.48 | 250 | 2.26 | 2000 | 0.40 | 0.55 | 2.7 | 149.22 | 0.58 |
| CORNER_134 | 0 | 1000 | 1.60 | 2000 | 0.80 | 0.96 | 3 | 823.43 | 2.26 |
| CORNER_134 | 0 | 1000 | 1.60 | 2000 | 0.80 | 0.96 | 3.3 | 784.59 | 2.75 |
| CORNER_134 | 0 | 1000 | 1.60 | 2000 | 0.80 | 0.96 | 3.6 | 732.6 | 3.19 |
| CORNER_134 | 0 | 1000 | 1.60 | 2000 | 0.80 | 0.96 | 3.9 | 673 | 3.53 |
| CORNER_134 | 0 | 1000 | 1.60 | 2000 | 0.80 | 0.96 | 4.2 | 620.31 | 3.85 |
| CORNER_134 | 0 | 1000 | 1.60 | 2000 | 0.80 | 0.96 | 4.5 | 559 | 4.01 |
| CORNER_134 | 0 | 1000 | 1.60 | 2000 | 0.80 | 0.96 | 4.8 | 507.91 | 4.16 |
| CORNER_134 | 0 | 1000 | 1.60 | 2000 | 0.80 | 0.96 | 5.1 | 464.96 | 4.30 |
| CORNER_134 | 0 | 1000 | 1.60 | 2000 | 0.80 | 0.96 | 5.4 | 409.16 | 4.16 |
| CORNER_134 | 0 | 1000 | 1.60 | 2000 | 0.80 | 0.96 | 5.7 | 357.3 | 3.92 |
| CORNER_134 | 0 | 1000 | 1.60 | 2000 | 0.80 | 0.96 | 6 | 327.07 | 3.94 |
| CORNER_135 | 0.24 | 1000 | 1.60 | 2000 | 0.80 | 0.96 | 3 | 717.88 | 1.87 |
| CORNER_135 | 0.24 | 1000 | 1.60 | 2000 | 0.80 | 0.96 | 3.3 | 644.03 | 2.09 |
| CORNER_135 | 0.24 | 1000 | 1.60 | 2000 | 0.80 | 0.96 | 3.6 | 582.71 | 2.31 |
| CORNER_135 | 0.24 | 1000 | 1.60 | 2000 | 0.80 | 0.96 | 3.9 | 504.7 | 2.34 |
| CORNER_135 | 0.24 | 1000 | 1.60 | 2000 | 0.80 | 0.96 | 4.2 | 454.8 | 2.46 |
| CORNER_135 | 0.24 | 1000 | 1.60 | 2000 | 0.80 | 0.96 | 4.5 | 407.82 | 2.53 |
| CORNER_135 | 0.24 | 1000 | 1.60 | 2000 | 0.80 | 0.96 | 4.8 | 371.4 | 2.62 |
| CORNER_135 | 0.24 | 1000 | 1.60 | 2000 | 0.80 | 0.96 | 5.1 | 341.76 | 2.72 |

**Table A-1 (continued)**
**FDS corner results**

| Case ID | Length (m) | HRR (kW) | Q* | HRRPUA | Diameter (m) | D* | $H_p$ (m) | Temperature Rise (°C) | $k_F$ |
|---|---|---|---|---|---|---|---|---|---|
| CORNER_135 | 0.24 | 1000 | 1.60 | 2000 | 0.80 | 0.96 | 5.4 | 314.13 | 2.79 |
| CORNER_135 | 0.24 | 1000 | 1.60 | 2000 | 0.80 | 0.96 | 5.7 | 285.12 | 2.78 |
| CORNER_135 | 0.24 | 1000 | 1.60 | 2000 | 0.80 | 0.96 | 6 | 267.73 | 2.90 |
| CORNER_136 | 1.48 | 1000 | 1.60 | 2000 | 0.80 | 0.96 | 3 | 421.26 | 0.89 |
| CORNER_136 | 1.48 | 1000 | 1.60 | 2000 | 0.80 | 0.96 | 3.3 | 345.48 | 0.87 |
| CORNER_136 | 1.48 | 1000 | 1.60 | 2000 | 0.80 | 0.96 | 3.6 | 299.21 | 0.89 |
| CORNER_136 | 1.48 | 1000 | 1.60 | 2000 | 0.80 | 0.96 | 3.9 | 256.08 | 0.87 |
| CORNER_136 | 1.48 | 1000 | 1.60 | 2000 | 0.80 | 0.96 | 4.2 | 228.42 | 0.89 |
| CORNER_136 | 1.48 | 1000 | 1.60 | 2000 | 0.80 | 0.96 | 4.5 | 199.33 | 0.86 |
| CORNER_136 | 1.48 | 1000 | 1.60 | 2000 | 0.80 | 0.96 | 4.8 | 178.27 | 0.86 |
| CORNER_136 | 1.48 | 1000 | 1.60 | 2000 | 0.80 | 0.96 | 5.1 | 162.39 | 0.86 |
| CORNER_136 | 1.48 | 1000 | 1.60 | 2000 | 0.80 | 0.96 | 5.4 | 144.69 | 0.83 |
| CORNER_136 | 1.48 | 1000 | 1.60 | 2000 | 0.80 | 0.96 | 5.7 | 133.02 | 0.83 |
| CORNER_137 | 0.24 | 250 | 0.17 | 250 | 1.13 | 0.55 | 1.2 | 371.85 | 0.90 |
| CORNER_137 | 0.24 | 250 | 0.17 | 250 | 1.13 | 0.55 | 1.5 | 285.62 | 0.92 |
| CORNER_137 | 0.24 | 250 | 0.17 | 250 | 1.13 | 0.55 | 1.8 | 245.62 | 1.11 |
| CORNER_137 | 0.24 | 250 | 0.17 | 250 | 1.13 | 0.55 | 2.1 | 221.57 | 1.37 |
| CORNER_137 | 0.24 | 250 | 0.17 | 250 | 1.13 | 0.55 | 2.4 | 207.76 | 1.75 |
| CORNER_137 | 0.24 | 250 | 0.17 | 250 | 1.13 | 0.55 | 2.7 | 193.17 | 2.07 |
| CORNER_137 | 0.24 | 250 | 0.17 | 250 | 1.13 | 0.55 | 3 | 184.28 | 2.52 |
| CORNER_137 | 0.24 | 250 | 0.17 | 250 | 1.13 | 0.55 | 3.3 | 171.92 | 2.81 |
| CORNER_137 | 0.24 | 250 | 0.17 | 250 | 1.13 | 0.55 | 3.6 | 161.54 | 3.10 |
| CORNER_137 | 0.24 | 250 | 0.17 | 250 | 1.13 | 0.55 | 3.9 | 152.29 | 3.39 |
| CORNER_137 | 0.24 | 250 | 0.17 | 250 | 1.13 | 0.55 | 4.2 | 144.7 | 3.70 |
| CORNER_137 | 0.24 | 250 | 0.17 | 250 | 1.13 | 0.55 | 4.5 | 135.81 | 3.86 |
| CORNER_138 | 1.48 | 250 | 0.17 | 250 | 1.13 | 0.55 | 1.2 | 437.98 | 1.45 |

**Table A-1 (continued)**
**FDS corner results**

| Case ID | Length (m) | HRR (kW) | Q* | HRRPUA | Diameter (m) | D* | $H_p$ (m) | Temperature Rise (°C) | $k_F$ |
|---|---|---|---|---|---|---|---|---|---|
| CORNER_138 | 1.48 | 250 | 0.17 | 250 | 1.13 | 0.55 | 1.5 | 317.89 | 1.21 |
| CORNER_138 | 1.48 | 250 | 0.17 | 250 | 1.13 | 0.55 | 1.8 | 240.22 | 1.05 |
| CORNER_138 | 1.48 | 250 | 0.17 | 250 | 1.13 | 0.55 | 2.1 | 194.58 | 1.01 |
| CORNER_138 | 1.48 | 250 | 0.17 | 250 | 1.13 | 0.55 | 2.4 | 163.11 | 0.99 |
| CORNER_138 | 1.48 | 250 | 0.17 | 250 | 1.13 | 0.55 | 2.7 | 140.23 | 0.98 |
| CORNER_140 | 0 | 250 | 0.40 | 500 | 0.80 | 0.55 | 1.5 | 736.61 | 3.62 |
| CORNER_140 | 0 | 250 | 0.40 | 500 | 0.80 | 0.55 | 1.8 | 665.48 | 5.19 |
| CORNER_140 | 0 | 250 | 0.40 | 500 | 0.80 | 0.55 | 2.1 | 572.97 | 5.95 |
| CORNER_140 | 0 | 250 | 0.40 | 500 | 0.80 | 0.55 | 2.4 | 494.37 | 6.41 |
| CORNER_140 | 0 | 250 | 0.40 | 500 | 0.80 | 0.55 | 2.7 | 423.18 | 6.45 |
| CORNER_140 | 0 | 250 | 0.40 | 500 | 0.80 | 0.55 | 3 | 365.62 | 6.41 |
| CORNER_140 | 0 | 250 | 0.40 | 500 | 0.80 | 0.55 | 3.3 | 313.16 | 6.07 |
| CORNER_140 | 0 | 250 | 0.40 | 500 | 0.80 | 0.55 | 3.6 | 277.55 | 6.06 |
| CORNER_140 | 0 | 250 | 0.40 | 500 | 0.80 | 0.55 | 3.9 | 246.42 | 5.95 |
| CORNER_140 | 0 | 250 | 0.40 | 500 | 0.80 | 0.55 | 4.2 | 222.82 | 5.96 |
| CORNER_140 | 0 | 250 | 0.40 | 500 | 0.80 | 0.55 | 4.5 | 199.23 | 5.75 |
| CORNER_140 | 0 | 250 | 0.40 | 500 | 0.80 | 0.55 | 4.8 | 182.86 | 5.78 |
| CORNER_140 | 0 | 250 | 0.40 | 500 | 0.80 | 0.55 | 5.1 | 168.14 | 5.76 |
| CORNER_140 | 0 | 250 | 0.40 | 500 | 0.80 | 0.55 | 5.4 | 156.03 | 5.79 |
| CORNER_140 | 0 | 250 | 0.40 | 500 | 0.80 | 0.55 | 5.7 | 144.01 | 5.70 |
| CORNER_140 | 0 | 250 | 0.40 | 500 | 0.80 | 0.55 | 6 | 135.45 | 5.78 |
| CORNER_141 | 0.24 | 250 | 0.40 | 500 | 0.80 | 0.55 | 1.5 | 427.84 | 1.13 |
| CORNER_141 | 0.24 | 250 | 0.40 | 500 | 0.80 | 0.55 | 1.8 | 354.85 | 1.34 |
| CORNER_141 | 0.24 | 250 | 0.40 | 500 | 0.80 | 0.55 | 2.1 | 309 | 1.60 |
| CORNER_141 | 0.24 | 250 | 0.40 | 500 | 0.80 | 0.55 | 2.4 | 280.89 | 1.94 |
| CORNER_141 | 0.24 | 250 | 0.40 | 500 | 0.80 | 0.55 | 2.7 | 254.1 | 2.23 |

**Table A-1 (continued)**
**FDS corner results**

| Case ID | Length (m) | HRR (kW) | Q* | HRRPUA | Diameter (m) | D* | $H_p$ (m) | Temperature Rise (°C) | $k_F$ |
|---|---|---|---|---|---|---|---|---|---|
| CORNER_141 | 0.24 | 250 | 0.40 | 500 | 0.80 | 0.55 | 3 | 230.21 | 2.47 |
| CORNER_141 | 0.24 | 250 | 0.40 | 500 | 0.80 | 0.55 | 3.3 | 212.01 | 2.74 |
| CORNER_141 | 0.24 | 250 | 0.40 | 500 | 0.80 | 0.55 | 3.6 | 196.3 | 3.00 |
| CORNER_141 | 0.24 | 250 | 0.40 | 500 | 0.80 | 0.55 | 3.9 | 178.57 | 3.10 |
| CORNER_141 | 0.24 | 250 | 0.40 | 500 | 0.80 | 0.55 | 4.2 | 165.03 | 3.25 |
| CORNER_141 | 0.24 | 250 | 0.40 | 500 | 0.80 | 0.55 | 4.5 | 152.58 | 3.36 |
| CORNER_141 | 0.24 | 250 | 0.40 | 500 | 0.80 | 0.55 | 4.8 | 141.65 | 3.45 |
| CORNER_141 | 0.24 | 250 | 0.40 | 500 | 0.80 | 0.55 | 5.1 | 134.02 | 3.64 |
| CORNER_142 | 1.48 | 250 | 0.40 | 500 | 0.80 | 0.55 | 1.5 | 385.21 | 0.93 |
| CORNER_142 | 1.48 | 250 | 0.40 | 500 | 0.80 | 0.55 | 1.8 | 282.68 | 0.87 |
| CORNER_142 | 1.48 | 250 | 0.40 | 500 | 0.80 | 0.55 | 2.1 | 211.86 | 0.79 |
| CORNER_142 | 1.48 | 250 | 0.40 | 500 | 0.80 | 0.55 | 2.4 | 176.87 | 0.81 |
| CORNER_142 | 1.48 | 250 | 0.40 | 500 | 0.80 | 0.55 | 2.7 | 146.06 | 0.78 |
| CORNER_144 | 0 | 1000 | 0.28 | 500 | 1.60 | 0.96 | 2.1 | 695.46 | 2.50 |
| CORNER_144 | 0 | 1000 | 0.28 | 500 | 1.60 | 0.96 | 2.4 | 642.65 | 3.20 |
| CORNER_144 | 0 | 1000 | 0.28 | 500 | 1.60 | 0.96 | 2.7 | 571.51 | 3.44 |
| CORNER_144 | 0 | 1000 | 0.28 | 500 | 1.60 | 0.96 | 3 | 515.01 | 3.69 |
| CORNER_144 | 0 | 1000 | 0.28 | 500 | 1.60 | 0.96 | 3.3 | 447.07 | 3.48 |
| CORNER_144 | 0 | 1000 | 0.28 | 500 | 1.60 | 0.96 | 3.6 | 390.19 | 3.26 |
| CORNER_144 | 0 | 1000 | 0.28 | 500 | 1.60 | 0.96 | 3.9 | 335.51 | 2.92 |
| CORNER_144 | 0 | 1000 | 0.28 | 500 | 1.60 | 0.96 | 4.2 | 295.35 | 2.73 |
| CORNER_144 | 0 | 1000 | 0.28 | 500 | 1.60 | 0.96 | 4.5 | 256.26 | 2.44 |
| CORNER_144 | 0 | 1000 | 0.28 | 500 | 1.60 | 0.96 | 4.8 | 228.86 | 2.31 |
| CORNER_144 | 0 | 1000 | 0.28 | 500 | 1.60 | 0.96 | 5.1 | 212.12 | 2.33 |
| CORNER_144 | 0 | 1000 | 0.28 | 500 | 1.60 | 0.96 | 5.4 | 196.63 | 2.34 |
| CORNER_144 | 0 | 1000 | 0.28 | 500 | 1.60 | 0.96 | 5.7 | 187.59 | 2.47 |

**Table A-1 (continued)**
**FDS corner results**

| Case ID | Length (m) | HRR (kW) | Q* | HRRPUA | Diameter (m) | D* | $H_p$ (m) | Temperature Rise (°C) | $k_F$ |
|---|---|---|---|---|---|---|---|---|---|
| CORNER_144 | 0 | 1000 | 0.28 | 500 | 1.60 | 0.96 | 6 | 177.56 | 2.54 |
| CORNER_146 | 0.24 | 1000 | 0.28 | 500 | 1.60 | 0.96 | 2.1 | 584.76 | 1.57 |
| CORNER_146 | 0.24 | 1000 | 0.28 | 500 | 1.60 | 0.96 | 2.4 | 533.19 | 1.93 |
| CORNER_146 | 0.24 | 1000 | 0.28 | 500 | 1.60 | 0.96 | 2.7 | 479.2 | 2.17 |
| CORNER_146 | 0.24 | 1000 | 0.28 | 500 | 1.60 | 0.96 | 3 | 427.94 | 2.30 |
| CORNER_146 | 0.24 | 1000 | 0.28 | 500 | 1.60 | 0.96 | 3.3 | 386.05 | 2.43 |
| CORNER_146 | 0.24 | 1000 | 0.28 | 500 | 1.60 | 0.96 | 3.6 | 355.35 | 2.61 |
| CORNER_146 | 0.24 | 1000 | 0.28 | 500 | 1.60 | 0.96 | 3.9 | 321.84 | 2.65 |
| CORNER_146 | 0.24 | 1000 | 0.28 | 500 | 1.60 | 0.96 | 4.2 | 293.66 | 2.69 |
| CORNER_146 | 0.24 | 1000 | 0.28 | 500 | 1.60 | 0.96 | 4.5 | 266.13 | 2.65 |
| CORNER_146 | 0.24 | 1000 | 0.28 | 500 | 1.60 | 0.96 | 4.8 | 248.91 | 2.77 |
| CORNER_146 | 0.24 | 1000 | 0.28 | 500 | 1.60 | 0.96 | 5.1 | 232.63 | 2.85 |
| CORNER_146 | 0.24 | 1000 | 0.28 | 500 | 1.60 | 0.96 | 5.4 | 218.24 | 2.92 |
| CORNER_146 | 0.24 | 1000 | 0.28 | 500 | 1.60 | 0.96 | 5.7 | 203.57 | 2.93 |
| CORNER_146 | 0.24 | 1000 | 0.28 | 500 | 1.60 | 0.96 | 6 | 193.24 | 3.04 |

**Table A-2**
**Wall configuration results**

| Case ID | Length (m) | HRR (kW) | Q* | HRRPUA | Diameter (m) | D* | $H_p$ (m) | Temperature Rise (°C) | $k_F$ |
|---|---|---|---|---|---|---|---|---|---|
| WALL_100 | 0 | 40 | 1.50 | 1000 | 0.23 | 0.27 | 0.9 | 321.23 | 0.77 |
| WALL_100 | 0 | 40 | 1.50 | 1000 | 0.23 | 0.27 | 1.2 | 212.61 | 0.88 |
| WALL_100 | 0 | 40 | 1.50 | 1000 | 0.23 | 0.27 | 1.5 | 164.09 | 1.05 |
| WALL_100 | 0 | 40 | 1.50 | 1000 | 0.23 | 0.27 | 1.8 | 136.87 | 1.25 |
| WALL_101 | 0.24 | 40 | 1.50 | 1000 | 0.23 | 0.27 | 0.9 | 244.89 | 0.51 |
| WALL_101 | 0.24 | 40 | 1.50 | 1000 | 0.23 | 0.27 | 1.2 | 169.95 | 0.62 |
| WALL_101 | 0.24 | 40 | 1.50 | 1000 | 0.23 | 0.27 | 1.5 | 126.49 | 0.68 |
| WALL_102 | 0.48 | 40 | 1.50 | 1000 | 0.23 | 0.27 | 0.9 | 242.92 | 0.51 |
| WALL_102 | 0.48 | 40 | 1.50 | 1000 | 0.23 | 0.27 | 1.2 | 168.64 | 0.61 |
| WALL_102 | 0.48 | 40 | 1.50 | 1000 | 0.23 | 0.27 | 1.5 | 128.67 | 0.70 |
| WALL_103 | 0.76 | 40 | 1.50 | 1000 | 0.23 | 0.27 | 0.9 | 243.52 | 0.51 |
| WALL_103 | 0.76 | 40 | 1.50 | 1000 | 0.23 | 0.27 | 1.2 | 173.82 | 0.64 |
| WALL_103 | 0.76 | 40 | 1.50 | 1000 | 0.23 | 0.27 | 1.5 | 130.66 | 0.72 |
| WALL_104 | 1 | 40 | 1.50 | 1000 | 0.23 | 0.27 | 0.9 | 222.05 | 0.44 |
| WALL_104 | 1 | 40 | 1.50 | 1000 | 0.23 | 0.27 | 1.2 | 153.36 | 0.53 |
| WALL_105 | 1.48 | 40 | 1.50 | 1000 | 0.23 | 0.27 | 0.9 | 238.41 | 0.49 |
| WALL_105 | 1.48 | 40 | 1.50 | 1000 | 0.23 | 0.27 | 1.2 | 162.85 | 0.58 |
| WALL_106 | 0 | 78 | 1.26 | 1000 | 0.32 | 0.35 | 1.2 | 322.59 | 0.85 |
| WALL_106 | 0 | 78 | 1.26 | 1000 | 0.32 | 0.35 | 1.5 | 229.12 | 0.91 |
| WALL_106 | 0 | 78 | 1.26 | 1000 | 0.32 | 0.35 | 1.8 | 181.83 | 1.02 |
| WALL_106 | 0 | 78 | 1.26 | 1000 | 0.32 | 0.35 | 2.1 | 142.6 | 1.02 |
| WALL_107 | 0.24 | 78 | 1.26 | 1000 | 0.32 | 0.35 | 1.2 | 255.08 | 0.60 |
| WALL_107 | 0.24 | 78 | 1.26 | 1000 | 0.32 | 0.35 | 1.5 | 179.41 | 0.62 |
| WALL_107 | 0.24 | 78 | 1.26 | 1000 | 0.32 | 0.35 | 1.8 | 145.4 | 0.71 |

**Table A-2 (continued)**
**Wall configuration results**

| Case ID | Length (m) | HRR (kW) | Q* | HRRPUA | Diameter (m) | D* | $H_p$ (m) | Temperature Rise (°C) | $k_F$ |
|---|---|---|---|---|---|---|---|---|---|
| WALL_108 | 0.48 | 78 | 1.26 | 1000 | 0.32 | 0.35 | 1.2 | 243.24 | 0.56 |
| WALL_108 | 0.48 | 78 | 1.26 | 1000 | 0.32 | 0.35 | 1.5 | 170.51 | 0.57 |
| WALL_108 | 0.48 | 78 | 1.26 | 1000 | 0.32 | 0.35 | 1.8 | 139.32 | 0.66 |
| WALL_109 | 0.76 | 78 | 1.26 | 1000 | 0.32 | 0.35 | 1.2 | 258.49 | 0.61 |
| WALL_109 | 0.76 | 78 | 1.26 | 1000 | 0.32 | 0.35 | 1.5 | 193.87 | 0.70 |
| WALL_109 | 0.76 | 78 | 1.26 | 1000 | 0.32 | 0.35 | 1.8 | 150.9 | 0.75 |
| WALL_110 | 1 | 78 | 1.26 | 1000 | 0.32 | 0.35 | 1.2 | 254.7 | 0.60 |
| WALL_110 | 1 | 78 | 1.26 | 1000 | 0.32 | 0.35 | 1.5 | 173.77 | 0.59 |
| WALL_110 | 1 | 78 | 1.26 | 1000 | 0.32 | 0.35 | 1.8 | 133.91 | 0.62 |
| WALL_111 | 1.48 | 78 | 1.26 | 1000 | 0.32 | 0.35 | 1.2 | 257.02 | 0.60 |
| WALL_111 | 1.48 | 78 | 1.26 | 1000 | 0.32 | 0.35 | 1.5 | 173.37 | 0.59 |
| WALL_111 | 1.48 | 78 | 1.26 | 1000 | 0.32 | 0.35 | 1.8 | 139.81 | 0.66 |
| WALL_112 | 0 | 250 | 0.95 | 1000 | 0.56 | 0.55 | 1.8 | 353.97 | 0.91 |
| WALL_112 | 0 | 250 | 0.95 | 1000 | 0.56 | 0.55 | 2.1 | 279.55 | 0.95 |
| WALL_112 | 0 | 250 | 0.95 | 1000 | 0.56 | 0.55 | 2.4 | 233.38 | 1.02 |
| WALL_112 | 0 | 250 | 0.95 | 1000 | 0.56 | 0.55 | 2.7 | 195.29 | 1.04 |
| WALL_112 | 0 | 250 | 0.95 | 1000 | 0.56 | 0.55 | 3 | 173.96 | 1.13 |
| WALL_112 | 0 | 250 | 0.95 | 1000 | 0.56 | 0.55 | 3.3 | 156 | 1.21 |
| WALL_112 | 0 | 250 | 0.95 | 1000 | 0.56 | 0.55 | 3.6 | 140.38 | 1.27 |
| WALL_113 | 0.24 | 250 | 0.95 | 1000 | 0.56 | 0.55 | 1.8 | 315.59 | 0.76 |
| WALL_113 | 0.24 | 250 | 0.95 | 1000 | 0.56 | 0.55 | 2.1 | 232.77 | 0.71 |
| WALL_113 | 0.24 | 250 | 0.95 | 1000 | 0.56 | 0.55 | 2.4 | 191.82 | 0.74 |
| WALL_113 | 0.24 | 250 | 0.95 | 1000 | 0.56 | 0.55 | 2.7 | 160.58 | 0.75 |

**Table A-2 (continued)**
**Wall configuration results**

| Case ID | Length (m) | HRR (kW) | Q* | HRRPUA | Diameter (m) | D* | $H_p$ (m) | Temperature Rise (°C) | $k_F$ |
|---|---|---|---|---|---|---|---|---|---|
| WALL_113 | 0.24 | 250 | 0.95 | 1000 | 0.56 | 0.55 | 3 | 140.95 | 0.79 |
| WALL_113 | 0.24 | 250 | 0.95 | 1000 | 0.56 | 0.55 | 3.3 | 125.51 | 0.83 |
| WALL_114 | 0.48 | 250 | 0.95 | 1000 | 0.56 | 0.55 | 1.8 | 272.52 | 0.60 |
| WALL_114 | 0.48 | 250 | 0.95 | 1000 | 0.56 | 0.55 | 2.1 | 204.65 | 0.58 |
| WALL_114 | 0.48 | 250 | 0.95 | 1000 | 0.56 | 0.55 | 2.4 | 174.15 | 0.63 |
| WALL_114 | 0.48 | 250 | 0.95 | 1000 | 0.56 | 0.55 | 2.7 | 142.85 | 0.62 |
| WALL_114 | 0.48 | 250 | 0.95 | 1000 | 0.56 | 0.55 | 3 | 127.06 | 0.66 |
| WALL_115 | 0.76 | 250 | 0.95 | 1000 | 0.56 | 0.55 | 1.8 | 255.32 | 0.55 |
| WALL_115 | 0.76 | 250 | 0.95 | 1000 | 0.56 | 0.55 | 2.1 | 208.08 | 0.59 |
| WALL_115 | 0.76 | 250 | 0.95 | 1000 | 0.56 | 0.55 | 2.4 | 175.45 | 0.64 |
| WALL_115 | 0.76 | 250 | 0.95 | 1000 | 0.56 | 0.55 | 2.7 | 143.69 | 0.62 |
| WALL_115 | 0.76 | 250 | 0.95 | 1000 | 0.56 | 0.55 | 3 | 128.95 | 0.68 |
| WALL_116 | 1 | 250 | 0.95 | 1000 | 0.56 | 0.55 | 1.8 | 268.5 | 0.59 |
| WALL_116 | 1 | 250 | 0.95 | 1000 | 0.56 | 0.55 | 2.1 | 214.1 | 0.62 |
| WALL_116 | 1 | 250 | 0.95 | 1000 | 0.56 | 0.55 | 2.4 | 184.49 | 0.69 |
| WALL_116 | 1 | 250 | 0.95 | 1000 | 0.56 | 0.55 | 2.7 | 156.14 | 0.72 |
| WALL_116 | 1 | 250 | 0.95 | 1000 | 0.56 | 0.55 | 3 | 136.69 | 0.75 |
| WALL_117 | 1.48 | 250 | 0.95 | 1000 | 0.56 | 0.55 | 1.8 | 287.9 | 0.66 |
| WALL_117 | 1.48 | 250 | 0.95 | 1000 | 0.56 | 0.55 | 2.1 | 227.56 | 0.68 |
| WALL_117 | 1.48 | 250 | 0.95 | 1000 | 0.56 | 0.55 | 2.4 | 189.26 | 0.72 |
| WALL_117 | 1.48 | 250 | 0.95 | 1000 | 0.56 | 0.55 | 2.7 | 157.63 | 0.73 |
| WALL_117 | 1.48 | 250 | 0.95 | 1000 | 0.56 | 0.55 | 3 | 136.34 | 0.75 |
| WALL_118 | 0 | 500 | 0.80 | 1000 | 0.80 | 0.73 | 2.1 | 367.22 | 0.73 |

**Table A-2 (continued)**
**Wall configuration results**

| Case ID | Length (m) | HRR (kW) | Q* | HRRPUA | Diameter (m) | D* | $H_p$ (m) | Temperature Rise (°C) | $k_F$ |
|---|---|---|---|---|---|---|---|---|---|
| WALL_118 | 0 | 500 | 0.80 | 1000 | 0.80 | 0.73 | 2.4 | 311.71 | 0.81 |
| WALL_118 | 0 | 500 | 0.80 | 1000 | 0.80 | 0.73 | 2.7 | 253.29 | 0.79 |
| WALL_118 | 0 | 500 | 0.80 | 1000 | 0.80 | 0.73 | 3 | 220.53 | 0.84 |
| WALL_118 | 0 | 500 | 0.80 | 1000 | 0.80 | 0.73 | 3.3 | 195.33 | 0.88 |
| WALL_118 | 0 | 500 | 0.80 | 1000 | 0.80 | 0.73 | 3.6 | 176.77 | 0.94 |
| WALL_118 | 0 | 500 | 0.80 | 1000 | 0.80 | 0.73 | 3.9 | 157.81 | 0.96 |
| WALL_118 | 0 | 500 | 0.80 | 1000 | 0.80 | 0.73 | 4.2 | 143.12 | 0.98 |
| WALL_118 | 0 | 500 | 0.80 | 1000 | 0.80 | 0.73 | 4.5 | 130.16 | 0.99 |
| WALL_119 | 0.24 | 500 | 0.80 | 1000 | 0.80 | 0.73 | 2.1 | 371.03 | 0.74 |
| WALL_119 | 0.24 | 500 | 0.80 | 1000 | 0.80 | 0.73 | 2.4 | 313.6 | 0.82 |
| WALL_119 | 0.24 | 500 | 0.80 | 1000 | 0.80 | 0.73 | 2.7 | 253.56 | 0.80 |
| WALL_119 | 0.24 | 500 | 0.80 | 1000 | 0.80 | 0.73 | 3 | 215.78 | 0.81 |
| WALL_119 | 0.24 | 500 | 0.80 | 1000 | 0.80 | 0.73 | 3.3 | 184.76 | 0.81 |
| WALL_119 | 0.24 | 500 | 0.80 | 1000 | 0.80 | 0.73 | 3.6 | 170.83 | 0.89 |
| WALL_119 | 0.24 | 500 | 0.80 | 1000 | 0.80 | 0.73 | 3.9 | 148.72 | 0.86 |
| WALL_119 | 0.24 | 500 | 0.80 | 1000 | 0.80 | 0.73 | 4.2 | 132.71 | 0.86 |
| WALL_120 | 0.48 | 500 | 0.80 | 1000 | 0.80 | 0.73 | 2.1 | 335.37 | 0.63 |
| WALL_120 | 0.48 | 500 | 0.80 | 1000 | 0.80 | 0.73 | 2.4 | 270.6 | 0.64 |
| WALL_120 | 0.48 | 500 | 0.80 | 1000 | 0.80 | 0.73 | 2.7 | 221.06 | 0.64 |
| WALL_120 | 0.48 | 500 | 0.80 | 1000 | 0.80 | 0.73 | 3 | 188.63 | 0.65 |
| WALL_120 | 0.48 | 500 | 0.80 | 1000 | 0.80 | 0.73 | 3.3 | 161.26 | 0.64 |
| WALL_120 | 0.48 | 500 | 0.80 | 1000 | 0.80 | 0.73 | 3.6 | 150.85 | 0.72 |
| WALL_120 | 0.48 | 500 | 0.80 | 1000 | 0.80 | 0.73 | 3.9 | 134.63 | 0.73 |

**Table A-2 (continued)**
**Wall configuration results**

| Case ID | Length (m) | HRR (kW) | Q* | HRRPUA | Diameter (m) | D* | $H_p$ (m) | Temperature Rise (°C) | $k_F$ |
|---|---|---|---|---|---|---|---|---|---|
| WALL_121 | 0.76 | 500 | 0.80 | 1000 | 0.80 | 0.73 | 2.1 | 355.61 | 0.69 |
| WALL_121 | 0.76 | 500 | 0.80 | 1000 | 0.80 | 0.73 | 2.4 | 284.68 | 0.70 |
| WALL_121 | 0.76 | 500 | 0.80 | 1000 | 0.80 | 0.73 | 2.7 | 218.36 | 0.62 |
| WALL_121 | 0.76 | 500 | 0.80 | 1000 | 0.80 | 0.73 | 3 | 186.38 | 0.64 |
| WALL_121 | 0.76 | 500 | 0.80 | 1000 | 0.80 | 0.73 | 3.3 | 159.99 | 0.63 |
| WALL_121 | 0.76 | 500 | 0.80 | 1000 | 0.80 | 0.73 | 3.6 | 145.28 | 0.67 |
| WALL_121 | 0.76 | 500 | 0.80 | 1000 | 0.80 | 0.73 | 3.9 | 133.34 | 0.71 |
| WALL_122 | 1 | 500 | 0.80 | 1000 | 0.80 | 0.73 | 2.1 | 325.28 | 0.60 |
| WALL_122 | 1 | 500 | 0.80 | 1000 | 0.80 | 0.73 | 2.4 | 258.33 | 0.60 |
| WALL_122 | 1 | 500 | 0.80 | 1000 | 0.80 | 0.73 | 2.7 | 204.86 | 0.56 |
| WALL_122 | 1 | 500 | 0.80 | 1000 | 0.80 | 0.73 | 3 | 177.63 | 0.59 |
| WALL_122 | 1 | 500 | 0.80 | 1000 | 0.80 | 0.73 | 3.3 | 156.35 | 0.61 |
| WALL_122 | 1 | 500 | 0.80 | 1000 | 0.80 | 0.73 | 3.6 | 137.92 | 0.61 |
| WALL_123 | 1.48 | 500 | 0.80 | 1000 | 0.80 | 0.73 | 2.1 | 373.55 | 0.75 |
| WALL_123 | 1.48 | 500 | 0.80 | 1000 | 0.80 | 0.73 | 2.4 | 290.53 | 0.72 |
| WALL_123 | 1.48 | 500 | 0.80 | 1000 | 0.80 | 0.73 | 2.7 | 243.25 | 0.74 |
| WALL_123 | 1.48 | 500 | 0.80 | 1000 | 0.80 | 0.73 | 3 | 210.09 | 0.77 |
| WALL_123 | 1.48 | 500 | 0.80 | 1000 | 0.80 | 0.73 | 3.3 | 176.32 | 0.74 |
| WALL_123 | 1.48 | 500 | 0.80 | 1000 | 0.80 | 0.73 | 3.6 | 154.66 | 0.75 |
| WALL_123 | 1.48 | 500 | 0.80 | 1000 | 0.80 | 0.73 | 3.9 | 136.86 | 0.75 |
| WALL_124 | 0 | 1000 | 0.67 | 1000 | 1.13 | 0.96 | 2.7 | 395.41 | 0.82 |
| WALL_124 | 0 | 1000 | 0.67 | 1000 | 1.13 | 0.96 | 3 | 334.16 | 0.83 |
| WALL_124 | 0 | 1000 | 0.67 | 1000 | 1.13 | 0.96 | 3.3 | 277.86 | 0.79 |

**Table A-2 (continued)**
**Wall configuration results**

| Case ID | Length (m) | HRR (kW) | Q* | HRRPUA | Diameter (m) | D* | $H_p$ (m) | Temperature Rise (°C) | $k_F$ |
|---|---|---|---|---|---|---|---|---|---|
| WALL_124 | 0 | 1000 | 0.67 | 1000 | 1.13 | 0.96 | 3.6 | 247.24 | 0.83 |
| WALL_124 | 0 | 1000 | 0.67 | 1000 | 1.13 | 0.96 | 3.9 | 223.61 | 0.87 |
| WALL_124 | 0 | 1000 | 0.67 | 1000 | 1.13 | 0.96 | 4.2 | 205.41 | 0.91 |
| WALL_124 | 0 | 1000 | 0.67 | 1000 | 1.13 | 0.96 | 4.5 | 186.42 | 0.93 |
| WALL_124 | 0 | 1000 | 0.67 | 1000 | 1.13 | 0.96 | 4.8 | 174.82 | 0.99 |
| WALL_124 | 0 | 1000 | 0.67 | 1000 | 1.13 | 0.96 | 5.1 | 160.73 | 1.00 |
| WALL_124 | 0 | 1000 | 0.67 | 1000 | 1.13 | 0.96 | 5.4 | 147.73 | 1.01 |
| WALL_124 | 0 | 1000 | 0.67 | 1000 | 1.13 | 0.96 | 5.7 | 139.67 | 1.05 |
| WALL_124 | 0 | 1000 | 0.67 | 1000 | 1.13 | 0.96 | 6 | 132.64 | 1.09 |
| WALL_125 | 0.24 | 1000 | 0.67 | 1000 | 1.13 | 0.96 | 2.7 | 442.93 | 0.99 |
| WALL_125 | 0.24 | 1000 | 0.67 | 1000 | 1.13 | 0.96 | 3 | 380.25 | 1.03 |
| WALL_125 | 0.24 | 1000 | 0.67 | 1000 | 1.13 | 0.96 | 3.3 | 316.55 | 0.99 |
| WALL_125 | 0.24 | 1000 | 0.67 | 1000 | 1.13 | 0.96 | 3.6 | 274.47 | 0.99 |
| WALL_125 | 0.24 | 1000 | 0.67 | 1000 | 1.13 | 0.96 | 3.9 | 237.4 | 0.96 |
| WALL_125 | 0.24 | 1000 | 0.67 | 1000 | 1.13 | 0.96 | 4.2 | 205.86 | 0.92 |
| WALL_125 | 0.24 | 1000 | 0.67 | 1000 | 1.13 | 0.96 | 4.5 | 182.13 | 0.89 |
| WALL_125 | 0.24 | 1000 | 0.67 | 1000 | 1.13 | 0.96 | 4.8 | 166.7 | 0.91 |
| WALL_125 | 0.24 | 1000 | 0.67 | 1000 | 1.13 | 0.96 | 5.1 | 153.7 | 0.93 |
| WALL_125 | 0.24 | 1000 | 0.67 | 1000 | 1.13 | 0.96 | 5.4 | 137.67 | 0.89 |
| WALL_125 | 0.24 | 1000 | 0.67 | 1000 | 1.13 | 0.96 | 5.7 | 131.09 | 0.94 |
| WALL_125 | 0.24 | 1000 | 0.67 | 1000 | 1.13 | 0.96 | 6 | 127.31 | 1.02 |
| WALL_126 | 0.48 | 1000 | 0.67 | 1000 | 1.13 | 0.96 | 2.7 | 349.66 | 0.67 |
| WALL_126 | 0.48 | 1000 | 0.67 | 1000 | 1.13 | 0.96 | 3 | 298.85 | 0.69 |

**Table A-2 (continued)**
**Wall configuration results**

| Case ID | Length (m) | HRR (kW) | Q* | HRRPUA | Diameter (m) | D* | $H_p$ (m) | Temperature Rise (°C) | $k_F$ |
|---|---|---|---|---|---|---|---|---|---|
| WALL_126 | 0.48 | 1000 | 0.67 | 1000 | 1.13 | 0.96 | 3.3 | 256.77 | 0.70 |
| WALL_126 | 0.48 | 1000 | 0.67 | 1000 | 1.13 | 0.96 | 3.6 | 222.37 | 0.69 |
| WALL_126 | 0.48 | 1000 | 0.67 | 1000 | 1.13 | 0.96 | 3.9 | 196.9 | 0.70 |
| WALL_126 | 0.48 | 1000 | 0.67 | 1000 | 1.13 | 0.96 | 4.2 | 184.21 | 0.76 |
| WALL_126 | 0.48 | 1000 | 0.67 | 1000 | 1.13 | 0.96 | 4.5 | 174.44 | 0.83 |
| WALL_126 | 0.48 | 1000 | 0.67 | 1000 | 1.13 | 0.96 | 4.8 | 166.39 | 0.91 |
| WALL_126 | 0.48 | 1000 | 0.67 | 1000 | 1.13 | 0.96 | 5.1 | 157.4 | 0.97 |
| WALL_126 | 0.48 | 1000 | 0.67 | 1000 | 1.13 | 0.96 | 5.4 | 146.72 | 0.99 |
| WALL_126 | 0.48 | 1000 | 0.67 | 1000 | 1.13 | 0.96 | 5.7 | 139.16 | 1.04 |
| WALL_126 | 0.48 | 1000 | 0.67 | 1000 | 1.13 | 0.96 | 6 | 133.61 | 1.11 |
| WALL_127 | 0.76 | 1000 | 0.67 | 1000 | 1.13 | 0.96 | 2.7 | 391.88 | 0.81 |
| WALL_127 | 0.76 | 1000 | 0.67 | 1000 | 1.13 | 0.96 | 3 | 336.43 | 0.84 |
| WALL_127 | 0.76 | 1000 | 0.67 | 1000 | 1.13 | 0.96 | 3.3 | 274.15 | 0.78 |
| WALL_127 | 0.76 | 1000 | 0.67 | 1000 | 1.13 | 0.96 | 3.6 | 239.89 | 0.79 |
| WALL_127 | 0.76 | 1000 | 0.67 | 1000 | 1.13 | 0.96 | 3.9 | 203.68 | 0.74 |
| WALL_127 | 0.76 | 1000 | 0.67 | 1000 | 1.13 | 0.96 | 4.2 | 180.02 | 0.73 |
| WALL_127 | 0.76 | 1000 | 0.67 | 1000 | 1.13 | 0.96 | 4.5 | 163.12 | 0.74 |
| WALL_127 | 0.76 | 1000 | 0.67 | 1000 | 1.13 | 0.96 | 4.8 | 152.35 | 0.78 |
| WALL_127 | 0.76 | 1000 | 0.67 | 1000 | 1.13 | 0.96 | 5.1 | 140.76 | 0.79 |
| WALL_127 | 0.76 | 1000 | 0.67 | 1000 | 1.13 | 0.96 | 5.4 | 133.1 | 0.83 |
| WALL_127 | 0.76 | 1000 | 0.67 | 1000 | 1.13 | 0.96 | 5.7 | 125.08 | 0.86 |
| WALL_128 | 1 | 1000 | 0.67 | 1000 | 1.13 | 0.96 | 2.7 | 425.6 | 0.92 |
| WALL_128 | 1 | 1000 | 0.67 | 1000 | 1.13 | 0.96 | 3 | 375.1 | 1.01 |

**Table A-2 (continued)**
**Wall configuration results**

| Case ID | Length (m) | HRR (kW) | Q* | HRRPUA | Diameter (m) | D* | $H_p$ (m) | Temperature Rise (°C) | $k_F$ |
|---|---|---|---|---|---|---|---|---|---|
| WALL_128 | 1 | 1000 | 0.67 | 1000 | 1.13 | 0.96 | 3.3 | 311.04 | 0.96 |
| WALL_128 | 1 | 1000 | 0.67 | 1000 | 1.13 | 0.96 | 3.6 | 271.05 | 0.97 |
| WALL_128 | 1 | 1000 | 0.67 | 1000 | 1.13 | 0.96 | 3.9 | 228.55 | 0.90 |
| WALL_128 | 1 | 1000 | 0.67 | 1000 | 1.13 | 0.96 | 4.2 | 198.78 | 0.87 |
| WALL_128 | 1 | 1000 | 0.67 | 1000 | 1.13 | 0.96 | 4.5 | 176 | 0.84 |
| WALL_128 | 1 | 1000 | 0.67 | 1000 | 1.13 | 0.96 | 4.8 | 158.08 | 0.83 |
| WALL_128 | 1 | 1000 | 0.67 | 1000 | 1.13 | 0.96 | 5.1 | 143.41 | 0.82 |
| WALL_128 | 1 | 1000 | 0.67 | 1000 | 1.13 | 0.96 | 5.4 | 131.42 | 0.82 |
| WALL_129 | 1.48 | 1000 | 0.67 | 1000 | 1.13 | 0.96 | 2.7 | 411.59 | 0.88 |
| WALL_129 | 1.48 | 1000 | 0.67 | 1000 | 1.13 | 0.96 | 3 | 332.12 | 0.82 |
| WALL_129 | 1.48 | 1000 | 0.67 | 1000 | 1.13 | 0.96 | 3.3 | 269.11 | 0.75 |
| WALL_129 | 1.48 | 1000 | 0.67 | 1000 | 1.13 | 0.96 | 3.6 | 232.69 | 0.75 |
| WALL_129 | 1.48 | 1000 | 0.67 | 1000 | 1.13 | 0.96 | 3.9 | 201.24 | 0.72 |
| WALL_129 | 1.48 | 1000 | 0.67 | 1000 | 1.13 | 0.96 | 4.2 | 178.8 | 0.72 |
| WALL_129 | 1.48 | 1000 | 0.67 | 1000 | 1.13 | 0.96 | 4.5 | 158.82 | 0.71 |
| WALL_129 | 1.48 | 1000 | 0.67 | 1000 | 1.13 | 0.96 | 4.8 | 145.22 | 0.72 |
| WALL_129 | 1.48 | 1000 | 0.67 | 1000 | 1.13 | 0.96 | 5.1 | 138.07 | 0.77 |
| WALL_129 | 1.48 | 1000 | 0.67 | 1000 | 1.13 | 0.96 | 5.4 | 128.53 | 0.78 |
| WALL_330 | 0 | 250 | 2.26 | 2000 | 0.40 | 0.55 | 1.8 | 367.03 | 0.76 |
| WALL_330 | 0 | 250 | 2.26 | 2000 | 0.40 | 0.55 | 2.1 | 273.01 | 0.75 |
| WALL_330 | 0 | 250 | 2.26 | 2000 | 0.40 | 0.55 | 2.4 | 224.9 | 0.81 |
| WALL_330 | 0 | 250 | 2.26 | 2000 | 0.40 | 0.55 | 2.7 | 190.61 | 0.85 |
| WALL_330 | 0 | 250 | 2.26 | 2000 | 0.40 | 0.55 | 3 | 167.63 | 0.92 |

**Table A-2 (continued)**
**Wall configuration results**

| Case ID | Length (m) | HRR (kW) | Q* | HRRPUA | Diameter (m) | D* | $H_p$ (m) | Temperature Rise (°C) | $k_F$ |
|---|---|---|---|---|---|---|---|---|---|
| WALL_330 | 0 | 250 | 2.26 | 2000 | 0.40 | 0.55 | 3.3 | 147.3 | 0.96 |
| WALL_330 | 0 | 250 | 2.26 | 2000 | 0.40 | 0.55 | 3.6 | 134.95 | 1.04 |
| WALL_360 | 0.24 | 250 | 2.26 | 2000 | 0.40 | 0.55 | 1.8 | 270.27 | 0.50 |
| WALL_360 | 0.24 | 250 | 2.26 | 2000 | 0.40 | 0.55 | 2.1 | 212.96 | 0.53 |
| WALL_360 | 0.24 | 250 | 2.26 | 2000 | 0.40 | 0.55 | 2.4 | 183.71 | 0.59 |
| WALL_360 | 0.24 | 250 | 2.26 | 2000 | 0.40 | 0.55 | 2.7 | 165.45 | 0.69 |
| WALL_360 | 0.24 | 250 | 2.26 | 2000 | 0.40 | 0.55 | 3 | 151.71 | 0.79 |
| WALL_360 | 0.24 | 250 | 2.26 | 2000 | 0.40 | 0.55 | 3.3 | 138.64 | 0.87 |
| WALL_360 | 0.24 | 250 | 2.26 | 2000 | 0.40 | 0.55 | 3.6 | 128.62 | 0.96 |
| WALL_390 | 1.48 | 250 | 2.26 | 2000 | 0.40 | 0.55 | 1.8 | 268.92 | 0.49 |
| WALL_390 | 1.48 | 250 | 2.26 | 2000 | 0.40 | 0.55 | 2.1 | 210.69 | 0.52 |
| WALL_390 | 1.48 | 250 | 2.26 | 2000 | 0.40 | 0.55 | 2.4 | 165.16 | 0.51 |
| WALL_390 | 1.48 | 250 | 2.26 | 2000 | 0.40 | 0.55 | 2.7 | 136.97 | 0.51 |
| WALL_310 | 0 | 250 | 0.17 | 250 | 1.13 | 0.55 | 1.2 | 352.01 | 0.78 |
| WALL_310 | 0 | 250 | 0.17 | 250 | 1.13 | 0.55 | 1.5 | 256.74 | 0.72 |
| WALL_310 | 0 | 250 | 0.17 | 250 | 1.13 | 0.55 | 1.8 | 211.79 | 0.78 |
| WALL_310 | 0 | 250 | 0.17 | 250 | 1.13 | 0.55 | 2.1 | 180.18 | 0.85 |
| WALL_310 | 0 | 250 | 0.17 | 250 | 1.13 | 0.55 | 2.4 | 158.24 | 0.93 |
| WALL_310 | 0 | 250 | 0.17 | 250 | 1.13 | 0.55 | 2.7 | 138.35 | 0.95 |
| WALL_340 | 0.24 | 250 | 0.17 | 250 | 1.13 | 0.55 | 1.2 | 440 | 1.47 |
| WALL_340 | 0.24 | 250 | 0.17 | 250 | 1.13 | 0.55 | 1.5 | 316.07 | 1.20 |
| WALL_340 | 0.24 | 250 | 0.17 | 250 | 1.13 | 0.55 | 1.8 | 249.23 | 1.15 |
| WALL_340 | 0.24 | 250 | 0.17 | 250 | 1.13 | 0.55 | 2.1 | 199.55 | 1.07 |

**Table A-2 (continued)**
**Wall configuration results**

| Case ID | Length (m) | HRR (kW) | Q* | HRRPUA | Diameter (m) | D* | $H_p$ (m) | Temperature Rise (°C) | $k_F$ |
|---|---|---|---|---|---|---|---|---|---|
| WALL_340 | 0.24 | 250 | 0.17 | 250 | 1.13 | 0.55 | 2.4 | 171.16 | 1.11 |
| WALL_340 | 0.24 | 250 | 0.17 | 250 | 1.13 | 0.55 | 2.7 | 145.08 | 1.06 |
| WALL_340 | 0.24 | 250 | 0.17 | 250 | 1.13 | 0.55 | 3 | 130.13 | 1.12 |
| WALL_370 | 1.48 | 250 | 0.17 | 250 | 1.13 | 0.55 | 1.2 | 422.03 | 1.29 |
| WALL_370 | 1.48 | 250 | 0.17 | 250 | 1.13 | 0.55 | 1.5 | 298.73 | 1.03 |
| WALL_370 | 1.48 | 250 | 0.17 | 250 | 1.13 | 0.55 | 1.8 | 240.36 | 1.05 |
| WALL_370 | 1.48 | 250 | 0.17 | 250 | 1.13 | 0.55 | 2.1 | 191.99 | 0.98 |
| WALL_370 | 1.48 | 250 | 0.17 | 250 | 1.13 | 0.55 | 2.4 | 157.49 | 0.92 |
| WALL_370 | 1.48 | 250 | 0.17 | 250 | 1.13 | 0.55 | 2.7 | 134.62 | 0.90 |
| WALL_320 | 0 | 250 | 0.40 | 500 | 0.80 | 0.55 | 1.5 | 349.42 | 0.77 |
| WALL_320 | 0 | 250 | 0.40 | 500 | 0.80 | 0.55 | 1.8 | 291.2 | 0.92 |
| WALL_320 | 0 | 250 | 0.40 | 500 | 0.80 | 0.55 | 2.1 | 245.51 | 1.03 |
| WALL_320 | 0 | 250 | 0.40 | 500 | 0.80 | 0.55 | 2.4 | 212.48 | 1.14 |
| WALL_320 | 0 | 250 | 0.40 | 500 | 0.80 | 0.55 | 2.7 | 183.66 | 1.20 |
| WALL_320 | 0 | 250 | 0.40 | 500 | 0.80 | 0.55 | 3 | 162.19 | 1.26 |
| WALL_320 | 0 | 250 | 0.40 | 500 | 0.80 | 0.55 | 3.3 | 147.39 | 1.36 |
| WALL_320 | 0 | 250 | 0.40 | 500 | 0.80 | 0.55 | 3.6 | 131.62 | 1.38 |
| WALL_350 | 0.24 | 250 | 0.40 | 500 | 0.80 | 0.55 | 1.5 | 355.7 | 0.80 |
| WALL_350 | 0.24 | 250 | 0.40 | 500 | 0.80 | 0.55 | 1.8 | 258.26 | 0.74 |
| WALL_350 | 0.24 | 250 | 0.40 | 500 | 0.80 | 0.55 | 2.1 | 199.07 | 0.70 |
| WALL_350 | 0.24 | 250 | 0.40 | 500 | 0.80 | 0.55 | 2.4 | 166.6 | 0.72 |
| WALL_350 | 0.24 | 250 | 0.40 | 500 | 0.80 | 0.55 | 2.7 | 143.84 | 0.76 |
| WALL_350 | 0.24 | 250 | 0.40 | 500 | 0.80 | 0.55 | 3 | 125.81 | 0.78 |

**Table A-2 (continued)**
**Wall configuration results**

| Case ID | Length (m) | HRR (kW) | Q* | HRRPUA | Diameter (m) | D* | $H_p$ (m) | Temperature Rise (°C) | $k_F$ |
|---|---|---|---|---|---|---|---|---|---|
| WALL_380 | 1.48 | 250 | 0.40 | 500 | 0.80 | 0.55 | 1.5 | 347.65 | 0.77 |
| WALL_380 | 1.48 | 250 | 0.40 | 500 | 0.80 | 0.55 | 1.8 | 265.09 | 0.78 |
| WALL_380 | 1.48 | 250 | 0.40 | 500 | 0.80 | 0.55 | 2.1 | 218.23 | 0.83 |
| WALL_380 | 1.48 | 250 | 0.40 | 500 | 0.80 | 0.55 | 2.4 | 183.15 | 0.86 |
| WALL_380 | 1.48 | 250 | 0.40 | 500 | 0.80 | 0.55 | 2.7 | 153.84 | 0.86 |
| WALL_380 | 1.48 | 250 | 0.40 | 500 | 0.80 | 0.55 | 3 | 135.17 | 0.89 |

**Table A-3**
**Open configuration results**

| Case ID | Length (m) | HRR (kW) | Q* | HRRPUA | Diameter (m) | D* | $H_p$ (m) | Temperature Rise (°C) | $k_F$ |
|---|---|---|---|---|---|---|---|---|---|
| BASE_100 | ∞ | 40 | 1.50 | 1000 | 0.23 | 0.27 | 0.9 | 247.59 | 0.52 |
| BASE_100 | ∞ | 40 | 1.50 | 1000 | 0.23 | 0.27 | 1.2 | 168.87 | 0.61 |
| BASE_101 | ∞ | 78 | 1.26 | 1000 | 0.32 | 0.35 | 1.2 | 265.27 | 0.63 |
| BASE_101 | ∞ | 78 | 1.26 | 1000 | 0.32 | 0.35 | 1.5 | 180.12 | 0.62 |
| BASE_101 | ∞ | 78 | 1.26 | 1000 | 0.32 | 0.35 | 1.8 | 140.05 | 0.66 |
| BASE_102 | ∞ | 250 | 0.95 | 1000 | 0.56 | 0.55 | 1.8 | 335.74 | 0.84 |
| BASE_102 | ∞ | 250 | 0.95 | 1000 | 0.56 | 0.55 | 2.1 | 241.4 | 0.75 |
| BASE_102 | ∞ | 250 | 0.95 | 1000 | 0.56 | 0.55 | 2.4 | 204.03 | 0.82 |
| BASE_102 | ∞ | 250 | 0.95 | 1000 | 0.56 | 0.55 | 2.7 | 166.36 | 0.80 |
| BASE_102 | ∞ | 250 | 0.95 | 1000 | 0.56 | 0.55 | 3 | 140.13 | 0.78 |
| BASE_103 | ∞ | 500 | 0.80 | 1000 | 0.80 | 0.73 | 2.1 | 453.62 | 1.02 |
| BASE_103 | ∞ | 500 | 0.80 | 1000 | 0.80 | 0.73 | 2.4 | 375.48 | 1.09 |
| BASE_103 | ∞ | 500 | 0.80 | 1000 | 0.80 | 0.73 | 2.7 | 305.81 | 1.08 |

**Table A-3 (continued)**
**Open configuration results**

| Case ID | Length (m) | HRR (kW) | Q* | HRRPUA | Diameter (m) | D* | $H_p$ (m) | Temperature Rise (°C) | $k_F$ |
|---|---|---|---|---|---|---|---|---|---|
| BASE_103 | ∞ | 500 | 0.80 | 1000 | 0.80 | 0.73 | 3 | 246.77 | 1.01 |
| BASE_103 | ∞ | 500 | 0.80 | 1000 | 0.80 | 0.73 | 3.3 | 198 | 0.90 |
| BASE_103 | ∞ | 500 | 0.80 | 1000 | 0.80 | 0.73 | 3.6 | 173.29 | 0.91 |
| BASE_103 | ∞ | 500 | 0.80 | 1000 | 0.80 | 0.73 | 3.9 | 150.62 | 0.88 |
| BASE_103 | ∞ | 500 | 0.80 | 1000 | 0.80 | 0.73 | 4.2 | 134.2 | 0.88 |
| BASE_104 | ∞ | 1000 | 0.67 | 1000 | 1.13 | 0.96 | 2.7 | 544.73 | 1.39 |
| BASE_104 | ∞ | 1000 | 0.67 | 1000 | 1.13 | 0.96 | 3 | 465.34 | 1.44 |
| BASE_104 | ∞ | 1000 | 0.67 | 1000 | 1.13 | 0.96 | 3.3 | 387.87 | 1.39 |
| BASE_104 | ∞ | 1000 | 0.67 | 1000 | 1.13 | 0.96 | 3.6 | 336.91 | 1.39 |
| BASE_104 | ∞ | 1000 | 0.67 | 1000 | 1.13 | 0.96 | 3.9 | 285.86 | 1.31 |
| BASE_104 | ∞ | 1000 | 0.67 | 1000 | 1.13 | 0.96 | 4.2 | 251.96 | 1.30 |
| BASE_104 | ∞ | 1000 | 0.67 | 1000 | 1.13 | 0.96 | 4.5 | 216.44 | 1.20 |
| BASE_104 | ∞ | 1000 | 0.67 | 1000 | 1.13 | 0.96 | 4.8 | 197.21 | 1.22 |
| BASE_104 | ∞ | 1000 | 0.67 | 1000 | 1.13 | 0.96 | 5.1 | 174.06 | 1.15 |
| BASE_104 | ∞ | 1000 | 0.67 | 1000 | 1.13 | 0.96 | 5.4 | 153.34 | 1.07 |
| BASE_104 | ∞ | 1000 | 0.67 | 1000 | 1.13 | 0.96 | 5.7 | 139.31 | 1.04 |
| BASE_104 | ∞ | 1000 | 0.67 | 1000 | 1.13 | 0.96 | 6 | 126.43 | 1.00 |

**Table A-4**
**Alternate corner surface results**

| Case ID | Length (m) | HRR (kW) | Q* | HRRPUA | Diameter (m) | D* | Hp (m) | Temperature Rise (°C) | kF | Surface Properties |
|---|---|---|---|---|---|---|---|---|---|---|
| CORNER_500 | 0 | 40 | | 1000 | 0.23 | | 0.9 | 989.20 | 3.91 | Adiabatic |
| CORNER_500 | 0 | 40 | | 1000 | 0.23 | | 1.2 | 797.28 | 6.55 | Adiabatic |
| CORNER_500 | 0 | 40 | | 1000 | 0.23 | | 1.5 | 572.53 | 7.58 | Adiabatic |
| CORNER_500 | 0 | 40 | | 1000 | 0.23 | | 1.8 | 436.40 | 8.41 | Adiabatic |
| CORNER_500 | 0 | 40 | | 1000 | 0.23 | | 2.1 | 339.78 | 8.84 | Adiabatic |
| CORNER_500 | 0 | 40 | | 1000 | 0.23 | | 2.4 | 283.60 | 9.69 | Adiabatic |
| CORNER_500 | 0 | 40 | | 1000 | 0.23 | | 2.7 | 237.77 | 10.22 | Adiabatic |
| CORNER_500 | 0 | 40 | | 1000 | 0.23 | | 3 | 205.94 | 10.92 | Adiabatic |
| CORNER_500 | 0 | 40 | | 1000 | 0.23 | | 3.3 | 176.85 | 11.19 | Adiabatic |
| CORNER_500 | 0 | 40 | | 1000 | 0.23 | | 3.6 | 156.43 | 11.72 | Adiabatic |
| CORNER_500 | 0 | 40 | | 1000 | 0.23 | | 3.9 | 138.09 | 12.00 | Adiabatic |
| CORNER_500 | 0 | 40 | | 1000 | 0.23 | | 4.2 | 125.15 | 12.57 | Adiabatic |
| CORNER_500 | 0 | 40 | | 1000 | 0.23 | | 4.5 | 112.23 | 12.78 | Adiabatic |
| CORNER_600 | 0 | 40 | | 1000 | 0.23 | | 0.9 | 703.52 | 2.45 | Gypsum |
| CORNER_600 | 0 | 40 | | 1000 | 0.23 | | 1.2 | 525.51 | 3.61 | Gypsum |
| CORNER_600 | 0 | 40 | | 1000 | 0.23 | | 1.5 | 381.90 | 4.20 | Gypsum |
| CORNER_600 | 0 | 40 | | 1000 | 0.23 | | 1.8 | 301.23 | 4.88 | Gypsum |
| CORNER_600 | 0 | 40 | | 1000 | 0.23 | | 2.1 | 236.02 | 5.16 | Gypsum |
| CORNER_600 | 0 | 40 | | 1000 | 0.23 | | 2.4 | 190.95 | 5.39 | Gypsum |
| CORNER_600 | 0 | 40 | | 1000 | 0.23 | | 2.7 | 154.18 | 5.37 | Gypsum |
| CORNER_600 | 0 | 40 | | 1000 | 0.23 | | 3 | 131.26 | 5.58 | Gypsum |
| CORNER_600 | 0 | 40 | | 1000 | 0.23 | | 3.3 | 112.45 | 5.70 | Gypsum |
| CORNER_700 | 0 | 40 | | 1000 | 0.23 | | 0.9 | 620.93 | 2.06 | Steel |

**Table A-4 (continued)**
**Alternate corner surface results**

| Case ID | Length (m) | HRR (kW) | Q* | HRRPUA | Diameter (m) | D* | Hp (m) | Temperature Rise (°C) | kF | Surface Properties |
|---|---|---|---|---|---|---|---|---|---|---|
| CORNER_700 | 0 | 40 | | 1000 | 0.23 | | 1.2 | 486.70 | 3.24 | Steel |
| CORNER_700 | 0 | 40 | | 1000 | 0.23 | | 1.5 | 348.51 | 3.69 | Steel |
| CORNER_700 | 0 | 40 | | 1000 | 0.23 | | 1.8 | 269.86 | 4.16 | Steel |
| CORNER_700 | 0 | 40 | | 1000 | 0.23 | | 2.1 | 206.22 | 4.24 | Steel |
| CORNER_700 | 0 | 40 | | 1000 | 0.23 | | 2.4 | 172.21 | 4.63 | Steel |
| CORNER_700 | 0 | 40 | | 1000 | 0.23 | | 2.7 | 143.67 | 4.84 | Steel |
| CORNER_700 | 0 | 40 | | 1000 | 0.23 | | 3 | 124.78 | 5.18 | Steel |
| CORNER_800 | 0 | 40 | | 1000 | 0.23 | | 0.9 | 711.12 | 2.48 | INERT |
| CORNER_800 | 0 | 40 | | 1000 | 0.23 | | 1.2 | 544.06 | 3.79 | INERT |
| CORNER_800 | 0 | 40 | | 1000 | 0.23 | | 1.5 | 387.49 | 4.29 | INERT |
| CORNER_800 | 0 | 40 | | 1000 | 0.23 | | 1.8 | 296.95 | 4.78 | INERT |
| CORNER_800 | 0 | 40 | | 1000 | 0.23 | | 2.1 | 232.66 | 5.06 | INERT |
| CORNER_800 | 0 | 40 | | 1000 | 0.23 | | 2.4 | 196.13 | 5.61 | INERT |
| CORNER_800 | 0 | 40 | | 1000 | 0.23 | | 2.7 | 162.77 | 5.82 | INERT |
| CORNER_800 | 0 | 40 | | 1000 | 0.23 | | 3 | 143.06 | 6.34 | INERT |
| CORNER_800 | 0 | 40 | | 1000 | 0.23 | | 3.3 | 125.08 | 6.67 | INERT |
| CORNER_800 | 0 | 40 | | 1000 | 0.23 | | 3.6 | 110.55 | 6.97 | INERT |
| CORNER_506 | 0 | 78 | | 1000 | 0.32 | | 1.2 | 937.93 | 4.26 | Adiabatic |
| CORNER_506 | 0 | 78 | | 1000 | 0.32 | | 1.5 | 755.03 | 5.87 | Adiabatic |
| CORNER_506 | 0 | 78 | | 1000 | 0.32 | | 1.8 | 599.27 | 6.95 | Adiabatic |
| CORNER_506 | 0 | 78 | | 1000 | 0.32 | | 2.1 | 451.77 | 6.96 | Adiabatic |
| CORNER_506 | 0 | 78 | | 1000 | 0.32 | | 2.4 | 366.58 | 7.32 | Adiabatic |

**Table A-4 (continued)**
**Alternate corner surface results**

| Case ID | Length (m) | HRR (kW) | Q* | HRRPUA | Diameter (m) | D* | Hp (m) | Temperature Rise (°C) | kF | Surface Properties |
|---|---|---|---|---|---|---|---|---|---|---|
| CORNER_506 | 0 | 78 | | 1000 | 0.32 | | 2.7 | 298.03 | 7.37 | Adiabatic |
| CORNER_506 | 0 | 78 | | 1000 | 0.32 | | 3 | 253.24 | 7.66 | Adiabatic |
| CORNER_506 | 0 | 78 | | 1000 | 0.32 | | 3.3 | 211.78 | 7.54 | Adiabatic |
| CORNER_506 | 0 | 78 | | 1000 | 0.32 | | 3.6 | 184.74 | 7.73 | Adiabatic |
| CORNER_506 | 0 | 78 | | 1000 | 0.32 | | 3.9 | 161.22 | 7.78 | Adiabatic |
| CORNER_506 | 0 | 78 | | 1000 | 0.32 | | 4.2 | 144.90 | 8.05 | Adiabatic |
| CORNER_506 | 0 | 78 | | 1000 | 0.32 | | 4.5 | 129.65 | 8.15 | Adiabatic |
| CORNER_506 | 0 | 78 | | 1000 | 0.32 | | 4.8 | 119.48 | 8.54 | Adiabatic |
| CORNER_506 | 0 | 78 | | 1000 | 0.32 | | 5.1 | 110.93 | 8.94 | Adiabatic |
| CORNER_606 | 0 | 78 | | 1000 | 0.32 | | 1.2 | 723.47 | 2.92 | Gypsum |
| CORNER_606 | 0 | 78 | | 1000 | 0.32 | | 1.5 | 586.06 | 4.02 | Gypsum |
| CORNER_606 | 0 | 78 | | 1000 | 0.32 | | 1.8 | 475.87 | 4.91 | Gypsum |
| CORNER_606 | 0 | 78 | | 1000 | 0.32 | | 2.1 | 368.07 | 5.11 | Gypsum |
| CORNER_606 | 0 | 78 | | 1000 | 0.32 | | 2.4 | 295.27 | 5.28 | Gypsum |
| CORNER_606 | 0 | 78 | | 1000 | 0.32 | | 2.7 | 236.15 | 5.19 | Gypsum |
| CORNER_606 | 0 | 78 | | 1000 | 0.32 | | 3 | 200.85 | 5.39 | Gypsum |
| CORNER_606 | 0 | 78 | | 1000 | 0.32 | | 3.3 | 173.14 | 5.56 | Gypsum |
| CORNER_606 | 0 | 78 | | 1000 | 0.32 | | 3.6 | 153.54 | 5.84 | Gypsum |
| CORNER_606 | 0 | 78 | | 1000 | 0.32 | | 3.9 | 132.53 | 5.78 | Gypsum |
| CORNER_606 | 0 | 78 | | 1000 | 0.32 | | 4.2 | 115.98 | 5.75 | Gypsum |
| CORNER_706 | 0 | 78 | | 1000 | 0.32 | | 1.2 | 711.60 | 2.85 | Steel |
| CORNER_706 | 0 | 78 | | 1000 | 0.32 | | 1.5 | 552.05 | 3.68 | Steel |

**Table A-4 (continued)**
**Alternate corner surface results**

| Case ID | Length (m) | HRR (kW) | Q* | HRRPUA | Diameter (m) | D* | Hp (m) | Temperature Rise (°C) | kF | Surface Properties |
|---|---|---|---|---|---|---|---|---|---|---|
| CORNER_706 | 0 | 78 | | 1000 | 0.32 | | 1.8 | 445.88 | 4.45 | Steel |
| CORNER_706 | 0 | 78 | | 1000 | 0.32 | | 2.1 | 352.24 | 4.78 | Steel |
| CORNER_706 | 0 | 78 | | 1000 | 0.32 | | 2.4 | 289.00 | 5.11 | Steel |
| CORNER_706 | 0 | 78 | | 1000 | 0.32 | | 2.7 | 237.02 | 5.22 | Steel |
| CORNER_706 | 0 | 78 | | 1000 | 0.32 | | 3 | 202.67 | 5.47 | Steel |
| CORNER_706 | 0 | 78 | | 1000 | 0.32 | | 3.3 | 172.09 | 5.51 | Steel |
| CORNER_706 | 0 | 78 | | 1000 | 0.32 | | 3.6 | 147.28 | 5.49 | Steel |
| CORNER_706 | 0 | 78 | | 1000 | 0.32 | | 3.9 | 125.25 | 5.31 | Steel |
| CORNER_706 | 0 | 78 | | 1000 | 0.32 | | 4.2 | 111.69 | 5.43 | Steel |
| CORNER_806 | 0 | 78 | | 1000 | 0.32 | | 1.2 | 648.49 | 2.50 | INERT |
| CORNER_806 | 0 | 78 | | 1000 | 0.32 | | 1.5 | 516.34 | 3.34 | INERT |
| CORNER_806 | 0 | 78 | | 1000 | 0.32 | | 1.8 | 411.66 | 3.96 | INERT |
| CORNER_806 | 0 | 78 | | 1000 | 0.32 | | 2.1 | 315.06 | 4.05 | INERT |
| CORNER_806 | 0 | 78 | | 1000 | 0.32 | | 2.4 | 254.63 | 4.23 | INERT |
| CORNER_806 | 0 | 78 | | 1000 | 0.32 | | 2.7 | 203.45 | 4.15 | INERT |
| CORNER_806 | 0 | 78 | | 1000 | 0.32 | | 3 | 171.51 | 4.26 | INERT |
| CORNER_806 | 0 | 78 | | 1000 | 0.32 | | 3.3 | 144.83 | 4.26 | INERT |
| CORNER_806 | 0 | 78 | | 1000 | 0.32 | | 3.6 | 126.47 | 4.37 | INERT |
| CORNER_512 | 0 | 250 | | 1000 | 0.56 | | 1.8 | 951.61 | 4.50 | Adiabatic |
| CORNER_512 | 0 | 250 | | 1000 | 0.56 | | 2.1 | 893.17 | 6.44 | Adiabatic |
| CORNER_512 | 0 | 250 | | 1000 | 0.56 | | 2.4 | 813.89 | 8.22 | Adiabatic |
| CORNER_512 | 0 | 250 | | 1000 | 0.56 | | 2.7 | 702.66 | 9.08 | Adiabatic |

**Table A-4 (continued)**
**Alternate corner surface results**

| Case ID | Length (m) | HRR (kW) | Q* | HRRPUA | Diameter (m) | D* | Hp (m) | Temperature Rise (°C) | kF | Surface Properties |
|---|---|---|---|---|---|---|---|---|---|---|
| CORNER_512 | 0 | 250 | | 1000 | 0.56 | | 3 | 619.65 | 9.99 | Adiabatic |
| CORNER_512 | 0 | 250 | | 1000 | 0.56 | | 3.3 | 552.16 | 10.84 | Adiabatic |
| CORNER_512 | 0 | 250 | | 1000 | 0.56 | | 3.6 | 499.47 | 11.75 | Adiabatic |
| CORNER_512 | 0 | 250 | | 1000 | 0.56 | | 3.9 | 430.52 | 11.49 | Adiabatic |
| CORNER_512 | 0 | 250 | | 1000 | 0.56 | | 4.2 | 375.33 | 11.27 | Adiabatic |
| CORNER_512 | 0 | 250 | | 1000 | 0.56 | | 4.5 | 323.10 | 10.67 | Adiabatic |
| CORNER_512 | 0 | 250 | | 1000 | 0.56 | | 4.8 | 286.26 | 10.46 | Adiabatic |
| CORNER_512 | 0 | 250 | | 1000 | 0.56 | | 5.1 | 256.52 | 10.34 | Adiabatic |
| CORNER_512 | 0 | 250 | | 1000 | 0.56 | | 5.4 | 227.91 | 9.98 | Adiabatic |
| CORNER_512 | 0 | 250 | | 1000 | 0.56 | | 5.7 | 204.83 | 9.74 | Adiabatic |
| CORNER_512 | 0 | 250 | | 1000 | 0.56 | | 6 | 188.21 | 9.77 | Adiabatic |
| CORNER_612 | 0 | 250 | | 1000 | 0.56 | | 1.8 | 724.82 | 2.91 | Gypsum |
| CORNER_612 | 0 | 250 | | 1000 | 0.56 | | 2.1 | 628.07 | 3.62 | Gypsum |
| CORNER_612 | 0 | 250 | | 1000 | 0.56 | | 2.4 | 536.80 | 4.13 | Gypsum |
| CORNER_612 | 0 | 250 | | 1000 | 0.56 | | 2.7 | 457.88 | 4.48 | Gypsum |
| CORNER_612 | 0 | 250 | | 1000 | 0.56 | | 3 | 389.49 | 4.66 | Gypsum |
| CORNER_612 | 0 | 250 | | 1000 | 0.56 | | 3.3 | 321.61 | 4.48 | Gypsum |
| CORNER_612 | 0 | 250 | | 1000 | 0.56 | | 3.6 | 276.29 | 4.48 | Gypsum |
| CORNER_612 | 0 | 250 | | 1000 | 0.56 | | 3.9 | 226.30 | 4.08 | Gypsum |
| CORNER_612 | 0 | 250 | | 1000 | 0.56 | | 4.2 | 192.56 | 3.88 | Gypsum |
| CORNER_612 | 0 | 250 | | 1000 | 0.56 | | 4.5 | 166.53 | 3.73 | Gypsum |
| CORNER_612 | 0 | 250 | | 1000 | 0.56 | | 4.8 | 150.42 | 3.79 | Gypsum |

**Table A-4 (continued)**
**Alternate corner surface results**

| Case ID | Length (m) | HRR (kW) | Q* | HRRPUA | Diameter (m) | D* | Hp (m) | Temperature Rise (°C) | kF | Surface Properties |
|---|---|---|---|---|---|---|---|---|---|---|
| CORNER_612 | 0 | 250 | | 1000 | 0.56 | | 5.1 | 135.46 | 3.79 | Gypsum |
| CORNER_612 | 0 | 250 | | 1000 | 0.56 | | 5.4 | 120.65 | 3.69 | Gypsum |
| CORNER_712 | 0 | 250 | | 1000 | 0.56 | | 1.8 | 732.06 | 2.95 | Steel |
| CORNER_712 | 0 | 250 | | 1000 | 0.56 | | 2.1 | 648.12 | 3.81 | Steel |
| CORNER_712 | 0 | 250 | | 1000 | 0.56 | | 2.4 | 583.05 | 4.72 | Steel |
| CORNER_712 | 0 | 250 | | 1000 | 0.56 | | 2.7 | 510.90 | 5.34 | Steel |
| CORNER_712 | 0 | 250 | | 1000 | 0.56 | | 3 | 444.33 | 5.75 | Steel |
| CORNER_712 | 0 | 250 | | 1000 | 0.56 | | 3.3 | 372.65 | 5.66 | Steel |
| CORNER_712 | 0 | 250 | | 1000 | 0.56 | | 3.6 | 322.51 | 5.72 | Steel |
| CORNER_712 | 0 | 250 | | 1000 | 0.56 | | 3.9 | 270.46 | 5.39 | Steel |
| CORNER_712 | 0 | 250 | | 1000 | 0.56 | | 4.2 | 235.77 | 5.32 | Steel |
| CORNER_712 | 0 | 250 | | 1000 | 0.56 | | 4.5 | 203.25 | 5.08 | Steel |
| CORNER_712 | 0 | 250 | | 1000 | 0.56 | | 4.8 | 180.78 | 5.03 | Steel |
| CORNER_712 | 0 | 250 | | 1000 | 0.56 | | 5.1 | 162.76 | 5.03 | Steel |
| CORNER_712 | 0 | 250 | | 1000 | 0.56 | | 5.4 | 145.24 | 4.90 | Steel |
| CORNER_712 | 0 | 250 | | 1000 | 0.56 | | 5.7 | 131.78 | 4.87 | Steel |
| CORNER_712 | 0 | 250 | | 1000 | 0.56 | | 6 | 121.18 | 4.90 | Steel |
| CORNER_812 | 0 | 250 | | 1000 | 0.56 | | 1.8 | 704.26 | 2.78 | INERT |
| CORNER_812 | 0 | 250 | | 1000 | 0.56 | | 2.1 | 612.32 | 3.48 | INERT |
| CORNER_812 | 0 | 250 | | 1000 | 0.56 | | 2.4 | 526.68 | 4.01 | INERT |
| CORNER_812 | 0 | 250 | | 1000 | 0.56 | | 2.7 | 440.90 | 4.22 | INERT |
| CORNER_812 | 0 | 250 | | 1000 | 0.56 | | 3 | 364.92 | 4.20 | INERT |

**Table A-4 (continued)**
**Alternate corner surface results**

| Case ID | Length (m) | HRR (kW) | Q* | HRRPUA | Diameter (m) | D* | Hp (m) | Temperature Rise (°C) | kF | Surface Properties |
|---|---|---|---|---|---|---|---|---|---|---|
| CORNER_812 | 0 | 250 | | 1000 | 0.56 | | 3.3 | 300.24 | 4.02 | INERT |
| CORNER_812 | 0 | 250 | | 1000 | 0.56 | | 3.6 | 259.64 | 4.07 | INERT |
| CORNER_812 | 0 | 250 | | 1000 | 0.56 | | 3.9 | 225.29 | 4.05 | INERT |
| CORNER_812 | 0 | 250 | | 1000 | 0.56 | | 4.2 | 201.23 | 4.15 | INERT |
| CORNER_812 | 0 | 250 | | 1000 | 0.56 | | 4.5 | 174.68 | 4.01 | INERT |
| CORNER_812 | 0 | 250 | | 1000 | 0.56 | | 4.8 | 156.22 | 4.01 | INERT |
| CORNER_812 | 0 | 250 | | 1000 | 0.56 | | 5.1 | 142.82 | 4.11 | INERT |
| CORNER_812 | 0 | 250 | | 1000 | 0.56 | | 5.4 | 130.53 | 4.16 | INERT |
| CORNER_812 | 0 | 250 | | 1000 | 0.56 | | 5.7 | 119.97 | 4.21 | INERT |
| CORNER_812 | 0 | 250 | | 1000 | 0.56 | | 6 | 112.64 | 4.38 | INERT |
| CORNER_518 | 0 | 500 | | 1000 | 0.80 | | 2.1 | 986.40 | 3.82 | Adiabatic |
| CORNER_518 | 0 | 500 | | 1000 | 0.80 | | 2.4 | 978.19 | 5.70 | Adiabatic |
| CORNER_518 | 0 | 500 | | 1000 | 0.80 | | 2.7 | 941.22 | 7.69 | Adiabatic |
| CORNER_518 | 0 | 500 | | 1000 | 0.80 | | 3 | 884.56 | 9.53 | Adiabatic |
| CORNER_518 | 0 | 500 | | 1000 | 0.80 | | 3.3 | 809.57 | 10.84 | Adiabatic |
| CORNER_518 | 0 | 500 | | 1000 | 0.80 | | 3.6 | 741.60 | 12.01 | Adiabatic |
| CORNER_518 | 0 | 500 | | 1000 | 0.80 | | 3.9 | 682.07 | 13.09 | Adiabatic |
| CORNER_518 | 0 | 500 | | 1000 | 0.80 | | 4.2 | 628.44 | 14.05 | Adiabatic |
| CORNER_518 | 0 | 500 | | 1000 | 0.80 | | 4.5 | 569.65 | 14.38 | Adiabatic |
| CORNER_518 | 0 | 500 | | 1000 | 0.80 | | 4.8 | 514.30 | 14.41 | Adiabatic |
| CORNER_518 | 0 | 500 | | 1000 | 0.80 | | 5.1 | 466.69 | 14.41 | Adiabatic |
| CORNER_518 | 0 | 500 | | 1000 | 0.80 | | 5.4 | 416.22 | 13.84 | Adiabatic |

**Table A-4 (continued)**
**Alternate corner surface results**

| Case ID | Length (m) | HRR (kW) | Q* | HRRPUA | Diameter (m) | D* | Hp (m) | Temperature Rise (°C) | kF | Surface Properties |
|---|---|---|---|---|---|---|---|---|---|---|
| CORNER_518 | 0 | 500 | | 1000 | 0.80 | | 5.7 | 364.69 | 12.78 | Adiabatic |
| CORNER_518 | 0 | 500 | | 1000 | 0.80 | | 6 | 329.49 | 12.39 | Adiabatic |
| CORNER_618 | 0 | 500 | | 1000 | 0.80 | | 2.1 | 774.42 | 2.54 | Gypsum |
| CORNER_618 | 0 | 500 | | 1000 | 0.80 | | 2.4 | 724.66 | 3.37 | Gypsum |
| CORNER_618 | 0 | 500 | | 1000 | 0.80 | | 2.7 | 667.83 | 4.16 | Gypsum |
| CORNER_618 | 0 | 500 | | 1000 | 0.80 | | 3 | 605.14 | 4.80 | Gypsum |
| CORNER_618 | 0 | 500 | | 1000 | 0.80 | | 3.3 | 534.84 | 5.13 | Gypsum |
| CORNER_618 | 0 | 500 | | 1000 | 0.80 | | 3.6 | 465.50 | 5.21 | Gypsum |
| CORNER_618 | 0 | 500 | | 1000 | 0.80 | | 3.9 | 402.51 | 5.13 | Gypsum |
| CORNER_618 | 0 | 500 | | 1000 | 0.80 | | 4.2 | 356.07 | 5.16 | Gypsum |
| CORNER_618 | 0 | 500 | | 1000 | 0.80 | | 4.5 | 313.52 | 5.07 | Gypsum |
| CORNER_618 | 0 | 500 | | 1000 | 0.80 | | 4.8 | 280.20 | 5.05 | Gypsum |
| CORNER_618 | 0 | 500 | | 1000 | 0.80 | | 5.1 | 251.33 | 5.00 | Gypsum |
| CORNER_618 | 0 | 500 | | 1000 | 0.80 | | 5.4 | 225.53 | 4.91 | Gypsum |
| CORNER_618 | 0 | 500 | | 1000 | 0.80 | | 5.7 | 202.76 | 4.79 | Gypsum |
| CORNER_618 | 0 | 500 | | 1000 | 0.80 | | 6 | 186.59 | 4.82 | Gypsum |
| CORNER_718 | 0 | 500 | | 1000 | 0.80 | | 2.1 | 743.95 | 2.38 | Steel |
| CORNER_718 | 0 | 500 | | 1000 | 0.80 | | 2.4 | 689.06 | 3.10 | Steel |
| CORNER_718 | 0 | 500 | | 1000 | 0.80 | | 2.7 | 619.09 | 3.66 | Steel |
| CORNER_718 | 0 | 500 | | 1000 | 0.80 | | 3 | 550.11 | 4.08 | Steel |
| CORNER_718 | 0 | 500 | | 1000 | 0.80 | | 3.3 | 484.88 | 4.35 | Steel |
| CORNER_718 | 0 | 500 | | 1000 | 0.80 | | 3.6 | 429.05 | 4.55 | Steel |

**Table A-4 (continued)**
**Alternate corner surface results**

| Case ID | Length (m) | HRR (kW) | Q* | HRRPUA | Diameter (m) | D* | Hp (m) | Temperature Rise (°C) | kF | Surface Properties |
|---|---|---|---|---|---|---|---|---|---|---|
| CORNER_718 | 0 | 500 | | 1000 | 0.80 | | 3.9 | 364.32 | 4.35 | Steel |
| CORNER_718 | 0 | 500 | | 1000 | 0.80 | | 4.2 | 318.69 | 4.30 | Steel |
| CORNER_718 | 0 | 500 | | 1000 | 0.80 | | 4.5 | 292.56 | 4.53 | Steel |
| CORNER_718 | 0 | 500 | | 1000 | 0.80 | | 4.8 | 268.92 | 4.72 | Steel |
| CORNER_718 | 0 | 500 | | 1000 | 0.80 | | 5.1 | 244.54 | 4.78 | Steel |
| CORNER_718 | 0 | 500 | | 1000 | 0.80 | | 5.4 | 221.60 | 4.77 | Steel |
| CORNER_718 | 0 | 500 | | 1000 | 0.80 | | 5.7 | 197.12 | 4.58 | Steel |
| CORNER_718 | 0 | 500 | | 1000 | 0.80 | | 6 | 182.84 | 4.67 | Steel |
| CORNER_818 | 0 | 500 | | 1000 | 0.80 | | 2.1 | 725.74 | 2.28 | INERT |
| CORNER_818 | 0 | 500 | | 1000 | 0.80 | | 2.4 | 671.59 | 2.97 | INERT |
| CORNER_818 | 0 | 500 | | 1000 | 0.80 | | 2.7 | 604.85 | 3.52 | INERT |
| CORNER_818 | 0 | 500 | | 1000 | 0.80 | | 3 | 553.89 | 4.13 | INERT |
| CORNER_818 | 0 | 500 | | 1000 | 0.80 | | 3.3 | 488.82 | 4.41 | INERT |
| CORNER_818 | 0 | 500 | | 1000 | 0.80 | | 3.6 | 437.03 | 4.69 | INERT |
| CORNER_818 | 0 | 500 | | 1000 | 0.80 | | 3.9 | 386.26 | 4.79 | INERT |
| CORNER_818 | 0 | 500 | | 1000 | 0.80 | | 4.2 | 339.88 | 4.78 | INERT |
| CORNER_818 | 0 | 500 | | 1000 | 0.80 | | 4.5 | 297.66 | 4.66 | INERT |
| CORNER_818 | 0 | 500 | | 1000 | 0.80 | | 4.8 | 267.39 | 4.68 | INERT |
| CORNER_818 | 0 | 500 | | 1000 | 0.80 | | 5.1 | 238.53 | 4.60 | INERT |
| CORNER_818 | 0 | 500 | | 1000 | 0.80 | | 5.4 | 215.76 | 4.57 | INERT |
| CORNER_818 | 0 | 500 | | 1000 | 0.80 | | 5.7 | 195.71 | 4.53 | INERT |
| CORNER_818 | 0 | 500 | | 1000 | 0.80 | | 6 | 180.32 | 4.56 | INERT |

**Table A-4 (continued)**
**Alternate corner surface results**

| Case ID | Length (m) | HRR (kW) | Q* | HRRPUA | Diameter (m) | D* | Hp (m) | Temperature Rise (°C) | kF | Surface Properties |
|---|---|---|---|---|---|---|---|---|---|---|
| CORNER_524 | 0 | 1000 | | 1000 | 1.13 | | 2.7 | 951.69 | 3.93 | Adiabatic |
| CORNER_524 | 0 | 1000 | | 1000 | 1.13 | | 3 | 919.43 | 5.14 | Adiabatic |
| CORNER_524 | 0 | 1000 | | 1000 | 1.13 | | 3.3 | 881.27 | 6.41 | Adiabatic |
| CORNER_524 | 0 | 1000 | | 1000 | 1.13 | | 3.6 | 841.32 | 7.71 | Adiabatic |
| CORNER_524 | 0 | 1000 | | 1000 | 1.13 | | 3.9 | 798.19 | 8.95 | Adiabatic |
| CORNER_524 | 0 | 1000 | | 1000 | 1.13 | | 4.2 | 764.25 | 10.37 | Adiabatic |
| CORNER_524 | 0 | 1000 | | 1000 | 1.13 | | 4.5 | 722.19 | 11.49 | Adiabatic |
| CORNER_524 | 0 | 1000 | | 1000 | 1.13 | | 4.8 | 688.21 | 12.76 | Adiabatic |
| CORNER_524 | 0 | 1000 | | 1000 | 1.13 | | 5.1 | 655.28 | 13.96 | Adiabatic |
| CORNER_524 | 0 | 1000 | | 1000 | 1.13 | | 5.4 | 611.41 | 14.47 | Adiabatic |
| CORNER_524 | 0 | 1000 | | 1000 | 1.13 | | 5.7 | 566.70 | 14.65 | Adiabatic |
| CORNER_524 | 0 | 1000 | | 1000 | 1.13 | | 6 | 520.60 | 14.45 | Adiabatic |
| CORNER_624 | 0 | 1000 | | 1000 | 1.13 | | 2.7 | 736.32 | 2.46 | Gypsum |
| CORNER_624 | 0 | 1000 | | 1000 | 1.13 | | 3 | 695.31 | 3.05 | Gypsum |
| CORNER_624 | 0 | 1000 | | 1000 | 1.13 | | 3.3 | 629.93 | 3.41 | Gypsum |
| CORNER_624 | 0 | 1000 | | 1000 | 1.13 | | 3.6 | 575.35 | 3.76 | Gypsum |
| CORNER_624 | 0 | 1000 | | 1000 | 1.13 | | 3.9 | 512.56 | 3.88 | Gypsum |
| CORNER_624 | 0 | 1000 | | 1000 | 1.13 | | 4.2 | 464.19 | 4.05 | Gypsum |
| CORNER_624 | 0 | 1000 | | 1000 | 1.13 | | 4.5 | 420.37 | 4.16 | Gypsum |
| CORNER_624 | 0 | 1000 | | 1000 | 1.13 | | 4.8 | 384.77 | 4.29 | Gypsum |
| CORNER_624 | 0 | 1000 | | 1000 | 1.13 | | 5.1 | 353.16 | 4.40 | Gypsum |
| CORNER_624 | 0 | 1000 | | 1000 | 1.13 | | 5.4 | 311.88 | 4.19 | Gypsum |

**Table A-4 (continued)**
**Alternate corner surface results**

| Case ID | Length (m) | HRR (kW) | Q* | HRRPUA | Diameter (m) | D* | Hp (m) | Temperature Rise (°C) | kF | Surface Properties |
|---|---|---|---|---|---|---|---|---|---|---|
| CORNER_624 | 0 | 1000 | | 1000 | 1.13 | | 5.7 | 280.59 | 4.08 | Gypsum |
| CORNER_624 | 0 | 1000 | | 1000 | 1.13 | | 6 | 259.16 | 4.12 | Gypsum |
| CORNER_724 | 0 | 1000 | | 1000 | 1.13 | | 2.7 | 661.07 | 2.05 | Steel |
| CORNER_724 | 0 | 1000 | | 1000 | 1.13 | | 3 | 608.91 | 2.42 | Steel |
| CORNER_724 | 0 | 1000 | | 1000 | 1.13 | | 3.3 | 550.34 | 2.69 | Steel |
| CORNER_724 | 0 | 1000 | | 1000 | 1.13 | | 3.6 | 502.52 | 2.97 | Steel |
| CORNER_724 | 0 | 1000 | | 1000 | 1.13 | | 3.9 | 452.05 | 3.12 | Steel |
| CORNER_724 | 0 | 1000 | | 1000 | 1.13 | | 4.2 | 418.07 | 3.38 | Steel |
| CORNER_724 | 0 | 1000 | | 1000 | 1.13 | | 4.5 | 385.29 | 3.58 | Steel |
| CORNER_724 | 0 | 1000 | | 1000 | 1.13 | | 4.8 | 360.73 | 3.84 | Steel |
| CORNER_724 | 0 | 1000 | | 1000 | 1.13 | | 5.1 | 344.84 | 4.23 | Steel |
| CORNER_724 | 0 | 1000 | | 1000 | 1.13 | | 5.4 | 325.25 | 4.50 | Steel |
| CORNER_724 | 0 | 1000 | | 1000 | 1.13 | | 5.7 | 305.80 | 4.71 | Steel |
| CORNER_724 | 0 | 1000 | | 1000 | 1.13 | | 6 | 286.86 | 4.88 | Steel |
| CORNER_824 | 0 | 1000 | | 1000 | 1.13 | | 2.7 | 657.46 | 2.03 | INERT |
| CORNER_824 | 0 | 1000 | | 1000 | 1.13 | | 3 | 598.72 | 2.36 | INERT |
| CORNER_824 | 0 | 1000 | | 1000 | 1.13 | | 3.3 | 552.18 | 2.71 | INERT |
| CORNER_824 | 0 | 1000 | | 1000 | 1.13 | | 3.6 | 504.15 | 2.99 | INERT |
| CORNER_824 | 0 | 1000 | | 1000 | 1.13 | | 3.9 | 449.01 | 3.09 | INERT |
| CORNER_824 | 0 | 1000 | | 1000 | 1.13 | | 4.2 | 406.43 | 3.22 | INERT |
| CORNER_824 | 0 | 1000 | | 1000 | 1.13 | | 4.5 | 365.44 | 3.27 | INERT |
| CORNER_824 | 0 | 1000 | | 1000 | 1.13 | | 4.8 | 341.64 | 3.51 | INERT |

**Table A-4 (continued)**
**Alternate corner surface results**

| Case ID | Length (m) | HRR (kW) | Q* | HRRPUA | Diameter (m) | D* | Hp (m) | Temperature Rise (°C) | kF | Surface Properties |
|---|---|---|---|---|---|---|---|---|---|---|
| CORNER_824 | 0 | 1000 | | 1000 | 1.13 | | 5.1 | 317.23 | 3.67 | INERT |
| CORNER_824 | 0 | 1000 | | 1000 | 1.13 | | 5.4 | 288.98 | 3.68 | INERT |
| CORNER_824 | 0 | 1000 | | 1000 | 1.13 | | 5.7 | 267.17 | 3.76 | INERT |
| CORNER_824 | 0 | 1000 | | 1000 | 1.13 | | 6 | 246.81 | 3.80 | INERT |

# B
# CHARACTERISTICS OF TRANSIENT FIRES FROM THE FIRE EVENTS DATABASE

## B.1 Characteristics of Transient Fires from the Fire Events Database

Table B-1 contains data from the EPRI Updated Fire Events Database from the 1990s and 2000s for general transient fires. The first six columns provide the fire ID, power level, ignition source, fire cause, damage extent, and additional information. Columns 7–9 present the categorization of the transient fires to determine whether the combustible material is integral to the ignition source. The following question is asked:

> Question 1: Does the ignition source on its own contain sufficient combustible material to be considered a significant transient combustible fire source? If so, the distance between ignition source and combustible material is 0, and the second question, regarding the locations of ignition source and transient combustible material, is not applicable. If not, the second question must be answered.

Columns 10–12 complete the categorization of the transient fires to determine whether the ignition source and combustible package were correlated or uncorrelated. The following question is asked:

> Question 2: Is the ignition source part of an activity that is likely to lead to the ignition source and sufficient combustible material for a transient combustible fire being close together (spatially correlated)? If the answer to the first question is yes, this is N/A.

A value of "1" is entered into the appropriate column. In some cases, when the answer was unclear, a value of "0.5" was placed in two columns to represent equal probability of each answer.

Two fire events were excluded from the transient analysis, fire IDs 504 and 20313. Fire ID 504 had an unusual transient ignition source—debris from the auxiliary boiler that ignited. Fire ID 20313 has no description; therefore, no insights could be derived.

The summing of the results and calculating the fractions that describe the transient fires are presented in Table B-2. Based on the results in Figure 4-4 (Chapter 4) and Table B-2, it is interesting to note that the low power conditions have a higher fraction of uncorrelated transient fires than the at-power conditions. The reason may be due to the type of work and housekeeping practices that occur during low power. Tables B-3 and B-4 contain a list of the ignition sources that are characterized as *correlated* and *uncorrelated* for the at-power and low-power conditions. For low-power conditions, the ignition sources consist of more heaters, weld machines, and equipment (for example, air compressor, floor scrubber) than in the full-power events, which may be related to the type of work performed at low-power conditions.

**Table B-1**
**Characterization of transient fires from the EPRI Updated Fire Events Database**

| Fire ID<br>Power Level (AP = At Power, LPSD = Low-Power-Shutdown) | | | | | Question 1<br>Does the ignition source on its own contain sufficient combustible material to be considered a significant transient combustible fire source? If so, the distance between ignition source and combustible material is 0, and the second question, regarding the locations of ignition source and transient combustible material, is not applicable. If not, the second question must be answered. | | | Question 2<br>Is the ignition source part of an activity that is likely to lead to the ignition source and sufficient combustible material for a transient combustible fire being close together (spatially correlated)? If the answer to the first question is yes, this is N/A. | | | |
|---|---|---|---|---|---|---|---|---|---|---|---|
| | Ignition Source | Fire Cause | Damage Extent | Additional Information | Yes | No | Reasoning | Yes | No | N/A | Reasoning |
| 236<br>LPSD | Water cooler cord - burnt insulation | Electrical failure - overheating materials | Confined to object of origin | Burnt wire connection on the backside of the cooler; water cooler and coffee pot plugged into extension cord; put out by unplugging; single cable, insulation on cord burned. | | 1 | One electrical cord does not contain sufficient combustible material. | 1 | | | A water cooler cord could ignite a nearby combustible, such as a trash can for water cups, and so on. |
| 238<br>AP | Overheating electrical wiring | Electrical failure - overheating materials | Confined to object of origin | Overload of electrical cables in laundry trailer portable heater; suppression by removing power. | | 1 | The overloaded cables within the portable heater do not contain sufficient combustible material. | 1 | | | The heater is likely to be close to other combustibles in association with an activity that requires heating for personal comfort. |
| 246<br>LPSD | Light string heated up wood reel and ignited | Personnel error - misuse of material ignited | Confined to room of origin | Light string lying on top of wood wire reel ignited; temporary electrical wiring. | | 1 | A light string does not contain sufficient combustible material. | 1 | | | Very little info provided; however, the intersection of combustible and temporary light string implies a correlated activity. |
| 259<br>AP | Temporary electrical wiring | Electrical failure - overheating materials | Confined to object of origin | No description provided. Fire Events Database attributes include high-level event description: temporary electrical wiring or equipment; light smoke coming from ignition source - minor or no visibility reduction in vicinity of fire. | | 1 | A minimal amount of temporary electrical wiring does not contain sufficient combustible material. | 1 | | | Due to the lack of description, assumed that the electrical wiring could have been located near to a combustible. |
| 20277<br>LPSD | Overheating electrical connections | Electrical failure - overheating materials | Confined to object of origin | Overheating at electrical connections caused fire. | | 1 | Electrical connections alone do not contain sufficient combustible material. | 1 | | | Based on the information provided and power mode (LPSD), assumed that work activities were in progress, and combustibles may be correlated. |
| 20289<br>LPSD | Clothing | Unknown | Unknown | Cloth; cellulosic materials including wood, paper or other solid transients; no information given as to ignition source. Fire was detected by roving fire watch. | | 1 | No information regarding ignition source; however, clothing does not contain an ignition source. Thus, this is classified as correlated (ignition source in contact with secondary combustibles). | 1 | | | Although the ignition source is not known, the secondary combustible (clothing or cloth) indicates work activity is likely. |
| 20297<br>LPSD | Electrical fault in temporary light | Electrical failure - overheating materials | Confined to the object of origin | Temporary light was left on and caused an electrical fault. Cable insulation burned. | | 1 | Temporary electrical wiring does not contain sufficient combustible material alone. | 1 | | | Due to the presence of temporary lighting and the operating mode (LPSD), it is likely that work activities were underway. Therefore, it is assumed that combustibles may be located nearby. |
| 20304<br>LPSD | Tea kettle (combustible liquid) | Electrical failure - overheating materials | Confined to the object of origin | Tea kettle with combustible liquid. Suppressed by fire watch during construction work during shutdown. | 1 | | The tea kettle contained combustible material. The ignition source was electrical failure. Consider the ignition source and combustible as integral. | | | 1 | |
| 50608<br>LPSD | Short in electrical cord | Electrical arcing or sparks (non-HEAF) | Confined to the object of origin (localized/single subcomponent) | A short duration fire occurred that was caused by a short in the electrical cord connections for a wetwell cleanup filter crusher and the temporary power supply “bang box.” The fire was due to faulty wiring in a three-way “pig” extension. | | 1 | A short in an electrical cord is the ignition source. The equipment being tested appears to be small (a subcomponent, it is reported) and, therefore, not a significant combustible itself. | 1 | | | Occurred during maintenance activities; therefore, the ignition source is considered correlated. |

**Table B-1 (continued)**
**Characterization of transient fires from the EPRI Updated Fire Events Database**

| Fire ID<br>Power Level (AP = At Power, LPSD = Low-Power-Shutdown) | | | | | Question 1<br>Does the ignition source on its own contain sufficient combustible material to be considered a significant transient combustible fire source? If so, the distance between ignition source and combustible material is 0, and the second question, regarding the locations of ignition source and transient combustible material, is not applicable. If not, the second question must be answered. | | | Question 2<br>Is the ignition source part of an activity that is likely to lead to the ignition source and sufficient combustible material for a transient combustible fire being close together (spatially correlated)? If the answer to the first question is yes, this is N/A. | | | |
|---|---|---|---|---|---|---|---|---|---|---|---|
| | **Ignition Source** | **Fire Cause** | **Damage Extent** | **Additional Information** | **Yes** | **No** | **Reasoning** | **Yes** | **No** | **N/A** | **Reasoning** |
| 125<br>AP | Floodlight burst (hot fragments ignited hose) | Electrical failure - overheating materials | Confined to part of room or area of origin | Contract employee reported burning smell and discovered fire inside a metal building. The fire was located in an area of plastic-covered hose being stored on the floor of the building. The fire, which reached a level requiring the plant fire brigade, was started by hot fragments of glass blown from the lamp in a nearby quartz halogen portable light. The fragments were not contained within the floodlight canister because the floodlight tempered glass door had been removed. Fire hose was used to extinguish fire. Fire was localized within a 3 ft area near the center of the building. Burning material was coiled cask pit transfer hose in plastic wrapping and several nylon strings. | | 1 | The ignited hose is separate from the floodlight, thus, by definition, a correlated ignition source. | 1 | | | The floodlight is in a temporary building, presumably erected for the same activity that involved the coiled hose. Therefore, there is reason to suppose that the hose was near the floodlight because they both were part of the same activity. |
| 515<br>LPSD | Temporary air compressor | Unknown | Unknown | Fire reported at the base of the unit aux air lock in a temporary air compressor. | | 1 | A typical small temporary air compressor does not contain sufficient combustible material to generate a significant HRR. | | 1 | | No activity is mentioned or implied that would cause there to be a sufficient nearby collection of combustible material. |
| 30314<br>AP | Altered extension cord | Electrical failure - overheating materials | Confined to structure of origin - Classified this way because the fire was in the stressing gallery, but the door was open to the aux building, and smoke and heat set off the fire detection system in the adjacent room. | At 17:00, one of the two 2000 watt heaters was energized in preparation for the next day's work activities. Over the next 10 hours, one of the extension cords heated up to the point that a fire started and ignited rhino cloth and herculite. The overloaded extension cord caught a radiation protection (RP) clothing bag that was on the cord. Heavy smoke was generated; fire detection and suppression systems operated. | | 1 | An extension cord alone does not contain sufficient combustible material. | 1 | | | Yes. The altered extension cord and the poor housekeeping practices contributed to this fire event. This is a correlated transient fire event where the ignition source and secondary combustibles were in close proximity |
| 30374<br>LPSD | Portable space heater | Electrical failure - overheating materials | Confined to object of origin | While performing coating repairs on a heat exchanger, a portable space heater was issued and hooked up. The heater was used to fast cure the applied coatings. The heater was shut off, and during that time, an inspection was performed on the west end of the heat exchanger. While the painter was walking back to the east end, he noticed smoke. It was determined that the heater malfunctioned and caught fire. | | 1 | The portable space heater does not contain sufficient combustible material. | | 1 | | Although this occurred during work activities, the review insights indicate that the space heater was not located near combustibles or the general work area. |

**Table B-1 (continued)**
**Characterization of transient fires from the EPRI Updated Fire Events Database**

| Fire ID<br>Power Level (AP = At Power, LPSD = Low-Power-Shutdown) | | | | | Question 1<br>Does the ignition source on its own contain sufficient combustible material to be considered a significant transient combustible fire source? If so, the distance between ignition source and combustible material is 0, and the second question, regarding the locations of ignition source and transient combustible material, is not applicable. If not, the second question must be answered. | | | Question 2<br>Is the ignition source part of an activity that is likely to lead to the ignition source and sufficient combustible material for a transient combustible fire being close together (spatially correlated)? If the answer to the first question is yes, this is N/A. | | | |
|---|---|---|---|---|---|---|---|---|---|---|---|
| | **Ignition Source** | **Fire Cause** | **Damage Extent** | **Additional Information** | **Yes** | **No** | **Reasoning** | **Yes** | **No** | **N/A** | **Reasoning** |
| 50796<br>LPSD | Floor scrubber battery | Electrical failure - overheating materials | Confined to object of origin | Battery on floor scrubber was smoking, and visible flames were observed. An I&C technician extinguished the fire by blowing on the flames. Flames were limited to the negative battery terminal of the lower battery. The I&C technician suspects that the terminal may have been loose, causing an overheat condition. Top of the battery was melted. | 0.5 | 0.5 | In this event, the fire was limited (as evident in extinguishment by blowing); however, the floor scrubber is a substantial piece of equipment, and thus a 50/50 probability is assigned. | | 0.5 | 0.5 | No evidence in the report of nearby combustibles or work activity. Therefore, assume activity is uncorrelated. |
| 50809<br>LPSD | Faulty plug – extension cord | Electrical failure - overheating materials | Confined to object of origin | Plant personnel noticed a bit of smoke between the main steam isolation valves. While searching for the source of the smoke, flames shot up from an electrical cord. Personnel extinguished the flame with a Class ABC extinguisher, which had been staged for welding activities. While personnel shot the fire with the extinguisher, another worker in the room unplugged the plug at the source to eliminate the electricity to the plug. After the fire was extinguished, plant personnel overhauled the electrical equipment that had burned and removed it from the area. The cause was found to be a faulty plug on a temporary light. | | 1 | The extension cord alone does not contain sufficient combustibles to generate a substantial fire. | 0.5 | 0.5 | | Assign a 50/50 split between correlated and uncorrelated. Event description mentioned welding activities, which would not likely involve nearby combustibles; however, the event description suggests a transition to welding activities. |
| 81<br>AP | Temporary lighting fixture | Overheated materials (lube oil, pump packing, thermal insulation, and so on) | Confined to object of origin | At 20:10 CST, a station operator detected a fire on top of a charcoal absorber bed in the augmented offgas system room. The site fire brigade was dispatched to the scene and extinguished the fire at 20:32 CST. Fire was caused by ignition of insulation by a temporary lighting fixture installed for maintenance activities. | | 1 | The light itself does not contain sufficient combustible material. The insulation also does not seem to contain sufficient combustible material. Therefore, the need for an additional combustible is postulated. | 1 | | | Yes, per the event description, work activities were in progress. |
| 20281<br>AP | Oil leaked from reservoir | Overheated materials (lube oil, pump packing, thermal insulation, and so on) | Unknown | Very little detail provided, summary of “oil that was leaking from a reservoir came in contact with some hot pipes and began to smoke.” | 0.5 | 0.5 | The oil source is assumed to be part of the same equipment that contains the hot pipe and insulation materials. The oil leak and insulation may or may not contain sufficient combustible material. 50% probability assigned. | | 0.5 | 0.5 | No activity is mentioned or implied that would cause there to be a sufficient nearby collection of combustible material. |

**Table B-1 (continued)**
**Characterization of transient fires from the EPRI Updated Fire Events Database**

| Fire ID<br>Power Level (AP = At Power, LPSD = Low-Power-Shutdown) | | | | | Question 1<br>Does the ignition source on its own contain sufficient combustible material to be considered a significant transient combustible fire source? If so, the distance between ignition source and combustible material is 0, and the second question, regarding the locations of ignition source and transient combustible material, is not applicable. If not, the second question must be answered. | | | Question 2<br>Is the ignition source part of an activity that is likely to lead to the ignition source and sufficient combustible material for a transient combustible fire being close together (spatially correlated)? If the answer to the first question is yes, this is N/A. | | | |
|---|---|---|---|---|---|---|---|---|---|---|---|
| | **Ignition Source** | **Fire Cause** | **Damage Extent** | **Additional Information** | **Yes** | **No** | **Reasoning** | **Yes** | **No** | **N/A** | **Reasoning** |
| 20303<br>LPSD | Smoldering oily rags on top of a drop light | Personnel error: misuse of heating devices | No damage | Rags used to clean the D/G fuel injectors were left on top of a turned-on light. The light was a plastic-coated metal trouble light. Oily rags were discovered smoldering on the top of a drop light (incandescent bulb). The fire was extinguished in the incipient stage. Damage was limited to the drop light cord and rags. | | 1 | The incandescent light bulb and rags represent a minimal combustible. | 1 | | | The rags were placed on the drop light bulb during maintenance. |
| 20336<br>AP | Rags, paper, foam (in yard) | Unknown | No damage | Little description available – minor rubbish fire. The point of origin was rags, paper, and foam. | 1 | | The ignition source is not noted, but it may be integral to the trash (such as oil-soaked rags). | | | 1 | |
| 20341<br>LPSD | Heater | Personnel error: misuse of heating devices | Unknown | Stress relief heater ignited paint on the floor. | | 1 | The stress-relief heater does not contain sufficient combustible material. The paint on the floor is not a sufficient combustible. | | 1 | | The welding stress relief heater is used to warm up areas near welds. It is deduced that the heater pad came in contact with the floor and briefly ignited the painted floor. Although this appears to be a correlated event, the painted floor is an unusual secondary combustible that is unlikely to contribute significantly to a fire of significant HRR and duration. Event assumed to be uncorrelated. |
| 20361<br>AP | 480 V extension cord | Electrical failure - overheating materials | Unknown | 480 V extension cord overheated from use of heavy amp machine. No damage other than the plug ends of the extension cord. | | 1 | The plug end of the extension cord overheated. This does not represent the potential for a significant fire unless combustibles are nearby. | 1 | | | There is little narrative provided, but it has been assumed that the extension cord is associated with a maintenance activity. |
| 20373<br>LPSD | Wiring in main condenser | Electrical failure - overheating materials | Unknown | This fire was during refueling, and it appears that there was welding within the condenser. | | 1 | The ignition source was the welding inside the main condenser. Insufficient combustibles on its own. | | 1 | | Controls during welding would preclude any extra combustibles stored nearby. |
| 422<br>AP | 480 V power outlet | Electrical failure - overheating materials | Confined to object of origin | Electrical fire on service building loading dock. A 480 V power outlet became overheated and caught fire. This outlet was to supply power for temporary freeze protection. | | 1 | The power outlet became overheated. This does not represent the potential for a significant fire unless combustibles are nearby. | | 1 | | This outlet was being used for temporary freeze protection, not for an activity that would have involved the collection of sufficient combustible material. |

**Table B-1 (continued)**
**Characterization of transient fires from the EPRI Updated Fire Events Database**

| Fire ID<br>Power Level (AP = At Power, LPSD = Low-Power-Shutdown) | | | | | Question 1<br>Does the ignition source on its own contain sufficient combustible material to be considered a significant transient combustible fire source? If so, the distance between ignition source and combustible material is 0, and the second question, regarding the locations of ignition source and transient combustible material, is not applicable. If not, the second question must be answered. | | | Question 2<br>Is the ignition source part of an activity that is likely to lead to the ignition source and sufficient combustible material for a transient combustible fire being close together (spatially correlated)? If the answer to the first question is yes, this is N/A. | | | |
|---|---|---|---|---|---|---|---|---|---|---|---|
| | **Ignition Source** | **Fire Cause** | **Damage Extent** | **Additional Information** | **Yes** | **No** | **Reasoning** | **Yes** | **No** | **N/A** | **Reasoning** |
| 10628<br>AP | Temporary air conditioner | Electrical arcing or sparks (non-high-energy arcing fault [HEAF]) | Confined to the object of origin (localized/single subcomponent) | An enclosed office was built in the bay of the diesel generator building. This office was built for the purpose of having an area to work on security equipment (cameras, monitors, and so on). The office was equipped with a window air conditioner unit to maintain a desirable temperature for human occupation and for the equipment. The facility had not been used for several years. It was determined that the facility needed to be demobilized. Craft personnel were in the process of removing the structure and the A/C unit when they noticed smoke and flames coming from the unit. They immediately responded to the unit with a fire extinguisher, put the fire out, and notified the main control room (MCR). Occurred during work, so the fire was quickly extinguished. | | 1 | An air conditioner would not contain sufficient combustible material to generate a large damaging HRR. | 1 | | | The enclosed area was in the process of being dismantled; therefore, for the purpose of this review, the demolition is akin to maintenance/work. |
| 30333<br>AP | Paint thinner | Overheated materials (lube oil, pump packing, thermal insulation, and so on) | Confined to the object of origin (localized/single subcomponent) | While coating activities were taking place in a confined space, the thinner being used to clean the spray gun ignited and caught fire. The painters performing the activities attempted to extinguish the fire for a few seconds but were unsuccessful; the fire brigade extinguished the fire. | | 1 | The ignition source is the spray gun and the paint thinner (flash point around 100°F) is the combustible. A small amount is put in contact with the gun, which would probably not produce a fire of sufficient HRR and duration. | 1 | | | The use of the spray gun is likely to be accompanied by transient combustibles, such as the paint thinner. Therefore, this event is classified as correlated. |
| 30418<br>LPSD | Forklift battery | Electrical failure - overheating materials | Confined to the object of origin (localized/single subcomponent) | Battery shorted and caught fire. The cause of the fire was that the tie-down bracket holding the battery came in contact with the positive terminal of the battery. Fire brigade was called but not needed; the forklift operator extinguished the fire. | | 1 | The battery for the forklift would not contain sufficient combustible material to be considered integral; additionally, the fire was on top of the battery. The highest HRR used for station batteries is 69 kW, and the forklift battery would have less combustible material. | 0.5 | 0.5 | | Unclear from the event narrative what the forklift activity was for. Assigned a 50/50 probability to account for possibility of nearby combustibles. |

**Table B-1 (continued)**
**Characterization of transient fires from the EPRI Updated Fire Events Database**

| Fire ID<br>Power Level (AP = At Power, LPSD = Low-Power-Shutdown) | | | | | Question 1<br>Does the ignition source on its own contain sufficient combustible material to be considered a significant transient combustible fire source? If so, the distance between ignition source and combustible material is 0, and the second question, regarding the locations of ignition source and transient combustible material, is not applicable. If not, the second question must be answered. | | | Question 2<br>Is the ignition source part of an activity that is likely to lead to the ignition source and sufficient combustible material for a transient combustible fire being close together (spatially correlated)? If the answer to the first question is yes, this is N/A. | | | |
|---|---|---|---|---|---|---|---|---|---|---|---|
| | **Ignition Source** | **Fire Cause** | **Damage Extent** | **Additional Information** | **Yes** | **No** | **Reasoning** | **Yes** | **No** | **N/A** | **Reasoning** |
| 30459<br>AP | Cardboard (chart box paper, spill kit box) | Overheated materials (lube oil, pump packing, thermal insulation, and so on) | Confined to the object of origin (localized/single subcomponent) | Operating rover was performing outside rounds at the LSH. When he entered the LSH, he noticed a funny smell. Investigation led him to the traveling screen control panel. When he opened up the back of the panel, he found a chart paper box and a spill kit box (both cardboard) on the floor. Both were smoldering. He pulled both boxes out of the panel and encountered a small amount of flame. He placed the two boxes on the floor and used a dry chemical fireextinguisher to extinguish the flame. | | 1 | The ignition source appears to have been something outside the boxes but within the control panel. There was no mention was made of self-igniting material in the boxes. The boxes and their contents are considered to constitute sufficient combustible material if ignited inside the control panel and allowed to burn. The chart paper box may have contained a stack or rolls of chart paper. The spill kit box may have contained components of a spill kit, such as pads, gloves, sorbent material, bags, instruction sheets, and safety glasses. | 1 | | | The presence of the boxes appears to be correlated with activities that involve the control panel and an associated chart recorder. |
| 30566<br>AP | Sweatshirt draped over a light caused the fire | Overheated materials (lube oil, pump packing, thermal insulation, and so on) | Confined to the object of origin (localized/single subcomponent) | A sweatshirt draped over a quartz light caught fire. Flaming combustion – external to the component. | | 1 | A light string combined with a sweatshirt does not contain sufficient combustible material. | 1 | | | The sweatshirt, draped over a quartz light on a lift, is not a sufficient combustible. However, other combustible material may be associated with the activity. |
| 30604<br>AP | Bird's nest in a pump exhaust caused heavy smoke | Other | Confined to object of origin | During a startup of the fire pump (FP) A diesel, the pump room very quickly filled with dense black smoke, which was seen coming from the point where the diesel joins the exhaust pipe. The operator stopped the pump using the hand switch on the front of the diesel and informed the main control room. Rusty screens on the FP diesel exhausts allowed biofouling, which created a hazardous condition in the FP room. Area operator reported no flames present, but remnants of a smoldering bird's nest were lodged in the exhaust manifold screen. | | 1 | The ignition of the bird's nest in the exhaust pipe does not represent a condition that may cause damage to secondary targets (appears likely that the exhaust pipe discharges to an outside area). | | 1 | | Although a test activity, it is unlikely that this event is correlated with a sufficient amount of combustible material. |

**Table B-1 (continued)**
**Characterization of transient fires from the EPRI Updated Fire Events Database**

| Fire ID<br>Power Level (AP = At Power, LPSD = Low-Power-Shutdown) | | | | | Question 1<br>Does the ignition source on its own contain sufficient combustible material to be considered a significant transient combustible fire source? If so, the distance between ignition source and combustible material is 0, and the second question, regarding the locations of ignition source and transient combustible material, is not applicable. If not, the second question must be answered. | | | Question 2<br>Is the ignition source part of an activity that is likely to lead to the ignition source and sufficient combustible material for a transient combustible fire being close together (spatially correlated)? If the answer to the first question is yes, this is N/A. | | | |
|---|---|---|---|---|---|---|---|---|---|---|---|
| | **Ignition Source** | **Fire Cause** | **Damage Extent** | **Additional Information** | **Yes** | **No** | **Reasoning** | **Yes** | **No** | **N/A** | **Reasoning** |
| 30717<br>AP | Lamp | Electrical failure - overheating materials | Confined to object of origin | While replacing a lamp, the lamp blew out and caught on fire. The switch became unusable. This caused the valve that supplies sample to the CT lab to close and not allow sample to flow. Fire was put out quickly with no other problems encountered. Flaming combustion – internal to the component; Light smoke coming from ignition source - minor or no visibility reduction in the vicinity of the fire; temperature at or close to ambient | | 1 | A lamp/light bulb does not contain sufficient combustible material. | | 1 | | No combustible material other than the lamp is mentioned. The lamp replacement activity is not expected to be associated with sufficient combustible material. Therefore, the locations of the ignition source and sufficient combustible are judged to be uncorrelated. |
| 30757<br>AP | Cigarette box | Unknown | Confined to object of origin | A cigarette box was on fire with shooting flames and bellowing smoke near the scrubber test shop. The cigarette box was next to a metal building with a wooden floor. A large Igloo water cooler was located to eventually put out the fire. | | 1 | A cigarette box by itself is not a sufficient combustible. | | 1 | | Smoking would not be associated with collection of extra combustibles. |
| 50504<br>LPSD | Strip heater | Overheated materials (lube oil, pump packing, thermal insulation, and so on) | Confined to the object of origin (localized/single subcomponent) | This condition report is to document a strip heater fire in the boric acid addition tank room. At 0854, the control room received a fire detection alarm with four detectors in alarm for the BAAT room. The SEO was dispatched to investigate, and the station fire alarm sounded to activate the fire brigade. The fire brigade responded; determined the source of the fire, which was one of the strip heaters; and de-energized all strip heaters. | | 1 | A strip heater alone does not contain sufficient combustible material. | | 1 | | No activity was ongoing nearby when the fire occurred. Sufficient combustible material was not ignited. Therefore, the location of an unspecified combustible is not correlated with the location of the ignition source. |
| 23<br>AP | Steam leak on electrical extension cord caused wetted lagging and insulation to ignite | Overheated materials (lube oil, pump packing, thermal insulation, and so on) | Confined to object of origin | A steam leak on an electrical extension cord started a fire on the lagging. The fire was put out with dry chemicals, but the fire reflashed and was put out by the fire brigade. The time from ignition and reflash to complete extinction was 40 minutes. | | 1 | The steam leak on an extension cord is the ignition source. The extension cord itself does not constitute an integral source. | 1 | | | Due to the presence of intermediate combustibles in the event, this is considered correlated. |
| 208<br>AP | Short in electrical cord | Electrical failure - overheating materials | Confined to object of origin | Very little information provided. Overcurrent of an internal short. The fire was put out by tripping the breaker and unplugging the cord. | | 1 | An electrical cord alone does not contain sufficient combustible material. | 0.5 | 0.5 | | The description does not refer to the electrical cord as an extension cord, which would have implied an activity. Therefore, a 50% probability of correlation is assigned. |
| 244<br>LPSD | Vacuum cleaner | Electrical failure - overheating materials | Confined to part of room or area of origin | Smoke observed in the turbine building (TB). Fire brigade responded and extinguished the vacuum cleaner. | 1 | | A vacuum cleaner may contain sufficient combustible material to qualify as integral. | | | 1 | |

**Table B-1 (continued)**
**Characterization of transient fires from the EPRI Updated Fire Events Database**

| Fire ID<br>Power Level (AP = At Power, LPSD = Low-Power-Shutdown) | | | | | Question 1<br>Does the ignition source on its own contain sufficient combustible material to be considered a significant transient combustible fire source? If so, the distance between ignition source and combustible material is 0, and the second question, regarding the locations of ignition source and transient combustible material, is not applicable. If not, the second question must be answered. | | | Question 2<br>Is the ignition source part of an activity that is likely to lead to the ignition source and sufficient combustible material for a transient combustible fire being close together (spatially correlated)? If the answer to the first question is yes, this is N/A. | | | |
|---|---|---|---|---|---|---|---|---|---|---|---|
| | **Ignition Source** | **Fire Cause** | **Damage Extent** | **Additional Information** | **Yes** | **No** | **Reasoning** | **Yes** | **No** | **N/A** | **Reasoning** |
| 20300<br>LPSD | Excess wire ignited by oven | Personnel error: misuse of heating devices | Confined to object of origin | Very little description provided. Excess wire was ignited by oven. | | 1 | Wire insulation does not contain sufficient combustible material. | 0.5 | 0.5 | | Unable to determine any more details from the event report. 50%/50% probability assigned to each. |
| 20301<br>AP | Plastic emergency lighting | Overheated materials (lube oil, pump packing, thermal insulation, and so on) | Confined to object of origin | Very little description provided. Initiating equipment was an emergency light and the initiating combustible was plastic. | | 1 | The emergency light appeared to have come in contact with plastic, resulting in an overheating condition. This would likely lead to melting of the plastic. The plastic associated with the emergency light would not be enough to generate a 317 kW fire. | | 1 | | Emergency lighting is permanently located in the plant for when power goes out. It is not purposely placed near work activities. Therefore, the location of an unspecified combustible is not correlated with the location of the ignition source. |
| 20326<br>LPSD | Trash | Personnel error: misuse of heating devices | No damage | Very little description of event. Misuse of heating device and trash are the only attributes mentioned in the fire event. | | 1 | An unspecified heating device is the ignition source, and trash is the combustible material. The heating device does not appear to constitute a sufficient combustible by itself. | 0.5 | 0.5 | | The heating device may have been in use at a work station that had a trash bin nearby. 50% probability assigned. |
| 266<br>AP | Vacuum cleaner | Unknown | Confined to object of origin | Vacuum cleaner caught on fire. Type of extinguisher not specified in report. At 1134, the control room was notified by the WWC of a vacuum cleaner fire on the TB mezzanine. A quality control inspector in the area put out the fire with a fire extinguisher and notified the WWC. An NAO was dispatched and verified that the fire was extinguished. The vacuum was removed from the TB and overhauled with 10 gallons of water. | 1 | | A vacuum cleaner may contain sufficient combustible material to qualify as integral. | | | 1 | |
| 350<br>LPSD | Portable plug in hot plate/linseed oil | Personnel error: misuse of heating devices | No damage | While on rounds, a contractor reported smelling smoke in the vicinity of the station air receivers. Upon investigation, he found a small fire on a hot plate in the vicinity of #2 MFP. The hot plate was being used to heat a linseed oil compound for sealing the #2 MFPT, which overflowed onto the hot plate and caught fire. The control room was informed, and the fire brigade was called. A fire extinguisher was brought to the scene, but the fire burned out before the extinguishing agent was applied. Fire duration was estimated at less than 5 minutes. | | 1 | The hot plate is the ignition source, and the linseed oil is a separate combustible material that may be near the hotplate for a work activity. | 1 | | | The hotplate involves activity that could involve other combustibles being placed nearby. |

**Table B-1 (continued)**
**Characterization of transient fires from the EPRI Updated Fire Events Database**

| Fire ID<br>Power Level (AP = At Power, LPSD = Low-Power-Shutdown) | Ignition Source | Fire Cause | Damage Extent | Additional Information | Question 1<br>Does the ignition source on its own contain sufficient combustible material to be considered a significant transient combustible fire source? If so, the distance between ignition source and combustible material is 0, and the second question, regarding the locations of ignition source and transient combustible material, is not applicable. If not, the second question must be answered. | | | Question 2<br>Is the ignition source part of an activity that is likely to lead to the ignition source and sufficient combustible material for a transient combustible fire being close together (spatially correlated)? If the answer to the first question is yes, this is N/A. | | | |
|---|---|---|---|---|---|---|---|---|---|---|---|
| | | | | | Yes | No | Reasoning | Yes | No | N/A | Reasoning |
| 10492<br>LPSD | Temporary 480 V power | Electrical arcing or sparks (non-HEAF) | Confined to the object of origin (broad/extensive damage) – classified this way due to personnel injury | While reworking temporary 480 V power to a temp electrohydraulic control (EHC) skid on the unit 2 turbine deck, an arc flash occurred. One of the two NSS supplemental electricians involved received minor burns to his right hand and arm. The employee was transported to UVA after being seen by the nurse. The cord and connectors were damaged. | | 1 | The temporary 480 V power to the temporary skid does not contain significant combustibles. | 1 | | | Due to location (near the EHC skid), it is assumed that the temporary power is near to hydraulic oil. Correlation with work is assumed. |
| 10555<br>LPSD | Arcing cable ignited rag | Electrical failure - overheating materials | No damage | During the night-shift, pre-heat cables, which were newly installed in the moisture separator room, were being tested and started arcing, causing a fire. A splitter (Y connector) that had one end not in use had bad insulation and was touching a scaffold. When power was applied, it started arcing and set a rag on fire. The smoke from the burning rag set off the smoke detectors. Two maintenance/modifications fire-watch personnel extinguished the fire. Fire ops and operations responded to the fire. Safety was notified, and there were no injuries to any personnel or plant equipment. Fire ops has requested that all heat wrap pads and cables be inspected before any further weld joints are heated. It was agreed upon that one fire-watch would be placed at each post heat wrap for the time remaining on each wrap that was in process at the time of this incident. Once the wraps were completed, a stand-down was held, and all pads and cables were inspected for damage and repaired as needed. | | 1 | An electrical cable does not contain sufficient combustible material. | 1 | | | Yes, heat and the combination of cables and rags constitute a correlated work scenario. |
| 30277<br>AP | Smoldering oily rags | Unknown | Confined to object of origin | Contractor reported to control room that there was a smoldering trash can fire that they discovered in the TB. They discharged a $CO_2$ extinguisher to combat the problem. FUS and TB 1 NPO dispatched. FUS reports a 55 gallon drum with smoldering oily rags was in the area of concern and there is no fire, Provisions are underway to remove the suspect rags from the drum. | 1 | | The oily rags in a 55 gallon drum constitute a sufficient integral ignition source and combustible. | | | 1 | |

**Table B-1 (continued)**
**Characterization of transient fires from the EPRI Updated Fire Events Database**

| Fire ID<br>Power Level (AP = At Power, LPSD = Low-Power-Shutdown) | | | | | Question 1<br>Does the ignition source on its own contain sufficient combustible material to be considered a significant transient combustible fire source? If so, the distance between ignition source and combustible material is 0, and the second question, regarding the locations of ignition source and transient combustible material, is not applicable. If not, the second question must be answered. | | | Question 2<br>Is the ignition source part of an activity that is likely to lead to the ignition source and sufficient combustible material for a transient combustible fire being close together (spatially correlated)? If the answer to the first question is yes, this is N/A. | | | |
|---|---|---|---|---|---|---|---|---|---|---|---|
| | **Ignition Source** | **Fire Cause** | **Damage Extent** | **Additional Information** | **Yes** | **No** | **Reasoning** | **Yes** | **No** | **N/A** | **Reasoning** |
| 30322<br>LPSD | Temp kidney loop pump heater | Overheated materials (lube oil, pump packing, thermal insulation, and so on) | Confined to the object of origin (localized/single subcomponent) | A temporary kidney loop oil heater caught on fire at the top heater element flange. The kidney loop pump and heater were placed in operation at 10:30 on 10/27/06 in unit track bay. The system was being monitored on the hour by a millwright and fire watch for system operation, temperature, and differential pressure. At 17:20 a millwright moving empty oil drums observed a temperature increase on the heater and a small fire at the top heater element flange. A fire extinguisher was used to put out the fire. | 1 | | The ignition source includes oil that could spill out and ignite. Consider this as an integral source. | | | 1 | |
| 30330<br>LPSD | Temp kidney loop pump heater | Overheated materials (lube oil, pump packing, thermal insulation, and so on) | Confined to the object of origin (localized/single subcomponent) | At approximately 22:20, a millwright reported to me that the kidney loop pump was not running and that the heater temperature was > 300 degrees, smoking, and he had shut off the power to the heater. He also stated that he saw a small flame coming out by the upper insulation. | 1 | | The ignition source includes oil that could spill out and ignite. Consider this as an integral source. | | | 1 | |
| 30350<br>AP | Trash can smoldering | Other | Confined to object of origin | On 7/26/04, a security officer contacted the control room at 06:08 hours, to inform them that an overfilled trash receptacle, located just east of the 4160 volt switchgear room, was producing large quantities of smoke. The fire brigade leader responded to the area to investigate. The brigade Leader was on scene 2 minutes (06:10 hours) after the incident was reported to the Control Room. The brigade leader observed smoke coming from the trash can, but did NOT see any visible flames and did not request the fire brigade to be activated. The security officer and the fire brigade leader extinguished the fire. One 5 lb dry chemical fire extinguisher and approximately 20 gallons of water were used. The smoldering fire was extinguished at 06:15 hours. | 1 | | The ignition source is not noted, but it may be integral to the trash (such as oil soaked rags). | | | 1 | |
| 30361<br>LPSD | Cardboard box against heater strip | Personnel error: misuse of heating devices | Confined to the object of origin (localized/single subcomponent) | A fire occurred in a metal gang box being used as a heater/temperature control for generator phase links. Cardboard boxes were placed in the box against the heater strip causing the boxes to catch on fire. Fire brigade responded to this event. | | 1 | The heater strip would not contain sufficient combustible material. The cardboard boxes are not integral to the heater strip. | 1 | | | The metal box next to the heater strip appears to have been a convenient place to put cardboard boxes. This is counted as an associated activity. |

**Table B-1 (continued)**
**Characterization of transient fires from the EPRI Updated Fire Events Database**

| Fire ID<br>Power Level (AP = At Power, LPSD = Low-Power-Shutdown) | | | | | Question 1<br>Does the ignition source on its own contain sufficient combustible material to be considered a significant transient combustible fire source? If so, the distance between ignition source and combustible material is 0, and the second question, regarding the locations of ignition source and transient combustible material, is not applicable. If not, the second question must be answered. | | | Question 2<br>Is the ignition source part of an activity that is likely to lead to the ignition source and sufficient combustible material for a transient combustible fire being close together (spatially correlated)? If the answer to the first question is yes, this is N/A. | | | |
|---|---|---|---|---|---|---|---|---|---|---|---|
| | **Ignition Source** | **Fire Cause** | **Damage Extent** | **Additional Information** | **Yes** | **No** | **Reasoning** | **Yes** | **No** | **N/A** | **Reasoning** |
| 30380<br>LPSD | Cigarette butt container | Overheated materials (lube oil, pump packing, thermal insulation, and so on) | Confined to the object of origin (localized/single subcomponent) | Cigarette butt container on the south end of the turbine deck caught on fire. The container was completely full, which caused a hole to melt into the top. The hole provided additional oxygen to support continuous combustion. Water was poured onto the container, which extinguished the fire immediately. There was no damage to any other equipment or injuries to plant personnel. | | 1 | A cigarette container itself is not a sufficient combustible. | | 1 | | Smoking would not be associated with collection of extra combustibles. |
| 30408<br>AP | Temporary valve label | Unknown | No damage | Found temporary valve label burning on valve bonnet after getting a report of something burning in area around waterbox outlet manway. | | 1 | The valve label is integral to the valve, but not a sufficient combustible. | | 1 | | No sufficient transient combustible is mentioned or implied. No activity is mentioned or implied. Therefore, there is no apparent correlation between the ignition source and a sufficient transient combustible. |
| 30421<br>LPSD | Welding rod ovens with paper instructions smoked | Other | Confined to object of origin | Three welding rod ovens were plugged in (energized) with operating instructions inside resulting in a contained burning of the paper. Personnel noticed the smoke and unplugged the ovens. | | 1 | The oven itself does not contain sufficient combustible material to become a significant fire. The paper instructions inside are not sufficient combustible material. | | 1 | | Since neither the oven nor the paper instructions constitute integral combustibles, and there is no mention of nearby combustibles, this has been classified as uncorrelated. |
| 30508<br>LPSD | Electrical fire in weld machine | Electrical failure - overheating materials | Confined to object of origin | When the crew returned from break, they re-energized the weld machine, and it immediately started smoking. On March 26 at 04:54 hours, a fire was reported in a welding machine in the TB feedwater heater corridor area by the work group using the machine. The MCR entered the fire procedure and made a PA announcement to evacuate the area and dispatched the fire brigade. The fire brigade arrived and reported a small electrical fire in a weld machine. The machine was de-energized and a $CO_2$ hand portable fire extinguisher was used to extinguish the residual flame. | | 1 | The welding machine would not contain sufficient combustible material. | | 1 | | Based on welding practices (minimizing combustibles) and the event report, this event has been classified as uncorrelated. |
| 30512<br>LPSD | Power cord in weld machine | Electrical failure - overheating materials | Confined to object of origin | At approximately 22:00, open flame was observed on the power cord leading to a weld machine. The weld machine was turned off, and the flame went out. Investigation revealed that one of the 100 V wires shorted out through the jacket and grounded to the wire mesh around the 240 V feed. Additionally, there was installed fire suppression, but it did not actuate as the fire was very small and not of sufficient intensity or duration to initiate wet pipe suppression. | | 1 | The power cord to welding machine would not contain sufficient combustible material. | | 1 | | Based on welding practices (minimizing combustibles) and the event report, this event has been classified as uncorrelated. |

**Table B-1 (continued)**
**Characterization of transient fires from the EPRI Updated Fire Events Database**

| Fire ID<br>Power Level (AP = At Power, LPSD = Low-Power-Shutdown) | Ignition Source | Fire Cause | Damage Extent | Additional Information | Question 1<br>Does the ignition source on its own contain sufficient combustible material to be considered a significant transient combustible fire source? If so, the distance between ignition source and combustible material is 0, and the second question, regarding the locations of ignition source and transient combustible material, is not applicable. If not, the second question must be answered. | | | Question 2<br>Is the ignition source part of an activity that is likely to lead to the ignition source and sufficient combustible material for a transient combustible fire being close together (spatially correlated)? If the answer to the first question is yes, this is N/A. | | | |
|---|---|---|---|---|---|---|---|---|---|---|---|
| | | | | | Yes | No | Reasoning | Yes | No | N/A | Reasoning |
| 30752<br>AP | Fire in oil bucket | Overheated materials (lube oil, pump packing, thermal insulation, and so on) | Confined to object of origin | Active fire in an oil bucket located at the TB 3rd floor. Immediate entry into fire brigade response procedure was initiated. A fire brigade qualified NEO in the control room at the time of the emergency line call was dispatched to perform a first assessment. 07:46 the fire was reported as "OUT" and announced over PA system and radio system. Command reports two $CO_2$ fire extinguishers were used to extinguish localized active fire. | 1 | | No ignition source is mentioned. Therefore, the source is assumed to be integral with the combustible (such as an oil-soaked rag). | | | 1 | |
| 50833<br>LPSD | Plastic light bulb enclosure | Personnel error: misuse of material ignited | Confined to the object of origin (localized/single subcomponent) | On 09/23/08 at approximately 04:42, smoke and visible flames were observed by two NDE inspectors who were entering the moisture separator to perform an inspection of downcomer piping under the false bottom. The source of the fire was identified at two incandescent light bulb enclosures (made of plastic) that came in contact with each other. The moisture separator safety watch, from a safe distance, put the fire out using a purple K dry chemical fire extinguisher. | | 1 | The plastic light bulb enclosures would not contain sufficient combustible material. | 1 | | | The presence of NDE inspectors, safety watch, and temporary lighting indicate the presence of maintenance or work activities. |
| | | | | **Sum=** | **10** | **44** | | **25.5** | **18.5** | **10** | |
| | | | | | $X_{int}$ | | | $X_{corr}$ | $X_{uncorr}$ | | |
| | | | | | 0.19 | | | 0.47 | 0.34 | | |

**Table B-2**
**Calculating results for characterization of transient fires**

| Result | Power Level | | |
|---|---|---|---|
| | **All Levels** | **At Power** | **Low Power** |
| Number of transient fires considered Integral (Question 1 answer = yes) | 10 | 5.5 | 4.5 |
| Number of transient fires NOT considered Integral (Question 1 answer = no) | 44 | 17.5 | 26.5 |
| Integral transient ignition sources, $x_{int}$ | 10/(10+44) = 0.19 | 5.5/(5.5+17.5) = 0.24 | 4.5/(4.5+26.5) = 0.15 |
| Number of transient fires considered correlated (Question 2 answer = yes) | 25.5 | 11.5 | 14 |
| Correlated ignition sources, $x_{corr}$ | 25.5/(10+44) = 0.47 | 11.5/(5.5+17.5) = 0.50 | 14/(4.5+26.5) = 0.45 |
| Number of transient fires considered uncorrelated (Question 2 answer = no) | 18.5 | 6 | 12.5 |
| Uncorrelated ignition sources, $x_{uncorr}$ | 18.5/(10+44) = 0.34 | 6/(5.5+17.5) = 0.26 | 12.5/(4.5+26.5) = 0.40 |

**Table B-3**
**Correlated and uncorrelated ignition sources for transient fires—at full power**

| At Power Ignition Source | Number of Correlated Transient Fires | Number of Uncorrelated Transient Fires |
|---|---|---|
| Short in electrical cord | 0.5 | 0.5 |
| Overheating electrical wiring | 1 | |
| Temporary electrical wiring | 1 | |
| Floodlight burst (hot fragments ignited hose) | 1 | |
| Altered extension cord | 1 | |
| Temporary lighting fixture | 1 | |
| 480 V extension cord | 1 | |
| Temporary air conditioner | 1 | |
| Paint thinner | 1 | |
| Cardboard (chart box paper, spill kit box) | 1 | |
| Sweatshirt draped over lift | 1 | |
| Steam leak on electrical extension cord caused wetted lagging and insulation to ignite | 1 | |

**Table B-3 (continued)**
**Correlated and uncorrelated ignition sources for transient fires—at full power**

| At Power Ignition Source | Number of Correlated Transient Fires | Number of Uncorrelated Transient Fires |
|---|---|---|
| Oil leaked from reservoir (0.5 considered integral) | | 0.5 |
| 480 V power outlet | | 1 |
| Bird's nest in pump exhaust | | 1 |
| Cigarette box | | 1 |
| Plastic emergency lighting | | 1 |
| Temporary valve label | | 1 |
| **Totals** | **11.5** | **6** |

**Table B-4**
**Correlated and uncorrelated ignition sources for transient fires—low power**

| Low Power Ignition Source | Number of Correlated Transient Fires | Number of Uncorrelated Transient Fires |
|---|---|---|
| Faulty plug – extension cord | 0.5 | 0.5 |
| Forklift battery | 0.5 | 0.5 |
| Excess wire ignited by oven | 0.5 | 0.5 |
| Trash | 0.5 | 0.5 |
| Water cooler cord - burnt insulation | 1 | |
| Light string heated up wood reel and ignited | 1 | |
| Overheating electrical connections | 1 | |
| Clothing | 1 | |
| Electrical fault in temporary light | 1 | |
| Short in electrical cord | 1 | |
| Smoldering oily rags on top of light | 1 | |
| Portable plug in hot plate/linseed oil | 1 | |
| Temporary 480 V power | 1 | |
| Arcing cable ignited rag | 1 | |
| Cardboard box against heater strip | 1 | |

**Table B-4 (continued)**
**Correlated and uncorrelated ignition sources for transient fires—low power**

| Low Power Ignition Source | Number of Correlated Transient Fires | Number of Uncorrelated Transient Fires |
|---|---|---|
| Plastic light bulb enclosure | 1 | |
| Temporary air compressor | | 1 |
| Portable space heater | | 1 |
| Floor scrubber battery (0.5 considered integral) | | 0.5 |
| Heater | | 1 |
| Wiring in main condenser | | 1 |
| Lamp | | 1 |
| Strip heater | | 1 |
| Cigarette butt container | | 1 |
| Welding rod ovens with paper instructions smoked | | 1 |
| Electrical fire in weld machine | | 1 |
| Power cord in weld machine | | 1 |
| **Totals** | **14** | **12.5** |

## B.2 MATLAB Files

The following code calculates Wp(r) for r=0.05 to 2 m for qcrit=6 to q=20:

**File: Trans_q_r_set.m**

```
qcrit=4 %qcrit in units of kW;
alpha=1.8;%alpha in gamma distribution for transient fires
beta=57.4;%beta in gamma distribution for transient firesr=0.5
f = @(Q) Q.^(alpha-1).*exp(-Q./beta)./(beta.^alpha.*gamma(alpha))
%Test1 = integral(f,0,inf)
rad=0.4
fileID=fopen('output-q_vs_r_vs_Wp_Xr4.txt', 'w');
for i=1:8
qcrit=qcrit+2
fprintf(fileID,'%6s %8.1f\n','qcrit=',qcrit);
fprintf(fileID,'%6s %10s\n','r(m)','Wp');
```

```
r=0
for j=1:40
r=r+0.05
ff = @(q) (4.*pi.*r.^2./rad).*(4.*q.*pi.*r.^2/rad).^(alpha-1).*exp(-
4.*q.*pi.*r.^2./rad./beta)./(beta.^alpha.*gamma(alpha))
Wp=1-integral(ff,0,qcrit)
A=[r; Wp];
fprintf(fileID,'%8.3f %9.6f\n',A);
end
end
fclose(fileID)
```

The following code calculates Wp(L) for L=0.1 to 2 m with 100,000 Monte Carlo steps:

**File: TransHRR_Random_Xr4_SD_part1.m**

```
%-- 3/19/2015 --%
%qcrit in units of kW; qcrit varies between qlow and qhigh
qlow=6;
qhigh=20;
alpha=1.8;%alpha in gamma distribution for transient fires
beta=57.4;%beta in gamma distribution for transient fires
f = @(Q) Q.^(alpha-1).*exp(-Q./beta)./(beta.^alpha.*gamma(alpha));
%Test1 = integral(f,0,inf)
rad=0.4;
size=100000;
fileID=fopen('output-Xr4_SD_part1.txt', 'w');
fprintf(fileID,'%6s %8.1f\r\n','qlow=',qlow);
fprintf(fileID,'%6s %8.1f\r\n','qhigh=',qhigh);
fprintf(fileID,'%23s %8.0f\r\n','Number of Realizations=',size);
fprintf(fileID,'%6s %10s %10s\r\n','L(m)','Wpave','StdDev');
L=0;
for j=1:20
Wptot=0;
L=L+0.1
```

```
WpSq=0;
for i=1:size;
X1=rand*L;
Y1=rand*L;
X2=rand*L;
Y2=rand*L;
r=sqrt((X1-X2)^2+(Y1-Y2)^2);
qcrit=(qhigh-qlow)*rand+qlow;
ff = @(q) (4.*pi.*r.^2./rad).*(4.*q.*pi.*r.^2/rad).^(alpha-1).*exp(-
4.*q.*pi.*r.^2./rad./beta)./(beta.^alpha.*gamma(alpha));
Wp=1-integral(ff,0,qcrit);
Wptot=Wptot+Wp;
WpSq=WpSq+Wp^2;
end
Wpave=Wptot/size;
%Equation 5A and Equation 40 to calculate the standard deviation of the
%average--Introduction to the Theory of Error by Yardley Beers
SDave=sqrt((WpSq-size*Wpave^2)/(size-1))/sqrt(size);
A=[L; Wpave;SDave];
fprintf(fileID,'%8.3f %9.6f %9.6f\r\n',A);
end
fclose(fileID)
```

The following code calculates Wp(L) for L=2.1 to 8 m with 100,000 Monte Carlo steps

**File: TransHRR_Random_Xr4_SD_part2.m**

```
%-- 3/19/2015 --%
%qcrit in units of kW; qcrit varies between qlow and qhigh
qlow=6;
qhigh=20;
alpha=1.8;%alpha in gamma distribution for transient fires
beta=57.4;%beta in gamma distribution for transient fires
f = @(Q) Q.^(alpha-1).*exp(-Q./beta)./(beta.^alpha.*gamma(alpha));
%Test1 = integral(f,0,inf)
```

```
rad=0.4;
size=100000;
fileID=fopen('output-Xr4_SD_part2.txt', 'w');
fprintf(fileID,'%6s %8.1f\r\n','qlow=',qlow);
fprintf(fileID,'%6s %8.1f\r\n','qhigh=',qhigh);
fprintf(fileID,'%23s %8.0f\r\n','Number of Realizations=',size);
fprintf(fileID,'%6s %10s %10s\r\n','L(m)','Wpave','StdDev');
L=2.0;
for j=1:60
Wptot=0;
L=L+0.1
WpSq=0;
for i=1:size;
X1=rand*L;
Y1=rand*L;
X2=rand*L;
Y2=rand*L;
r=sqrt((X1-X2)^2+(Y1-Y2)^2);
qcrit=(qhigh-qlow)*rand+qlow;
ff = @(q) (4.*pi.*r.^2./rad).*(4.*q.*pi.*r.^2/rad).^(alpha-1).*exp(-
4.*q.*pi.*r.^2./rad./beta)./(beta.^alpha.*gamma(alpha));
Wp=1-integral(ff,0,qcrit);
Wptot=Wptot+Wp;
WpSq=WpSq+Wp^2;
end
Wpave=Wptot/size;
%Equation 5A and Equation 40 to calculate the standard deviation of the
%average--Introduction to the Theory of Error by Yardley Beers
SDave=sqrt((WpSq-size*Wpave^2)/(size-1))/sqrt(size);
A=[L; Wpave;SDave];
fprintf(fileID,'%8.3f %9.6f %9.6f\r\n',A);
end
fclose(fileID)
```

# C
# LIQUID SPILL FIRE TEST NAMING CONVENTION AND SPILL HEAT RELEASE RATE PROFILES

## C.1 NIJ Test Naming Convention

In order to efficiently present and discuss the results from the large number of tests conducted in this research, a naming convention was developed to fully describe the pertinent variables considered in each test. An alphanumeric code was developed to identify the following parameters [1]:

- The test type and identification number
- The confinement (confined or unconfined)
- The substrate
- The liquid type
- The liquid depth (confined scenarios) or quantity (unconfined scenarios)
- The liquid area (confined scenarios) or spread time (unconfined scenarios)

The alphanumeric key is provided in Figure C-1. This alphanumeric code is used to identify all tests within the NIJ report [1].

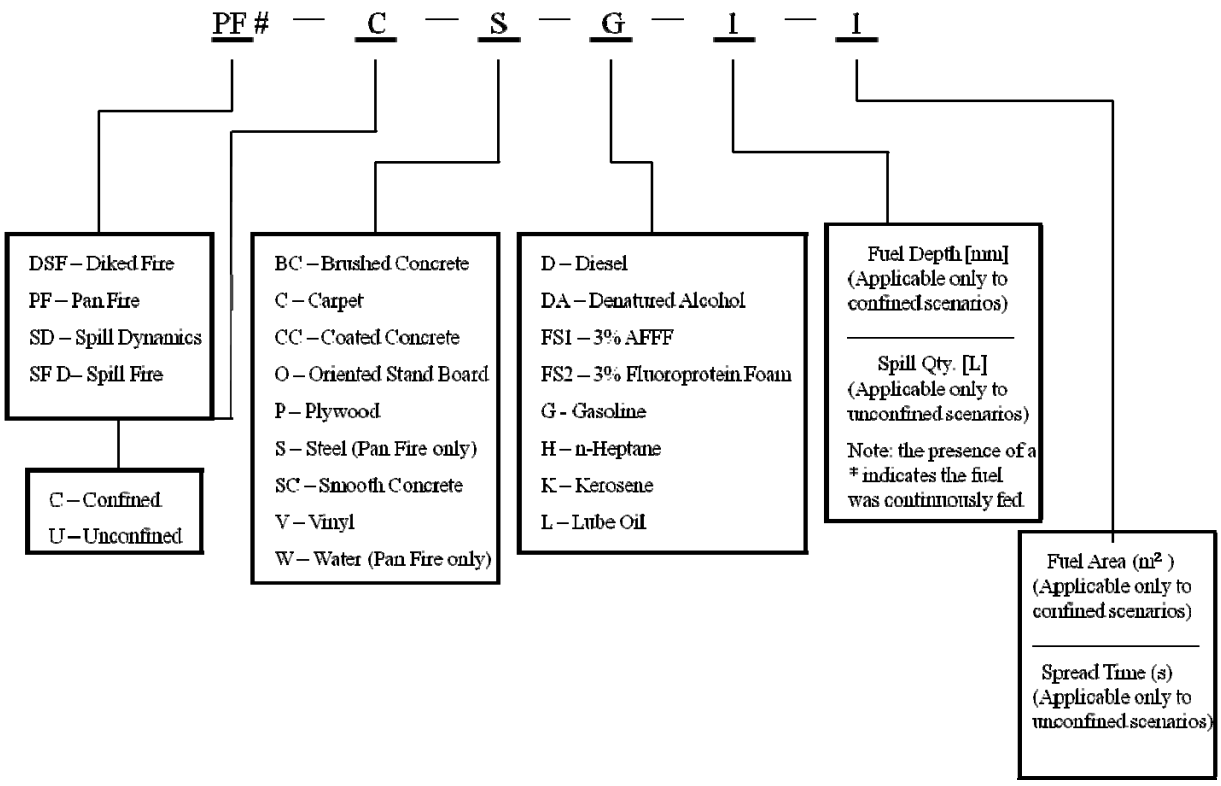


**Figure C-1**
**Key to alphanumeric test identification code**

As an example, the legend of Figure 5-10d identifies one of the tests shown as PF65-C-S-K-1-0.37. Based on Figure C-1, this is a pan fire test with a sequential number of 65 that is confined and had a steel substrate. The fuel is kerosene, the spill depth is 1 mm, and the pan area is 0.37 m² (that is, the 0.3 m diameter pan).

## C.2 Spill Fire Heat Release Rates

The calculation of the HRR profile using the integral model presented in Section 6.2.2.2 is not a simple calculation that can be implemented in a spreadsheet as needed. Rather, the model is best implemented using a solution algorithm, either within a spreadsheet as a macro or as a stand-alone program. However, the solution for a given set of parameters is identical. In this regard, a solution to the integral model, defined as a set of time and HRR values, for different volumes of flammable or combustible liquids commonly found in commercial NPPs provides a useful reference and allows the model to be applied directly. The purpose of this appendix is to provide this solution set for gasoline, kerosene, and lubricating oil. These fuels represent a significant fraction of the liquid fuels found in commercial NPPs for which fire scenarios are typically developed. The following volumes are considered in this appendix:

- 0.1 L (0.0265 gal)
- 0.25 L (0.066 gal)
- 0.5 L (0.13 gal)
- 1.0 L (0.265 gal)

- 2.0 L (0.53 gal)
- 5.0 L (1.32 gal)
- 10.0 L (2.65 gal)
- 15.0 L (3.97 gal)
- 20.0 L (5.29 gal)
- 25.0 L (6.61 gal)
- 37.8 L (10.0 gal)

The HRR profiles for spill fires involving these liquids and liquid volumes are provided using the integral model described in Section 6.2.2.2. The model parameters provided in Tables 6-1 and 5-5 are used to develop the HRR profiles. Three HRR profiles are provided for each scenario. The first is the expected HRR profile as determined using the recommended or average value for the model parameters. The second is an upper-bound HRR, determined using the approach described in Section 6.1.3.3. In this case, the model parameters are biased to yield a maximum heat release. The third is a minimum-bound HRR, determined using the approach described in Section 6.1.3.3. In this case, the model parameters are biased to yield a minimum HRR.

### *C.2.1 Gasoline Spill Fires*

The baseline model parameters for the gasoline spill fires are obtained from Tables 6-1 and 5-5 and are as follows:

- Density: 740 kg/m³
- Heat of combustion: 43,700 kJ/kg
- Mass burning rate: 0.055 kg/m²-s, with a range of 0.053–0.057 kg/m²-s
- Empirical diameter constant: 2.1 $m^{-1}$, with a range of 1.8–2.4 $m^{-1}$

The fuel depth for an unconfined gasoline spill fire is 0.71 mm for gasoline according to Table 5-4. This is nearly equal to the average value of 0.72 mm for all fuels. The maximum and minimum spill depth range for gasoline is 0.48–1.1 mm according to Table 5-4 and is used in place of the generic spill depth range of all fuels. The depth coefficient for the gasoline spill fires is computed using the minimum, average, and maximum bound correlations provided in Section 6.1.3.3.2.

**Table C-1**
**Gasoline spill fire depth coefficients**

| Depth Coefficient Function | Spill Depth Coefficient for: | | |
|---|---|---|---|
| | Minimum Spill Depth (0.48 mm) | | Minimum Spill Depth (0.48 mm) |
| Minimum | **0.168**[†] | Minimum | **0.168**[†] |
| Average | 0.274 | Average | 0.274 |
| Maximum | 0.571 | Maximum | 0.571 |

[†] Bold values indicate minimum-minimum, average-average, and maximum-maximum values that are used in the solutions provided in this appendix.

The HRR development time is 10 seconds, and the spread rate over the liquid surface is 10 cm/s, the same values used to validate the model with gasoline fires in Sections 6.1.3.1 and 6.1.3.2. Table C-2 summarizes the minimum, average, and maximum spill diameters and HRRPUA for each spill volume considered. The HRRs per unit area are determined from the product of the maximum mass burning rate, the depth coefficient, and the empirical diameter coefficient. Note that the maximum diameter fire scenario corresponds to the minimum HRRPUA because the depth coefficient variation is greater than the empirical diameter coefficient variation.

**Table C-2**
**Gasoline spill fire diameter and heat release rates per unit area**

| Spill Volume (L) | Diameter (m) | | | Heat Release Rate per Unit Area (kW/m²) | | |
|---|---|---|---|---|---|---|
| | Maximum | Average | Minimum | Minimum | Average | Maximum |
| 0.1 | 0.52 | 0.42 | 0.34 | 236 | 536 | 1,229 |
| 0.25 | 0.81 | 0.66 | 0.54 | 300 | 688 | 1,596 |
| 0.50 | 1.15 | 0.94 | 0.76 | 341 | 787 | 1,847 |
| 1.0 | 1.63 | 1.33 | 1.08 | 369 | 858 | 2,035 |
| 2.0 | 2.30 | 1.88 | 1.52 | 384 | 896 | 2,145 |
| 5.0 | 3.64 | 2.97 | 2.41 | 389 | 912 | 2,195 |
| 10.0 | 5.15 | 4.21 | 3.40 | 390 | 914 | 2,201 |
| 15.0 | 6.31 | 5.15 | 4.17 | 390 | 914 | 2,202 |
| 20.0 | 7.28 | 5.95 | 4.81 | 390 | 914 | 2,202 |
| 25.0 | 8.14 | 6.65 | 5.38 | 390 | 914 | 2,202 |
| 37.8 | 10.0 | 8.18 | 6.61 | 390 | 914 | 2,202 |

The results for gasoline spill fires with volumes ranging from 0.1 to 37.8 L are summarized in Figures C-2 through C-12. Tabular data (Tables C-7 through C-17) at approximately 5 second increments are provided in Section C.2.5 for each HRR profile shown in Figures C-2 through C-12.

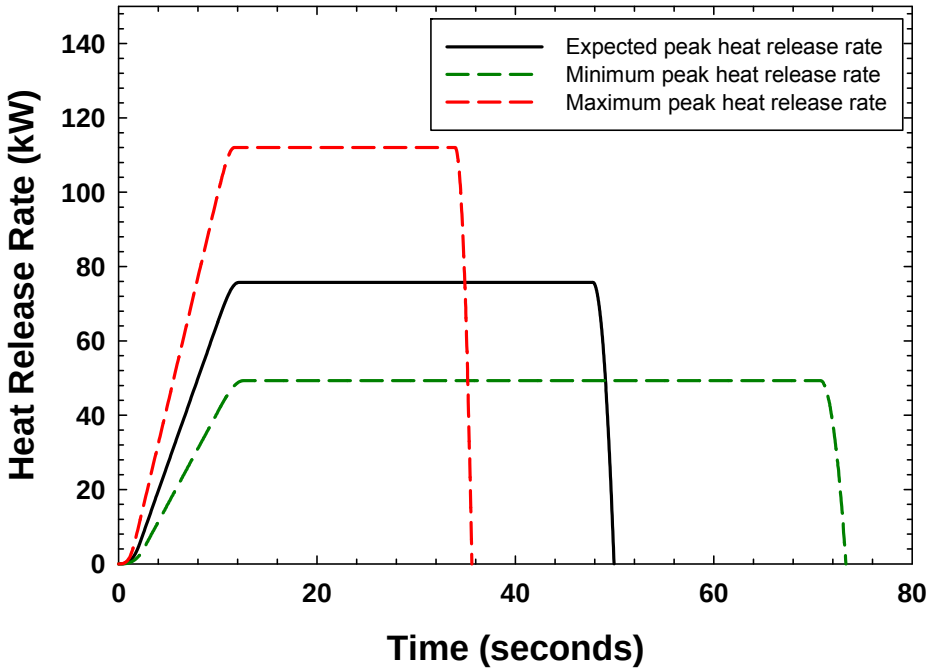


**Figure C-2**
**HRR profiles for a 0.1 L gasoline spill fire scenario**

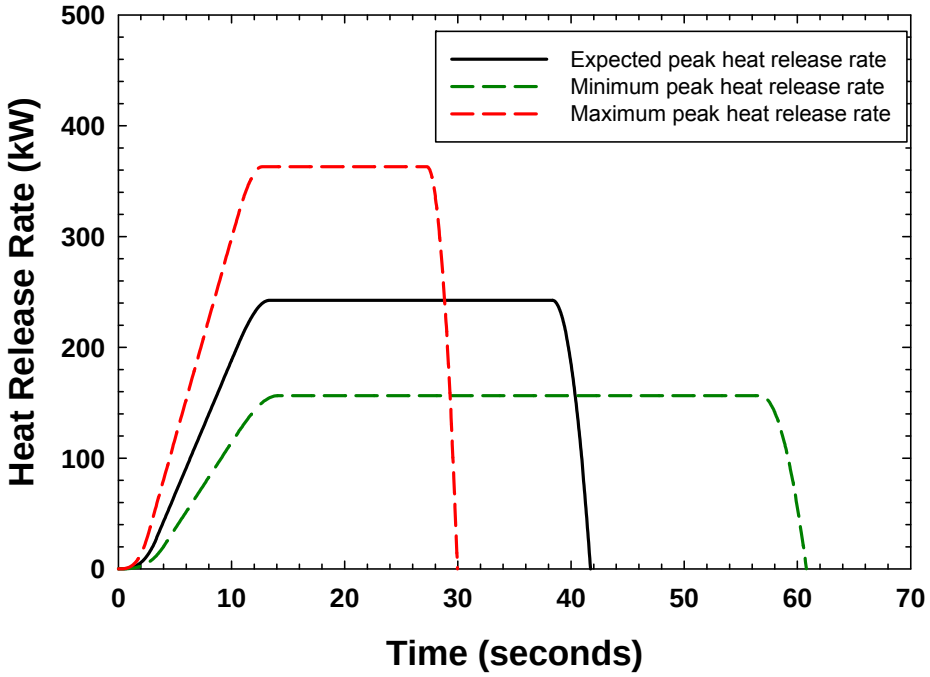


**Figure C-3**
**HRR profiles for a 0.25 L gasoline spill fire scenario**

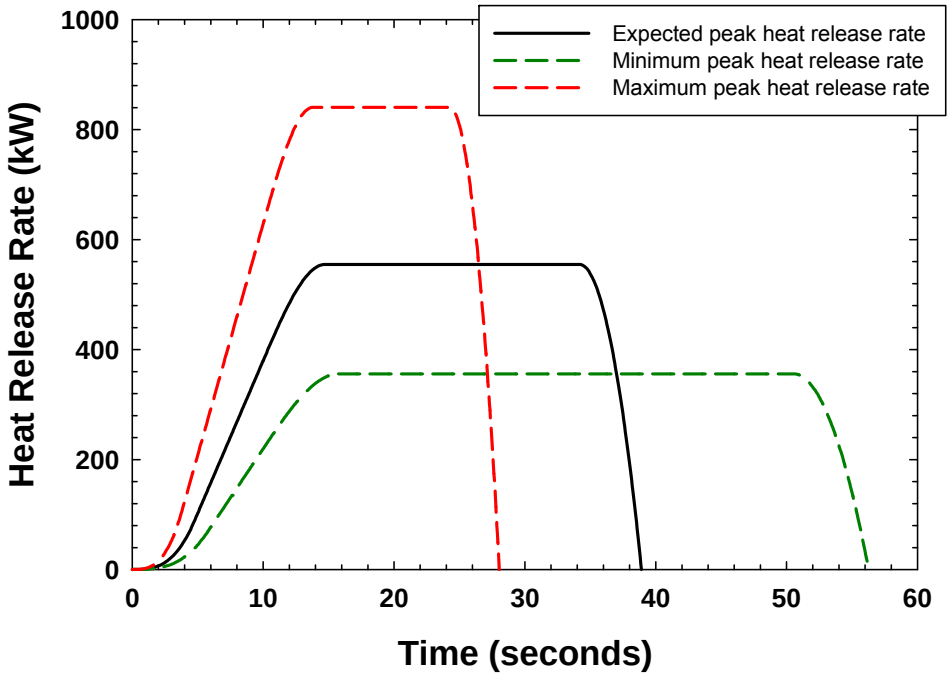


**Figure C-4**
**HRR profiles for a 0.5 L gasoline spill fire scenario**

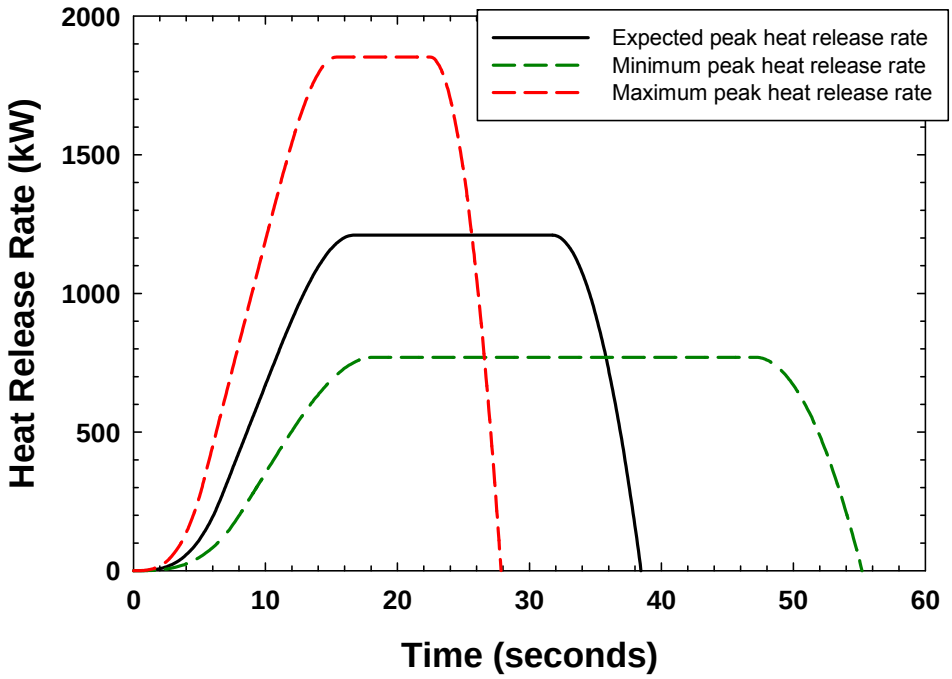


**Figure C-5**
**HRR profiles for a 1.0 L gasoline spill fire scenario**

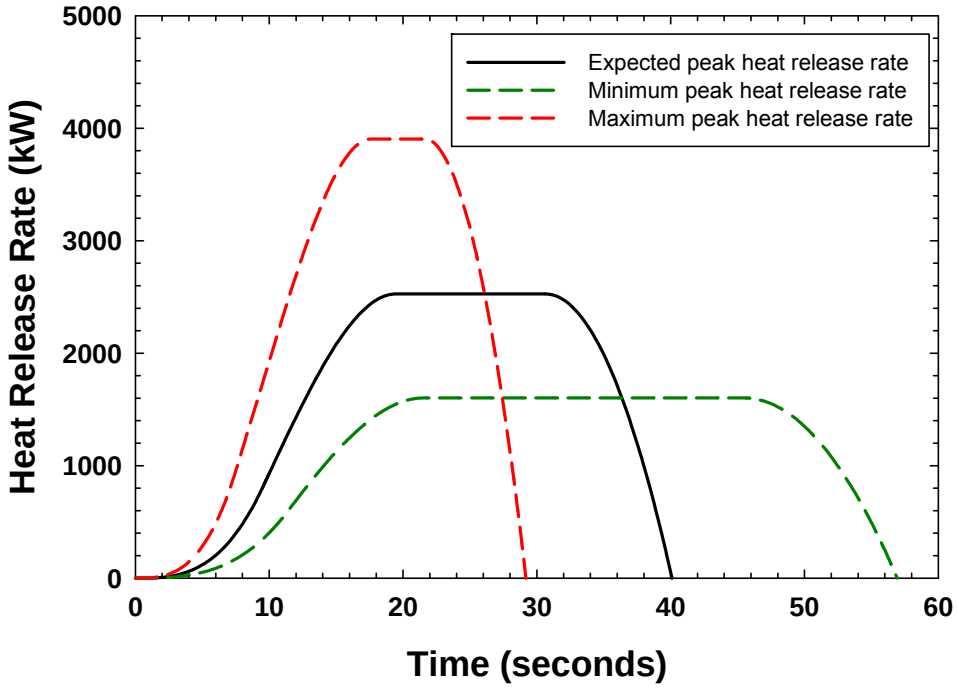


**Figure C-6**
**HRR profiles for a 2.0 L gasoline spill fire scenario**

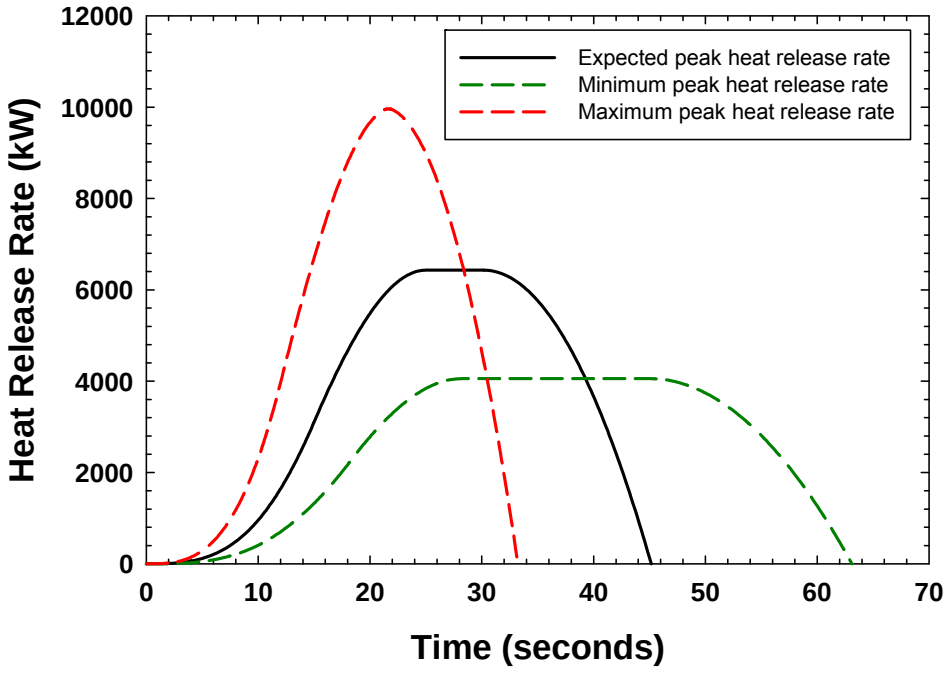


**Figure C-7**
**HRR profiles for a 5.0 L gasoline spill fire scenario**

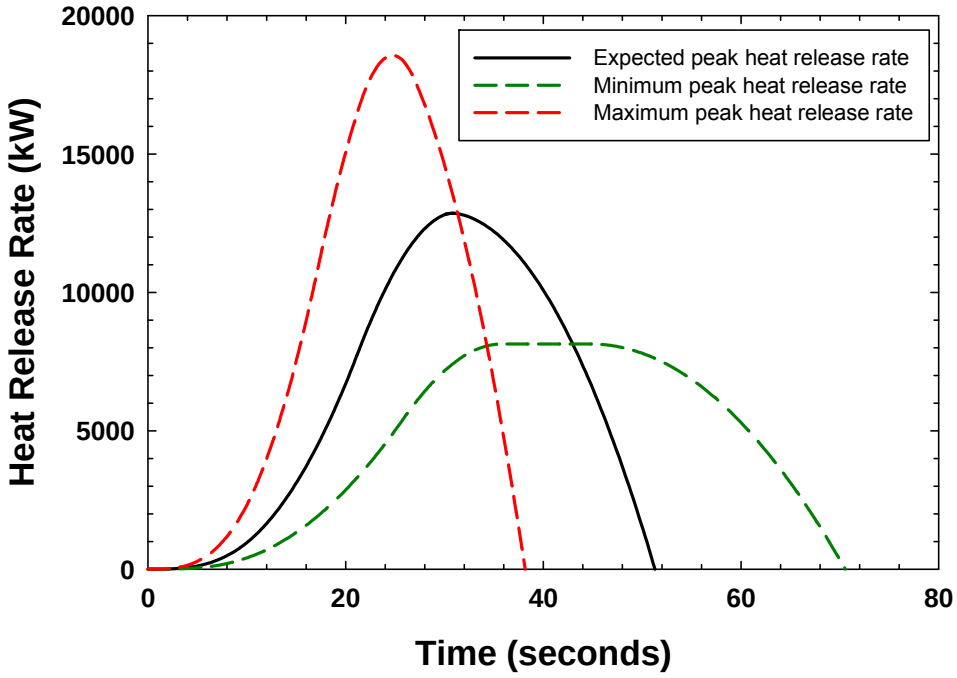


**Figure C-8**
**HRR profiles for a 10.0 L gasoline spill fire scenario**

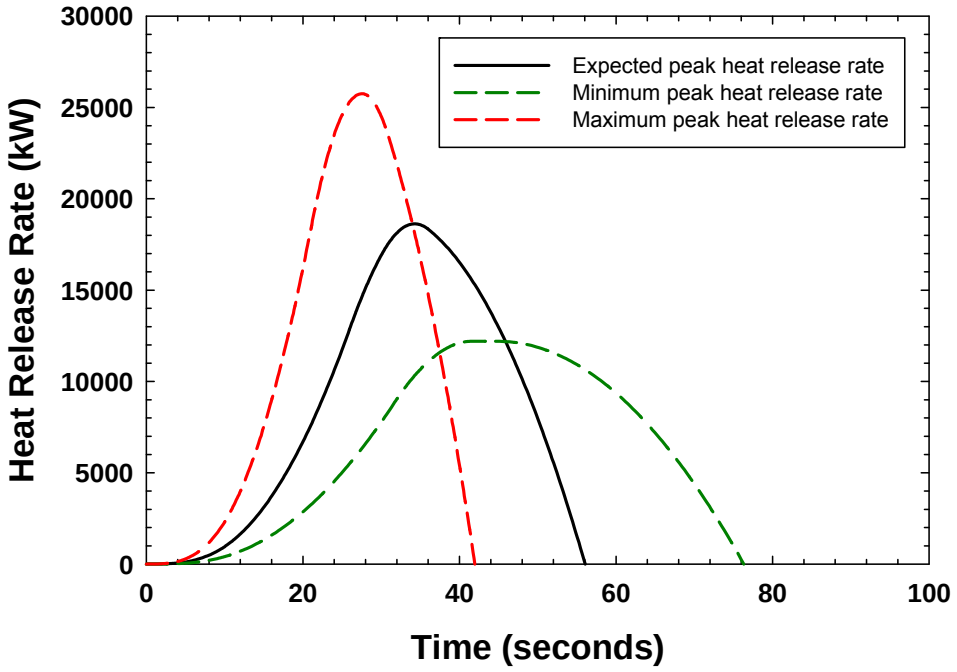


**Figure C-9**
**HRR profiles for a 15.0 L gasoline spill fire scenario**

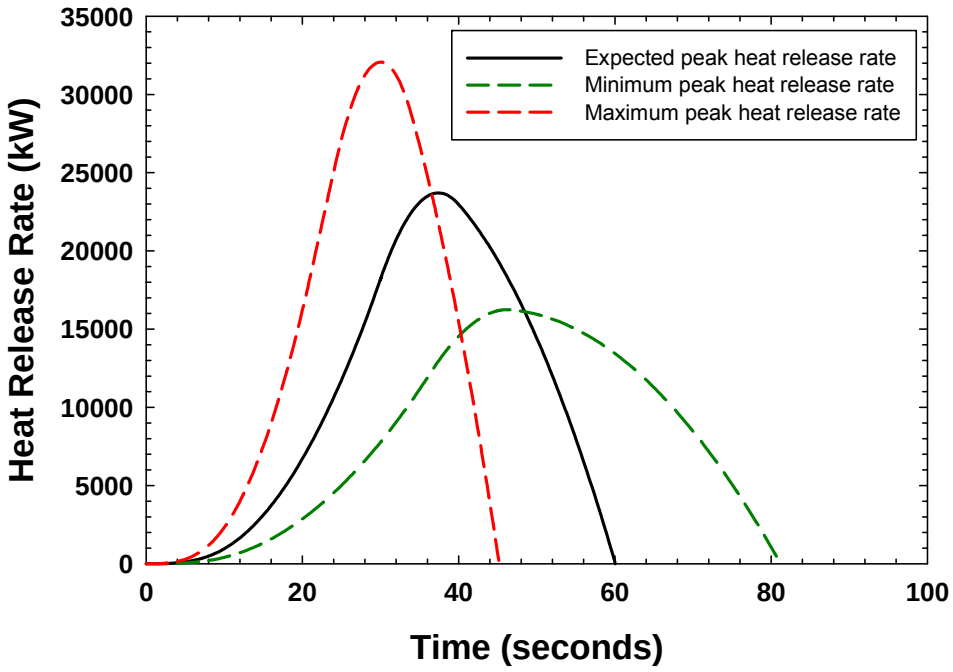


**Figure C-10**
**HRR profiles for a 20.0 L gasoline spill fire scenario**

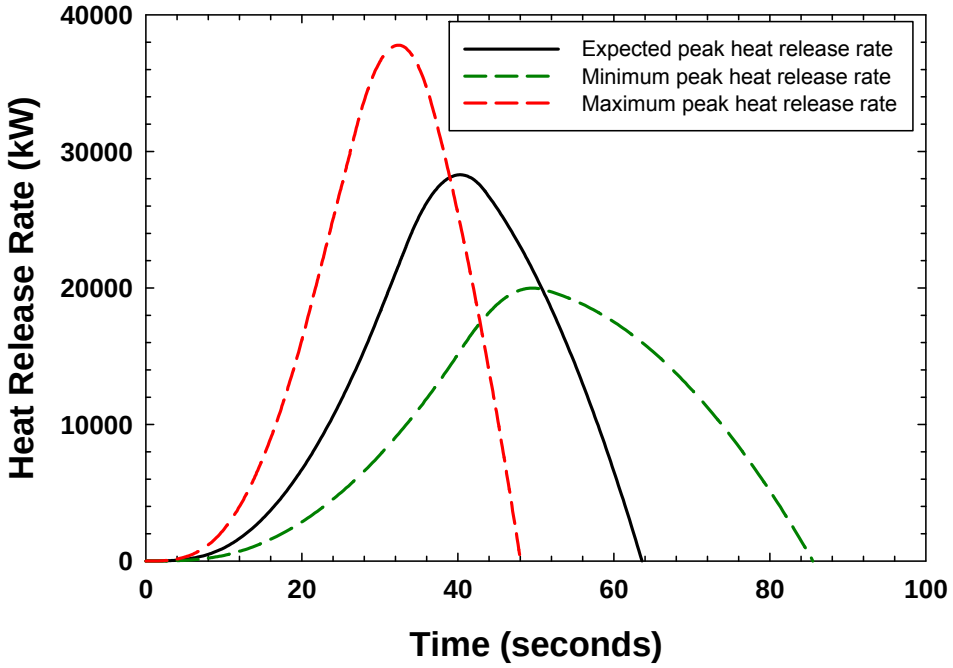


**Figure C-11**
**HRR profiles for a 25.0 L gasoline spill fire scenario**

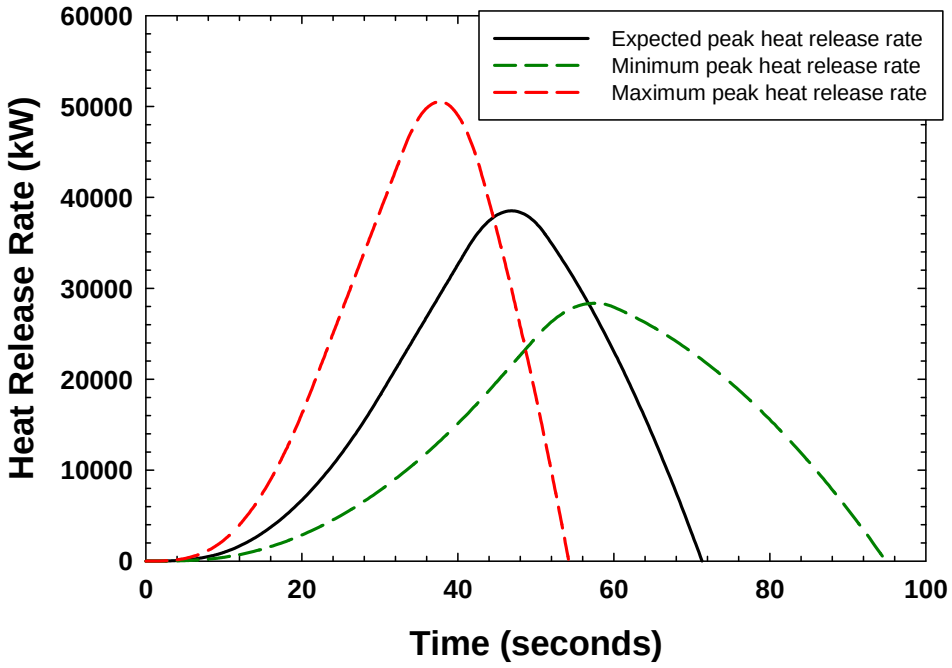


**Figure C-12**
**HRR profiles for a 37.8 L gasoline spill fire scenario**

### *C.2.2 Kerosene Spill Fires*

The baseline model parameters for the kerosene spill fires are obtained from Tables 6-1 and 5-5 and are as follows:

- Density: 820 kg/m³
- Heat of combustion: 32,200 kJ/kg
- Mass burning rate: 0.039 kg/m²-s, with a range of 0.036–0.042 kg/m²-s
- Empirical diameter constant: 3.5 $m^{-1}$, with a range of 2.7–4.3 $m^{-1}$

The fuel depth for an unconfined kerosene spill fire is 1.01 mm according to Table 5-4. The maximum and minimum spill depth range for kerosene is 0.91–1.2 mm according to Table 5-4 and is used in place of the generic spill depth range of all fuels. The depth coefficient for the kerosene spill fires is computed using the minimum, average, and maximum bound correlations provided in Section 6.1.3.3.2.

**Table C-3**
**Kerosene spill fire depth coefficients**

| Depth Coefficient Function | Spill Depth Coefficient for: | | |
|---|---|---|---|
| | Minimum Spill Depth (0.91 mm) | | Minimum Spill Depth (0.91 mm) |
| Minimum | **0.176**[†] | Minimum | **0.176**[†] |
| Average | 0.373 | Average | 0.373 |
| Maximum | 0.817 | Maximum | 0.817 |

[†]Bold values indicate minimum-minimum, average-average, and maximum-maximum values that are used in the solutions provided in this appendix.

The HRR development time is 15 seconds, and the spread rate over the liquid surface is 5 cm/s, the same values used to validate the model with kerosene fires in Section 6.1.3.3.5. Table C-4 summarizes the minimum, average, and maximum spill diameters and HRRPUA for each spill volume considered. The HRRs per unit area are determined from the product of the maximum mass burning rate, the depth coefficient, and the empirical diameter coefficient. Note that the maximum diameter fire scenario corresponds to the minimum HRRPUA because the depth coefficient variation is greater than the empirical diameter coefficient variation.

**Table C-4**
**Kerosene spill fire diameter and heat release rates per unit area**

| Spill Volume (L) | Diameter (m) | | | Heat Release Rate per Unit Area (kW/m²) | | |
|---|---|---|---|---|---|---|
| | Maximum | Average | Minimum | Minimum | Average | Maximum |
| 0.1 | 0.37 | 0.36 | 0.33 | 130 | 360 | 933 |
| 0.25 | 0.59 | 0.56 | 0.52 | 163 | 436 | 1,104 |
| 0.50 | 0.84 | 0.79 | 0.73 | 183 | 475 | 1,185 |
| 1.0 | 1.18 | 1.12 | 1.03 | 196 | 497 | 1,224 |
| 2.0 | 1.67 | 1.59 | 1.46 | 202 | 505 | 1,236 |
| 5.0 | 2.64 | 2.51 | 2.3 | 204 | 507 | 1,239 |
| 10.0 | 3.74 | 3.55 | 3.26 | 204 | 507 | 1,239 |
| 15.0 | 4.58 | 4.35 | 3.99 | 204 | 507 | 1,239 |
| 20.0 | 5.29 | 5.02 | 4.61 | 204 | 507 | 1,239 |
| 25.0 | 5.91 | 5.61 | 5.15 | 204 | 507 | 1,239 |
| 37.8 | 7.27 | 6.9 | 6.33 | 204 | 507 | 1,239 |

The results for kerosene spill fires with volumes ranging from 0.1 to 37.8 L are summarized in Figures C-13 through C-23. Tabular data (Tables C-18 through C-28) at approximately 10 second increments are provided in Section C.2.5 for each HRR profile shown in Figures C-13 through C-23.

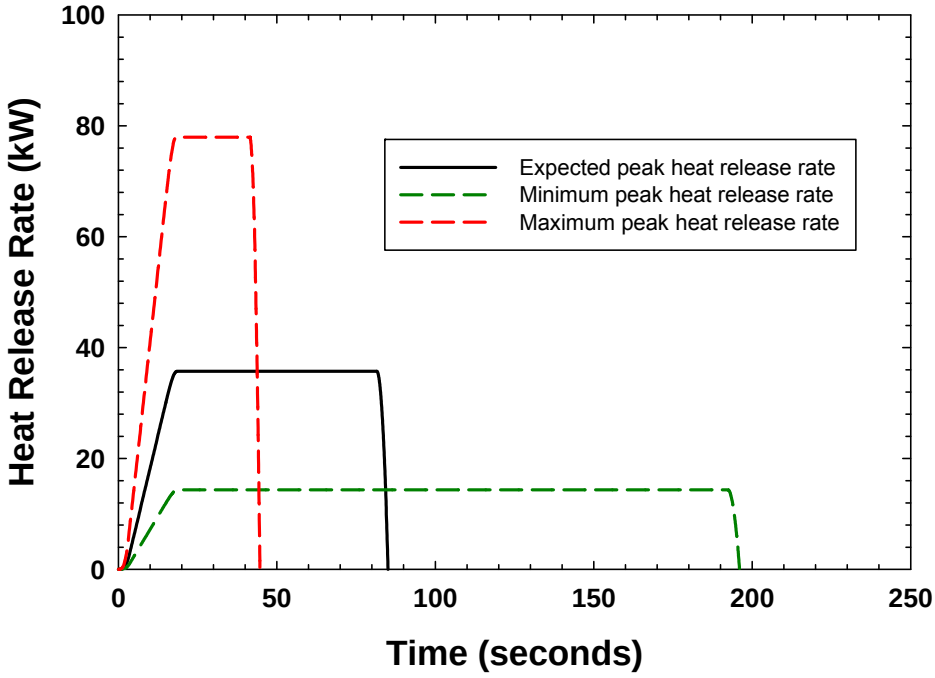


**Figure C-13**
**HRR profiles for a 0.1 L kerosene spill fire scenario**

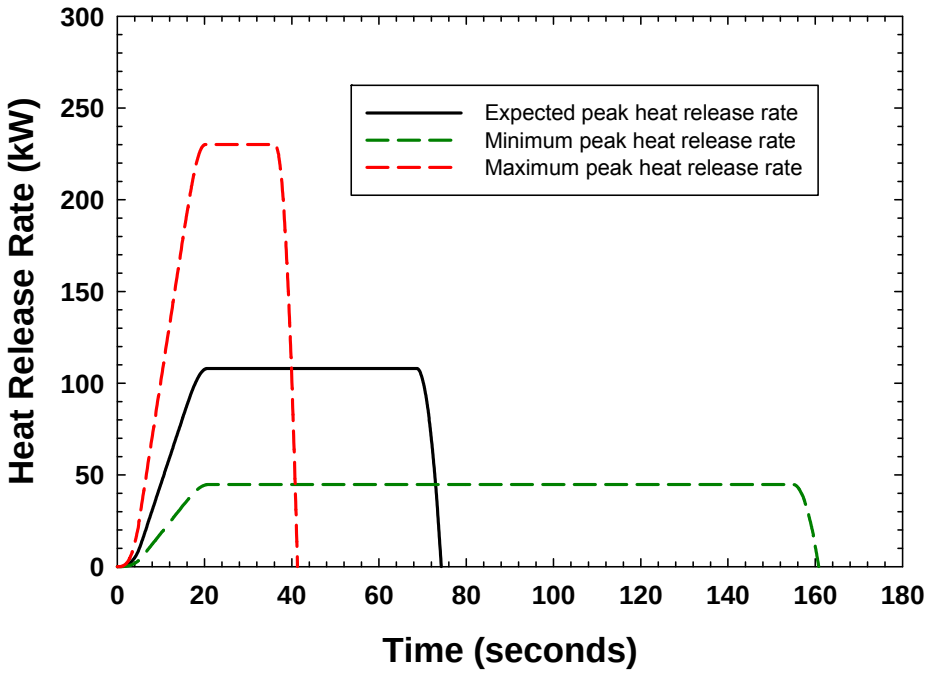


**Figure C-14**
**HRR profiles for a 0.25 L kerosene spill fire scenario**

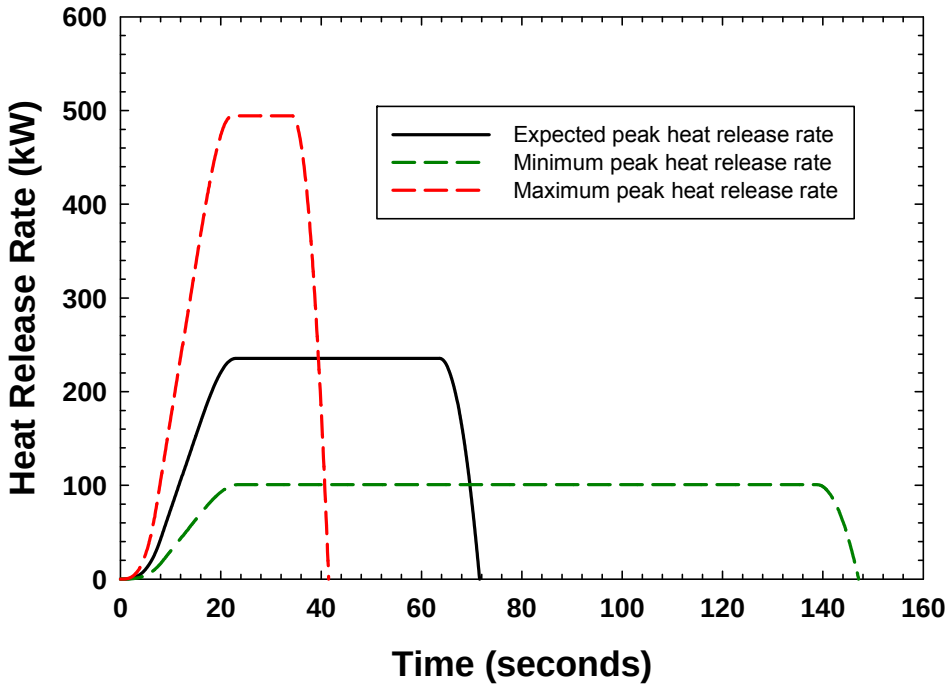


**Figure C-15**
**HRR profiles for a 0.5 L kerosene spill fire scenario**

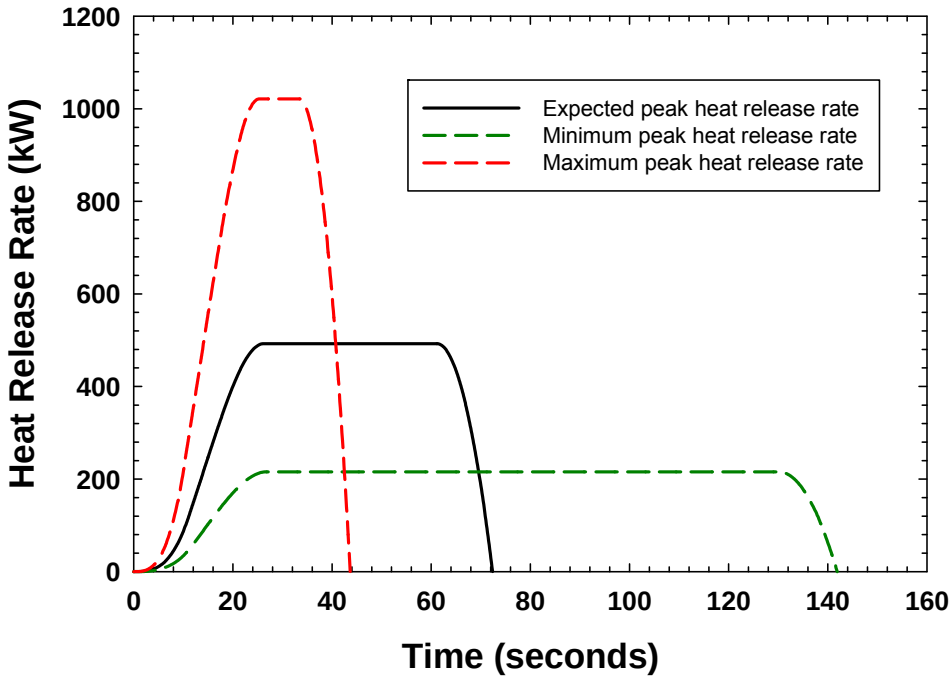


**Figure C-16**
**HRR profiles for a 1.0 L kerosene spill fire scenario**

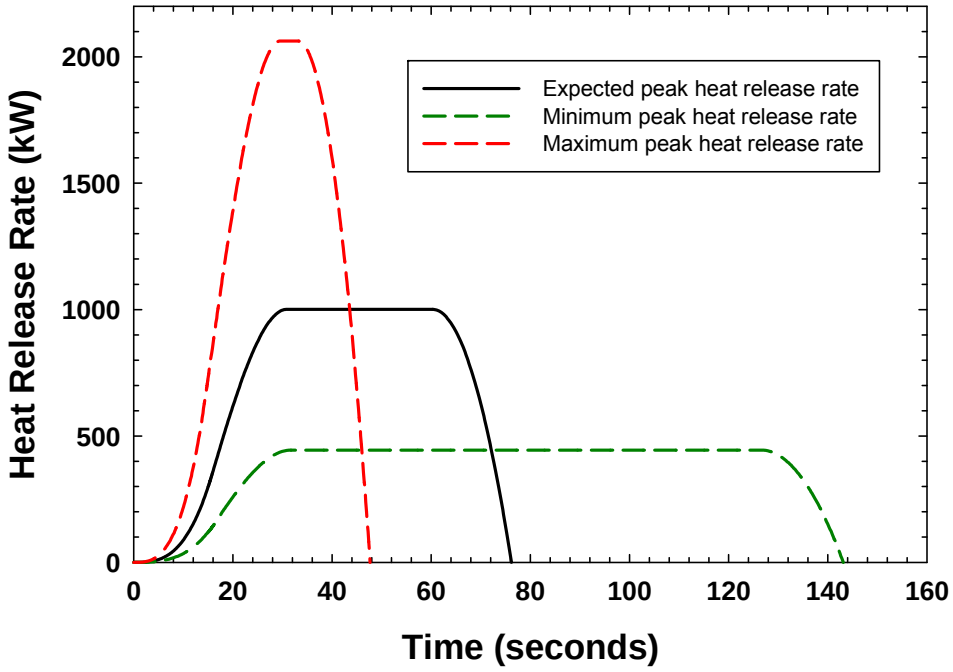


**Figure C-17**
**HRR profiles for a 2.0 L kerosene spill fire scenario**

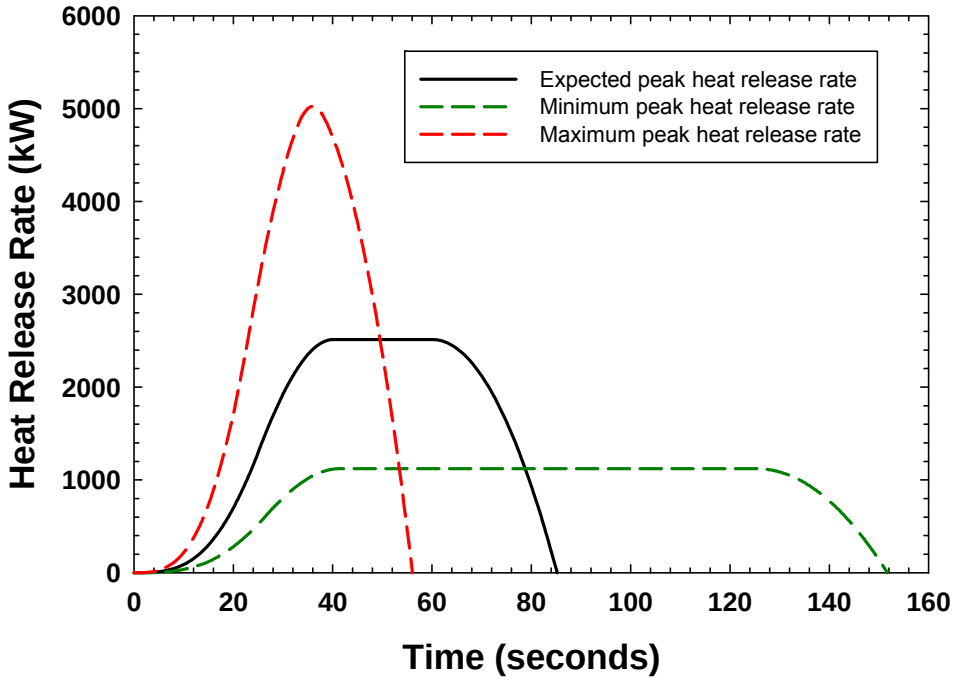


**Figure C-18**
**HRR profiles for a 5.0 L kerosene spill fire scenario**

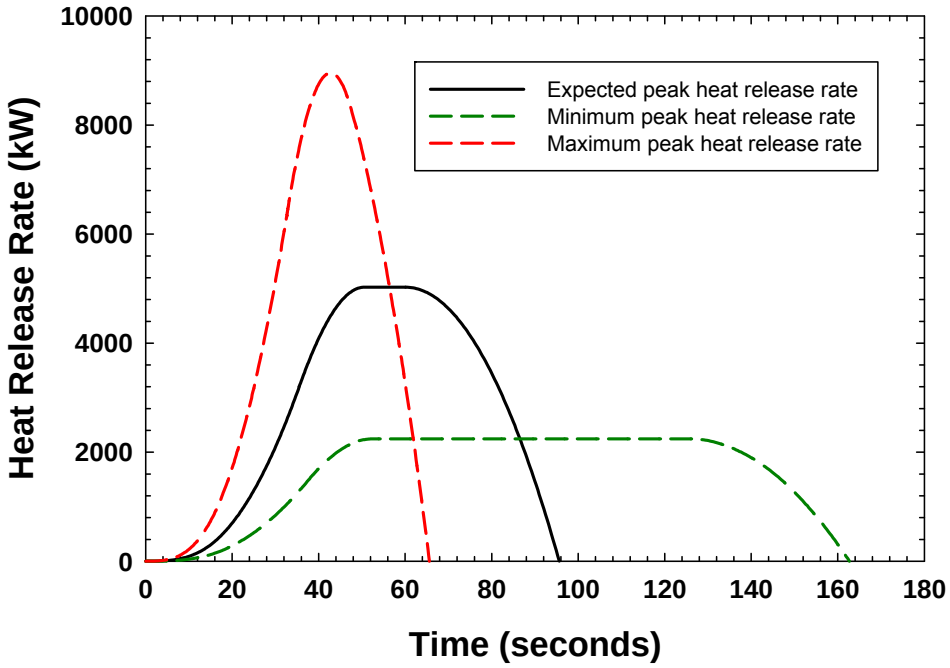


**Figure C-19**
**HRR profiles for a 10.0 L kerosene spill fire scenario**

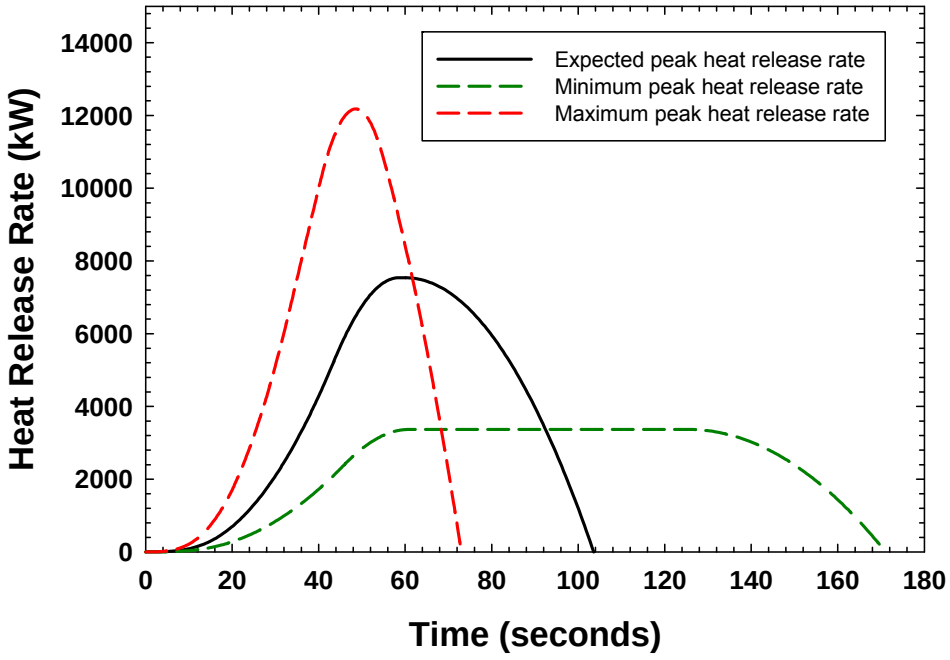


**Figure C-20**
**HRR profiles for a 15.0 L kerosene spill fire scenario**

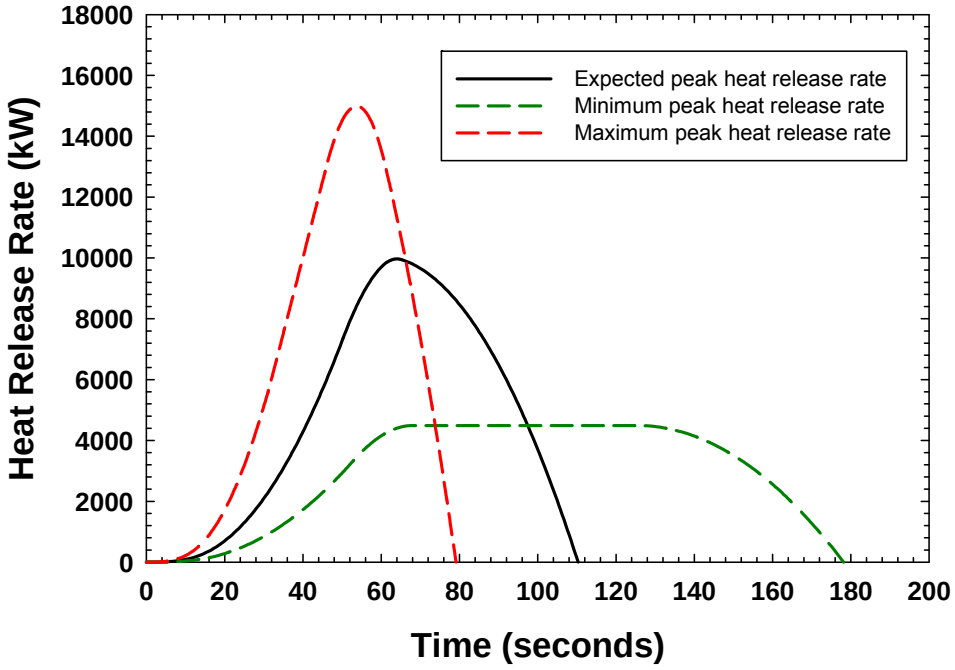


**Figure C-21**
**HRR profiles for a 20.0 L kerosene spill fire scenario**

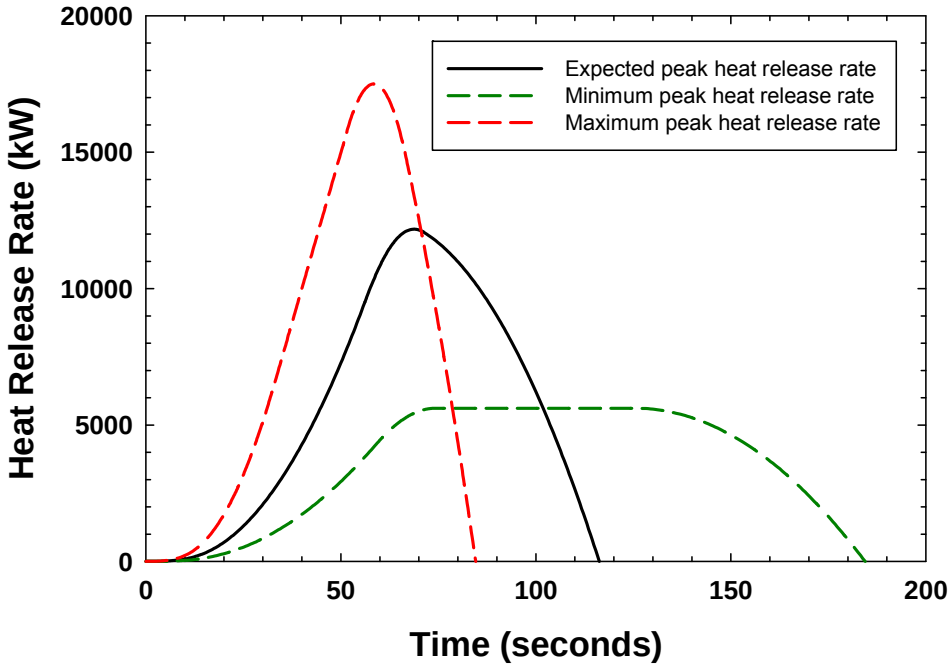


**Figure C-22**
**HRR profiles for a 25.0 L kerosene spill fire scenario**

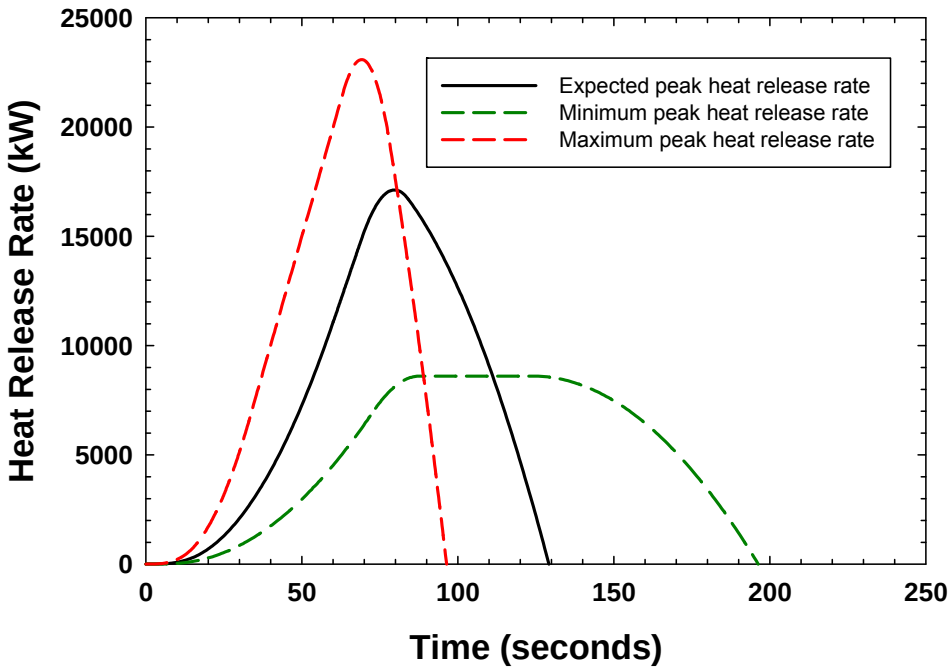


**Figure C-23**
**HRR profiles for a 37.8 L kerosene spill fire scenario**

### *C.2.3 Lubricating Oil Spill Fires (Minimum Depth Coefficient)*

The baseline model parameters for the lubricating oil spill fires with the depth coefficient minimized are obtained from Tables 6-1 and 5-5 and are as follows:

- Density: 970 kg/m³ (average value for fuel oil per Table 6-1)
- Heat of combustion: 39,700 kJ/kg
- Mass burning rate: 0.035 kg/m²-s, with a range of 0.032–0.038 kg/m²-s
- Empirical diameter constant: 1.7 $m^{-1}$, with a range of 1.1–2.3 $m^{-1}$

The fuel depth for an unconfined lubricating oil spill fire is 1.54 mm according to Table 5-4. The maximum and minimum spill depth range for lubricating oil is 0.86–2.4 mm according to Table 5-4. The depth coefficient is 0.2, which is the minimum depth coefficient for lubricating oil spills with a depth between 1 and 2 mm.

The HRR development time is 15 seconds and the spread rate over the liquid surface is 5 cm/s, the same values used to validate the model with kerosene fires in Section 6.1.3.3.5. Table C-5 summarizes the minimum, average, and maximum spill diameters and HRRPUA for each spill volume considered. The HRRs per unit area are determined from the product of the maximum mass burning rate, the depth coefficient, and the empirical diameter coefficient. Note that the minimum diameter fire scenario corresponds to the minimum HRRPUA because the depth coefficient variation is less than the empirical diameter coefficient variation.

**Table C-5**
**Lubricating oil spill fire diameter and heat release rates per unit area – depth coefficient minimized**

| Spill Volume (L) | Diameter (m) | | | Heat Release Rate per Unit Area (kW/m²) | | |
|---|---|---|---|---|---|---|
| | Minimum | Average | Maximum | Minimum | Average | Maximum |
| 0.1 | 0.23 | 0.29 | 0.38 | 88 | 107 | 124 |
| 0.25 | 0.36 | 0.45 | 0.61 | 124 | 150 | 171 |
| 0.50 | 0.52 | 0.64 | 0.86 | 155 | 185 | 209 |
| 1.0 | 0.73 | 0.91 | 1.22 | 187 | 219 | 245 |
| 2.0 | 1.03 | 1.29 | 1.72 | 216 | 247 | 273 |
| 5.0 | 1.63 | 2.03 | 2.72 | 241 | 269 | 295 |
| 10.0 | 2.3 | 2.88 | 3.85 | 250 | 276 | 300 |
| 15.0 | 2.82 | 3.52 | 4.71 | 253 | 277 | 301 |
| 20.0 | 3.26 | 4.07 | 5.44 | 253 | 278 | 302 |
| 25.0 | 3.64 | 4.55 | 6.08 | 254 | 278 | 302 |
| 37.8 | 4.48 | 5.59 | 7.48 | 254 | 278 | 302 |

The results for lubricating oil spill fires with volumes ranging from 0.1 to 37.8 L are summarized in Figures C-24 through C-34 when the depth coefficient is minimized. Tabular data (Tables C-29 through 39) at key points on the HRR profile are provided in Section C.2.5 for each HRR profile shown in Figures C-24 through C-34.

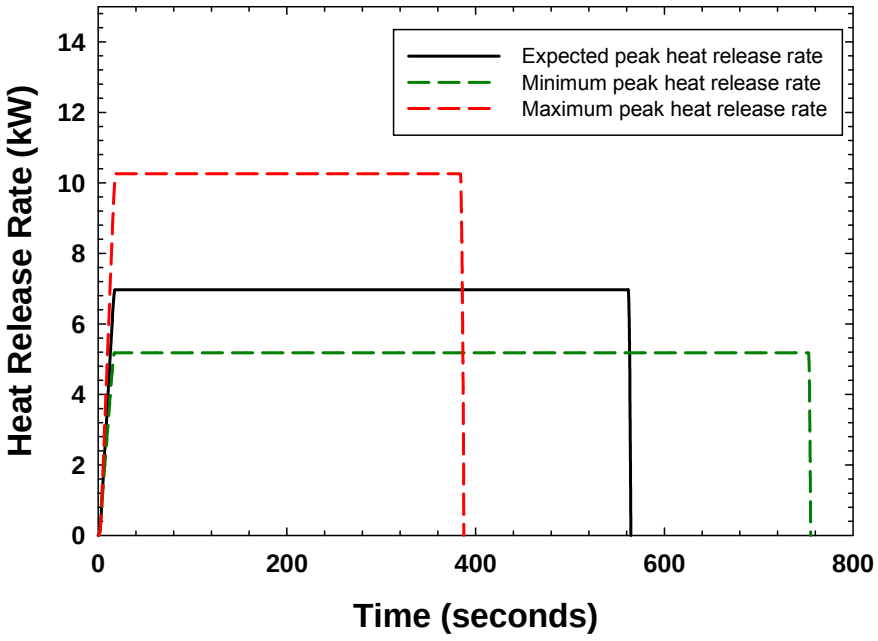


**Figure C-24**
**HRR profiles for a 0.1 L lubricating oil spill fire scenario – depth coefficient minimized**

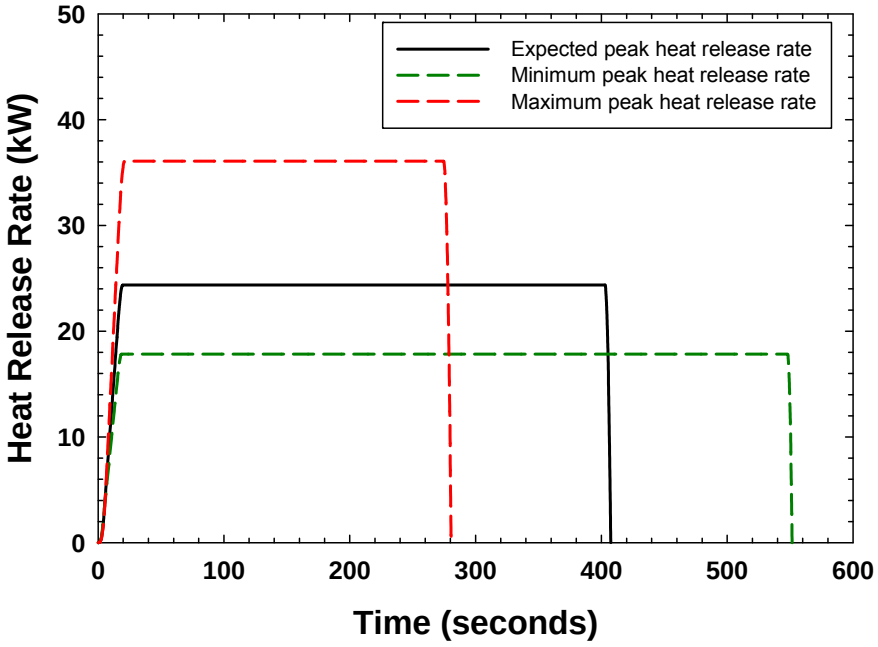


**Figure C-25**
**HRR profiles for a 0.25 L lubricating oil spill fire scenario – depth coefficient minimized**

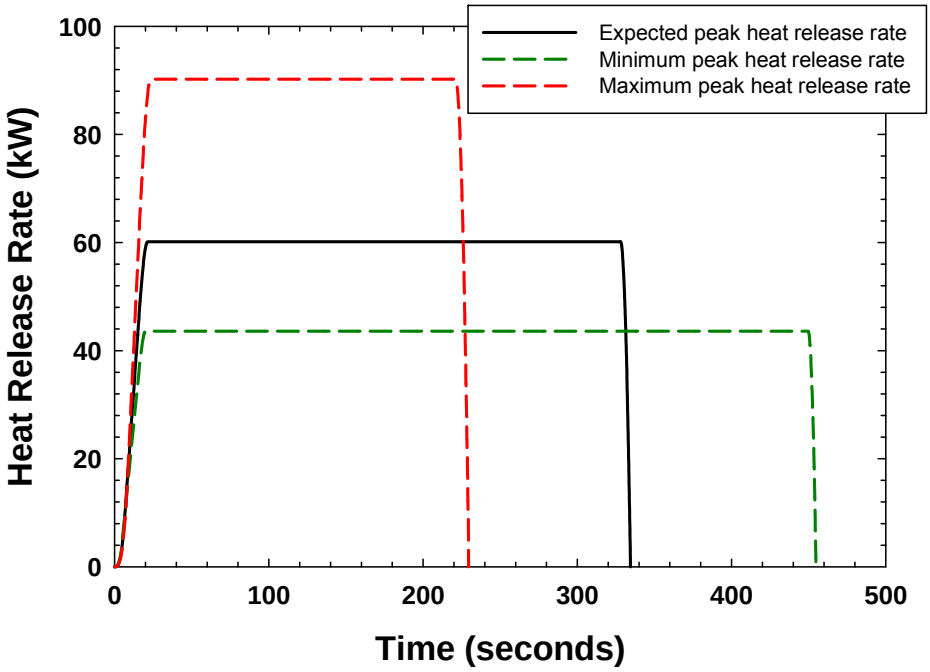


**Figure C-26**
**HRR profiles for a 0.5 L lubricating oil spill fire scenario – depth coefficient minimized**

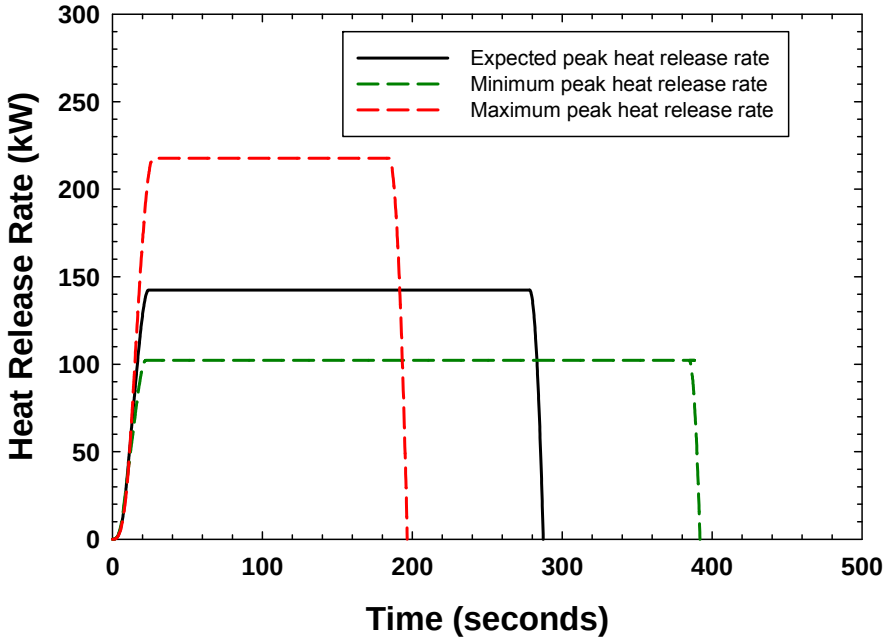


**Figure C-27**
**HRR profiles for a 1.0 L lubricating oil spill fire scenario – depth coefficient minimized**

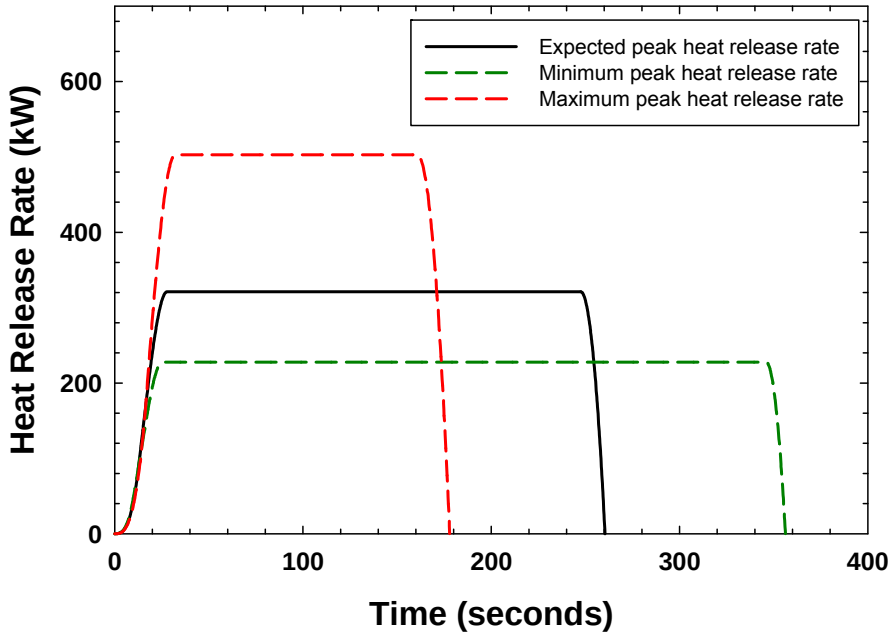


**Figure C-28**
**HRR profiles for a 2.0 L lubricating oil spill fire scenario – depth coefficient minimized**

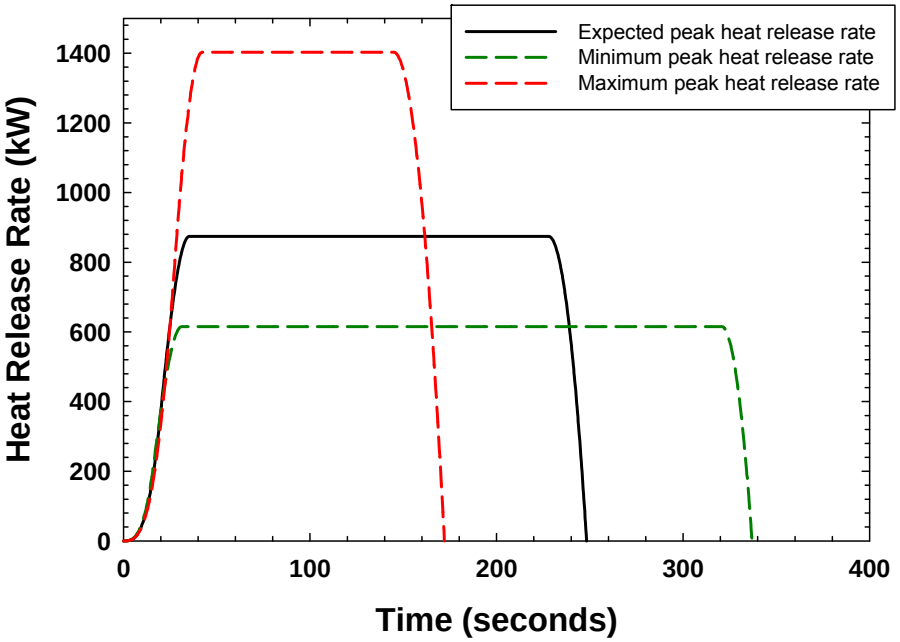


**Figure C-29**
**HRR profiles for a 5.0 L lubricating oil spill fire scenario – depth coefficient minimized**

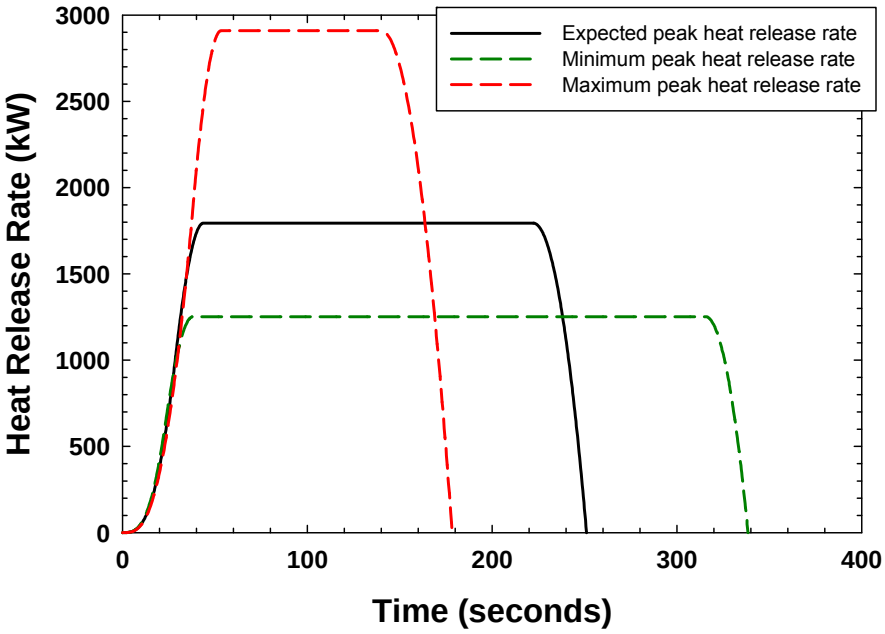


**Figure C-30**
**HRR profiles for a 10.0 L lubricating oil spill fire scenario – depth coefficient minimized**

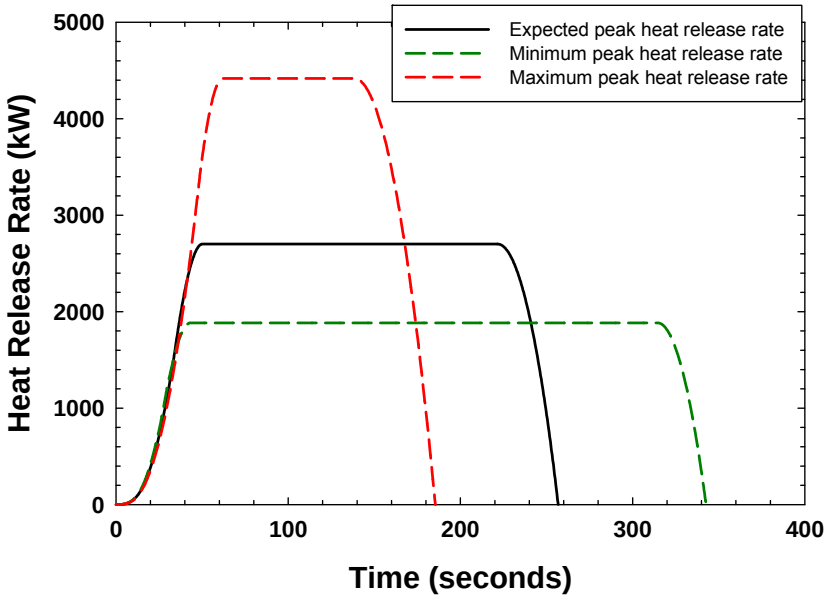


**Figure C-31**
**HRR profiles for a 15.0 l lubricating oil spill fire scenario – depth coefficient minimized**

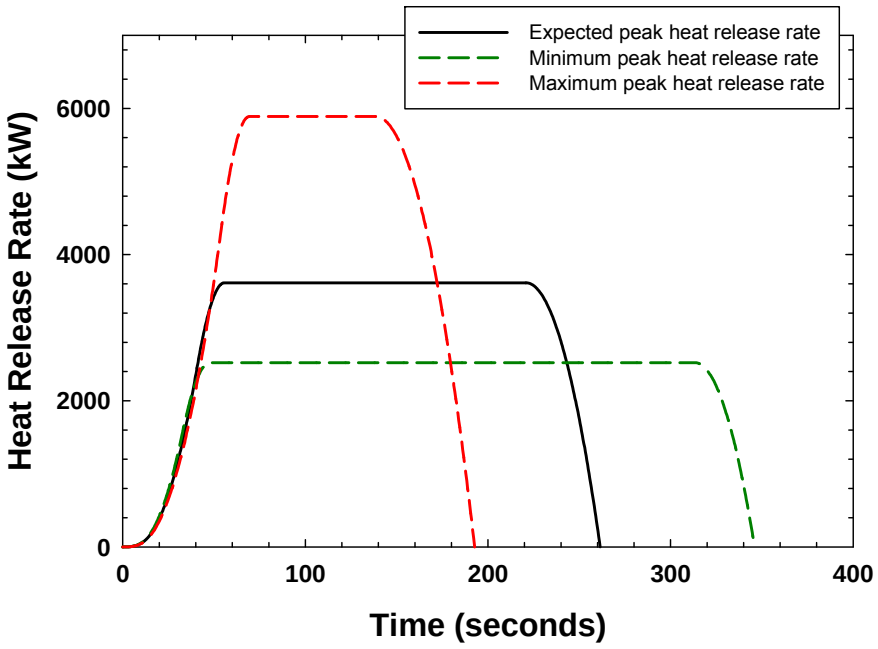


**Figure C-32**
**HRR profiles for a 20.0 L lubricating oil spill fire scenario – depth coefficient minimized**

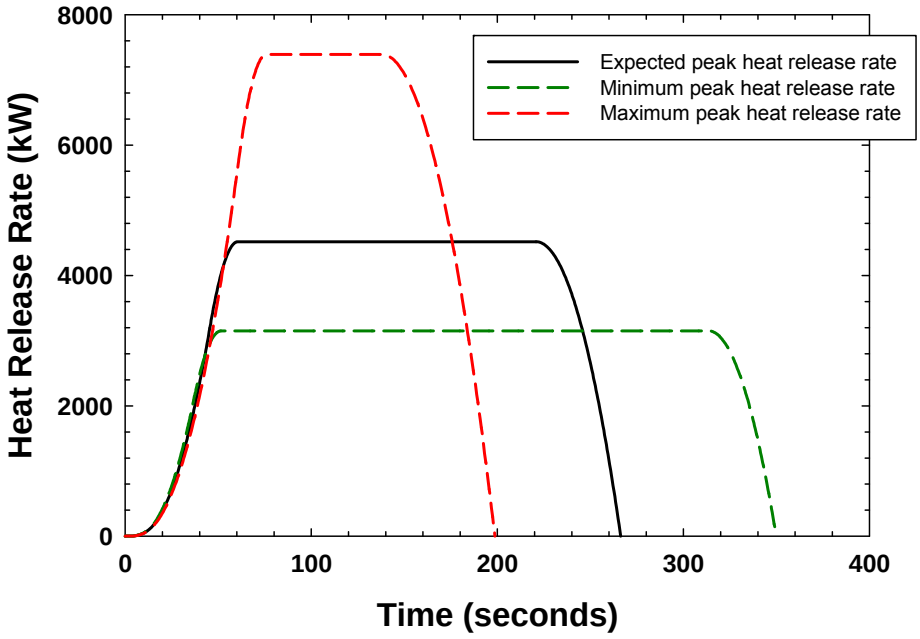


**Figure C-33**
**HRR profiles for a 25.0 L lubricating oil spill fire scenario – depth coefficient minimized**

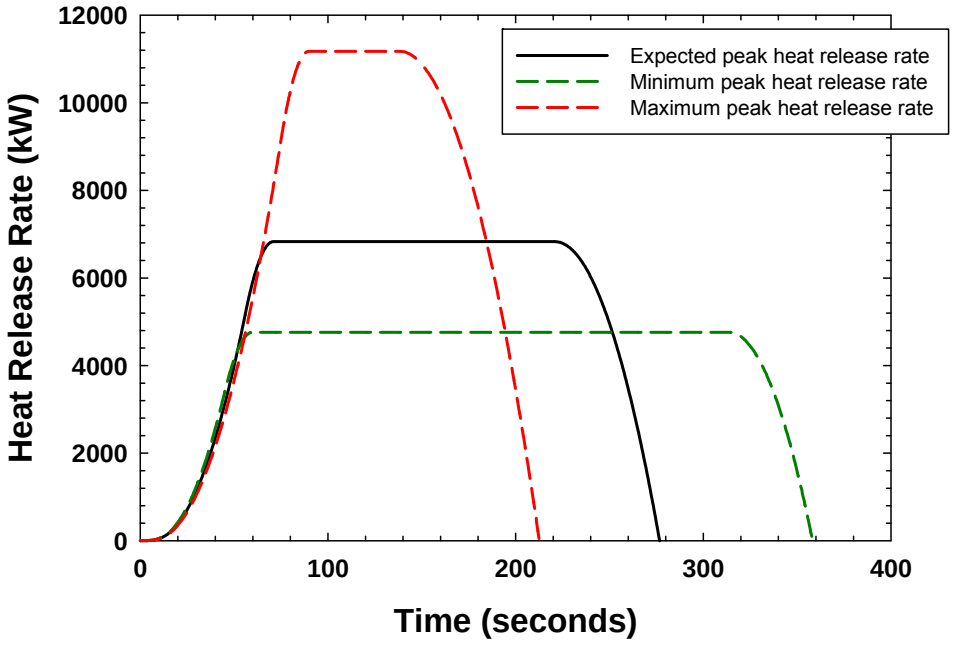


**Figure C-34**
**HRR profiles for a 37.8 L lubricating oil spill fire scenario – depth coefficient minimized**

### *C.2.4 Lubricating Oil Spill Fires (Maximum Depth Coefficient)*

The baseline model parameters for the lubricating oil spill fires with the depth coefficient maximized are obtained from Tables 6-1 and 5-5 are as follows:

- Density: 970 kg/m³ (average value for fuel oil per Table 6-1)
- Heat of combustion: 39,700 kJ/kg
- Mass burning rate: 0.035 kg/m²-s, with a range of 0.032–0.038 kg/m²-s
- Empirical diameter constant: 1.7 $m^{-1}$, with a range of 1.1–2.3 $m^{-1}$

The fuel depth for an unconfined lubricating oil spill fire is 1.54 mm according to Table 5-4. The maximum and minimum spill depth range for lubricating oil is 0.86–2.4 mm according to Table 5-4. The depth coefficient is 1.0, which is the maximum depth coefficient for lubricating oil spills with a depth between 1 and 2 mm.

The HRR development time is 15 seconds, and the spread rate over the liquid surface is 5 cm/s, the same values used to validate the model with kerosene fires in Section 6.1.3.3.5. Table C-6 summarizes the minimum, average, and maximum spill diameters and HRRPUA for each spill volume considered. The HRRs per unit area are determined from the product of the maximum mass burning rate, the depth coefficient, and the empirical diameter coefficient. Note that the minimum diameter fire scenario corresponds to the minimum HRRPUA because the depth coefficient variation is less than the empirical diameter coefficient variation.

**Table C-6**
**Lubricating oil spill fire diameter and heat release rates per unit area – depth coefficient maximized**

| Spill Volume (L) | Diameter (m) | | | Heat Release Rate per Unit Area (kW/m²) | | |
|---|---|---|---|---|---|---|
| | Minimum | Average | Maximum | Minimum | Average | Maximum |
| 0.1 | 0.38 | 0.29 | 0.23 | 438 | 537 | 620 |
| 0.25 | 0.61 | 0.45 | 0.36 | 620 | 748 | 856 |
| 0.50 | 0.86 | 0.64 | 0.52 | 777 | 924 | 1,047 |
| 1.0 | 1.22 | 0.91 | 0.73 | 937 | 1,093 | 1,226 |
| 2.0 | 1.72 | 1.29 | 1.03 | 1,079 | 1,233 | 1,367 |
| 5.0 | 2.72 | 2.03 | 1.63 | 1,207 | 1,346 | 1,473 |
| 10.0 | 3.85 | 2.88 | 2.3 | 1,252 | 1,379 | 1,501 |
| 15.0 | 4.71 | 3.52 | 2.82 | 1,263 | 1,386 | 1,506 |
| 20.0 | 5.44 | 4.07 | 3.26 | 1,267 | 1,388 | 1,508 |
| 25.0 | 6.08 | 4.55 | 3.64 | 1,269 | 1,389 | 1,508 |
| 37.8 | 7.48 | 5.59 | 4.48 | 1,270 | 1,389 | 1,509 |

The results for lubricating oil spill fires with volumes ranging from 0.1 to 37.8 L are summarized in Figures C-35 through C-45 when the depth coefficient is maximized. Tabular data (Tables C-40 through C-50) at approximately 10 second intervals are provided in Section C.2.5 for each HRR profile shown in Figures C-35 through C-45.

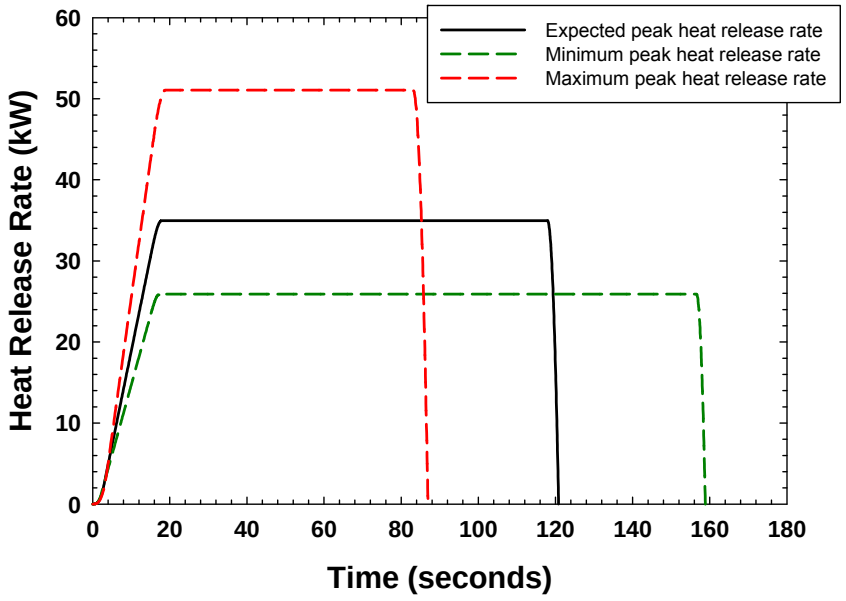


**Figure C-35**
**HRR profiles for a 0.1 L lubricating oil spill fire scenario – depth coefficient minimized**

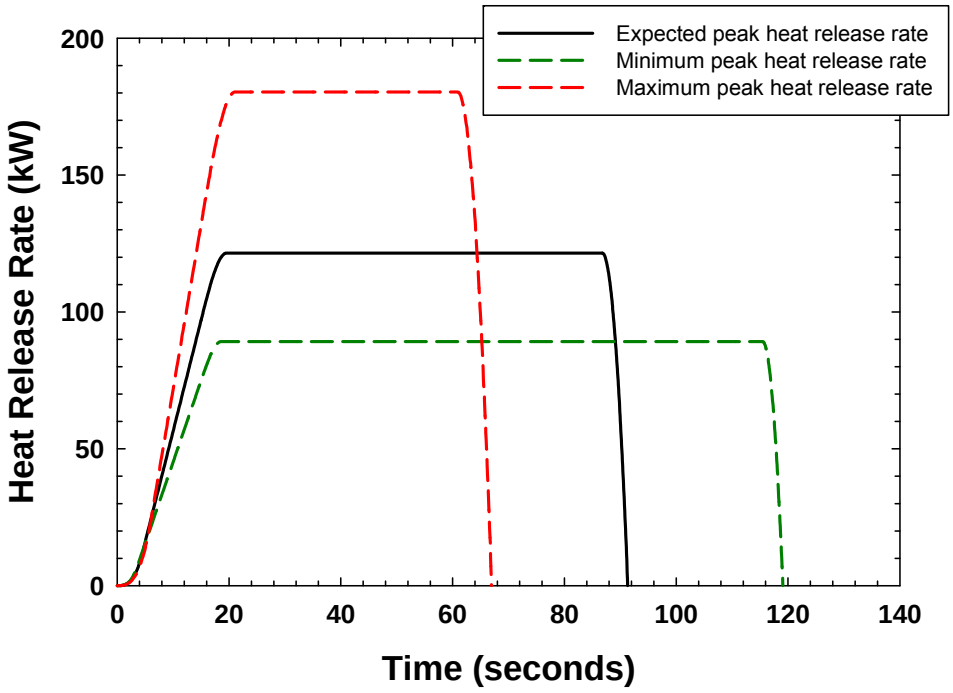


**Figure C-36**
**HRR profiles for a 0.5 L lubricating oil spill fire scenario – depth coefficient maximized**

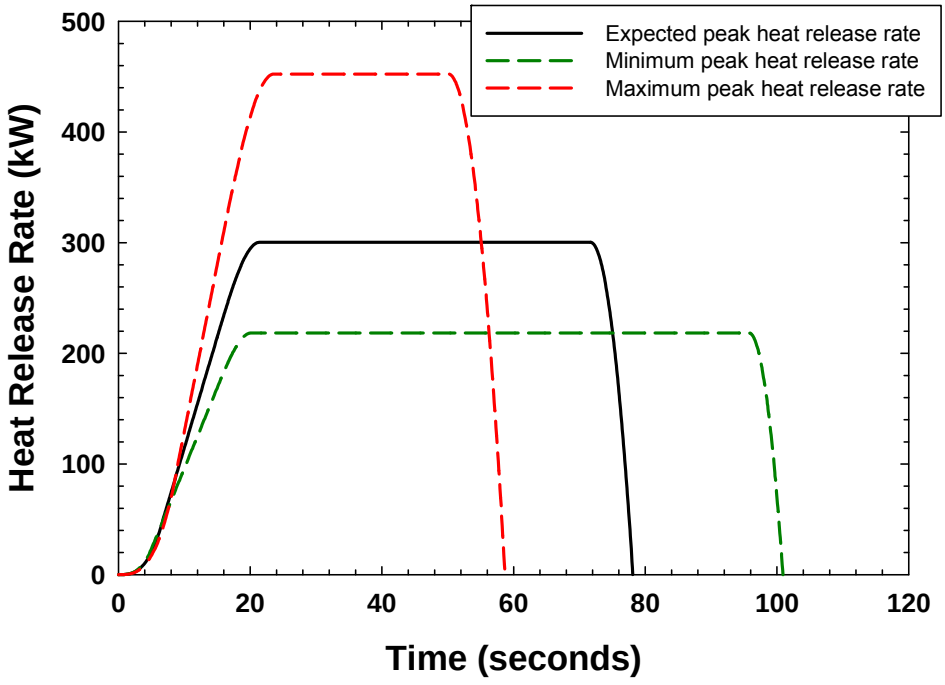


**Figure C-37**
**HRR profiles for a 0.5 L lubricating oil spill fire scenario – depth coefficient maximized**

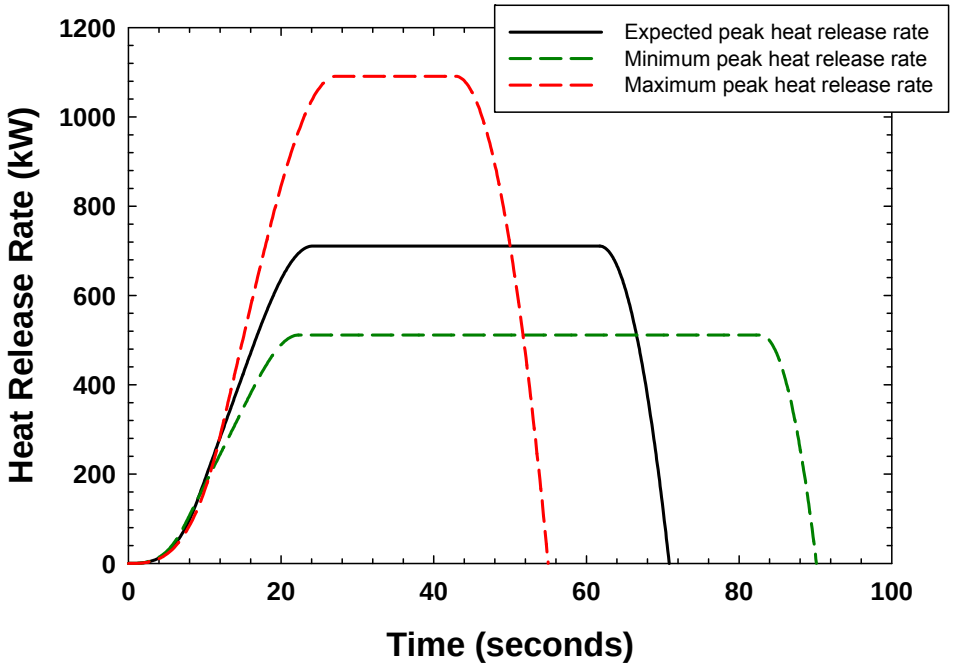


**Figure C-38**
**HRR profiles for a 1.0 L lubricating oil spill fire scenario – depth coefficient maximized**

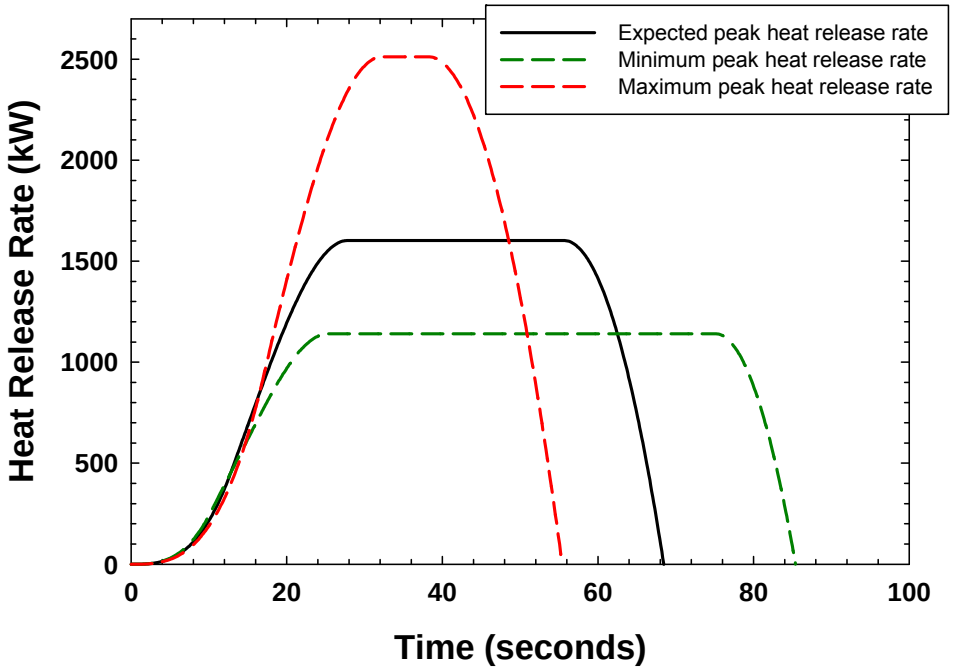


**Figure C-39**
**HRR profiles for a 2.0 L lubricating oil spill fire scenario – depth coefficient maximized**

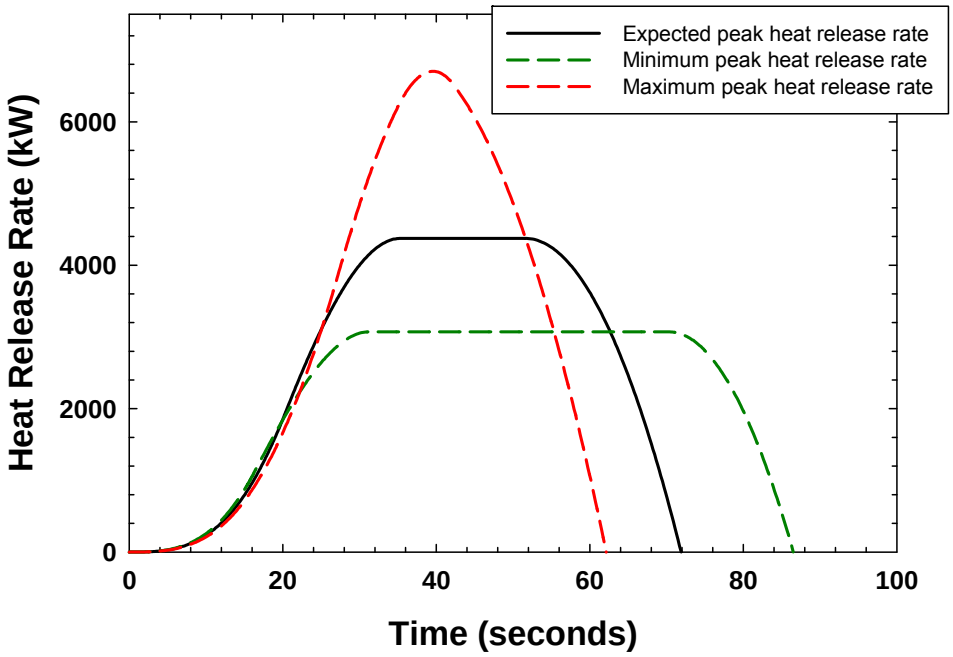


**Figure C-40**
**HRR profiles for a 5.0 L lubricating oil spill fire scenario – depth coefficient maximized**

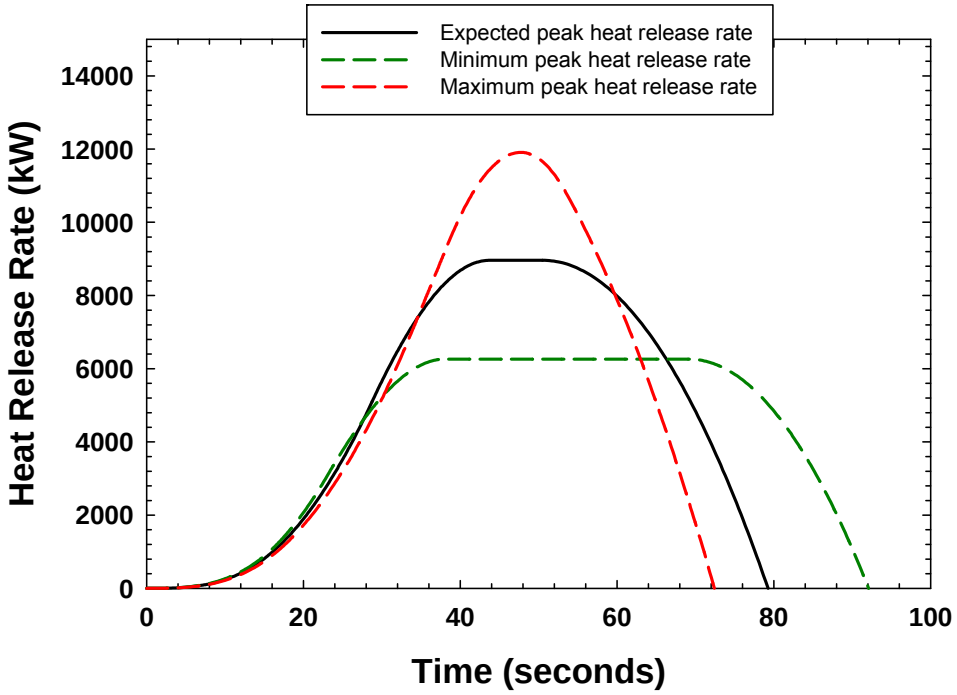


**Figure C-41**
**HRR profiles for a 10.0 L lubricating oil spill fire scenario – depth coefficient maximized**

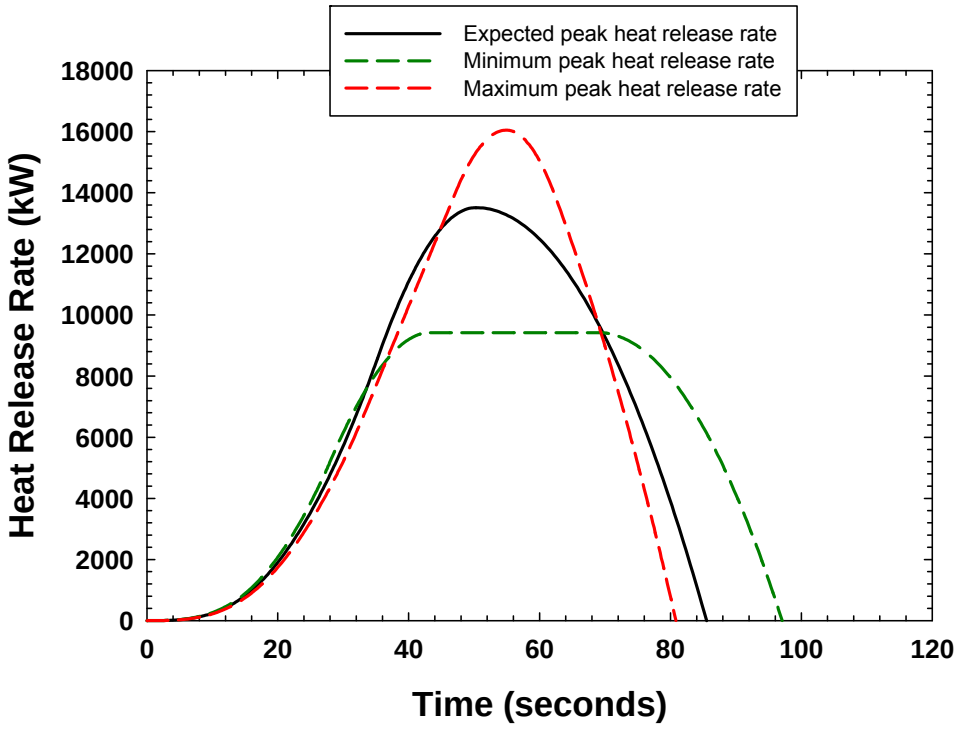


**Figure C-42**
**HRR profiles for a 15.0 L lubricating oil spill fire scenario – depth coefficient maximized**

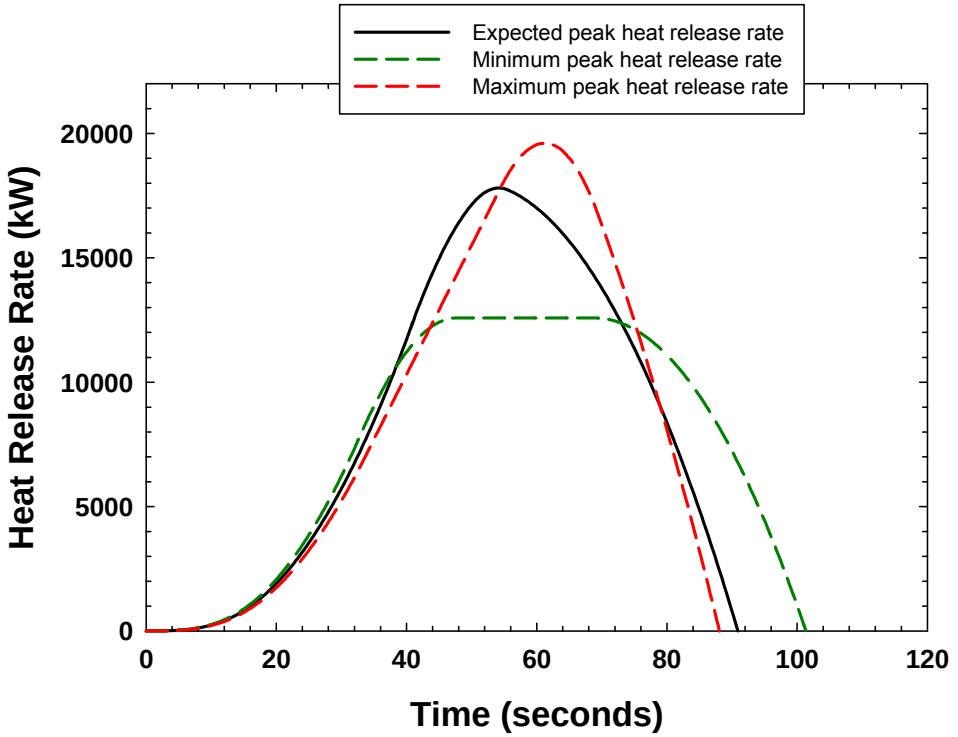


**Figure C-43**
**HRR profiles for a 20.0 L lubricating oil spill fire scenario – depth coefficient maximized**

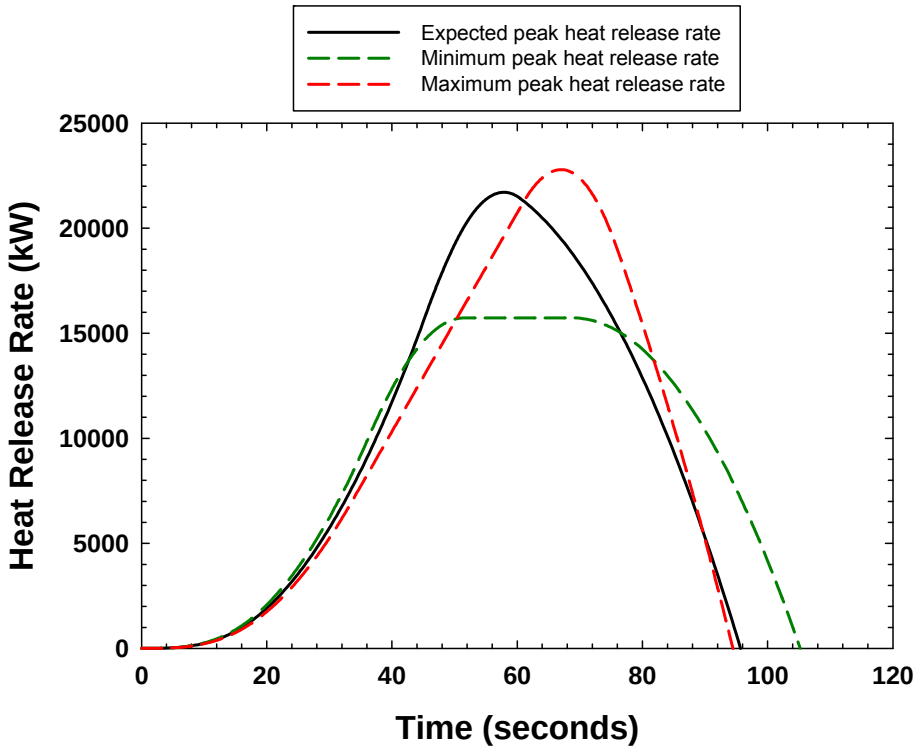


**Figure C-44**
**HRR profiles for a 25.0 L lubricating oil spill fire scenario – depth coefficient maximized**

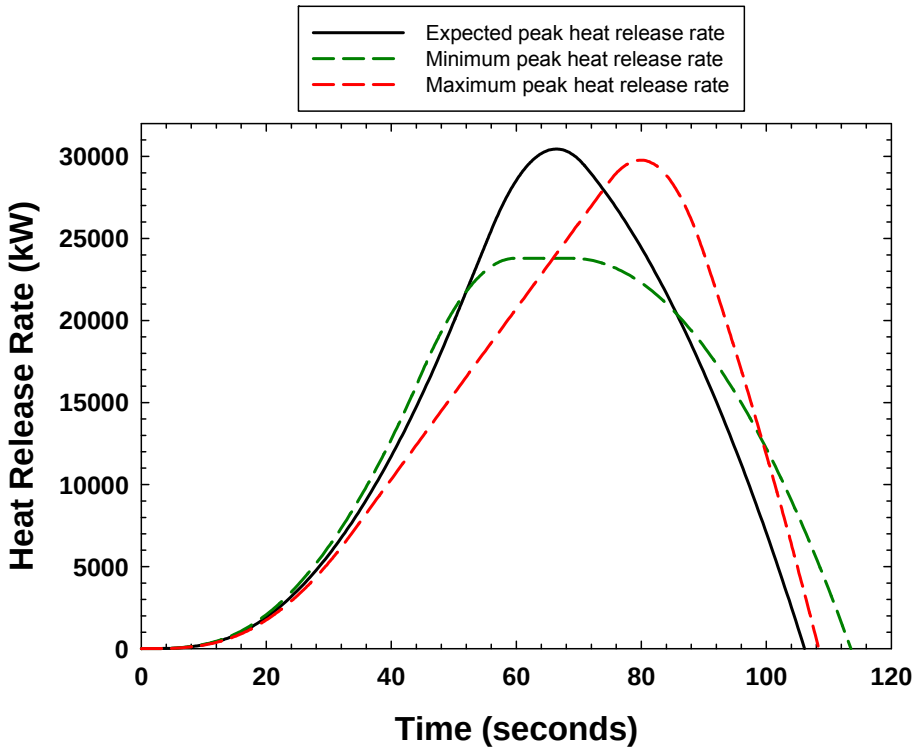


**Figure C-45**
**HRR profiles for a 37.8 L lubricating oil spill fire scenario – depth coefficient maximized**

Note that the scenario that results in the maximum HRR shown in Figure C-45 is the intermediate or expected scenario. This occurs because the fire diameter effects are diminishing, and at the volume considered, the maximum HRR occurs at an intermediate spill thickness.

### *C.2.5 Tabular Heat Release Rate Data*

Tables C-7 through C-50 provide tabular heat release rate data corresponding to Figures C-2 through C-45. The data are provided at approximately 5 second increments for gasoline spill fires, 10 second increments for kerosene and lubricating oil spill fire scenarios with the depth coefficient maximized for lubricating oil fires, and at key points on the HRR profile for the lubricating oil spill fires with the depth coefficient minimized.

**Table C-7**
**Tabular HRR data for Figure C-2**

| Minimum Heat Release Rate | | Expected Heat Release Rate | | Maximum Heat Release Rate | |
|---|---|---|---|---|---|
| Time (s) | Heat Release Rate (kW) | Time (s) | Heat Release Rate (kW) | Time (s) | Heat Release Rate (kW) |
| 0.0 | 0 | 0.0 | 0 | 0.0 | 0 |
| 5.0 | 16 | 5.0 | 27 | 4.9 | 43 |
| 10.0 | 41 | 10.0 | 65 | 10.0 | 99 |
| 14.9 | 49 | 15.0 | 76 | 15.0 | 112 |
| 20.1 | 49 | 20.0 | 76 | 19.9 | 112 |
| 24.8 | 49 | 25.0 | 76 | 25.0 | 112 |
| 30.0 | 49 | 30.0 | 76 | 30.2 | 112 |
| 35.3 | 49 | 35.0 | 76 | 35.0 | 69 |
| 39.9 | 49 | 40.0 | 76 | 35.6 | 0 |
| 45.2 | 49 | 45.0 | 76 | | |
| 50.4 | 49 | 50.0 | 0 | | |
| 55.1 | 49 | | | | |
| 60.3 | 49 | | | | |
| 65.5 | 49 | | | | |
| 70.2 | 49 | | | | |
| 73.4 | 0 | | | | |

**Table C-8**
**Tabular HRR data for Figure C-3**

| Minimum Heat Release Rate | | Expected Heat Release Rate | | Maximum Heat Release Rate | |
|---|---|---|---|---|---|
| **Time (s)** | **Heat Release Rate (kW)** | **Time (s)** | **Heat Release Rate (kW)** | **Time (s)** | **Heat Release Rate (kW)** |
| 0.0 | 0 | 0.0 | 0 | 0.0 | 0 |
| 5.0 | 35 | 4.9 | 66 | 5.0 | 115 |
| 10.0 | 114 | 10.0 | 188 | 10.0 | 298 |
| 14.9 | 156 | 15.1 | 242 | 15.0 | 363 |
| 19.6 | 156 | 20.1 | 242 | 20.0 | 363 |
| 25.2 | 156 | 25.1 | 242 | 25.1 | 363 |
| 29.9 | 156 | 30.1 | 242 | 30.0 | 0 |
| 35.0 | 156 | 35.1 | 242 | | |
| 40.1 | 156 | 40.0 | 184 | | |
| 45.2 | 156 | 41.7 | 0 | | |
| 50.3 | 156 | | | | |
| 55.0 | 156 | | | | |
| 60.0 | 54 | | | | |
| 60.8 | 0 | | | | |

**Table C-9**
**Tabular HRR data for Figure C-4**

| Minimum Heat Release Rate | | Expected Heat Release Rate | | Maximum Heat Release Rate | |
|---|---|---|---|---|---|
| **Time (s)** | **Heat Release Rate (kW)** | **Time (s)** | **Heat Release Rate (kW)** | **Time (s)** | **Heat Release Rate (kW)** |
| 0.0 | 0 | 0.0 | 0 | 0.0 | 0 |
| 5.0 | 45 | 5.0 | 102 | 5.0 | 211 |
| 10.0 | 219 | 10.0 | 380 | 10.0 | 627 |
| 15.0 | 352 | 14.9 | 555 | 15.0 | 840 |
| 19.9 | 356 | 20.2 | 555 | 20.1 | 840 |
| 25.1 | 356 | 25.0 | 555 | 25.0 | 807 |
| 30.0 | 356 | 30.1 | 555 | 28.1 | 0 |
| 35.2 | 356 | 35.0 | 537 | | |
| 40.1 | 356 | 38.9 | 0 | | |
| 45.3 | 356 | | | | |
| 50.2 | 356 | | | | |
| 55.0 | 139 | | | | |
| 56.3 | 0 | | | | |

**Table C-10**
**Tabular HRR data for Figure C-5**

| Minimum Heat Release Rate | | Expected Heat Release Rate | | Maximum Heat Release Rate | |
|---|---|---|---|---|---|
| **Time (s)** | **Heat Release Rate (kW)** | **Time (s)** | **Heat Release Rate (kW)** | **Time (s)** | **Heat Release Rate (kW)** |
| 0.0 | 0 | 0.0 | 0 | 0.0 | 0 |
| 5.1 | 50 | 5.0 | 114 | 5.0 | 267 |
| 10.0 | 352 | 10.0 | 669 | 10.0 | 1,188 |
| 15.1 | 691 | 15.0 | 1,163 | 15.0 | 1,847 |
| 20.2 | 770 | 20.0 | 1,210 | 20.1 | 1,852 |
| 25.1 | 770 | 25.0 | 1,210 | 25.0 | 1,443 |
| 30.0 | 770 | 30.1 | 1,210 | 27.9 | 0 |
| 34.9 | 770 | 35.0 | 919 | | |
| 40.1 | 770 | 38.5 | 0 | | |
| 45.0 | 770 | | | | |
| 50.0 | 670 | | | | |
| 55.1 | 30 | | | | |
| 55.2 | 0 | | | | |
| 0.0 | 0 | | | | |

**Table C-11**
**Tabular HRR data for Figure C-6**

| Minimum Heat Release Rate | | Expected Heat Release Rate | | Maximum Heat Release Rate | |
|---|---|---|---|---|---|
| **Time (s)** | **Heat Release Rate (kW)** | **Time (s)** | **Heat Release Rate (kW)** | **Time (s)** | **Heat Release Rate (kW)** |
| 0.0 | 0 | 0.0 | 0 | 0.0 | 0 |
| 5.0 | 50 | 5.0 | 119 | 5.0 | 285 |
| 10.0 | 402 | 10.0 | 931 | 10.0 | 1,923 |
| 15.0 | 1,125 | 15.0 | 2,080 | 15.0 | 3,599 |
| 20.0 | 1,572 | 20.0 | 2,526 | 20.0 | 3,904 |
| 25.1 | 1,601 | 25.0 | 2,526 | 25.0 | 3,113 |
| 30.1 | 1,601 | 30.1 | 2,526 | 29.2 | 0 |
| 35.1 | 1,601 | 35.1 | 1,968 | | |
| 40.2 | 1,601 | 40.1 | 0 | | |
| 44.9 | 1,601 | | | | |
| 50.0 | 1,345 | | | | |
| 55.1 | 471 | | | | |
| 56.9 | 0 | | | | |
| 0.0 | 0 | | | | |

**Table C-12**
**Tabular HRR data for Figure C-7**

| Minimum Heat Release Rate | | Expected Heat Release Rate | | Maximum Heat Release Rate | |
|---|---|---|---|---|---|
| **Time (s)** | **Heat Release Rate (kW)** | **Time (s)** | **Heat Release Rate (kW)** | **Time (s)** | **Heat Release Rate (kW)** |
| 0.0 | 0 | 0.0 | 0 | 0.0 | 0 |
| 5.0 | 51 | 5.0 | 119 | 5.0 | 287 |
| 10.0 | 407 | 10.0 | 955 | 10.0 | 2,299 |
| 15.0 | 1,327 | 15.1 | 3,149 | 15.0 | 6,655 |
| 20.0 | 2,784 | 20.1 | 5,511 | 20.0 | 9,667 |
| 25.0 | 3,841 | 25.0 | 6,429 | 25.1 | 8,963 |
| 30.1 | 4,056 | 30.0 | 6,429 | 30.0 | 4,665 |
| 35.1 | 4,056 | 35.0 | 5,770 | 33.2 | 0 |
| 40.1 | 4,056 | 40.1 | 3,628 | | |
| 45.1 | 4,056 | 45.2 | 0 | | |
| 50.0 | 3,738 | | | | |
| 55.1 | 2,784 | | | | |
| 60.0 | 1,262 | | | | |
| 63.1 | 0 | | | | |

**Table C-13**
**Tabular HRR data for Figure C-8**

| Minimum Heat Release Rate | | Expected Heat Release Rate | | Maximum Heat Release Rate | |
|---|---|---|---|---|---|
| **Time (s)** | **Heat Release Rate (kW)** | **Time (s)** | **Heat Release Rate (kW)** | **Time (s)** | **Heat Release Rate (kW)** |
| 0.0 | 0 | 0.0 | 0 | 0.0 | 0 |
| 5.0 | 51 | 5.0 | 120 | 5.0 | 288 |
| 10.0 | 408 | 10.0 | 957 | 10.0 | 2,305 |
| 15.0 | 1,338 | 15.0 | 3,129 | 15.1 | 7,663 |
| 20.1 | 2,892 | 20.1 | 6,756 | 20.0 | 15,029 |
| 25.0 | 4,991 | 25.0 | 10,803 | 25.0 | 18,546 |
| 30.1 | 7,183 | 30.0 | 12,806 | 30.0 | 14,586 |
| 35.1 | 8,117 | 35.0 | 12,200 | 35.1 | 6,680 |
| 40.0 | 8,133 | 40.0 | 10,062 | 38.2 | 0 |
| 45.1 | 8,132 | 45.1 | 6,471 | | |
| 50.0 | 7,807 | 50.1 | 1,427 | | |
| 55.1 | 6,831 | 51.3 | 0 | | |
| 60.0 | 5,302 | | | | |
| 65.2 | 3,057 | | | | |
| 70.0 | 322 | | | | |
| 70.6 | 0 | | | | |

**Table C-14**
**Tabular HRR data for Figure C-9**

| Minimum Heat Release Rate | | Expected Heat Release Rate | | Maximum Heat Release Rate | |
|---|---|---|---|---|---|
| **Time (s)** | **Heat Release Rate (kW)** | **Time (s)** | **Heat Release Rate (kW)** | **Time (s)** | **Heat Release Rate (kW)** |
| 0.0 | 0 | 0.0 | 0 | 0.0 | 0 |
| 5.0 | 51 | 5.0 | 120 | 5.0 | 288 |
| 10.0 | 408 | 10.0 | 957 | 10.0 | 2,306 |
| 15.0 | 1,317 | 15.1 | 3,170 | 15.1 | 7,629 |
| 20.1 | 2,907 | 20.0 | 6,739 | 20.1 | 16,318 |
| 25.1 | 5,046 | 25.3 | 12,080 | 25.0 | 24,596 |
| 30.0 | 7,787 | 30.0 | 16,925 | 30.1 | 24,473 |
| 35.1 | 10,678 | 35.0 | 18,577 | 35.1 | 16,635 |
| 40.1 | 12,113 | 40.0 | 16,543 | 40.1 | 5,220 |
| 45.1 | 12,198 | 45.2 | 12,799 | 42.0 | 0 |
| 50.2 | 11,846 | 50.0 | 7,947 | | |
| 55.2 | 10,871 | 55.1 | 1,470 | | |
| 60.3 | 9,270 | 56.1 | 0 | | |
| 65.0 | 7,202 | | | | |
| 70.0 | 4,392 | | | | |
| 75.1 | 956 | | | | |
| 76.4 | 0 | | | | |

**Table C-15**
**Tabular HRR data for Figure C-10**

| Minimum Heat Release Rate | | Expected Heat Release Rate | | Maximum Heat Release Rate | |
|---|---|---|---|---|---|
| **Time (s)** | **Heat Release Rate (kW)** | **Time (s)** | **Heat Release Rate (kW)** | **Time (s)** | **Heat Release Rate (kW)** |
| 0.0 | 0 | 0.0 | 0 | 0.0 | 0 |
| 5.0 | 51 | 5.0 | 120 | 5.0 | 288 |
| 10.0 | 408 | 10.0 | 957 | 10.0 | 2306 |
| 15.0 | 1333 | 15.0 | 3105 | 15.0 | 7521 |
| 20.0 | 2876 | 20.0 | 6682 | 20.0 | 16222 |
| 25.1 | 5036 | 25.0 | 11689 | 25.1 | 27208 |
| 30.1 | 7815 | 30.0 | 18186 | 30.1 | 32060 |
| 35.1 | 11213 | 34.9 | 23059 | 35.1 | 26673 |
| 40.0 | 14542 | 40.0 | 22992 | 40.1 | 15265 |
| 45.0 | 16175 | 45.0 | 19423 | 45.0 | 739 |
| 50.3 | 15900 | 50.0 | 14402 | 45.2 | 0 |
| 55.1 | 14957 | 55.0 | 7927 | | |
| 60.0 | 13432 | 60.1 | 0 | | |
| 65.2 | 11153 | | | | |
| 70.1 | 8423 | | | | |
| 75.0 | 5112 | | | | |
| 80.2 | 919 | | | | |
| 81.2 | 0 | | | | |

**Table C-16**
**Tabular HRR data for Figure C-11**

| Minimum Heat Release Rate | | Expected Heat Release Rate | | Maximum Heat Release Rate | |
|---|---|---|---|---|---|
| **Time (s)** | **Heat Release Rate (kW)** | **Time (s)** | **Heat Release Rate (kW)** | **Time (s)** | **Heat Release Rate (kW)** |
| 0.0 | 0 | 0.0 | 0 | 0.0 | 0 |
| 5.0 | 51 | 5.0 | 120 | 5.0 | 288 |
| 10.0 | 408 | 10.0 | 957 | 10.0 | 2,306 |
| 14.9 | 1,307 | 15.0 | 3,128 | 15.0 | 7,521 |
| 20.1 | 2,912 | 20.1 | 6,752 | 20.0 | 16,222 |
| 25.1 | 5,033 | 25.1 | 11,829 | 25.0 | 27,247 |
| 30.3 | 7,936 | 29.9 | 18,070 | 30.0 | 36,563 |
| 35.2 | 11,279 | 35.1 | 25,284 | 35.0 | 36,157 |
| 40.1 | 15,215 | 40.1 | 28,283 | 40.0 | 25,438 |
| 45.0 | 18,786 | 45.1 | 25,767 | 45.1 | 10,585 |
| 50.0 | 19,972 | 50.1 | 20,712 | 48.1 | 0 |
| 54.9 | 19,079 | 55.0 | 14,492 | | |
| 60.1 | 17,452 | 60.0 | 6,590 | | |
| 65.0 | 15,330 | 63.6 | 0 | | |
| 70.2 | 12,412 | | | | |
| 75.1 | 9,086 | | | | |
| 80.3 | 4,877 | | | | |
| 85.2 | 346 | | | | |
| 85.5 | 0 | | | | |

**Table C-17**
**Tabular HRR data for Figure C-12**

| Minimum Heat Release Rate | | Expected Heat Release Rate | | Maximum Heat Release Rate | |
|---|---|---|---|---|---|
| **Time (s)** | **Heat Release Rate (kW)** | **Time (s)** | **Heat Release Rate (kW)** | **Time (s)** | **Heat Release Rate (kW)** |
| 0.0 | 0 | 0.0 | 0 | 0.0 | 0 |
| 5.0 | 51 | 5.0 | 120 | 5.0 | 288 |
| 10.0 | 408 | 10.0 | 957 | 10.0 | 2,306 |
| 15.2 | 1,382 | 15.0 | 3,128 | 15.0 | 7,521 |
| 20.1 | 2,893 | 20.1 | 6,752 | 20.0 | 16,222 |
| 25.0 | 4,985 | 25.1 | 11,829 | 25.1 | 27,431 |
| 30.2 | 7,873 | 29.9 | 18,070 | 30.0 | 38,368 |
| 35.1 | 11,171 | 35.1 | 25,542 | 35.1 | 48,839 |
| 40.3 | 15,349 | 40.1 | 32,725 | 40.1 | 48,941 |
| 45.0 | 19,717 | 45.0 | 38,043 | 45.1 | 36,085 |
| 50.0 | 24,618 | 50.1 | 37,119 | 50.0 | 18,162 |
| 55.1 | 27,961 | 55.0 | 30,920 | 54.2 | 0 |
| 60.1 | 27,877 | 60.0 | 23,004 | | |
| 65.3 | 25,587 | 65.1 | 13,635 | | |
| 70.2 | 22,848 | 70.1 | 2,813 | | |
| 75.1 | 19,527 | 71.3 | 0 | | |
| 80.3 | 15,323 | | | | |
| 85.1 | 10,797 | | | | |
| 90.0 | 5,689 | | | | |
| 94.9 | 0 | | | | |

**Table C-18**
**Tabular HRR data for Figure C-13**

| Minimum Heat Release Rate | | Expected Heat Release Rate | | Maximum Heat Release Rate | |
|---|---|---|---|---|---|
| Time (s) | Heat Release Rate (kW) | Time (s) | Heat Release Rate (kW) | Time (s) | Heat Release Rate (kW) |
| 0.0 | 0 | 0.0 | 0 | 0.0 | 0 |
| 10.0 | 7 | 10.1 | 18 | 10.1 | 41 |
| 20.5 | 14 | 19.8 | 36 | 20.1 | 78 |
| 30.9 | 14 | 29.9 | 36 | 30.1 | 78 |
| 39.6 | 14 | 40.0 | 36 | 40.1 | 78 |
| 50.0 | 14 | 50.1 | 36 | 44.7 | 0 |
| 60.4 | 14 | 60.2 | 36 | | |
| 70.8 | 14 | 70.2 | 36 | | |
| 79.5 | 14 | 80.3 | 36 | | |
| 89.9 | 14 | 85.1 | 0 | | |
| 100.3 | 14 | | | | |
| 109.0 | 14 | | | | |
| 119.4 | 14 | | | | |
| 129.8 | 14 | | | | |
| 140.3 | 14 | | | | |
| 150.7 | 14 | | | | |
| 159.3 | 14 | | | | |
| 169.8 | 14 | | | | |
| 180.2 | 14 | | | | |
| 190.6 | 14 | | | | |
| 196.1 | 0 | | | | |

**Table C-19**
**Tabular HRR data for Figure C-14**

| Minimum Heat Release Rate | | Expected Heat Release Rate | | Maximum Heat Release Rate | |
|---|---|---|---|---|---|
| **Time (s)** | **Heat Release Rate (kW)** | **Time (s)** | **Heat Release Rate (kW)** | **Time (s)** | **Heat Release Rate (kW)** |
| 0.0 | 0 | 0.0 | 0 | 0.0 | 0 |
| 10.0 | 18 | 10.0 | 45 | 10.0 | 100 |
| 20.0 | 44 | 20.1 | 108 | 20.0 | 230 |
| 30.3 | 45 | 30.2 | 108 | 30.1 | 230 |
| 39.7 | 45 | 40.3 | 108 | 40.0 | 104 |
| 50.4 | 45 | 50.4 | 108 | 41.4 | 0 |
| 59.8 | 45 | 60.0 | 108 | | |
| 70.5 | 45 | 70.0 | 102 | | |
| 79.9 | 45 | 74.3 | 0 | | |
| 90.6 | 45 | | | | |
| 100.0 | 45 | | | | |
| 110.7 | 45 | | | | |
| 120.1 | 45 | | | | |
| 130.8 | 45 | | | | |
| 140.2 | 45 | | | | |
| 149.5 | 45 | | | | |
| 160.1 | 11 | | | | |
| 160.8 | 0 | | | | |

**Table C-20**
**Tabular HRR data for Figure C-15**

| Minimum Heat Release Rate | | Expected Heat Release Rate | | Maximum Heat Release Rate | |
|---|---|---|---|---|---|
| **Time (s)** | **Heat Release Rate (kW)** | **Time (s)** | **Heat Release Rate (kW)** | **Time (s)** | **Heat Release Rate (kW)** |
| 0.0 | 0 | 0.0 | 0 | 0.0 | 0 |
| 10.0 | 30 | 10.0 | 74 | 10.1 | 172 |
| 20.0 | 93 | 20.0 | 220 | 20.0 | 474 |
| 29.1 | 101 | 30.3 | 235 | 30.1 | 494 |
| 40.7 | 101 | 40.0 | 235 | 40.1 | 178 |
| 49.9 | 101 | 50.2 | 235 | 41.5 | 0 |
| 60.3 | 101 | 60.4 | 235 | | |
| 70.7 | 101 | 70.1 | 81 | | |
| 79.9 | 101 | 71.6 | 0 | | |
| 90.3 | 101 | | | | |
| 99.6 | 101 | | | | |
| 109.9 | 101 | | | | |
| 120.3 | 101 | | | | |
| 130.7 | 101 | | | | |
| 140.1 | 98 | | | | |
| 147.2 | 0 | | | | |

**Table C-21**
**Tabular HRR data for Figure C-16**

| Minimum Heat Release Rate | | Expected Heat Release Rate | | Maximum Heat Release Rate | |
|---|---|---|---|---|---|
| **Time (s)** | **Heat Release Rate (kW)** | **Time (s)** | **Heat Release Rate (kW)** | **Time (s)** | **Heat Release Rate (kW)** |
| 0.0 | 0 | 0.0 | 0 | 0.0 | 0 |
| 10.1 | 35 | 10.0 | 87 | 10.0 | 213 |
| 20.1 | 171 | 20.1 | 401 | 20.1 | 870 |
| 29.9 | 216 | 30.1 | 493 | 30.1 | 1,021 |
| 40.3 | 216 | 40.2 | 493 | 40.1 | 590 |
| 50.6 | 216 | 50.3 | 493 | 43.7 | 0 |
| 60.9 | 216 | 60.1 | 493 | | |
| 70.2 | 216 | 70.0 | 185 | | |
| 80.5 | 216 | 72.4 | 0 | | |
| 90.9 | 216 | | | | |
| 100.1 | 216 | | | | |
| 110.5 | 216 | | | | |
| 120.8 | 216 | | | | |
| 130.1 | 216 | | | | |
| 140.0 | 63 | | | | |
| 141.9 | 0 | | | | |

**Table C-22**
**Tabular HRR data for Figure C-17**

| Minimum Heat Release Rate | | Expected Heat Release Rate | | Maximum Heat Release Rate | |
|---|---|---|---|---|---|
| **Time (s)** | **Heat Release Rate (kW)** | **Time (s)** | **Heat Release Rate (kW)** | **Time (s)** | **Heat Release Rate (kW)** |
| 0.0 | 0 | 0.0 | 0 | 0.0 | 0 |
| 10.1 | 36 | 10.1 | 89 | 10.1 | 219 |
| 20.0 | 259 | 20.1 | 622 | 20.1 | 1,399 |
| 30.1 | 440 | 30.1 | 999 | 30.0 | 2,062 |
| 40.3 | 444 | 40.0 | 1,001 | 40.1 | 1,587 |
| 50.7 | 444 | 50.0 | 1,001 | 47.7 | 0 |
| 60.1 | 444 | 60.0 | 1,001 | | |
| 70.6 | 444 | 70.0 | 628 | | |
| 80.0 | 444 | 76.2 | 0 | | |
| 90.5 | 444 | | | | |
| 100.9 | 444 | | | | |
| 110.3 | 444 | | | | |
| 120.8 | 444 | | | | |
| 130.1 | 423 | | | | |
| 140.0 | 153 | | | | |
| 143.2 | 0 | | | | |

**Table C-23**
**Tabular HRR data for Figure C-18**

| Minimum Heat Release Rate | | Expected Heat Release Rate | | Maximum Heat Release Rate | |
|---|---|---|---|---|---|
| **Time (s)** | **Heat Release Rate (kW)** | **Time (s)** | **Heat Release Rate (kW)** | **Time (s)** | **Heat Release Rate (kW)** |
| 0.0 | 0 | 0.0 | 0 | 0.0 | 0 |
| 10.1 | 36 | 10.1 | 90 | 10.1 | 220 |
| 20.0 | 282 | 20.1 | 703 | 20.1 | 1,719 |
| 30.1 | 807 | 30.1 | 1,929 | 30.1 | 4,325 |
| 40.1 | 1,117 | 40.1 | 2,512 | 40.0 | 4,696 |
| 50.7 | 1,122 | 50.1 | 2,512 | 50.2 | 2,329 |
| 60.7 | 1,122 | 60.1 | 2,512 | 56.1 | 0 |
| 70.8 | 1,122 | 70.1 | 2,110 | | |
| 80.0 | 1,122 | 80.2 | 904 | | |
| 90.1 | 1,122 | 85.2 | 0 | | |
| 100.1 | 1,122 | | | | |
| 110.2 | 1,122 | | | | |
| 120.3 | 1,122 | | | | |
| 130.0 | 1,086 | | | | |
| 140.1 | 770 | | | | |
| 150.2 | 131 | | | | |
| 151.7 | 0 | | | | |

**Table C-24**
**Tabular HRR data for Figure C-19**

| Minimum Heat Release Rate | | Expected Heat Release Rate | | Maximum Heat Release Rate | |
|---|---|---|---|---|---|
| **Time (s)** | **Heat Release Rate (kW)** | **Time (s)** | **Heat Release Rate (kW)** | **Time (s)** | **Heat Release Rate (kW)** |
| 0.0 | 0 | 0.0 | 0 | 0.0 | 0 |
| 10.1 | 36 | 10.1 | 90 | 10.1 | 220 |
| 19.9 | 278 | 19.9 | 689 | 19.9 | 1,685 |
| 30.0 | 843 | 30.0 | 2,087 | 30.0 | 5,087 |
| 40.1 | 1,705 | 40.0 | 4,087 | 40.0 | 8,751 |
| 50.0 | 2,221 | 50.1 | 5,023 | 50.1 | 7,507 |
| 60.4 | 2,244 | 60.0 | 5,024 | 60.1 | 3,248 |
| 70.6 | 2,244 | 70.0 | 4,631 | 65.7 | 0 |
| 80.1 | 2,244 | 80.3 | 3,392 | | |
| 90.3 | 2,244 | 90.3 | 1,394 | | |
| 100.5 | 2,244 | 95.6 | 0 | | |
| 110.7 | 2,244 | | | | |
| 120.2 | 2,244 | | | | |
| 130.1 | 2,206 | | | | |
| 140.3 | 1,885 | | | | |
| 150.4 | 1,237 | | | | |
| 160.1 | 303 | | | | |
| 162.7 | 0 | | | | |

**Table C-25**
**Tabular HRR data for Figure C-20**

| Minimum Heat Release Rate | | Expected Heat Release Rate | | Maximum Heat Release Rate | |
|---|---|---|---|---|---|
| **Time (s)** | **Heat Release Rate (kW)** | **Time (s)** | **Heat Release Rate (kW)** | **Time (s)** | **Heat Release Rate (kW)** |
| 0.0 | 0 | 0.0 | 0 | 0.0 | 0 |
| 10.1 | 36 | 10.1 | 90 | 10.1 | 220 |
| 20.2 | 290 | 20.1 | 710 | 20.1 | 1,718 |
| 30.1 | 849 | 30.1 | 2,110 | 30.0 | 5,109 |
| 40.3 | 1,752 | 40.1 | 4,303 | 40.1 | 10,025 |
| 50.0 | 2,840 | 50.1 | 6,774 | 50.1 | 12,104 |
| 60.1 | 3,363 | 60.0 | 7,537 | 60.2 | 8,365 |
| 70.5 | 3,366 | 70.1 | 7,138 | 70.1 | 2,165 |
| 80.2 | 3,366 | 80.1 | 5,942 | 73.0 | 0 |
| 90.5 | 3,366 | 90.1 | 3,949 | | |
| 100.1 | 3,366 | 100.1 | 1,158 | | |
| 110.5 | 3,366 | 103.6 | 0 | | |
| 120.1 | 3,366 | | | | |
| 130.3 | 3,325 | | | | |
| 140.4 | 2,999 | | | | |
| 150 | 2,384 | | | | |
| 160.1 | 1,422 | | | | |
| 170.2 | 133 | | | | |
| 171.1 | 0 | | | | |

**Table C-26**
**Tabular HRR data for Figure C-21**

| Minimum Heat Release Rate | | Expected Heat Release Rate | | Maximum Heat Release Rate | |
|---|---|---|---|---|---|
| **Time (s)** | **Heat Release Rate (kW)** | **Time (s)** | **Heat Release Rate (kW)** | **Time (s)** | **Heat Release Rate (kW)** |
| 0.0 | 0 | 0.0 | 0 | 0.0 | 0 |
| 10.1 | 36 | 10.1 | 90 | 10.1 | 220 |
| 20.3 | 293 | 20.3 | 726 | 20.1 | 1,718 |
| 30.2 | 853 | 30.2 | 2,118 | 30.0 | 5,109 |
| 40.0 | 1,725 | 40.0 | 4,285 | 40.1 | 10,044 |
| 50.3 | 2,961 | 50.2 | 7,347 | 50.1 | 14,535 |
| 60.1 | 4,161 | 60.0 | 9,696 | 60.0 | 13,561 |
| 70.2 | 4,488 | 70.2 | 9,643 | 70.1 | 7,311 |
| 80.5 | 4,488 | 80.1 | 8,453 | 79.2 | 0 |
| 90.3 | 4,488 | 90.0 | 6,479 | | |
| 100.0 | 4,488 | 100.4 | 3,577 | | |
| 110.4 | 4,488 | 110.3 | 0 | | |
| 120.1 | 4,488 | | | | |
| 130.0 | 4,451 | | | | |
| 140.1 | 4,136 | | | | |
| 150.2 | 3,496 | | | | |
| 160.2 | 2,533 | | | | |
| 170.3 | 1,245 | | | | |
| 178.2 | 0 | | | | |

**Table C-27**
**Tabular HRR data for Figure C-22**

| Minimum Heat Release Rate | | Expected Heat Release Rate | | Maximum Heat Release Rate | |
|---|---|---|---|---|---|
| Time (s) | Heat Release Rate (kW) | Time (s) | Heat Release Rate (kW) | Time (s) | Heat Release Rate (kW) |
| 0.0 | 0 | 0.0 | 0 | 0.0 | 0 |
| 10.1 | 36 | 10.1 | 90 | 10.1 | 220 |
| 20.3 | 293 | 20.4 | 732 | 20.1 | 1,718 |
| 30.0 | 842 | 30.2 | 2,132 | 30.0 | 5,109 |
| 40.2 | 1,741 | 40.1 | 4,309 | 40.1 | 10,037 |
| 50.3 | 2,970 | 50.4 | 7,404 | 50.1 | 14,996 |
| 60.1 | 4,453 | 60.0 | 10,832 | 60.1 | 17,408 |
| 70.1 | 5,508 | 70.1 | 12,148 | 70.1 | 12,465 |
| 80.3 | 5,610 | 80.2 | 10,955 | 80.1 | 4,332 |
| 90.0 | 5,610 | 90.1 | 8,976 | 84.6 | 0 |
| 100.2 | 5,610 | 100.0 | 6,213 | | |
| 110.5 | 5,610 | 110.4 | 2,486 | | |
| 120.2 | 5,610 | 116.3 | 0 | | |
| 130.0 | 5,574 | | | | |
| 140.1 | 5,259 | | | | |
| 150.1 | 4,620 | | | | |
| 160.2 | 3,657 | | | | |
| 170.3 | 2,370 | | | | |
| 180.3 | 758 | | | | |
| 184.5 | 0 | | | | |

**Table C-28**
**Tabular HRR data for Figure C-23**

| Minimum Heat Release Rate | | Expected Heat Release Rate | | Maximum Heat Release Rate | |
|---|---|---|---|---|---|
| Time (s) | Heat Release Rate (kW) | Time (s) | Heat Release Rate (kW) | Time (s) | Heat Release Rate (kW) |
| 0.0 | 0 | 0.0 | 0 | 0.0 | 0 |
| 10.1 | 37 | 10.1 | 90 | 10.1 | 220 |
| 20.2 | 293 | 20.0 | 693 | 20.1 | 1,718 |
| 30.0 | 855 | 30.3 | 2,151 | 30.0 | 5,109 |
| 40.4 | 1,792 | 40.3 | 4,347 | 40.0 | 10,013 |
| 50.2 | 2,999 | 50.2 | 7,327 | 50.0 | 14,988 |
| 60.1 | 4,520 | 60.1 | 11,092 | 60.0 | 19,962 |
| 70.4 | 6,473 | 70.1 | 15,266 | 70.1 | 23,040 |
| 80.1 | 8,161 | 80.0 | 17,119 | 80.2 | 17,483 |
| 90.3 | 8,606 | 90.4 | 15,342 | 90.1 | 7,411 |
| 100.3 | 8,606 | 100.3 | 12,558 | 96.4 | 0 |
| 110.3 | 8,606 | 110.2 | 8,990 | | |
| 120.4 | 8,606 | 120.1 | 4,637 | | |
| 130.1 | 8,537 | 129.2 | 0 | | |
| 140.3 | 8,151 | | | | |
| 150.5 | 7,428 | | | | |
| 160.7 | 6,368 | | | | |
| 170.1 | 5,081 | | | | |
| 180.3 | 3,370 | | | | |
| 190.5 | 1,322 | | | | |
| 196.3 | 0 | | | | |

**Table C-29**
**Tabular HRR data for Figure C-24**

| Minimum Heat Release Rate | | Expected Heat Release Rate | | Maximum Heat Release Rate | |
|---|---|---|---|---|---|
| Time (s) | Heat Release Rate (kW) | Time (s) | Heat Release Rate (kW) | Time (s) | Heat Release Rate (kW) |
| 0.0 | 0 | 0.0 | 0 | 0.0 | 0 |
| 17.3 | 5 | 17.9 | 7 | 18.9 | 10 |
| 752.8 | 5 | 561.7 | 7 | 383.8 | 10 |
| 755.1 | 0 | 564.6 | 0 | 387.7 | 0 |

**Table C-30**
**Tabular HRR data for Figure C-25**

| Minimum Heat Release Rate | | Expected Heat Release Rate | | Maximum Heat Release Rate | |
|---|---|---|---|---|---|
| Time (s) | Heat Release Rate (kW) | Time (s) | Heat Release Rate (kW) | Time (s) | Heat Release Rate (kW) |
| 0.0 | 0 | 0.0 | 0 | 0.0 | 0 |
| 9.1 | 8 | 19.5 | 24 | 21.1 | 36 |
| 18.6 | 18 | 402.9 | 24 | 274.6 | 36 |
| 548.0 | 18 | 407.4 | 0 | 280.7 | 0 |
| 551.6 | 0 | | | | |

**Table C-31**
**Tabular HRR data for Figure C-26**

| Minimum Heat Release Rate | | Expected Heat Release Rate | | Maximum Heat Release Rate | |
|---|---|---|---|---|---|
| Time (s) | Heat Release Rate (kW) | Time (s) | Heat Release Rate (kW) | Time (s) | Heat Release Rate (kW) |
| 0.0 | 0 | 0.0 | 0 | 0.0 | 0 |
| 10.1 | 19 | 21.4 | 60 | 23.6 | 90 |
| 20.2 | 44 | 328.1 | 60 | 221.2 | 90 |
| 449.7 | 44 | 334.5 | 0 | 229.8 | 0 |
| 454.9 | 0 | | | | |

**Table C-32**
**Tabular HRR data for Figure C-27**

| Minimum Heat Release Rate | | Expected Heat Release Rate | | Maximum Heat Release Rate | |
|---|---|---|---|---|---|
| Time (s) | Heat Release Rate (kW) | Time (s) | Heat Release Rate (kW) | Time (s) | Heat Release Rate (kW) |
| 0.0 | 0 | 0.0 | 0 | 0.0 | 0 |
| 11.1 | 42 | 12.0 | 56 | 13.6 | 79 |
| 22.3 | 102 | 24.1 | 142 | 27.2 | 218 |
| 384.7 | 102 | 278.3 | 142 | 184.6 | 218 |
| 392.0 | 0 | 287.4 | 0 | 196.8 | 0 |

**Table C-33**
**Tabular HRR data for Figure C-28**

| Minimum Heat Release Rate | | Expected Heat Release Rate | | Maximum Heat Release Rate | |
|---|---|---|---|---|---|
| Time (s) | Heat Release Rate (kW) | Time (s) | Heat Release Rate (kW) | Time (s) | Heat Release Rate (kW) |
| 0.0 | 0 | 0.0 | 0 | 0.0 | 0 |
| 12.5 | 85 | 13.8 | 113 | 16.0 | 155 |
| 25.2 | 228 | 27.7 | 321 | 32.1 | 503 |
| 336.4 | 228 | 241.0 | 321 | 157.0 | 503 |
| 356.3 | 0 | 260.5 | 0 | 178.0 | 0 |

**Table C-34**
**Tabular HRR data for Figure C-29**

| Minimum Heat Release Rate | | Expected Heat Release Rate | | Maximum Heat Release Rate | |
|---|---|---|---|---|---|
| Time (s) | Heat Release Rate (kW) | Time (s) | Heat Release Rate (kW) | Time (s) | Heat Release Rate (kW) |
| 0.0 | 0 | 0.0 | 0 | 0.0 | 0 |
| 10.1 | 52 | 10.1 | 48 | 10.1 | 43 |
| 20.0 | 370 | 24.1 | 578 | 31.0 | 1028 |
| 31.3 | 615 | 35.3 | 874 | 42.2 | 1403 |
| 321.0 | 615 | 228.2 | 874 | 145.2 | 1402 |
| 337.1 | 0 | 248.3 | 0 | 172.1 | 0 |

**Table C-35**
**Tabular HRR data for Figure C-30**

| Minimum Heat Release Rate | | Expected Heat Release Rate | | Maximum Heat Release Rate | |
|---|---|---|---|---|---|
| Time (s) | Heat Release Rate (kW) | Time (s) | Heat Release Rate (kW) | Time (s) | Heat Release Rate (kW) |
| 0.0 | 0 | 0.0 | 0 | 0.0 | 0 |
| 10.1 | 53 | 10.1 | 49 | 10.1 | 44 |
| 20.1 | 416 | 23.7 | 608 | 29.8 | 1013 |
| 30.1 | 1049 | 35.8 | 1555 | 45.5 | 2613 |
| 37.9 | 1251 | 43.6 | 1794 | 53.3 | 2910 |
| 315.6 | 1251 | 222.4 | 1794 | 140.0 | 2910 |
| 326.2 | 986 | 235.6 | 1414 | 157.7 | 2294 |
| 338.6 | 0 | 251.1 | 0 | 178.5 | 0 |

**Table C-36**
**Tabular HRR data for Figure C-31**

| Minimum Heat Release Rate | | Expected Heat Release Rate | | Maximum Heat Release Rate | |
|---|---|---|---|---|---|
| Time (s) | Heat Release Rate (kW) | Time (s) | Heat Release Rate (kW) | Time (s) | Heat Release Rate (kW) |
| 0.0 | 0 | 0.0 | 0 | 0.0 | 0 |
| 10.1 | 53 | 10.1 | 49 | 10.1 | 45 |
| 20.0 | 415 | 22.7 | 543 | 27.2 | 810 |
| 30.0 | 1229 | 37.0 | 1921 | 48.9 | 3430 |
| 39.9 | 1836 | 46.9 | 2647 | 58.8 | 4351 |
| 43.2 | 1883 | 50.2 | 2701 | 62.1 | 4417 |
| 314.5 | 1883 | 221.6 | 2701 | 138.4 | 4417 |
| 328.1 | 1449 | 238.5 | 2078 | 161.0 | 3399 |
| 342.8 | 0 | 256.8 | 0 | 185.5 | 0 |

**Table C-37**
**Tabular HRR data for Figure C-32**

| Minimum Heat Release Rate | | Expected Heat Release Rate | | Maximum Heat Release Rate | |
|---|---|---|---|---|---|
| Time (s) | Heat Release Rate (kW) | Time (s) | Heat Release Rate (kW) | Time (s) | Heat Release Rate (kW) |
| 0.0 | 0 | 0.0 | 0 | 0.0 | 0 |
| 10.1 | 54 | 10.1 | 49 | 10.1 | 45 |
| 20.1 | 421 | 22.4 | 529 | 26.4 | 750 |
| 30.1 | 1259 | 37.1 | 1952 | 48.9 | 3446 |
| 40.1 | 2251 | 48.2 | 3301 | 61.9 | 5502 |
| 47.6 | 2519 | 55.7 | 3614 | 69.4 | 5889 |
| 313.5 | 2519 | 220.8 | 3614 | 138.4 | 5889 |
| 330.2 | 1864 | 241.6 | 2674 | 166.2 | 4357 |
| 346.1 | 0 | 261.5 | 0 | 192.8 | 0 |

**Table C-38**
**Tabular HRR data for Figure C-33**

| Minimum Heat Release Rate | | Expected Heat Release Rate | | Maximum Heat Release Rate | |
|---|---|---|---|---|---|
| Time (s) | Heat Release Rate (kW) | Time (s) | Heat Release Rate (kW) | Time (s) | Heat Release Rate (kW) |
| 0.0 | 0 | 0.0 | 0 | 0.0 | 0 |
| 10.1 | 54 | 10.1 | 49 | 10.1 | 45 |
| 20.1 | 424 | 22.3 | 520 | 26.0 | 721 |
| 30.0 | 1246 | 36.3 | 1857 | 47.1 | 3167 |
| 40.0 | 2478 | 49.1 | 3729 | 64.5 | 6404 |
| 50.1 | 3138 | 59.1 | 4505 | 74.5 | 7376 |
| 51.4 | 3149 | 60.5 | 4517 | 75.9 | 7391 |
| 303.0 | 3149 | 214.4 | 4517 | 135.4 | 7391 |
| 326.3 | 2763 | 236.7 | 3964 | 159.2 | 6485 |
| 350.0 | 0 | 266.3 | 0 | 198.8 | 0 |

**Table C-39**
**Tabular HRR data for Figure C-34**

| Minimum Heat Release Rate | | Expected Heat Release Rate | | Maximum Heat Release Rate | |
|---|---|---|---|---|---|
| Time (s) | Heat Release Rate (kW) | Time (s) | Heat Release Rate (kW) | Time (s) | Heat Release Rate (kW) |
| 0.0 | 0 | 0.0 | 0 | 0.0 | 0 |
| 10.1 | 54 | 10.1 | 49 | 10.1 | 45 |
| 20.1 | 419 | 22.0 | 497 | 25.2 | 661 |
| 30.2 | 1267 | 35.9 | 1799 | 45.5 | 2921 |
| 40.0 | 2555 | 49.4 | 3871 | 65.3 | 6695 |
| 50.1 | 4136 | 61.2 | 6101 | 80.1 | 10269 |
| 59.8 | 4761 | 70.9 | 6830 | 89.8 | 11175 |
| 313.5 | 4761 | 220.8 | 6830 | 137.9 | 11175 |
| 337.3 | 3424 | 250.5 | 4911 | 177.6 | 8036 |
| 358.3 | 0 | 276.8 | 0 | 212.7 | 0 |

**Table C-40**
**Tabular HRR data for Figure C-35**

| Minimum Heat Release Rate | | Expected Heat Release Rate | | Maximum Heat Release Rate | |
|---|---|---|---|---|---|
| Time (s) | Heat Release Rate (kW) | Time (s) | Heat Release Rate (kW) | Time (s) | Heat Release Rate (kW) |
| 0.0 | 0 | 0.0 | 0 | 0.0 | 0 |
| 10.0 | 15 | 10.0 | 19 | 10.1 | 26 |
| 20.1 | 26 | 20.9 | 35 | 20.1 | 51 |
| 29.8 | 26 | 29.9 | 35 | 30.4 | 51 |
| 41.0 | 26 | 39.9 | 35 | 40.1 | 51 |
| 50.7 | 26 | 49.9 | 35 | 49.7 | 51 |
| 60.5 | 26 | 59.9 | 35 | 60.6 | 51 |
| 70.2 | 26 | 69.9 | 35 | 70.3 | 51 |
| 80.0 | 26 | 79.9 | 35 | 80.5 | 51 |
| 89.7 | 26 | 89.9 | 35 | 87.0 | 0 |
| 100.9 | 26 | 99.9 | 35 | | |
| 109.2 | 26 | 109.9 | 35 | | |

**Table C-40 (continued)**
**Tabular HRR data for Figure C-35**

| Minimum Heat Release Rate | | Expected Heat Release Rate | | Maximum Heat Release Rate | |
|---|---|---|---|---|---|
| Time (s) | Heat Release Rate (kW) | Time (s) | Heat Release Rate (kW) | Time (s) | Heat Release Rate (kW) |
| 120.4 | 26 | 120.0 | 17 | | |
| 130.1 | 26 | 120.8 | 0 | | |
| 139.9 | 26 | | | | |
| 149.6 | 26 | | | | |
| 158.9 | 0 | | | | |

**Table C-41**
**Tabular HRR data for Figure C-36**

| Minimum Heat Release Rate | | Expected Heat Release Rate | | Maximum Heat Release Rate | |
|---|---|---|---|---|---|
| Time (s) | Heat Release Rate (kW) | Time (s) | Heat Release Rate (kW) | Time (s) | Heat Release Rate (kW) |
| 0.0 | 0 | 0.0 | 0 | 0.0 | 0 |
| 10.0 | 45 | 10.1 | 57 | 10.0 | 72 |
| 20.6 | 89 | 20.2 | 121 | 20.1 | 178 |
| 30.3 | 89 | 30.3 | 121 | 30.2 | 180 |
| 39.9 | 89 | 40.4 | 121 | 40.2 | 180 |
| 49.6 | 89 | 49.8 | 121 | 50.2 | 180 |
| 60.3 | 89 | 60.6 | 121 | 60.1 | 180 |
| 70.0 | 89 | 70.0 | 121 | 67.0 | 0 |
| 79.6 | 89 | 80.1 | 121 | | |
| 90.3 | 89 | 90.0 | 60 | | |
| 100.0 | 89 | 91.3 | 0 | | |
| 109.7 | 89 | | | | |
| 119.1 | 0 | | | | |

**Table C-42**
**Tabular HRR data for Figure C-37**

| Minimum Heat Release Rate | | Expected Heat Release Rate | | Maximum Heat Release Rate | |
|---|---|---|---|---|---|
| Time (s) | Heat Release Rate (kW) | Time (s) | Heat Release Rate (kW) | Time (s) | Heat Release Rate (kW) |
| 0.0 | 0 | 0.0 | 0 | 0.0 | 0 |
| 10.1 | 97 | 10.0 | 115 | 10.0 | 129 |
| 20.1 | 218 | 20.0 | 295 | 20.1 | 415 |
| 30.0 | 218 | 30.5 | 300 | 30.0 | 452 |
| 40.6 | 218 | 40.0 | 300 | 40.0 | 452 |
| 49.6 | 218 | 50.1 | 300 | 50.1 | 452 |
| 60.2 | 218 | 60.1 | 300 | 58.7 | 0 |
| 70.1 | 218 | 70.2 | 300 | | |
| 80.6 | 218 | 78.1 | 0 | | |
| 90.5 | 218 | | | | |
| 100.0 | 72 | | | | |
| 100.9 | 0 | | | | |

**Table C-43**
**Tabular HRR data for Figure C-38**

| Minimum Heat Release Rate | | Expected Heat Release Rate | | Maximum Heat Release Rate | |
|---|---|---|---|---|---|
| Time (s) | Heat Release Rate (kW) | Time (s) | Heat Release Rate (kW) | Time (s) | Heat Release Rate (kW) |
| 0.0 | 0 | 0.0 | 0 | 0.0 | 0 |
| 10.1 | 177 | 10.0 | 188 | 10.1 | 169 |
| 20.0 | 490 | 20.0 | 636 | 20.0 | 843 |
| 30.2 | 511 | 30.1 | 711 | 30.0 | 1,091 |
| 39.9 | 511 | 39.9 | 711 | 40.0 | 1,091 |
| 50.2 | 511 | 50.1 | 711 | 50.0 | 711 |
| 59.9 | 511 | 60.3 | 711 | 55.0 | 0 |
| 70.2 | 511 | 70.0 | 122 | | |
| 79.9 | 511 | 70.9 | 0 | | |
| 90.0 | 20 | | | | |
| 90.2 | 0 | | | | |

**Table C-44**
**Tabular HRR data for Figure C-39**

| Minimum Heat Release Rate | | Expected Heat Release Rate | | Maximum Heat Release Rate | |
|---|---|---|---|---|---|
| Time (s) | Heat Release Rate (kW) | Time (s) | Heat Release Rate (kW) | Time (s) | Heat Release Rate (kW) |
| 0.0 | 0 | 0.0 | 0 | 0.0 | 0 |
| 10.1 | 246 | 10.0 | 217 | 10.1 | 191 |
| 20.0 | 971 | 20.0 | 1,195 | 20.1 | 1,414 |
| 29.8 | 1,140 | 30.1 | 1,603 | 30.1 | 2,470 |
| 40.2 | 1,140 | 40.1 | 1,603 | 40.1 | 2,481 |
| 50.2 | 1,140 | 50.1 | 1,603 | 50.1 | 1,316 |
| 59.7 | 1,140 | 60.0 | 1,418 | 55.4 | 0 |
| 70.1 | 1,140 | 68.5 | 0 | | |
| 80.1 | 878 | | | | |
| 85.4 | 0 | | | | |

**Table C-45**
**Tabular HRR data for Figure C-40**

| Minimum Heat Release Rate | | Expected Heat Release Rate | | Maximum Heat Release Rate | |
|---|---|---|---|---|---|
| Time (s) | Heat Release Rate (kW) | Time (s) | Heat Release Rate (kW) | Time (s) | Heat Release Rate (kW) |
| 0.0 | 0 | 0.0 | 0 | 0.0 | 0 |
| 10.1 | 261 | 10.1 | 238 | 10.1 | 214 |
| 20.0 | 1,847 | 20.0 | 1,856 | 20.0 | 1,661 |
| 30.1 | 3,054 | 30.1 | 4,013 | 30.1 | 4,864 |
| 40.3 | 3,072 | 40.0 | 4,374 | 40.0 | 6,698 |
| 50.4 | 3,072 | 50.1 | 4,374 | 50.2 | 4,817 |
| 60.1 | 3,072 | 60.1 | 3,603 | 60.2 | 991 |
| 70.2 | 3,072 | 70.1 | 752 | 62.2 | 0 |
| 80.0 | 1,966 | 71.9 | 0 | | |
| 86.5 | 0 | | | | |

**Table C-46**
**Tabular HRR data for Figure C-41**

| Minimum Heat Release Rate | | Expected Heat Release Rate | | Maximum Heat Release Rate | |
|---|---|---|---|---|---|
| Time (s) | Heat Release Rate (kW) | Time (s) | Heat Release Rate (kW) | Time (s) | Heat Release Rate (kW) |
| 0.0 | 0 | 0.0 | 0 | 0.0 | 0 |
| 10.1 | 266 | 10.1 | 244 | 10.1 | 222 |
| 20.1 | 2,083 | 20.1 | 1,921 | 20.1 | 1,750 |
| 30.1 | 5,247 | 30.1 | 5,705 | 30.0 | 5,150 |
| 39.9 | 6,260 | 40.0 | 8,683 | 40.0 | 10,151 |
| 50.1 | 6,260 | 50.0 | 8,963 | 50.0 | 11,734 |
| 60.1 | 6,260 | 60.0 | 7,987 | 59.9 | 7,931 |
| 70.0 | 6,250 | 70.1 | 4,818 | 70.0 | 1,806 |
| 79.9 | 4,877 | 79.3 | 0 | 72.4 | 0 |
| 90.0 | 1,076 | | | | |
| 92.1 | 0 | | | | |

**Table C-47**
**Tabular HRR data for Figure C-42**

| Minimum Heat Release Rate | | Expected Heat Release Rate | | Maximum Heat Release Rate | |
|---|---|---|---|---|---|
| Time (s) | Heat Release Rate (kW) | Time (s) | Heat Release Rate (kW) | Time (s) | Heat Release Rate (kW) |
| 0.0 | 0 | 0.0 | 0 | 0.0 | 0 |
| 10.1 | 267 | 10.1 | 246 | 10.1 | 224 |
| 20.0 | 2,077 | 20.1 | 1,921 | 20.1 | 1,750 |
| 30.0 | 6,148 | 30.2 | 5,801 | 30.2 | 5,281 |
| 40.1 | 9,209 | 40.0 | 11,109 | 40.0 | 10,289 |
| 50.1 | 9,421 | 50.1 | 13,512 | 50.0 | 15,215 |
| 59.9 | 9,421 | 59.8 | 12,528 | 60.0 | 15,040 |
| 70.0 | 9,406 | 70.0 | 9,275 | 70.0 | 8,987 |
| 79.9 | 7,988 | 80.2 | 3,750 | 79.9 | 867 |
| 90.0 | 4,122 | 85.5 | 0 | 80.9 | 0 |
| 97.1 | 0 | | | | |

**Table C-48**
**Tabular HRR data for Figure C-43**

| Minimum Heat Release Rate | | Expected Heat Release Rate | | Maximum Heat Release Rate | |
|---|---|---|---|---|---|
| Time (s) | Heat Release Rate (kW) | Time (s) | Heat Release Rate (kW) | Time (s) | Heat Release Rate (kW) |
| 0.0 | 0 | 0.0 | 0 | 0.0 | 0 |
| 10.1 | 267 | 10.1 | 246 | 10.1 | 224 |
| 20.1 | 2,103 | 20.1 | 1,945 | 20.0 | 1,750 |
| 30.0 | 6,192 | 30.2 | 5,798 | 30.1 | 5,268 |
| 39.9 | 11,190 | 40.2 | 11,839 | 40.1 | 10,340 |
| 50.1 | 12,578 | 50.0 | 17,143 | 50.1 | 15,534 |
| 60.1 | 12,578 | 60.3 | 16,945 | 60.1 | 19,558 |
| 70.1 | 12,558 | 69.8 | 13,877 | 70.2 | 16,201 |
| 80.2 | 11,038 | 80.3 | 8,156 | 80.1 | 8,044 |
| 90.3 | 7,099 | 89.9 | 925 | 88.1 | 0 |
| 100.1 | 986 | 90.9 | 0 | | |
| 101.4 | 0 | | | | |

**Table C-49**
**Tabular HRR data for Figure C-44**

| Minimum Heat Release Rate | | Expected Heat Release Rate | | Maximum Heat Release Rate | |
|---|---|---|---|---|---|
| Time (s) | Heat Release Rate (kW) | Time (s) | Heat Release Rate (kW) | Time (s) | Heat Release Rate (kW) |
| 0.0 | 0 | 0.0 | 0 | 0.0 | 0 |
| 10.1 | 267 | 10.1 | 246 | 10.1 | 225 |
| 19.9 | 2,052 | 19.9 | 1,876 | 20.0 | 1,749 |
| 30.0 | 6,221 | 30.2 | 5,847 | 30.1 | 5,261 |
| 40.0 | 12,374 | 40.3 | 11,943 | 40.1 | 10,380 |
| 49.9 | 15,659 | 50.0 | 19,217 | 50.2 | 15,628 |
| 59.9 | 15,723 | 60.1 | 21,500 | 60.0 | 20,735 |
| 69.9 | 15,709 | 70.3 | 18,143 | 70.0 | 22,365 |
| 80.1 | 14,212 | 80.2 | 12,752 | 80.0 | 15,503 |
| 89.9 | 10,434 | 90.0 | 5,243 | 90.0 | 5,217 |
| 100.1 | 4,094 | 95.7 | 0 | 94.5 | 0 |
| 105.2 | 0 | | | | |

**Table C-50**
**Tabular HRR data for Figure C-45**

| Minimum Heat Release Rate | | Expected Heat Release Rate | | Maximum Heat Release Rate | |
|---|---|---|---|---|---|
| Time (s) | Heat Release Rate (kW) | Time (s) | Heat Release Rate (kW) | Time (s) | Heat Release Rate (kW) |
| 0.0 | 0 | 0.0 | 0 | 0.0 | 0 |
| 10.1 | 267 | 10.1 | 246 | 10.1 | 225 |
| 20.1 | 2,094 | 20.3 | 1,986 | 20.0 | 1,749 |
| 29.9 | 6,169 | 30.1 | 5,793 | 30.0 | 5,258 |
| 40.0 | 12,767 | 40.3 | 11,970 | 40.2 | 10,405 |
| 50.1 | 20,668 | 50.2 | 20,091 | 50.1 | 15,557 |
| 60.1 | 23,789 | 60.1 | 28,610 | 60.4 | 20,924 |
| 70.1 | 23,768 | 70.0 | 29,801 | 70.3 | 26,076 |
| 80.4 | 22,181 | 80.1 | 24,382 | 80.1 | 29,764 |
| 90.3 | 18,308 | 90.3 | 16,590 | 90.0 | 24,085 |
| 99.7 | 12,463 | 100.1 | 6,911 | 100.1 | 11,784 |
| 110.4 | 3,214 | 106.1 | 0 | 108.4 | 0 |
| 113.5 | 0 | | | | |

## C.3 Statistical Analysis

The model bias is evaluated using the statistical model provided in NUREG-1934 [2]. In this study, the "Experimental" value ($E$) is defined by the results discussed in Section 5-4. The "Modeled" value ($M$) will be the predicted quantity using any of the four discussed methods (1 through 4). The following expressions are used to define the statistical analysis:

$$E|\theta \sim N(\theta, \sigma_E^2);\ \tilde{\sigma}_E = \sigma_E/\theta \qquad \textbf{Eq. C-1}$$

$$M|\theta \sim N(\delta\theta, \sigma_M^2);\ \tilde{\sigma}_M = \sigma_M/\delta\theta \qquad \textbf{Eq. C-2}$$

$$\overline{\ln\left(\frac{M}{E}\right)} = \frac{1}{n}\sum_{i=1}^{n} \ln\left(\frac{M_i}{E_i}\right) \qquad \textbf{Eq. C-3}$$

$$\tilde{\sigma}_M^2 + \tilde{\sigma}_E^2 = \frac{1}{1-n}\sum_{i=1}^{n}\left[\ln\left(\frac{M_i}{E_i}\right) - \overline{\ln\left(\frac{M}{E}\right)}\right]^2 \qquad \textbf{Eq. C-4}$$

$$\boldsymbol{\delta} = \exp\left(\overline{\ln\left(\frac{M}{E}\right)} + \frac{\tilde{\sigma}_M^2}{2} - \frac{\tilde{\sigma}_E^2}{2}\right) \qquad \textbf{Eq. C-5}$$

Where:

$N(\mu, \sigma^2)$ indicates a normal distribution with mean, $\mu$, and standard deviation, $\sigma$.

The quantities $\theta$, $E$, and $M$ are the True, Experimental, and Modeled quantities of interest. In this case, $E$ and $M$ are defined as the peak heat release rate, or the burning duration.

The relative standard deviations, $\tilde{\sigma}_E$ and $\tilde{\sigma}_M$, are necessary in this framework and represent the fraction of the measured quantity that can be attributed to uncertainty.

The quantity $\tilde{\sigma}_E$ is considered an input to the statistical model and can be estimated from prior analysis (0.1 is assumed, corresponding to 10% experimental uncertainty).

The model bias, $\delta$, is the primary quantity of interest for this study since it describes the relative ratio between a predicted outcome and an observed experimental outcome.

Values of $\delta$ greater than 1.0 demonstrate model over-prediction of a quantity, and values less than 1.0 demonstrate model under-prediction of a quantity. A value of 1.0 exactly would indicate that the model predicts an identical outcome as the experimental observations, on average.

## C.4 References

1. Grant No. 2008-DN-BX-K168, *Fire Dynamics and Forensic Analysis of Liquid Fuel Fires, Final Report,* Mealy, C., Benfer, M., and Gottuk, D., Hughes Associates, Inc., Baltimore, MD, February 18, 2011.
2. *Nuclear Power Plant Fire Modeling Analysis Guidelines (NPP FIRE MAG*). NUREG-1934 and EPRI 1023259. U.S. Nuclear Regulatory Commission, Office of Nuclear Regulatory Research (RES), Washington, D.C. and Electric Power Research Institute (EPRI), Palo Alto, CA: 2012.

**Export Control Restrictions**

Access to and use of EPRI Intellectual Property is granted with the specific understanding and requirement that responsibility for ensuring full compliance with all applicable U.S. and foreign export laws and regulations is being undertaken by you and your company. This includes an obligation to ensure that any individual receiving access hereunder who is not a U.S. citizen or permanent U.S. resident is permitted access under applicable U.S. and foreign export laws and regulations. In the event you are uncertain whether you or your company may lawfully obtain access to this EPRI Intellectual Property, you acknowledge that it is your obligation to consult with your company's legal counsel to determine whether this access is lawful. Although EPRI may make available on a case-by-case basis an informal assessment of the applicable U.S. export classification for specific EPRI Intellectual Property, you and your company acknowledge that this assessment is solely for informational purposes and not for reliance purposes. You and your company acknowledge that it is still the obligation of you and your company to make your own assessment of the applicable U.S. export classification and ensure compliance accordingly. You and your company understand and acknowledge your obligations to make a prompt report to EPRI and the appropriate authorities regarding any access to or use of EPRI Intellectual Property hereunder that may be in violation of applicable U.S. or foreign export laws or regulations.

**The Electric Power Research Institute Inc.,** (EPRI, www.epri.com) conducts research and development relating to the generation, delivery and use of electricity for the benefit of the public. An independent, nonprofit organization, EPRI brings together its scientists and engineers as well as experts from academia and industry to help address challenges in electricity, including reliability, efficiency, affordability, health, safety and the environment. EPRI also provides technology, policy and economic analyses to drive long-range research and development planning, and supports research in emerging technologies. EPRI's members represent approximately 90 percent of the electricity generated and delivered in the United States, and international participation extends to more than 30 countries. EPRI's principal offices and laboratories are located in Palo Alto, Calif.; Charlotte, N.C.; Knoxville, Tenn.; and Lenox, Mass.

Together...Shaping the Future of Electricity

***Program:***

Risk and Safety Management Program



3002005303

**Electric Power Research Institute**
3420 Hillview Avenue, Palo Alto, California 94304-1338 • PO Box 10412, Palo Alto, California 94303-0813 USA
800.313.3774 • 650.855.2121 • askepri@epri.com • www.epri.com